

**LOW ALTITUDE ATMOSPHERIC TURBULENCE  
LO-LOCAT PHASE III INTERIM REPORT  
VOLUME II. INSTRUMENTATION AND DATA PROCESSING  
DETAILS, GUST VELOCITY DATA, AND TEST LOG**

*K. R. MONSON, G. W. JONES, R. H. MIELKE, et al.*

\*\*\* Export controls have been removed \*\*\*

This document is subject to special export controls and each transmittal to foreign governments or foreign nationals may be made only with prior approval of the Air Force Flight Dynamics Laboratory (FDTE), Wright-Patterson Air Force Base, Ohio 45433.

FOREWORD

This report is an interim summary of the low-level critical air turbulence research work conducted from 17 April 1968 through 8 January 1969 under Contract Number F33615-68-C-1468 (LO-LOCAT PHASE III). The report was prepared by The Boeing Company, Wichita Division for the Air Force Flight Dynamics Laboratory, Wright-Patterson Air Force Base, Ohio.


The LO-LOCAT PHASE III Project is part of Advanced Development Program 682E (ALLCAT) and, as such, is under the direction of the ADP 682E Program Director, Mr. E. Brazier, and the Technical Coordinator, Mr. Neal V. Loving. Mr. Jan N. Garrison, FDTE, is the Air Force Project Engineer.

Research is being conducted under the Boeing supervision of Mr. F. K. Atnip, Program Manager. Mr. C. F. Peterson is the Project Pilot. Mr. D. B. Marshall is in charge of Instrumentation; Mr. H. H. Depew is directing the Data Processing; and Mr. J. D. Gault is in charge of Data Analysis; Mr. W. B. Moreland (Boeing-Seattle) is directing meteorological forecasts and analysis; Airplane maintenance and inspection are the responsibility of Mr. J. Strain and Mr. J. Bonawitz, respectively.

Acknowledgment is made for the assistance of the following Boeing-Wichita personnel: Dr. T. Swaney, Structural Loads; Messrs. C. J. Gamm and J. Robertson, Instrumentation; Messrs. D. E. Gunter and J. W. Jones, Data Analysis; Messrs. W. F. Wenzlaff, C. P. Dennis, and L. D. Hager, Data Processing; and Mr. B. Dorland, Industrial Graphics. The following Boeing-Seattle personnel are providing meteorological forecasts and analysis: Messrs. R. Martin, R. Clancy, and K. Knechtel.

This report was submitted by the authors 26 May 1969.

This technical report has been reviewed and is approved.

  
GORDON R. NEEGAARD,  
Major, USAF  
Chief, Design Criteria Branch  
Structures Division  
Air Force Flight Dynamics Laboratory

## ABSTRACT

The contents of this report describe accomplishments during the first half of the Low-Level Critical Air Turbulence (LO-LOCAT) Phase III program. Data that were obtained during flight over routes near McConnell Air Force Base, Kansas, and Edwards Air Force Base, California, are presented. Also included are time histories of some of the larger magnitude gust velocities recorded over the Peterson Field, Colorado route. Approximately 72 hours of low-level (0-1000 feet) turbulence and associated meteorological data recorded from August 16, 1968, through January 8, 1969, are presented. The turbulence environment is analyzed in terms of gust velocity primary peaks, amplitude samples, rms values, maximum values and derived equivalent gusts. Mathematical expressions for turbulence spectra and scale length statistics, and correlations between atmospheric gust velocities and meteorological and geophysical phenomena are shown. The most predominant characteristics of these data are the increases in rms values, scale lengths, Taylor micro scales and maximum gust values as compared to the LO-LOCAT Phases I and II data. These differences are attributed to the increased speed of the Phase III airplane which is providing a better definition of the longer wavelengths of atmospheric turbulence. This report consists of two volumes. Volume I contains a discussion of data acquisition and quality, along with a preliminary analysis of turbulence and meteorological data. Instrumentation details, calibrations and checks, data processing, gust velocity data (power spectra, peak and amplitude count, etc.) and test logs are presented in Volume II.

(Distribution of this abstract is unlimited)

# *Contrails*



# Contrails

## TABLE OF CONTENTS

		PAGE NO.
VOLUME I		
SECTION I	INTRODUCTION	1
SECTION II	DATA ACQUISITION	3
SECTION III	DATA QUALITY	19
SECTION IV	METEOROLOGICAL DATA ANALYSIS	52
SECTION V	PRELIMINARY TURBULENCE ANALYSIS	94
SECTION VI	BREN TOWER FLYBY	223
SECTION VII	SUMMARY	229
VOLUME II		
APPENDIX I	INSTRUMENTATION DETAILS	1
	AIRPLANE AND GUST PROBE INSTRUMENTATION	1
	Airspeed	1
	Angular Rates	1
	Accelerations	1
	Pitch, Roll and Yaw Angles	2
	Angles of Attack and Sideslip	2
	Pressure Altitude	2
	Surface Positions	3
	Ground Surface Temperature	3
	Outside Air Temperature	3
	Heading	3
	Ground Speed and Drift Angle	3
	Absolute Altitude	3
	Photographic Coverage	3
	Gust Probe Temperatures	4
	SIGNAL CONDITIONING AND RECORDING	4
	Instrumentation Power Control	4
	Signal Conditioning	4
	Transducer Power Supply	5
	Sub-Carrier Oscillator Package	5
	Magnetic Tape Recorder	5
	Standardization Control Panel and Preflight Timer	5
	Time Coordination	5
	MOBILE GROUND STATION - QUICK LOOK SYSTEM	7
	Tape Recorder - Reproducer	7
	Discriminator System	7
	Time Code Reader	7
	Oscillograph	7
	Communication Radio	7

TABLE OF CONTENTS		PAGE NO.
APPENDIX II	INSTRUMENTATION CALIBRATIONS AND CHECKS	12
	CALIBRATION IN THE LABORATORY AND AT THE AIRPLANE	12
	WIND TUNNEL STATIC CALIBRATION OF THE PROBE	12
	CAMERA BORESIGHT	14
	INFLIGHT CALIBRATION OF GUST PROBE ANGLES OF ATTACK AND SIDESLIP	15
	RADAR ALTIMETER CHECK	17
	GROUND SPEED VERIFICATION	18
	WIND TUNNEL DYNAMIC CALIBRATION OF THE GUST PROBE	18
	GUST PROBE AND BOOM NATURAL FREQUENCY DETERMINATION	20
	AIRSPEED CALIBRATION	21
	RADIOMETER (GROUND SURFACE TEMPERATURE) CALIBRATION	24
	OUTSIDE AIR TEMPERATURE (OAT) CALIBRATION	27
APPENDIX III	DATA PROCESSING	61
	GROUND STATION EQUIPMENT	61
	DATA PLAYBACK	62
	COMPUTER PROGRAMS	65
	MULTIPLE REGRESSION	88
APPENDIX IV	GUST VELOCITY POWER SPECTRA AND ASSOCIATED DATA	105
	POWER SPECTRA	106
	HOMOGENEITY	106
	COHERENCY	106
	EXPERIMENTAL TO MATHEMATICAL COMPARISONS	107
	ISOTROPY	107
APPENDIX V	GUST VELOCITY PEAK, AMPLITUDE AND LEVEL CROSSING COUNT DATA	252
APPENDIX VI	TEST LOG	277
REFERENCES		298

## LIST OF ILLUSTRATIONS

<u>FIGURE NO.</u>	<u>VOLUME II TITLE</u>	<u>PAGE NO.</u>
I-1	Recording System Block Diagram	9
I-2	Instrumentation Power Control Block Diagram	10
I-3	Mobile Ground Station Instrumentation System	11
II-1	Front View of Camera Installation	31
II-2	Front View of Camera Installation with Aerodynamic Fairing Installed	31
II-3	Rear View of Camera Installation	32
II-4	Boresight Calibration Target Stand	33
II-5	Side View of Boresight Calibration Setup	34
II-6	Calculation of Target Spacing	34
II-7	Top View of Boresight Calibration Setup	35
II-8	Camera Boresight Calibration for Angle of Attack	36
II-9	Camera Boresight Calibration for Angle of Sideslip	37
II-10	Confetti Hopper Installation in C-135 Airplane - Aft View	38
II-11	C-135 Airplane Confetti Discharge Duct-Left Exterior Side View	38
II-12	Sample Frame of Confetti Film	39
II-13	Radial Template Used to Determine the Point of Emanation of Confetti Streaks	40
II-14	Typical Film Frame Showing Point of Emanation Obtained through use of the Radial Template	40
II-15	Gust Boom and Probe Installation on T-33A Airplane	41
II-16	Gust Probe Head and Pressure Port Identification	41
II-17	Angle of Attack Calibration for 0.4 Mach	42

## LIST OF ILLUSTRATIONS

<u>FIGURE NO.</u>	<u>VOLUME II TITLE</u>	<u>PAGE NO.</u>
II-18	Angle of Attack Calibration for 0.5 Mach	43
II-19	Angle of Attack Calibration for 0.6 Mach	44
II-20	Angle of Sideslip Calibration for 0.4 Mach	45
II-21	Angle of Sideslip Calibration for 0.5 Mach	46
II 22	Angle of Sideslip Calibration for 0.6 Mach	47
II 23	Airplane Flight Path over Cheney Reservoir	48
II-24	Time History of Terrain Height from Radar Altimeter Data	49
II-25	Probe Vertical Acceleration Time History-Natural Frequency Determination	50
II-26	Probe Lateral Acceleration Time History-Natural Frequency Determination	51
II-27	Probe Vertical Acceleration Time History-Natural Frequency Determination	52
II-28	Probe Lateral Acceleration Time History-Natural Frequency Determination	52
II-29	Probe Vertical Acceleration PSD-Natural Frequency Determination	53
II-30	Probe Lateral Acceleration PSD-Natural Frequency Determination	53
II-31	Probe Vertical Acceleration PSD-Natural Frequency Determination	53
II-32	Probe Lateral Acceleration PSD-Natural Frequency Determination	53
II-33	Smoky Hill Gunnery and Bomb Range Features in Area of Tower No. 2	54
II-34	Airspeed Calibration-Tower Flyby Arrangement	55
II-35	Thermometers for Measuring Water Temperature	56
II-36	OAT Probe Installation of T-33 Airplane	57
II-37	OAT Calibration from Smoky Hill Tower Flyby	58
II-38	Cedar Vale Remote Weather Station	59

## LIST OF ILLUSTRATIONS

<u>FIGURE NO.</u>	<u>VOLUME II TITLE</u>	<u>PAGE NO.</u>
II-39	OAT Calibration from Cedar Vale Fly-Bys	60
III-1	Ground Station Equipment Diagram	93
III-2	Low Level Turbulence Data Processing Sequence	94
III-3	Compensation	95
III-4	Flow Diagram of Data Processing Steps	96
III-5	Analytical and Statistical Calculations	97
III-6	Ideal Filter	98
III-7	Ormsby Filter	98
III-8	Martin-Graham Filter	98
III-9	Comparison of Ormsby and Martin-Graham Filters	99
III-10	Two Pass Filter	99
III-11	Aliasing	100
III-12	Example of High Pass Filtering Sequence	101
III-13	Martin-Graham Transfer Function	102
III-14	Martin-Graham Time Function	103
III-15	Linear Extension	104
III-16	Folded Extension	104
III-17	Folded-Inverted Extension	104
IV-1 thru V-144	Turbulence Spectra Data	108 thru 251
V-1 thru V-12	Gust Velocity Peak and Level Crossing Distributions	253 thru 264
V-13 thru V-24	Gust Velocity Peak, Amplitude and Level Crossing Probability Distributions	265 thru 276

## LIST OF TABLES

## VOLUME II

<u>TABLE NO.</u>	<u>TITLE</u>	<u>PAGE NO.</u>
I-1	Instrumentation Arrangement	6
II-1	Calibration Details	29
II-2	Airspeed Calibration Variables Recorded	22
II-3	Instrumentation and Equipment	23
II-4	Recorded Data for Airspeed Calibration	23
II-5	OAT Calibration Temperatures for Cedar Vale Test	28
III-1	Digitizer and Strip Chart Formats	63
III-2	Filter Constants	78
III-3	Filter Guidelines	79
III-4	F - Values for $\nu_2$ Degrees of Freedom	89
VI-1	Test Log	279
VI-2	Low Turbulence Data Samples	297

Symbols and Abbreviations :

A	Regression coefficient ,
A thru H, J, K	Coefficients in the equation for angle of attack.
A' thru H', J', K'	Coefficients in the equation for angle of sideslip.
A(n)	Complex finite transform.
$\tilde{A}(n)$	Complex conjugate of A(n).
a	“Universal Constant” in the longitudinal gust velocity component spectrum expression, constant in $\alpha$ equation; and shape parameter used in spectra mathematical expressions.
B	Air stability ratio.
b	Constant in $\beta$ equation, also a constant in gust velocity rms distribution equation.
$b_n$	Real part of Fourier transform.
C	Constant in the Lumley-Panofsky equation.
c	Mean aerodynamic chord,
c.g.	Airplane center of gravity.
$C_{L_\alpha}$	Airplane lift curve slope in 1/radians .
cpf	Cycles per foot.
cps	Cycles per second.
D	Distance from airplane c.g. to measurement location in feet.
d	Degrees of freedom, distance traveled in statute miles, differential.
db	Decibel
$E_{AR}$	Actual energy per unit area radiated from a real surface .
$E_{BB}$	Energy per unit area radiated from a black body.

## NOTATIONS

$E_R$	Incoming radiant energy.
$E_\alpha$	Total crossings of the level $\alpha$ .
$F$	F-ratio or F-test of significance in regression analysis.
$F(f)$	Fourier transform modulus.
$f$	Frequency in cps; function.
$f_b$	Frequency of occurrence in band $b$ .
$f_c$	The highest frequency of a low-pass filter whose amplitude is passed with unity gain (cutoff frequency) in cps.
$f_N$	Nyquist or folding frequency in cps.
fps	Feet per second.
$f_s$	Sampling frequency in samples per second.
$f_\alpha$	A significant frequency present in the spectrum in cps.
$G_f$	Gust factor.
$G_S$	Ground speed in feet per second.
$g$	Earth's gravitational constant at sea level = 32.174 ft./sec. <sup>2</sup>
$H$	Altitude above the earth's surface in feet, true altitude in feet.
$H_c$	Calibrated pressure altitude in feet.
$H(f)$	Transfer function of the filter.
Hg	Symbol for the element Mercury.
$H_I, H_1$	Indicated pressure altitude in feet.
$\overline{H_N(f)}$	Constrained transfer function.
$H_P$	Pressure altitude in feet.
$h$	True heading in degrees.



$h_m$	Magnetic heading in degrees.
$h_n$	Filter weights at time $t \pm n \Delta t$ .
$\overline{h_n}$	Constrained filter weights.
$h(t, \tau)$	Time domain weighting function.
$h_0$	Constant in empirical scale length equation.
$i$	Counter, time series sample.
ips	Inches per second.
IAS	Indicated airspeed.
IRIG	Inter-range Instrumentation Group
in.	Inches .
$j$	Square root of minus one.
$K_{a,b}$	Constants.
KIAS	Knots indicated airspeed.
$K_g$	Gust alleviation factor.
$K_t$	Ram recovery factor for OAT probe
$k$	Spatial frequency in cpf; also defines order of the derivative of the transfer function $H(f)$ .
$k_1, k_2, k_3$	Truncated standard deviation frequency limits corresponding to 0.04, 0.667 and 10 cps, respectively, in cycles per foot.
$L$	Turbulence scale length in feet.
$L_f$	Minimum focal range of the camera lens in feet.
$L_h$	Constant in empirical scale length equation.
$l$	Distance from probe tip to accelerometers in feet.
$M$	True Mach Number.

## NOTATIONS

$M_s$	Magnitude of the center of the step pressure.
$m$	Maximum lag = $f_N / \Delta f$ , slope of a line, number of functions of the input variables, and meters.
$mb$	Millibar
$mm$	Millimeter.
$N$	Total number, conditions, data points, samples, peaks, bands.
NBFM	Narrow band frequency modulation.
$N_0$	Characteristic frequency from power spectral density - cpf.
$N_{OL}$	Number of crossings of the zero level.
$N_p$	Total number of peaks per mile. (characteristic frequency).
$N_{pe}$	Total number of peaks obtained using extrapolation technique.
$N_\alpha$	Crossings per mile of the level $\alpha$ .
$n$	Acceleration in g units, also a counter, number of data points, shape parameter in spectra mathematical expressions.
OAT	Outside air temperature in °F.
$O_n$	Run test observation of the mean.
$O'_n$	Run test observation of the mean square
PSD	Power spectral density.
$P_s$	Static pressure in inches of mercury.
$P_{s_i}$	Indicated static pressure in inches of mercury.
$P_o$	Static pressure at sea level under standard conditions - 29.921 inches of mercury.
$P_\alpha$	Level crossing probability
$Q$	Number of independent variables in the regression equation.
$q_c$	Calibrated impact pressure in inches of mercury.

## NOTATIONS

$q_I$	Indicated impact pressure in inches of mercury.
$R_A$	Radar altitude, feet
$R$	Richardson number.
$[R]$	Rotation matrix used to transform measurements from the airplane reference axis to the earth reference axes.
$R_1$	Value of least square line at a given wind speed.
rms	Root mean square.
$R_d$	Distance from c.g. to camera lens in feet.
$R(\tau)$	Gust velocity covariance function.
$R(\tau)/R(0)$	Gust velocity autocorrelation function where $\tau = 0 \dots \tau_L$ .
$S$	Airplane planform wing area in $\text{ft.}^2$ , horizontal distance in miles.
SCO	Subcarrier oscillator
$S_T$	True solar time of day - hours.
$S_{SE}$	Sine of solar elevation.
$T$	Period of time function in seconds.
$T_a$	Ambient air temperature in degrees Rankine.
$T_{AR}$	Actual temperature of real surface in degrees Rankine.
$T_{BB}$	Temperature of black body in degrees Rankine.
Temp.	Temperature.
$T_G$	Ground surface temperature in degrees Fahrenheit.
$T_I$	Calibrated outside air temperature in degrees Rankine.
$T_L$	Lower time limit of weighting function in seconds.
$T_o$	Temperature at sea level under standard conditions (518.69 degrees Rankine).

## NOTATIONS

$T_{rad}$	Surface temperature as recorded by radiometer.
$T_U$	Upper time limit of weighting function in seconds.
$t$	Time in sec., also standardized variable.
$U_{de}$	Derived equivalent gust velocity in fps.
$\left. \begin{array}{l} U_U \\ U_V \\ U_W \end{array} \right\}$	Probe motion terms
$u$	Longitudinal gust velocity in fps, positive aft.
$V$	True airspeed or ground speed in fps.
$V_e$	Equivalent airspeed in fps.
$V_F$	Confetti fall rate in fps.
$V_G$	Ground speed in fps
$V_i$	Indicated airspeed.
$V_{SL}$	Confetti fall rate at sea level in fps.
$V_T$	True airspeed in fps.
$\{V\}$	Represents the matrix of true airspeed components and corrections for pitch and yaw rate.
$v$	Lateral gust velocity in fps, positive to the right.
$W$	Airplane weight in pounds, wind speed in fps.
$WA$	Wind angle, angle in degrees between airplane ground track and wind vector.
$W_D$	Wind direction in degrees azimuth.
$\overline{W_E}$	Average easterly winds in fps.
$\overline{W_N}$	Average northerly winds in fps.
$w$	Vertical gust velocity in fps, positive upward.

$x$	Amplitude.
$x_b$	Mid-band value.
$x_i$	$i$ th value of $x$ , predictors, coefficient of simple linear correlation, and value of gust velocity rms at a given wind speed.
$x(i)$	Amplitude values of the time series.
$x_k(t_i)$	$k^{\text{th}}$ record included in the ensemble averaging scheme.
$\tilde{X}_q$	Smoothed values.
$x(t)$	Sampled value of time series.
$x_t^*$	Filter output data at equi-spaced intervals.
$x^*(t)$	Sampled value of low-pass filtered time series.
$\tilde{x}(t)$	Sampled value of high-pass filtered time series.
$X_\alpha$	Level of gust velocity - fps.
$Y$	Dependent variable, regression function
$y$	Intercept of $y$ axis, random variable.
$Z_i$	Input variable.
%	Percent.
$\alpha$	Angle of attack in degrees, levels of gust velocity used in level crossing procedure; confidence limit.
$\beta$	Angle of sideslip in degrees.
$\Gamma$	Lapse rate in degrees Fahrenheit/ft. (+ indicates temperature decrease with increasing altitude).
$\Gamma_d$	Dry adiabatic lapse rate.
$\gamma$	Ratio of specific heats for air = 1.40.
$\gamma^2(k)$	Coherency function.
$\Delta$	Incremental or difference.

## NOTATIONS

$\Delta f$	A change in frequency in cps, also the width between where the filter transfer function equals one and zero.
$\Delta h$	Static pressure error in feet.
$\Delta H$	Distance above or below reference point $H_{IT}$ , also difference in terrain elevation-in feet.
$\Delta N_{ZCG}$	Incremental load factor in acceleration units.
$\Delta P_S$	Static pressure error in inches of mercury.
$\Delta P_S/q_I$	Pressure coefficient - dimensionless
$\Delta P_{SP}$	Static pressure position error correction inches of Mercury.
$\Delta P_\alpha$	Angle of attack differential pressure in inches of mercury.
$\Delta P_\beta$	Angle of sideslip differential pressure in inches of mercury.
$\Delta t$	Time interval between data samples in seconds.
$\Delta W/\Delta H$	Vertical wind gradient in fps/ft.
$\Delta W_{DH}$	Number of degrees of wind direction change between start and end of data sample.
$\Delta w_H$	Horizontal wind gradient in ft./sec./mi.
$\Delta \alpha$	Total angle of attack correction in degrees.
$\Delta \alpha_{FR}$	Angle of attack correction due to confetti fall rate in degrees.
$\Delta \alpha_{PL}$	Angle of attack correction due to measurement location in degrees.
$\Delta \alpha_{PR}$	Angle of attack correction due to aircraft rate of pitch in degrees.
$\Delta \beta$	Total angle of sideslip correction in degrees.
$\Delta \beta_{FR}$	Angle of sideslip correction due to confetti fall rate in degrees.

# Contrails

## NOTATIONS

$\Delta\beta_{PL}$	Angle of sideslip correction due to measurement location in degrees.
$\Delta\beta_{YR}$	Angle of sideslip correction due to aircraft rate of yaw in degrees.
$\Delta\psi$	Error in angle of yaw.
$\delta$	Drift angle in degrees.
$\epsilon$	Viscous dissipation rate in $\text{ft}^2/\text{sec}^3$ filter constant, and emissivity factor.
$\epsilon_C$	Emissivity of surface used for calibration.
$\epsilon_R$	Emissivity of a real surface.
$\eta$	Kolmogorov microscale.
$\theta$	Pitch angle in degrees.
$\dot{\theta}$	Rate of pitch in degrees/sec.
$\lambda$	Taylor turbulence microscale length.
$\mu$	Air viscosity in $\text{lb. sec./ft.}^2$ , also mean value, airplane mass ratio.
$\mu_1, \mu_2$	Constant used in gust velocity rms distribution equation.
$\mu_x(t)$	Ensemble average time function
$\nu$	Kinematic viscosity, degrees of freedom.
$\pi$	3.1416 . . . .
$\rho$	Air density in $\text{slugs/ft.}^3$
$\rho_0$	Air density at sea level under standard conditions - .002378 $\text{slugs/ft.}^3$ .
$\sigma$	Standard deviation of a statistical sample; standard deviation in fps from gust velocity spectra between 0.0416 and 10 cps; air density ratio; Stefan-Boltzman constant.
$\sigma_D$	Standard deviation about a least square line.
$\sigma_L$	Standard deviation of level crossing distribution.
$\sigma_N$	Standard deviation of noise.

## NOTATIONS

$\sigma_n$	Standard deviation of vertical acceleration.
$\sigma_{pe}$	Standard deviation of primary peaks obtained using extrapolated value of $N_{pe}$ .
$\sigma_R$	Standard deviation of recorded data.
$\sigma_T$	Standard deviation in fps obtained from the gust velocity spectra between 0.667 and 10 cps.
$\sigma_t$	Standard deviation of the gust velocity time series in fps.
$\sigma_{tm}$	Minimum valid $\sigma_t$
$\sigma_Y$	Standard deviation of Y.
$\sigma_y$	Standard deviation of y.
$\sigma_\alpha$	Standard deviation of angle of attack differential pressure in inches of Hg.
$\sigma_\beta$	Standard deviation of sideslip differential pressure in inches of Hg.
$\sigma_o$	Standard deviation (dispersion of the distribution) of gust velocity rms.
$\sigma_{oc}$	Corrected standard deviation of gust velocity rms.
$\sigma_1$	Standard deviation of the time derivative of the associated function.
$\sigma_2, \sigma_3$	Constant used in rms gust velocity distribution equation.
$\tau$	Lag time for the weighting operation convolution in seconds.
$\tau_L$	Maximum correlation distance where $\tau_L = mV$ .
$\Phi$	One-dimensional gust velocity power spectral density.
$\phi$	Roll angle in degrees.
$\chi$	Chi statistic.
$\psi$	Yaw angle in degrees.
$\dot{\psi}$	Rate of yaw in degrees per second.
$\omega$	Frequency in radians per second.
$\omega_o$	Break frequency - radians per second.



## NOTATIONS

### SUBSCRIPTS AND SUPERSSCRIPTS:

b	Band number.
Corr.	Corrected value.
D	Based on the Dryden equation.
e	Extrapolated value.
filt.	Filtered value.
H	Horizontal.
i	Sample number.
N	Noise.
n	Counter.
$\kappa$	Based on the von Karman equation.
max	Indicates maximum value.
min	Indicates minimum value.
P	Peak count or, based on the Lumley- Panofsky equation.
R	Recorded data.
T	Truncated, obtained from wind tunnel instrumentation, obtained from tower.
t	From the gust velocity time series.
u	From the longitudinal gust velocity component.
v	From the lateral gust velocity component.
w	From the vertical gust velocity component.
x	Longitudinal.
y	Lateral.
z	Vertical.

NOTATIONS

SUBSCRIPTS AND SUPERSSCRIPTS (CONT.):

- o Initial value.
- I Pertaining to quadrant 1
- II Pertaining to quadrant 2
- III Pertaining to quadrant 3
- IV Pertaining to quadrant 4
- $\alpha$  Related to level crossing count; also refers to significant frequency content present in the data.

Primes indicate Hanned estimates unless otherwise noted.

Overbars depict time means.

- 2 Refers to starting point of leg
- 3 Refers to ending point of leg
- 32 Refers to difference between start and end.

## APPENDIX I

## INSTRUMENTATION DETAILS

This appendix presents a description of instrumentation being used to obtain data during the LO-LOCAT Phase III program. A detailed description of the instrumentation equipment, installations, locations, wiring diagrams, and operating procedures are published in References I-1 and I-2 for the airplane and mobile ground station systems, respectively.

AIRPLANE AND GUST PROBE INSTRUMENTATION

Instrumentation installed in the airplane and gust probe is discussed below in relation to the specific parameters being measured.

Airspeed

A Rosemount Type 831V5 differential pressure transducer is installed in the probe to measure impact pressure. The output of this transducer is conditioned and recorded on two channels. One channel is for coarse airspeed measurement and the other for the fine airspeed measurement. The nonlinearity and hysteresis are less than 0.75 percent of full scale output. Thermal zero and sensitivity shift are held to less than 0.1 percent full scale by temperature regulation of the probe transducer compartment. High natural frequency and low sensitivity to accelerations ensure optimum dynamic response to airspeed changes. The maximum estimated transducer error is 0.5 percent of full scale range.

Angular Rates

Sub-miniature precision rate gyros, Sanders Associates, Inc., Model GPE-1 are installed in the probe to sense rates of yaw and pitch. The rate of roll gyro and Sanders Model RGSEA rate gyro system electronics are installed in the airplane armament section. Data pick-offs are rotary differential transformers. The 0.65 degree maximum displacement at full scale of 15 degrees/second results in a minimum of cross-coupling error and a high signal-to-noise ratio. The gyro system electronics consists of demodulators, amplifiers, chokes, and reference transformers. A gain adjustment is supplied in the amplifier to ensure an optimum output level.

Temperature-compensated damping is provided within each gyro by viscous forces from the shearing of silicone oil. The gyro enclosure is temperature controlled to ensure stability of damping and output signal. Hysteresis of the gyro output is less than 0.1 percent of full scale. Threshold and resolution are less than 0.01 degree/second. The maximum estimated error, in percent of full scale, including nonlinearity is +2 percent.

Accelerations

Linear servo accelerometers, Kistler Instrument Corporation Model 303M122, are installed in the probe to measure vertical, lateral, and longitudinal accelerations. Identical units are installed at the airplane c.g., airplane station 237, to measure vertical and lateral accelerations.

The unit incorporates a "self test coil" which is used to check instrument performance. A current

applied to this coil imparts a force to the seismic mass which simulates the force caused by an external acceleration. Resolution of the sensor is better than 0.1 percent of full scale with nonlinearity and hysteresis values such that the overall error is less than  $\pm 1$  percent.

## Pitch, Roll and Yaw Angles

A three-axis vertical and azimuth stable platform, Lear Siegler Instrument Company Model AN/ASN-50, is installed at the base of the gust boom. This platform provides freedom of rotation about the roll, yaw, and pitch axes. The AN/ASN-50 attitude group is designed to serve as a central gyroscopic reference subsystem. Outputs are provided for roll, pitch, and azimuth information. The vertical reference portion provides gyro-stabilized data referenced to the earth. The azimuth reference signal is obtained from a vertically stabilized directional gyroscope. Being vertically stabilized, the azimuth output is free of intercardinal heading, pitch, and bank errors associated with all nonstabilized directional gyroscopes.

Test records of the components indicate vertical gyro drift performance well within 15 deg./hr. for the system. Random azimuth heading gyro drift rates have been observed to be less than 0.2 deg./hr. The following is a summary of the performance specification for the system:

- Bench Vertical Error  $\pm 0.25$  deg., maximum
- Free Vertical Drift  $\pm 10$  deg./hr., maximum
- Erection Rate  $1.3 \pm 0.5$  deg./min.
- Erection Gradient  $2.6 \pm 1.0$  deg./min.
- Roll Follow-up Rate 360 deg./sec.
- Yaw Follow-up Rate 180 deg./sec.

## Angles of Attack and Sideslip

These data are derived from differential pressure data obtained from pressure transducers mounted in the heated probe. The differential pressure transducers are connected by short, balanced cavities to the probes oriented on the probe head along the vertical and horizontal planes. Dual transducers are installed for each differential pressure, providing high and low sensitivities. The high sensitivity pressure transducer is a Rosemount Engineering Company Model 831V1. The low sensitivity transducer is a Statham Instruments, Inc. Model PM 131. Maximum errors are  $\pm 0.5$  percent and  $\pm 1.0$  percent of full scale, respectively.

## Pressure Altitude

A pressure transducer, Statham Instruments Inc. Model PA208, 0-15 psia, is mounted in the section of the probe adjacent to the static pressure ports for detection of pressure altitude.

The transducer has an inherently low sensitivity to accelerations. To further minimize this effect, it is oriented such that the axis most sensitive to acceleration is parallel to the probe longitudinal axis. Thermal zero and sensitivity shift are minimized by temperature regulation of the probe

transducer compartment. The transducer error, including nonlinearity and hysteresis, is less than  $\pm 1$  percent of full scale range.

## Surface Positions

Left and right aileron, left elevator, and rudder potentiometer type position transducers, New England Model 78PS, are installed on the hinge centerline of the airplane control surfaces. Transducer errors are less than  $\pm 3$  percent of full scale.

## Ground Surface Temperature

A radiation thermometer, Barnes Engineering Company Model PRT 4, is used to sense ground surface temperatures. The instrument operates by comparing the incoming radiation from the surface being examined with radiation emitted by an internal radiation reference standard. The instrument consists of an optical head mounted to look downward and an electronic unit that contains solid state processing and power circuits. The maximum system error throughout the range of ground temperatures is approximately  $\pm 4^{\circ}\text{C}$ .

## Outside Air Temperature

A Rosemount Model 102E OAT probe, with exposed platinum elements for fast response, is installed on the side of the airplane fuselage to measure absolute air temperature. The probe has an average response time constant of 0.025 seconds. Overall maximum error is estimated at  $\pm 0.5^{\circ}\text{C}$ .

## Heading

Heading data are recorded by paralleling the airplanes AN/ARN-14 heading indicating system. Transducer error is less than  $\pm 2$  percent of full scale.

## Ground Speed and Drift Angle

An AN/APN-153 Doppler radar system is installed on the airplane for measuring drift angle and ground speed. Error of the system is less than  $\pm 2$  percent of full scale.

## Absolute Altitude

Altitude of the test airplane above the terrain is determined from a Minneapolis Honeywell Model HG9050 radar altimeter. Maximum errors are estimated to be 7.5 feet plus 3 percent of altitude between 100 and 500 feet and 11 feet plus 3 percent of altitude between 500 and 1000 feet.

## Photographic Coverage

An Automax G-1 (35mm) camera with a 4 inch lens was installed in the nose section above the gust boom for use during sideslip calibration flights. This camera was used to photograph confetti dropped from a KC-135 aircraft.

## Gust Probe Temperatures

Thermistor elements are used to measure the probe temperatures at the probe head, instrument carrier and manifold ring. Signal outputs are recorded on NB/FM magnetic tape and used as a reference check on the transducer heater circuits, as well as a possible "trouble shooting" aid for the instrumentation in the gust probe.

## SIGNAL CONDITIONING AND RECORDING

The following electronic apparatus are utilized in supplying electrical power, conditioning the transducer output signals, and recording the data on magnetic tape for subsequent reduction and analysis. A block diagram of this equipment is shown in Figure I-1.

### Instrumentation Power Control

A Jack and Heinz Model F45-3 2500 VA inverter (400 cps-3 phase), a Leland Model SE-7 750 VA inverter (60 cps - single phase), and an ATR Manufacturing Co., Inc. Model RSE 115V inverter (60 cps - single phase) are installed to provide electrical power for the instrumentation equipment by electrical tie-in with the airplane power system. A master instrumentation power switch controls the power relays. This enables the pilot to have complete control of the instrumentation power. The instrumentation power control is shown in Figure I-2.

### Signal Conditioning

Each transducer output is passed through signal conditioners to provide the required input to the Sub-Carrier Oscillator (SCO). The signal conditioners also perform the secondary function of providing drift and sensitivity correction voltages to the SCO's on command from the Standardization Control Panel (SCP).

The signal conditioner mounting chassis accomodates up to 25 signal conditioner modules. Since each module serves two parameters, the maximum capability is 50 parameters per chassis.

The modules are used in conjunction with the transducers as a device for facilitating:

- Transducer balance
- Transducer bias
- Transducer excitation
- Transducer standardization
- System zero drift checks
- System sensitivity drift checks

The module is packaged as a printed circuit card containing all components required for two channels of data. The units are designed specifically for the NBFM system.



## Transducer Power Supply

The transducer power supply, a Neff Model 302, converts 115V, 400 cps airplane power to regulated 18 volts DC power. The power supply provides 18V DC to the NBFM system for drift and sensitivity correction, and for transducer excitation.

## Sub-Carrier Oscillator Package

Each data input is connected to an individual Teledynamics SCO. The SCO's convert the data inputs into frequency modulated sub-carrier signals. These signals are then combined in the mixer amplifier to form a composite signal which is recorded on magnetic tape.

The SCO's are solid state and interchangeable in the mounting chassis. One Band 1 SCO is required for automatic correction commands. This SCO is installed in the SCO package containing the reference oscillator. SCO's operating in Bands 5 through 11 are used for data except for that package containing the correction and reference units. In this package, Band 11 is restricted to reference use. The reference oscillator being used presents a stable 7.35 Kc reference signal for flutter compensation of the tape record/reproduce process.

## Magnetic Tape Recorder

An Ampex (Model AR 200) one inch magnetic tape recorder installed in the aft cockpit area is the primary data gathering system. System arrangement consists of 4 tracks of NB/FM data, 1 track of time recording, and 1 track of audio (Pilot's Interphone and Radio). The tape recorder has a recording speed of 3-3/4 inches per second and uses 10-1/2 inch tape reels with a total capacity of 4600 feet of 1 mil thick magnetic tape.

The arrangement of the individual recorded parameters by track and band is presented in Table I-1.

## Standardization Control Panel and Preflight Timer

The Standardization Control Panel (SCP) and Preflight Timer were designed to provide preflight and inflight standardization control for the NBFM data system. Outputs from the SCP actuate relays in the signal conditioner in a prescribed sequence such that reference voltages are applied to the recording system. The output sequence may be produced automatically or each reference voltage may be selected individually through a manual selector switch.

## Time Coordination

An Astrodata Model 6100 time code generator (TCG) supplies elapsed time to the data tape recorder. The TCG also provides pulses for camera framing during sideslip calibration flights.

The generator accumulates time data to 23 hours, 59 minutes and 59 seconds which is supplied as an output in the form of a serial binary amplitude modulated 1000 cps carrier for recording on magnetic tape. The TCG is controlled by an integral one megacycle crystal controlled oscillator with a stability of 3 parts in  $10^8$  or one second per month.

TABLE I-1

INSTRUMENTATION ARRANGEMENT

No.	Description	Track	Band
1	Probe Temperature No. 3	5	3
2	Right Hand Aileron Position	5	4
3	Angle of Pitch	5	5
4	Ground Surface Temperature	5	6
5	Angle of Sideslip Hi-Sensitivity	5	7
6	Angle of Sideslip Lo-Sensitivity	5	8
7	Rate of Roll	5	9
8	Vertical Acceleration Probe	5	10
9	Probe Temperature No. 2	7	3
10	Left Hand Aileron Position	7	4
11	Angle of Yaw	7	5
12	Rudder Position	7	6
13	Angle of Attack Hi-Sensitivity	7	7
14	Angle of Attack Lo-Sensitivity	7	8
15	Rate of Pitch	7	9
16	Camera Pulse	7	10
17	Longitudinal Acceleration Probe	7	11
18	Probe Temperature No. 1	9	3
19	Left Hand Elevator Position	9	4
20	Angle of Roll	9	5
21	Doppler Drift Angle	9	6
22	Radar Altitude	9	7
23	Aircraft Heading	9	8
24	Doppler Ground Speed	9	9
25	Rate of Yaw	9	10
26	Lateral Acceleration-Probe	9	11
27	Auto-Cal Signal	11	1
28	Condition and Event	11	2
29	Outside Air Temperature	11	5
30	Indicated Airspeed Fine	11	6
31	Indicated Airspeed Coarse	11	7
32	Pressure Altitude	11	8
33	Lateral Acceleration - Aircraft C.G.	11	9
34	Vertical Acceleration - Aircraft C.G.	11	10
35	Flutter Compensation	11	11
36	Pilot's Comments - Voice	12	--
37	Elapsed Time - TCG	13	--



## MOBILE GROUND STATION - QUICK LOOK SYSTEM

Equipment located in the mobile ground station is discussed below. A diagram of the system is presented in Figure I-3.

### Tape Recorder - Reproducer

Data tapes are played back on an Ampex FR 1300 at 30 inches per second, which is 8 times record speed. The FR 1300 is a 1 inch, 14 track system with IRIG head configuration. Frequency response bandwidth at 30 ips is 150 cps to 150,000 cps  $\pm 3$ db. Four reproduce and two record amplifiers are provided. Data from any of the 14 tracks may be selected for reproduce through a 14 X 4 switch assembly. Record amplifiers can be inserted into any of the 14 positions available. Equalizers are provided for 3-3/4 and 30 ips operation.

### Discriminator System

A discriminator system consisting of 11 Electro-Mechanical Research Model 267 data discriminators and one Electro-Mechanical Research Model 267R reference discriminator is provided. Channel selectors are fixed at 8 times IRIG proportional band frequencies, for bands 1 through 11. The reference discriminator, used for tape flutter compensation, requires IRIG Band 11, times 8, as an input.

### Time Code Reader

A Systron-Donner Model HI-150R Time Code Reader is provided to decode and display the elapsed time code recorded on-board the aircraft. The code being used is switch selectable on the front panel. A slow code, in BCD time of day format, is available as an output for providing timing information on strip chart recorders.

### Oscillograph

A Consolidated Electrodynamics Corporation Model 5-124 oscillograph is provided to permit strip chart recordings of up to 14 selected inputs. Discriminator and time code reader outputs are selectable through a patch panel.

### Communication Radio

An AN/ARC-34 UHF radio is provided to allow communications with the airplane and the control tower. A blade antenna for the radio is installed on the roof of the van.

A complement of electronic equipment is provided to aid in establishing the quality of the recorded data, and to assess the performance of the various equipment items. The following items are included:

- Oscilloscope, Hewlett-Packard Model 130C
- Digital Voltmeter, Hewlett-Packard Model 3440
- Frequency Counter, CMC Model 603A

# *Contrails*

Only 115V, 60 cps power is required to operate the equipment installed in the mobile data van. This power is brought into the van through an external power receptacle to a load center for distribution. Provision is also made for bringing 28V DC power into the van through a second external receptacle. Distribution is made to an outlet on a test bench to be used in performing functional checks of airborne equipment items. Maximum current drain, with all equipment operating and with the AN/ARC-34 radio receiver-transmitter in "TRANSMIT" mode is approximately 19.3 amps at 110 volts.

The complete system is installed in a 1967 Chevrolet Model S-108 Sports Van.

# Contrails

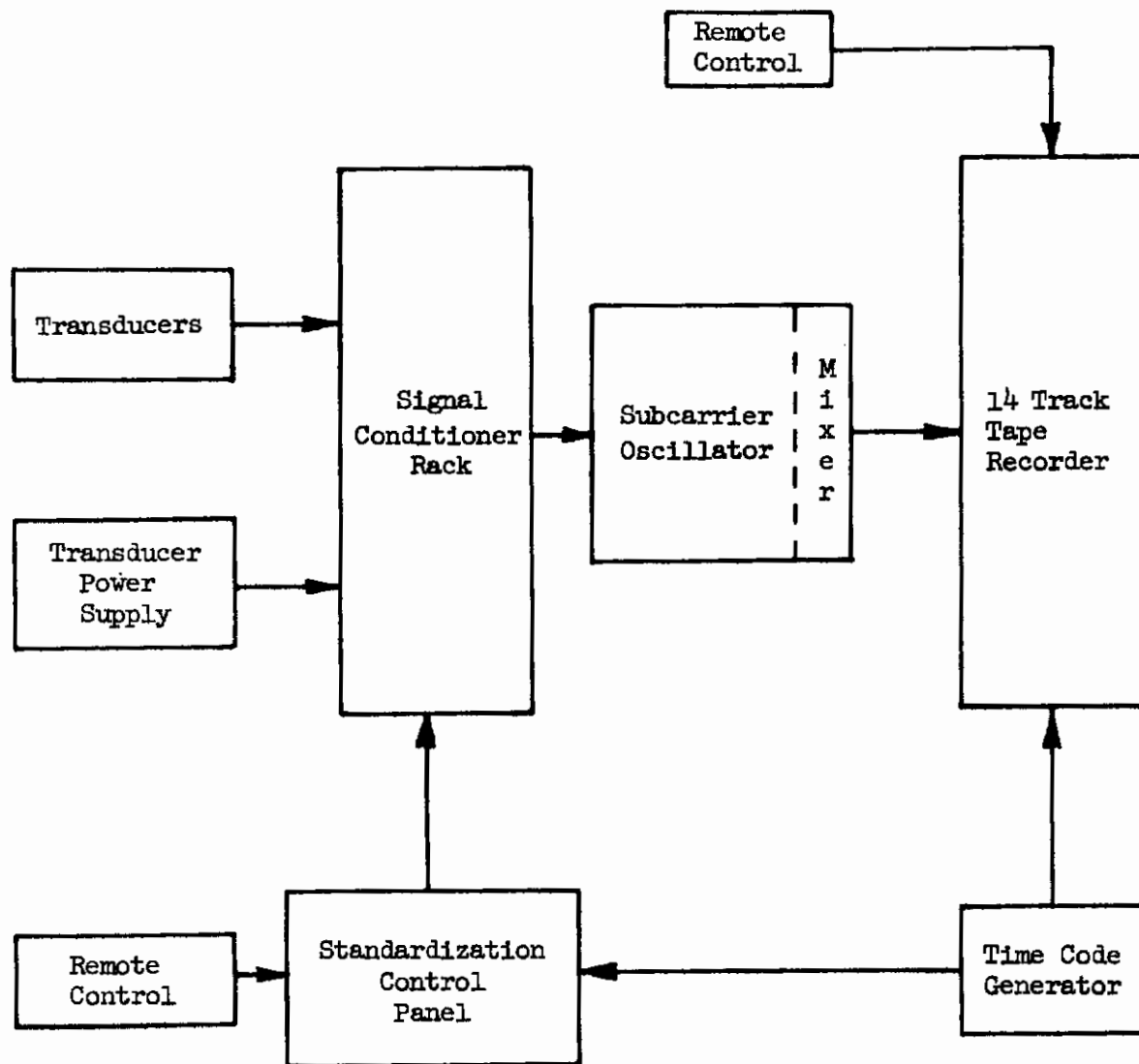


Figure I-1 Recording System Block Diagram

# Contrails

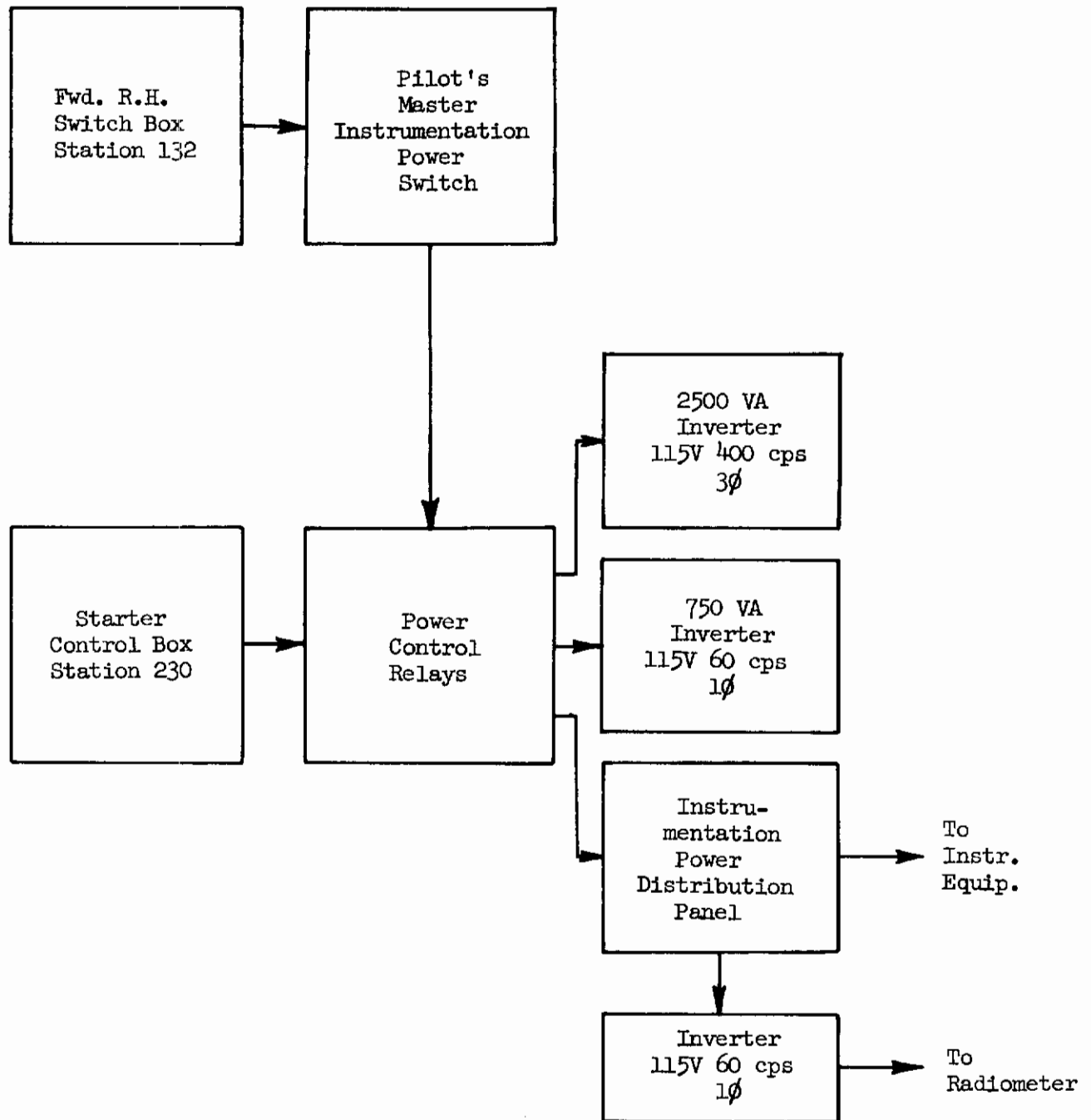


Figure I-2 Instrumentation Power Control Block Diagram



APPENDIX II

INSTRUMENTATION CALIBRATIONS AND CHECKS

This appendix contains details of the methods and procedures used to calibrate and maintain the instrumentation. Calibrations of instrumentation transducers are accomplished by exposing each transducer to expected environmental changes. Transducer frequency response characteristics are evaluated. Recalibrations and ground checks are accomplished periodically to verify that responses have not changed. Calibration details are given in Table II-1, located at the end of this appendix. The calibrations are used to convert the recorded electrical signals into units of the parameter being measured. The final calibration curve consists of a comparison of the input to the ratio of transducer response to a calibration reference. Calibration standards used to accomplish the calibrations are listed in Table II-1. The accuracy of each calibration is shown.

CALIBRATIONS IN THE LABORATORY AND AT THE AIRPLANE

Calibration of pressure transducers was accomplished before and after installation in the probe to ensure that plumbing system errors did not exist and to check the systems for leaks after installation. The "open-wire" platinum sensing element of the OAT transducer was calibrated to determine sensitivity. Circuitry wiring was included in the laboratory calibration. The radiation thermometer was calibrated in the laboratory using a "near-black-body" to which inflight corrections were made. Calibration of the airplane heading measurement was accomplished following installation of instrumentation and in conjunction with the usual compass swing. Since the electrical output of this system is sinusoidal, it was necessary to perform the calibration by heading quadrant. Calibration of the AN/APN-153 Doppler radar system was accomplished using the built-in, self-test circuit of the system. Potentiometers installed at the control surfaces were calibrated on location using Boeing-designed inclinometers. Laboratory calibration of the radar altimeter was run for altitude ranges applicable to each route.

WIND TUNNEL STATIC CALIBRATION OF THE PROBE

The following pressure coefficients were computed from the data recorded during the wind tunnel calibration (Reference II-1):

$$\frac{q_I - q_c}{q_c} ; \frac{P_{s1} - P_s}{q_c} ; \frac{\Delta P_\alpha}{q_c} \quad \frac{\Delta P_\beta}{q_c}$$

Quadratic equations for  $\alpha$  and  $\beta$  were derived by a least-squares, second order fit of  $\Delta P_\alpha / q_c$ ,  $\Delta P_\beta / q_c$ , and M data.

# Contrails

The equation for  $\alpha$  in the general form is:

$$\alpha = (a_1 + a_2 \frac{\Delta P_\alpha}{q_c} + a_3 \frac{\Delta P_\beta}{q_c} + a_4 M)^2 \quad (II-1)$$

which after expansion becomes:

$$\begin{aligned} \alpha = & A + B \frac{\Delta P_\alpha}{q_c} + C M + D \frac{\Delta P_\beta}{q_c} + E \frac{\Delta P_\alpha}{q_c} M + F \frac{\Delta P_\alpha}{q_c} \frac{\Delta P_\beta}{q_c} \\ & + G M \frac{\Delta P_\beta}{q_c} + H \left( \frac{\Delta P_\alpha}{q_c} \right)^2 + J M^2 + K \left( \frac{\Delta P_\beta}{q_c} \right)^2 \end{aligned} \quad (II-2)$$

The  $\alpha$  equation coefficients based on the wind tunnel data are as follows:

MACH NO. RANGE	A	B	C	D	E	F	G	H	J	K
.3 ≤ M < .6	-.616	10.348	1.607	.143	-1.922	.067	-.446	-.037	-1.115	.014
.6 ≤ M < .75	-2.721	7.197	8.349	.099	3.383	.154	-.359	.040	-6.529	-.022
.75 ≤ M ≤ .95	.913	.296	-2.200	-.201	12.581	.238	.054	.002	1.087	.011

Likewise, the general equation for  $\beta$  is:

$$\beta = (b_1 + b_2 \frac{\Delta P_\beta}{q_c} + b_3 \frac{\Delta P_\alpha}{q_c} + b_4 M)^2 \quad (II-3)$$

which when expanded becomes:

$$\begin{aligned} \beta = & A' + B' \frac{\Delta P_\beta}{q_c} + C' M + D' \frac{\Delta P_\alpha}{q_c} + E' \frac{\Delta P_\beta}{q_c} M + F' \frac{\Delta P_\beta}{q_c} \frac{\Delta P_\alpha}{q_c} \\ & + G' M \frac{\Delta P_\alpha}{q_c} + H' \left( \frac{\Delta P_\beta}{q_c} \right)^2 + J' M^2 + K' \left( \frac{\Delta P_\alpha}{q_c} \right)^2 \end{aligned} \quad (II-4)$$

The coefficients for the  $\beta$  equations determined from the wind tunnel data are:

MACH NO. RANGE	A'	B'	C'	D'	E'	F'	G'	H'	J'	K'
.3 $\leq$ M < .6	.196	10.507	-1.574	.046	-2.462	-.090	.173	.114	1.521	-.018
.6 $\leq$ M < .75	-3.132	5.904	8.412	.208	5.242	-.006	-.108	.114	-5.778	-.081
.75 $\leq$ M $\leq$ .95	-1.525	.624	3.793	.108	12.212	-.030	.031	.091	-2.435	-.131

### CAMERA BORESIGHT

A boresight calibration was performed on the 35 mm movie camera which was installed for the inflight calibration of angles of attack and sideslip. Due to space limitations in the T-33 airplane, only one camera was installed. The camera was rigidly mounted on the airplane centerline looking forward, as shown in Figures II-1 through II-3. Dimensionally, the center of the camera lens was located at Body Station 30.969, Buttock Line 0.0 and Water Line 104.95.

The method used in the boresight calibration was that of locating a target stand (Figure II-4) at known positions in front of the airplane and exposing a few feet of film. The airplane was located inside a hangar in an area that was free from drafts and in a position such that an area 100 feet directly in front of the airplane was clear.

It was necessary to elevate the nose of the airplane three degrees (Figure II-5) so that the target stand could be used to calibrate angles below the camera level. Since the target stand was not perpendicular to the elevated airplane center line, the target spacing was adjusted so that the targets were located at one degree intervals, as viewed by the camera. Target spacing was calculated as shown in Figure II-6. The targets were fixed to a common movable vertical beam on the target stand permitting attack angles to remain fixed in relation to each other for all angles of sideslip. The targets were moved to positions along a line perpendicular to, and either side of, the initial position (Figure II-7). A theodolite located directly below the camera was used to determine the angle between each position and the airplane center line. The targets were plumbed and elevation adjusted at each position using the theodolite and a "Y" level.

Data recorded during the calibration consisted of manual target position readings and 35 mm film positives of the targets. The film positives were projected on a screen and target positions were determined relative to horizontal and vertical lines drawn between fiducial markers. These measurements were then plotted versus the corresponding calculated angles of attack and sideslip (Figures II-8 and II-9). Equations determined from these plots are shown on each plot and were used in the angle of attack and sideslip calibration.



## INFLIGHT CALIBRATION OF GUST PROBE ANGLES OF ATTACK AND SIDESLIP

Inflight calibration of gust probe angle of attack ( $\alpha$ ) and angle of sideslip ( $\beta$ ) measurements was performed on the T-33A test airplane using the confetti cloud technique. The purpose of this calibration was to check the sensitivities and intercepts obtained from the wind tunnel calibration and to determine the effect of the fuselage generated pressure field on  $\alpha$  and  $\beta$ .

The confetti cloud calibration technique consisted of flying the test airplane through a steady stream of one-half inch square fluorescent orange paper particles. Confetti was dispensed from a C-135 support airplane into the path of the test airplane. The confetti hopper installation in the support airplane and an exterior view of the confetti discharge duct are shown in Figures II-10 and II-11.

The optimum position of the test airplane in the confetti stream was approximately two miles aft and slightly below the support airplane. Testing was accomplished at 0.4, 0.5, and 0.6 Mach numbers. After the test airplane was positioned in the confetti stream, various attack and sideslip angles were established and motion pictures of the confetti were taken. Angle of attack was established by variation of airspeed and altitude while angle of sideslip was established utilizing the rudder.

The motion pictures were taken with the boresighted, forward-looking 35 mm movie camera rigidly mounted in the nose of the test airplane.

The confetti particles appear as streaks emanating from a point on the movie film. The position of the point of emanation relative to the intersection of horizontal and vertical lines drawn between the camera fiducial marks indicates the direction of the relative wind. The streaks are caused by the change in relative angular location of the confetti particles with respect to the camera lens during the time the shutter is open.

The film was viewed one frame at a time and the best frame for each condition was selected for determining the point of emanation. An example frame is shown in Figure II-12. Each frame of film selected was projected on a screen and the point of emanation determined using the radial template shown in Figure II-13. This was done by aligning the radial lines on the template with the confetti streaks on the film and marking the location of the template center point. Vertical and horizontal distances of this point from crossed lines drawn between the camera fiducial marks ( $D_{\alpha}$  and  $D_{\beta}$ ) were then determined (Figure II-14). This procedure was repeated 15 times for each frame selected and the average point of emanation was determined. These average distances were converted to angle of attack and angle of sideslip, respectively, by applying the camera boresight equations presented in Figures II-8 and II-9. Angles of attack and sideslip calculated using the boresight equations were then corrected for confetti fall rate, rate of pitch, rate of yaw and probe location.

# Contrails

The fall rate was determined by measuring the time required for confetti samples to fall a known distance near ground level and then applying a correction for the change in air density with altitude. Two types of confetti with different fall rates were used during this testing. Fall rates for each type of confetti were determined from the following equation:

$$V_F = \frac{V_{SL}}{\sqrt{\sigma}} \quad (\text{II-5})$$

Where:

$$V_{SL} = 3.809 \text{ ft./sec. for type one (light orange)}$$

$$V_{SL} = 3.367 \text{ ft./sec. for type two (bright orange)}$$

Corrections to angle of attack were made using the following equations:

Fall Rate Correction

$$\Delta \alpha_{FR} = \left| \frac{V_F}{V_T} \cos \phi \right| 57.3 \quad (\text{II-6})$$

Pitch Rate Correction

$$\Delta \alpha_{PR} = \frac{\dot{\theta}(R_d + L_f)}{V_T} = \frac{47.17 \dot{\theta}}{V_T} \quad (\text{II-7})$$

Probe Location Correction

$$\Delta \alpha_{PL} = \frac{D \dot{\theta}}{V_T} = \frac{26.57 \dot{\theta}}{V_T} \quad (\text{II-8})$$

Total Angle of Attack Correction

$$\Delta \alpha = \Delta \alpha_{FR} + \Delta \alpha_{PR} - \Delta \alpha_{PL} \quad (\text{II-9})$$

Corrections to angle of sideslip were made utilizing the following equations:

Fall Rate Correction

$$\Delta \beta_{FR} = \frac{V_F}{V_T} (\sin \phi) 57.3 \quad (\text{II-10})$$

Yaw Rate Correction

$$\Delta \beta_{YR} = \frac{\dot{\psi}(R_d + L_f)}{V_T} = \frac{47.17 \dot{\psi}}{V_T} \quad (\text{II-11})$$

## Probe Location Correction

$$\Delta\beta_{PL} = \frac{D\dot{\psi}}{V_T} = \frac{26.57\dot{\psi}}{V_T} \quad (\text{II-12})$$

## Total Angle of Sideslip Correction

$$\Delta\beta = \Delta\beta_{FR} + \Delta\beta_{YR} + \Delta\beta_{PL} \quad (\text{II-13})$$

Differential pressure data from the gust probe (Figure II-15) were recorded during the angle of attack and sideslip calibrations. These pressure data were nondimensionalized by use of the following formulas:

$$\frac{\Delta P_\alpha}{q_c} = \frac{P_2 - P_1}{q_c} \quad (\text{II-14})$$

$$\frac{\Delta P_\beta}{q_c} = \frac{P_3 - P_4}{q_c} \quad (\text{II-15})$$

Pressures  $P_1$  through  $P_4$  and total pressure ( $P_5$ ) are identified in Figure II-16.

The pressure coefficients were then plotted as functions of angle of attack or angle of sideslip ( $\Delta P_\alpha / q_c$  vs.  $\alpha$  or  $\Delta P_\beta / q_c$  vs.  $\beta$ ) for a constant Mach number. The best straight line from a similar plot obtained during the wind tunnel calibration was then placed on the flight data plot for comparison. The purpose of this comparison was to determine any differences between wind tunnel and inflight  $\alpha$  and  $\beta$  sensitivities and intercepts caused by installation of the probe on the T-33A airplane. These data are presented in Figures II-17 through II-22. No significant differences between wind tunnel and flight data were indicated.

Results of this testing indicate that  $\alpha$  and  $\beta$  are not affected by the fuselage pressure field, therefore, wind tunnel derived equations for  $\alpha$  and  $\beta$  (equations II-2 and II-4) are used.

## RADAR ALTIMETER CHECK

The airplane was flown over Cheney Reservoir, in central Kansas, to check the radar altimeter. This was done by comparing the known height of the dam with that indicated by the radar altitude data. For this check, the pressure altitude was maintained constant. The airplane flight path is shown in Figure II-23.

The terrain height, as indicated by the radar altimeter, is shown in Figure II-24. The data show the height of the dam to be 45 feet on the land side. The top of the dam is indicated 27 feet above the water on the water side. The surveyed heights of the dam, above the land and above the water level were 60 and 35 feet, respectively. The radar altimeter recorded the height of the dam as about 75 percent of actual.

The difference between actual and recorded dam height is probably due to response time limitations of the radar altimeter. The airplane was flying at a ground speed of 450 fps as it passed over the dam. At this speed the dam was within the field of view of the radar altimeter for only about 0.2 seconds. According to the manufacturer's specifications, nominal altitude response time for a step change is 0.1 second. Thus the two steps recorded for the dam within 0.2 second is approaching the limitations of the system. This is substantiated by noting the lag in radar altimeter response in Figure II-24. According to these data, the airplane was over the dam for approximately 0.5 second. Considering the response time of the system and the time in which the dam was within the field of view of the radar altimeter, the operation of the unit is considered to be satisfactory.

## GROUND SPEED VERIFICATION

The check was accomplished by recording the time required for the airplane to fly a distance of four statute miles. The actual ground speed was computed from these data and compared to the Doppler ground speed as recorded on the data acquisition system's magnetic tape. This procedure was repeated and, in both cases, the recorded ground speed was within 0.25 percent of the actual ground speed. The results are shown below.

<u>Run No.</u>	<u>Recorded Ground Speed (fps)</u>	<u>Actual Ground Speed (fps)</u>
1	600.0	598.5
2	600.9	601.6

The ground speed indicator in the cockpit read approximately 603 fps during these runs.

## WIND TUNNEL DYNAMIC CALIBRATION OF THE GUST PROBE

The gust probe head being used for the LO-LOCAT Phase III Program is the one previously used on JB-52H AF 61-023. In 1964, this probe head was calibrated in the Cornell Aeronautical Laboratories (CAL) eight-foot transonic wind tunnel to determine the dynamic response of the angles of sideslip and attack. The tests were conducted over a Mach number range from .5 to .95. The probe was mounted on a dynamic test rig which supplied combinations of rotation and translation at various frequencies. For this testing, the rig was adjusted to give as near sinusoidal motion as possible for frequencies from 4 to 12 cps at various amplitudes. Induced angle of attack (input) differential pressure was computed considering both the pressure resulting from pitch angle and that due to probe tip velocity. The corresponding sensed differential pressure (output) was measured by probe instrumentation. Due to probe symmetry, it was not necessary to calibrate the sideslip plane.

Overall frequency response, i.e., the response due to combined aerodynamic and transduction (tubing and transducer) effects, was determined. To isolate the aerodynamic effects from the transduction effects, ground testing was conducted with the gust probe installed on the B-52 airplane.

The difference between the transfer function obtained from the wind tunnel and ground tests established that portion of the frequency response attributable to aerodynamic effects. The test procedures, analysis methods and results are given in Reference II-2.

The transduction effects for the Phase III probe were determined from ground testing and Fourier transform techniques and were added to the known aerodynamic effects obtained from the wind tunnel testing to obtain the overall frequency response characteristics. The procedure used in obtaining the transduction effects is discussed below.

With the probe installed on the airplane, the system was subjected to shock pressures of various magnitudes by pressurizing the individual ports and then rupturing a thin membrane in the pressure line to give an instantaneous drop (step) in pressure. The pressure steps were recorded by NBFM on magnetic tape and reproduced in the form of time history plots.

The approximate center of the pressure step was first determined manually from the step plots. The block of data samples between 0.15 and 0.30 seconds before and after the approximate center point was then averaged by computer to identify the exact center point. The magnitude ( $M_S$ ) of the exact center of the pressure step was calculated as follows:

$$M_S = \frac{N_{A_1} + N_{A_2}}{2} \quad (\text{II-16})$$

Where:  $N_{A_1}$  = Average of samples between 0.15 and 0.30 seconds  
prior to approximate center point

$N_{A_2}$  = Average of samples between 0.15 and 0.30 seconds  
after approximate center point

The computer then picked the data sample with a magnitude nearest to  $M_S$ . This allowed the determination of exact start and stop times for the step analysis.

The transform of the recorded pressure fluctuation was computed from 0.5 seconds before the center of the the step to 0.5 seconds after the center of the step.

In order to obtain the transfer function for transduction effects, the Fourier series coefficients of the recorded pressure fluctuation (output) was divided by the coefficients of a square wave.



# Contrails

Since the square wave is an odd function with a period of  $2\pi$ , it may be represented as:

$$f(x) = \sum_{n=1}^{\infty} b_n \sin nx \quad (\text{II-17})$$

$$\text{where } b_n = \frac{2}{\pi} \int_0^{\pi} f(x) \sin nx \, dx \quad (\text{II-18})$$

For  $0 < x < \pi$ ,  $y = P/2$  where  $P$  is the magnitude of the step pressure input. Therefore,

$$\begin{aligned} b_n &= \frac{P}{\pi} \int_0^{\pi} \sin nx \, dx \\ &= \frac{P}{\pi n} \left[ 1 - \cos(\pi n) \right] \\ &= \frac{2P}{\pi n} \quad \text{when } n \text{ is odd} \\ &= 0 \quad \text{when } n \text{ is even} \end{aligned} \quad (\text{II-19})$$

Thus the Fourier series of the input amplitude may be expressed as:

$$f(x) = \frac{2P}{\pi} \left[ \sin x + \frac{\sin 3x}{3} + \frac{\sin 5x}{5} + \dots \right] \quad (\text{II-20})$$

The transduction effects determined using this method were found to be approximately the same as those for the B-52 testing. Therefore, the gain factor determined during the B-52 testing is also applicable to the LO-LOCAT Phase III testing. The reciprocal of the gain factor is used as the frequency response compensation for  $\alpha$  and  $\beta$  in processing the Phase III LO-LOCAT data.

## GUST PROBE AND BOOM NATURAL FREQUENCY DETERMINATION

The gust probe and boom assembly was designed to have a natural frequency greater than 10 cps. If the natural frequency of the assembly were between .04 and 10 cps, the power spectral density of gust velocity, which is being analyzed over this frequency range, would be adversely affected.

The probe and boom assembly installed on JB-52H, AF 61-023, had a measured natural frequency of 14.5 cps. The probe and boom assemblies used during Phases I and II of the LO-LOCAT Program had natural frequencies of approximately 15.6 cps. The Phase III probe consists of the probe head previously installed on JB-52H, AF 61-023, and a probe shell used during LO-LOCAT Phases I and II. A boom that was used during Phases I and II was shortened for Phase III usage. Therefore, it was expected that the natural frequency of the Phase III assembly should be 15.6 cps or greater. However, due to the fact that attachment to the airplane is necessarily somewhat different for the T-33 than for the C-131 aircraft, a check was made to determine the natural frequency of the assembly for the Phase III Program.

With the gust probe and boom installed on the airplane, the boom was struck sharply by hand and then the vibration was allowed to damp out. Gust probe vertical and lateral accelerations were recorded and plotted as time histories. These plots are shown in Figures II-25 through II-28. The boom was struck three different times. Figure II-25 shows the vertical acceleration response when the boom was hit vertically. Figure II-26 shows the lateral acceleration response when the boom was hit laterally. Figures II-27 and II-28 show the responses of the vertical and lateral accelerometers, respectively, when the boom was struck at an angle of 45 degrees with respect to the vertical and lateral axes.

As can be seen from these acceleration time histories, a beat frequency is present, indicating the presence of two predominant frequencies. This is more obvious in the vertical acceleration traces but is also noted in the lateral acceleration response. Because of this beat frequency, power spectral densities of the accelerations were computed. The PSD plots are shown in Figures II-29 through II-32. The two predominant frequencies are seen to be at 16.7 and 18.5 cps in both the vertical and lateral directions. The 16.7 cps frequency is the more predominant of the two in the lateral direction. In the vertical direction, the power contributed by each frequency is approximately the same. In neither case, however, is there any significant power contribution between the frequencies of .04 and 10 cps.

## AIRSPEED CALIBRATION

Airspeed calibration data for the T-33 gust probe system was recorded during tower flybys on 15 August 1968. The fly-bys were conducted using Tower No. 2 at the Smoky Hill Gunnery and Bomb Range. The Smoky Hill Range is located southwest of Salina, Kansas; listed on the Salina Sectional Aeronautical Chart as restricted area R-3601. Authorization to use the range tower was coordinated through McConnell Air Force Base. A delay of one day in the schedule was encountered because of the crash of an F-105 on the range the day prior to the scheduled calibration flight.

The weather conditions in the test area at sunrise (0645 CDT) were marginal for this type of testing but were forecasted to improve. During the first flyby, at 0740 CDT, and two succeeding flybys, the pilot experienced visibility problems because of rain showers south of the tower. The rain showers rapidly dissipated, however, and no further problems occurred due to adverse weather. The wind speed increased from five knots to approximately eight knots by completion of the calibration at 0805 CDT. A sustained gust occurred at 0800 CDT, lasting approximately two to four minutes, increasing the wind speed to 12 knots. The ambient temperature was 70° F until the last flyby at which time the temperature had increased to 71°F. Pressure altitude slowly

decreased from 1750 feet to 1745 feet by the end of the testing at which time the sky had cleared with only scattered high level clouds remaining over the test area.

Photographs and motion pictures were taken to pictorially record the test. The pertinent elements of the range concerning this test are shown in Figure II-33. A line through the white tire marker and No. 1 strafe target defines the approximate 320 degree heading flown. The tower was located (by a field survey) 720 feet from the proposed flight path, as shown in Figure II-33.

The calibration procedure consisted of flying the T-33 airplane by the tower at airspeeds which bracket the airspeed expected to be flown during the LO-LOCAT Phase III Program. When the airplane crossed a specified point opposite the tower, its height above or below a reference point in the tower was determined, as shown in Figure II-34.

The calibration was initiated by flying at 300 KIAS. As the T-33 passed by the tower, the pilot read his cockpit indicators. The tower observer recorded the height above or below the reference point. One ground observer was used to determine if the flight path was over target No. 1. The passes were made from south to north. Additional passes were made increasing the airspeed by 25 knots until V max was attained. Maximum airspeed was 420 knots (using a shallow dive) for the T-33 in the configuration for this program. The decreased maximum velocity, specified as 505 knots at sea level in the -1 handbook, is attributed to the protruding radar altimeter and Doppler radar antennas.

Data were recorded by the pilot, tower observer, and NBFM instrumentation system on board the airplane. Table II-2 lists measurements recorded for each flyby. The values for each measurement were recorded at the call of "MARK" from the tower observer as the airplane passed through the point directly in front of the tower.

TABLE II-2

AIRSPEED CALIBRATION VARIABLES RECORDED

Method of Recording		
Pilot	Tower Observer	NBFM System
Pilot's airspeed	$\Delta H$ (ref. line)	Coord. No.
Pilot's altitude	Clock time	$P_{SI}$
Coord. No. at "MARK"	Altimeter	$q_I$
	Wind speed	OAT
	Wind direction	
	Air temperature	
	Metro. conditions	



# Contrails

The instrumentation and equipment involved in this test are listed in Table II-3. Additional details concerning the gust probe and instrumentation are available in Reference I-1.

TABLE II-3  
INSTRUMENTATION AND EQUIPMENT

Measurement	Transducer Number	Manufacturer
Pilot's airspeed	AF 55-30735-01	KOLLSMAN TAYLOR NO. 3132 - - - VCA THE BOEING CO. STATHAM ROSEMOUNT ROSEMOUNT
Pilot's altitude	AF 60-1204-01	
Tower altitude	FT 8347-32	
Wind speed	FT 7542 (anemometer)	
Wind and direction	ML-433A/PM (anemometer)	
Ambient temperature	14-4490 (liquid thermometer)	
SCR	SCR 9488 (gust probe)	
Static pressure	FT 24872-02	
Dynamic pressure	FT 55002-02 (-03)	
Outside air temp.	FT 24748-04 (type 102-E)	
Time correlation	9364	

A listing of the recorded data for each fly-by is presented in Table II-4. The true altitude, (H), of the airplane was determined from the tower data by:

$$H = H_{I_T} + \Delta H + \Delta h \quad (\text{II-21})$$

where:

- $\Delta H$  = height of airplane from reference
- $\Delta h$  = tower altimeter instrument error
- $H_{I_T}$  = indicated altitude from tower altimeter

TABLE II-4  
RECORDED DATA FOR AIRSPEED CALIBRATION

Pass	Pilot			Observer							NBFM		
	C/N	V <sub>1</sub>	H	$\Delta H$	TOD	Alt.	W	Dir.	Air Temp °F	Metro Cond.	P <sub>SI</sub>	q <sub>I</sub>	OAT
1	32:41	280	--	+55	0740	1750	6	SW	70	RWN S-SW	28.270	3.82	93.2
2	34:20	300	1680	+45	0742	1750	6	SW	70	RWN S-SW	28.310	4.22	95.1
3	35:56	300	1680	+15	0744	1750	7	SW	70	RWN S-SW	28.335	4.31	95.3
4	41:44	320	--	0	0749	1750	7	SW	70	Clearing	28.290	4.76	99.3
5	44:18	345	1680	-10	0751	1750	7	SW	70	Clearing	28.325	5.70	103.7
6	47:25	360	1780	+20	0755	1745	8	SW	70	Clear	28.345	6.31	107.0
7	50:44	390	1780	+10	0758	1745	9	SW	70	Clear	28.420	7.31	110.8
8	54:15	400	1780	0	0801	1745	12	SW	70	Clear	28.480	7.87	113.4
9	57:57	420	1760	0	0805	1745	8	SW	71	Clear	28.510	8.38	116.4

# Contrails

Comparison of the static pressure corresponding to the true altitude with the static pressure recorded from the gust probe was accomplished and a static pressure position error,  $\Delta P_{SP}$ , was calculated by:

$$\Delta P_{SP} = P_{S_I} - P_S \quad (II-22)$$

where:

$$\begin{aligned} \Delta P_{SP} &= \text{static pressure position error, in. H}_g \\ P_S &= \text{true static pressure, in. H}_g \\ P_{S_I} &= \text{indicated static pressure, in. H}_g \end{aligned}$$

## RADIOMETER (GROUND SURFACE TEMPERATURE) CALIBRATION

The radiometer was checked during flight by comparing the recorded temperature with a known surface temperature. For this purpose the airplane was flown over Cheney Reservoir, northwest of Wichita, Kansas. Observers in a boat measured the actual water temperature with calibrated thermometers. A diagram of the approximate flight path and locations where actual water temperatures were recorded is shown in Figure II-23. At each location, the water temperatures were recorded at 1, 3, 5, 7, and 12 inches below the surface. Thermometers suspended from a float (Figure II-35) were used for this purpose. The temperatures varied less than  $\pm 1^\circ\text{F}$  with depth below the water surface at each temperature check point location. The average value of the water temperature at each location was as follows:

- Point "A" 75.9°F
- Point "B" 76.9°F
- Point "C" 77.0°F

The radiometer has a field of view subtended by an angle of approximately  $2^\circ$ . For this particular test the airplane was flown approximately 750 feet above the water surface. This means that the field of view of the radiometer is a circular area with a diameter of approximately 26 feet. The temperature data from the radiometer were recorded on magnetic tape and sampled at a rate of 100 samples/second. Very little variation was noted in the individual data points along the flight path.

The average water temperature, as recorded manually by the observers in a boat, was 76.6°F while the average temperature recorded by the radiometer was 66.4°F. However, there are two corrections which must be made to the radiometer readings. This results from the fact that the radiometer references all incoming radiation to that emitted by a black body held at a constant temperature within the unit itself. Since real surfaces are not black bodies (i.e., emissivity  $< 1.0$ ) the radiometer recorded temperatures must be appropriately altered.

# Contrails

One correction is derived from a consideration of the following basic principles of radiation heat transfer:

$$E_{AR} = \epsilon_R \sigma T_{AR}^4 \quad (II-23)$$

and

$$E_{BB} = \sigma T_{BB}^4 \quad (II-24)$$

where:

$E_{AR}$  = actual energy per unit area radiated from a real surface at temp.  $T_{AR}$

$\epsilon_R$  = emissivity of the real surface

$\sigma$  = Stefan-Boltzman constant

$T_{AR}$  = actual temperature of the real surface

$E_{BB}$  = energy per unit area radiated from a black body at temperature  $T_{BB}$

$T_{BB}$  = temperature of a black body

As mentioned previously, the surface temperature recorded by the radiometer ( $T_G$ ) is the temperature of a surface assumed to be a black body, as the incoming radiant energy ( $E_R$ ) is assumed to be emitted from a black body.

$$\text{i.e., } E_R = E_{BB} = \epsilon_R \sigma T_{AR}^4 = \sigma T_{BB}^4 = \sigma T_G^4 \quad (II-25)$$

$$\text{or } T_{AR} = \epsilon_R^{-1/4} T_G \quad (II-26)$$

Thus the temperatures recorded by the radiometer must be corrected for emissivity of the surface by Equation II-26. According to Reference II-3, the emissivity of water at the temperature recorded during this inflight check is approximately 0.953.  $T_G$  for this test was 526.1°R or 66.4° F. Substituting these values into Equation II-26 yields a value for  $T_{AR}$  of 532.4° R or 72.7° F. As noted previously, the actual water temperature was 76.6° F or 3.9° F greater than  $T_{AR}$ . The cause of this discrepancy is the method used in calibrating the radiometer and requires a second correction to be made to the recorded temperatures. This correction is made to compensate for the emissivity of the calibration equipment.

The unit was calibrated by use of a piece of black painted aluminum placed within a cubical enclosure for which the temperature could be accurately controlled. The enclosure was insulated and composed of solid walls except for a small window in one side and a hole in the top through which the radiometer could view the black aluminum target. The temperature of the target was allowed to stabilize at various values and the corresponding temperatures indicated by the radiometer were recorded. The radiometer output was then plotted versus actual temperature, giving a calibration curve for the unit.

# Contrails

The calibration equipment setup is not a black body and therefore has an emissivity less than 1.0. By surmising that the difference of 3.9°F between the actual water temperature and that calculated from the radiometer during the inflight check condition is due to the black body assumption for the calibration equipment, the emissivity of the calibration equipment was calculated to be 0.972.

This value was found by noting that:

$$T_G = \epsilon_C^{-1/4} T_{rad} \quad (II-27)$$

where:

$\epsilon_C$  = emissivity of the calibration equipment

$T_{rad}$  = surface temperature as recorded by the radiometer

Equation II-27, which can be derived in the same manner as Equation II-26, is then substituted into Equation II-26 to yield:

$$T_{AR} = \epsilon_R^{-1/4} \epsilon_C^{-1/4} T_{rad} \quad (II-28)$$

$\epsilon_C$  was calculated by substituting in the appropriate values for the inflight check condition.

$$\epsilon_R = 0.953$$

$$T_{AR} = 536.3 \text{ } ^\circ\text{R}$$

$$T_{rad} = 526.1 \text{ } ^\circ\text{R}$$

These two corrections for emissivity were put into the computer program to correct all ground surface temperature readings. The emissivity,  $\epsilon_R$ , is 0.953 for the water leg at the Edwards Air Force Base route. This value is based on an assumed water temperature of approximately 50°F and Reference II-3. Also from Reference II-3, an emissivity value of 0.900 is used for all other legs at all routes. This value is an average of the many different surfaces comprising the land terrains. Using these values of emissivity, a value of 0.972 for  $\epsilon_C$ , and converting the units in Equations II-28 such that the temperatures are in degrees F, the corrections made to the surface temperatures recorded by the radiometers are:

For water

$$T_{AR} = 1.0200 T_{rad} + 9.2 \quad (II-29)$$

For land

$$T_{AR} = 1.0343 T_{rad} + 15.8 \quad (II-30)$$

## OUTSIDE AIR TEMPERATURE (OAT) CALIBRATION

The OAT calibration was conducted concurrently with the airspeed calibration test. This part of the test consisted of comparing the ambient air temperature at the tower with the ambient temperature computed from the airplane temperature probe. Calibration of the OAT probe during flight environment resulted in several valuable checks of the temperature probe system. First, the static calibration performed in the lab was confirmed. Second, the recovery factor was determined for the probe in use. And finally, if any installation effects occurred, they could be corrected or accounted for by correction factors.

The probe used for this installation was a Rosemount Model 102E. The position of the probe installation and the exterior appearance is shown in Figure II-36.

Using the results of the airspeed calibration, the relationship of Figure II-37 was developed. The values of the temperature ratio  $T_I / T_a$  are plotted versus  $M^2$ . A linear fit of the data points results in the expression for temperature rise due to air friction:

$$T_a = \frac{T_I}{K_a + 0.2 K_t M^2} \quad (\text{II-31})$$

where:

$K_t$  = recovery factor

$K_a$  = correction factor

The resulting expression of Figure II-37 gives rise to the following values for the constants:

$$K_t = 0.98$$

$$K_a = 1.0075$$

thus:

$$\frac{T_I}{T_a} = 0.196M^2 + 1.0075 \quad (\text{II-32})$$

The temperature probe element installed during the airspeed calibration was found to have failed during a subsequent data flight (No. 13). A new probe element was installed and during data flight No. 37, a check calibration test was conducted. This test was flown in proximity to the remote weather detachment stationed at Cedar Vale, Kansas. The temperature data recorded during the calibration from a balloon sounding is presented in Table II-5.

TABLE II-5

OAT CALIBRATION TEMPERATURES FOR CEDAR VALE TEST

Altitude (Feet)	Temperature ( ° C)
0	18.8
250	18.4
750	17.7
1000	17.9

The remote weather station at Cedar Vale is shown in Figure II-38. Analysis of the Cedar Vale test data resulted in the calibration curve of Figure II-39. Like Figure II-37, this data yields a recovery factor of 0.98 and a correction factor of 0.995.



TABLE II-I  
CALIBRATION DETAILS

MEASUREMENT	CALIBRATION RANGE	CALIBRATION STANDARD	ACCURACY
Pressure Transducers			
Airspeed	Fine 4.5 to 8.4 in-Hg Coarse 0-13.9 in-Hg	Texas Instrument Quartz Pressure Gage	.015% of Reading
Sideslip and Attack Differential Pressures	±5.1 in-Hg	Texas Instrument Quartz Pressure Gage	.015% of Reading
Altitude	30.5 to 16.2 in-Hg	Ideal Aeromsmith Model 1015-C Barometer	±.006 in-Hg
Temperature Transducers			
Outside Air Temperature	-76 to 140°F	Leads and Northrup Platinum Resistance Thermometer-in-Conjunction with Mueller Bridge	±.1° C
Ground Surface Temperature	-20 to 120°F	Rosemount Linear Bridge Model 414L	±.2° C
Angular Positions			
Airplane Heading	0 to 360°	Airplane System Output (AN/ARN-14)	± 3% of 0 to 180° Reading
Airplane Drift Angle	±40°	Doppler Radar (AN/APN-153) Calibrations are run against indicator settings.	±.2% of Indicator Reading
Rudder Position	±30°	Bubble Protractor	±.1% of Full Scale
Aileron Position	±20°		
Elevator Position	-16° to 26°		
Attitude Gyros			
Angles of Pitch and Roll	±20° (Static) 0.05 to 3 cps (Dynamic)	Humphrey Gyro Test Stand Frequency-Genisco Rate Table Amplitude-Brush Instruments Position Standard	±3 Minutes ± 2% of Calibration Frequency ±3°

TABLE II-I  
CALIBRATION DETAILS (Cont'd)

MEASUREMENT	CALIBRATION RANGE	CALIBRATION STANDARD	ACCURACY
<b>Attitude Gyros (Contd.)</b>			
Angle of Yaw	±20° (Static)	Humphrey Gyro Test Stand	±3 Minutes
	0.05 to 3 cps (Dynamic)	Frequency-Genisco Oscillating Table	±2% of Calibration Frequency
		Amplitude-Genisco Oscillating Table	±3°
<b>Rate Gyros</b>			
Rates of Pitch, Roll and Yaw	±15° /Sec (Static)	Genisco Rate Table	±.1% of Calibration Setting
	0.04 to 10 cps (Dynamic)	Genisco Oscillating Table and Micro Gee Oscillating Table	±1% (Amplitude) ±2° (Phase Angle)
<b>Accelerometers</b>			
Gust Probe-Vertical	-4 to 6 g's (Static)	Genisco Rate Table	±.1% of Calibration Setting
Airplane CG-Vertical	0.04 to 10 cps (Dynamic)	Micro Gee Linear Acceleration Table	±1% (Amplitude) ±2° (Phase Angle)
	±2g's (Static)	Genisco Rate Table	±.1% of Calibration Setting
Airplane CG-Lateral	0.04 to 10 cps (Dynamic)	Micro Gee Linear Acceleration Table	± 1% (Amplitude) ±2° (Phase Angle)
	±1g (Static)	Genisco Rate Table	±.1% of Calibration Setting
Gust Probe-Longitudinal	0.04 to 10 cps (Dynamic)	Micro Gee Linear Acceleration Table	± 1% (Amplitude) ±2° (Phase Angle)
	80 to 800 kts	Doppler Radar (AN/APN-153) Calibrations are run against indicator settings.	±.17% of Indicator Reading
Radar Altimeter	0 to 2500 Ft.	Calibrated versus indicator and self test circuit	1 Ft. ±.5% of Indicator Reading



# Contrails



Figure II-1 Front View of Camera Installation

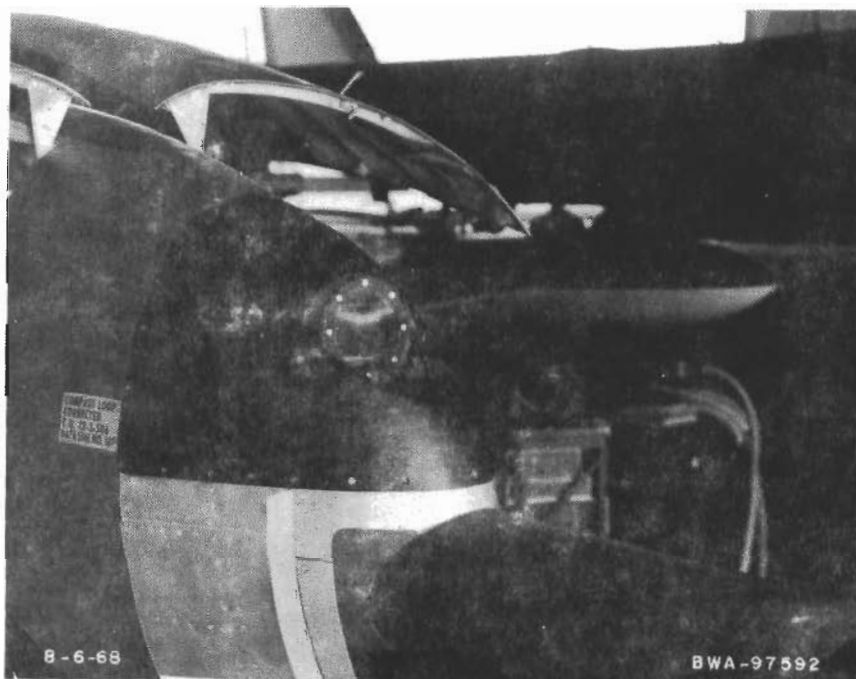


Figure II-2 Front View of Camera Installation with Aerodynamic Fairing Installed

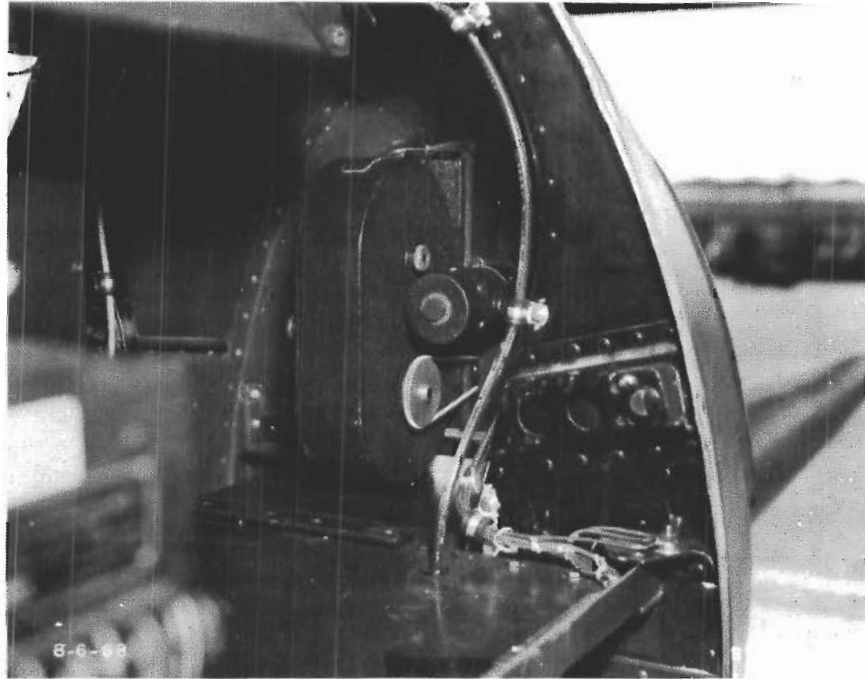


Figure II-3 Rear View of Camera Installation

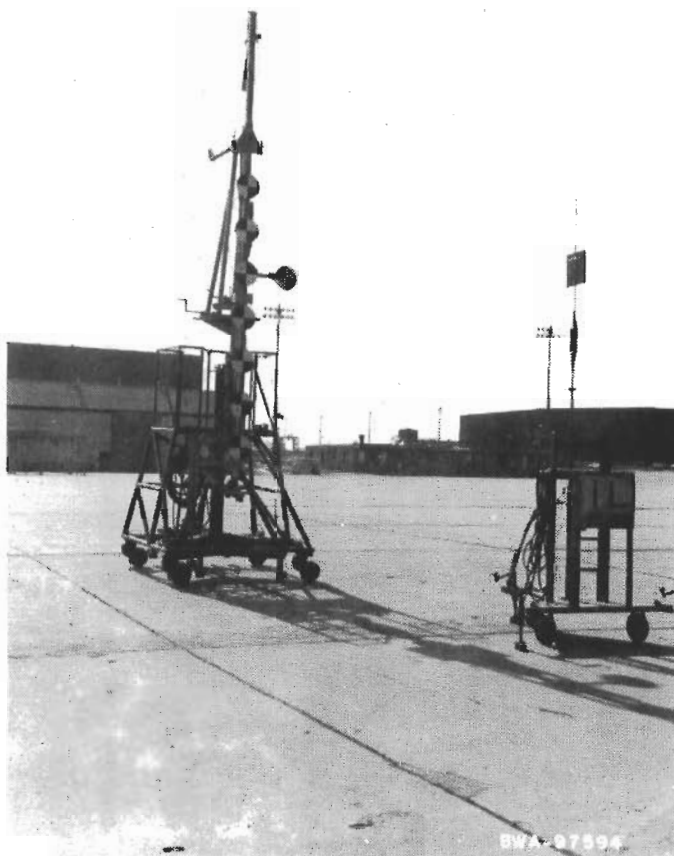


Figure II-4 Boresight Calibration Target Stand

# Contrails

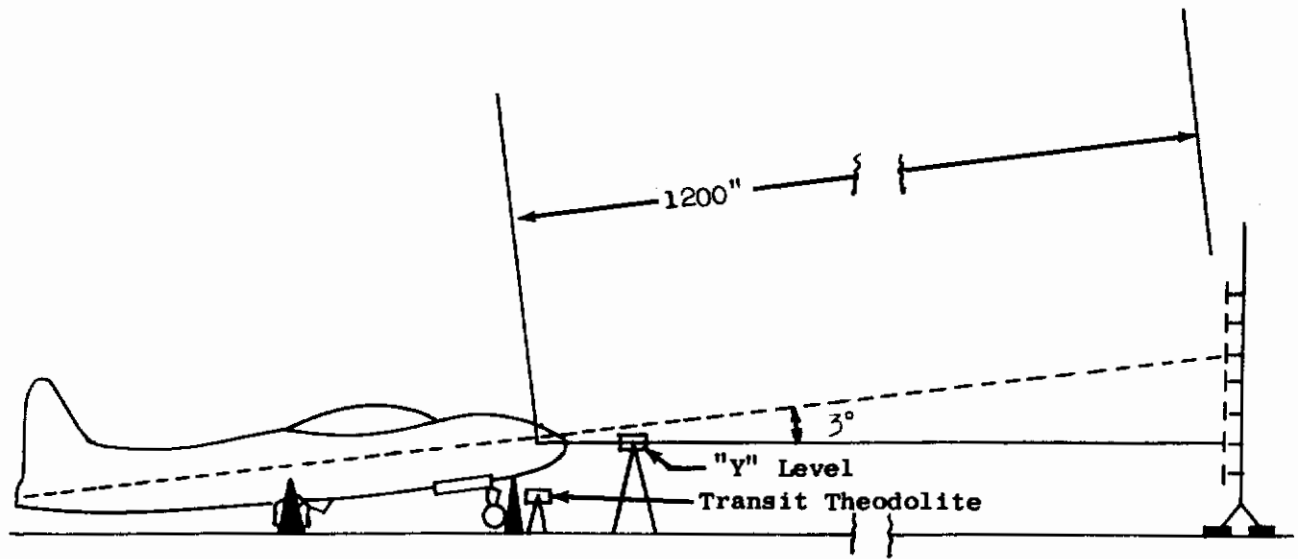


Figure II-5 Side View of Boresight Calibration Setup

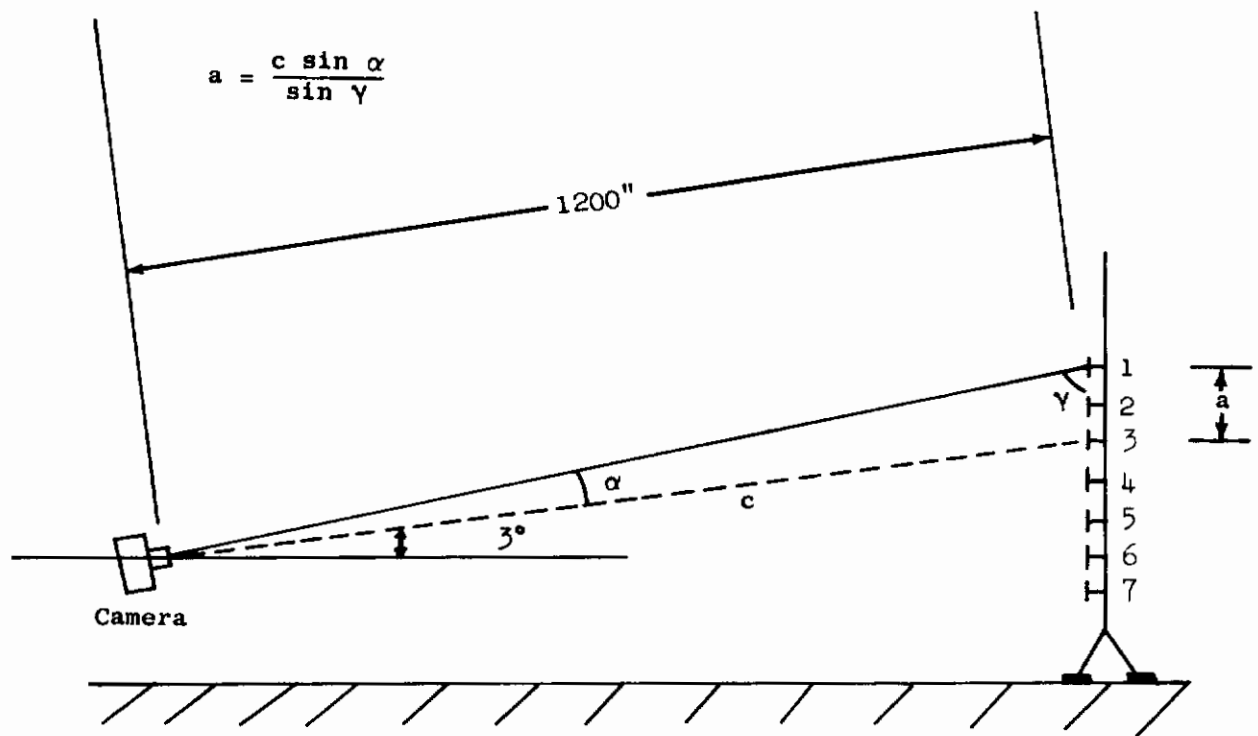


Figure II-6 Calculation of Target Spacing

# Contrails

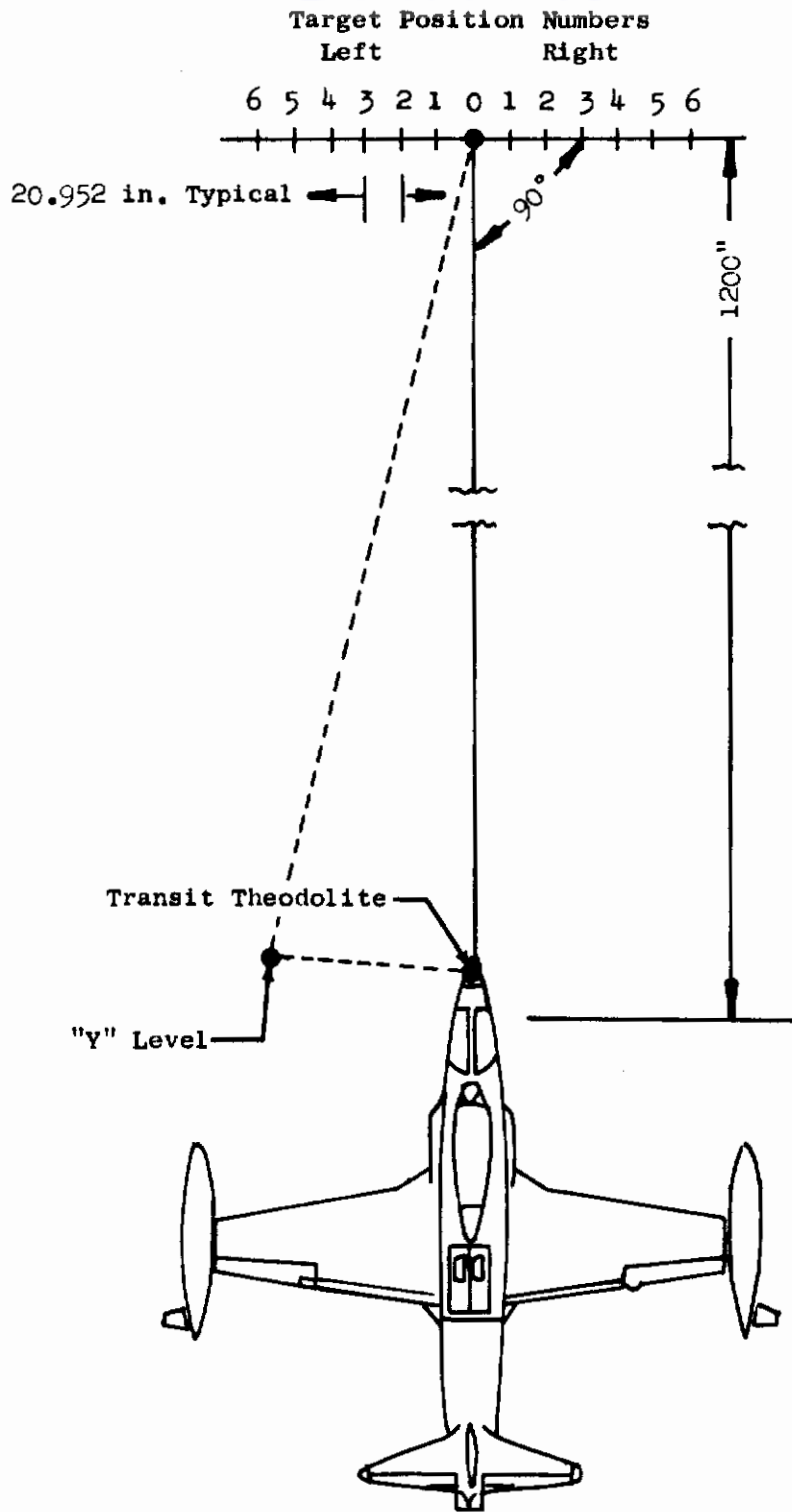


Figure II-7 Top View of Boresight Calibration Setup



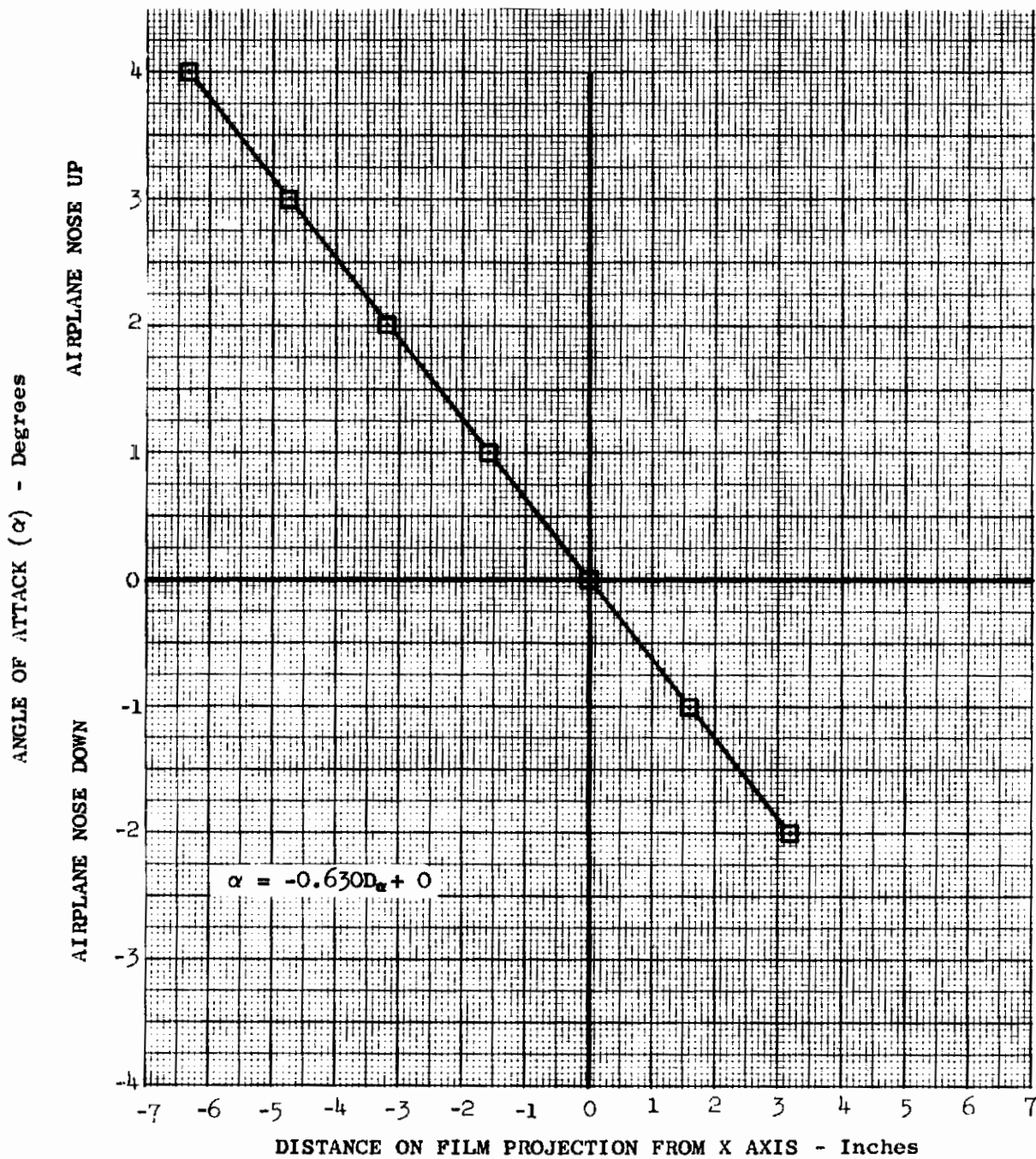


Figure II-8 Camera Boresight Calibration for Angle of Attack

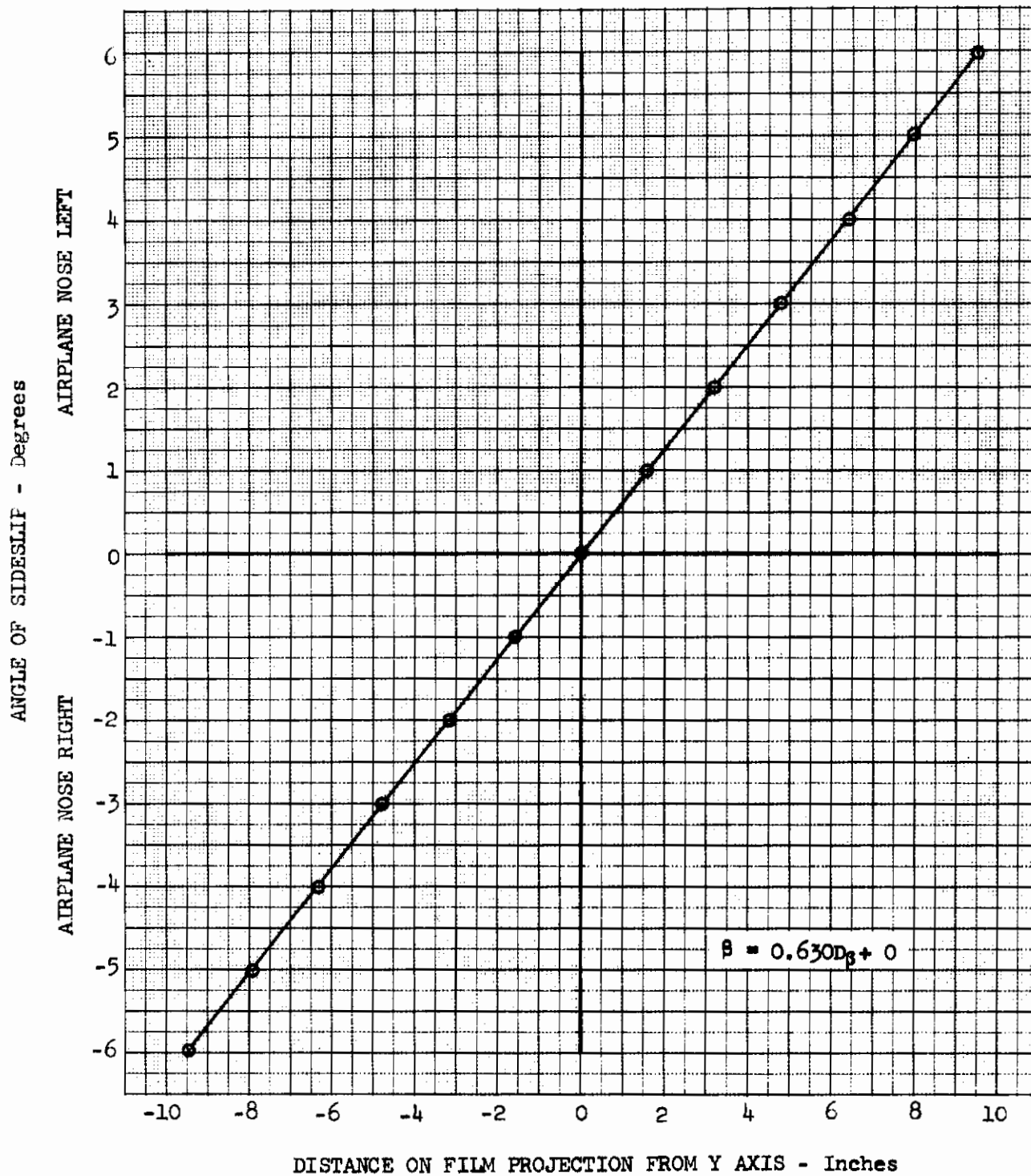


Figure II-9 Camera Boresight Calibration for Angle of Sideslip



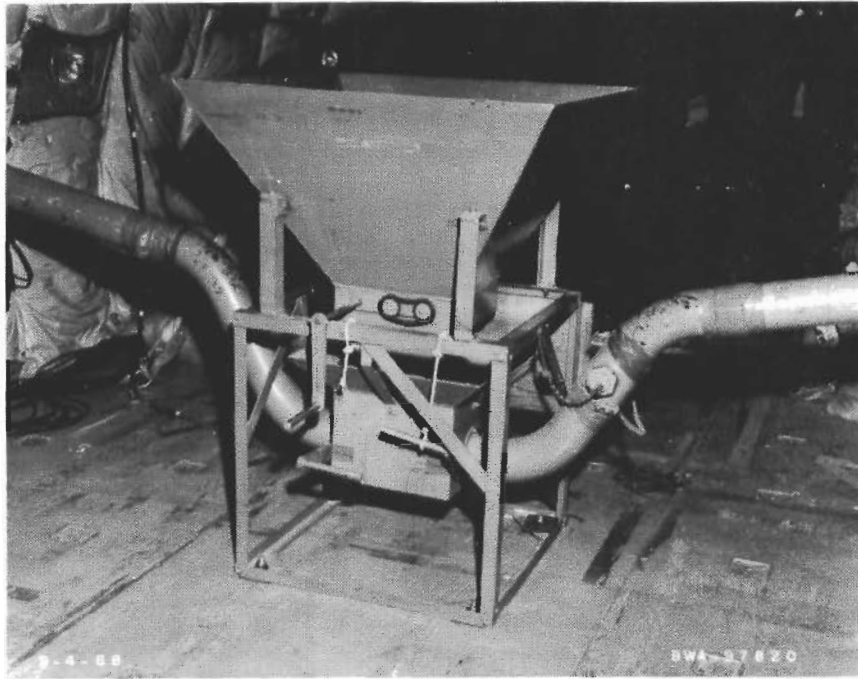


Figure II-10 Confetti Hopper Installation in C-135 Airplane -  
Aft View

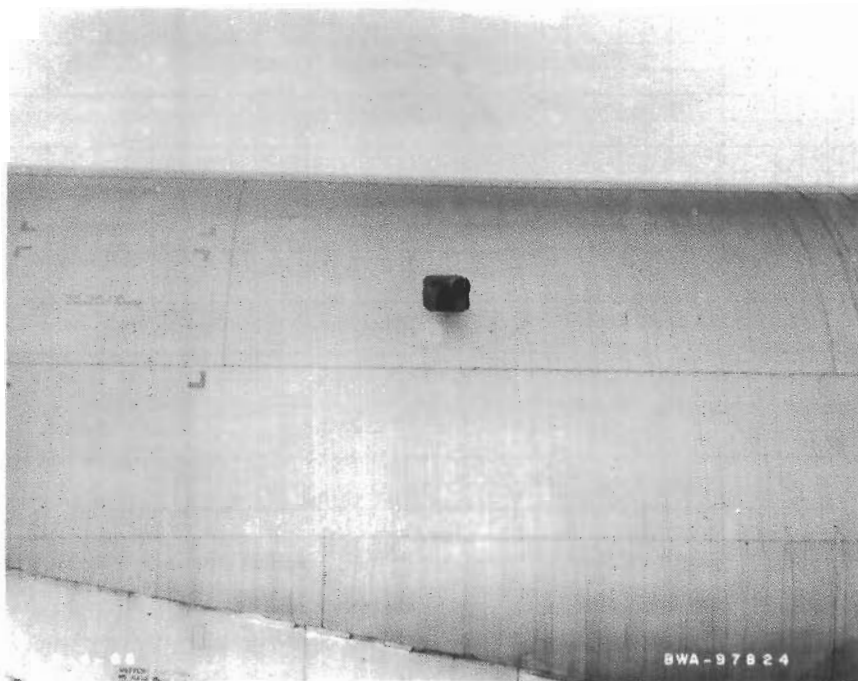


Figure II-11 C-135 Airplane Confetti Discharge Duct - Left  
Exterior Side View



Point of Emination  
of Confetti Streaks

C-135 Confetti  
Dispensing Airplane



Figure II-12 Sample Frame of Confetti Film

# Contrails

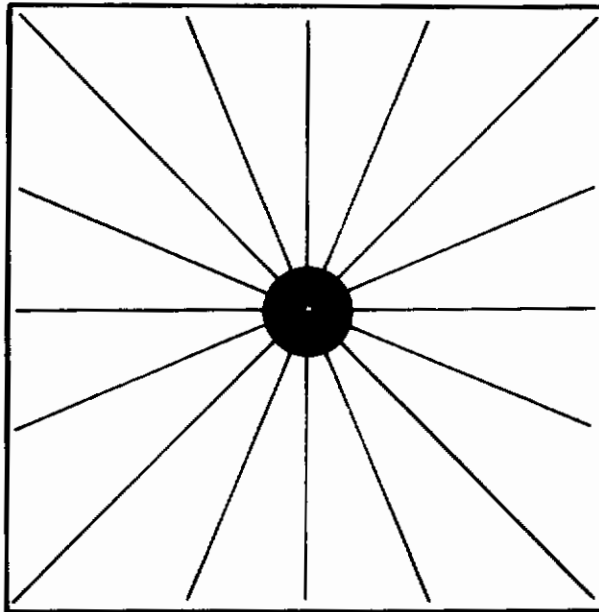


Figure II-13 Radial Template Used to Determine the Point of Emanation of the Confetti Streaks

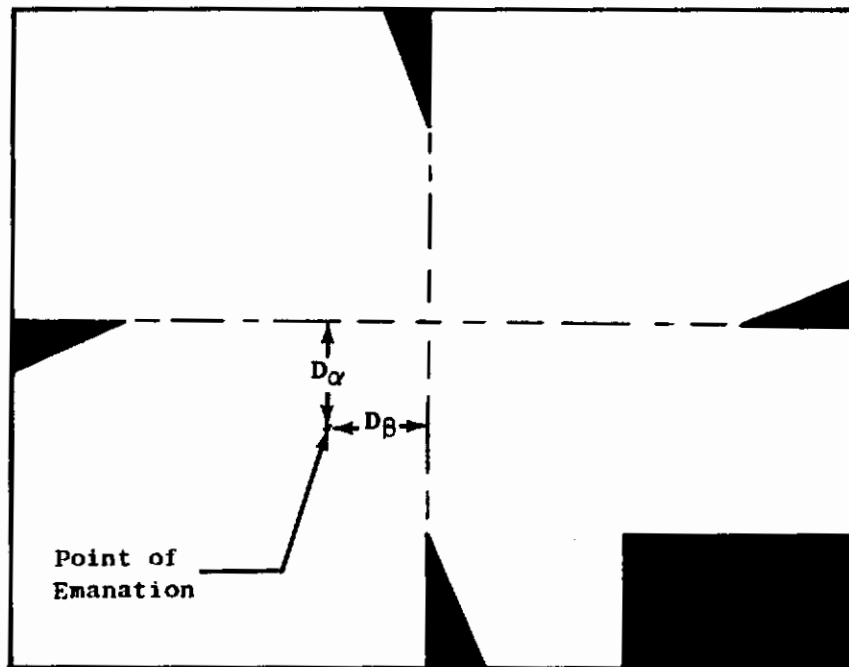


Figure II-14 Typical Film Frame Showing Point of Emanation Obtained through Use of the Radial Template

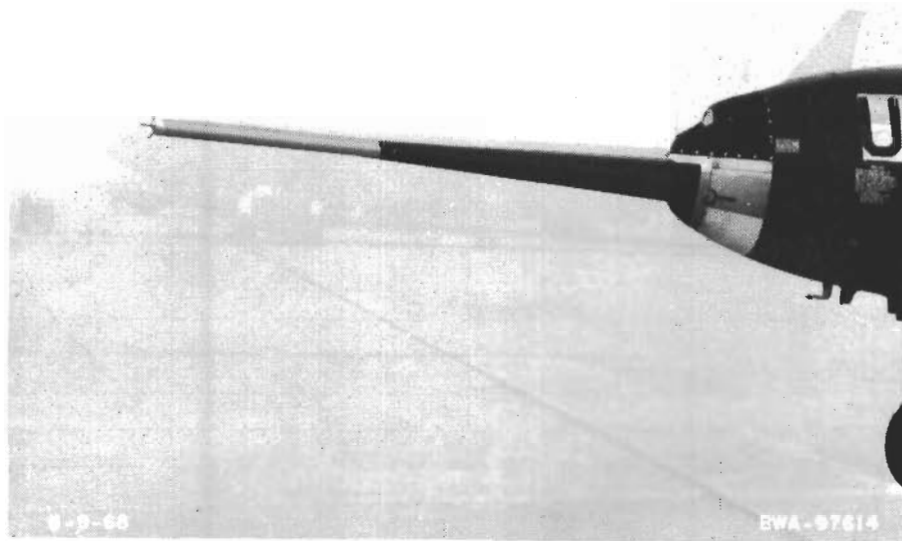


Figure II-15 Gust Boom and Probe Installation on T-33A Airplane

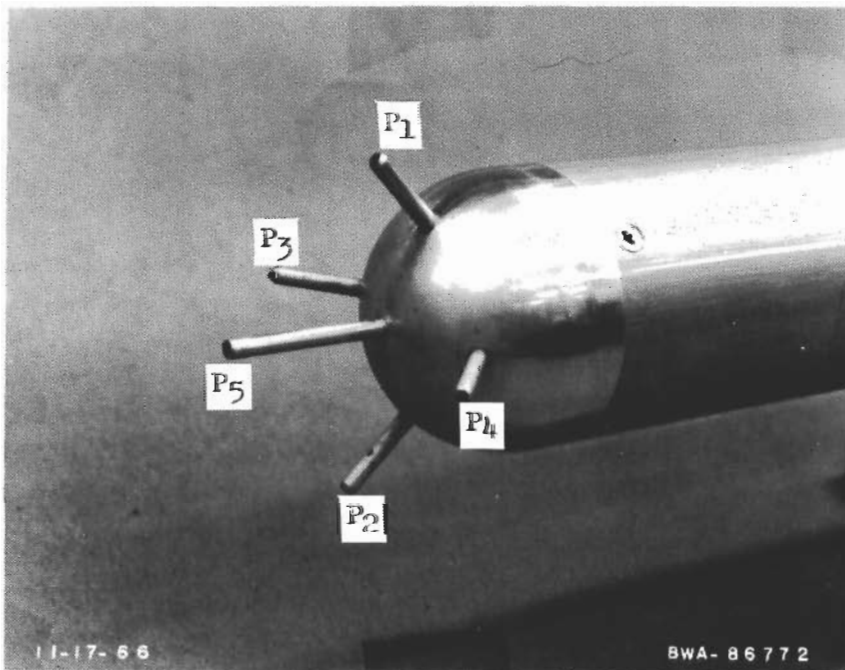


Figure II-16 Gust Probe Head and Pressure Port Identification

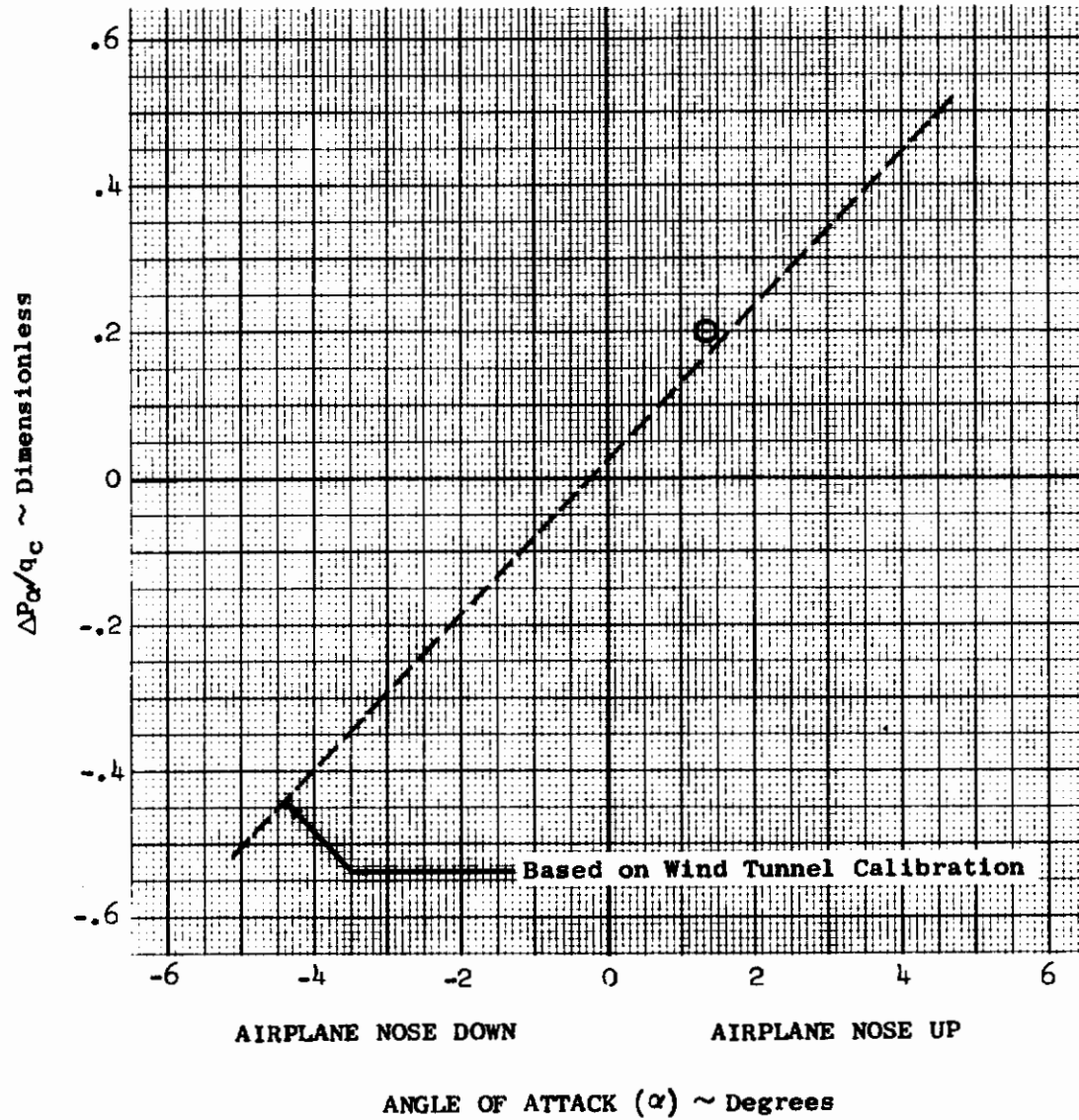


Figure II-17 Angle of Attack Calibration for .4 Mach



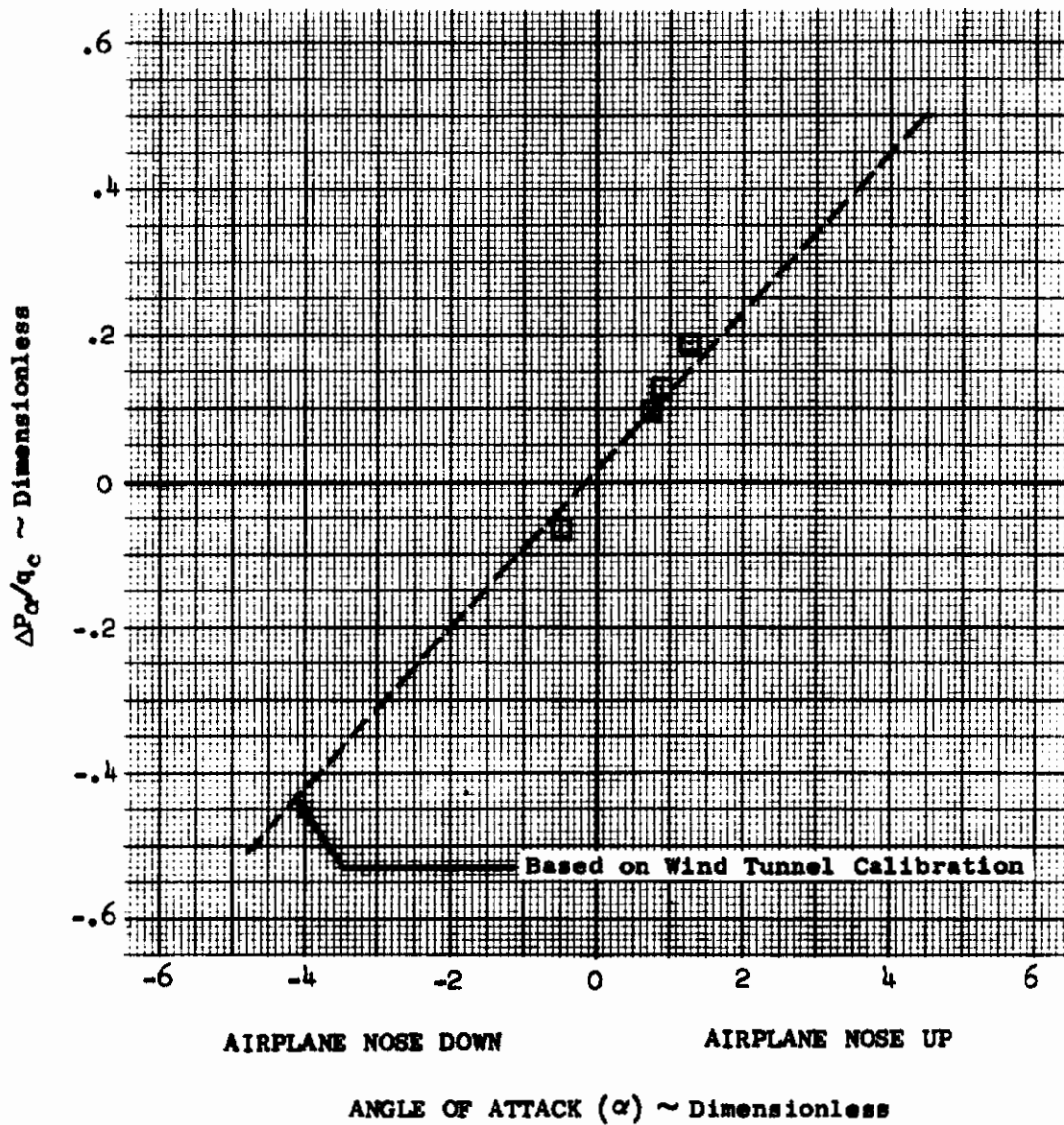


Figure II-18 Angle of Attack Calibration for .5 Mach

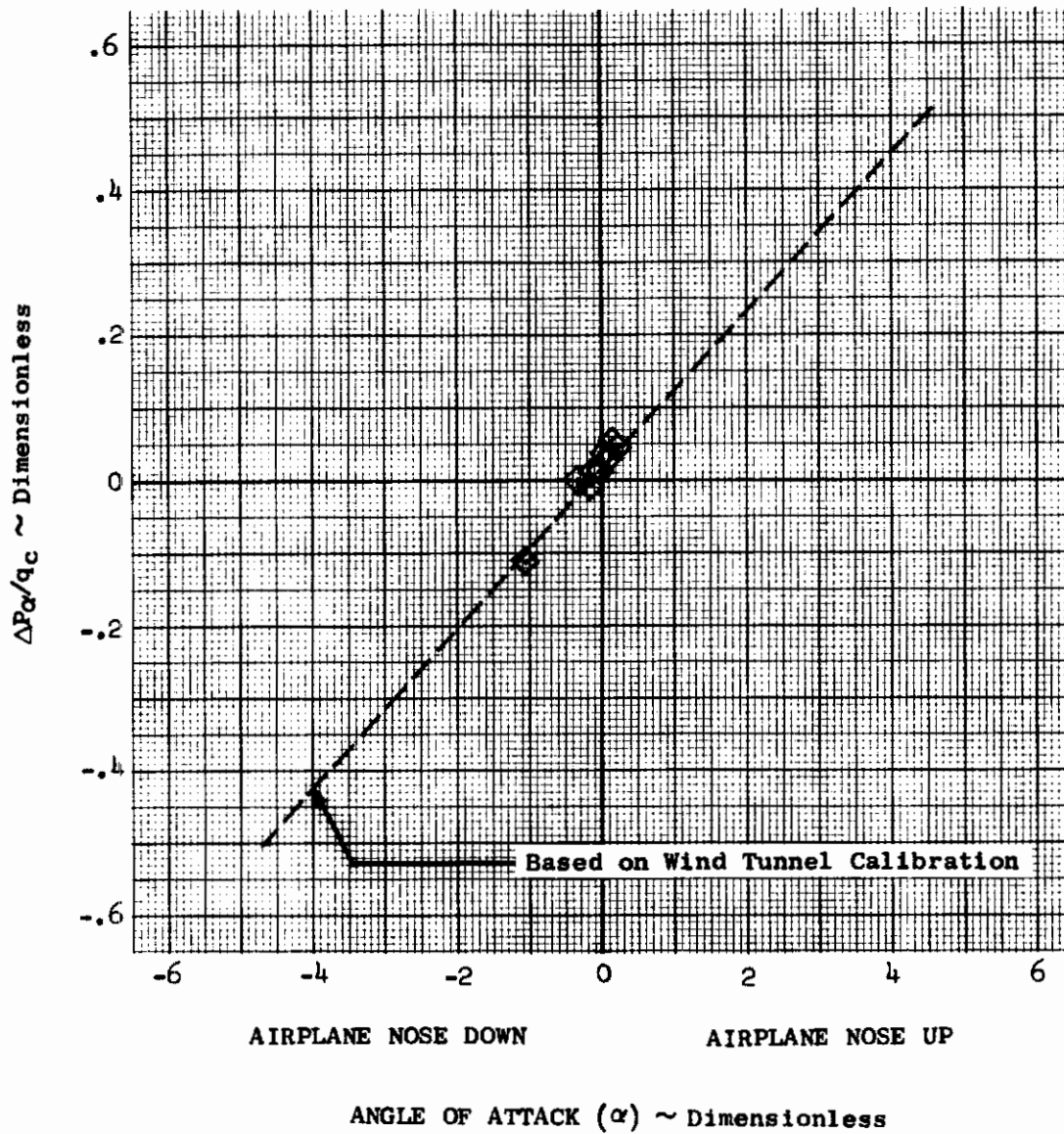


Figure II-19 Angle of Attack Calibration for .6 Mach



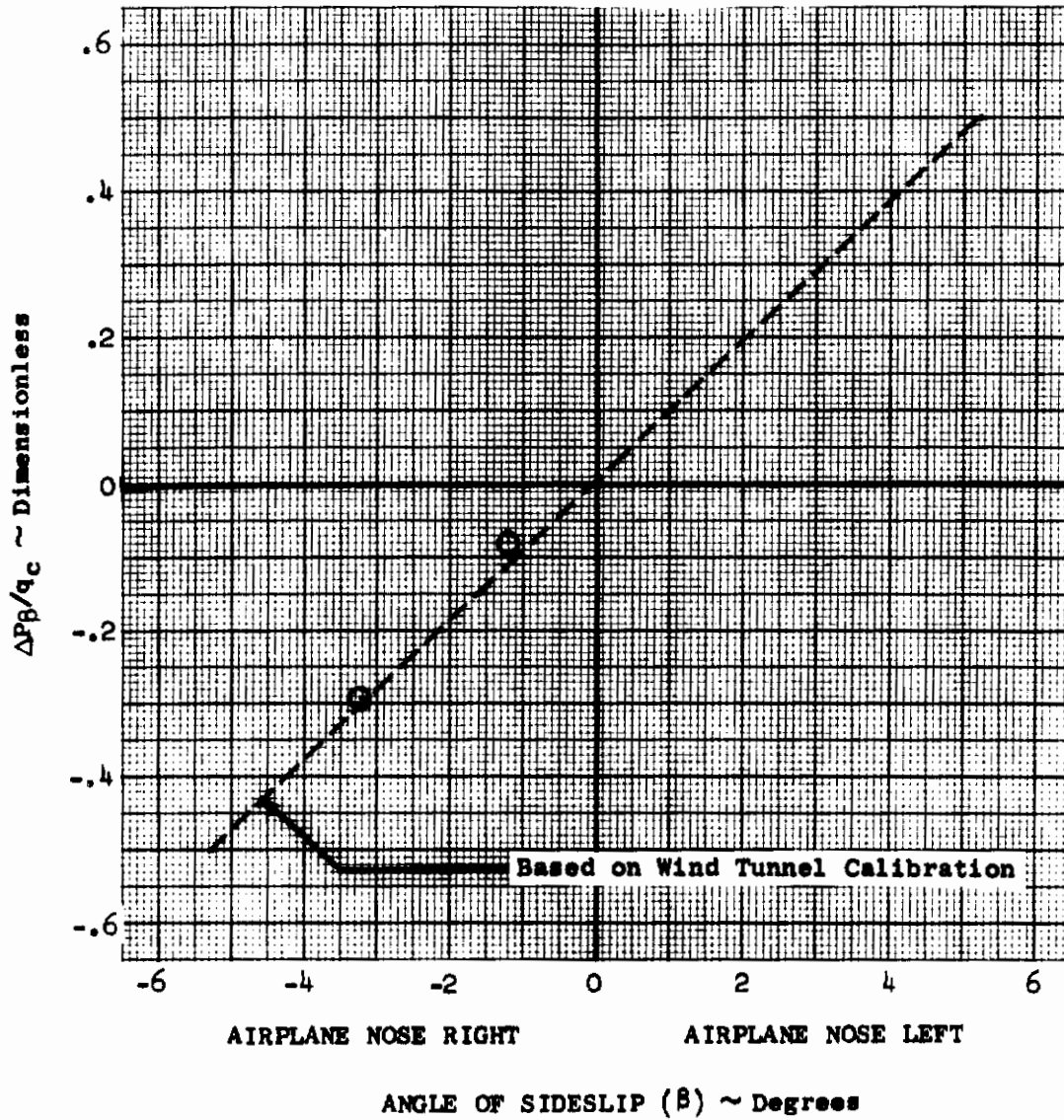


Figure II-20 Angle of Sideslip Calibration for .4 Mach

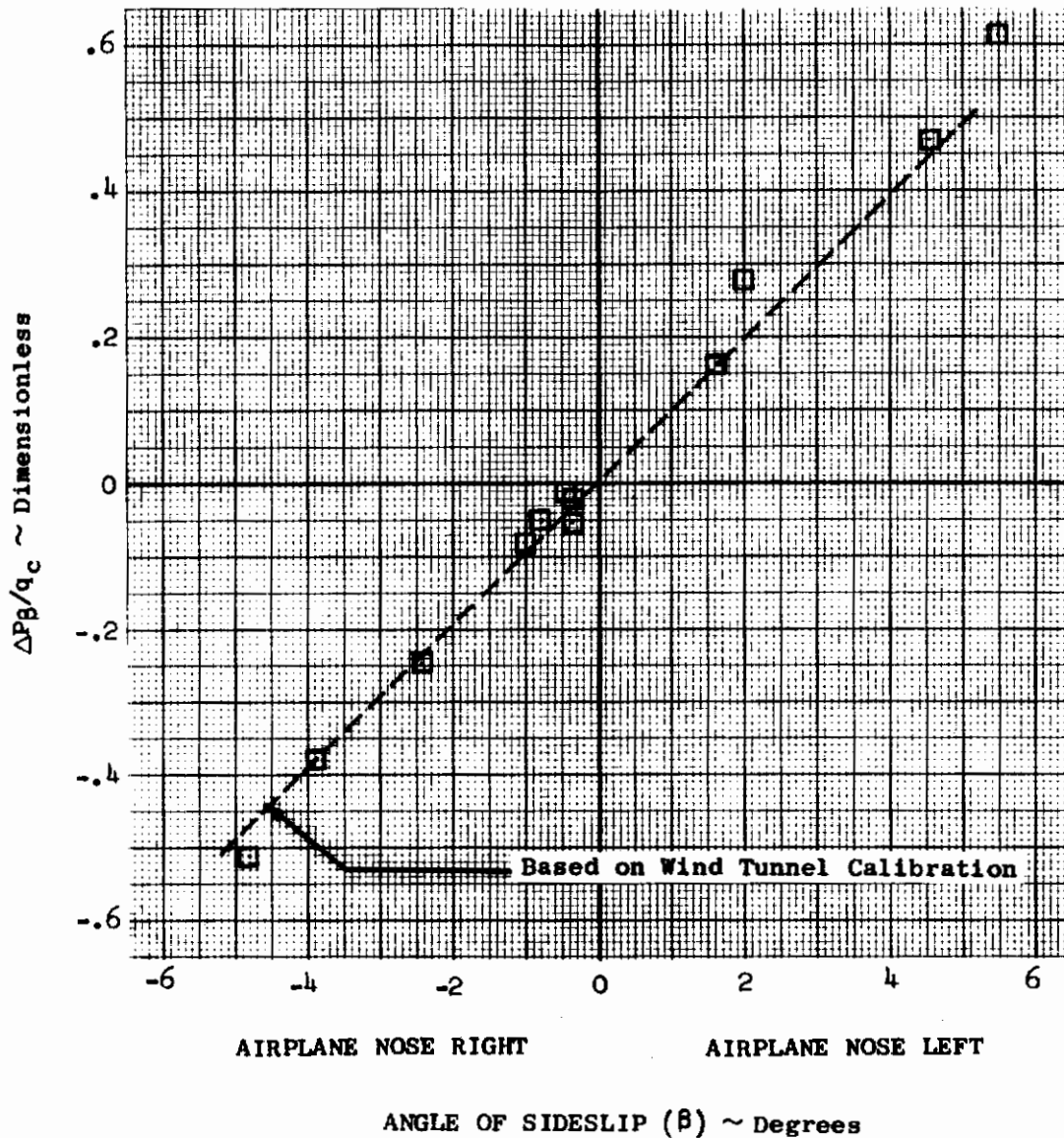


Figure II-21 Angle of Sideslip Calibration for .5 Mach



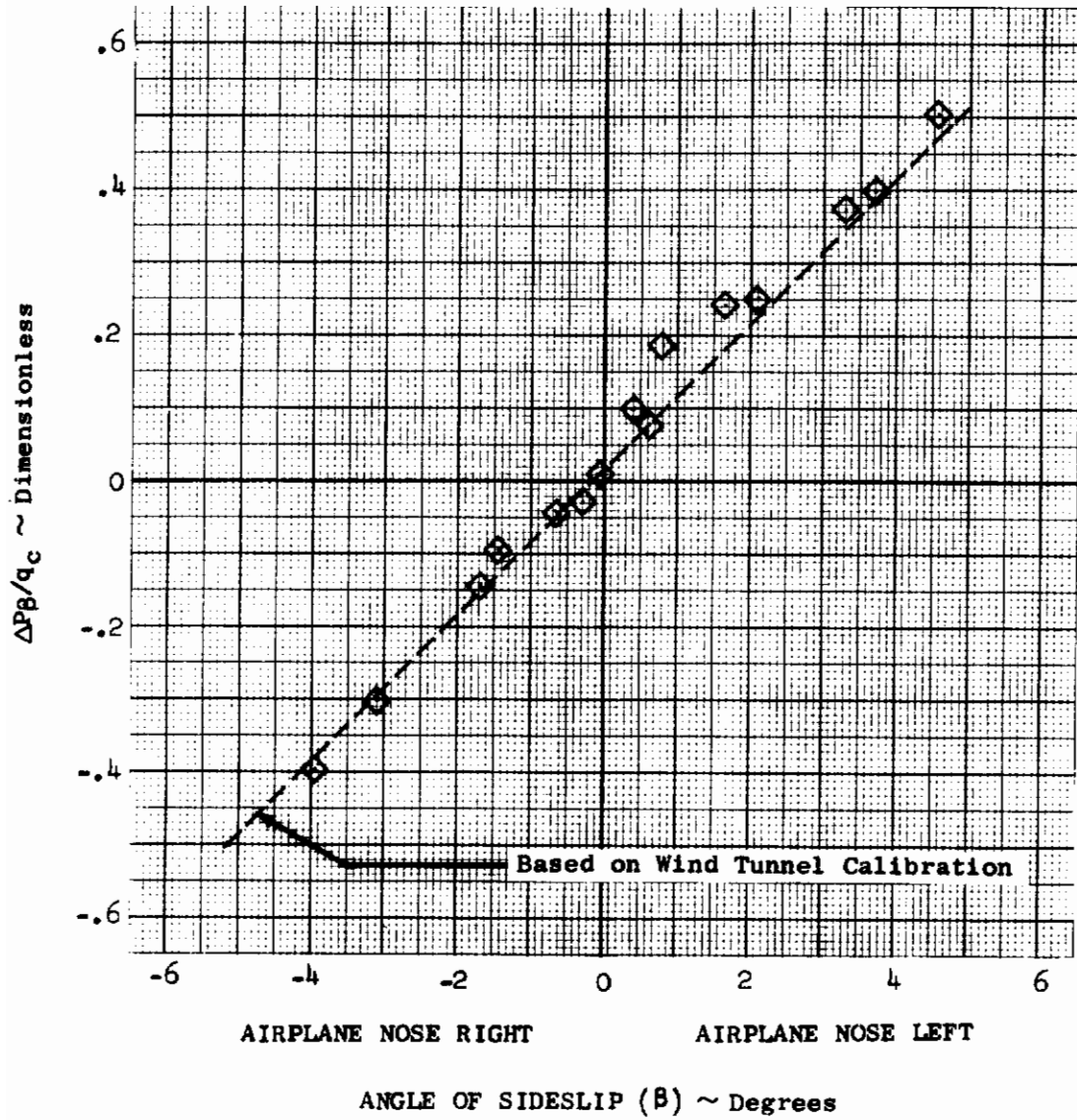


Figure II-22 Angle of Sideslip Calibration for .6 Mach

# Contrails

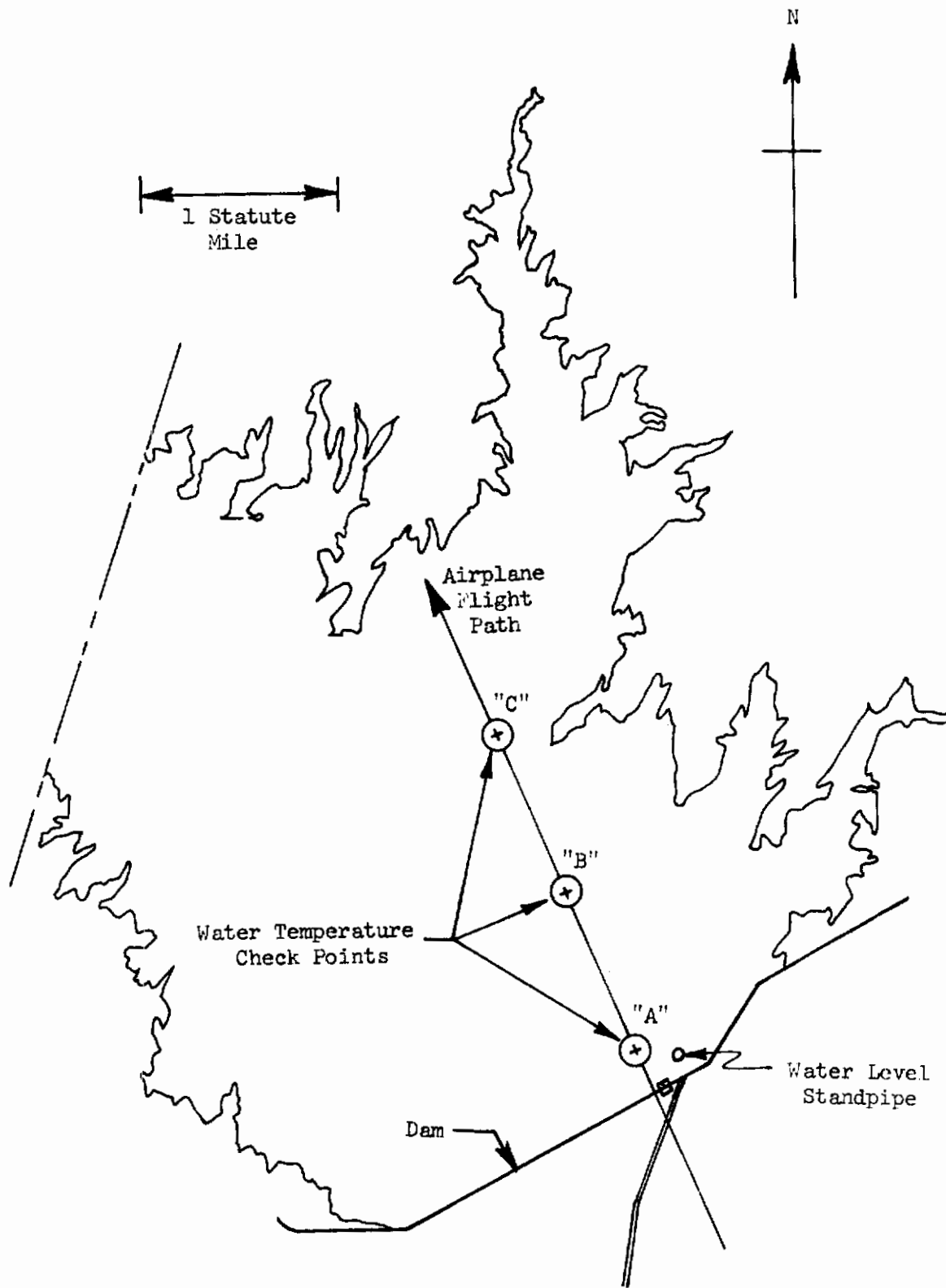


Figure II-23 Airplane Flight Path over Cheney Reservoir

# Contrails

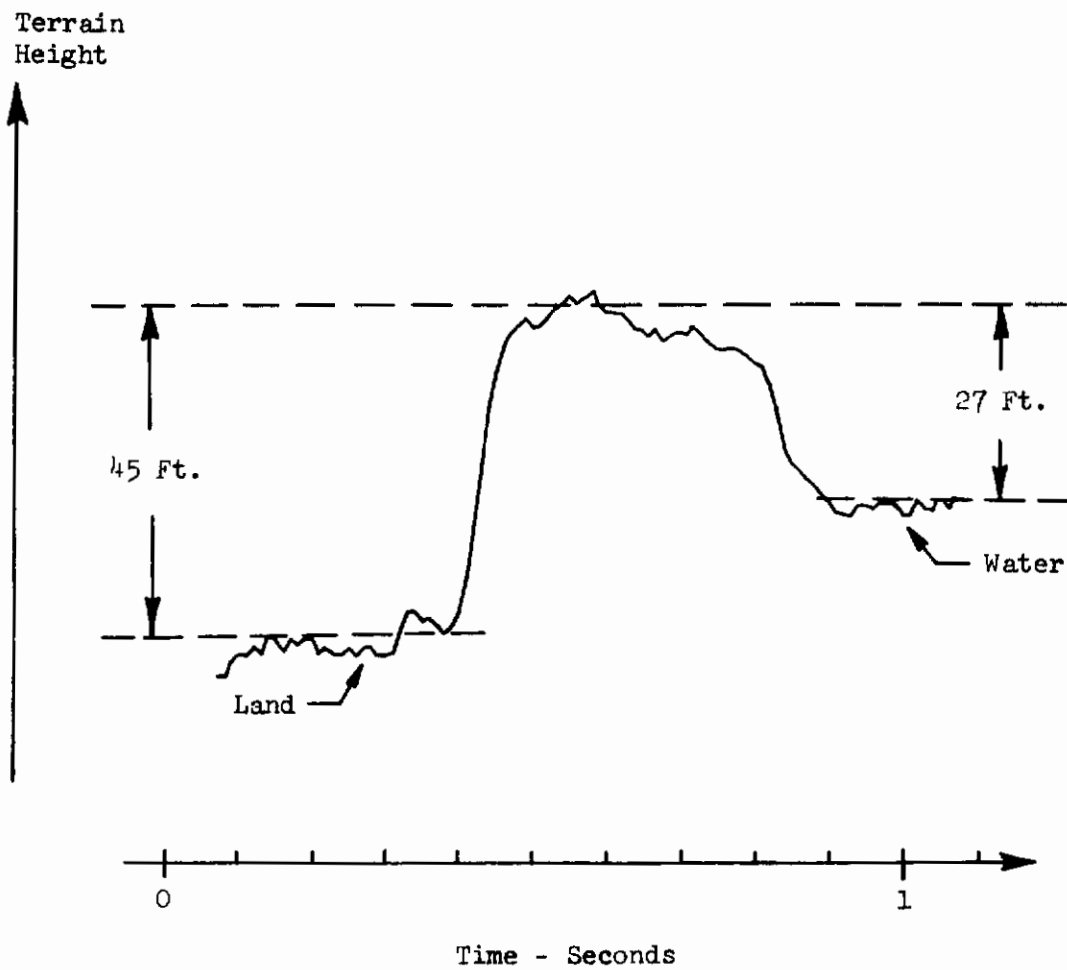


Figure II-24 Time History of Terrain Height from Radar Altimeter Data

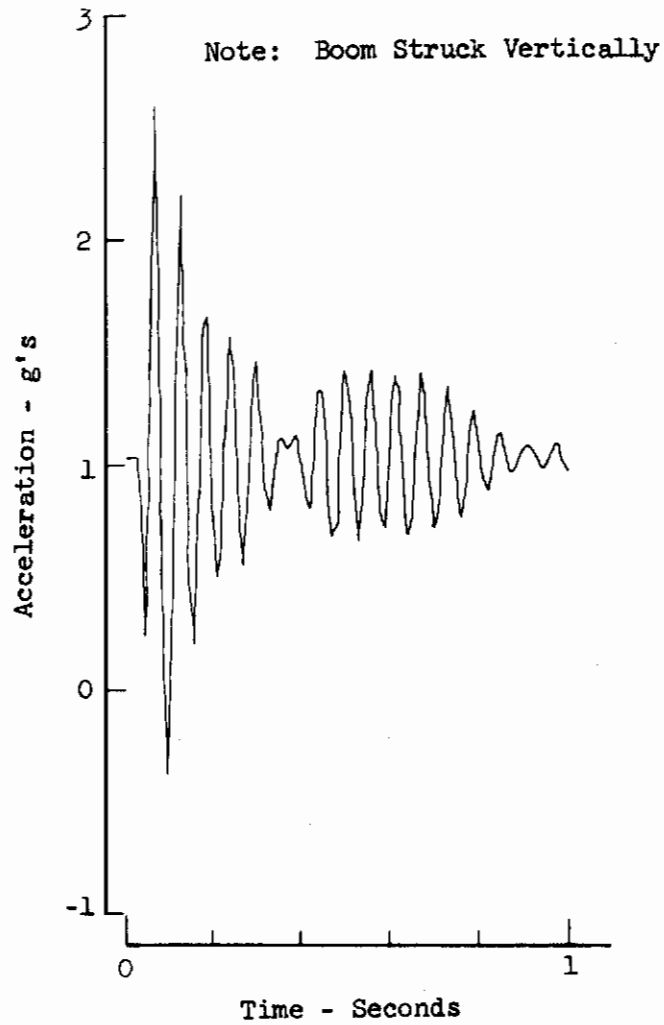


Figure II-25 Probe Vertical Acceleration Time History - Natural Frequency Determination

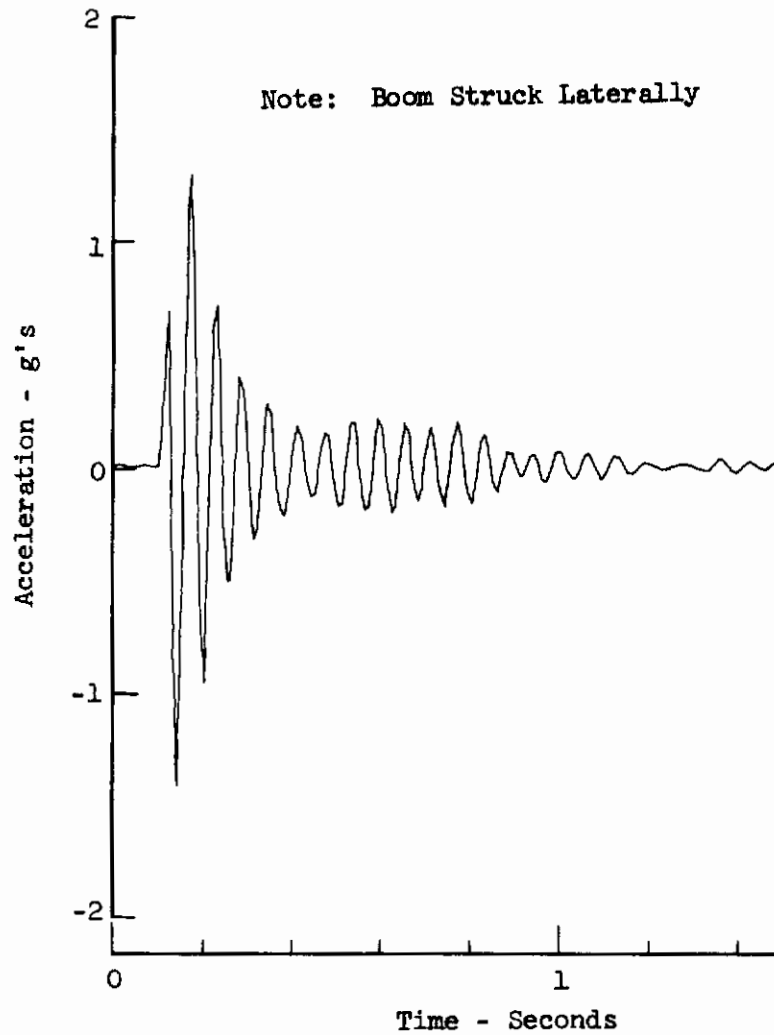


Figure II-26 Probe Lateral Acceleration Time History - Natural Frequency Determination

# Contrails

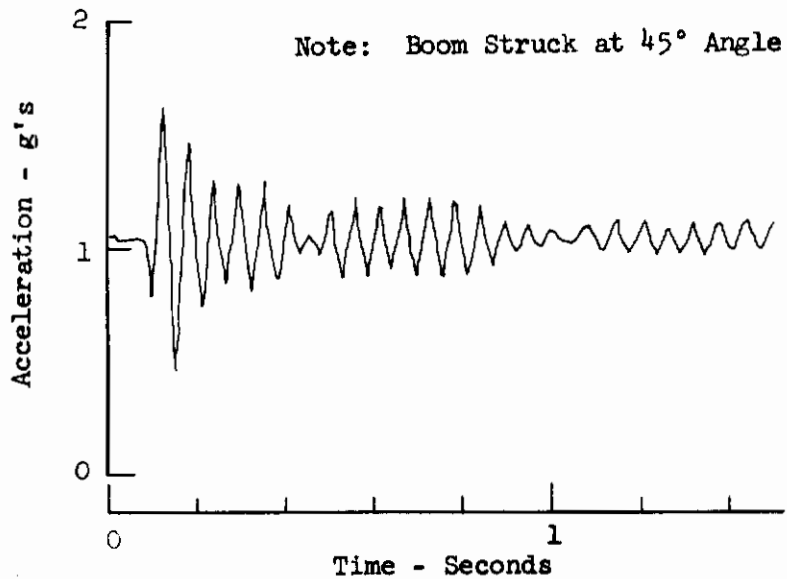


Figure II-27 Probe Vertical Acceleration Time History - Natural Frequency Determination

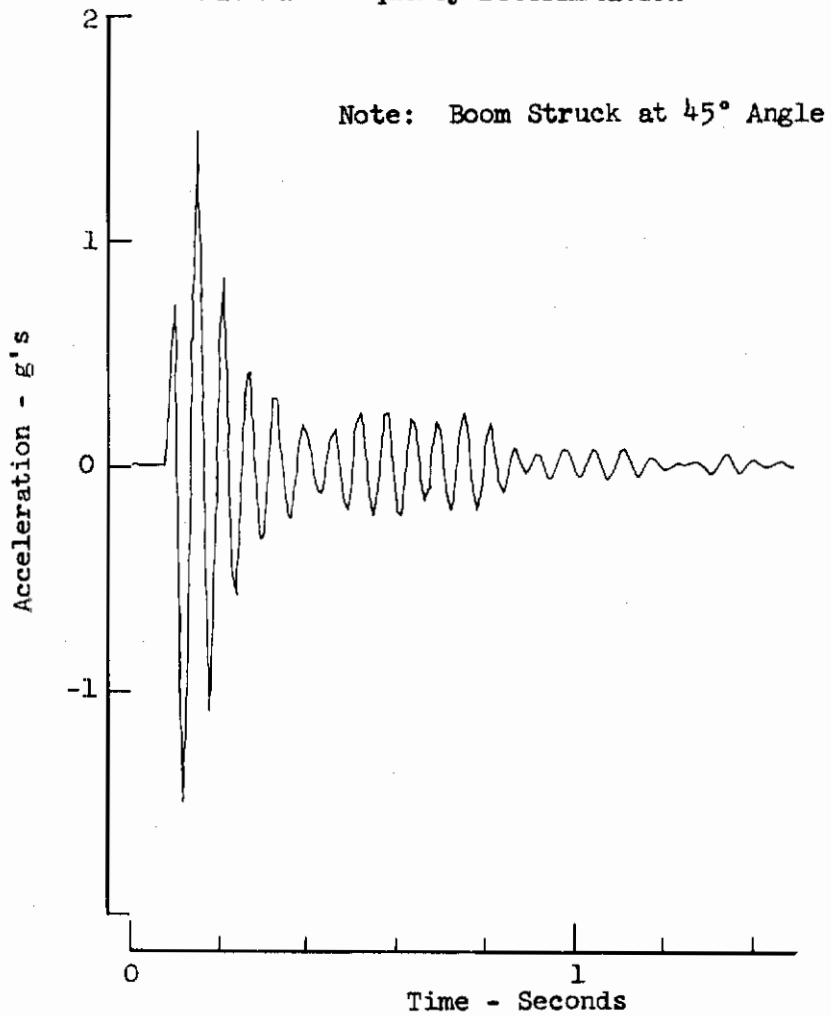


Figure II-28 Probe Lateral Acceleration Time History - Natural Frequency Determination



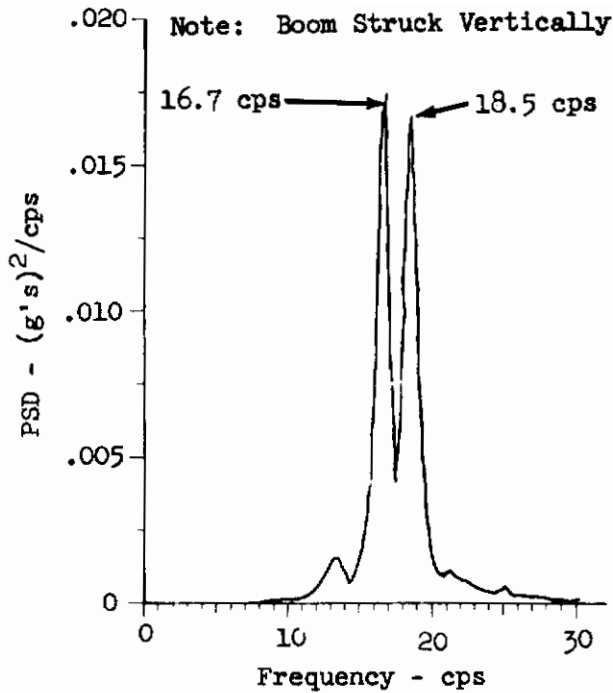


Fig. II-29 Probe Vertical Acceleration PSD - Natural Frequency Determination

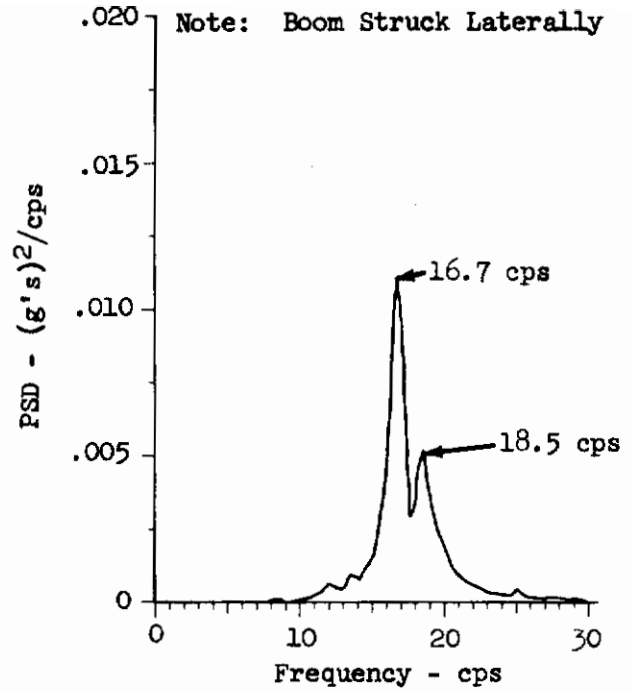


Fig. II-30 Probe Lateral Acceleration PSD - Natural Frequency Determination

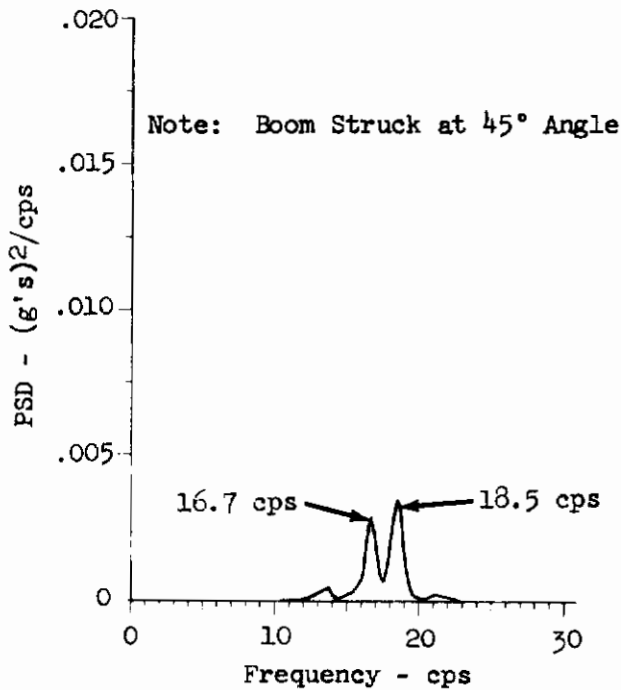


Fig. II-31 Probe Vertical Acceleration PSD - Natural Frequency Determination

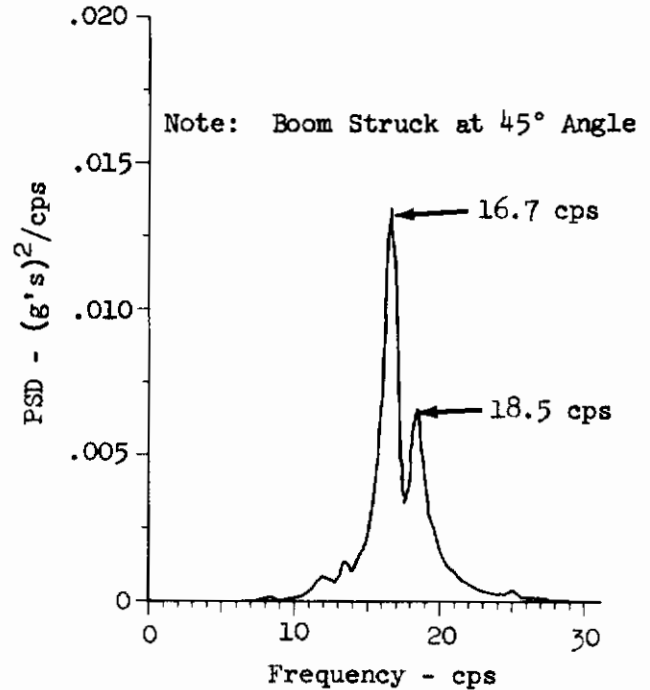


Fig. II-32 Probe Lateral Acceleration PSD - Natural Frequency Determination

# Contrails

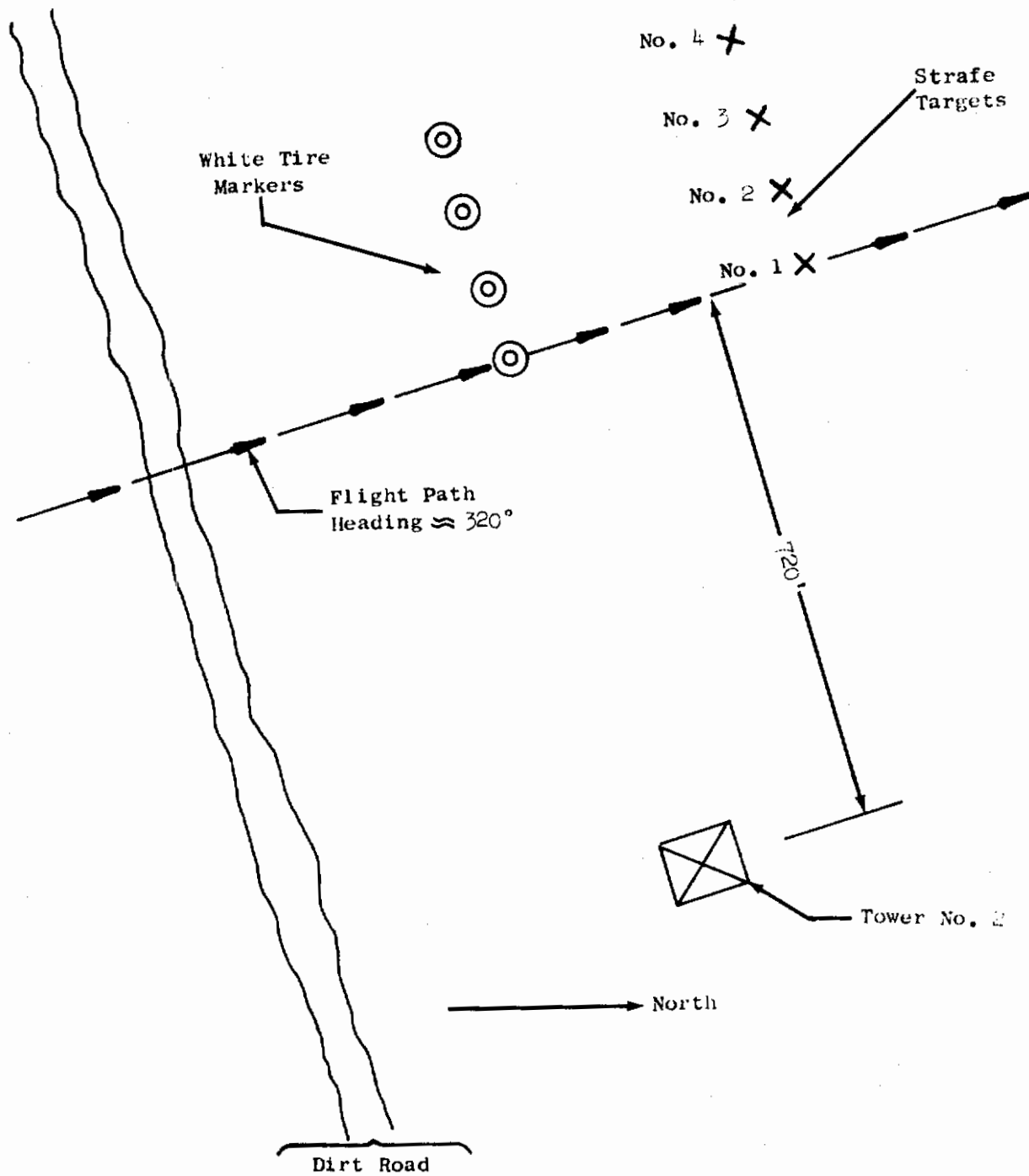


Figure II-33 Smoky Hill Gunnery and Bomb Range Features in Area of Tower No. 2

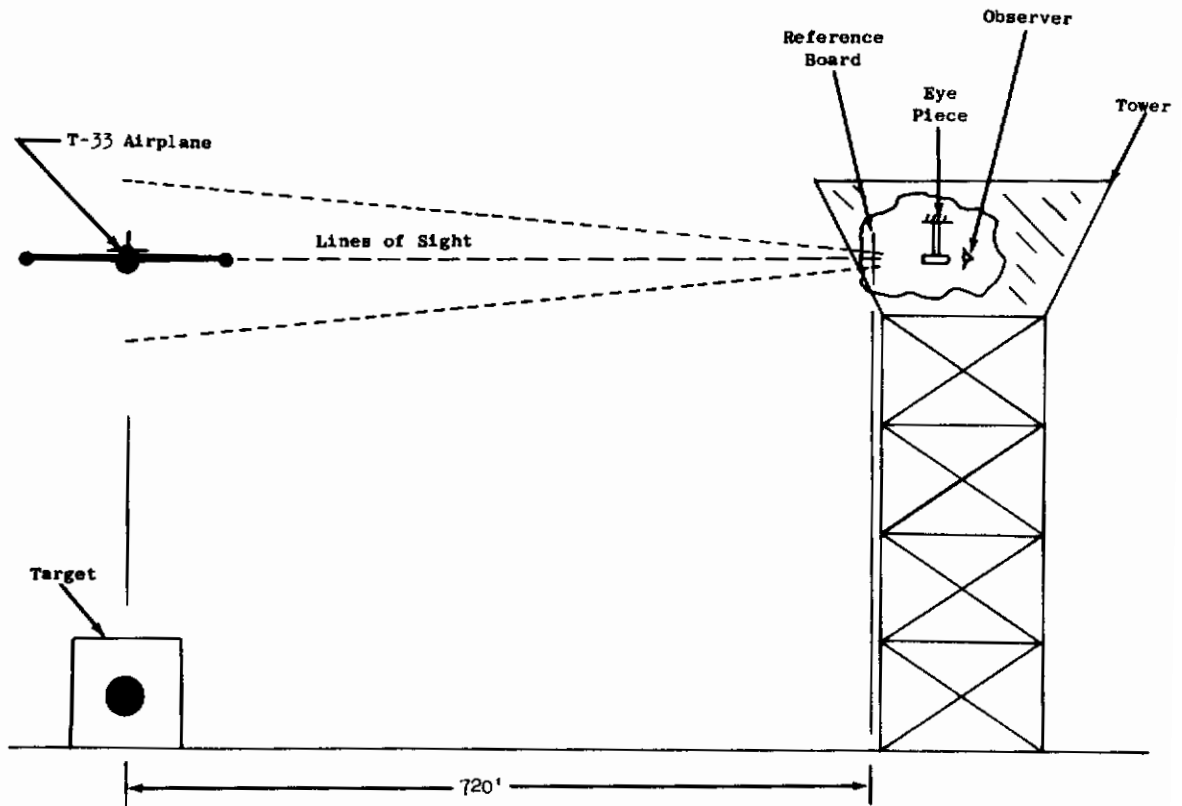


Figure II-34 Airspeed Calibration - Tower Flyby Arrangement

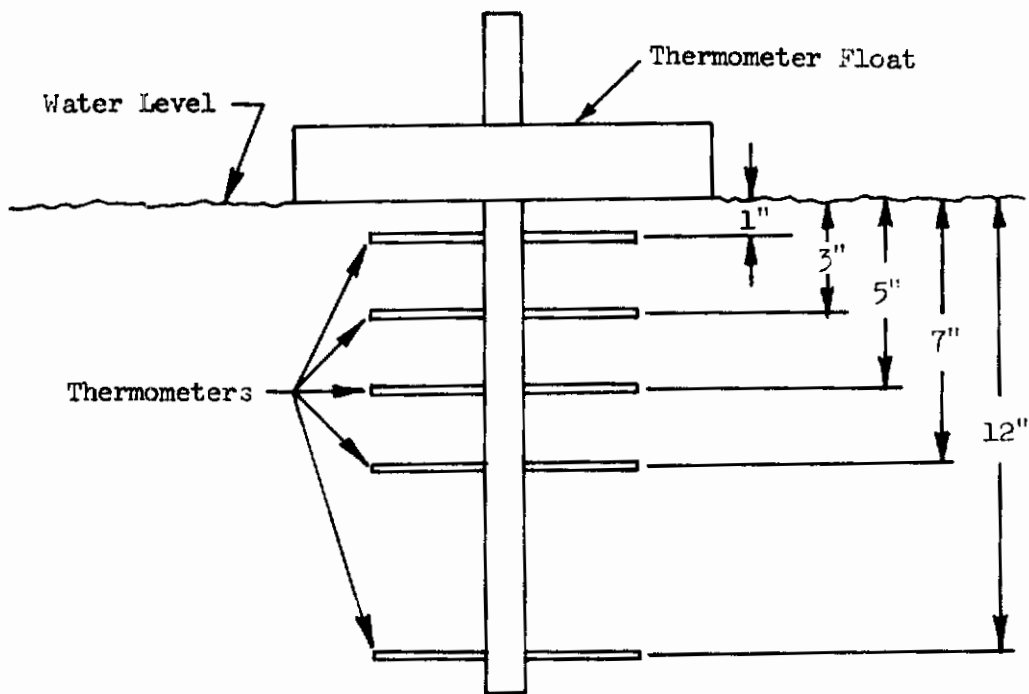


Figure II-35 Thermometers for Measuring Water Temperature

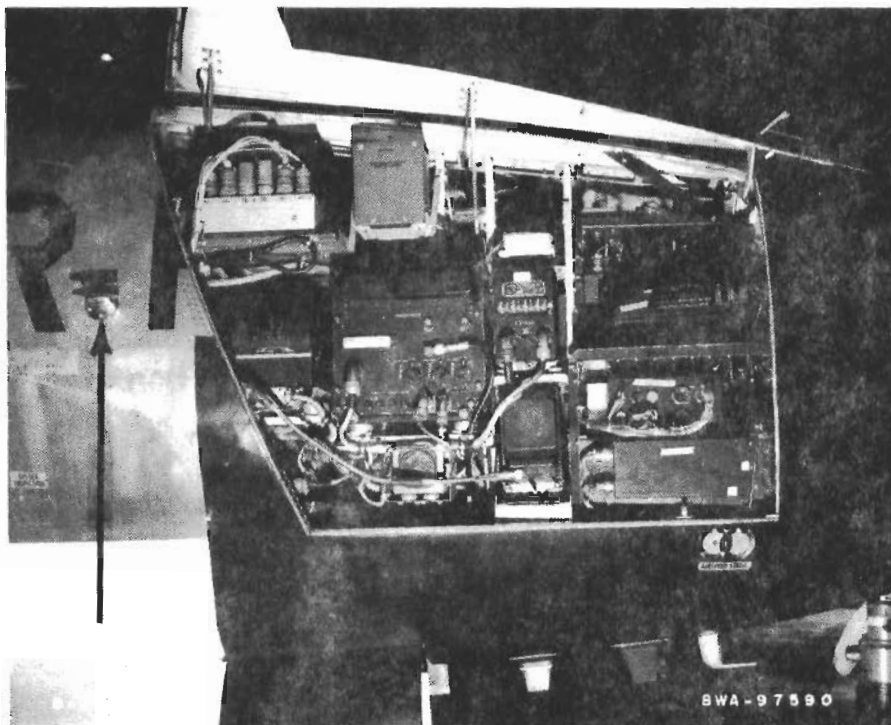


Figure II-36 OAT Probe Installation on T-33 Airplane

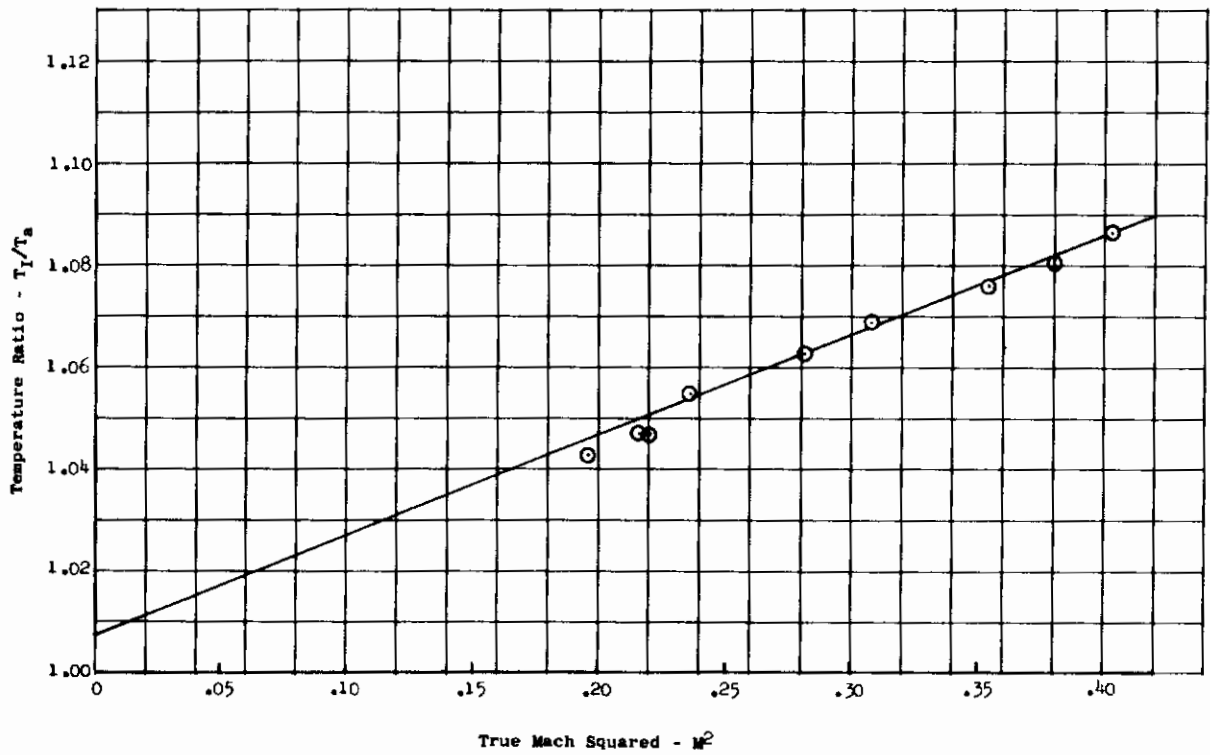


Figure II-37 OAT Calibration from Smoky Hill Tower Flyby



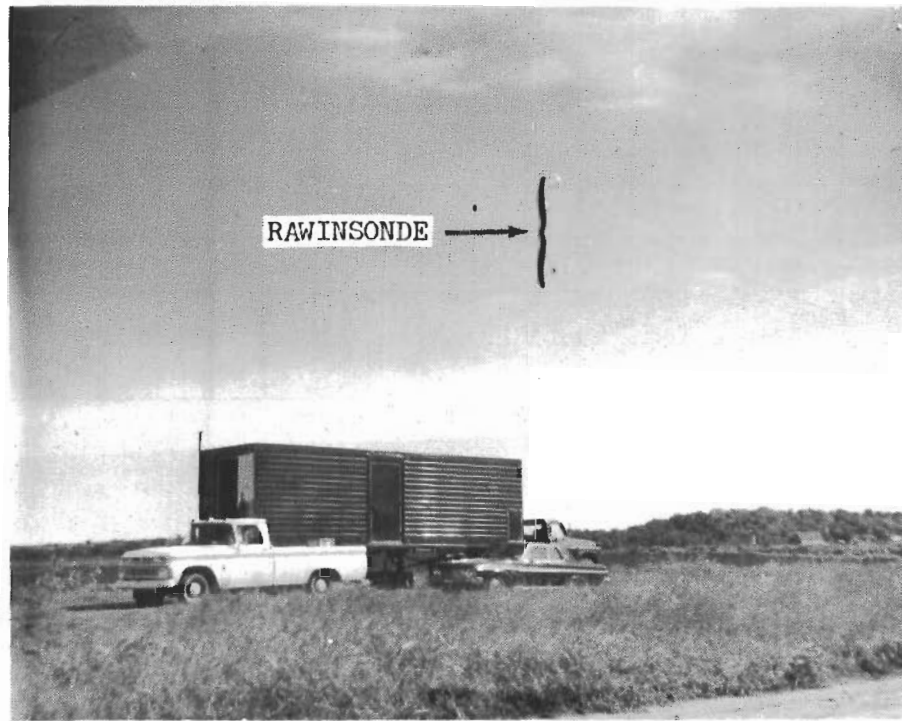
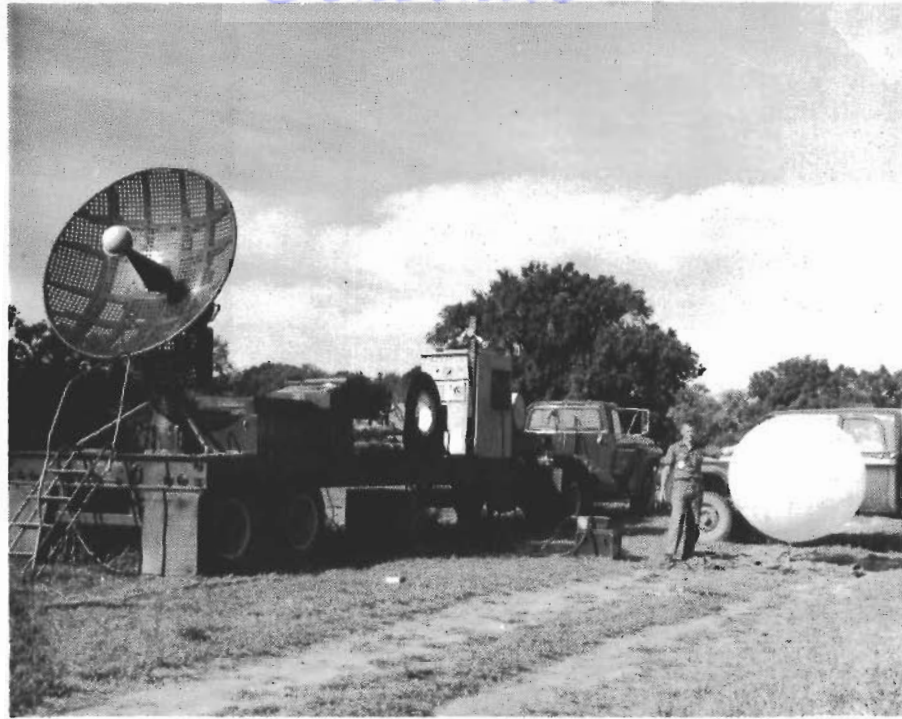


Figure II-38 Cedar Vale Remote Weather Station

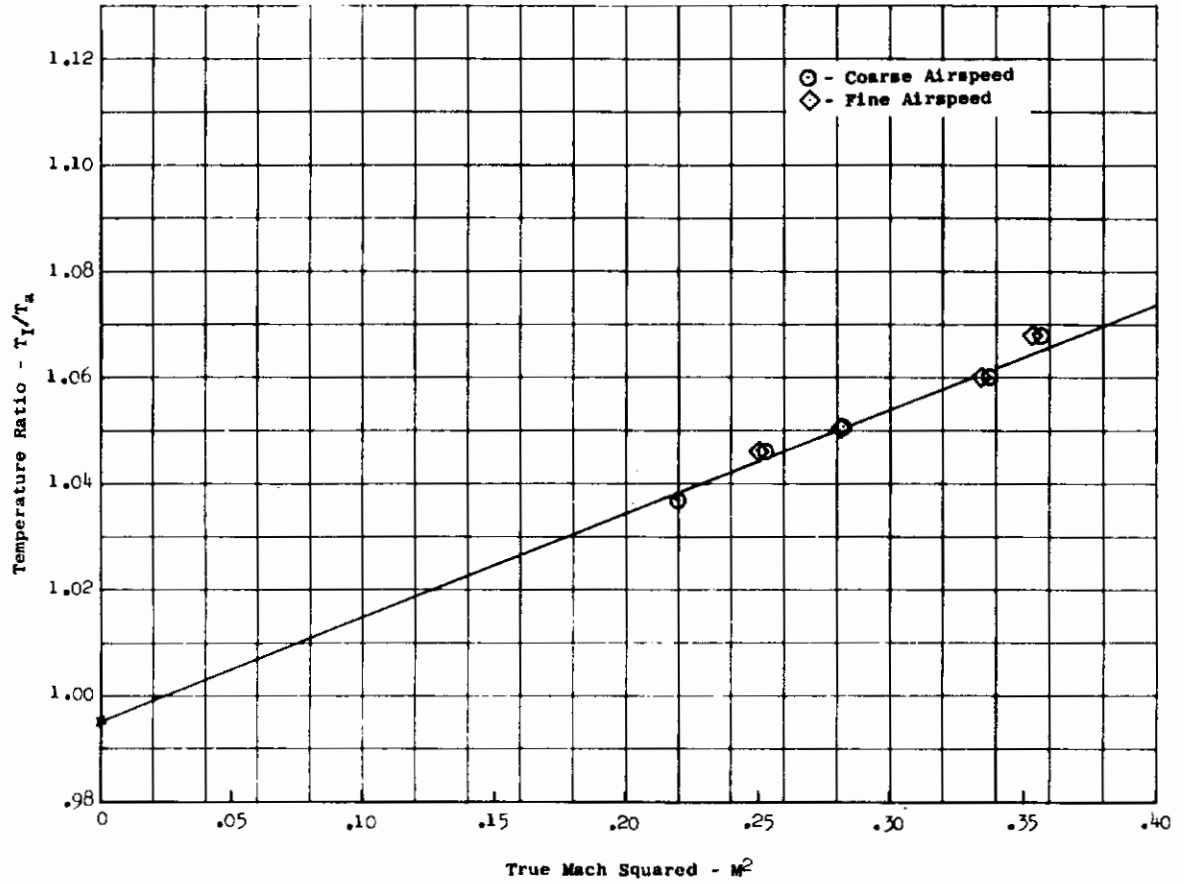


Figure II-39 OAT Calibration from Cedar Vale Flybys

## APPENDIX III

### DATA PROCESSING

Data processing is accomplished primarily by the use of digital computing equipment. The frequency response compensation of angle of attack and sideslip measurements is accomplished with analog computer. Analog compensation networks are spot-checked on the digital computer for accuracy verification.

The data processing equipment provides precise time correlation through the use of linear phase filters, sample and hold features to assure simultaneous sampling and time correlation of data during analog-to-digital conversion, reduced tape playback time, and automatic plotting and printing. Automatic methods are employed that precisely correct the data for undesirable transducer frequency response characteristics, transducer zero drift, and data system zero drift and sensitivity changes.

The central computing facility IBM 360-65 digital computer is used for the bulk of the computations. Magnetic tape units, magnetic discs, printers and card reader/punch equipment are available.

Digital techniques employed in the computer programs utilize recently developed algorithms for regression analysis, Fourier analysis, numerical integration and digital filtering. Optimum sampling rates are used to minimize integration drift errors and eliminate aliasing.

### GROUND STATION EQUIPMENT

Recovery of data recorded on the airborne portion of the NBFM system is provided through the use of the following ground station data processing equipment. Figure III-1 illustrates the basic flow of data through the ground station. All data processing is accomplished at a tape playback speed of 30 inches per second which is eight times the record speed.

#### Tape Playback Unit Mincom G-114

The tape record/reproduce system serves as a unity transfer data link; that is, it ensures that the output of the ground station tape reproducer is identical to the input to the airborne recorder. Phase linearity is important and the Mincom G-114 excels in this respect. Tape speed control is used to force the reproducer to run synchronized at eight times the airborne recorder speed. The frequency response of the Mincom G-114 at 30 inches per second is 150 to 150,000 cps.

#### Time Decoder

Elapsed time is extracted from the flight tape by an Astrodata Model 6220 time decoder. Parallel 27 bit binary time words are carried with the digitized data. Slow serial code binary coded decimal (BCD) time appears on all strip chart information. The high accuracy 1000 cps carrier of the time code is used for servo speed control of the tape reproducer.

## FM Discriminators

Twenty NBFM subcarriers are demodulated simultaneously using Astrodata Model 404 discriminators. All data channels are time correlated within one millisecond, including the effects of recording oscillators and ground equipment. The capability to maintain precise time correlation is used in combining several measurements for the gust calculations. Data output filters in the discriminators are of the linear phase type. The minimum cutoff frequency is 22 cps (175 cps at eight-to-one playback). Attenuation beyond the cutoff frequency is 36 db per octave. Tape flutter effects are corrected electronically in the FM discriminators.

## Analog Computer

An EAI Model TR-48 analog computer is used to correct for transducer frequency response characteristics. This computer consists of 32 operational amplifiers, 20 integrators, three multipliers, two function generators, 40 potentiometers, two comparators, and an x-y plotter. Computer outputs are compatible with FM discriminator outputs for simultaneous digitizing.

## Analog-to-Digital Converter

A Beckman Model 210 analog-to-digital converter simultaneously samples 20 measurements and converts them to digital equivalents at rates up to 24,000 conversions per second. Simultaneous sampling is required to maintain time correlation of the data. The output of the converter is 10 binary bits plus sign for a conversion accuracy of  $\pm 0.1$  percent.

The optimum sampling rate for the analog to digital conversion can be selected. This ensures that the measurement is adequately described without burdening the digital computer with unnecessary data samples.

## Digital Computer

A CDC 3200 is used to format the output of the Beckman 210 data converter. The computer operates on 24-bit binary words and contains 16,000 words of memory. The peripheral equipment consists of four Model 607 tape units that operate at 150 inches per second and write tapes at a bit density of either 556 bits per inch or 800 bits per inch; a card reader that reads 1200 cards per minute; a 500 line per minute printer; and a digital incremental plotter capable of providing a fully annotated plot in two minutes.

## DATA PLAYBACK

Digitizer and strip chart formats are presented in Table III-1. Format number one is used for processing of all data. In the event data go off scale, these data are reprocessed using Format two (coarse measurement). Format number 3 is used for periodic data checks in the form of a strip chart. All NBFM variables are digitized at a rate of 100 samples/second. Details of the NBFM ground station are given in Figure III-1.

## Data Flow

Data processing is initiated when the data tapes are received. The block diagram in Figure III-2 represents the data processing sequence.

TABLE III-1

DIGITIZER AND STRIP CHART FORMATS

FORMAT 1				FORMAT 2				FORMAT 3			
POS. DIG.	MEAS.	TK	BD	DIG. POS.	MEAS.	TK	BD	DIG. POS.	MEAS.	TK	BD
1	$\phi$	9	5	1	$\phi$	9	5	1	Probe Temp. 1	9	3
2	$\psi$	7	5	2	$\psi$	7	5	2	Probe Temp. 2	7	3
3	$\theta$	5	5	3	$\theta$	5	5	3	Probe Temp. 3	5	3
4	OAT	11	5	4	OAT	11	5	4	Rt. Ail. Pos.	5	4
5	$\delta$	9	6	5	$\delta$	9	6	5	Lt. Ail. Pos.	7	4
6	$T_G$	5	6	6	$T_G$	5	6	6	Lt. Elev. Pos.	9	4
7	$q_I$ fine	11	6	7	$q_I$ coarse	11	7	7	Rud. Pos.	7	6
8	H	9	7	8	H	9	7	8			
9	$\Delta P_\beta$ fine	5	7	9	$\Delta P_\beta$ coarse	5	8	9			
10	$\Delta P_\alpha$ fine	7	7	10	$\Delta P_\alpha$ coarse	7	8	10			
11	$P_S$	11	8	11	$P_S$	11	8	11			
12	h	9	8	12	h	9	8	12			
13	$\dot{\phi}$	5	9	13	$\dot{\phi}$	5	9	13			
14	$\dot{\theta}$	7	9	14	$\dot{\theta}$	7	9	14	$n_y$ cg	11	9
15	V	9	9	15	V	9	9	15			
16	$\dot{\psi}$	9	10	16	$\dot{\psi}$	9	10	16			
17	$n_z$	5	10	17	$n_z$	5	10	17	$n_z$ cg	11	10
18				18				18			
19	$n_x$	9	11	20	$n_x$	7	11	19	Flutter	11	11
20	$n_y$	9	11	20	$n_y$	9	11	20			



# Contrails

The turbulence samples are automatically identified to eliminate the tedious and time consuming manual editing of the flight tape. The specific data to be processed from a particular flight are selected prior to the playback of the flight tape through the ground station.

Block No. 1 of Figure III-2 represents standardization cycle corrections. Standardization cycles to correct for any zero or sensitivity drift during flight are taken at preflight and repeated before each data sample is recorded. Prior to processing recorded data, an automatic correction command signal activates the discriminator servos to correct for zero drift, whether the changes occurred in the airborne or the ground station equipment. Changes in sensitivity are corrected mathematically.

In Block No. 2 the analog computer is scaled so that the voltage representation of the individual parameters does not exceed the voltage range or frequency limitations of the computing and recording equipment. For maximum accuracy, the signal voltages on the analog computer representing the variables and their derivatives are as large as possible without causing the equipment to overload.

The ground station demodulates the airborne recorded frequency-modulated carrier signals into individual measurements in Block No. 3. Each measurement is a continuous time history form of data used in calculating either a meteorological parameter or one of the turbulence (i.e., gust velocity) components.

In Block No. 4 compensation for the probe frequency response characteristics, determined during the dynamic calibration of the probe, is made. The explicit function chosen is the mirror image of the undesirable portion of the frequency response. This assures an output response equal to unity.

For a probe measurement with a frequency response characteristic as shown in Figure III-3 a transfer function was used having the general form:

$$\frac{\text{Output}}{\text{Input}} (\omega) = \frac{b}{a} \left[ \frac{(j\omega/a\omega_0) + 1}{(j\omega/b\omega_0) + 1} \right] \quad (\text{III-1})$$

with a corresponding phase relationship of:

$$\psi (\omega) = \tan^{-1} (\omega/a\omega_0) - \tan^{-1} (\omega/b\omega_0) \quad (\text{III-2})$$

where a and b are constants selected to regulate the width of the compensation response and  $\omega_0$  is the break frequency in radians per second. For a "lead" type compensation a = 1 and b < 1 whereas for a "lag" type compensation a < 1 and b = 1.

In Block No. 5 the data are converted from analog to digital form at the rate of 100 samples per second and stored on magnetic tape. This sampling rate results in a Nyquist frequency,  $f_N$ , of 50 cps. The highest frequency up to which appreciable power can exist without causing aliasing is



found from the relationship:

$$f_{\max} = 2f_N - f_i \quad (\text{III-3})$$

With  $f_N = 50$  cps and  $f_i = 10$  cps the maximum frequency content allowable is 90 cps. Use of the ground station analog filter, which attenuates all frequencies above 22 cps with a roll-off of 36 db per octave, precludes any possibility of aliasing in the frequency range of interest, viz., zero to ten cps. The surveys associated with each data sample are digitized separately for computation of atmospheric properties.

Computer programs are used in the order and combination indicated in Figures III-4 and III-5. Control information and constants are input by the individual programs. The various computer programs are discussed in the following paragraphs

## COMPUTER PROGRAMS

### Program 1

The digital data obtained from Block 5 are converted to engineering units in Program 1 (Block 6). After these data are converted to engineering units they are stored on tape for input to the proper computer programs of Block No. 7.

Although not part of Program 1, the three angular attitude measurements are filtered by employing a low-pass Ormsby filter weight function discussed under Program 3. Also, pressure altitude and outside air temperature are smoothed using the equation:

$$\tilde{X}_q = \frac{1}{q} \sum_{i=1}^q X_i, \quad q \leq 100, \quad (\text{III-4})$$

$$\tilde{X}_q = \frac{1}{100} \sum_{i=q-99}^q X_i, \quad q > 100, \quad (\text{III-5})$$

where  $q$  is the data sample index

## Program 2

This program calculates the three-dimensional orthogonal gust velocity time history components relative to the direction of the initial flight path and determines the environmental meteorological parameters.

Gust velocities are calculated using the following general equation:

$$-\begin{pmatrix} u \\ v \\ w \end{pmatrix} = [R] [V] - ([R] [V])_{\substack{t=0 \\ \psi=0}} - g \int_0^t [R] \begin{pmatrix} n_x \\ n_y \\ n_z \end{pmatrix} dt + \begin{pmatrix} 0 \\ 0 \\ g \int_0^t dt \end{pmatrix} \quad (\text{III-6})$$

The rotation matrix used to translate the measurements from the airplane reference axes to the earth reference axes is:

$$[R] = \begin{bmatrix} -\cos \psi \cos \theta & \sin \psi \cos \phi & \sin \psi \sin \phi \\ \sin \psi \cos \theta & -\cos \psi \sin \theta \sin \phi & +\cos \psi \sin \theta \cos \phi \\ \sin \theta & \cos \psi \cos \phi & \cos \psi \sin \phi \\ & +\sin \psi \sin \theta \sin \phi & -\sin \psi \sin \theta \cos \phi \\ & -\sin \phi \cos \theta & \cos \phi \cos \theta \end{bmatrix} \quad (\text{III-7})$$

The matrix of true airspeed components corrected for pitch and yaw is:

$$[V] = \begin{pmatrix} V_T \cos \beta \cos \alpha \\ V_T \sin \beta + 1 \dot{\psi} / 57.296 \\ -V_T \sin \alpha + 1 \dot{\theta} / 57.296 \end{pmatrix} \quad (\text{III-8})$$

The method used for numerical integration is Simpson's rule, in conjunction with Simpson's half-rule to maintain the original sampling interval.

$$\left. \begin{aligned} \int_{i-2}^{i-1} x dt &= \frac{\Delta t}{12} \left[ 5x_{i-2} + 8x_{i-1} - x_i \right] \\ \int_{i-2}^i x dt &= \frac{\Delta t}{3} \left[ x_{i-2} + 4x_{i-1} + x_i \right] \end{aligned} \right\} \quad (\text{III-9})$$

True airspeed is calculated using the following equations:

$$V_T = 109.6 \left\{ \frac{T_I \left[ \left( \frac{q_c}{P_s} + 1 \right)^{2/7} - 1 \right]}{K_a - K_t + K_t \left( \frac{q_c}{P_s} + 1 \right)^{2/7}} \right\}^{1/2} \quad \text{(III-10)}$$

where:

$$T_I = OAT + 459.688 \quad \text{(III-11)}$$

$$q_c = q_I + \Delta P_s \quad \text{(III-12)}$$

$$P_s = P_{s_I} - \Delta P_s \quad \text{(III-13)}$$

The angles of pitch, yaw, and roll ( $\theta$ ,  $\psi$ , and  $\phi$  respectively) are determined either from direct measurement or from associated rate measurements ( $\dot{\theta}$ ,  $\dot{\psi}$ , and  $\dot{\phi}$ ) using the trapezoidal integration rule. Angles of attack and sideslip are calculated using the following:

$$\alpha = A + B \frac{\Delta P_\alpha}{q_c} + C M + D \frac{\Delta P_\beta}{q_c} + E \frac{\Delta P_\alpha}{q_c} M + F \frac{\Delta P_\alpha}{q_c} \frac{\Delta P_\beta}{q_c} \quad \text{(III-14)}$$

$$+ G M \frac{\Delta P_\beta}{q_c} + H \left( \frac{\Delta P_\alpha}{q_c} \right)^2 + J M^2 + K \left( \frac{\Delta P_\beta}{q_c} \right)^2$$

$$\beta = A' + B' \frac{\Delta P_\beta}{q_c} + C' M + D' \frac{\Delta P_\alpha}{q_c} + E' \frac{\Delta P_\beta}{q_c} M + F' \frac{\Delta P_\beta}{q_c} \frac{\Delta P_\alpha}{q_c} \quad \text{(III-15)}$$

$$+ G' M \frac{\Delta P_\alpha}{q_c} + H' \left( \frac{\Delta P_\beta}{q_c} \right)^2 + J' M^2 + K' \left( \frac{\Delta P_\alpha}{q_c} \right)^2$$

Basic information, which consists of the maximum and its time of occurrence, the minimum and its time of occurrence, the arithmetic mean, the standard deviation, and the rms are listed for each of the three gust components, ground speed, and true airspeed.

The meteorological parameters are determined from the two surveys and the data sample. The surveys define the vertical gradient parameters and the first five seconds and the last five seconds of the data sample determine the horizontal gradient parameters. Winds are defined as positive

# Contrails

from the north and east. Heading and drift angle are analyzed to determine the wind quadrant:

Quadrant

I	$0^\circ < (h + \delta) < 90^\circ$
II	$270^\circ < (h + \delta) < 360^\circ$
III	$180^\circ < (h + \delta) < 270^\circ$
IV	$90^\circ < (h + \delta) < 180^\circ$
If $(h + \delta) < 0^\circ$ add $360^\circ$	

Magnetic heading is corrected to true heading:

$$h = h_m + \Delta h \quad \text{(III-16)}$$

where ,  $\Delta h$  is magnetic variation

North and east wind components are calculated by:

Quadrant I:  $W_{N_I} = -G_S \sin(90 - h - \delta) + V_T \sin(90 - h) \quad \text{(III-17)}$

$$W_{E_I} = -G_S \cos(90 - h - \delta) + V_T \cos(90 - h) \quad \text{(III-18)}$$

Quadrant II:  $W_{N_{II}} = -G_S \sin(h + \delta - 270) + V_T \sin(h - 270) \quad \text{(III-19)}$

$$W_{E_{II}} = G_S \cos(h + \delta - 270) - V_T \cos(h - 270) \quad \text{(III-20)}$$

Quadrant III:  $W_{N_{III}} = G_S \sin(270 - h - \delta) - V_T \sin(270 - h) \quad \text{(III-21)}$

$$W_{E_{III}} = G_S \cos(270 - h - \delta) - V_T \cos(270 - h) \quad \text{(III-22)}$$

Quadrant IV:  $W_{N_{IV}} = G_S \sin(h + \delta - 90) - V_T \sin(h - 90) \quad \text{(III-23)}$

$$W_{E_{IV}} = -G_S \cos(h + \delta - 90) + V_T \cos(h - 90) \quad \text{(III-24)}$$

Average north and east wind components are calculated by:

$$\bar{W}_N = \frac{1}{N} \sum_{i=1}^N W_{N_i} \quad \text{(III-25)}$$

$$\bar{W}_E = \frac{1}{N} \sum_{i=1}^N W_{E_i} \quad \text{(III-26)}$$

Average winds are calculated:

$$\bar{W} = [(\bar{W}_N)^2 + (\bar{W}_E)^2]^{1/2} \quad \text{(III-27)}$$

If heading data is unavailable:

$$\bar{W} = [V_T^2 + G_S^2 - 2V_T G_S \cos \delta]^{1/2} \quad \text{(III-28)}$$

Wind direction is determined as follows:

$$0^\circ < \tan^{-1} \left| \frac{\bar{W}_N}{\bar{W}_E} \right| < 90^\circ$$

# Contrails

When:  $\bar{W}_N > 0$  and  $\bar{W}_E > 0$ :

$$W_D = 90^\circ - \tan^{-1} \left| \frac{\bar{W}_N}{\bar{W}_E} \right| \quad (\text{III-29})$$

When:  $\bar{W}_N < 0$  and  $\bar{W}_E > 0$ :

$$W_D = 90^\circ + \tan^{-1} \left| \frac{\bar{W}_N}{\bar{W}_E} \right| \quad (\text{III-30})$$

When:  $\bar{W}_N < 0$  and  $\bar{W}_E < 0$ :

$$W_D = 270^\circ - \tan^{-1} \left| \frac{\bar{W}_N}{\bar{W}_E} \right| \quad (\text{III-31})$$

When:  $\bar{W}_N > 0$  and  $\bar{W}_E < 0$ :

$$W_D = 270^\circ + \tan^{-1} \left| \frac{\bar{W}_N}{\bar{W}_E} \right| \quad (\text{III-32})$$

The flight path referenced wind angle is calculated using the following equation:

If:  $|V_T \cos \bar{\delta}| \leq G_s$

$$WA = [ \sin^{-1} (V_T \sin \bar{\delta}) / \bar{W} ] \quad (\text{III-33})$$

If:  $|V_T \cos \bar{\delta}| > G_s$  and  $\bar{\delta}$  is positive

$$WA = 180 - [ \sin^{-1} (V_T \sin \bar{\delta}) / \bar{W} ] \quad (\text{III-34})$$

If:  $|V_T \cos \bar{\delta}| > G_s$  and  $\bar{\delta}$  is negative

$$WA = -180 - [ \sin^{-1} (V_T \sin \bar{\delta}) / \bar{W} ] \quad (\text{III-35})$$

Vertical temperature gradient is calculated:

$$\frac{\Delta T}{\Delta H} = \frac{\bar{T}_1 - \bar{T}_{10}}{\bar{H}_{10} - \bar{H}_1} \quad (\text{III-36})$$

Either the radar or pressure altitude measurement is used in the determination of H, depending on terrain roughness. Subscripts 1 and 10 refer to survey samples obtained at 100 feet and 1000 feet respectively.

Vertical wind gradients are calculated:

$$\frac{\Delta W_{Ez}}{\Delta H} = \frac{\bar{W}_{E1} - \bar{W}_{E10}}{\bar{H}_{10} - \bar{H}_1} \quad (\text{III-37})$$

$$\frac{\Delta W_{Nz}}{\Delta H} = \frac{\bar{W}_{N1} - \bar{W}_{N10}}{\bar{H}_{10} - \bar{H}_1} \quad (\text{III-38})$$

$$\frac{\Delta W_z}{\Delta H} = \left[ \left( \frac{\Delta W_{Ez}}{\Delta H} \right)^2 + \left( \frac{\Delta W_{Nz}}{\Delta H} \right)^2 \right]^{1/2} \quad (\text{III-39})$$

$$\frac{\Delta W_{Dz}}{\Delta H} = [ W_{D1} - W_{D10} ] / \Delta H \quad (\text{III-40})$$

# Contrails

Richardson number is calculated:

$$R = \left( \frac{g}{T_a} \right) \frac{(\Gamma_d - \frac{\Delta T}{\Delta H})}{(\Delta W / \Delta H)^2} \quad (\text{III-41})$$

Where dry adiabatic lapse rate:

$$\Gamma_d = .0055^\circ \text{F} / \text{ft}$$

Air stability ( $\Delta T_s$ ) and the stability ratio B, are determined by the following equations:

$$\Delta T_s = -1000 (\Delta T / \Delta H) \quad (\text{III-42})$$

$$B = \frac{g}{T_a} \left( \frac{H}{W} \right)^2 \left( \Gamma_d - \frac{\Delta T}{\Delta H} \right) \quad (\text{III-43})$$

The atmospheric stability category is then determined as follows:

$$-\Delta T_s < 2^\circ \text{F} / 1000 \text{ ft. Very Stable}$$

$$2^\circ \text{F} / 1000 \text{ ft.} \leq -\Delta T_s < 5^\circ \text{F} / 1000 \text{ ft. Stable}$$

$$5^\circ \text{F} / 1000 \text{ ft.} \leq -\Delta T_s < 6^\circ \text{F} / 1000 \text{ ft. Neutral}$$

$$-\Delta T_s \geq 6^\circ \text{F} / 1000 \text{ ft. Unstable}$$

The horizontal pressure gradient is computed, considering differences in terrain and absolute altitudes between the beginning and end of the data sample.

$$H_c = \frac{1 - (P_s / 29.9213) \cdot 1902546}{.6875 (10)^{-5}} \quad (\text{III-44})$$

$$S = G_s \left( \frac{270}{5280} \right) \quad (\text{III-45})$$

$$\Delta P_H = \frac{29.9213}{S} \left\{ \left[ 1 - .6875 (10)^{-5} H_{c3} \right]^{5.256115} - \left[ 1 - .6875 (10)^{-5} (H_{c2} + \Delta H_{32}) \right]^{5.256115} \right\} \quad (\text{III-46})$$

where the subscripts 2 and 3 refer to the starting and ending 5 seconds of the data sample respectively.

$$\Delta H_{32} = (H_{t3} - H_{t2}) + R_{A3} - R_{A2} \quad (\text{III-47})$$

$\Delta H_{32}$  represents the difference between airplane MSL altitude at the start of the data sample and at the end of the data sample.



# Contrails

The horizontal temperature gradient is calculated:

$$\Delta T_H = \frac{T_{a3} + \Delta H_{32} \Gamma - T_{a2}}{S} \quad (\text{III-48})$$

Where:

$$\Gamma = .00356 \text{ }^\circ\text{F} / \text{ft}$$

The horizontal wind north and east component gradients are calculated:

$$\frac{\Delta W_{EH}}{S} = \frac{\bar{W}_{E3} - \bar{W}_{E2}}{S} \quad (\text{III-49})$$

$$\frac{\Delta W_{NH}}{S} = \frac{\bar{W}_{N3} - \bar{W}_{N2}}{S} \quad (\text{III-50})$$

The horizontal wind velocity gradients are calculated:

$$\frac{\Delta W_H}{S} = \left[ \left( \frac{\Delta W_{EH}}{S} \right)^2 + \left( \frac{\Delta W_{NH}}{S} \right)^2 \right]^{1/2} \quad (\text{III-51})$$

The horizontal wind directional gradients are calculated:

$$\frac{\Delta W_{DH}}{S} = \frac{W_{D3} - W_{D2}}{S} \quad (\text{III-52})$$

Ambient temperature and static pressure are averaged for each sample. In addition, the average air density ( $\bar{\rho}$ ) and average air viscosity ( $\bar{\mu}$ ) are computed:

$$\bar{\rho} = .041187 \left( \frac{\bar{P}_a}{\bar{T}_a} \right) \quad (\text{III-53})$$

$$\bar{\mu} = .317 (10)^{-10} (\bar{T}_a)^{3/2} \left( \frac{734.7}{\bar{T}_a + 216} \right) \quad (\text{III-54})$$

The surface temperature measurement is corrected for emissivity, averaged over the data sample and categorized with the meteorological data.

Meteorological data are listed in tabular form and punched in IBM cards for later use. The cards are used to put data on the combined tapes and for input to the statistical correlation and distribution program.

Two special listings are available. They are:

- The calculated means for  $\psi$ ,  $\theta$ ,  $\phi$ ,  $n_x$ ,  $n_y$ , and  $n_z$  listed on-line and
- All tagged data listed on-line (The tagged data listing consists of the measurement name, type of tag, and the time at which the tag occurred.)

## Program 3

### Digital Filtering

Drift is removed from computed gust velocities by employing a digital filter to attenuate amplitudes at frequencies below 0.046 cps. An explanation of the theory, application and ensuing errors of the digital filter used during this program follows.

### Filter Design

The filtering process consists of smoothing the original data with a low frequency curve which has been low-pass filtered above 0.046 cps. The low frequency smoothed curve is then subtracted from the original data to yield final gust velocities that are high-pass filtered below 0.046 cps and have a zero mean. A simple method to illustrate this high-pass filter effect is to take:

$$\tilde{x}(t) = x(t) - x^*(t) \quad (\text{III-55})$$

as the sampled filter output where  $x(t)$  is the sampled input to a low-pass filter and  $x^*(t)$  is the output of the low-pass filter.

The linear smoothing operation for continuous time data by means of the weighting function  $h(\tau)$  with finite time limits  $T_L$  and  $T_U$  is given as:

$$x^*(t) = \int_{T_L}^{T_U} h(\tau) x(t - \tau) d\tau \quad (\text{III-56})$$

The linear smoothing operation for discrete data at equi-spaced intervals  $\Delta t$  can be given as:

$$x_t^* = \sum_{n=-N}^N h_n x_{(t+n\Delta t)} \quad (\text{III-57})$$

where  $h_n$  are the  $2N + 1$  filter weights,  $x_{(t+n\Delta t)}$  are the input data samples and  $x_t^*$  are the output data samples.

# Contrails

An ideal low-pass filter, by definition, is one that passes all frequencies  $f \leq |f_c|$  without change and deletes all frequencies  $f > |f_c|$ . This filter is shown in Figure III-6.

The corresponding weight function is:

$$h(t) = \int_{-f_c}^{f_c} H(f) e^{j2\pi ft} df \quad (III-58)$$

$$= \frac{\sin 2\pi f_c t}{\pi t} \quad (III-59)$$

where:  $j = \sqrt{-1}$

The ideal filter is not physically realizable because of the jump discontinuities at  $f = \pm f_c$ . If the truncated Fourier series of  $H(f)$  is used to approximate  $H(f)$ , then, due to the Gibbs phenomenon, large oscillations persist in the neighborhood of  $\pm f_c$ . Furthermore, the amplitude of these oscillations remains constant with increasing  $N$ .

A more practical approach is to design a filter such that  $H(f)$  is non-zero on some interval  $(f_c, f_c + \Delta f)$  where  $\Delta f > 0$ . Any unwanted frequencies which appear in the interval are passed (though somewhat attenuated) by the approximating filter. One filter of this type was presented by Ormsby (Reference III-1) and is shown in Figure III-7.

The transfer function of this filter is:

$$H(f) = \begin{cases} 1 & |f| \leq f_c \\ 0 & |f| > (f_c + \Delta f) \\ \frac{f + f_c + \Delta f}{\Delta f} & -(f_c + \Delta f) \leq f < -f_c \\ \frac{f_c + \Delta f - f}{\Delta f} & f_c < f < f_c + \Delta f \end{cases} \quad (III-60)$$

# Contrails

H(f) has a linear roll-off between  $\pm f_c$  and  $\pm(f_c + \Delta f)$ . The time domain function is obtained by taking the Fourier transform of H(f):

$$h(t) = \int_{-\infty}^{\infty} H(f) e^{j2\pi f t} df \quad (\text{III-61})$$

$$= \frac{\sin \pi \Delta f t \sin \pi (2f_c + \Delta f) t}{\pi^2 \Delta f t^2} \quad (\text{III-62})$$

and applying a well-known trigonometric identity to get:

$$h(t) = \frac{\cos 2\pi f_c t - \cos 2\pi (f_c + \Delta f) t}{2\Delta f (\pi t)^2} \quad (\text{III-63})$$

The discrete case is given as:

$$h_n = \frac{\cos 2\pi n \Delta t f_c - \cos 2\pi n \Delta t (f_c + \Delta f)}{2\Delta f (\Delta t \pi n)^2} \quad (\text{III-64})$$

where:  $n = \pm 1, \pm 2, \dots, \pm N$

$$\text{and } h_{n=0} = \frac{2f_c + \Delta f}{f_s} \quad (\text{III-65})$$

where  $f_s$  is the sampling rate ( $f_s = 1/\Delta t$ ).

Certain trends given as general polynomial time forms and considered as desirable data components require constraints on the basic weights in order to pass without error. If a time function does contain a polynomial content, it is not band-limited and should be constrained so that the sampled values of the polynomial content are passed without error. Therefore, to prevent trend type errors, constraints must be applied to the weighting function to satisfy:

$$\begin{aligned} \frac{d^k H(f)}{df^k} &= 0 \quad \left| \quad f = 0 \quad \text{for } k \geq 1 \right. \\ &= 1 \quad \left| \quad f = 0 \quad \text{for } k = 0 \right. \end{aligned} \quad (\text{III-66})$$

For  $k = 0$ , as is the case for our filter, this is accomplished by modifying the  $h_n$  weights so that:

$$\sum_{n=-N}^N h_n = 1 \quad (\text{III-67})$$

The simplest way to satisfy Equation III-65 is to use the new weights:

$$\bar{h}_n = h_n + \frac{1 - \sum_{n=-N}^N h_n}{2N+1} \quad (\text{III-68})$$

which forces the transfer function to have unity gain at zero frequency.

A filter was developed independently by Martin and Graham which is shown in Figure III-8 (Reference III-2 through III-4).

The transfer function of this filter is:

$$H(f) = \begin{cases} 1 & |f| \leq f_c \\ 0 & |f| \geq (f_c + \Delta f) \\ \frac{1}{2} \left[ 1 + \cos \pi \left( \frac{f-f_c}{\Delta f} \right) \right] & f_c < f < (f_c + \Delta f) \\ \frac{1}{2} \left[ 1 + \cos \pi \left( \frac{f+f_c}{\Delta f} \right) \right] & -(f_c + \Delta f) < f < -f_c \end{cases} \quad (\text{III-69})$$

The Fourier transform of H(f) is:

$$h(t) = \frac{\cos(\pi \Delta f t) \sin \pi (2f_c + \Delta f) t}{\pi t (1 - 4 \Delta f^2 t^2)} \quad (\text{III-70})$$

which after applying a trigonometric identity and simplifying gives:

$$h(t) = \frac{\sin 2\pi f_c t + \sin 2\pi (f_c + \Delta f) t}{2\pi t (1 - 4 \Delta f^2 t^2)} \quad (\text{III-71})$$

The discrete form for this filter is given as:

$$h_n = \frac{1}{2\pi n \Delta t} \left( \frac{\sin 2\pi (f_c + \Delta f) n \Delta t + \sin 2\pi f_c n \Delta t}{1 - 4(\Delta f n \Delta t)^2} \right) \quad (\text{III-72})$$

where  $n = \pm 1, \pm 2, \dots, \pm N$ , and  $h_{n=0} = \frac{2f_c + \Delta f}{f_s}$  (III-73)

Constraints are applied to these filter weights in the identical manner as for the Ormsby filter. For both the Ormsby and Martin-Graham filters,  $h_n = h_n$ , so that only values of  $h_n$  for  $n = 1, 2, \dots, N$  need be calculated.

Comparison of the Ormsby and Martin-Graham filters reveals better performance using the latter filter for small values of  $N$ , because of less effect due to Gibbs' phenomenon. Another factor favoring the Martin-Graham is its relative steepness, that is, the filter rolls off slowly at  $f_c$ , very rapidly at  $1/2(2f_c \pm \Delta f)$  and slowly at  $f_c + \Delta f$ . This is evidenced in Figure III-9.

## Filter Application

To apply digital filtering to a set of data, the data values are first obtained by taking equally spaced samples of the function. Experimentation with gust data indicated low frequency drift error to be, as a general rule, in the frequency range 0 to  $1/T$  cps, where  $T$  was the total length of time, 270 seconds, of the turbulence sample. This was usually  $< 0.04$  cps, the lowest frequency of interest present in the data.

Next, practical values for  $f_c, \Delta f$ , and  $N$  were determined. The value for  $N$  was limited by the amount of computer storage available and a reasonable computation time. Too small a  $\Delta f$  or too small a value of  $N$  will cause excessive "overshoot" at the filter corner frequencies. In extreme cases, this overshoot will carry through a wide range of the spectrum.

The sampling frequency,  $f_s = 1/\Delta t$ , must be greater than twice the highest significant frequency present in the data to prevent aliasing. However, too large a value of  $f_s$  will reduce the time width of the filter weighting function since  $T_{filt} = N \Delta t = N/f_s$ . The only remedy is to increase  $N$ , which is usually impractical, or to decrease  $f_s$  (increase  $\Delta t$ ). The sampling frequency is decreased by pre-filtering the data through a preliminary low-pass filter that has:

$$f_{c_1} \geq f_{c_2}$$

and

$$f_{c_2} + \Delta f \leq f_{s_2}$$

Where:

$f_{c_1}$  = cut-off frequency of the preliminary low-pass filter

$f_{c_2}$  = cut-off frequency of the final low-pass filter

$\Delta f_1$  = the preliminary filter roll-off, and

$f_{s_2}$  = sampling frequency of the data to the final low-pass filter



# Contrails

The requirements of this initial filter were that the frequencies to be passed by the final low-pass filter remain unchanged and that the gain of the filter transfer function be zero at  $f_{s_2} \pm (f_{c_2} + \Delta f_2)$ . See Figure III-10. The zero gain requirement is necessary so that there will be not be significant frequencies present above the Nyquist (folding) frequency.

$$f_{N_2} = \frac{1}{2\Delta t_2} = \frac{f_{s_2}}{2} \quad (\text{III-74})$$

If the zero gain requirement is not observed and by virtue of  $\Delta t_2$  the spectrum is limited to  $f_{N_2}$ , such that  $f_{N_2} < f_m$ , aliasing will be present in the spectrum a distance  $f_m - f_{N_2}$  below the Nyquist frequency. Should this folded distance extend beyond zero the aliased spectrum will re-fold again at zero frequency. This successive folding at  $f_{N_2}$  and zero frequency will continue until  $f_m$  is reached. An example of this aliasing is shown in Figure III-11 where  $f_m > f_N$ .

Hence, referring again to Figure III-10, if the preliminary filter gain is zero in the neighborhood of  $2f_{N_2} = f_{s_2}$  no aliases will occur in the interval  $(0, f_{c_1} + \Delta f_2)$  and no aliasing error will be introduced by changing  $\Delta t$ . Aliases that occur at frequencies in the output of the preliminary filter greater than  $f_{c_2} + \Delta f_2$  are of no concern since they will be filtered out by the final low-pass filter.

The discrete expression for the double filter is:

$$x_t^* = \sum_{n_2=-N_2}^{N_2} h_{n_2} \sum_{n_1=-N_1}^{N_1} h_{n_1} x_{(t+n_1\Delta t_1+n_2\Delta t_2)} \quad (\text{III-75})$$

Filtered high-pass data at sampling frequency  $f_{s_1}$  are obtained by interpolating between samples of the low-pass data series with sampling frequency  $f_{s_2}$  and subtracting from the original data series with sampling frequency  $f_{s_1}$ . Recall that  $f_{s_2} < f_{s_1}$ , consequently, to keep interpolation errors to a minimum,  $f_{s_2}$  is chosen large enough to reconstruct the highest frequency passed by the low-pass filter. Refer to Figure III-12 for an example of the various steps.

The following guidelines may be used to determine  $f_s$ ,  $\Delta f$ , and  $N$ , given  $f_c$ , for a resultant overshoot  $\leq 1$  percent and an interpolation error  $\leq 1$  percent.

- $f_s \geq 20 (f_c + \Delta f)$  to reconstruct the highest frequency passed
- $\Delta f \geq 0.015 f_s$
- $N \geq \frac{1.05 f_s}{\Delta f}$

Empirical error bounds for the Ormsby and Martin-Graham filters in terms of  $N$ ,  $\Delta f$ , and  $\Delta t$  are given as follows:

- Ormsby  $\epsilon = \frac{0.012}{N \Delta f \Delta t} \quad (\text{III-76})$

● Martin-Graham 
$$\epsilon = \frac{1}{5\pi} \ln \frac{4N^2 (\Delta f \Delta t)^2}{4N^2 (\Delta f \Delta t)^2 - 1} \quad (\text{III-77})$$

The filter constants chosen for the Low Level Critical Air Turbulence Program and the associated errors are summarized in Table III-2.

TABLE III-2

FILTER CONSTANTS

Filter Constant	CALCULATED GUST VELOCITIES		ATTITUDE ANGLES
	Prelim. Filter "O"	Final Filter "M-G"	Low Pass Filter "O"
$f_c$	0.2	0.01	4.0
$\Delta f$	1.66	0.036	5.0
$f_s$	100	2	100
$\Delta t$	0.01	0.5	0.01
$N$	50	70	20
$\epsilon$	1.45%	1.09%	1.2%

The frequency content of the final output (high-pass) data was attenuated no more than 3 db at the lowest frequency of interest, which for calculated gust velocities is 0.04 cps. It was necessary to use a preliminary filter in order to decrease the value of N and keep computation time to a minimum.

Many values of  $f_c$ ,  $N$ ,  $f_s$  and  $\Delta f$  were tried until a reasonably optimum combination was selected. A comparison of the constants chosen for this program to those established by the three guidelines is presented in Table III-3. Two exceptions noted in the table are:

- The preliminary filter violated the third guideline, i.e., ( $N = 50$ )  $< 63$ . This was not critical since the error associated with  $N = 50$  fell outside the region of interest, namely  $f > f_{c2} + \Delta f_2 = 0.046$  cps.
- The filter for attitudes violated the first guideline, i.e., ( $f_s = 100$ )  $< 180$ . This violation was not critical because, first, interpolation was not required and, second, the filter has a relatively "slow" roll-off.

Plots of the calculated gust velocity final low-pass filter transfer function and associated time function are shown in Figures III-13 and III-14 respectively. The expression for the constrained Martin-Graham transfer function of Figure III-13 is given by:

$$\overline{H_N}(f) = \sum_{n=-N}^N \overline{h_n} \cos(2\pi f n \Delta t) \quad \text{(III-78)}$$

TABLE III-3

FILTER GUIDELINES

Guideline	CALCULATED GUST VELOCITIES		ATTITUDE ANGLES
	Prelim. Filter	Final Filter	Low Pass Filter
$f_s \geq 20(f_c + \Delta f)$	37.2 (100)	1 (2)	180 (100)
$\Delta f \geq 0.015 f_s$	1.5 (1.66)	.03 (.036)	1.5 (5.0)
$N \geq 1.05 f_s / \Delta f$	63 (50)	64 (70)	21 (20)

Note: Values in parenthesis are actual values of  $f_s$ ,  $\Delta f$  and  $N$  used for LO-LOCAT program

Data Extension

When data are filtered,  $N$  values are lost from the beginning and end of the time series because of the required non-circular sums of the lagged products required by equation III-57. Several schemes may be used to extend the data so that the output time history length equals the input time history length:

- One scheme, shown in Figure III-15 is to put  $N$  values on the beginning and end of the original time series, each value equal to the first and last values of the data, respectively.
- A second scheme is to fold the first and last  $N$  values of the time series about the first and last data samples, respectively, as shown in Figure III-16.
- A third scheme is to fold and invert the first and last  $N$  values about the first and last data samples, respectively, as shown in Figure III-17.

The choice of scheme to use is dependent upon the predominant data trend of the original data series, particularly in the first and last  $N$  values. The low frequency drift in the majority of turbulence samples is approximately linear. Therefore, for the Low Level Critical Air Turbulence Program, the folding and inverting technique is used so that minimum error is introduced, and then only in the extreme one-third end of the extension.

## Program 4

The frequency analysis program calculates power spectral densities, cross-spectral densities, and correlation functions. The raw estimate of the power spectral density is defined as the periodogram given by:

$$\Phi(n) = 2N\Delta t [A(n) \tilde{A}(n)] \quad \text{for } n = 0, 1, 2, \dots, N \quad (\text{III-79})$$

where  $A(n)$  is the complex finite Fourier transform of  $x(i)$  defined as:

$$A(n) = \frac{1}{N} \sum_{i=0}^{N-1} x(i) e^{-j2\pi ni/N} \quad (\text{III-80})$$

and  $j = \sqrt{-1}$ . The tilde denotes the complex conjugate. The Fourier transform is calculated using the computationally efficient and accurate Cooley-Tukey fast Fourier transform algorithm.

The spectral estimate is derived by splitting  $x(i)$  into a number of segments taking modified periodograms (distorted by the  $(\sin x)/x$  spectral window) of these segments, and finally averaging these modified periodograms to obtain the estimate of  $\Phi(f)$ . These averaged estimates are further refined according to the formula:

$$\Phi'(n) = .25 \Phi(n-1) + .5 \Phi(n) + .25 \Phi(n+1) \quad (\text{III-81})$$

If  $A_x(n)$  and  $A_y(n)$  are the finite Fourier transforms of  $x(i)$  any  $y(i)$ , respectively, the cross periodogram is given by:

$$\Phi_{xy}(n) = 2N\Delta t [A_x(n) \tilde{A}_y(n)] \quad (\text{III-82})$$

The real part is the cospectrum and the imaginary part is the quadrature spectrum. Modified cross periodograms are calculated for each pair of segments, averaged and smoothed to obtained refined estimates of  $\Phi_{xy}(n)$ .

The autocorrelation is defined as the real part of the inverse Fourier transform of the (real) periodogram:

$$R(i) = \sum_{n=0}^{N-1} \Phi(n) e^{2\pi inj/N} \quad (\text{III-83})$$

# Contrails

Cross correlations are obtained in a similar manner, except that this is a complex quantity, as is the cross spectrum:

$$R_{xy}(1) = \sum_{n=0}^{N-1} \Phi_{xy}(n) e^{2\pi i n j / N} \quad (\text{III-84})$$

All power spectral densities are normalized with respect to  $\sigma_t^2$ , given by

$$\sigma_t^2 = \frac{1}{N} \sum_{i=1}^N (x_i - \bar{x})^2 \quad (\text{III-85})$$

where:

$$\bar{x} = \frac{1}{27000} \sum_{i=1}^{27000} x_i \quad (\text{III-86})$$

All spectral estimates are computed for frequency intervals of 0.0416 cps converted to spatial frequency (cpf):

$$\Phi(k) = \Phi(f)(v) \quad (\text{III-87})$$

The coherency between lateral and longitudinal and between lateral and vertical gust velocity components is determined:

$$\gamma_{xy}^2(k) = \frac{[\Phi_{xy}(k)]^2}{\Phi_x(k) \Phi_y(k)} \quad (\text{III-88})$$

The characteristic frequency is calculated as:

$$N_0 = \frac{\sigma_1}{\sigma} \text{ c p f} \quad (\text{III-89})$$

# Contrails

Where:

$$\sigma = \left[ \int_{k_1}^{k_3} \Phi(k) dk \right]^{1/2} \quad (\text{III-90})$$

$$\sigma_1 = \left[ \int_{k_1}^{k_3} k^2 \Phi(k) dk \right]^{1/2} \quad (\text{III-91})$$

$$k_1 = 0.04 / (V)$$

$$k_3 = 10 / (V)$$

A truncated sigma,  $\sigma_T$ , in the inertial subrange is also calculated by means of Equation III-89 between the limits of .667 to 10 cps.

Mathematical expressions are calculated for each PSD for comparison to experimental data. The following equations are used:

von Karman -

$$L_{Kv} = .110 \left( \frac{\sigma_t}{\sigma_T} \right)_v^3 \left( \frac{1}{k_2^{2/3}} - \frac{1}{k_3^{2/3}} \right)^{3/2} \quad (\text{III-92})$$

$$L_{Ku} = .0717 \left( \frac{\sigma_t}{\sigma_T} \right)_u^3 \left( \frac{1}{k_2^{2/3}} - \frac{1}{k_3^{2/3}} \right)^{3/2} \quad (\text{III-93})$$

$$\left[ \frac{\Phi_v(k)}{\sigma_{t_v}^2} \right]_k = \frac{L_{Kv} [2 + 377.5 (L_{Kv} k)^2]}{[1 + 70.78 (L_{Kv} k)^2]^{11/6}} \quad (\text{III-94})$$

$$\left[ \frac{\Phi_u(k)}{\sigma_{t_u}^2} \right]_k = \frac{4 L_{Ku}}{[1 + 70.78 (L_{Ku} k)^2]^{5/6}} \quad (\text{III-95})$$



# Contrails

Dryden -

$$L_{Dv} = .152 \left( \frac{\sigma_t}{\sigma_T} \right)^2 \left( \frac{1}{k_2} - \frac{1}{k_3} \right) \quad (\text{III-96})$$

$$L_{Du} = .101 \left( \frac{\sigma_t}{\sigma_T} \right)^2 \left( \frac{1}{k_2} - \frac{1}{k_3} \right) \quad (\text{III-97})$$

$$\left[ \frac{\Phi_v(k)}{\sigma_{t_v}^2} \right]_D = \frac{L_{Dv} [2 + 6(2\pi L_{Dv} k)^2]}{[1 + (2\pi L_{Dv} k)^2]^2} \quad (\text{III-98})$$

$$\left[ \frac{\Phi_u(k)}{\sigma_{t_u}^2} \right]_D = \frac{4L_{Du}}{1 + (2\pi L_{Du} k)^2} \quad (\text{III-99})$$

where  $k_2 = .667/V$

Panofsky -

$$C = .172 \left( \frac{\sigma_t}{\sigma_T} \right)_u \left( \frac{1}{k_2^{2/3}} - \frac{1}{k_3^{2/3}} \right)^{1/2} \quad (\text{III-100})$$

$$\left[ \frac{\Phi_u(k)}{\sigma_{t_u}^2} \right]_P = \frac{11800}{C^2 [1 + (2950 k)^{5/3}]} \quad (\text{III-101})$$

Ratios of experimental to mathematical values are plotted against frequency.

The homogeneity of the individual gust components is determined by dividing the power spectrum of the middle third of each sample by the power spectrum of the entire sample. Isotropic characteristics are determined by dividing the unnormalized power spectra of the longitudinal and vertical gust components by the unnormalized power spectrum of the lateral gust component.

## Program 5

A peak count is performed for each turbulence sample, where a peak is defined as the greatest positive or negative excursion of the data between adjacent crossings of the mean. Peaks are counted in 40 bands of two fps. A cumulative probability distribution is calculated for each sample. The standard deviation of the peak count and characteristic frequency is calculated as follows:

$$\sigma_{pe} = \left[ \sum_{b=1}^N \frac{f_b(x_b)^2}{N_{pe}} \right]^{1/2} \quad (\text{III-102})$$

$$N_F = 19.55 \frac{N_{pe}}{V} \quad (\text{III-103})$$

All gust velocity components are amplitude counted for each sample. Amplitude count refers to the counting and accumulation of the number of data points falling between selected values. The values in this specific case are 40 bands of two fps, about the arithmetic mean. The cumulative probability distribution, between the limits of zero and one, versus gust velocity from zero to 60 feet/second, and the probability density are computed using classical techniques as found in Reference III-5.

The number of level crossings of  $x(t)$  at the value  $x(t) = \alpha$  is computed for  $\alpha = 0, \pm 2, \pm 4, \pm 6, \dots$ . The number of crossings per mile with a positive slope is given by:

$$N_{\alpha} = 19.55 \frac{E_{\alpha}}{V} \quad (\text{III-104})$$

where  $E_{\alpha}$  is the number of crossings of  $x(t)$  with positive slope of the level  $\alpha$ . The probability and probability density are calculated for these data.

Run tests considering mean-square as well as mean observations are determined for 100 periodic segments in each turbulence sample. A turbulence sample (27,000 data points) is segmented into 200 parts, each containing 135 data points. The mean and mean-square value for each odd numbered (1,3,5,...199) segment is calculated as follows:

$$O_n = \frac{1}{135} \sum_{i=a}^b x_i \quad (\text{III-105})$$

$$O'_n = \frac{1}{135} \sum_{i=a}^b x_i^2 \quad (\text{III-106})$$

where the limits  $a$  and  $b$  represent the beginning and ending data point number of the segment being considered, and are determined from:

# *Contrails*

$$a = 135n - 134 \quad \text{(III-107)}$$

$$b = 135n \quad \text{(III-108)}$$

where n is the segment number (1, 3, 5, ... 199)

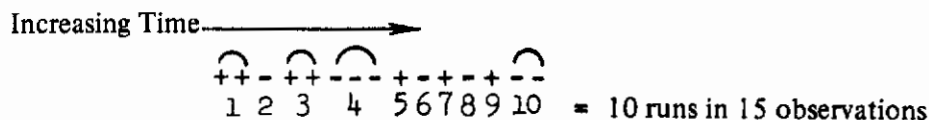
Each observation ( $O_n$  and  $O_n'$ ) is compared with a mean and given a sign: + when the observation is > the mean and - when the observation is < the mean. The means are defined as:

$$\bar{x} = \frac{1}{27000} \sum_{i=1}^{27000} x_i \quad \text{(III-109)}$$

$$\bar{x}^2 = \frac{1}{27000} \sum_{i=1}^{27000} x_i^2 \quad \text{(III-110)}$$

The number of runs is defined as the number of sets of like signs.

Example:



The number of runs and whether or not the sample was accepted as stationary at the 0.02 level of significance for both mean ( $O_n$ ) and mean-square ( $O_n'$ ) observations are determined.

The expected number of runs is found from the following:

$$\mu = \frac{2N_1N_2}{N_1 + N_2} + 1 \quad \text{(III-111)}$$

$$\sigma = \left[ \frac{2N_1N_2(2N_1N_2 - N_1 - N_2)}{(N_1 + N_2)^2(N_1 + N_2 - 1)} \right]^{1/2} \quad \text{(III-112)}$$

where:

$N_1$  = Total number of positive ( $O_n$  or  $O_n'$ )

$N_2$  = Total number of negative ( $O_n$  or  $O_n'$ )

Expected number of runs (E.N.O.R.) is found from:

$$\text{E.N.O.R.} = (\mu \pm 2.326\sigma) - 0.5 \quad (\text{III-113})$$

(2.326 corresponds to 0.02 level of significance)

If the actual number of runs falls between the two values of E.N.O.R., the stationarity hypothesis is accepted at the 0.02 level of significance.

In addition to listings of the peak and amplitude count distributions a master tape is created that accumulates distributions by category for later input to the statistical correlation and distribution program. A listing indicates the categories and number of samples per category on the master tape.

The control deck permits changing band definition and sample selection.

## Program 6

The program uses the rms gust velocities and selected meteorological parameters as input and calculates for each category and pooled category the following statistics:

- Cumulative distribution
- Cumulative probability distribution
- Probability density
- Arithmetic mean
- Root-mean-square
- Standard deviation
- Chi-square with associated level of significance
- Slope and y-intercept, using classical least squares techniques, of the linear relationship of the mid-class interval squared versus the  $\text{Log}_e$  of the probability density.
- The cumulative distributions for requested categories using the peak and amplitude count data accumulated on the master tape of Program 5

## Program 7

The Taylor microscale, Kolmogorov scale, and viscous dissipation rate were calculated as follows:

### Taylor Microscale

$$\lambda = 4.4309 \left[ \left( \frac{\mu}{\rho} \right) \cdot \left( \frac{L_{K_u}}{\sigma_{t_u}} \right) \right]^{1/2} \quad (\text{III-114})$$

### Kolmogorov Scale

$$\eta = \left( \frac{\nu^3}{\epsilon} \right)^{1/4} \quad (\text{III-115})$$

### Viscous Dissipation Rate

$$\epsilon = .761 \frac{\sigma_{t_u}^3}{L_{K_u}} \quad (\text{III-116})$$

MULTIPLE REGRESSION

The method used for multiple regression analysis is basically that of Reference III-6, which has been modified to process a greater number of independent variables. This digital computer method determines regression coefficients such that the sum of the squares of the dependent variable residuals (actual value minus regression estimate) is a minimum. The dependent variable, Y, is expressed as a linear function of a number of predictors X<sub>i</sub> (where i= 1, 2, 3, ...n) according to:

$$Y = A_0 + A_1 X_1 + A_2 X_2 + \dots + A_n X_n$$

where A<sub>i</sub> represents the regression coefficients.

If the input variables (designated Z<sub>i</sub>) are used directly as the X<sub>i</sub> in this equation, the result is a fairly simple linear expression. However, the power of this mathematical tool is greatly enhanced by the fact that each X<sub>i</sub> can be made an arbitrary linear or nonlinear function of any or all of the Z<sub>i</sub> variables. In some cases the functions to be tried for a particular X can be inferred from scatter diagrams. If this trend cannot be determined, the only recourse then is trial and error; this trial-and-error process, however, can be conducted in a very systematic manner. If, for instance, m number of functions of the input variables are put into "hold" positions as intermediate variables, an operation called "expand" will generate m(m+3)/2 independent variables. These independent variables consist of the original m functions, their squares, and all the combinations of cross products of the m functions taken two at a time. If, for instance, the m functions chosen are various powers (positive or negative, integers or fractions) of the input variables, the cross products yield a large range of exponents to be tested. The regression analysis program has been modified to handle values of m as high as 19, which generates 209 independent variables. The upper limit of m is determined by the computer's storage capability. The present limit was adopted so as not to jeopardize fast turnaround time on the computer.

The stepwise regression makes use of analysis of variance, Reference III-7, a statistical technique for resolving the total variability of a set of data into systematic and random components. It estimates the components of variance due to systematic and random causes, and leads to significance tests of these components. The most frequently used test of significance in regression analyses is the F-test based on the F-ratio. In the most general terms F is the ratio of two independent estimates of what on the null hypothesis is the same variance. Given a number of groups of data, the ratio of the two estimates of variance becomes the ratio of the mean square of group means to the mean square of individuals.

At each step of entry or removal the regression program calculates entry F-ratios for the variables not in the regression and removal F-ratios for the variables already in the regression. In this application the numerator of the F-ratio is the reduction in variations explainable by adding the variable, and the denominator is the residual variations between regression and the actual values after the variable is added. More explicitly,

$$F = \frac{\left[ \sum_{i=1}^N (\hat{Y}_i - \bar{Y})^2_{\text{Before}} - \sum_{i=1}^N (\hat{Y}_i - \bar{Y})^2_{\text{After}} \right] / \nu_1}{\sum_{i=1}^N (Y_i - \hat{Y}_i)^2 / \nu_2} \quad \text{(III-117)}$$



Where  $\hat{y}$  is the residual value, N is the number of input records and the subscripts "before" and "after" refer to the entry or removal of a regression variable. The degrees of freedom associated with the numerator and denominator respectively are  $\nu_1$  and  $\nu_2$ . In this case  $\nu_1$  equals 1, since only two groups are involved. (Therefore F in this instance is equivalent to  $t^2$ , where t is the statistic known as Student's t.) The degrees of freedom  $\nu_2$  equals  $N-Q-1$ , where Q is the number of independent variables in the regression equation after the entry or removal step.

If a variable has a high F-ratio of entry, it is highly correlated with variations in the dependent variable that are not explained by the other variables in the regression equation. If a variable has a low F-ratio of removal, the trends can be more adequately explained by the other variables of the equation. What is considered a high F-ratio depends on the level of significance desired. The level of significance is the risk of making the incorrect inference that an improvement in goodness of fit is significant when it is actually insignificant. As an example, the F-ratio corresponding to a level of significance of 0.05 (5 percent) is 3.84 for an infinite sample size. The F-ratios required to achieve a given significance level are relatively insensitive to the sample size until very low levels are demanded.

In applying the F-test for significance, the basic assumption is made that the variable under study is normally distributed. If the dependent-variable observations are normally distributed about the regression estimate, the F-ratio possesses an F-distribution, selected values of which (assuming that  $\nu_1=1$ ) are included in Table III-4 derived from Reference III-8. For a given data sample size the table shows what level of significance can be ascribed to an entry F-ratio for a particular variable.

The regression analysis program requires the specification of F-ratio criteria for entry and removal. The criterion for removal must be less than or equal to the criterion for entry. If, for example, an F-ratio of 2.71 is specified for both entry and removal, corresponding to a risk of 0.10, the following logic is used to select a variable for the next regression step:

1. Removal F-ratios are calculated for each variable in the regression equation.
2. The variable having the smallest F-ratio is removed from the equation if the F-ratio is less than 2.71. If this occurs, a regression step is printed and the removal F-ratios are recalculated and compared with 2.71 until no further removal instruction is obtained.

TABLE III-4. F-VALUES FOR  $\nu_2$  DEGREES OF FREEDOM

$\nu_2 = 20$	$\nu_2 = 30$	$\nu_2 = 40$	$\nu_2 = 60$	$\nu_2 = 120$	$\nu_2 = \infty$	Level of Significance (risk)	Confidence level (percent)
0.472	0.466	0.463	0.461	0.458	0.455	0.50	50
1.40	1.38	1.36	1.35	1.34	1.32	0.25	75
2.97	2.88	2.84	2.79	2.75	2.71	0.10	90
4.35	4.17	4.08	4.00	3.92	3.84	0.05	95
5.87	5.57	5.42	5.29	5.15	5.02	0.025	97.5
8.10	7.56	7.31	7.08	6.85	6.63	0.01	99
9.94	9.18	8.83	8.49	8.18	7.88	0.005	99.5
14.82	13.29	12.61	11.97	11.38	10.83	0.001	99.9
					12.12	0.0005	99.95
					15.14	0.0001	99.99
					19.51	$10^{-5}$	99.999
					23.93	$10^{-6}$	99.9999

3. Entry F-ratios are calculated for each variable not in the regression equation.
4. The variable having the greatest F-ratio is entered in the regression equation if the F-ratio is greater than 2.71. A regression step is printed and logic instructions 1 through 4 are repeated until no variables can be removed from or entered into the regression equation. When this occurs, the last regression step printed provides information concerning the final regression equation.

The regression analysis uses analysis of variance based on the F-distribution to assess the significance of possible variables. If a data sample is biased in any way, the F-ratio associated with a particular variable may not be an adequate criterion of its significance. For example, if turbulence avoidance techniques are practiced, a spurious inverse correlation of turbulence with airspeed will be noted. Therefore, reliance must not be placed entirely on the F-ratio criterion. Other criteria that have proved useful are:

- Reduction in the standard error of the estimate upon entry of the variable
- Increase in the multiple correlation coefficient upon entry of the variable
- Correlation coefficients between the dependent and independent variables
- Correlation coefficients between the entering variable and the other variables in the equation
- Sign and magnitude of the regression coefficients of the entering variable
- Changes in sign and magnitude of the regression coefficients of the variables already in the equation, as a result of the new variable
- The uncertainty in the accuracy of measurement of the variable
- Patterns of consistency between dependent variables and different data groups
- Known or assumed physical characteristics of the variable in question

Another measure of the significance of an independent variable is the contribution it makes to changes in the dependent variable. Given a regression equation as above, the contribution made by  $X_1$  to a possible change in  $Y$  is equal to the product of  $A_1$  and the possible range of values of  $X_1$ .

The standard error of the estimate is given by:

$$\sqrt{\frac{1}{N-Q-1} \sum_{i=1}^N (Y_i - \hat{Y}_i)^2} \quad (\text{III-118})$$

Correlation coefficients are obtained from the relationship:

$$\frac{\sum_{i=1}^N (X_i - \bar{X})(Y_i - \bar{Y})}{\sqrt{\sum_{i=1}^N (X_i - \bar{X})^2 \sum_{i=1}^N (Y_i - \bar{Y})^2}} \quad (\text{III-119})$$

These simple linear correlation coefficients are frequently of limited use in establishing that two variables are functionally related. Two variables may be strongly related, yet have a low correlation coefficient if the relationship is not linear.

If  $Y$  denotes the regression function of a random variable  $y$  with respect to  $X_i$ , the coefficient of multiple correlation between  $y$  and the  $X_i$  is defined as the coefficient of simple linear correlation between  $y$  and  $Y$ . Its value is equal to the ratio of their standard deviations, i.e.,  $\sigma_Y / \sigma_y$ . The coefficient of multiple correlation ranges from zero to +1. Its square equals the ratio of explained variance to total variance.

The normalized standard error  $E_i$  of a regression coefficient is the standard error divided by the value  $A_i$  of the coefficient. It can be applied to determine confidence intervals for the regression coefficients. For a given level of significance,  $\alpha$ , the  $(1-2\alpha)$  confidence limits for the true value of  $A_i$  are  $(1 \pm t_{\alpha} E_i) A_i$ , where  $T_{\alpha}$  (the upper or lower  $\alpha$  points) has a student's  $t$  distribution with  $\nu_2$  degrees of freedom. For an infinite sample size  $t$  has a standard normal distribution. The 90-percent confidence limits for a regression coefficient are lower limit  $(1 - 1.64 E_i) A_i$ , upper limit  $(1 + 1.64 E_i) A_i$ .

The conditions under which a regression equation may be used to estimate a functional relationship are determined from the way the equation is derived. The coefficients of the regression equation are those that minimize the sum-of-squares of deviations of observed values of the dependent variable from the values predicted by the regression. This assumes that errors need be considered only in the dependent variable—that is, the observed value of the dependent variable that deviates from the corresponding true value, and not the value of any other variable. If this is true, then the regression of the dependent variable on the independent variables is the best estimate of the underlying functional relationship. However, the regression of the dependent variable on the independent variables can be the best estimate of the functional relationship only if all values of the independent variables are determined without error and if the only variations that arise are unsystematic errors in measurement of the dependent variables. If this is not the case, the regression gives a biased estimate of the true relationship, the bias being dependent upon the errors of measurement of the independent variables and the ranges they span.

In practice, it is not necessary to insist too rigorously on the absence of errors in the measured values of the independent variables. If these errors are small compared with the ranges covered and with the errors in the dependent variable, the regression equation still gives a reasonable estimate of the functional relationship.

The fact that a trend is highly correlated is no guarantee that it is not biased. Since the regression information does not provide an indication of bias, all trends have been analyzed on the basis of the known or assumed physical characteristics of each independent variable. Independent variables

exhibiting unreasonable trends have been excluded from the final regression equations. The regression equations, although providing reasonable estimates, may contain bias and should be applied with caution.

Observed values of turbulence may be biased because of pilot technique, flight restrictions, or mission profiles. Bias is used here to mean an untrue trend caused by nonrandom sampling.

## Input Variables

The following variables are being used as inputs to the regression analysis for all phases of the program.

- Day of year
- Time of day
- Absolute altitude
- Richardson number
- Wind speed
- Vertical wind shear
- Horizontal wind shear
- Vertical wind direction gradient
- Horizontal wind direction gradient
- Lapse rate
- Horizontal temperature gradient
- Sine of solar elevation
- Time of day function
- Ground temperature
- Terrain rms
- Terrain wavelength
- Wind angle
- Vertical delta wind angle
- Horizontal delta wind angle
- Horizontal pressure gradient

In addition, the following variables are included in the Phase III analysis.

- 500 mb height
- 500 mb wind speed
- 500 mb temperature
- 700 mb height
- 700 mb wind speed
- 700 mb temperature
- 850 mb height
- 850 mb wind speed
- 850 mb temperature
- 850 mb dew point
- 250 feet wind direction
- 250 feet temperature
- 250 feet dew point
- 750 feet wind direction
- 750 feet wind speed
- 750 feet temperature
- 750 feet dew point
- 1000 feet wind direction
- 1000 feet wind speed
- 1000 feet temperature
- 1000 feet dew point
- Surface temperature
- Surface wind speed
- Cloud cover
- Showalter stability index
- Global Weather Center gust forecast
- Flight altitude temperature
- Flight altitude dew point
- Flight altitude wind speed
- 1000 feet above flight altitude temperature
- 1000 feet above flight altitude dew point
- 1000 feet above flight altitude wind direction
- 1000 feet above flight altitude wind speed



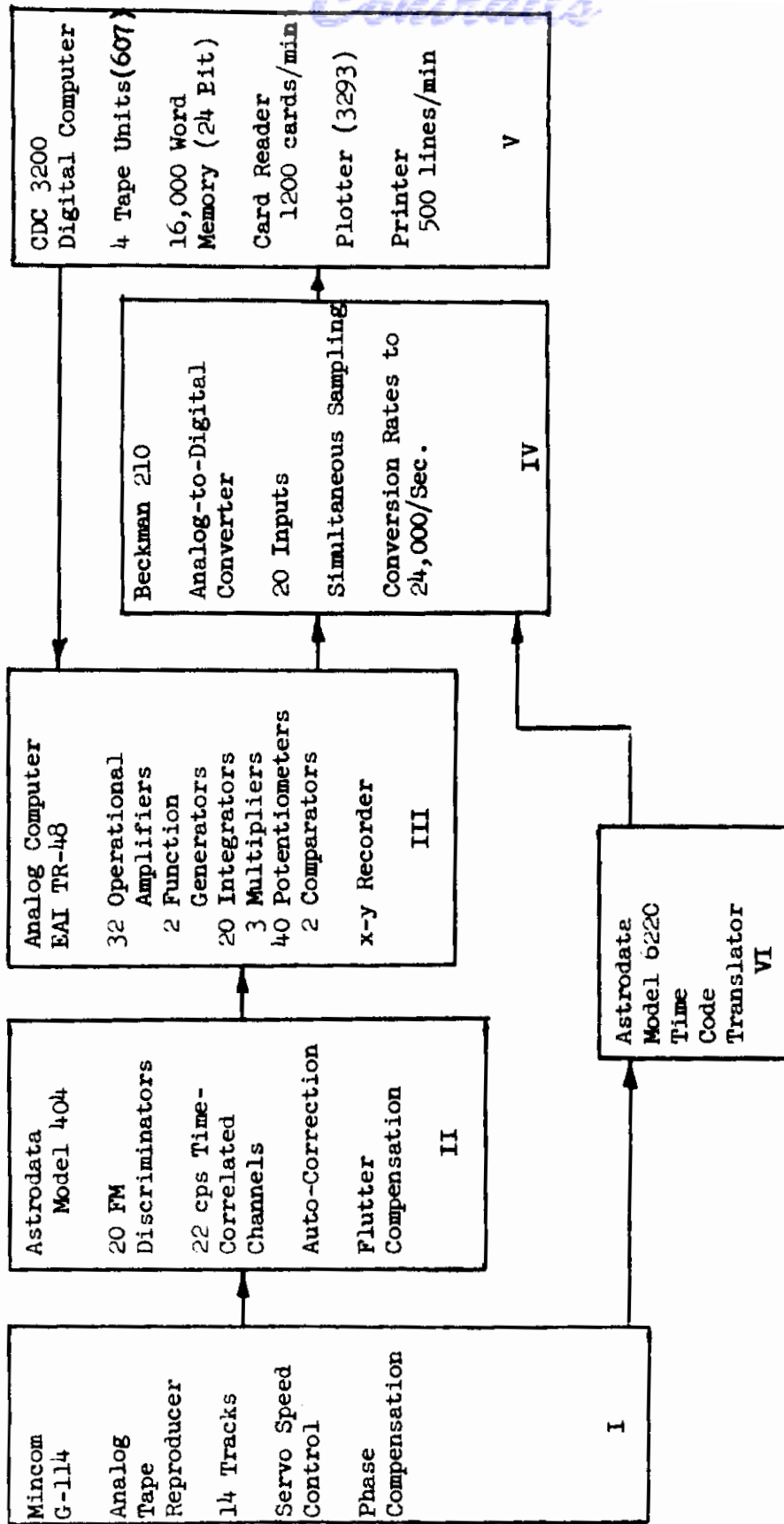


Figure III-1 Ground Station Equipment Diagram

*Continuals*

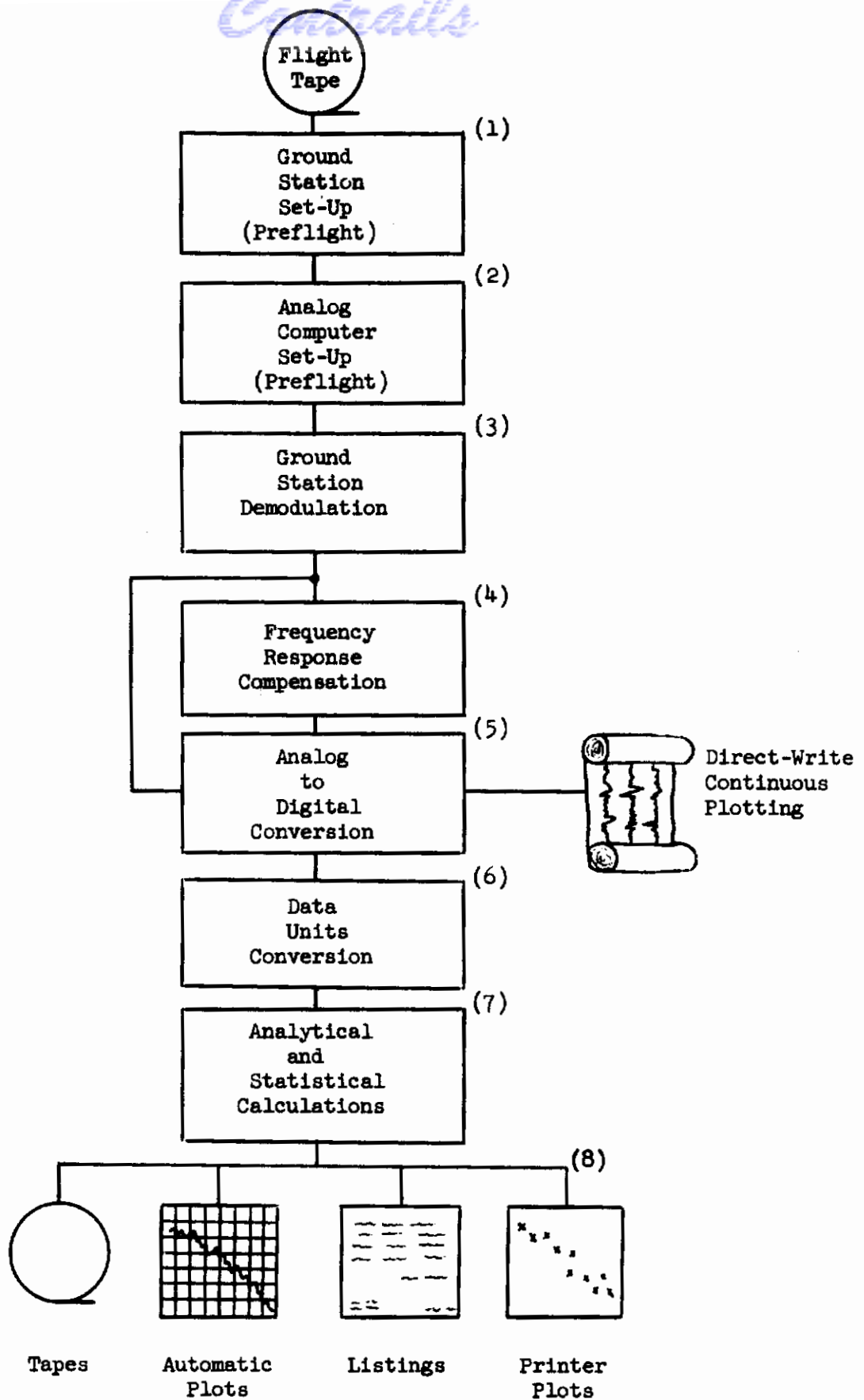


Figure III-2 Low Level Turbulence Data Processing Sequence



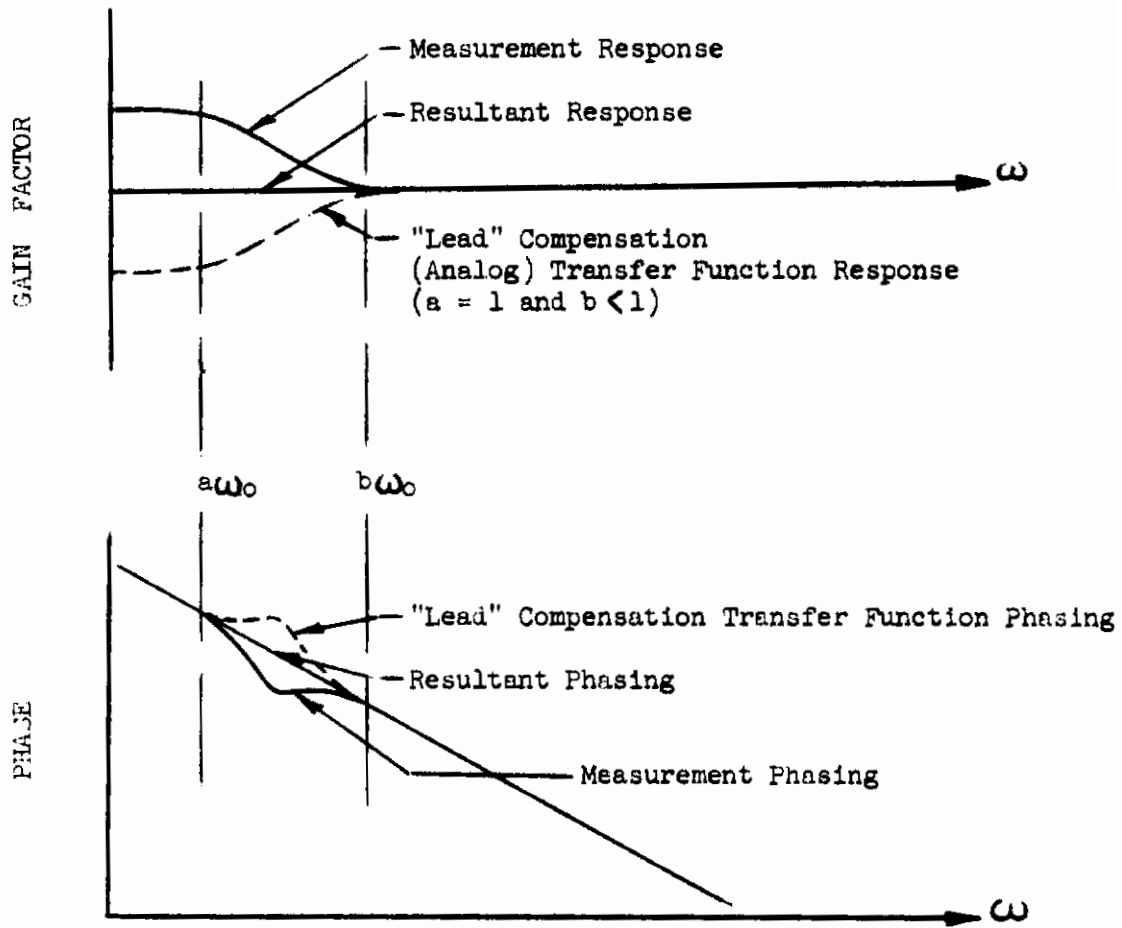


Figure III-3 Compensation

# Contrails

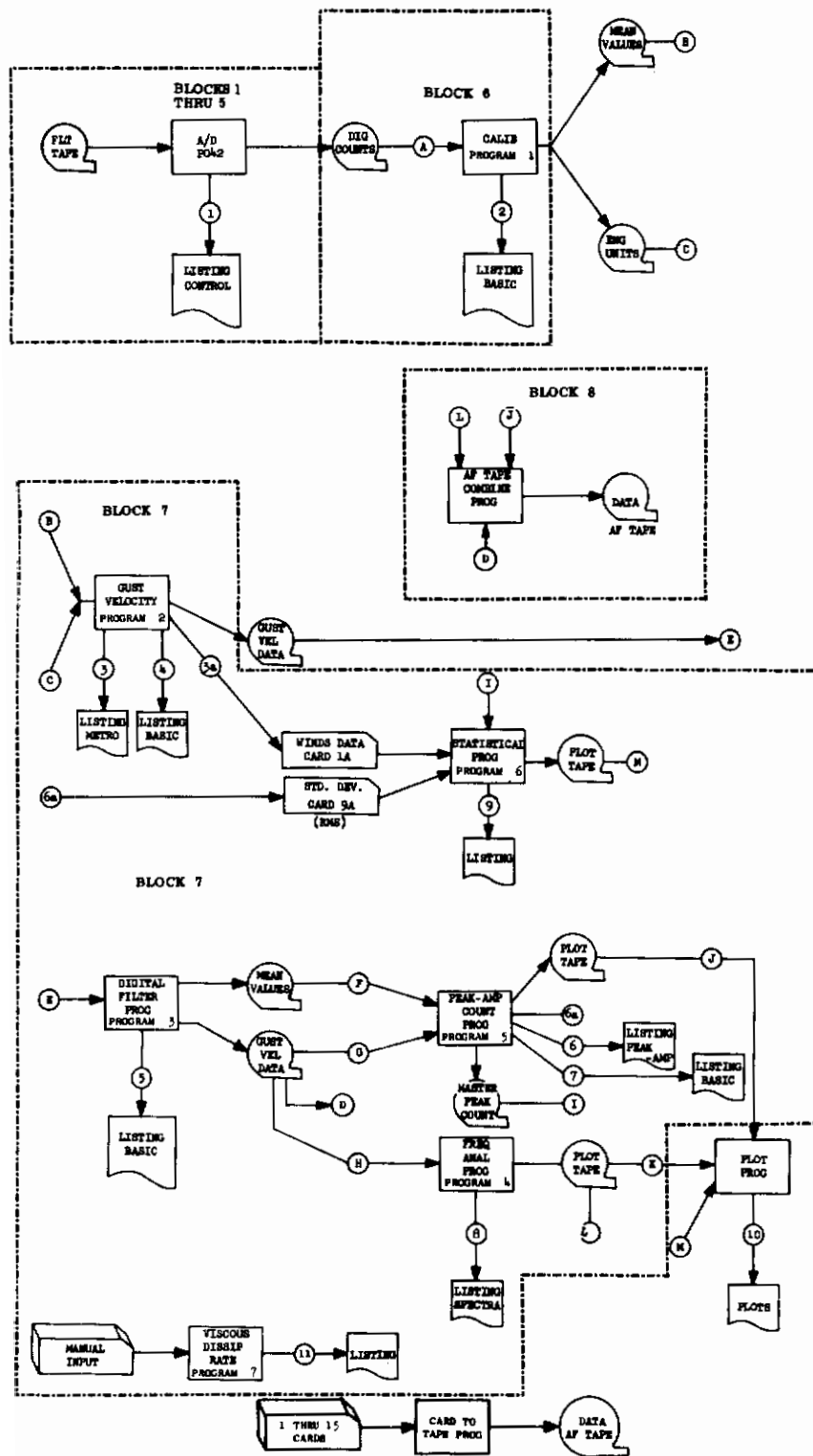


Figure III-4 Flow Diagram of Data Processing Steps

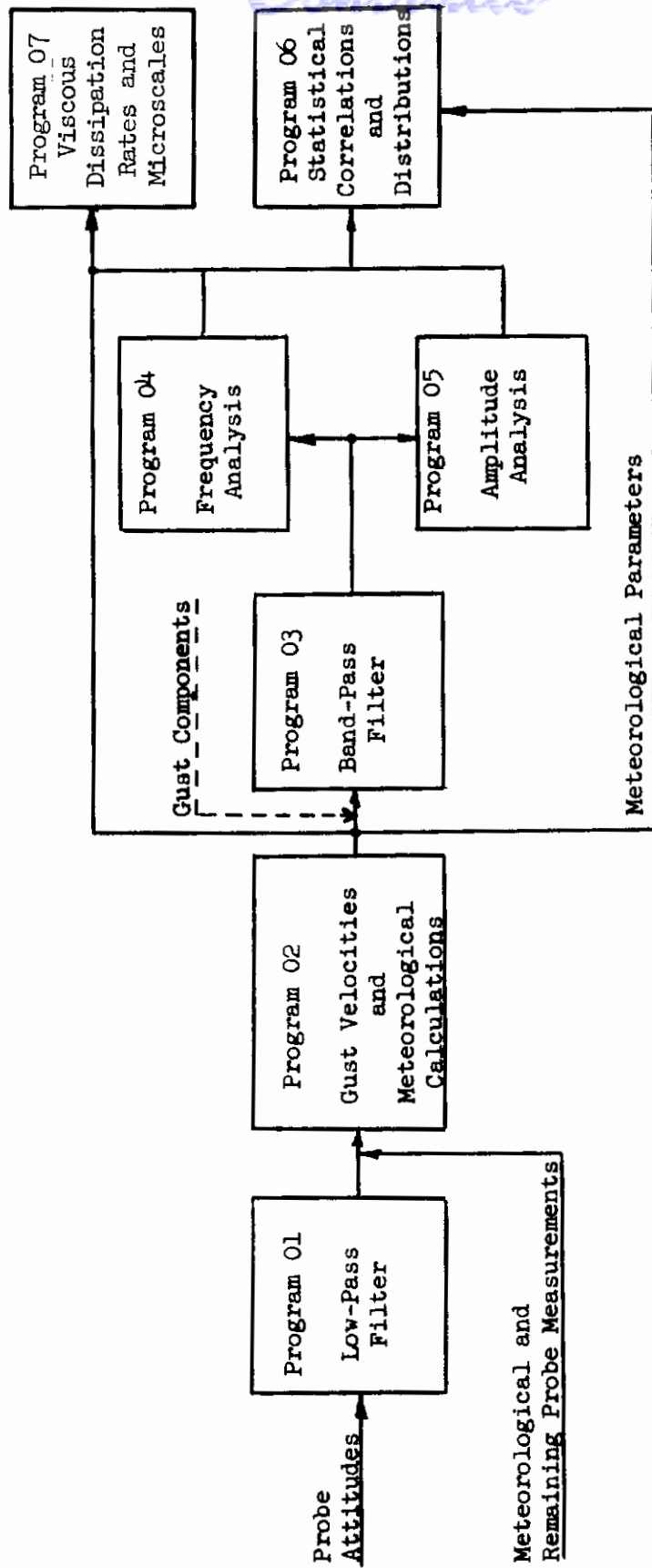


Figure III-5 Analytical and Statistical Calculations

# Contrails

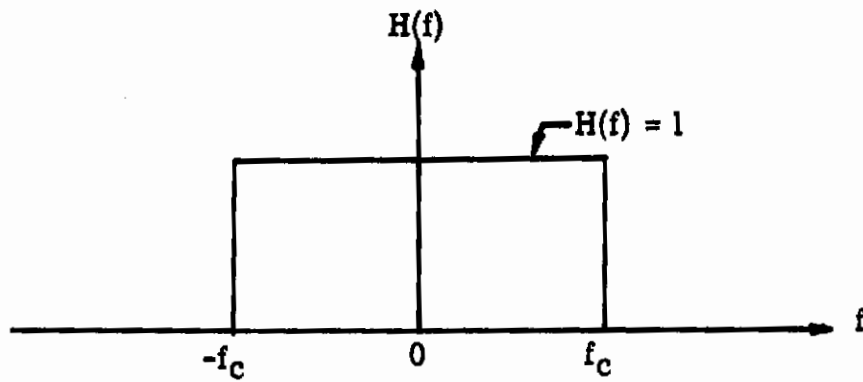


Figure III-6 Ideal Filter

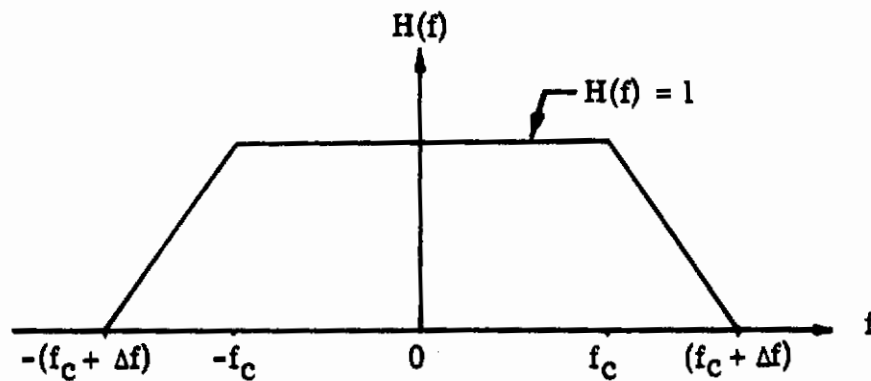


Figure III-7 Ormsby Filter

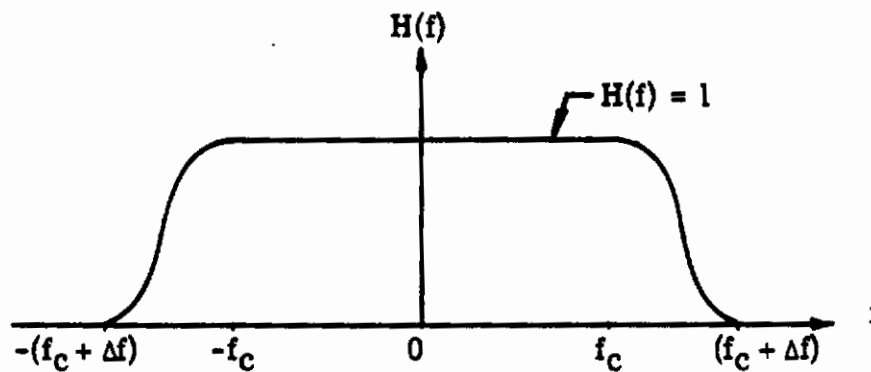


Figure III-8 Martin-Graham Filter

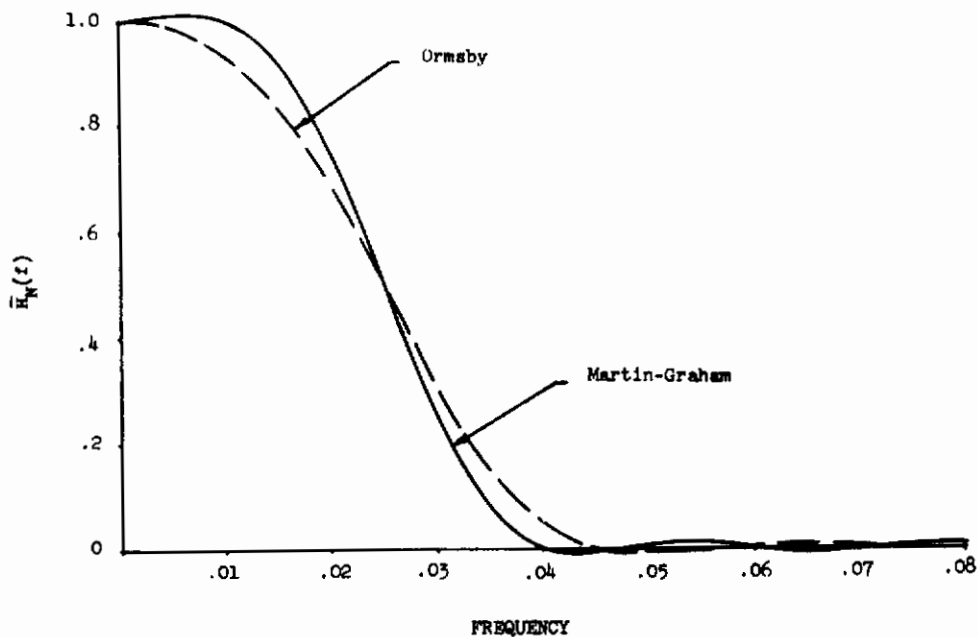


Figure III-9 Comparison of Ormsby and Martin-Graham Filters

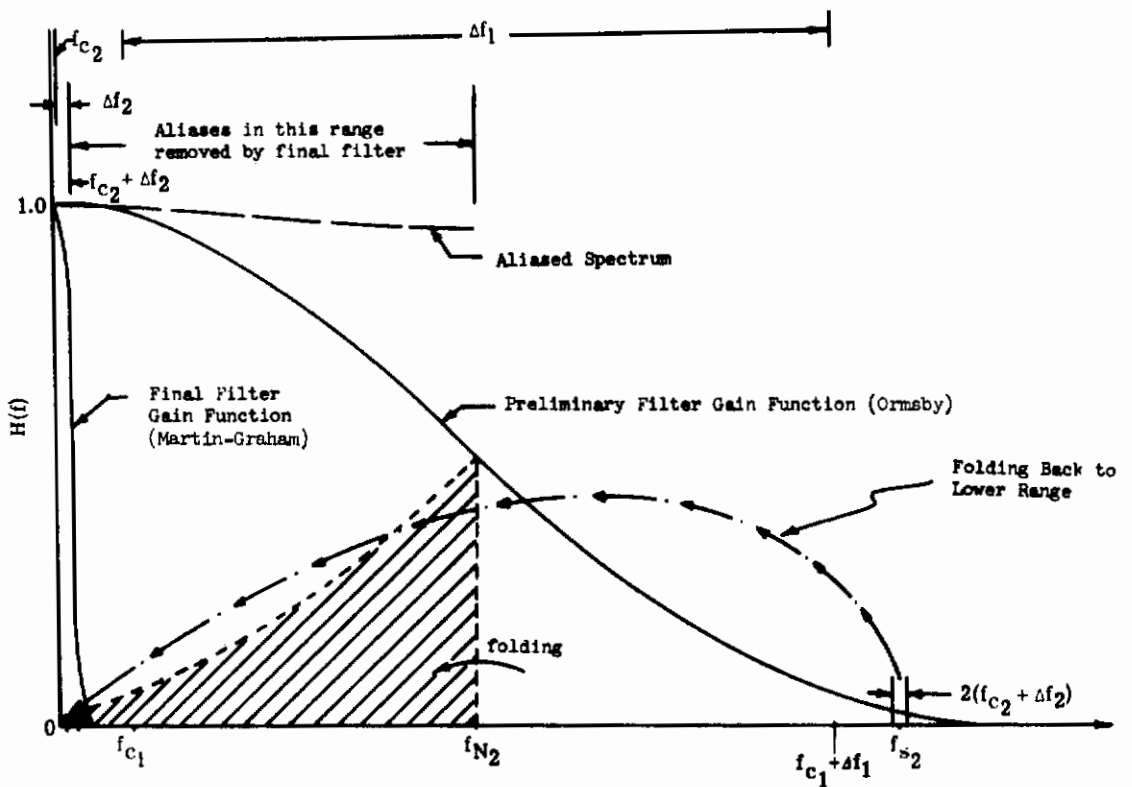


Figure III-10 Two Pass Filter

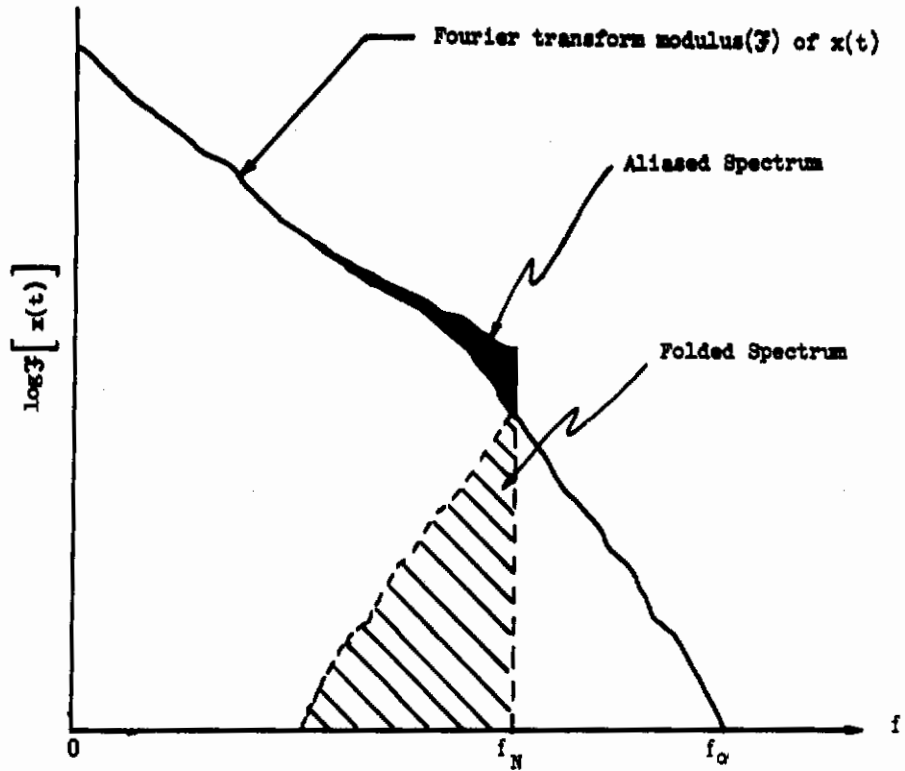


Figure III-11 Aliasing



Legend:

A - Unfiltered Computed Gust Velocity (100 samples per second)

B - 'A' After Low-pass Filtering (2 samples per second)

$f_c = 0.2$  cps

$f_t = 1.86$  cps

C - 'B' After Low-pass Filtering (2 samples per second)

$f_c = 0.01$  cps

$f_t = 0.046$  cps

D - Final Data, 'A' Minus 'C', Resulting in High Pass Filtered Computed Gust Velocity (100 samples per second)

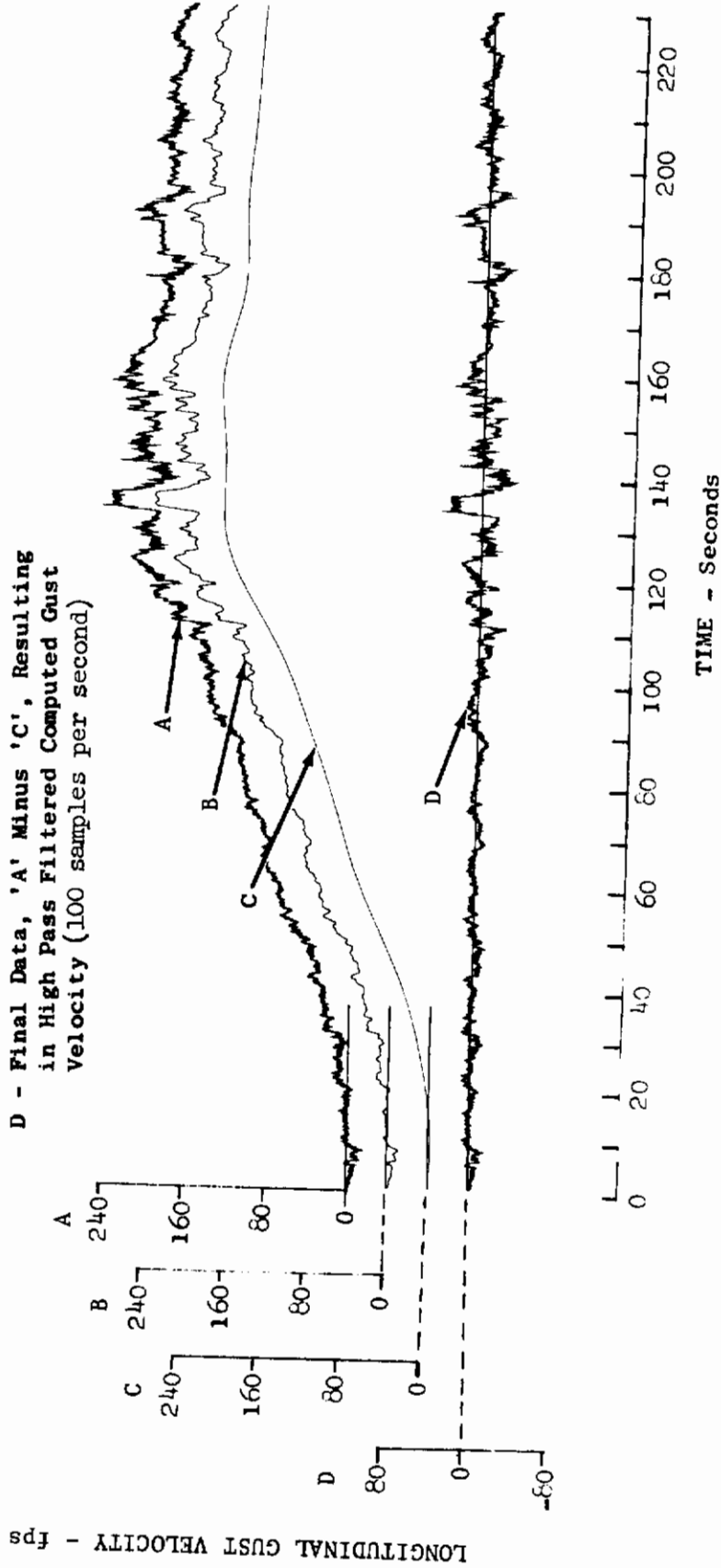


Figure III-12 Example of High Pass Filtering Sequence

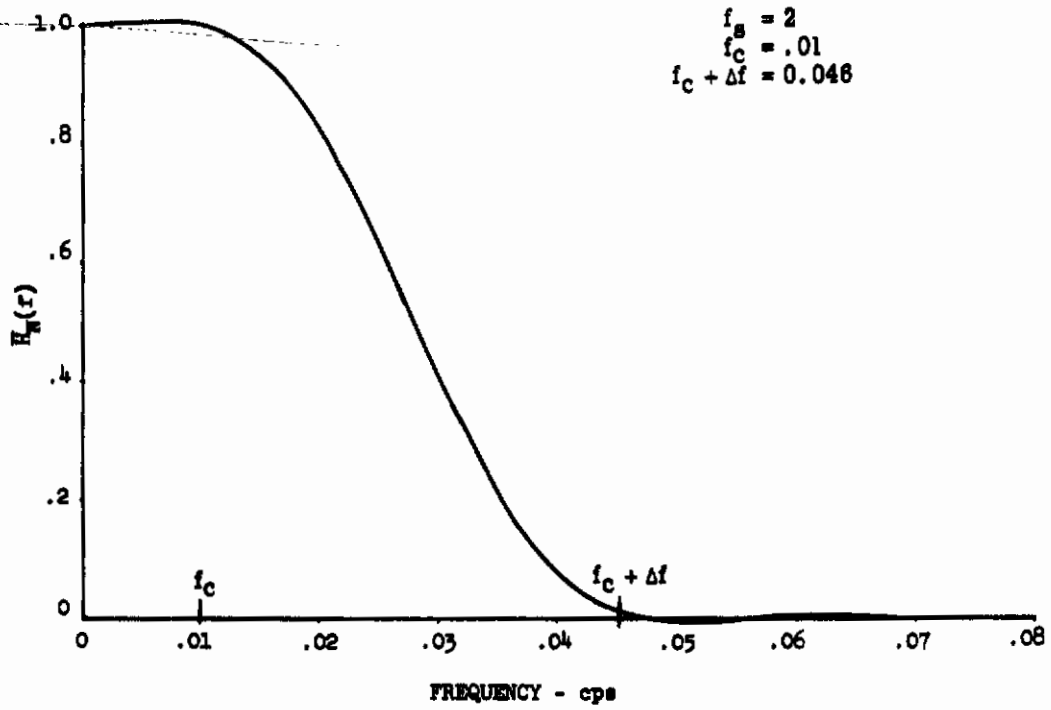


Figure III-13 Martin-Graham Transfer Function

# Contrails

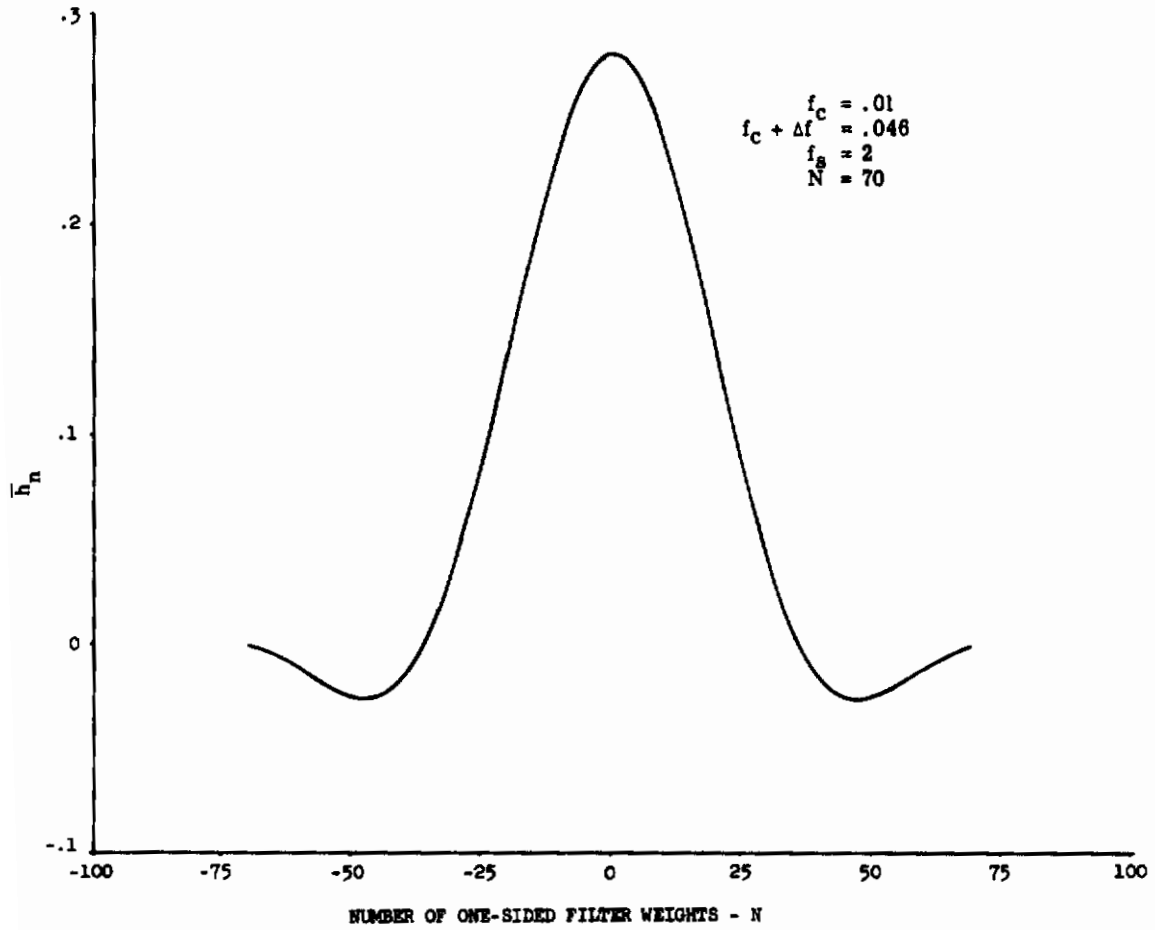


Figure III-14 Martin-Graham Time Function

# Contrails

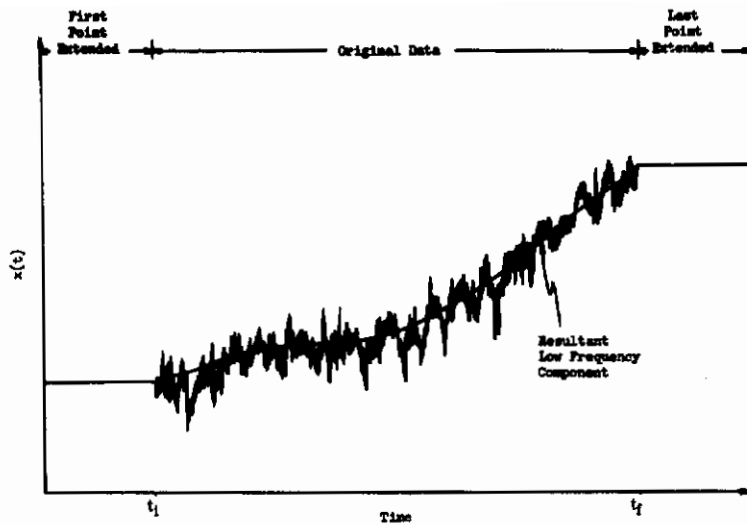


Figure III-15 Linear Extension

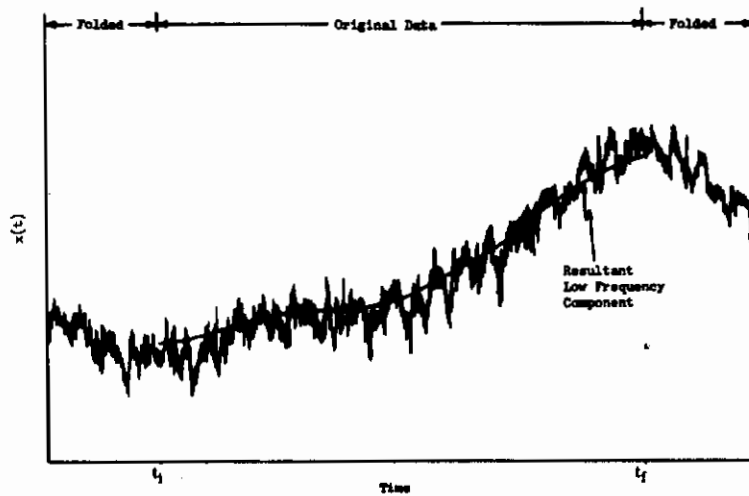


Figure III-16 Folded Extension

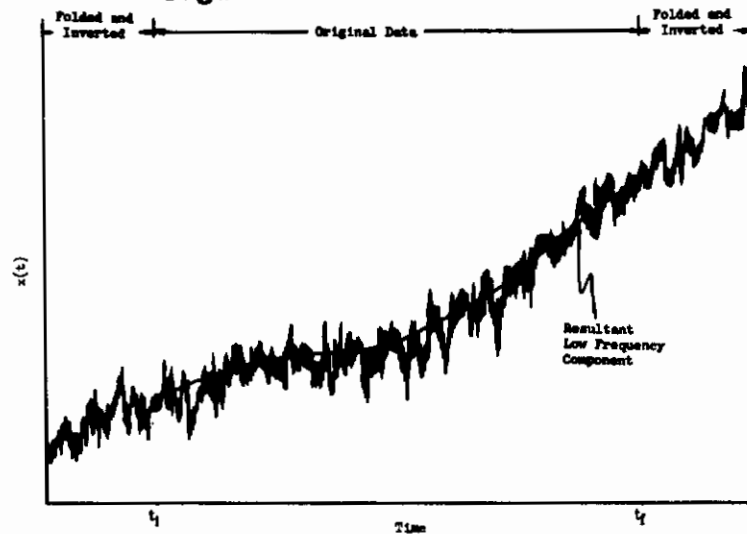


Figure III-17 Folded - Inverted Extension

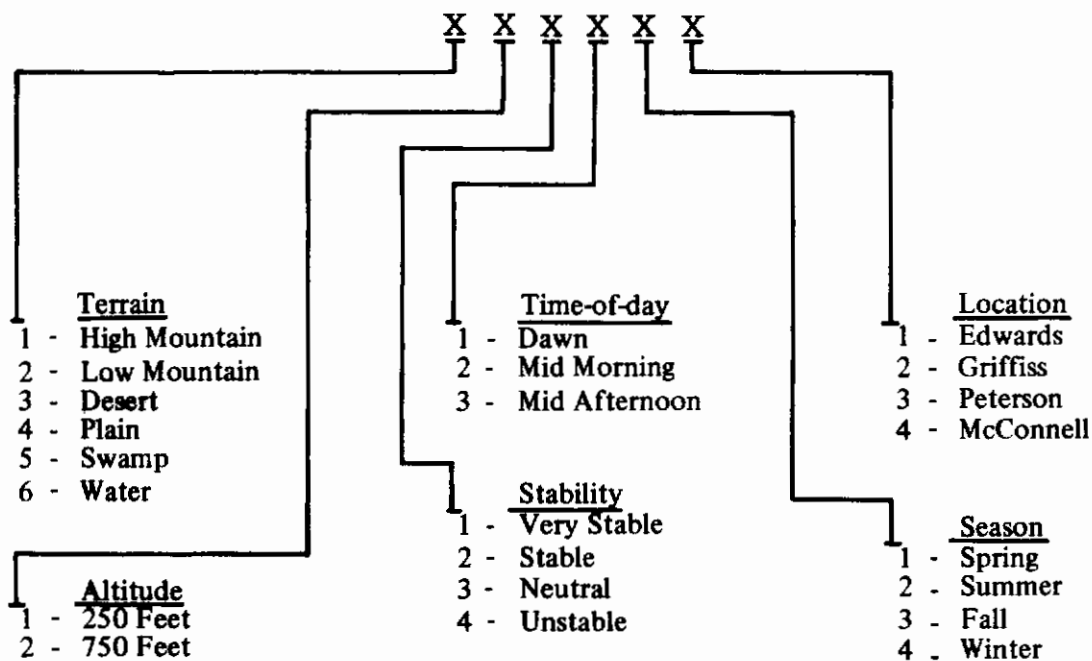
## APPENDIX IV

### GUST VELOCITY POWER SPECTRA AND ASSOCIATED DATA

Gust velocity power spectra and associated spectra data showing homogeneity, isotropy, and coherency characteristics, and experimental-to-mathematical comparisons are contained herein. The data are presented in order by test and leg number and are for the samples of data considered to be homogeneous.

The following is a brief explanation of each set of data, how it was obtained, and definition of abbreviated notes and scale identifications.

The six digit category number is used to define the type of terrain, flight altitude above the terrain, atmospheric stability, time of day, season and geographic location. Each digit in the category number is defined as follows:



## POWER SPECTRA

The ordinate scale, normalized PSD - 1/cpf, is the power,  $\phi(k)$ , normalized by  $\sigma_t^2$ . The  $\sigma_t$  values listed are the standard deviations calculated from the time series. The L values are scale lengths based on equations derived from von Karman's mathematical spectra. The spatial frequency is calculated as follows:  $k = \frac{f}{V}$ . WA is the wind angle in degrees measured with respect to the ground track of the airplane.

LO-LOCAT turbulence sample lengths were established to give a compromise between statistical confidence and turbulence stationarity considerations. Aliasing was prevented by the use of a high sampling rate to give a large frequency span between the break-point of the low-pass filter and the Nyquist frequency. The break-point of low-pass filters used was 22 cps and the Nyquist frequency was set at 50 cps. With negligible aliasing, the stability of uniformly spaced power spectral density estimates may be judged by analogy with a chi-square variate with d degrees of freedom, where:

$$d \approx \frac{2n\Delta f}{f_N} \quad (IV-1)$$

With  $N=27,000$ ,  $\Delta f = .046$  and  $f_N = 50$ , approximately 45 degrees of freedom were obtained.

Statistical reliability may also be evaluated by defining an interval of confidence on either side of the measured spectrum. The interval indicates the amount of variation that may be expected in the spectrum. Based on 90 percent confidence and a single time history, the interval is defined by:

$$\Phi_{90} = \exp \left[ \frac{1}{4.343} \left( \frac{300m}{6n-3m} \right)^{1/2} \right] \quad (IV-2)$$

This interval was approximately  $\pm 42$  percent for individual data samples.

## HOMOGENEITY

The homogeneity check PSD ratio was obtained by dividing the power spectra for the middle third of the data sample by the power spectra of the entire sample. This ratio is a measure of the degree of homogeneity (stationarity), which for perfect homogeneity will approach 1.0

## COHERENCY

The u-w and v-u coherency is a measure of the statistical independence between the v and w, and v and u gust velocity components. Ideally, the components are statistically independent and the coherency should be equal to zero. However, due to statistical variations in the power



spectra and cross spectra calculations, and electronic noise in the experimental data the coherency can only approximate zero.

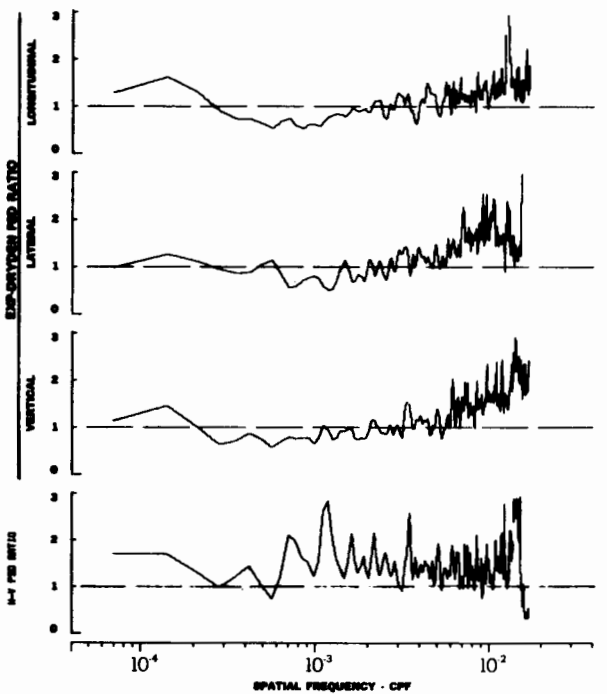
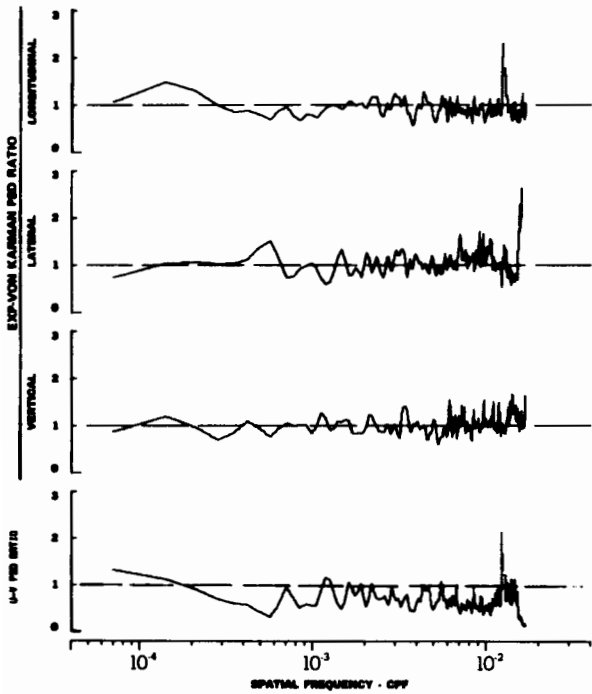
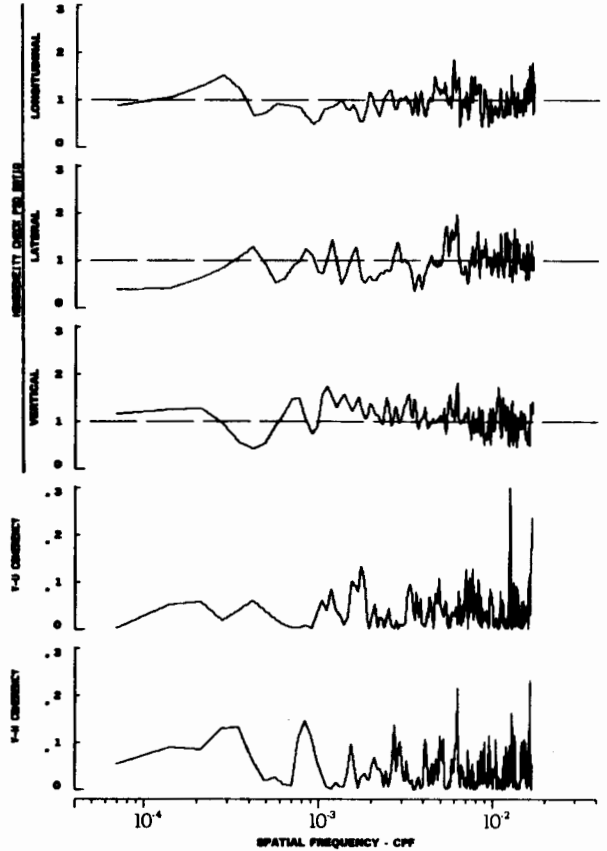
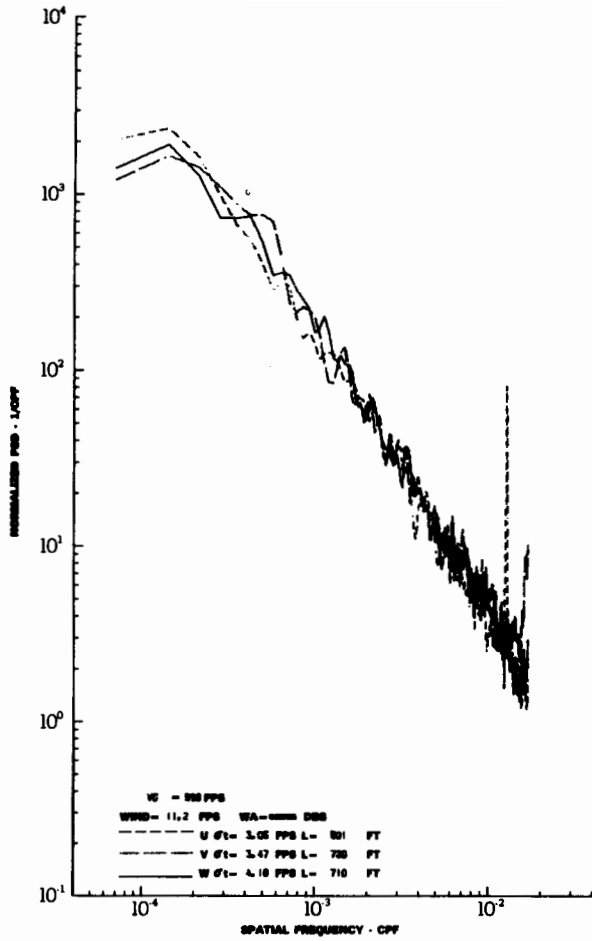
## EXPERIMENTAL TO MATHEMATICAL COMPARISONS

Experimental-to-von Karman and Dryden mathematical spectra relationships are illustrated by plotting the ratio of the experimental spectra to mathematical spectra for each component. Perfect agreement is indicated when either the experimental-von Karman PSD ratio or experimental-Dryden PSD ratio is equal to 1.0.

## ISOTROPY

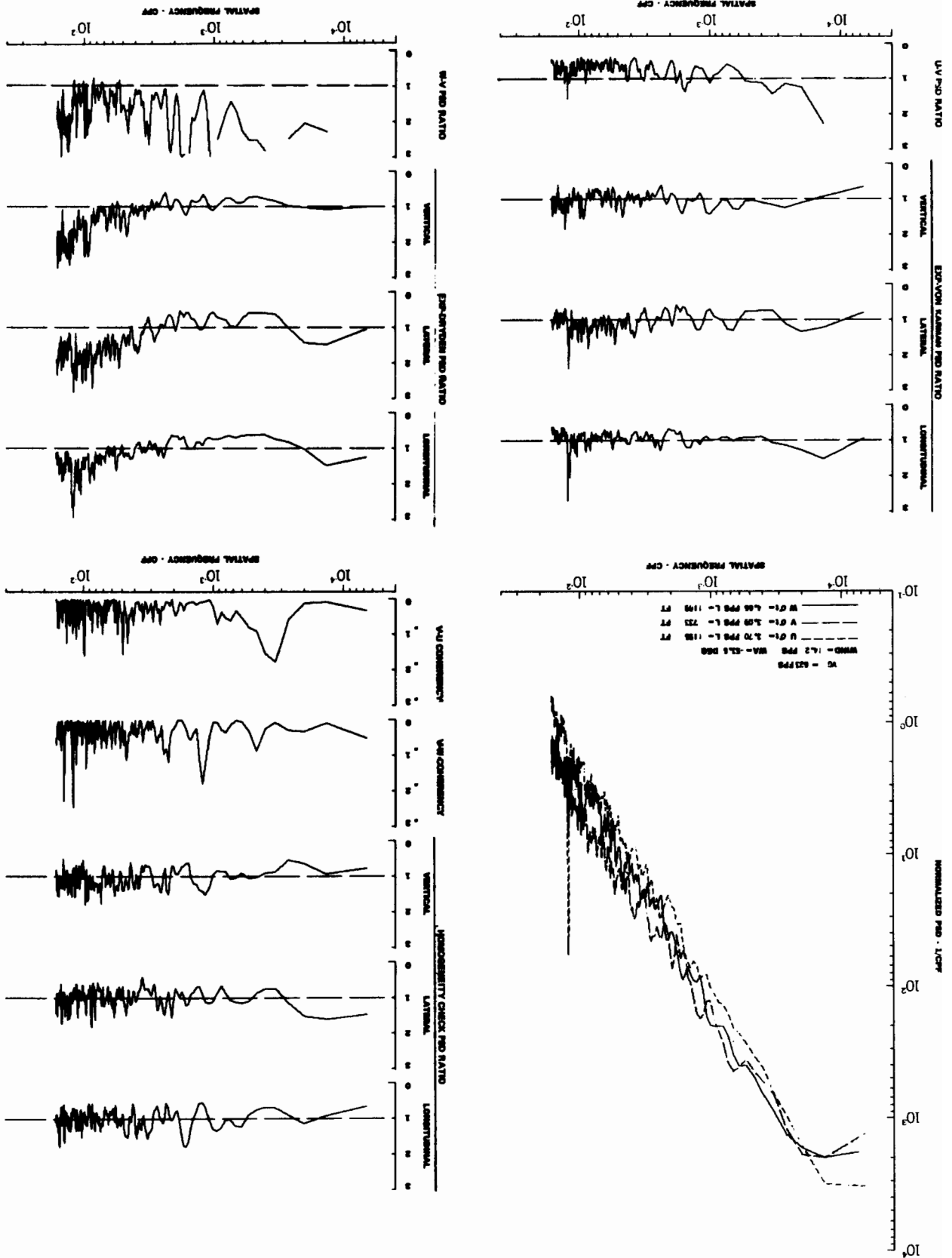
The isotropic characteristics are depicted by plotting the ratio of unnormalized power spectra of vertical and longitudinal gust velocity to lateral gust velocity versus spatial frequency. Perfect isotropy is indicated when the w-v PSD ratio is equal to 1.0 throughout the frequency range and the u-v PSD ratio is equal to approximately 2.0 at the low frequencies and 0.75 at the high frequencies. The frequency at which the u-v ratio is equal to 2.0 depends on the scale of turbulence. This is discussed in detail in Section V of Volume I.

# Contrails



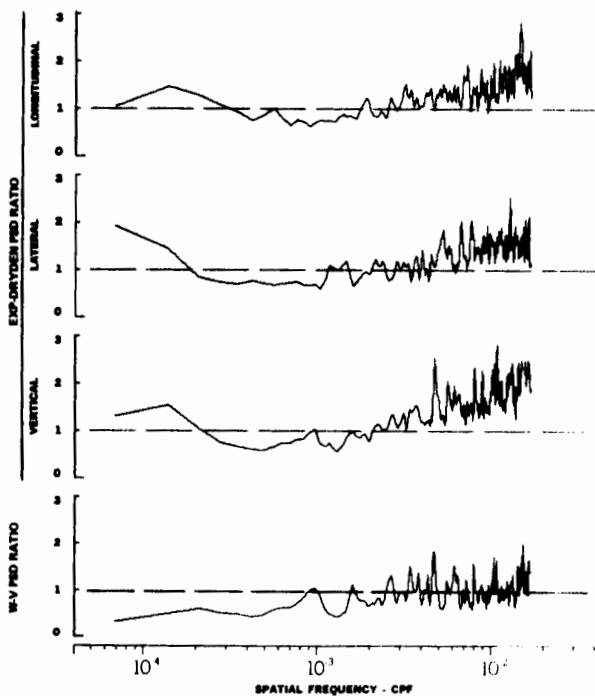
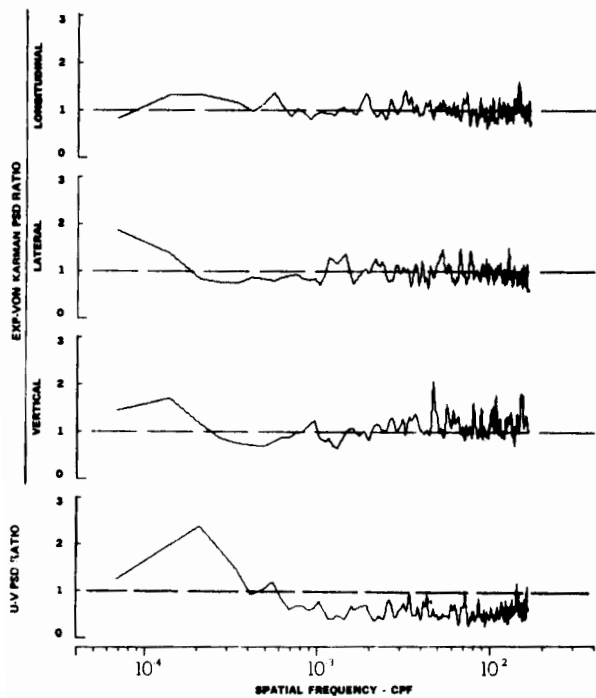
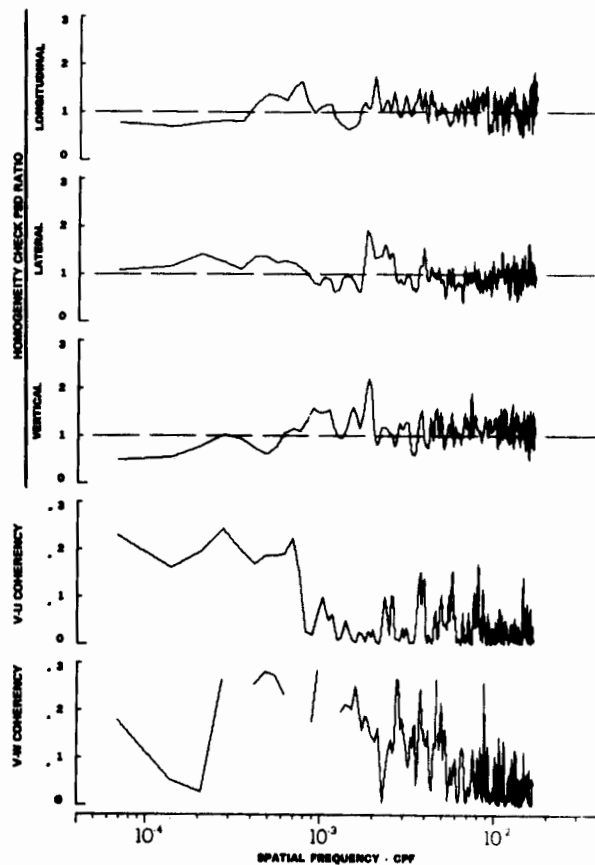
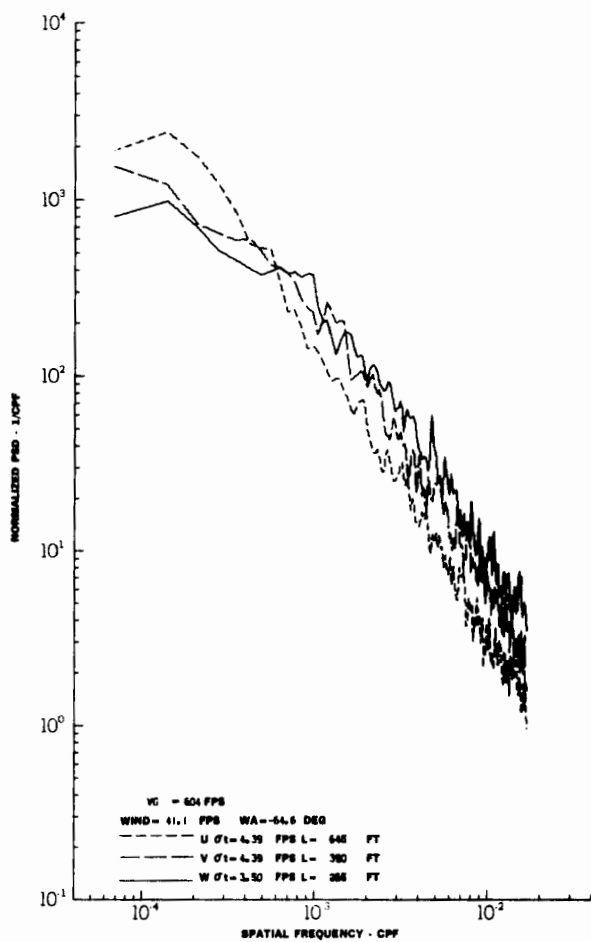
TURBULENCE SPECTRA DATA FOR TEST 17, LEG 1, CATEGORY 424324  
 FIGURE IV-1

**109**  
**TURBULENCE SPECTRA DATA FOR TEST 17, LEG 3, CATEGORY 424324**  
**FIGURE IV-2**

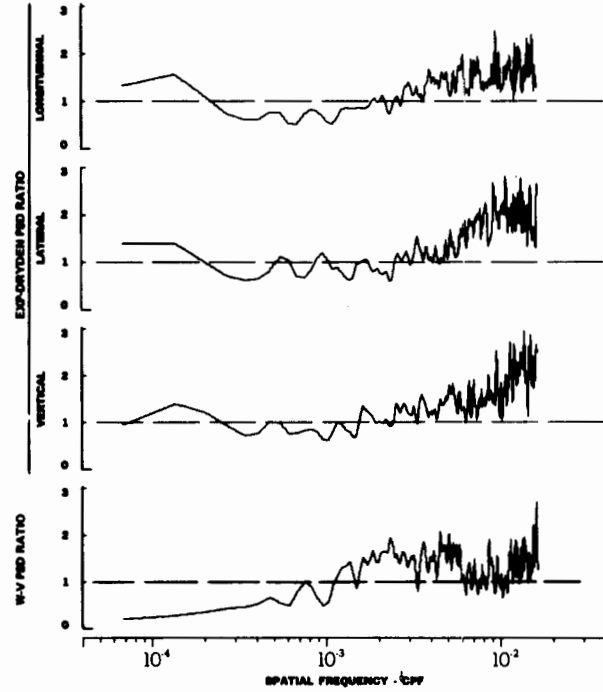
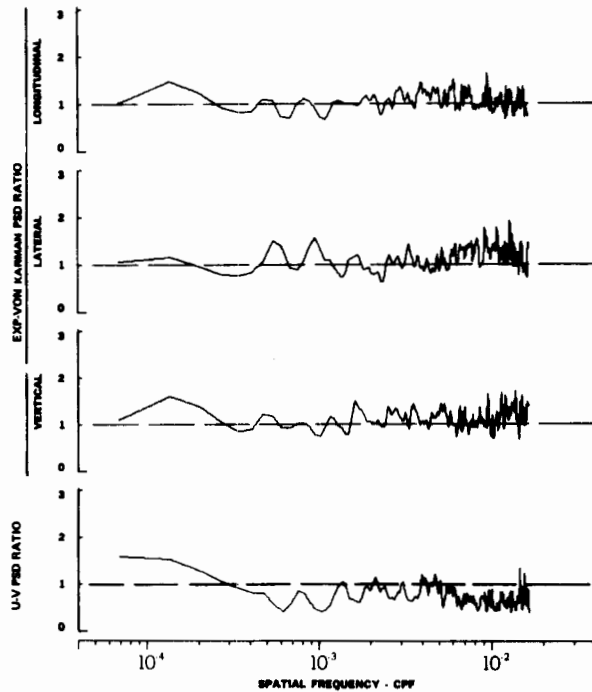
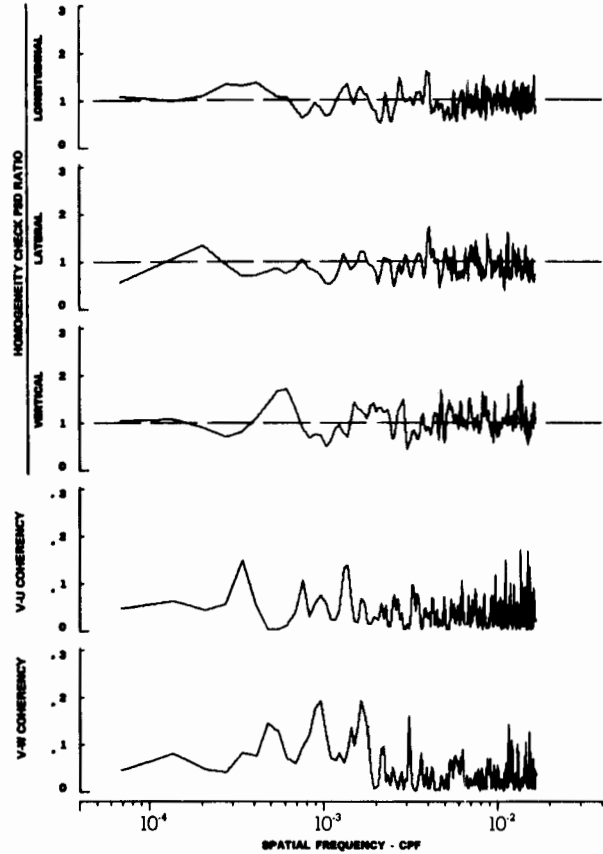
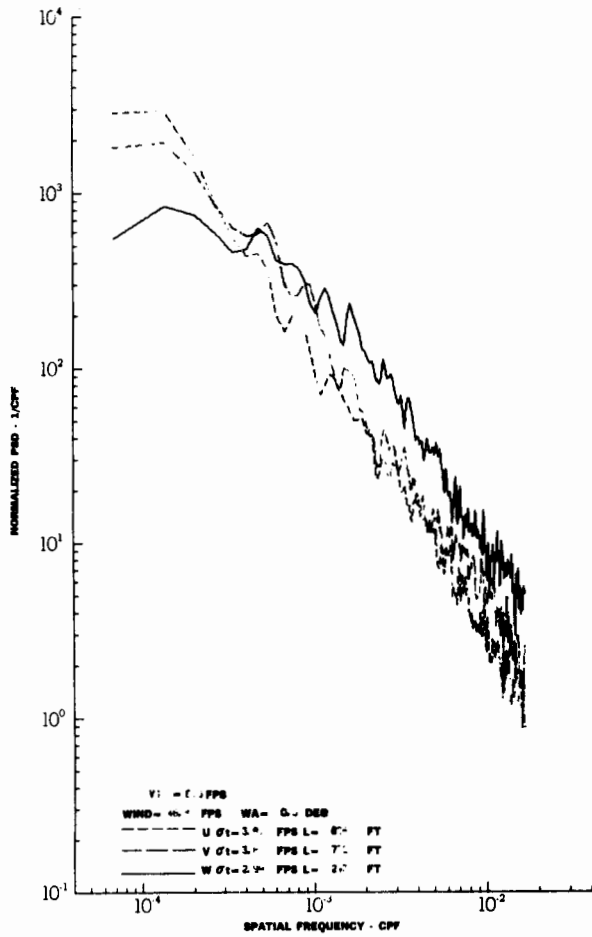




# Contrails



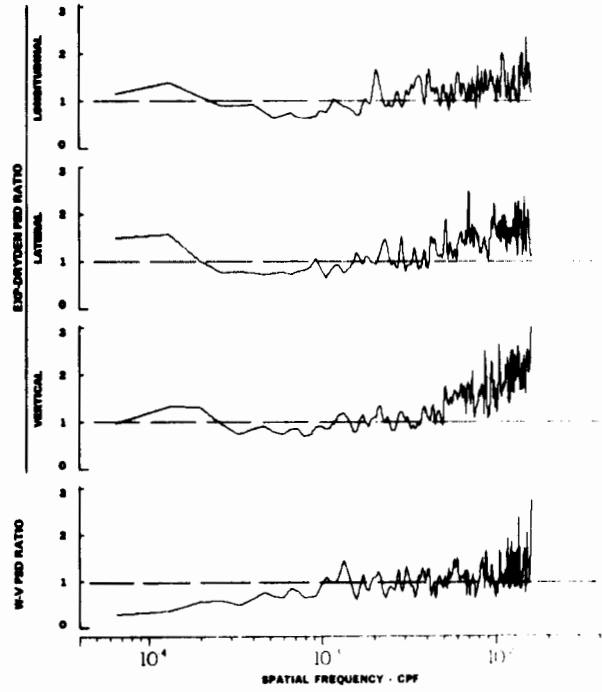
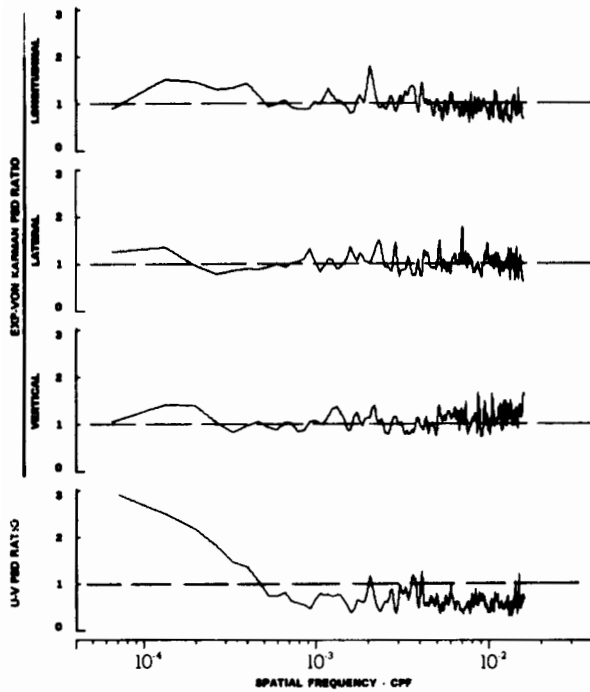
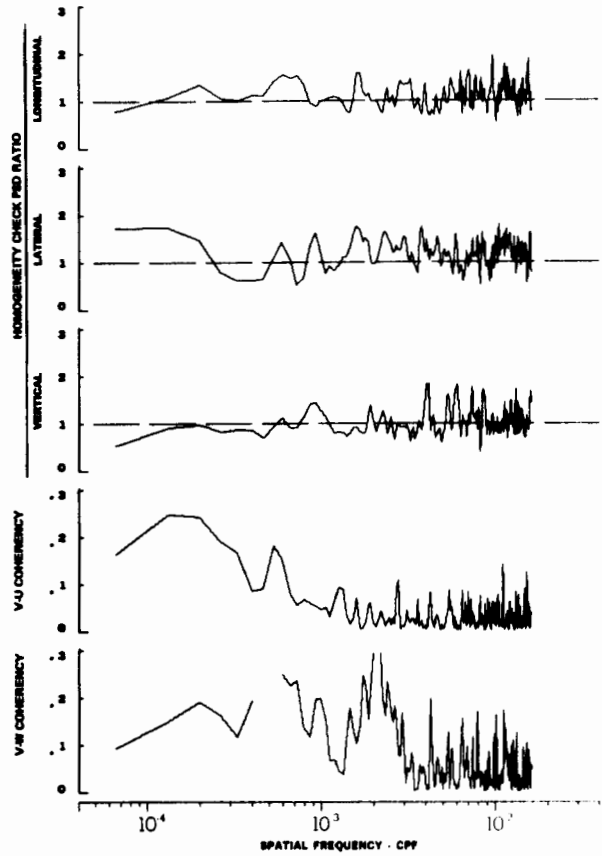
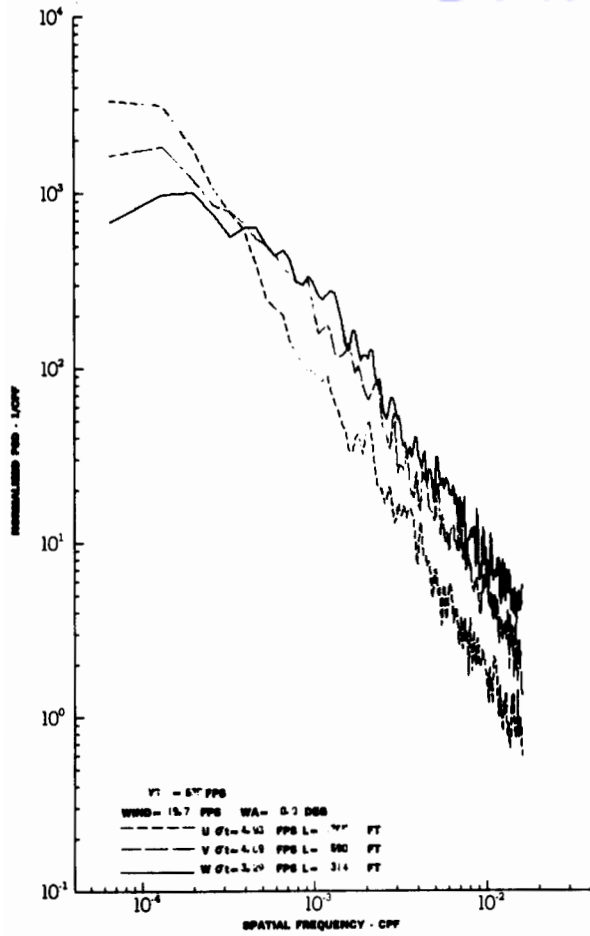
TURBULENCE SPECTRA DATA FOR TEST 23, LEG 7, CATEGORY 413224  
FIGURE IV-4



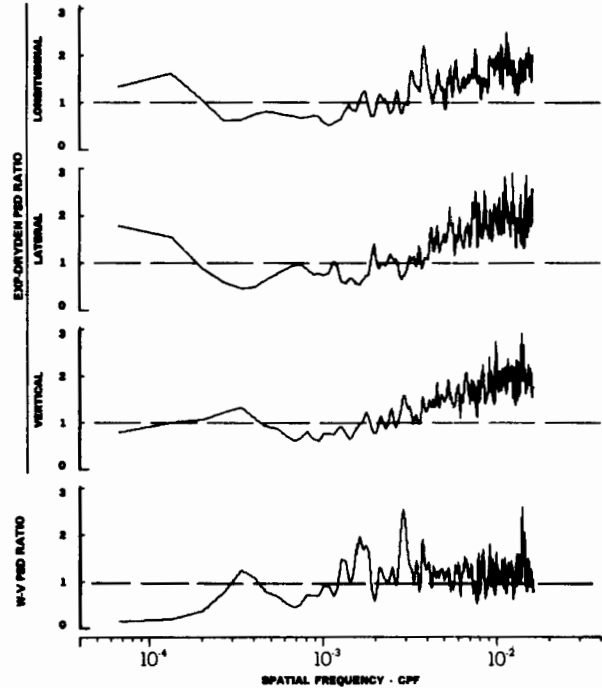
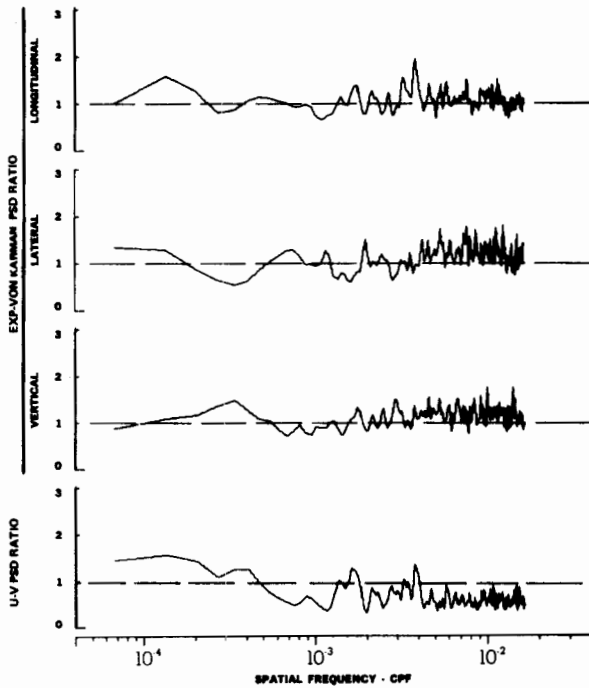
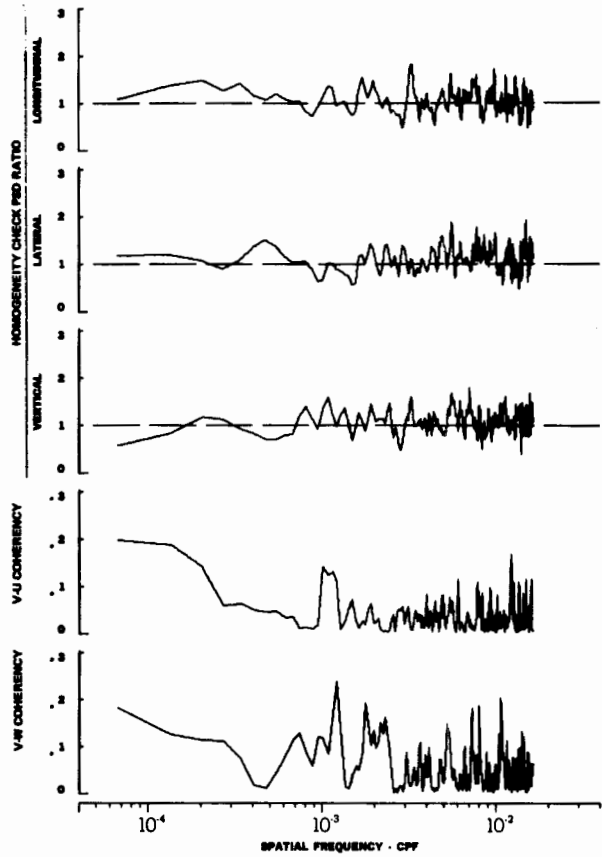
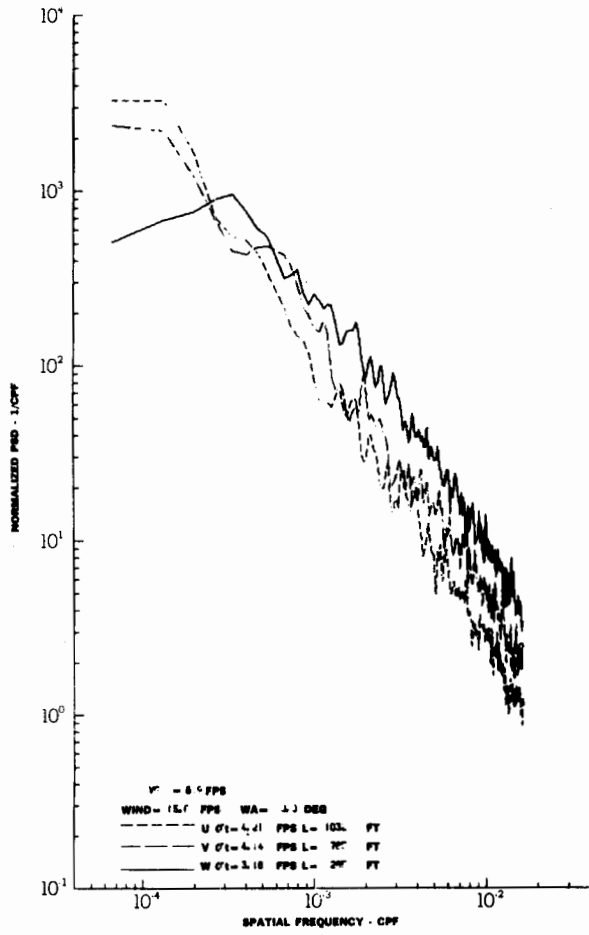
TURBULENCE SPECTRA DATA FOR TEST 24, LEG 2, CATEGORY 414324

FIGURE IV-5



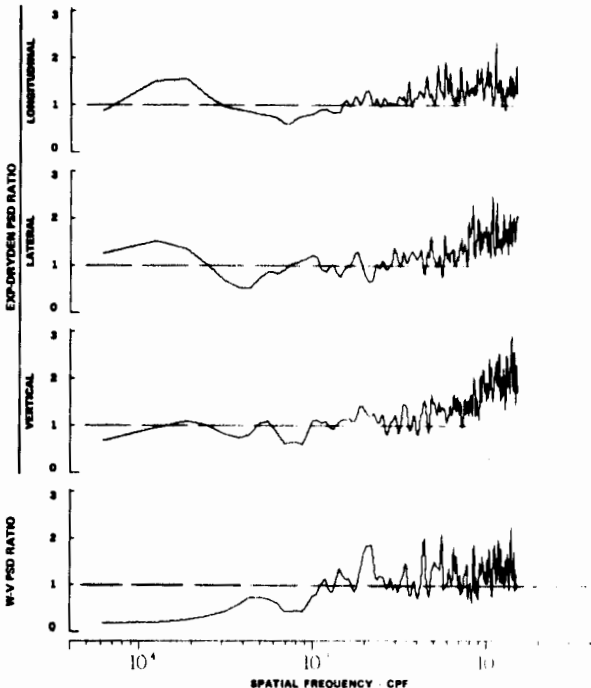
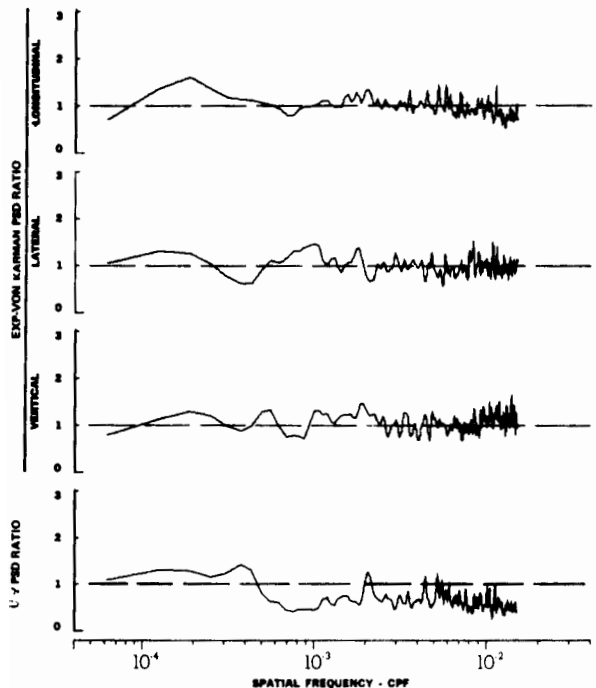
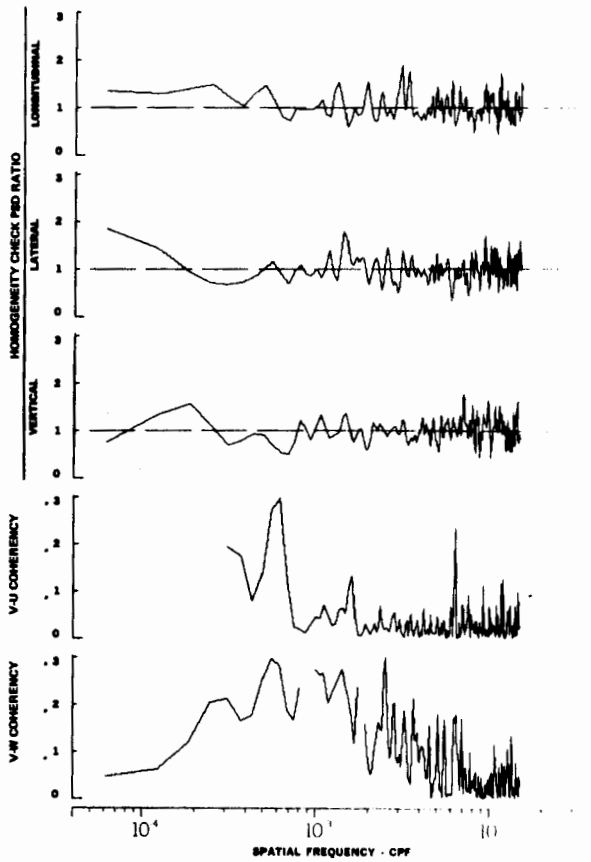
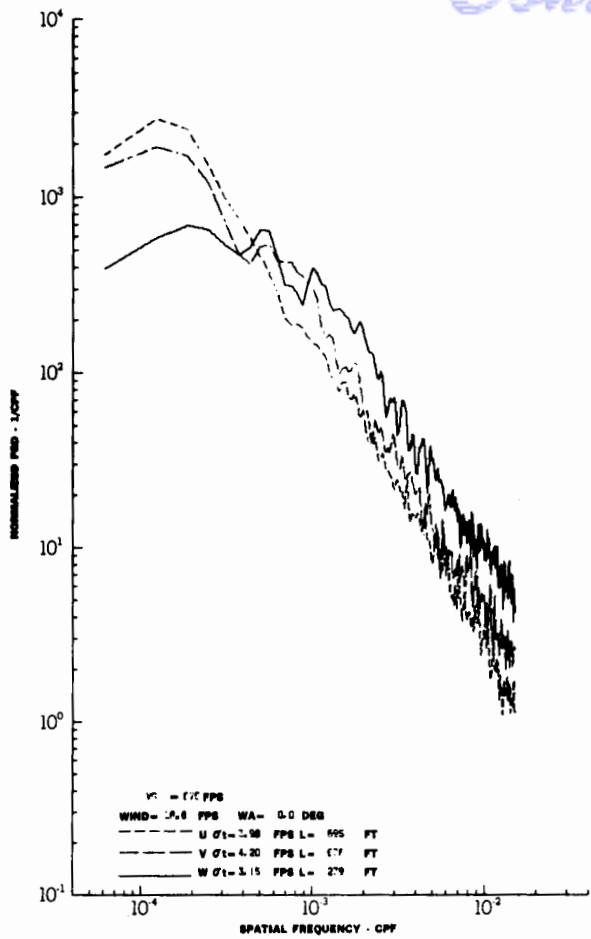


TURBULENCE SPECTRA DATA FOR TEST 24, LEG 4, CATEGORY 414324  
FIGURE IV-6



TURBULENCE SPECTRA DATA FOR TEST 24, LEG 6, CATEGORY 418324  
FIGURE IV-7

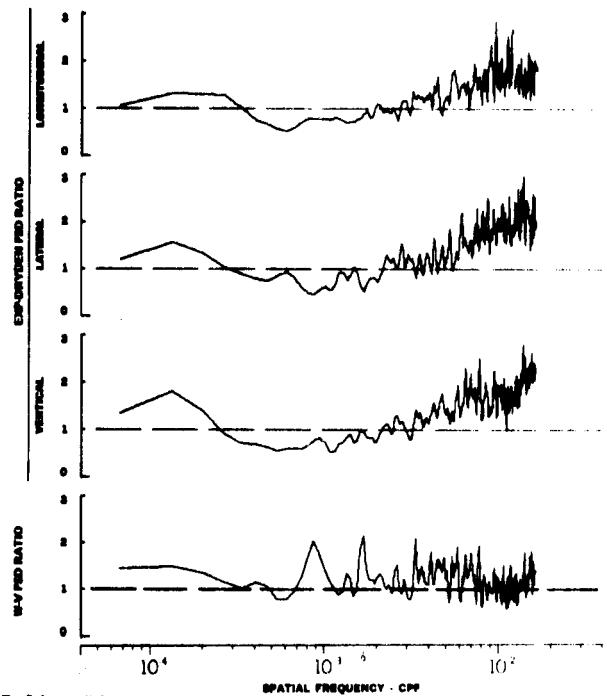
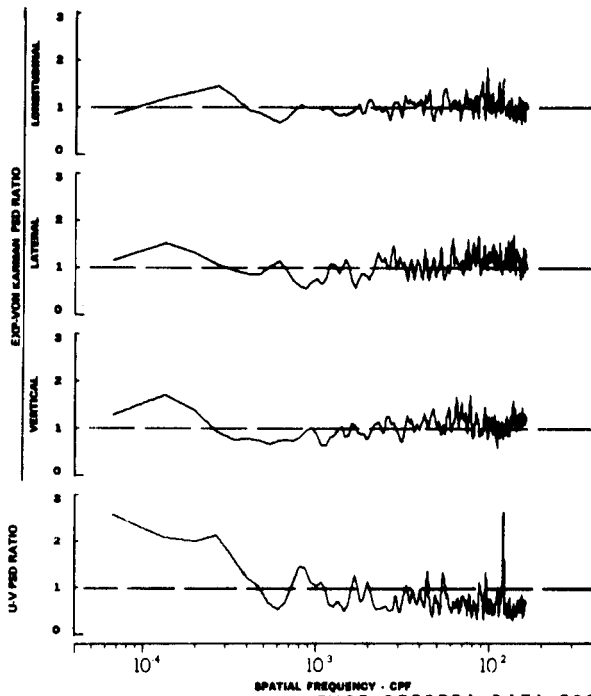
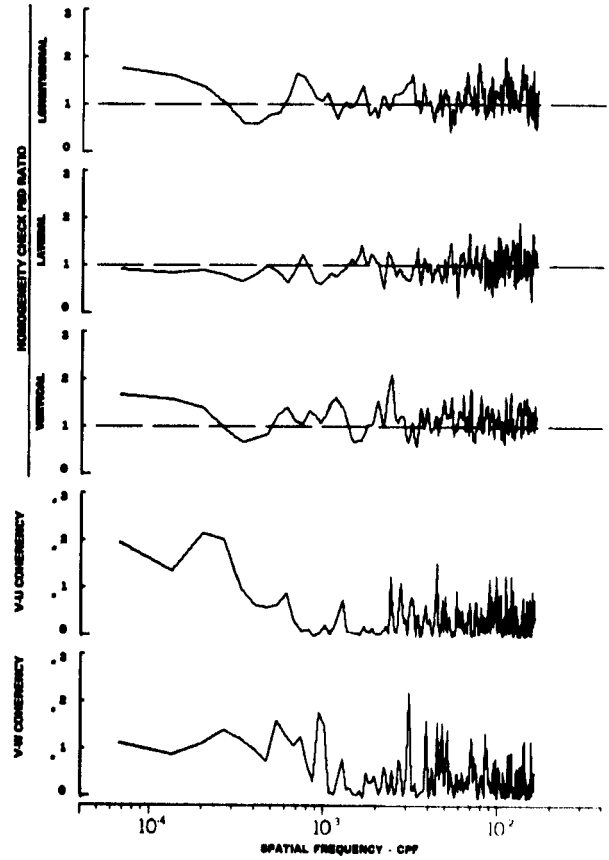
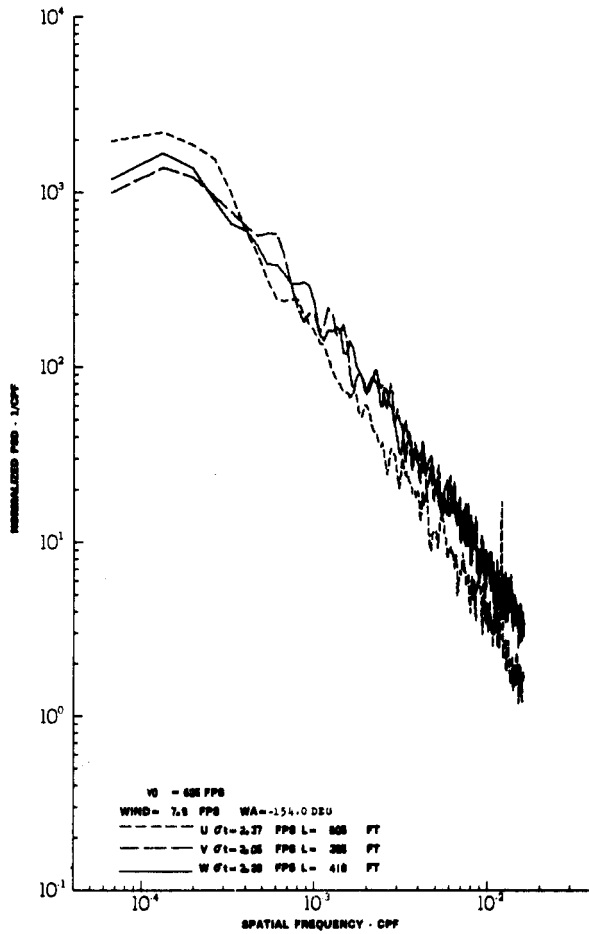
# Contrails



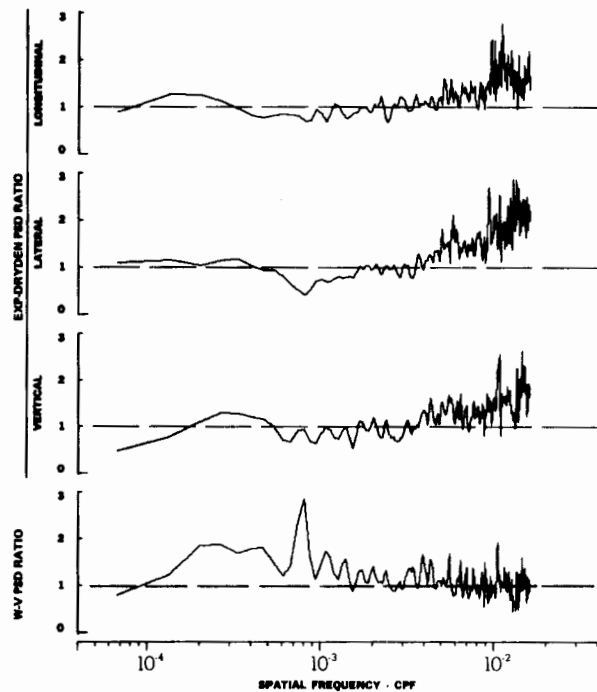
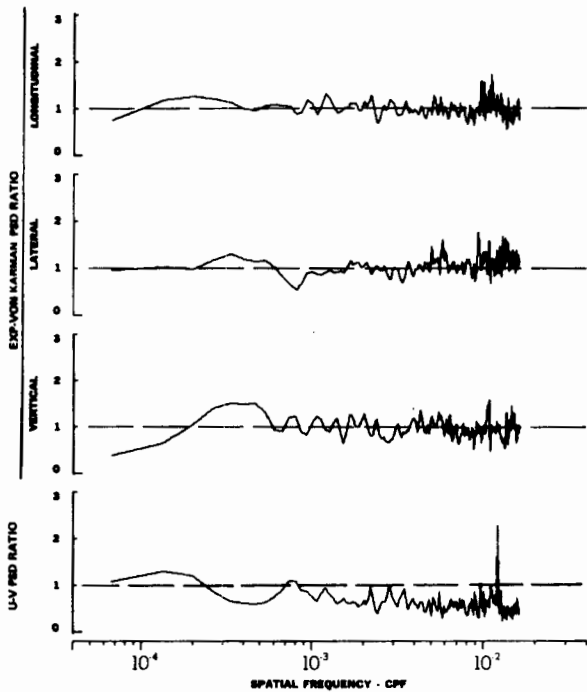
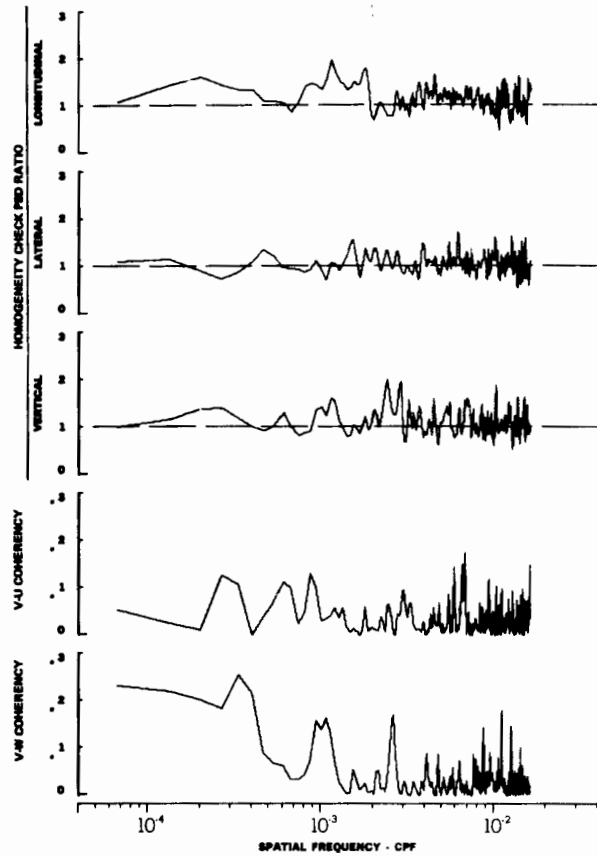
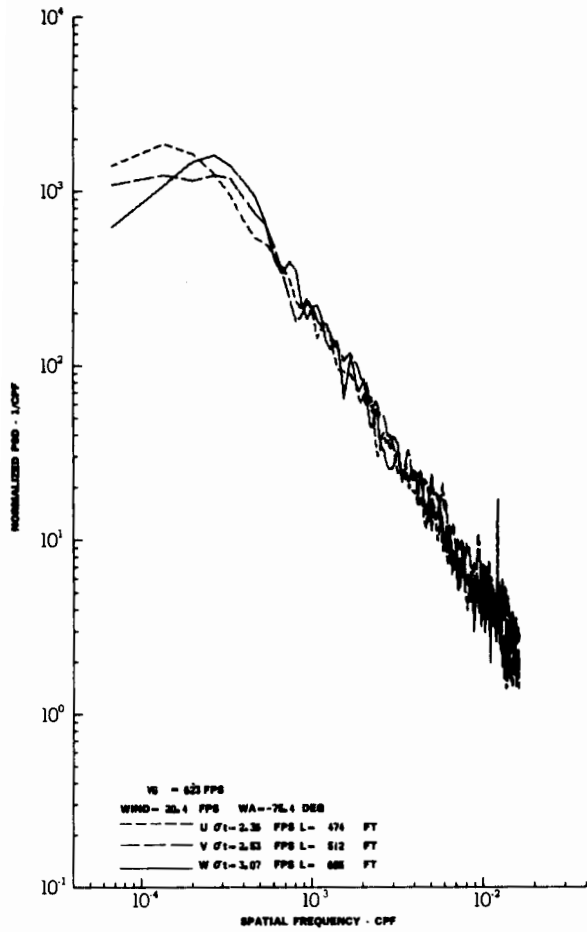
TURBULENCE SPECTRA DATA FOR TEST 24, LEG 8, CATEGORY 414324  
FIGURE IV-8



# Contrails

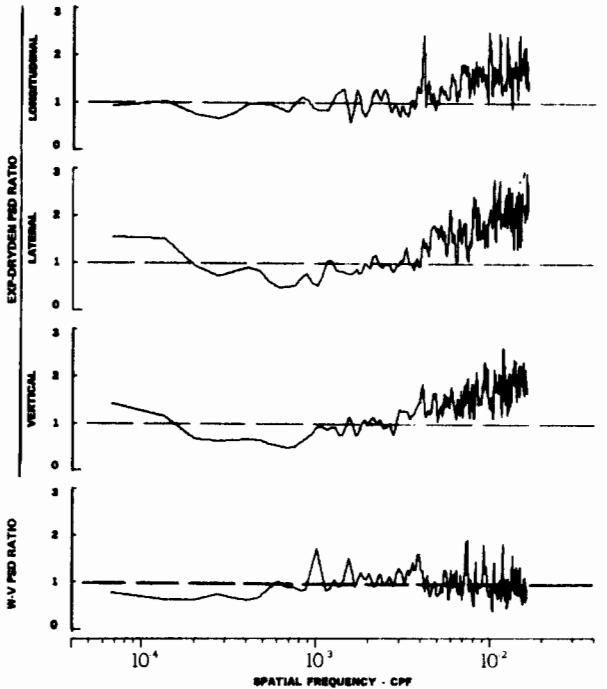
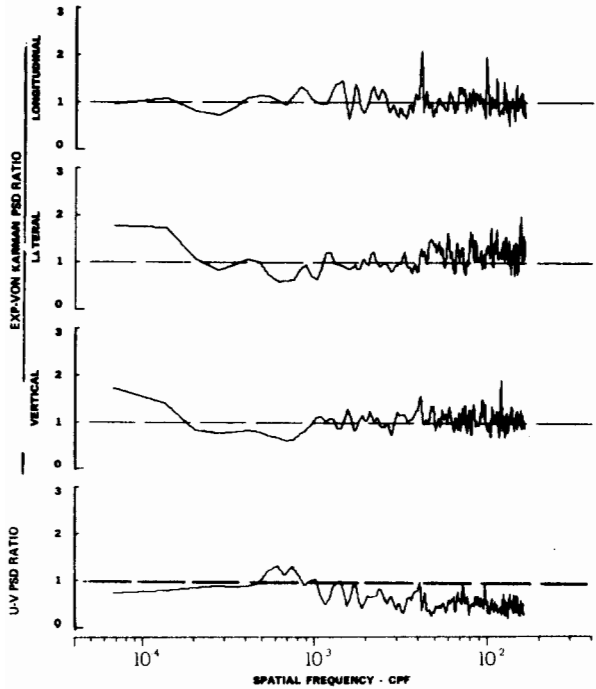
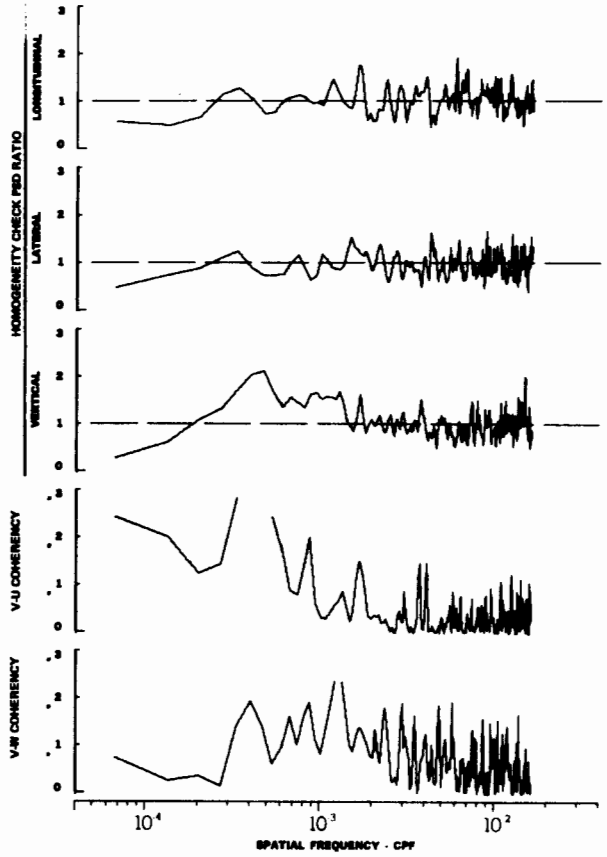
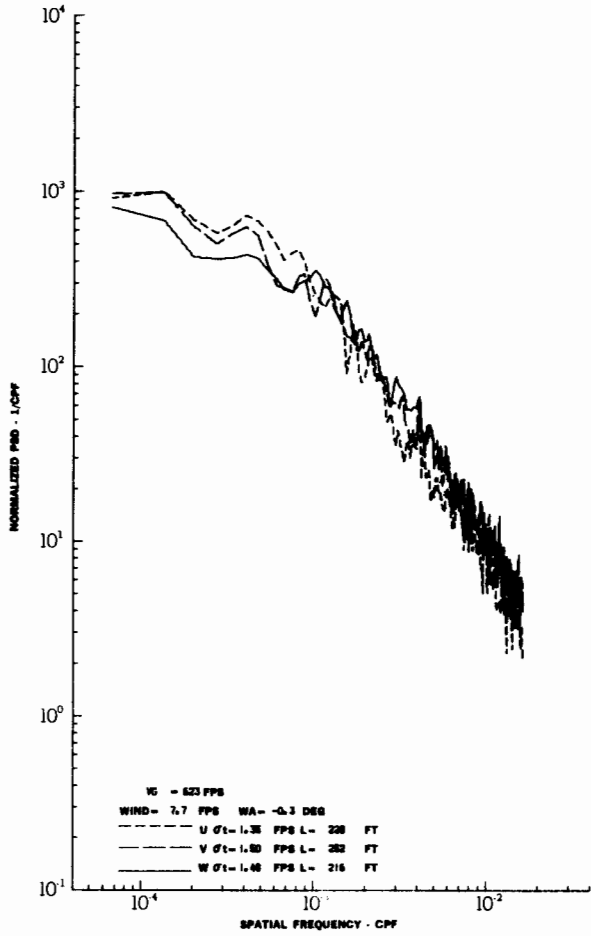


TURBULENCE SPECTRA DATA FOR TEST 26, LEG 6, CATEGORY 422224  
FIGURE IV-10

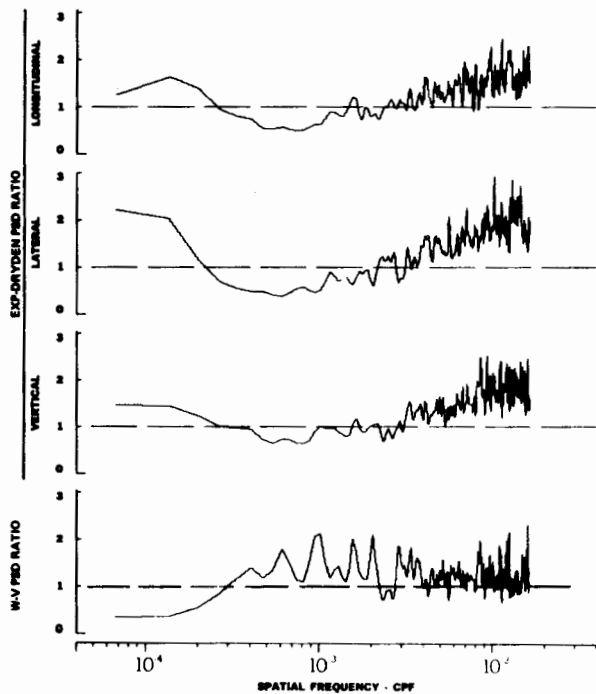
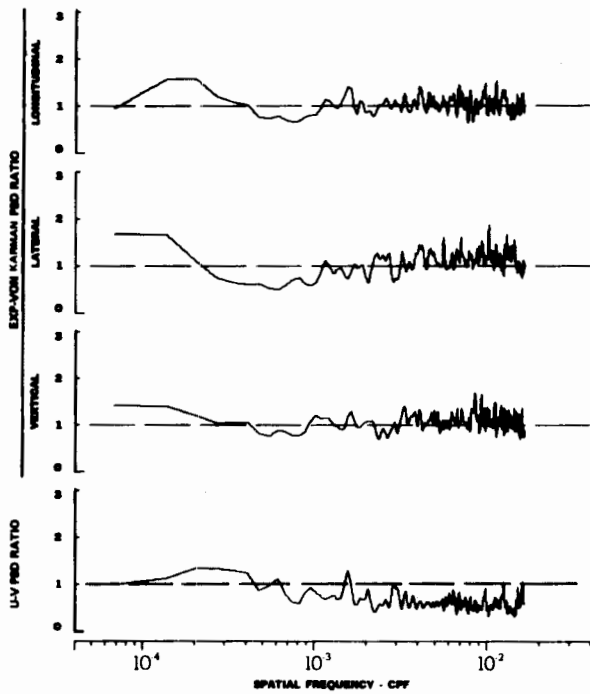
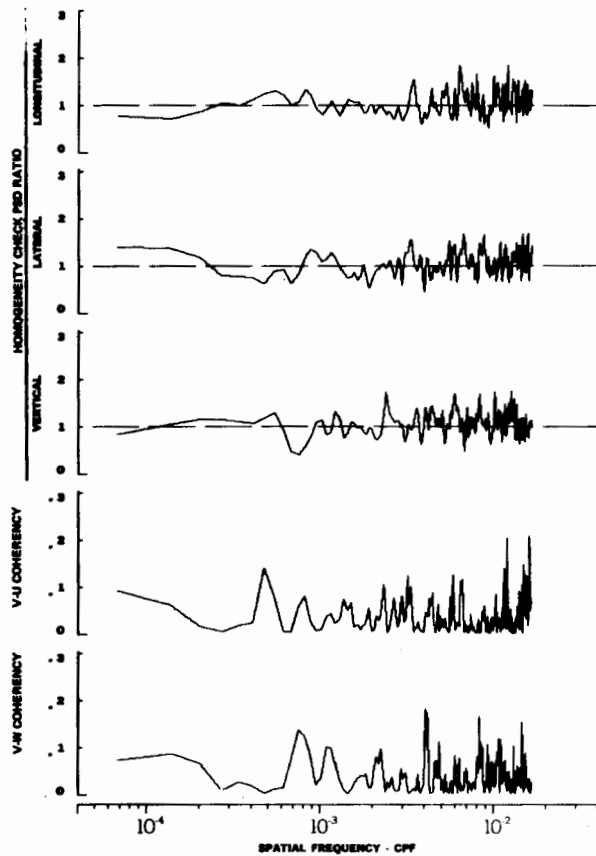
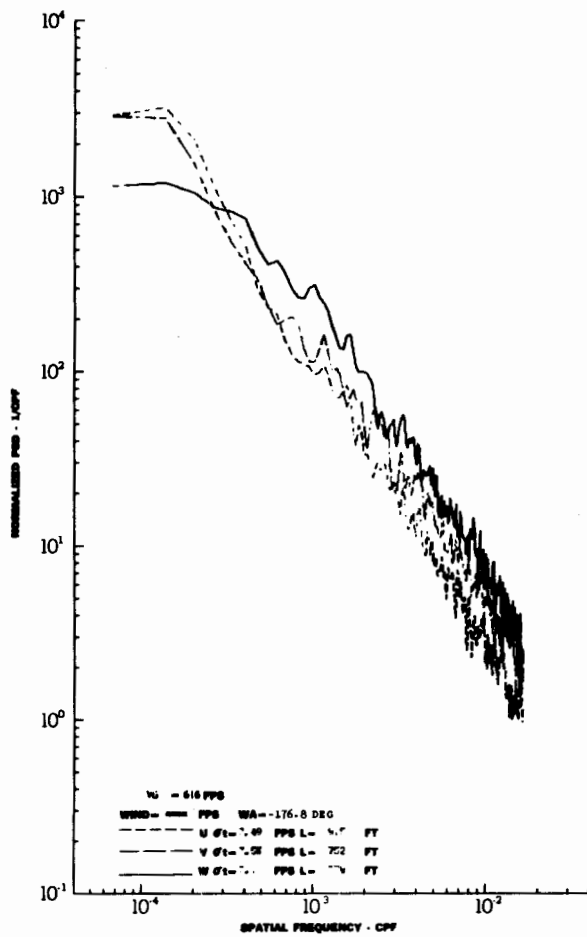


TURBULENCE SPECTRA DATA FOR TEST 26, LEG 8, CATEGORY 423224  
 FIGURE IV-11

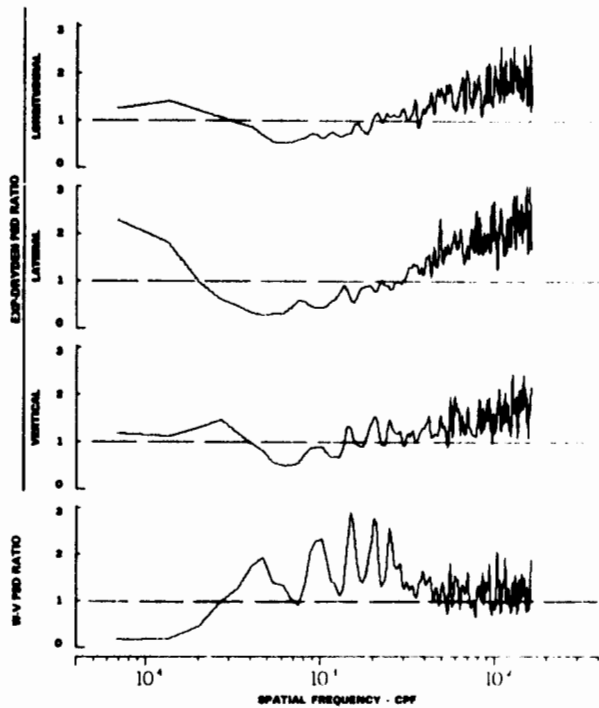
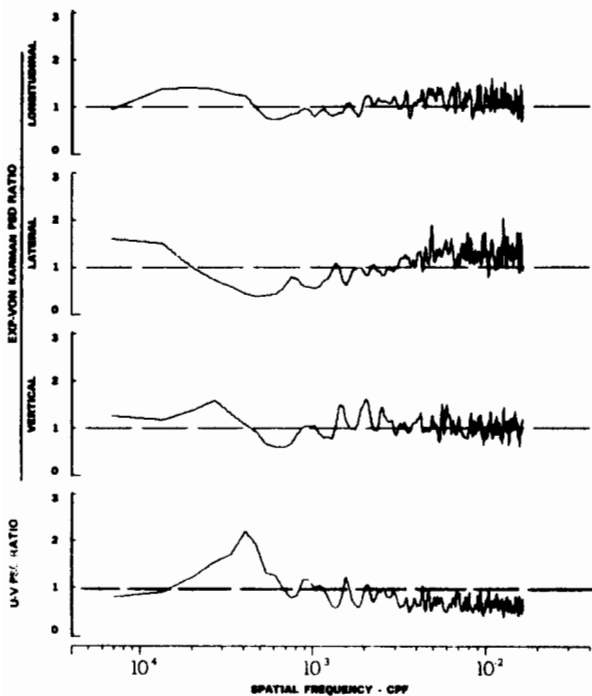
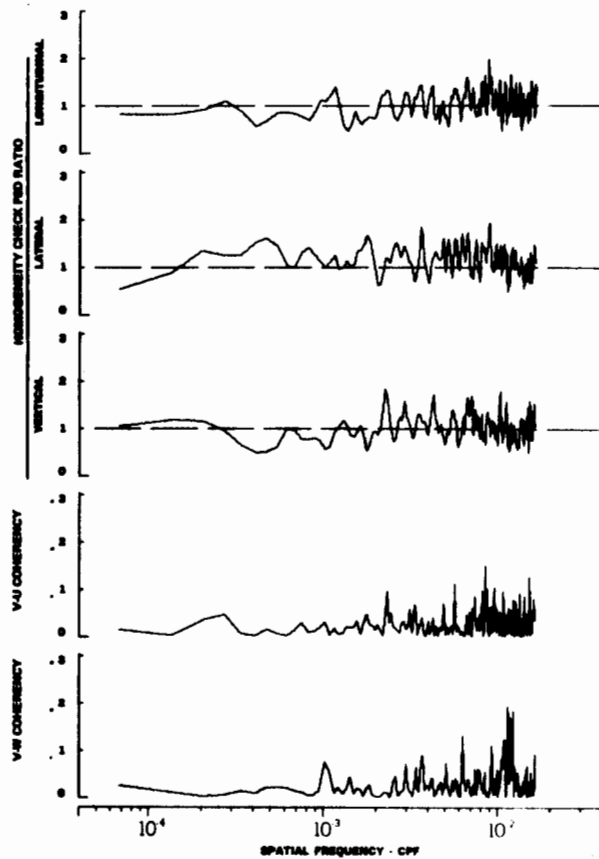
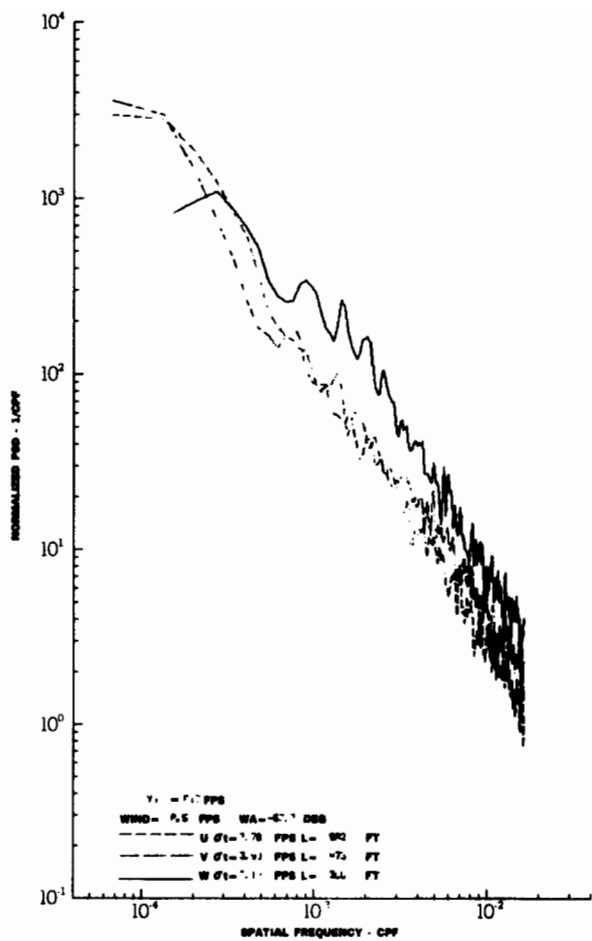




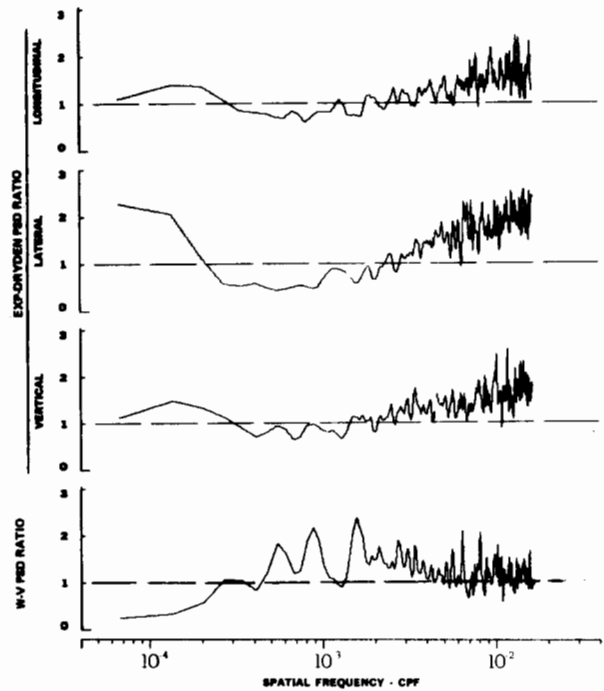
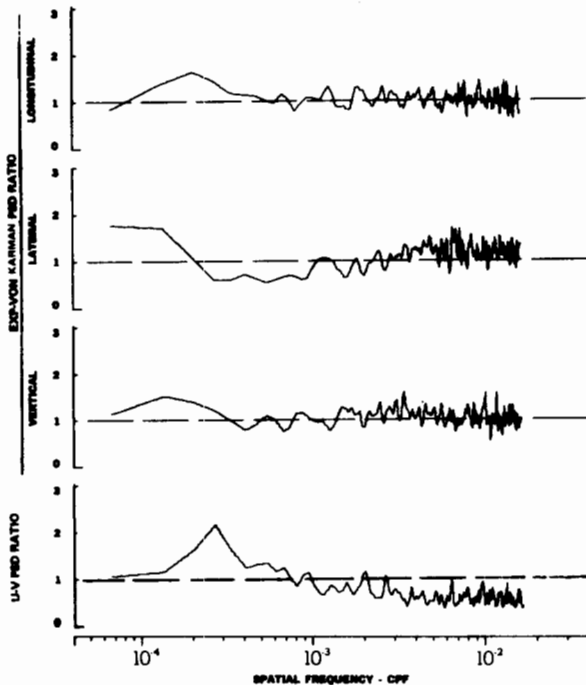
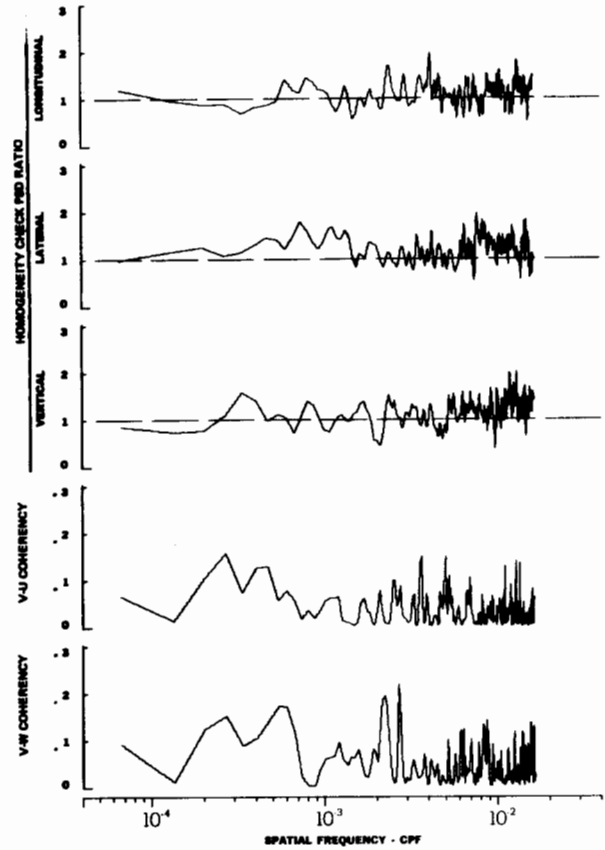
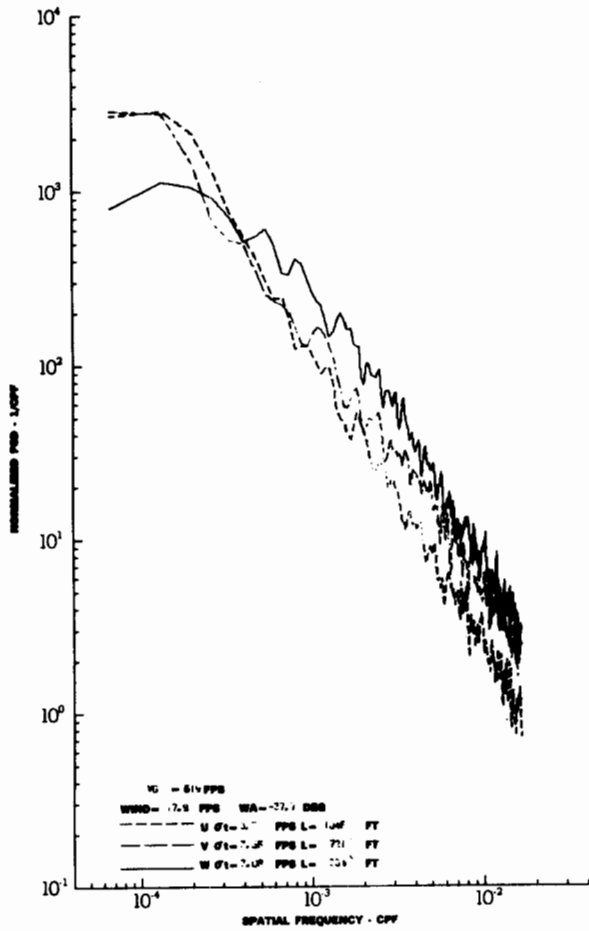
TURBULENCE SPECTRA DATA FOR TEST 28, LEG 2, CATEGORY 411224  
FIGURE IV-12



TURBULENCE SPECTRA DATA FOR TEST 29, LEG 1, CATEGORY 414324  
 FIGURE IV-13



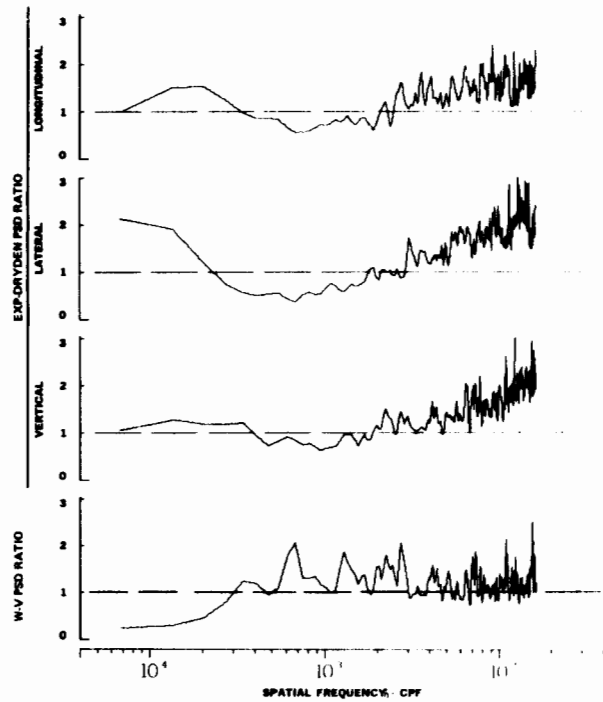
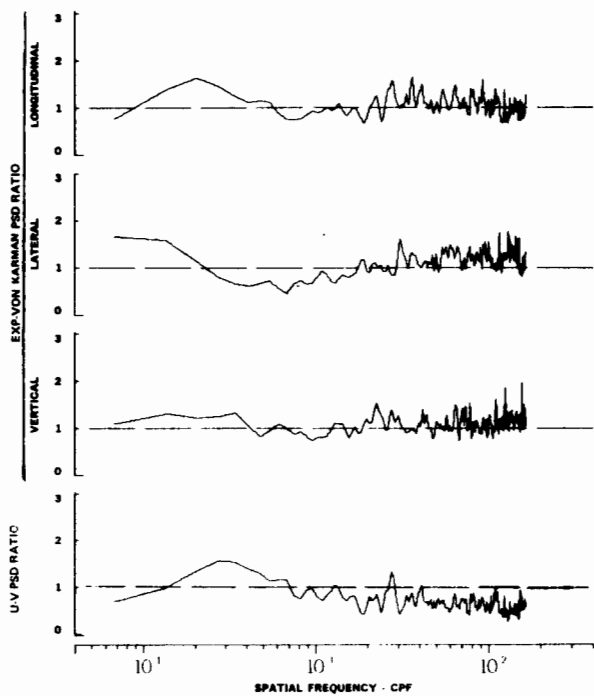
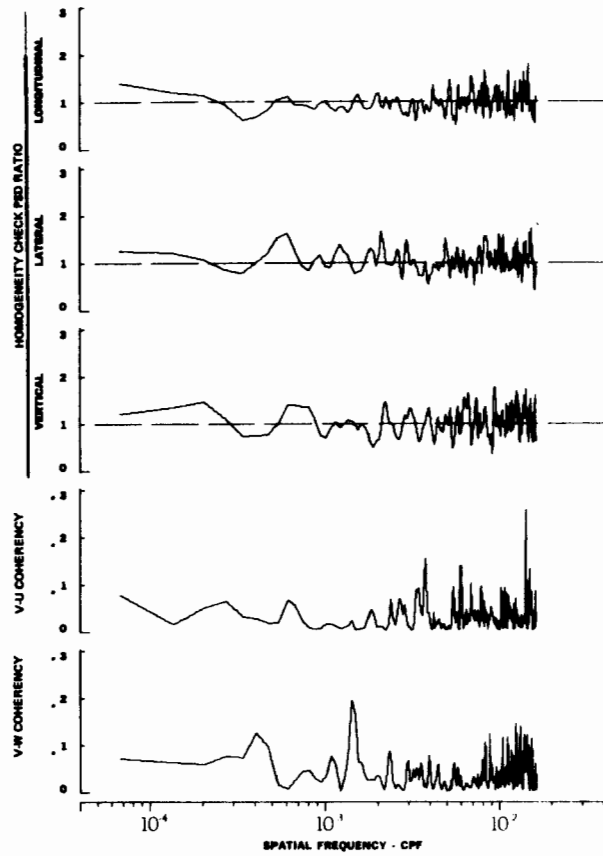
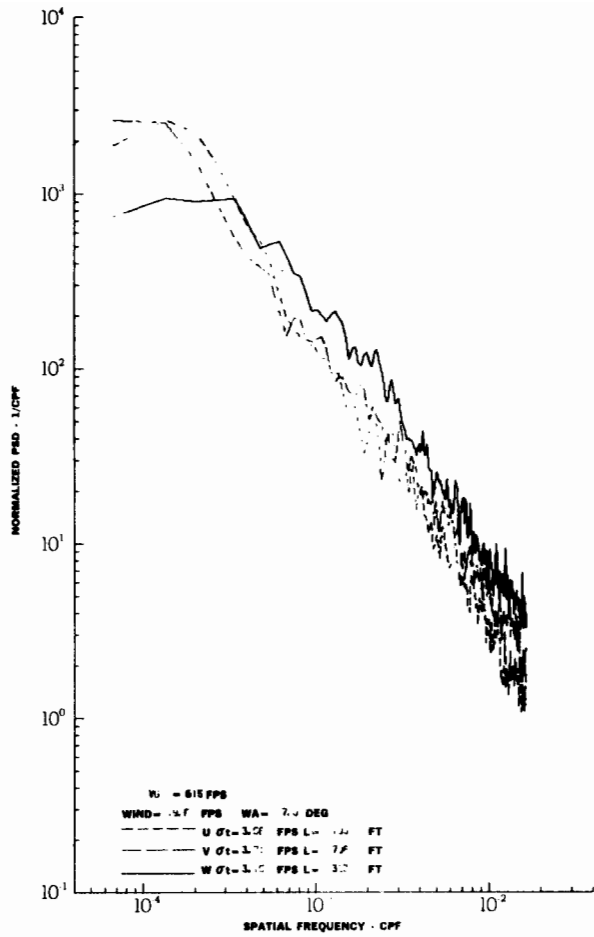
TURBULENCE SPECTRA DATA FOR TEST 29, LEG 3, CATEGORY 414324  
 FIGURE IV-14



TURBULENCE SPECTRA DATA FOR TEST 29, LEG 5, CATEGORY 414324

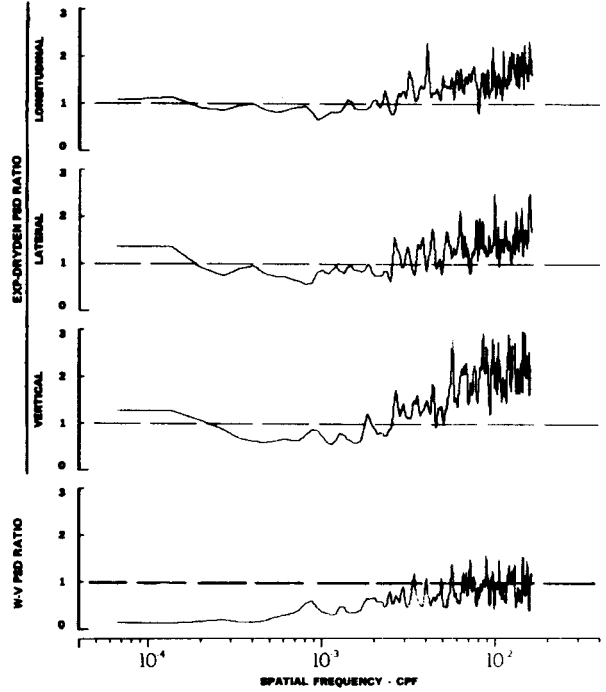
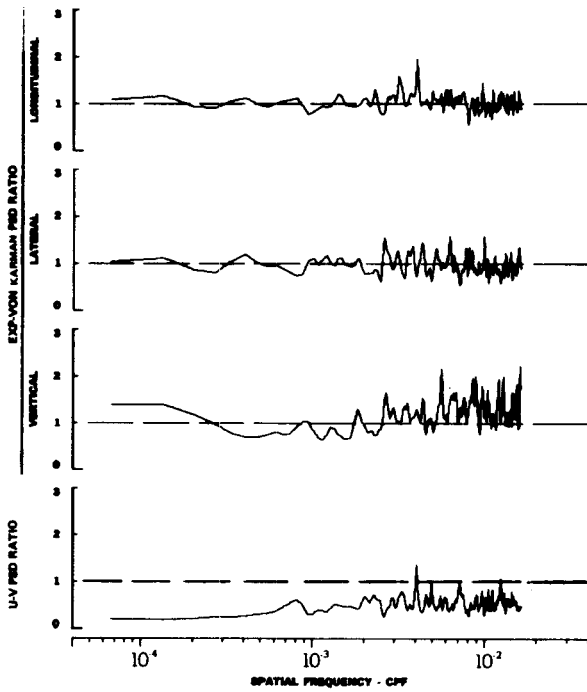
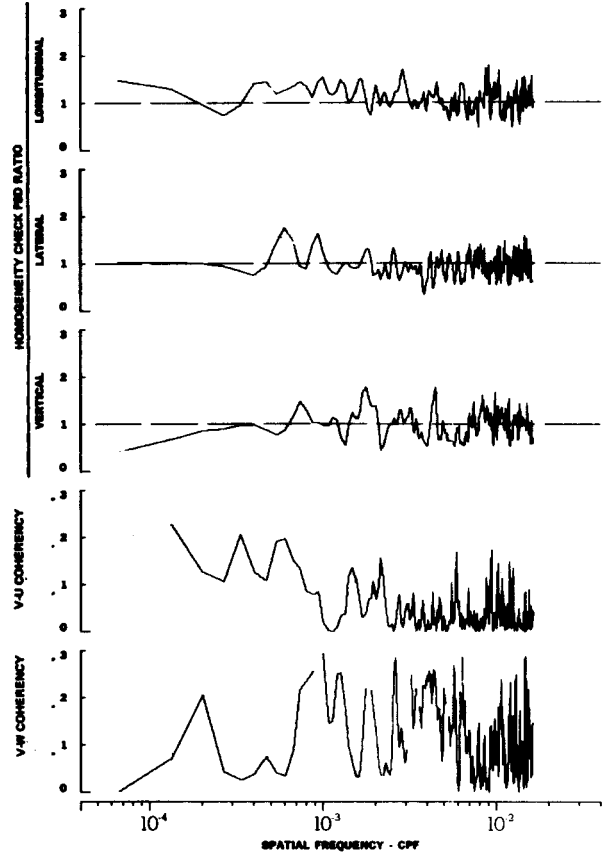
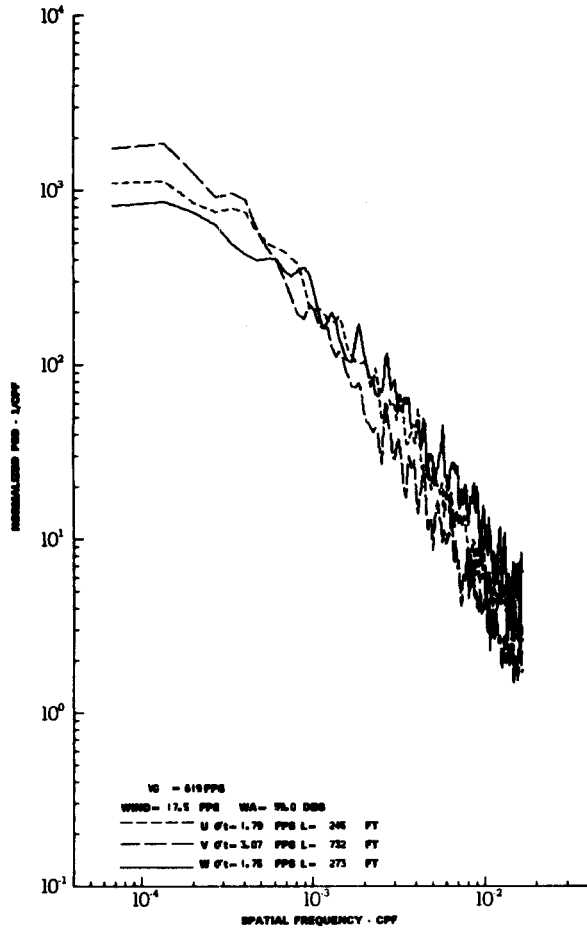
FIGURE IV-15

# Contrails



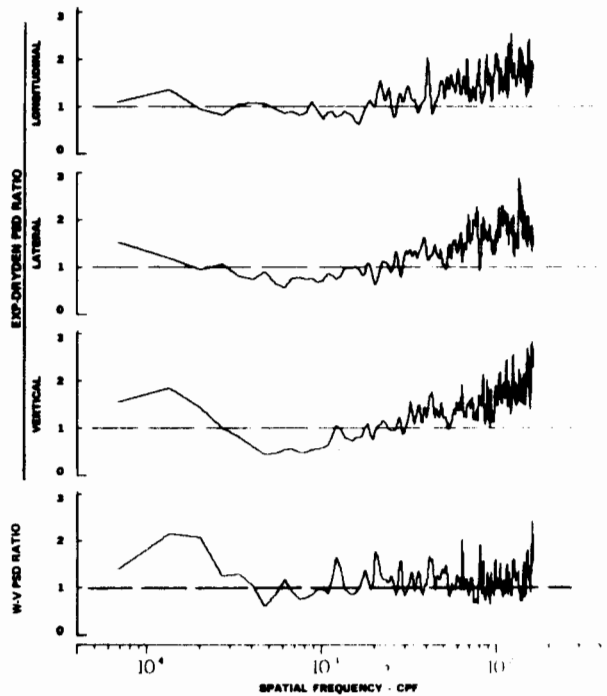
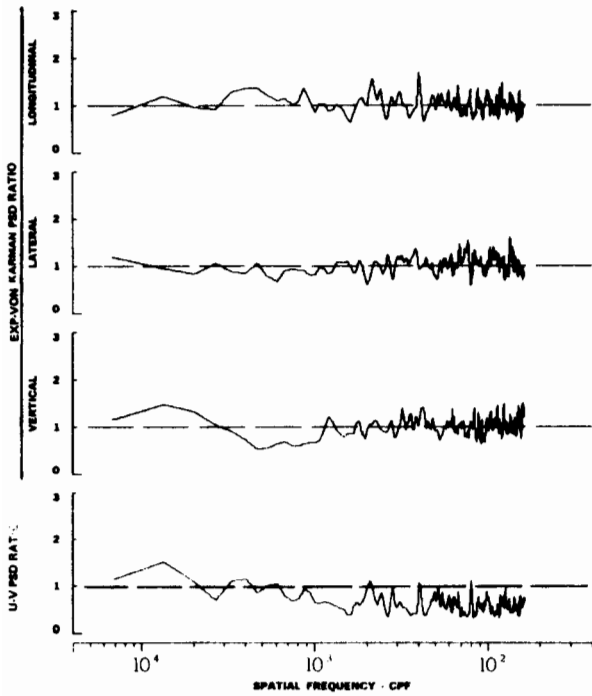
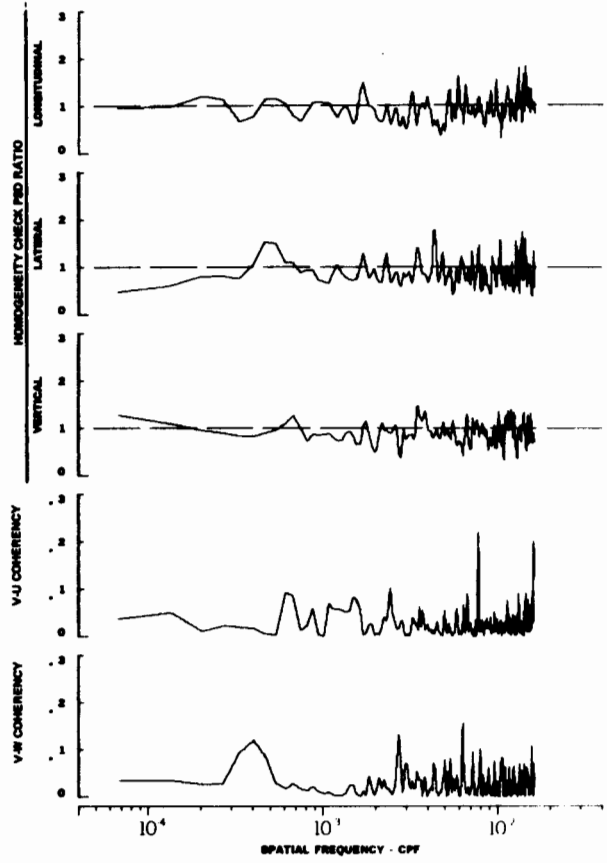
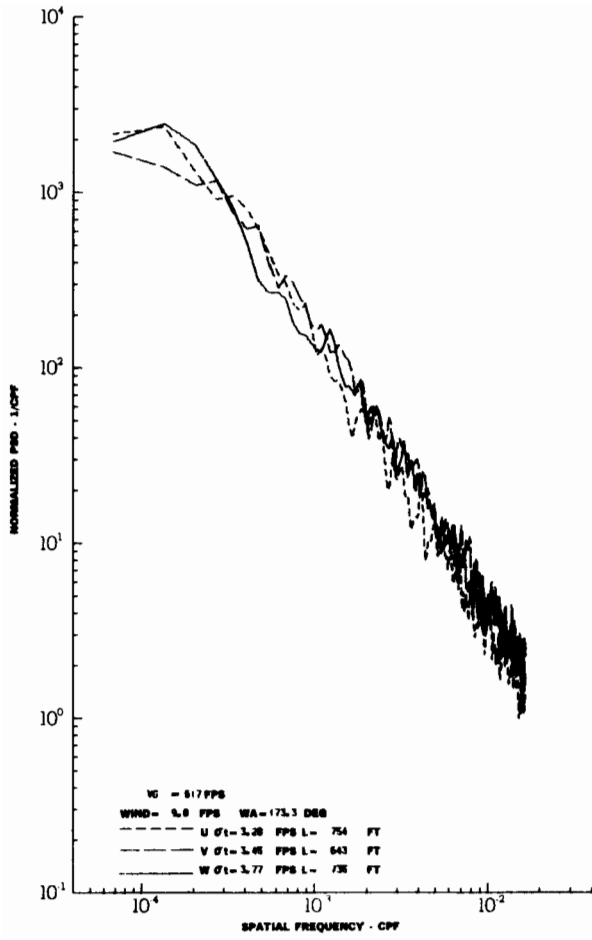
TURBULENCE SPECTRA DATA FOR TEST 29, LEG 7, CATEGORY 414324

FIGURE IV-16



TURBULENCE SPECTRA DATA FOR TEST 31, LEG 7, CATEGORY 421224

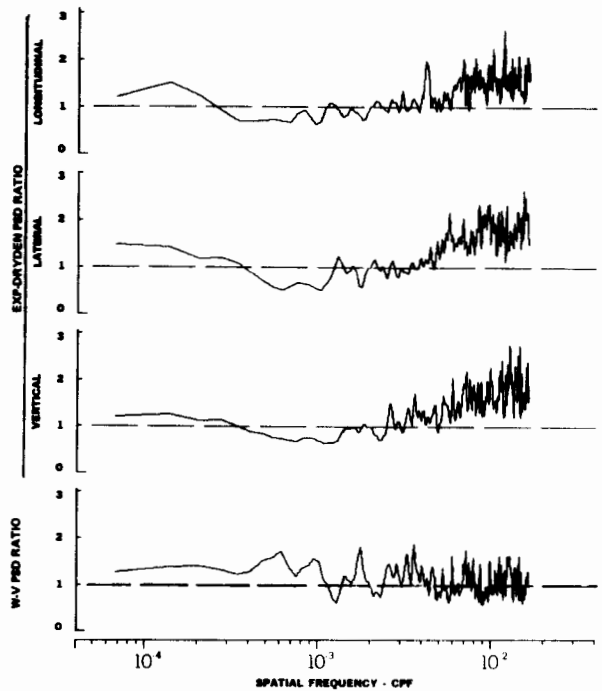
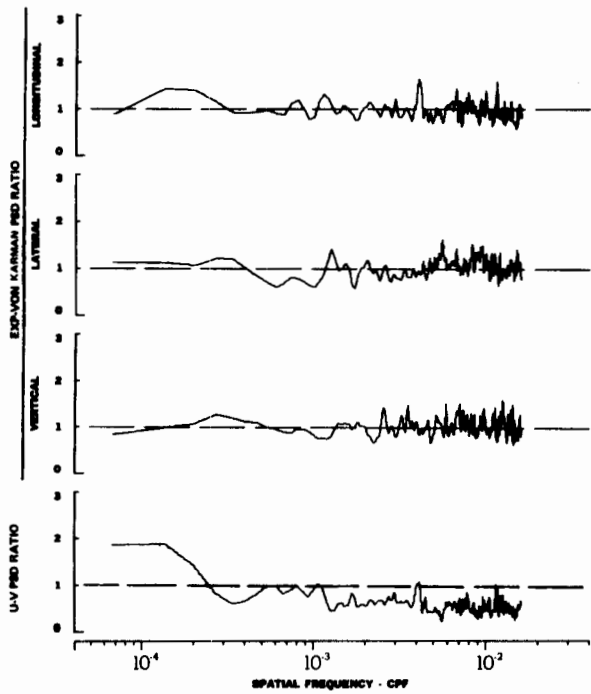
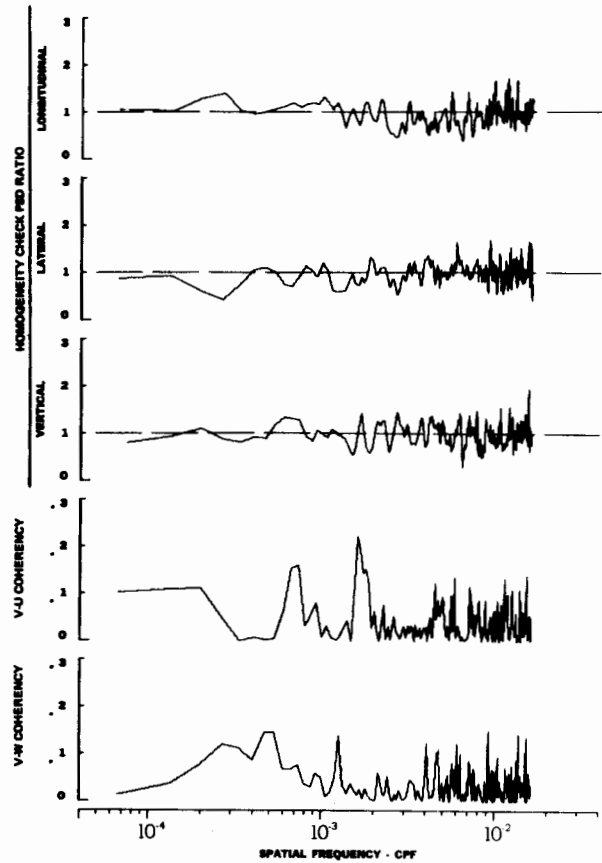
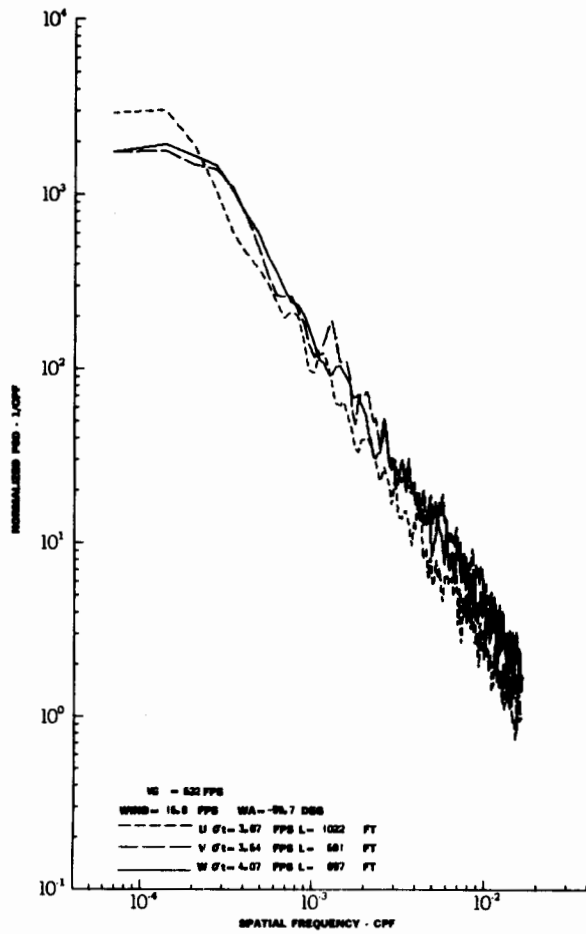
FIGURE IV-17



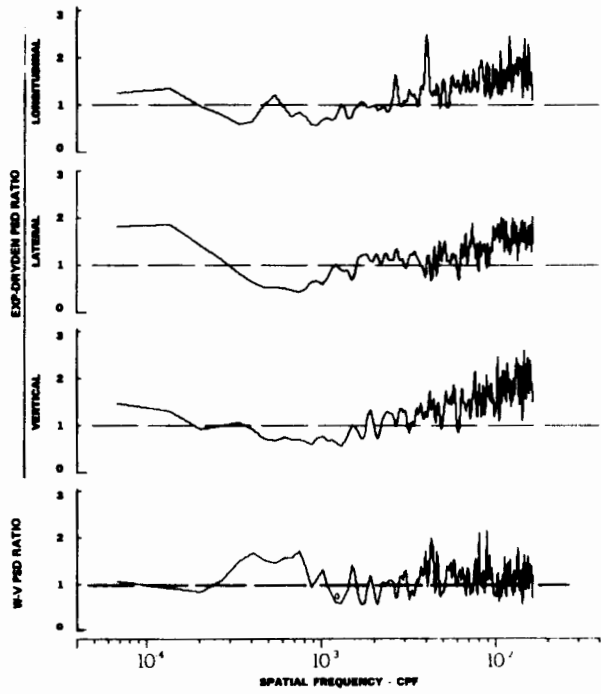
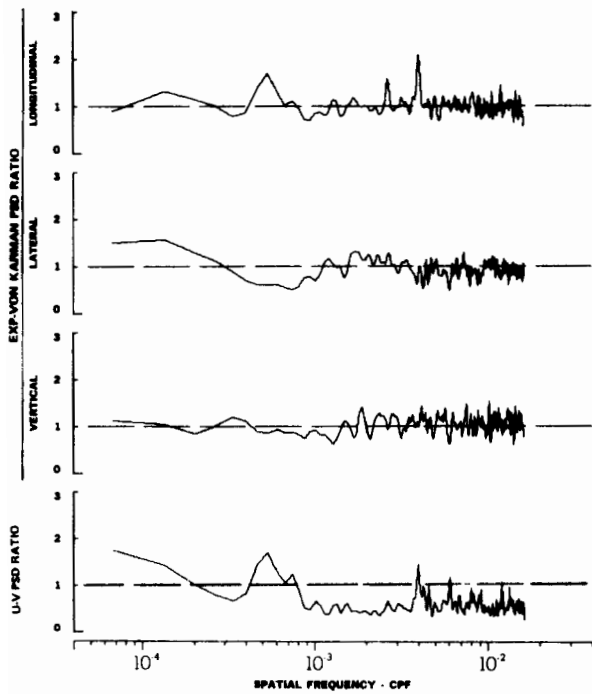
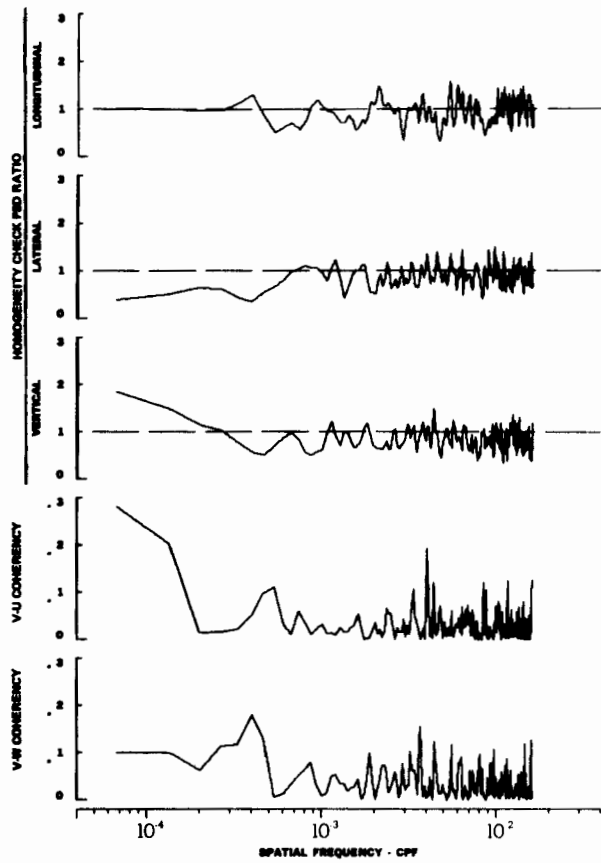
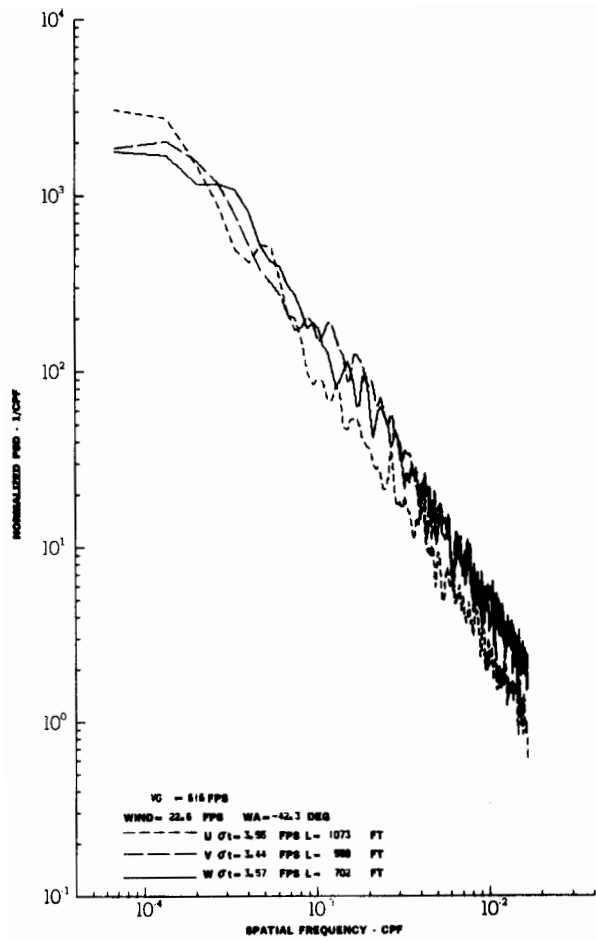
TURBULENCE SPECTRA DATA FOR TEST 32, LEG 2, CATEGORY 424324

FIGURE IV-18



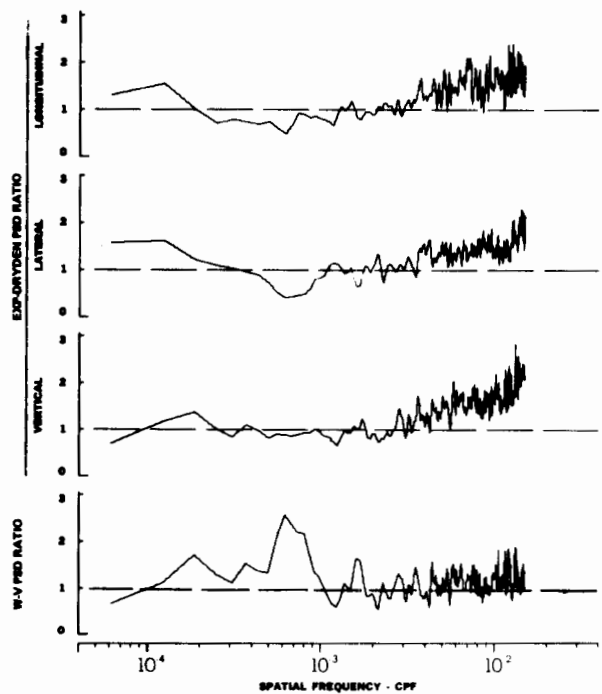
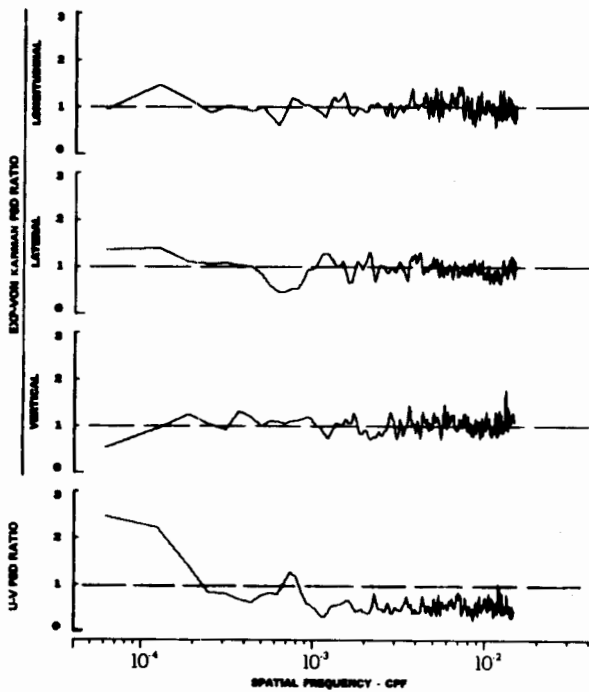
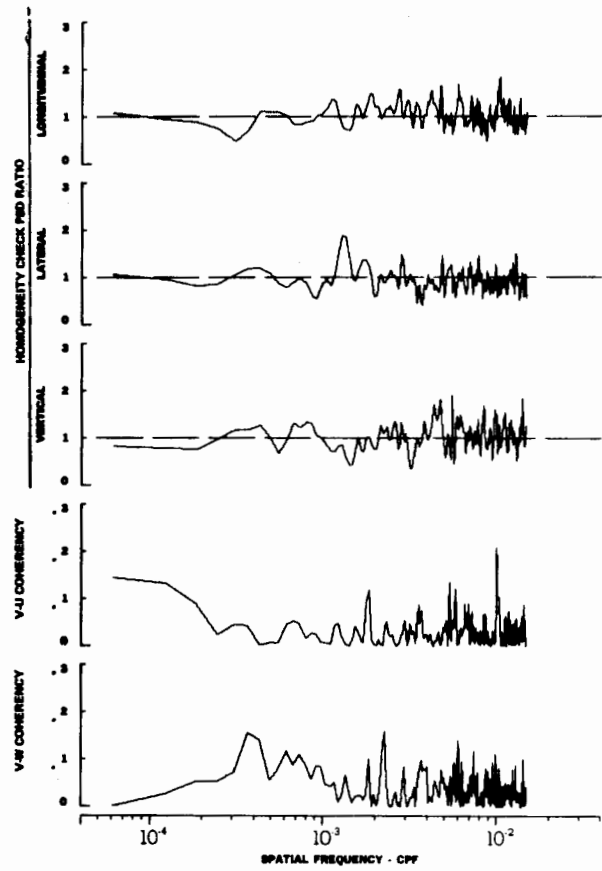
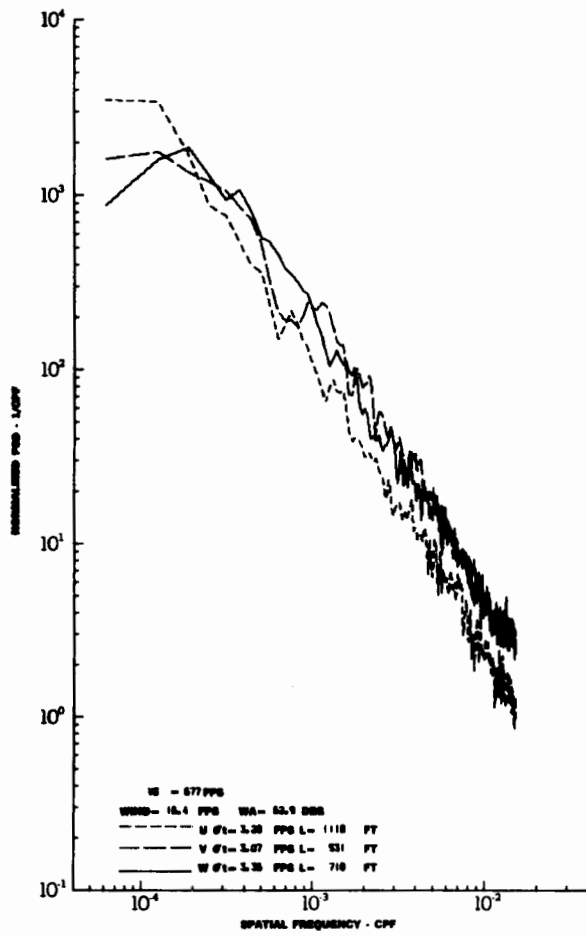


TURBULENCE SPECTRA DATA FOR TEST 32, LEG 4, CATEGORY 423324  
 FIGURE IV-19



TURBULENCE SPECTRA DATA FOR TEST 32, LEG 6, CATEGORY 424324

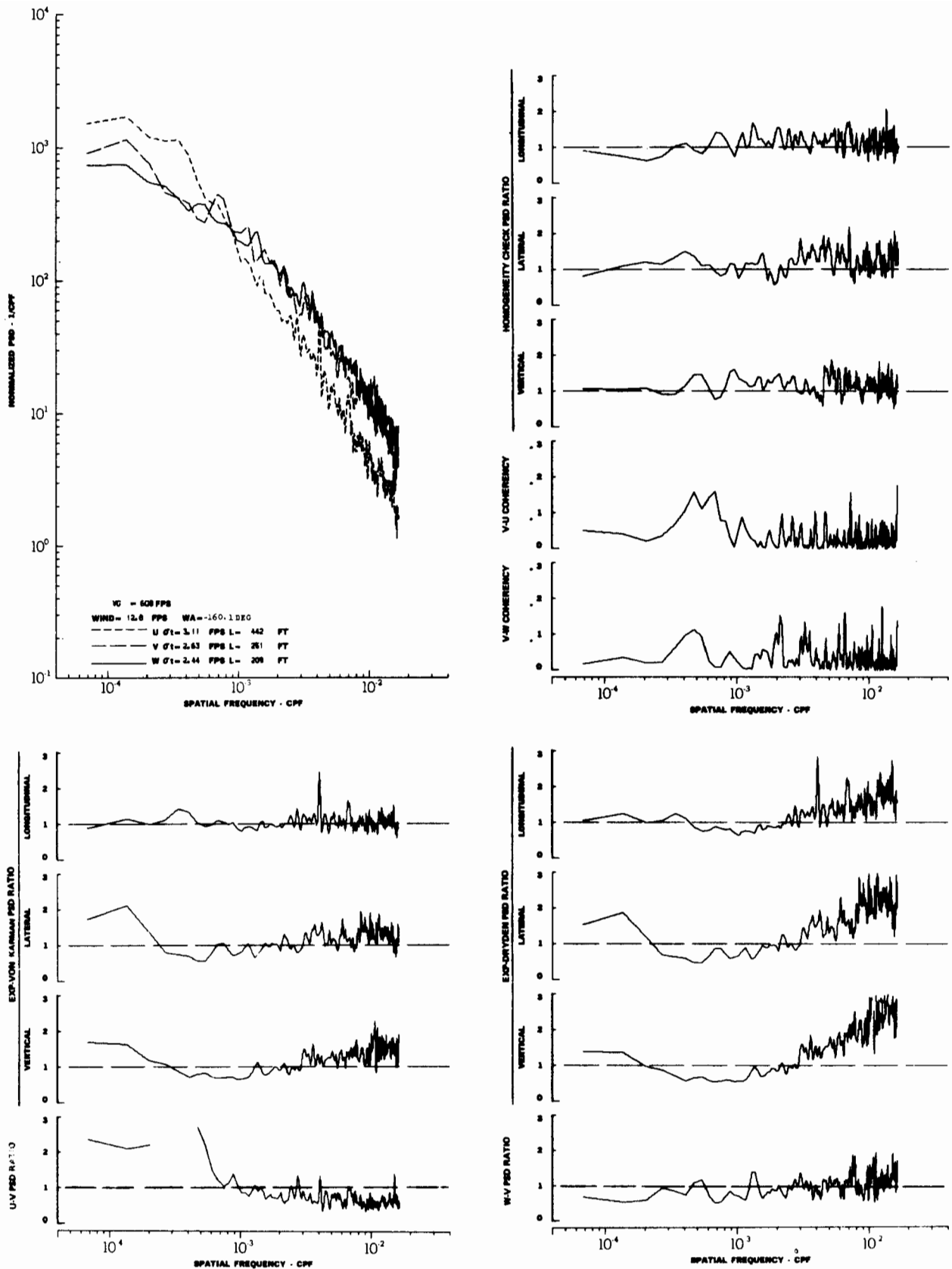
FIGURE IV-20



TURBULENCE SPECTRA DATA FOR TEST 32, LEG 8, CATEGORY 424324

FIGURE IV-21

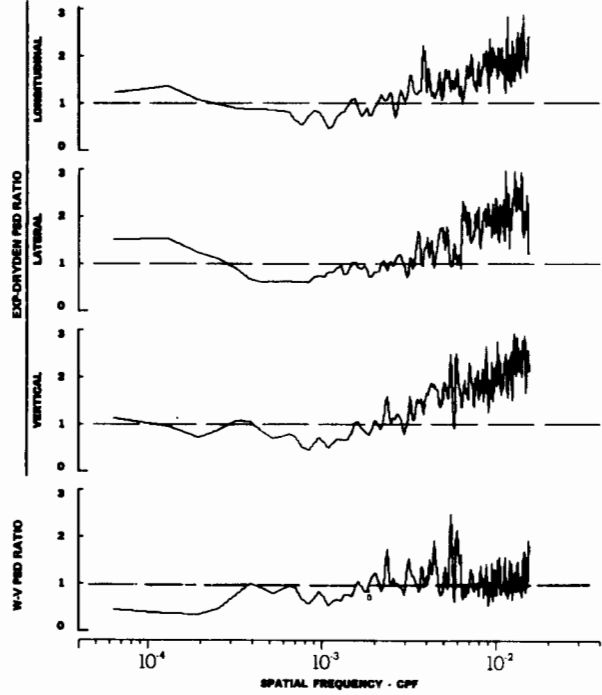
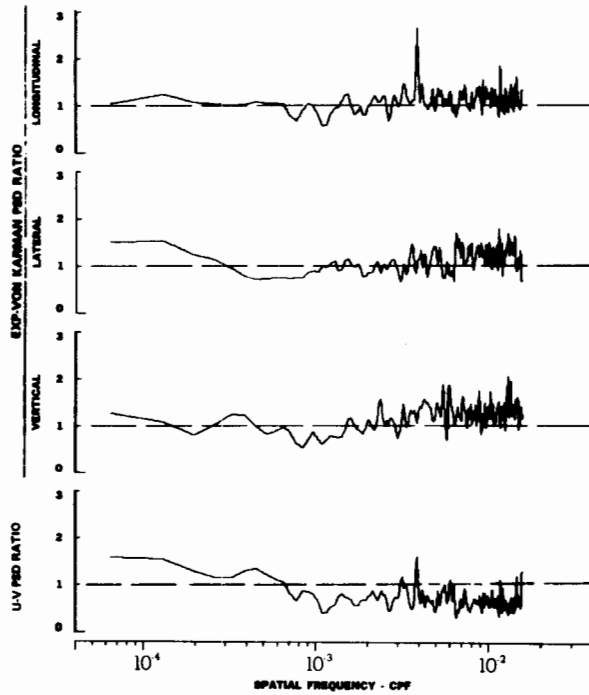
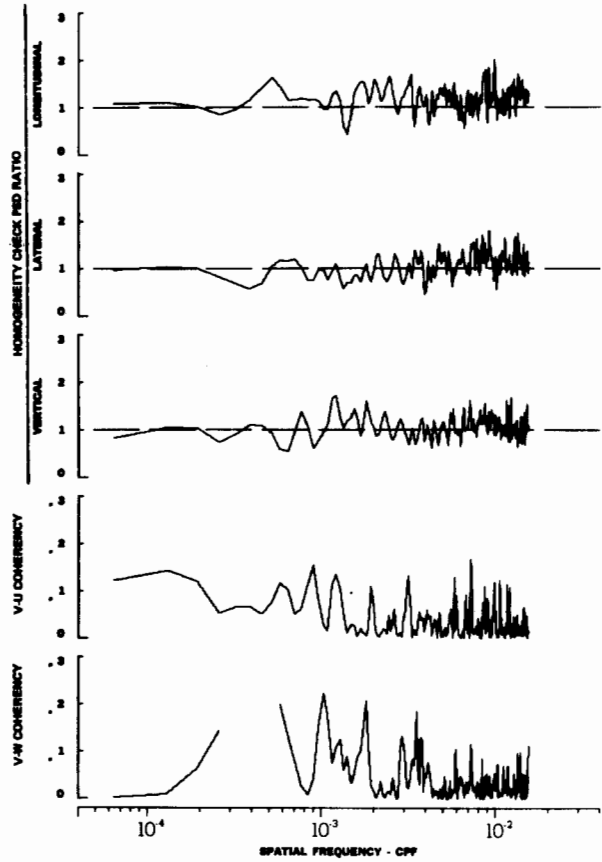
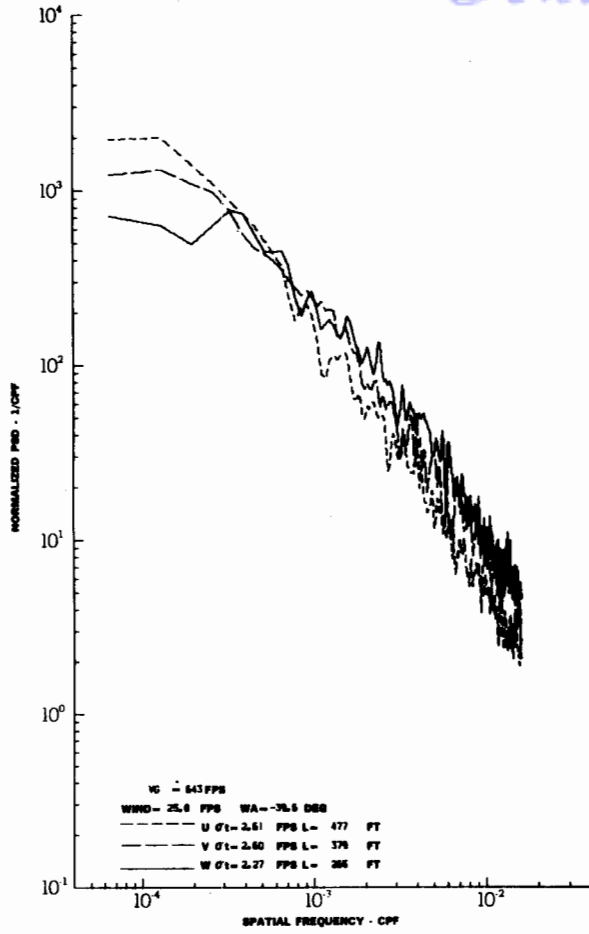
# Contrails



TURBULENCE SPECTRA DATA FOR TEST 34, LEG 2, CATEGORY 411224

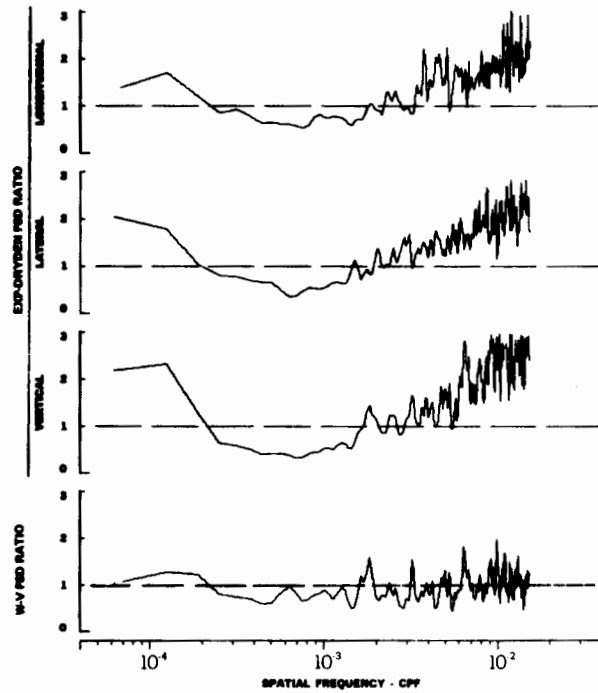
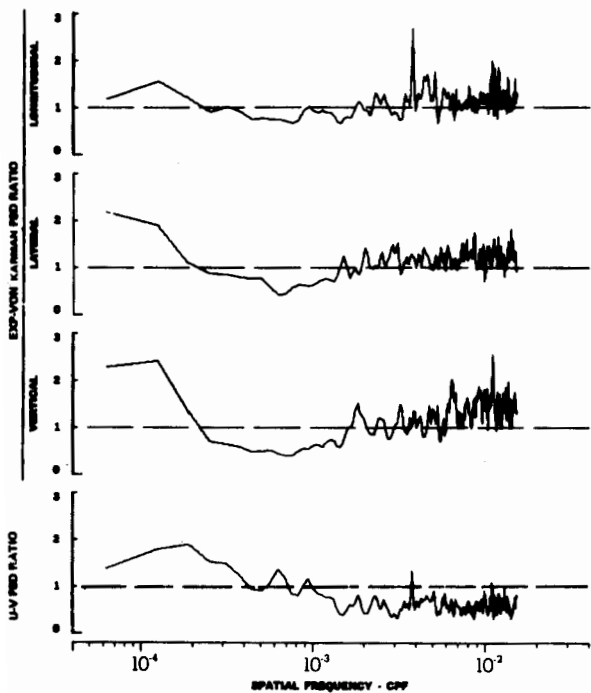
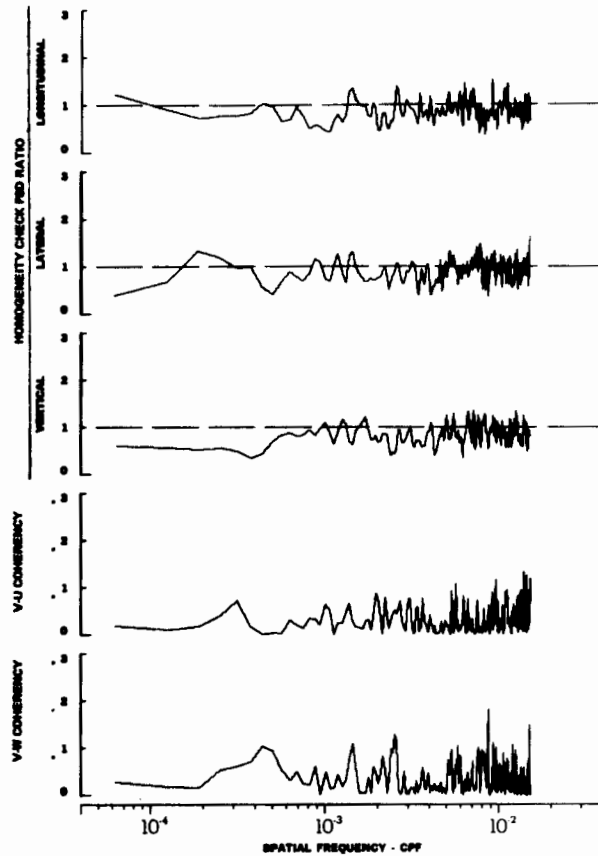
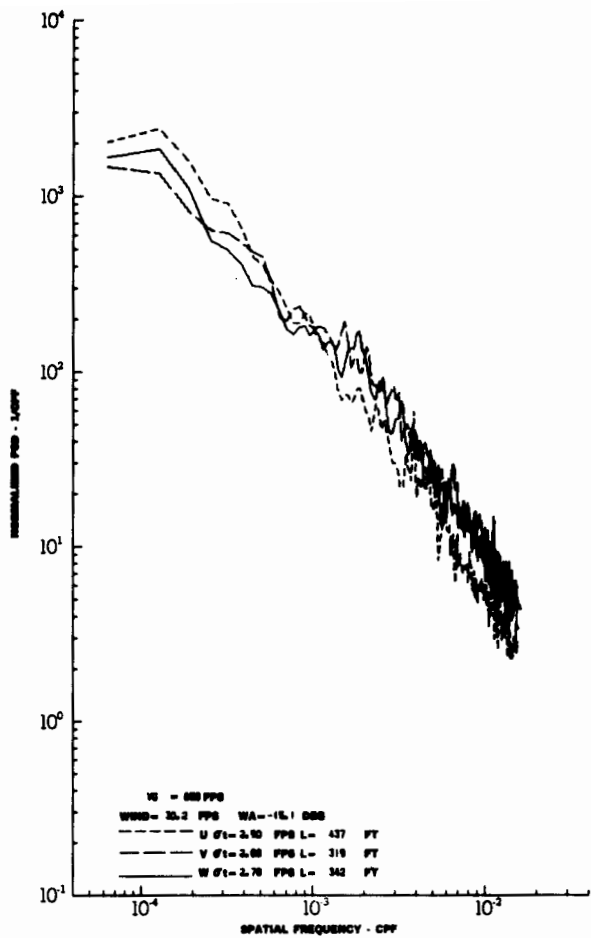
FIGURE IV-22

# Contrails



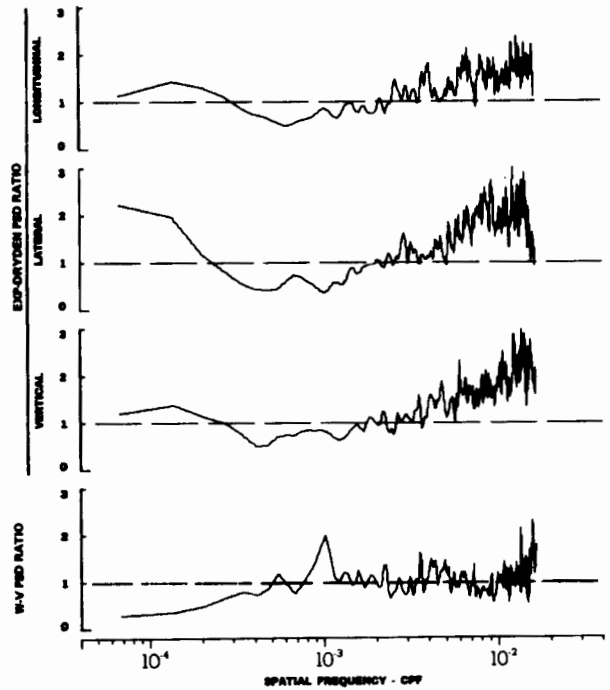
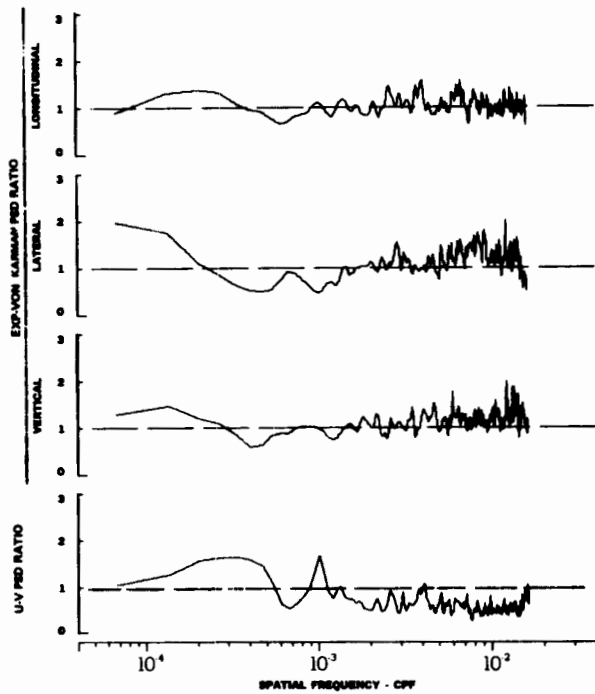
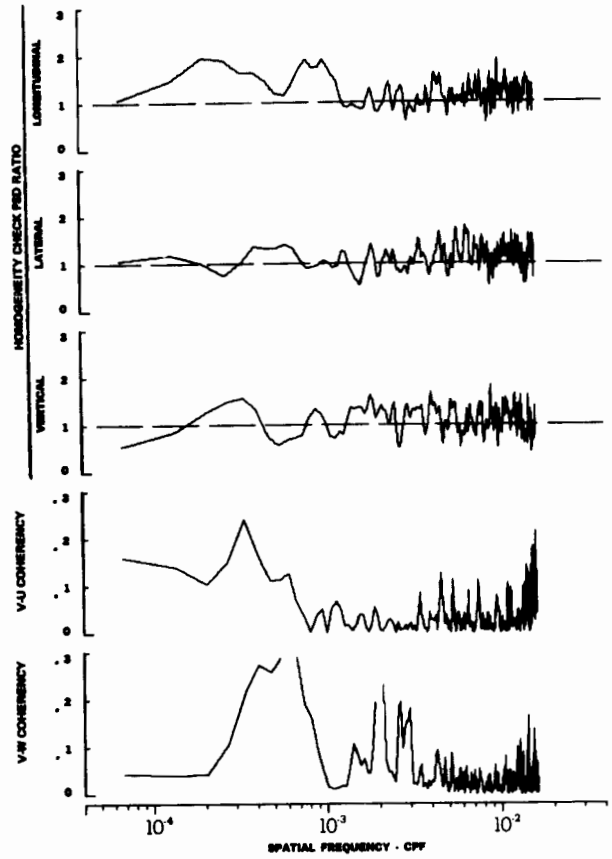
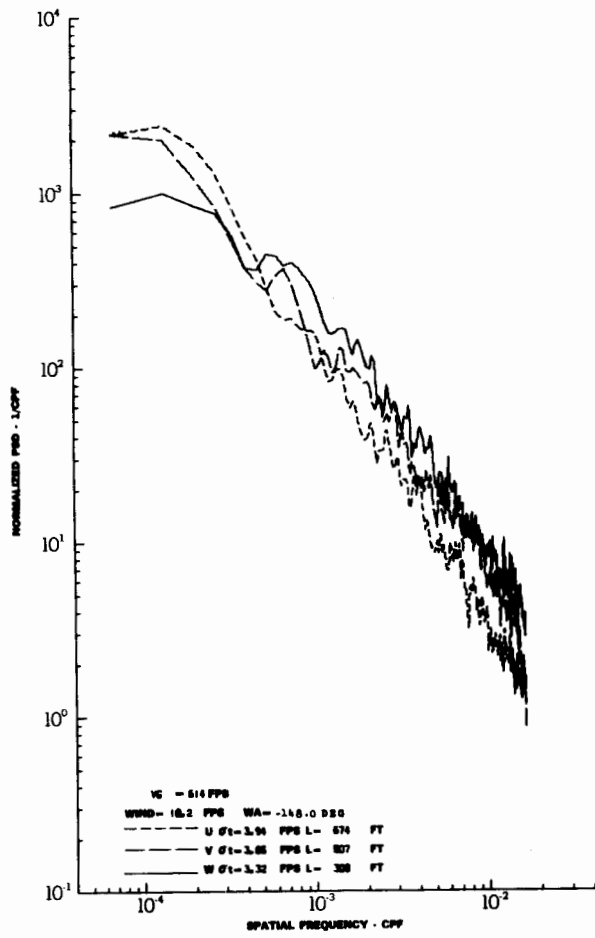
TURBULENCE SPECTRA DATA FOR TEST 34, LEG 4, CATEGORY 412224

FIGURE IV-23



TURBULENCE SPECTRA DATA FOR TEST 34, LEG 6, CATEGORY 413224

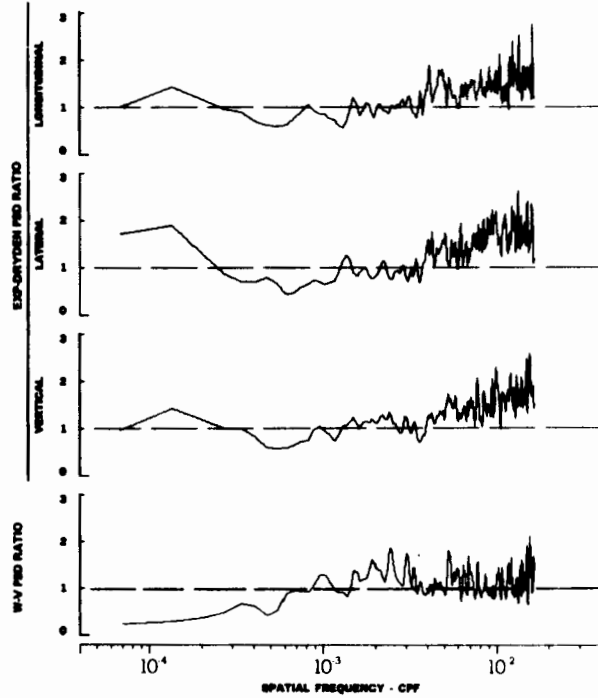
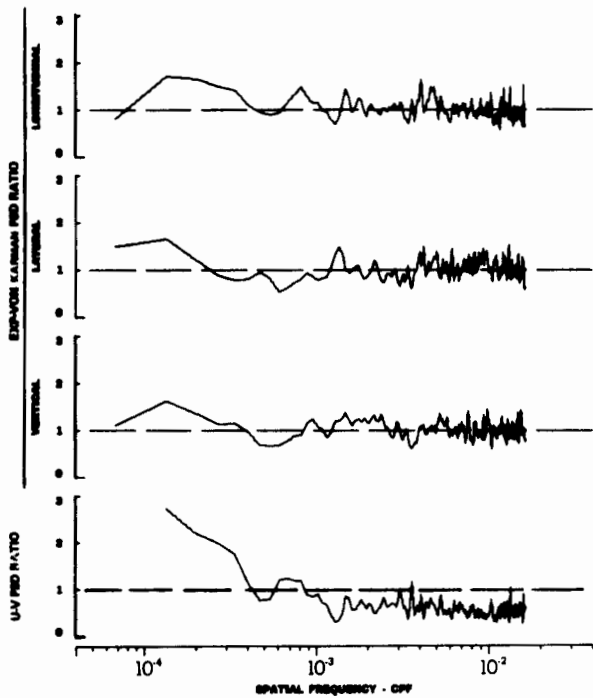
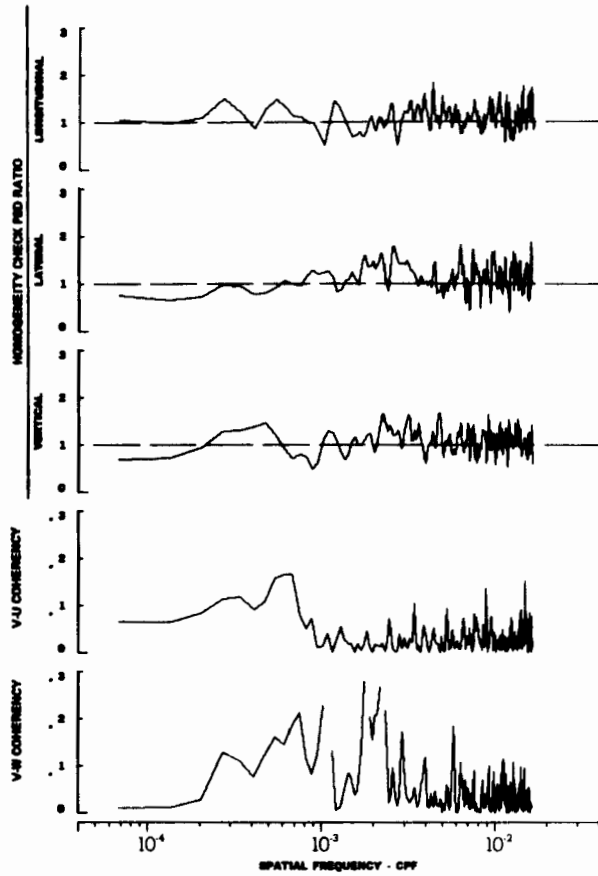
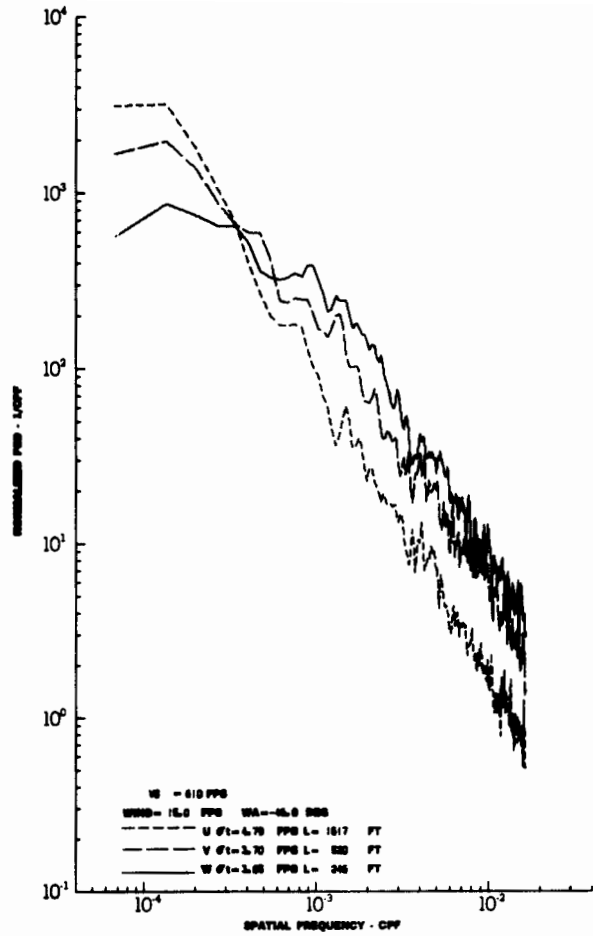
FIGURE IV-24



TURBULENCE SPECTRA DATA FOR TEST 35, LEG 1, CATEGORY 411324

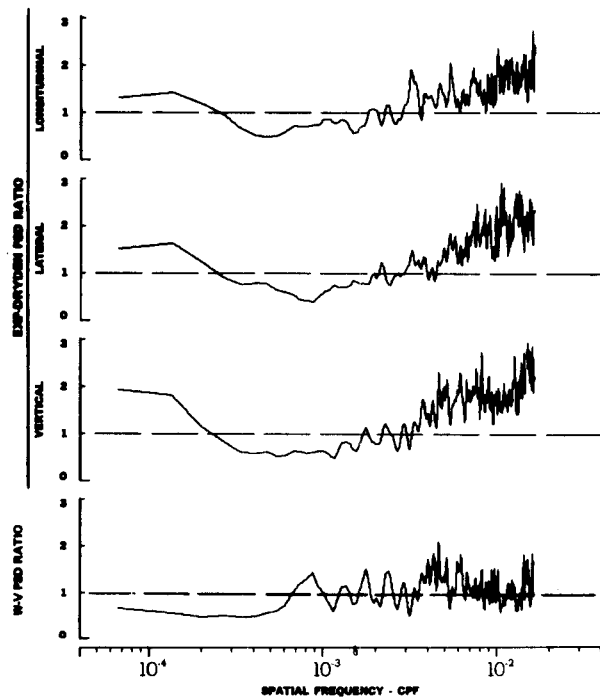
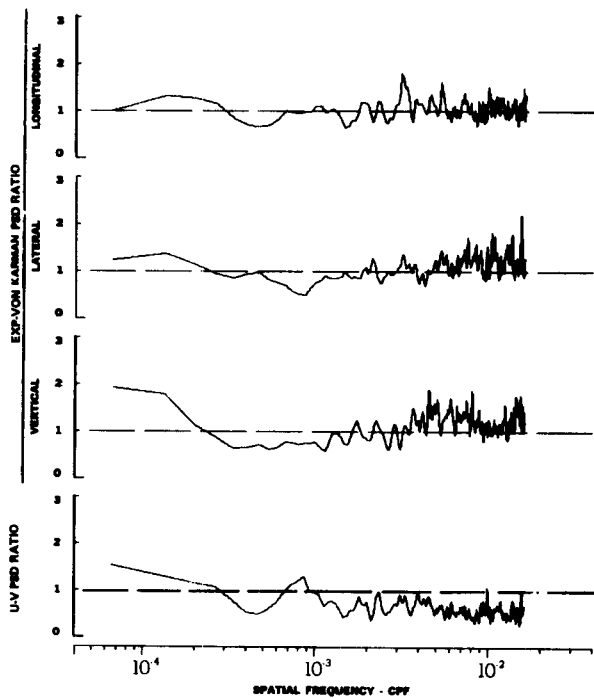
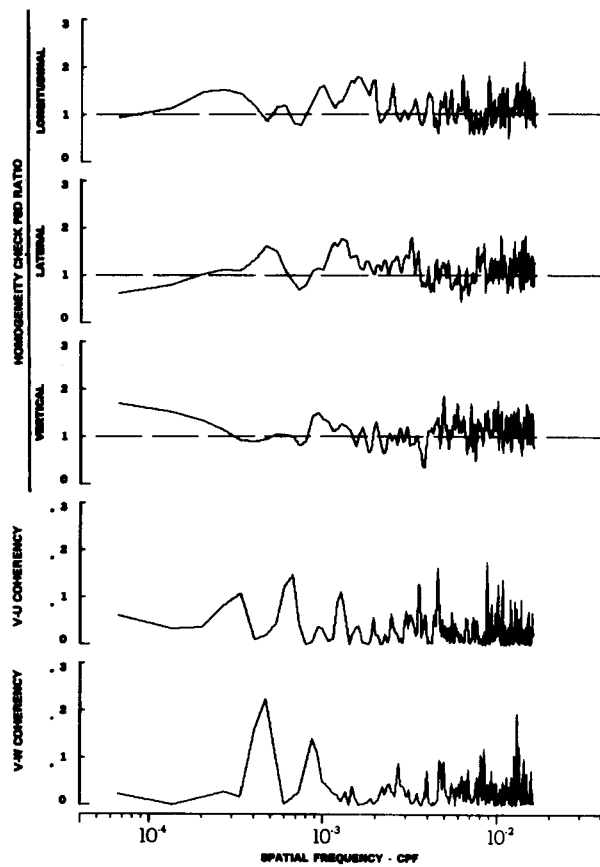
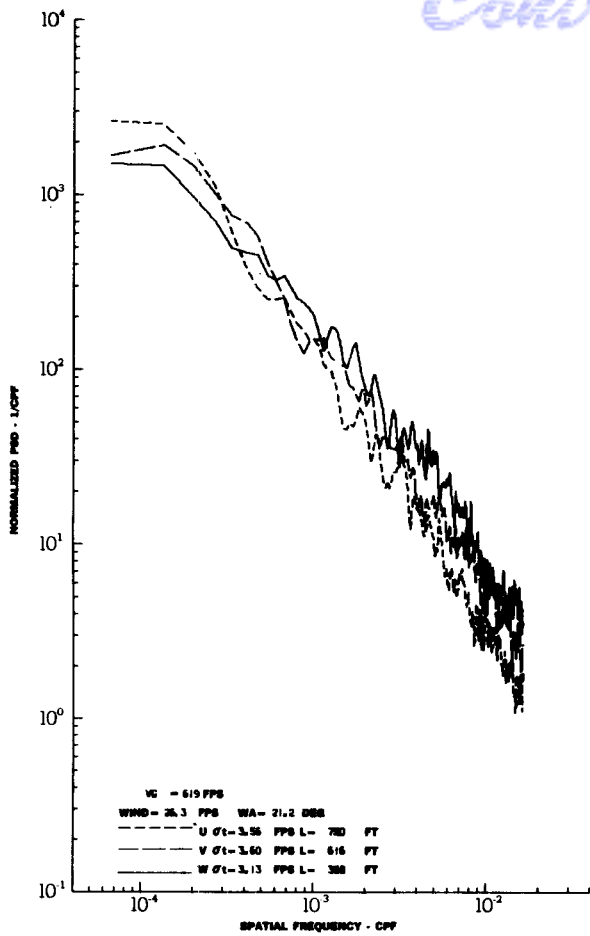
FIGURE IV-25





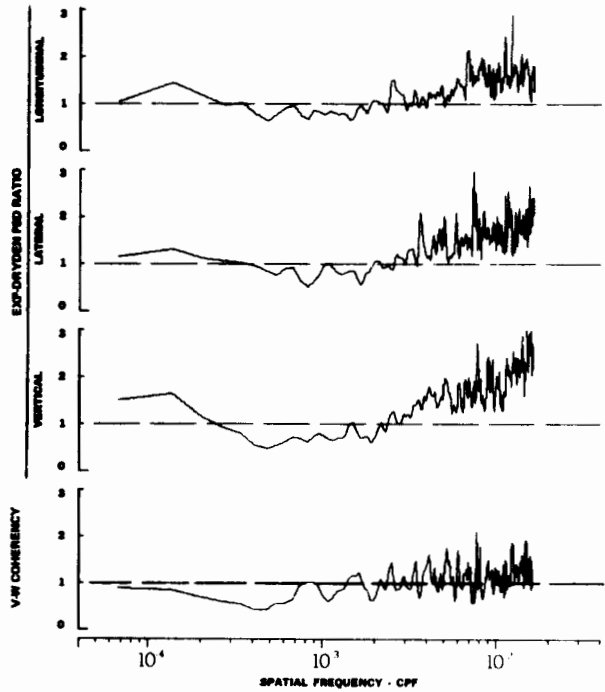
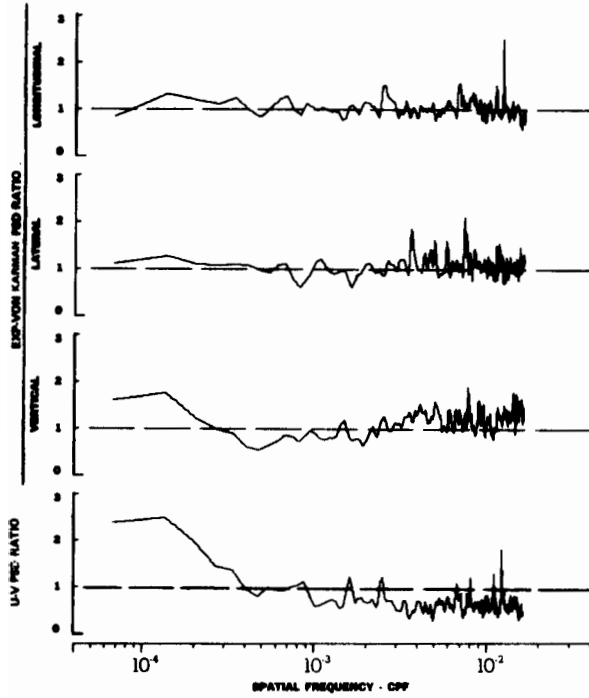
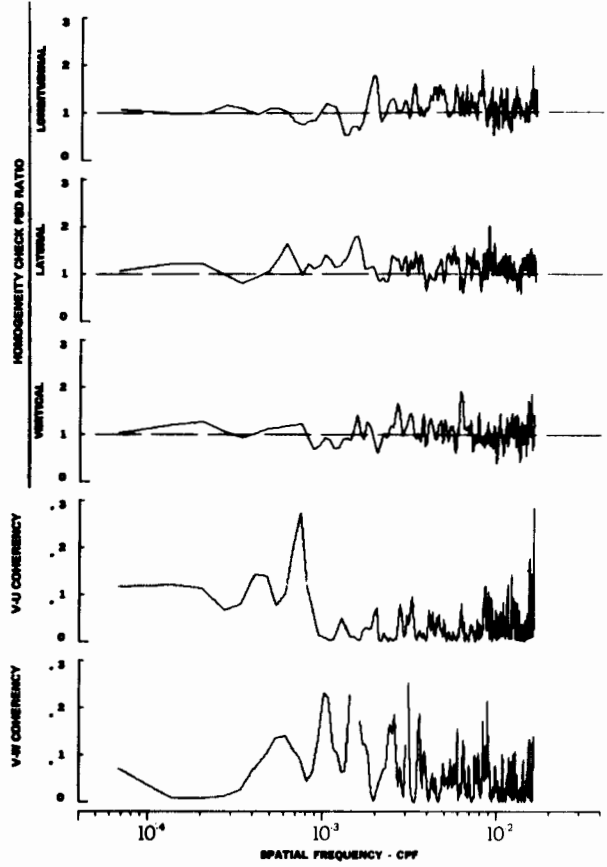
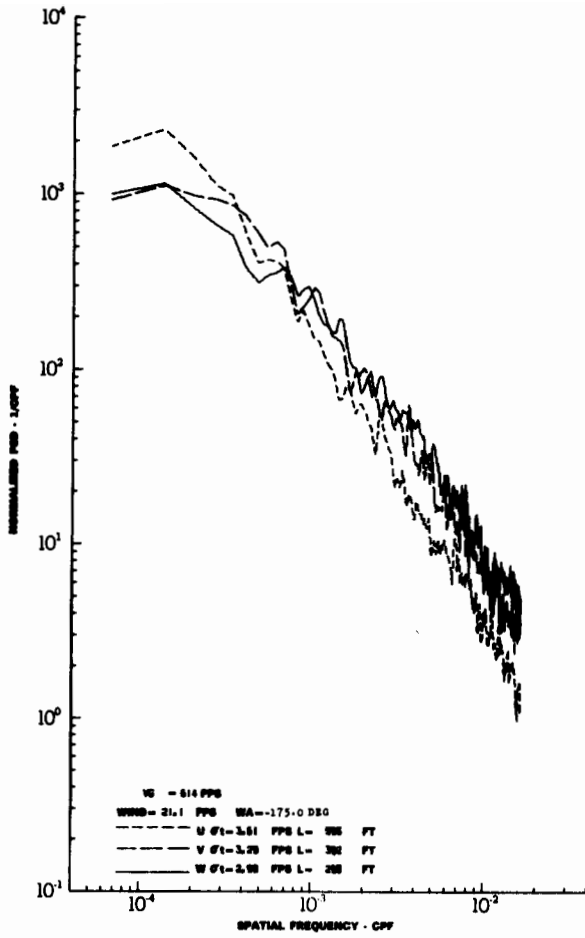
TURBULENCE SPECTRA DATA FOR TEST 35, LEG 3, CATEGORY 413324

FIGURE IV-26



TURBULENCE SPECTRA DATA FOR TEST 35, LEG 5, CATEGORY 413324

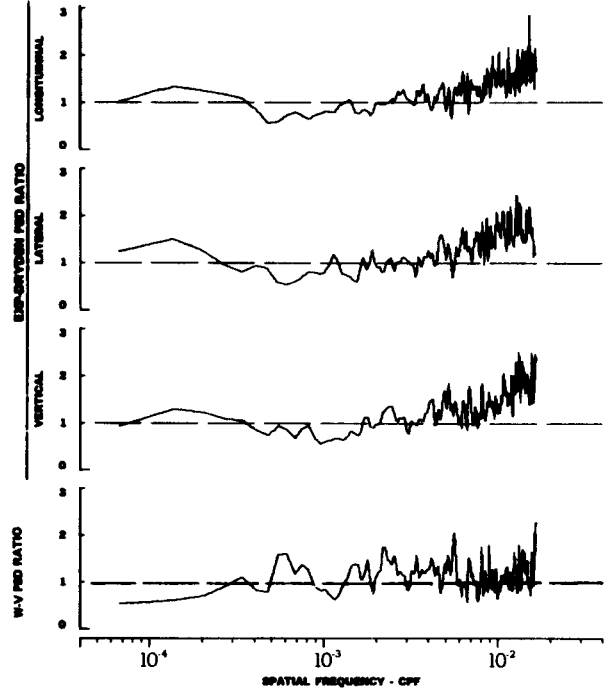
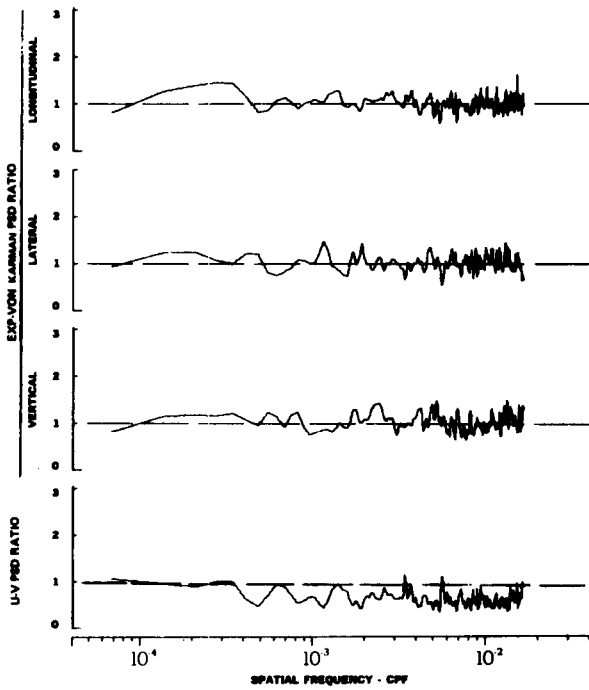
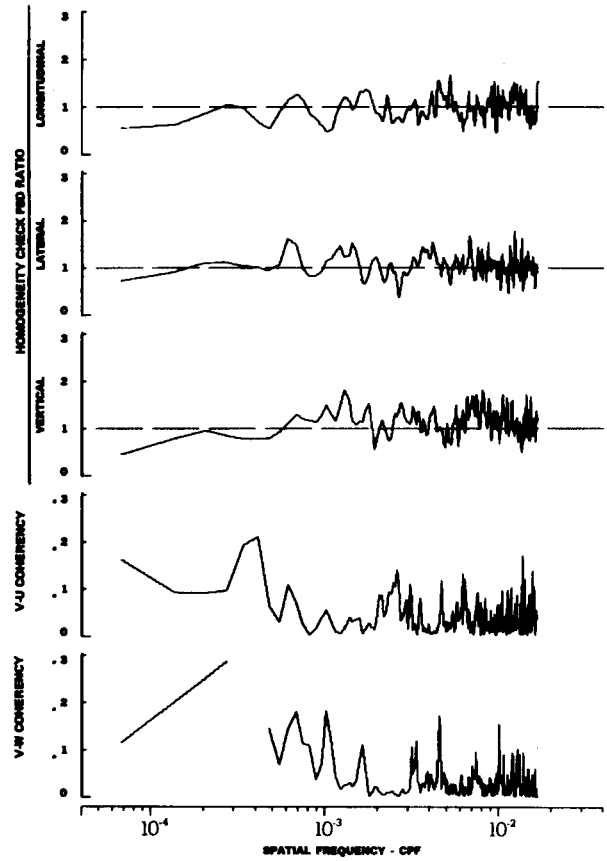
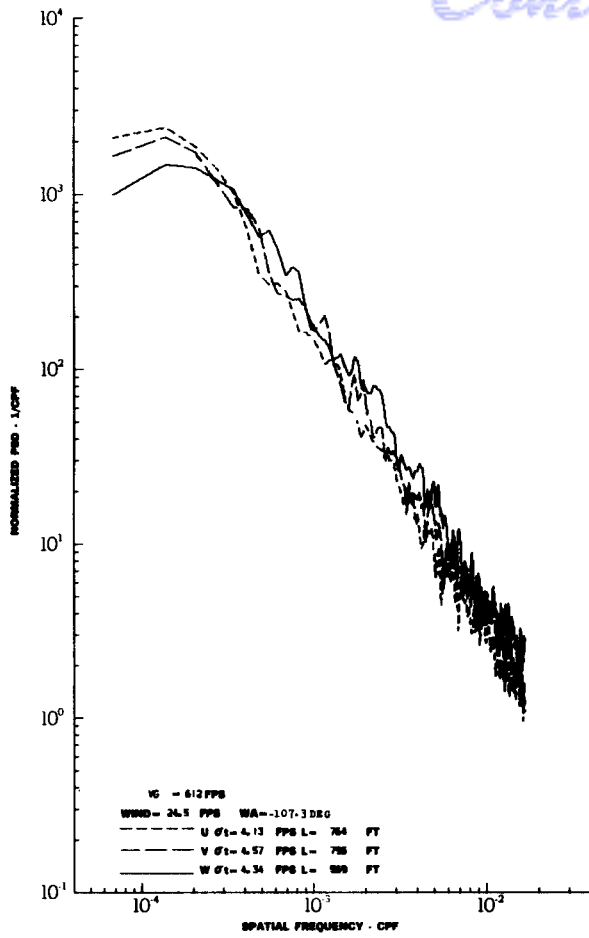
FIGURE IV-27



TURBULENCE SPECTRA DATA FOR TEST 37, LEG 7, CATEGORY 422224

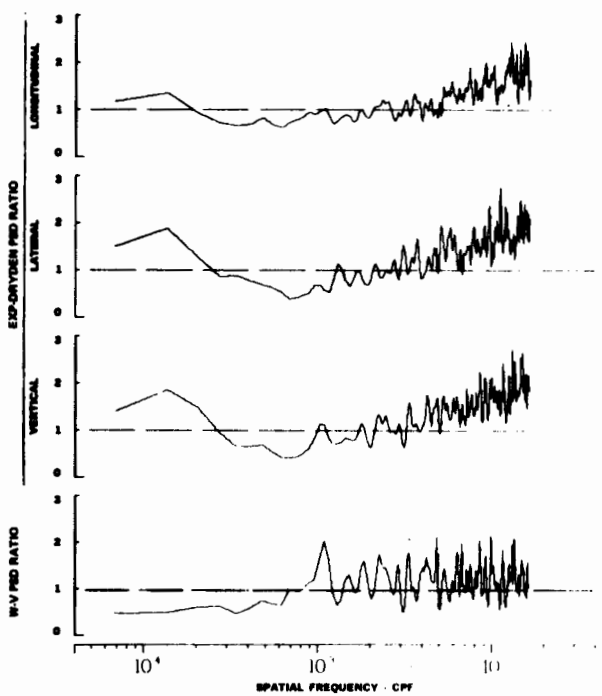
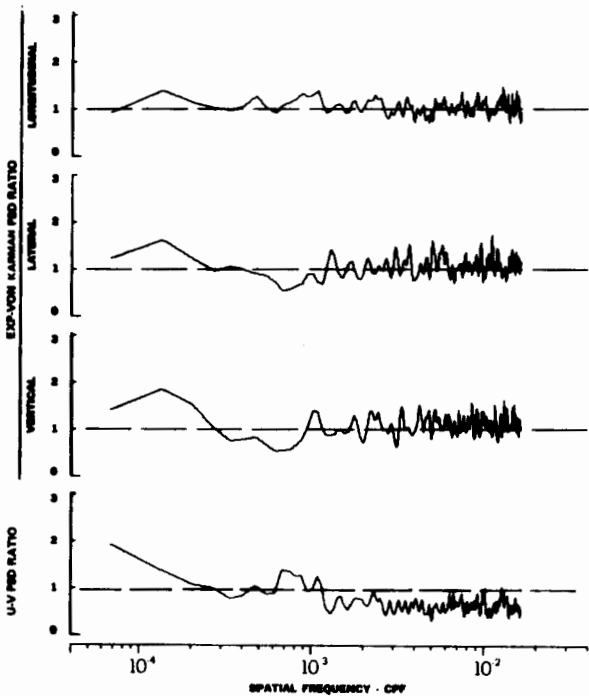
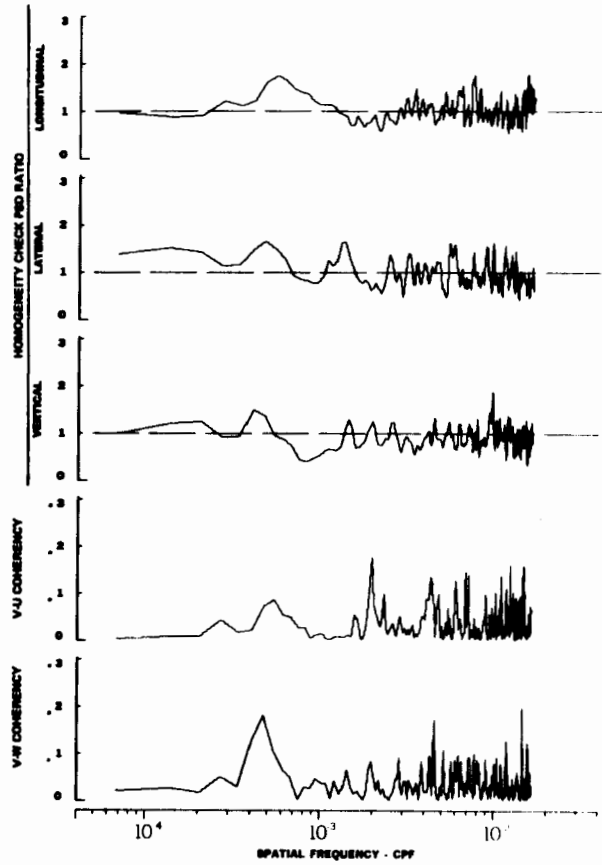
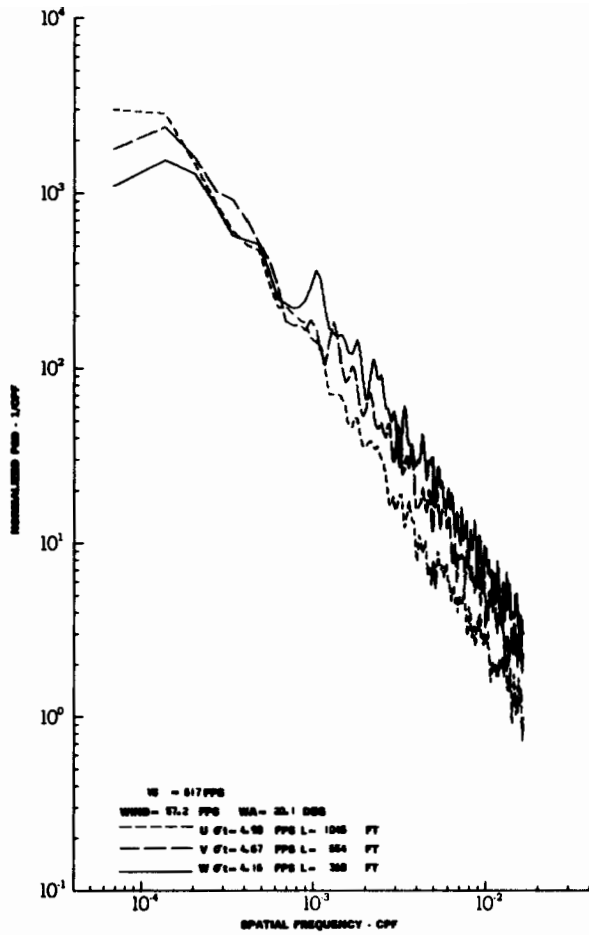
FIGURE IV-28

# Contrails



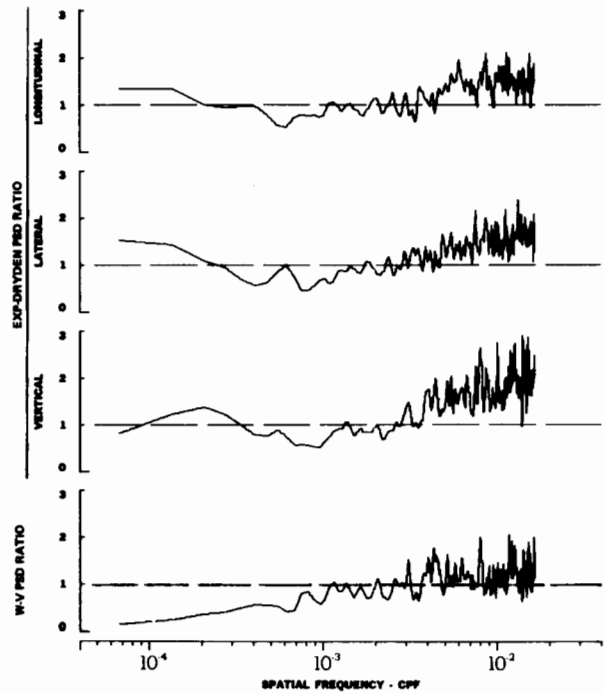
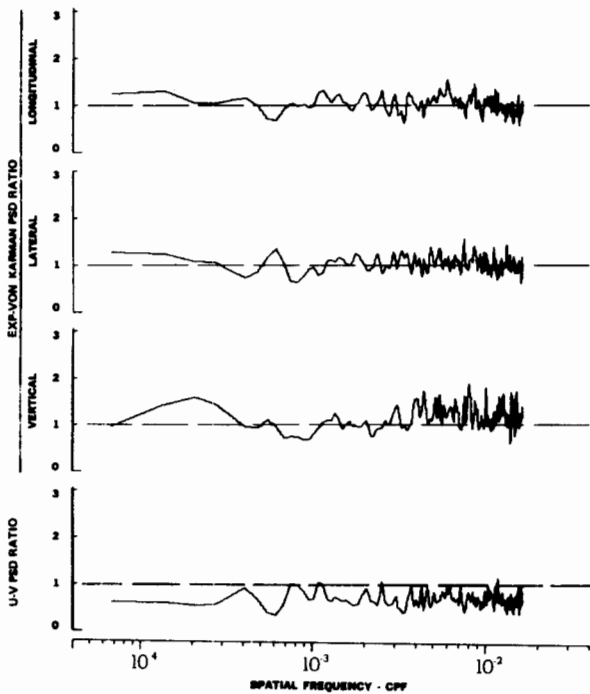
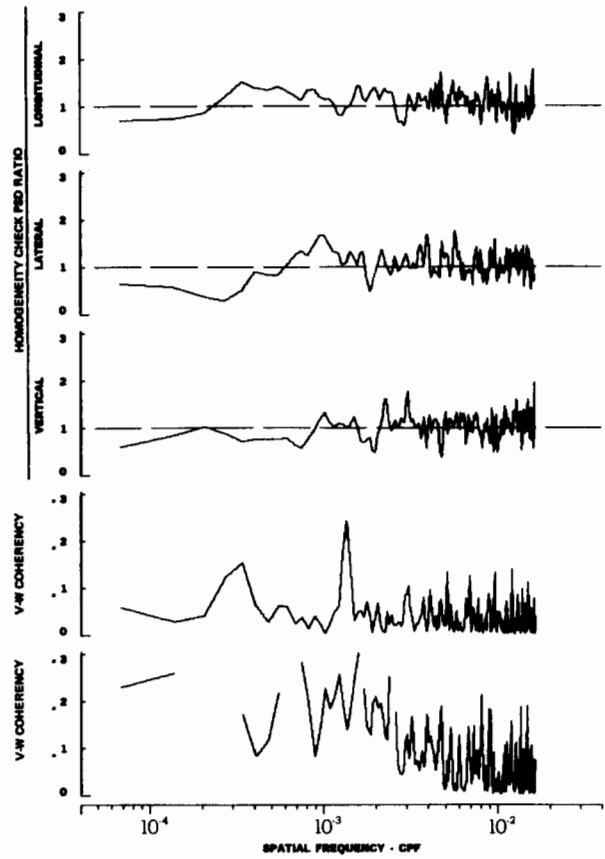
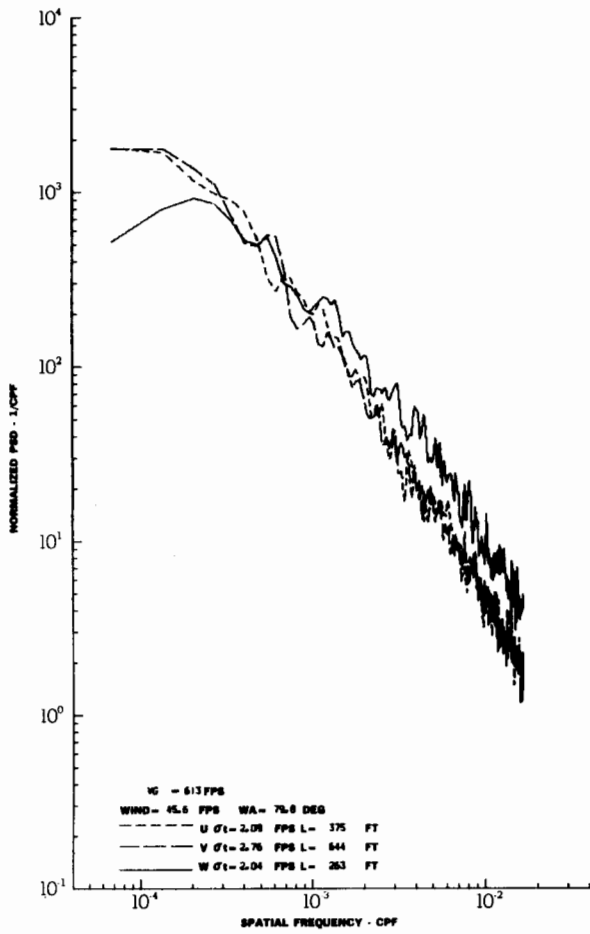
TURBULENCE SPECTRA DATA FOR TEST 38, LEG 2, CATEGORY 424324

FIGURE IV-29



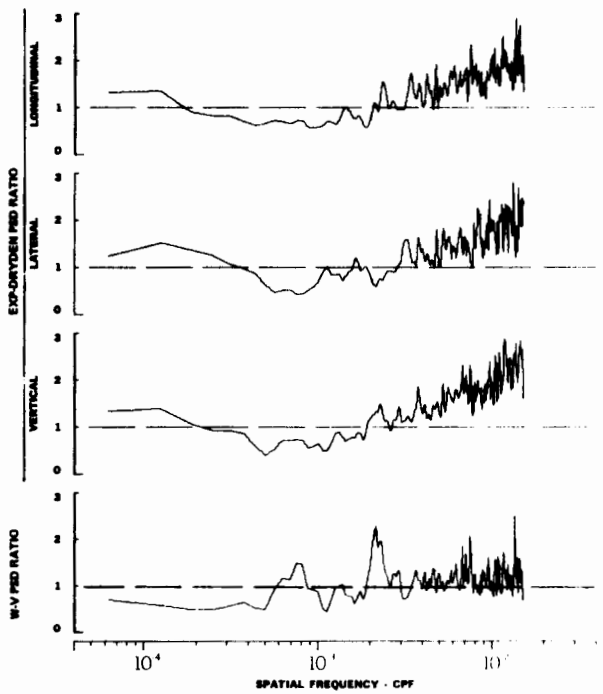
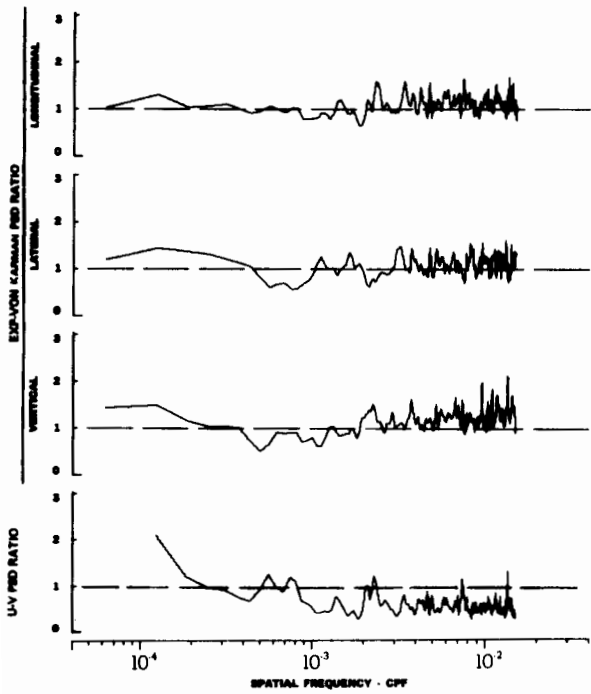
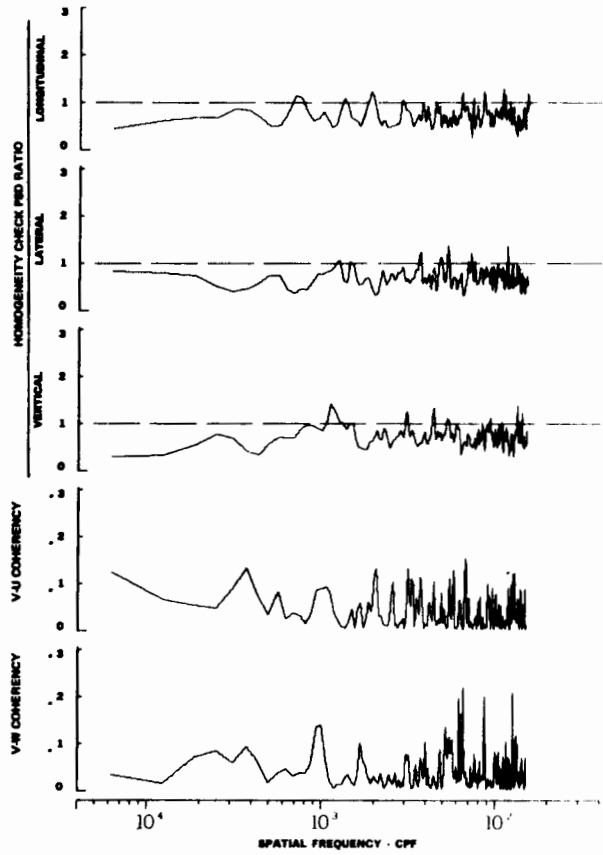
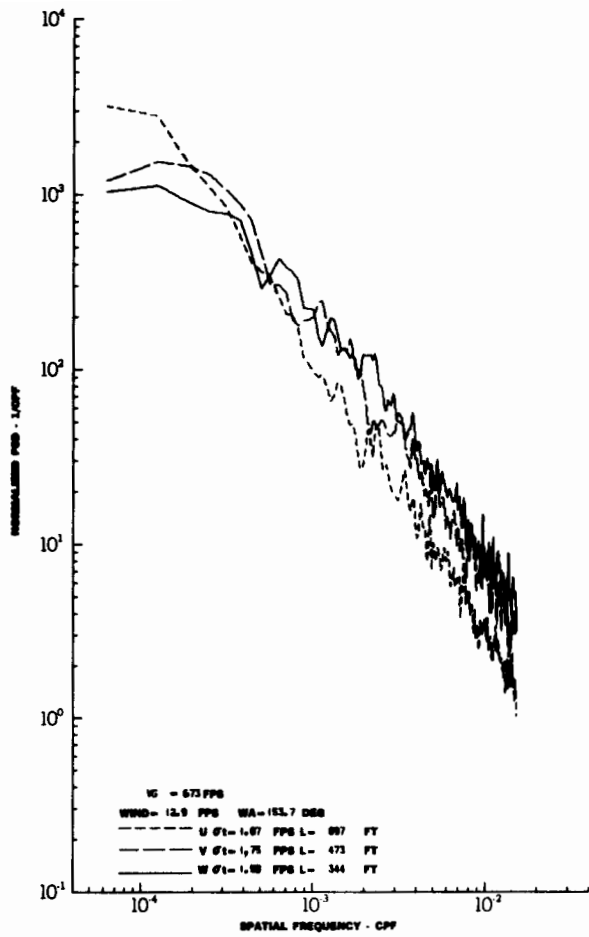
TURBULENCE SPECTRA DATA FOR TEST 38, LEG 4, CATEGORY 423324

FIGURE IV-30



TURBULENCE SPECTRA DATA FOR TEST 38, LEG 6, CATEGORY 423324

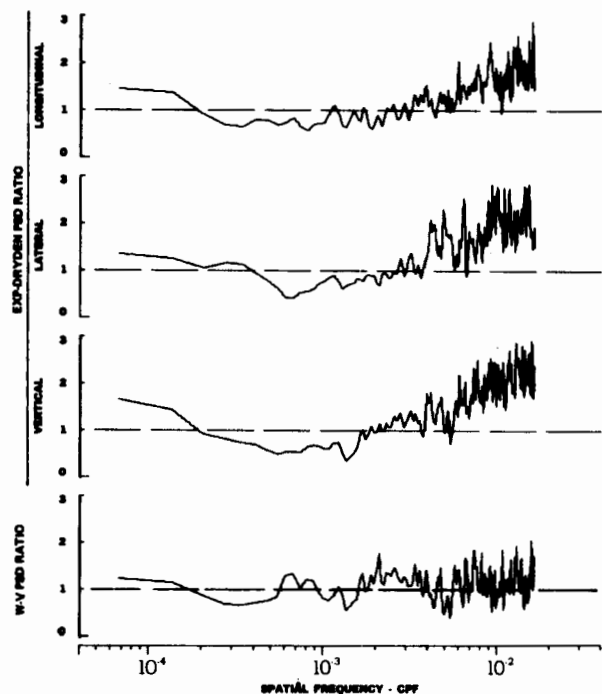
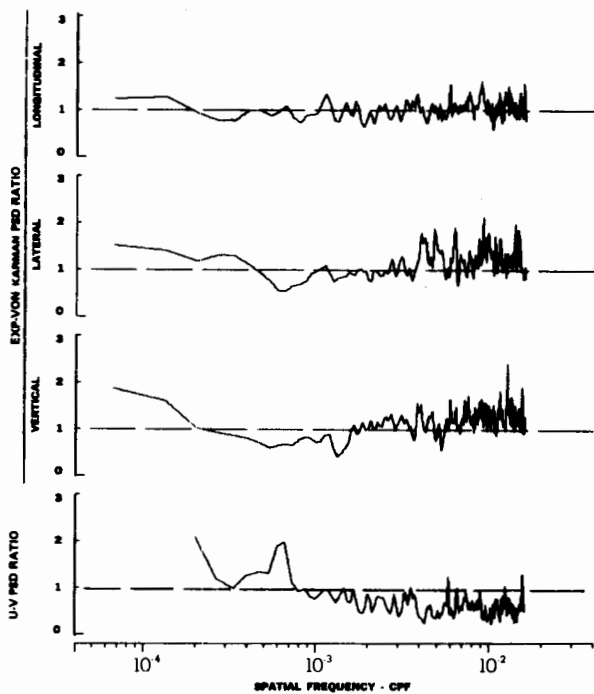
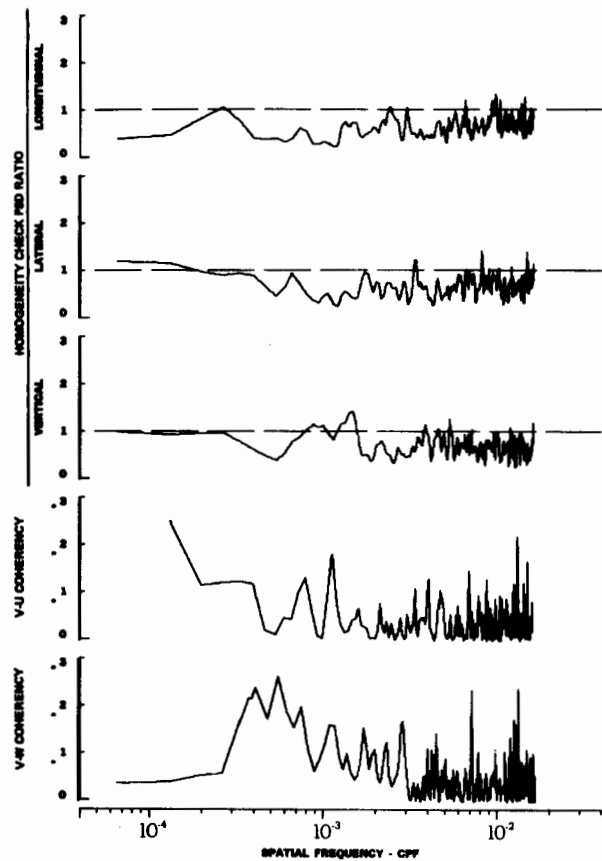
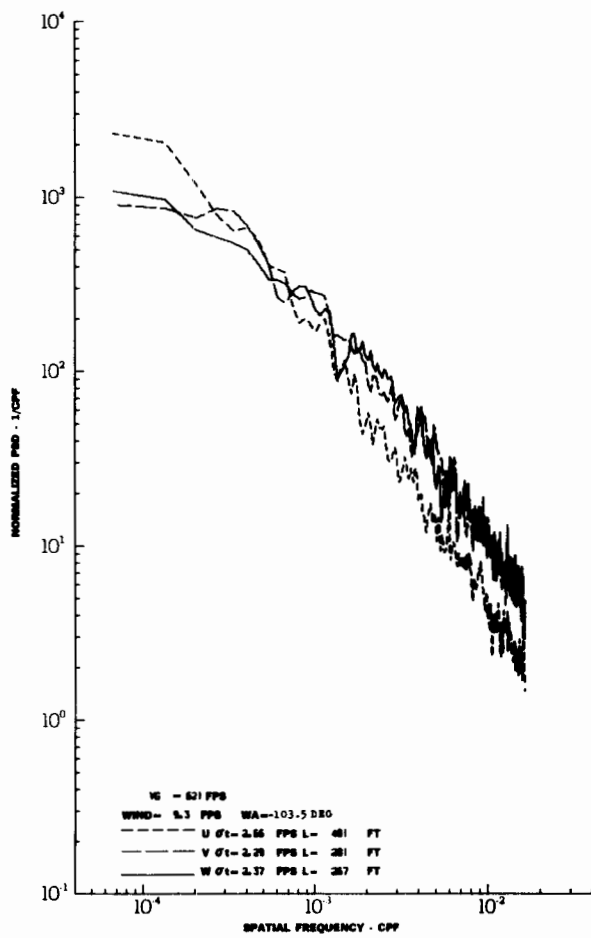
FIGURE IV-31



TURBULENCE SPECTRA DATA FOR TEST 38, LEG 8, CATEGORY 424324

FIGURE IV-32

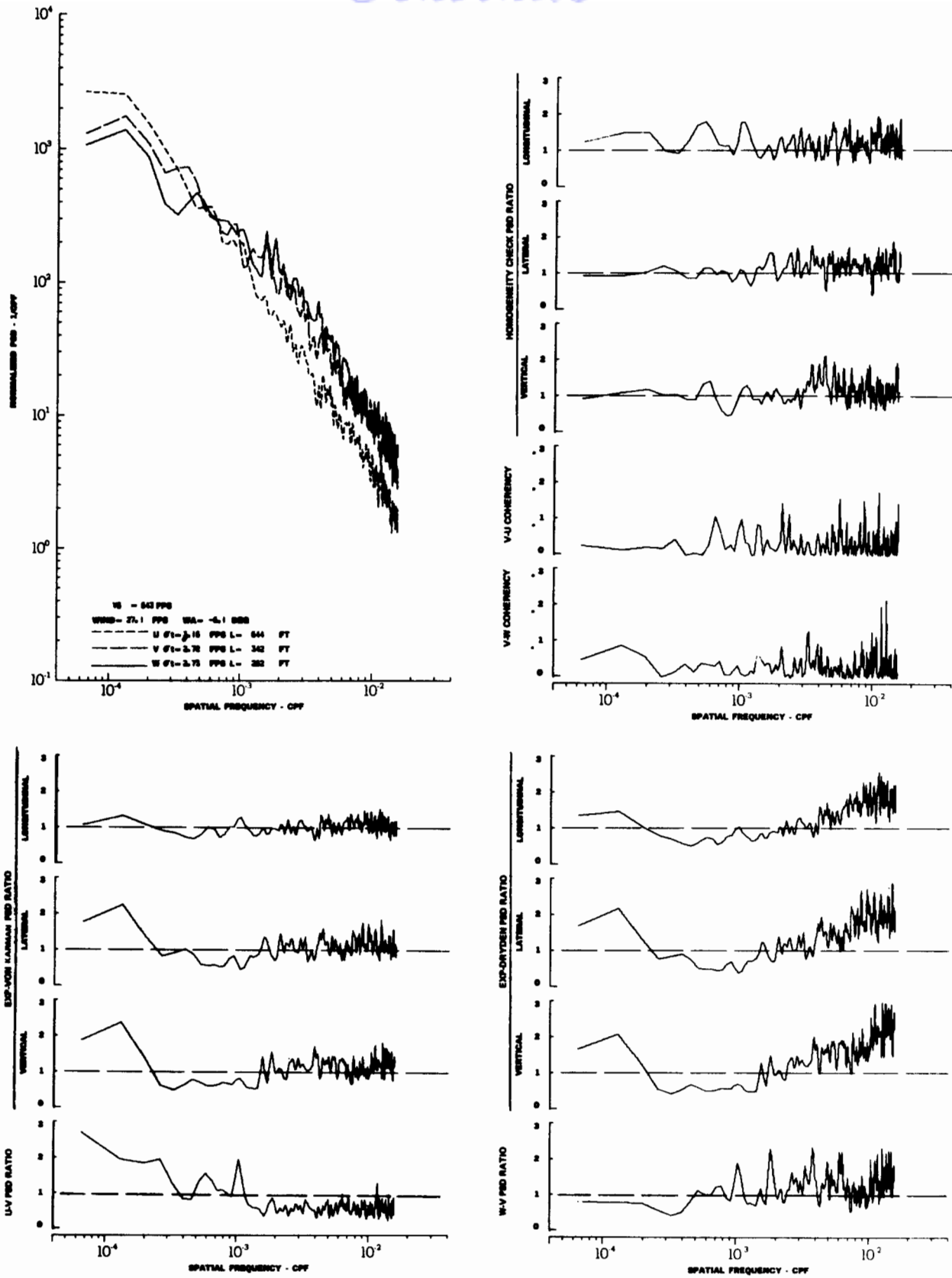




TURBULENCE SPECTRA DATA FOR TEST 40, LEG 2, CATEGORY 411234

FIGURE IV-33

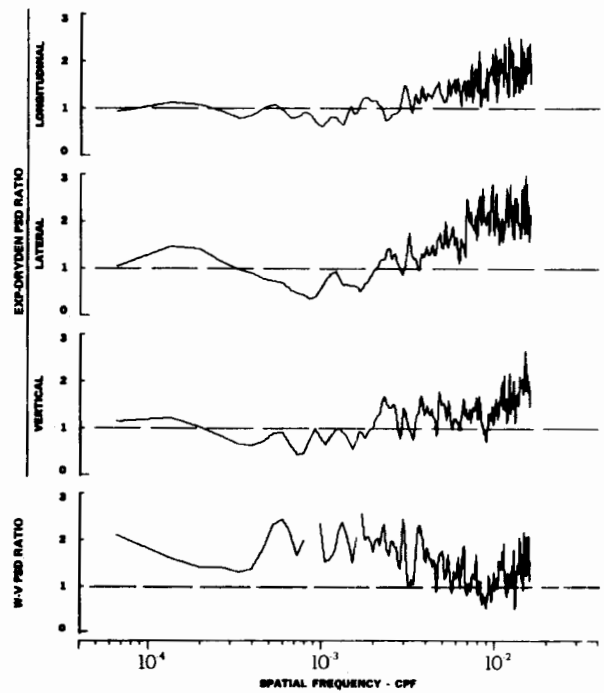
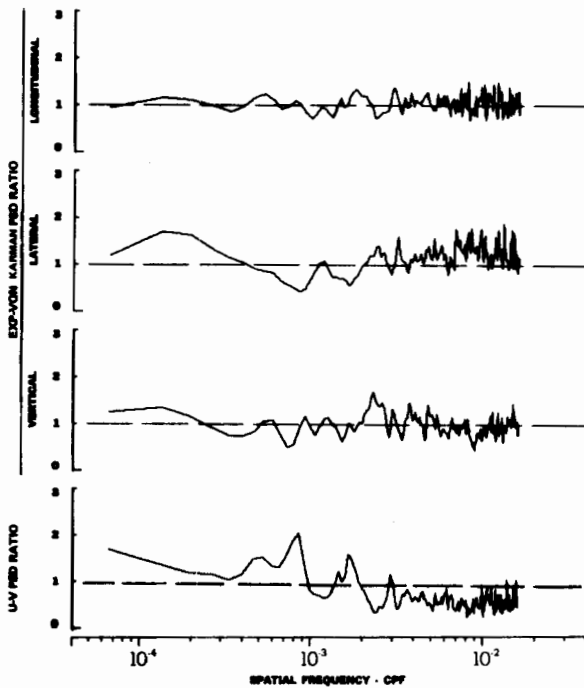
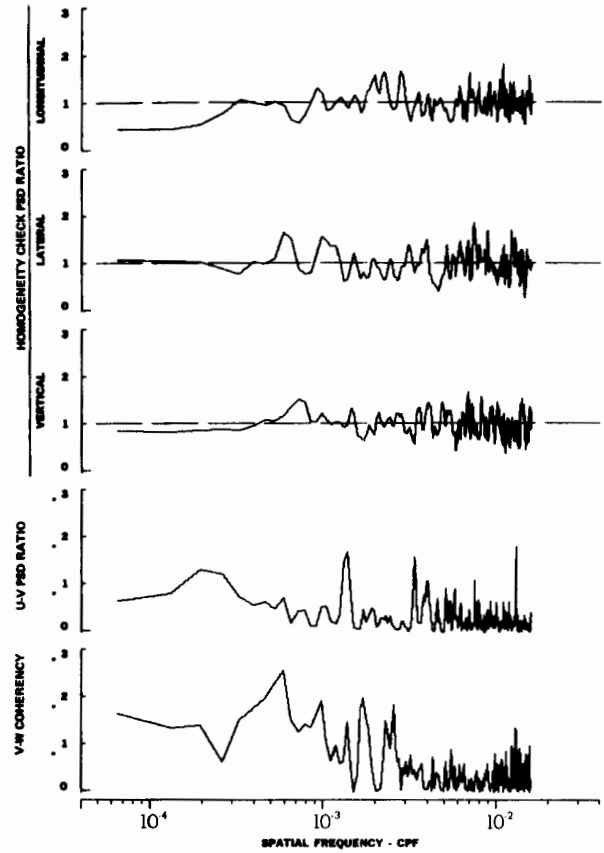
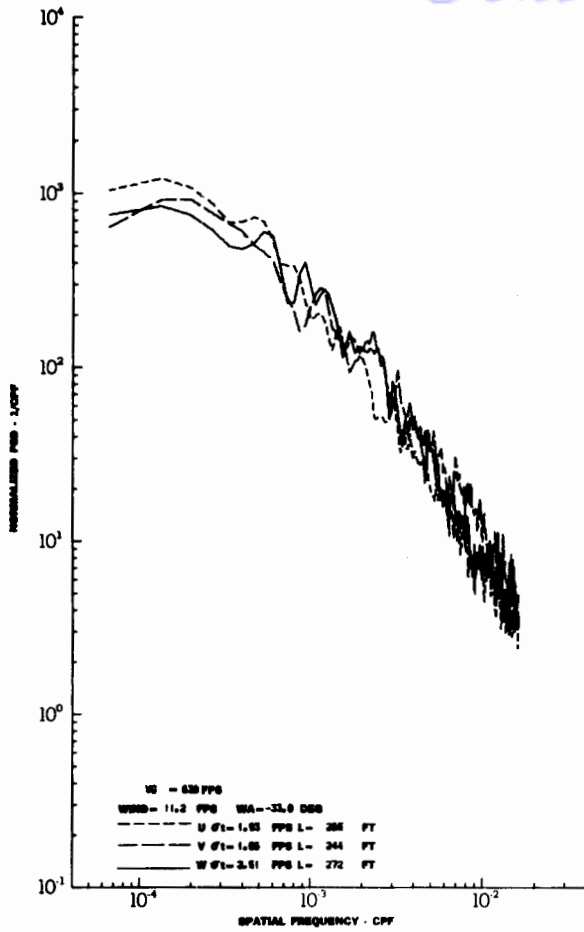
# Contrails



TURBULENCE SPECTRA DATA FOR TEST 40, LEG 4, CATEGORY 412234

FIGURE IV-34

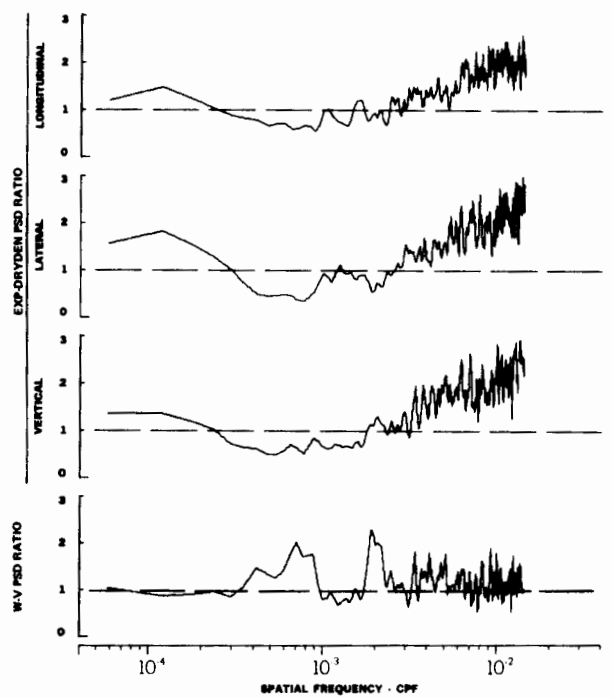
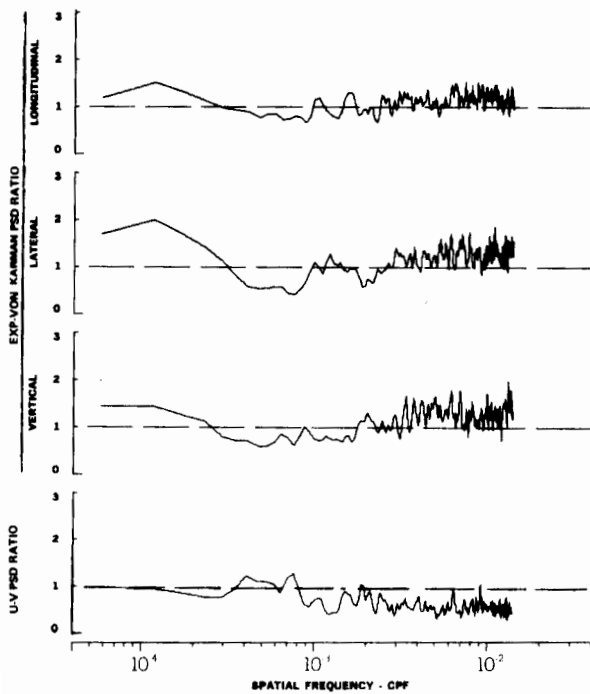
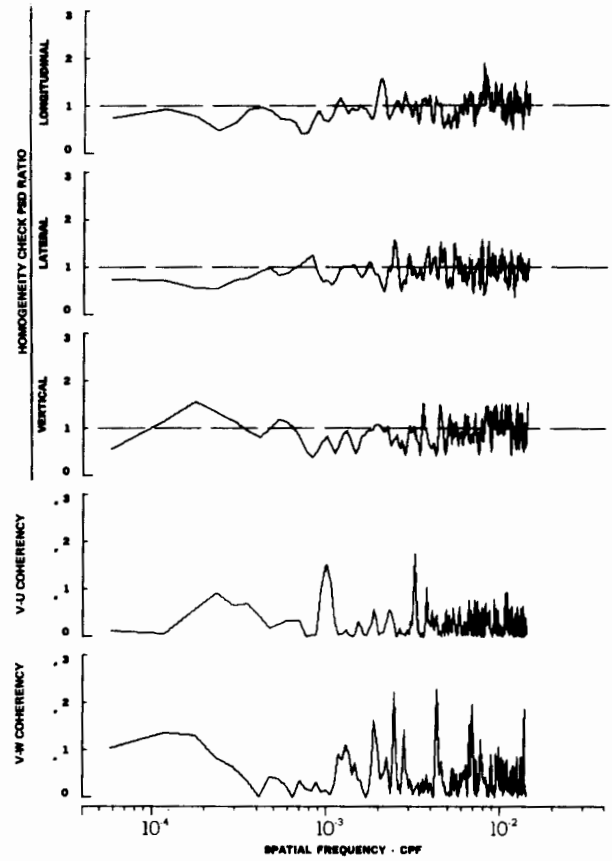
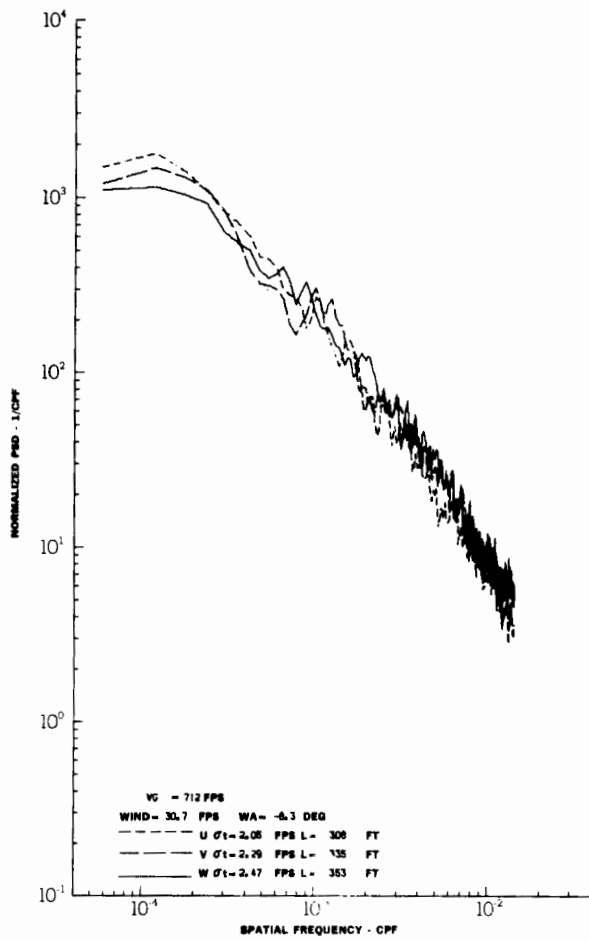
# Contrails



TURBULENCE SPECTRA DATA FOR TEST 40, LEG 6, CATEGORY 412234

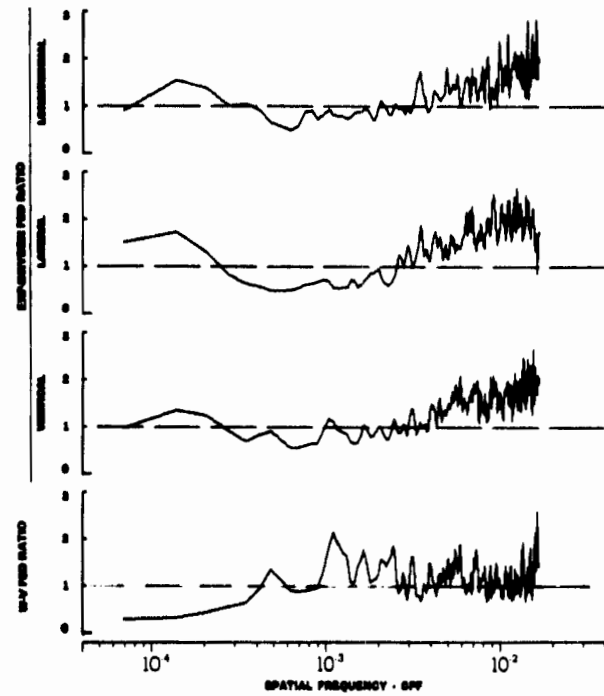
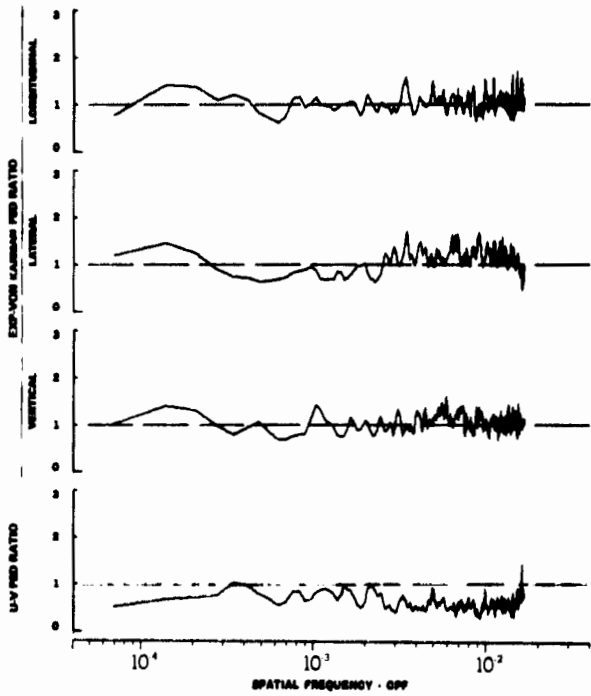
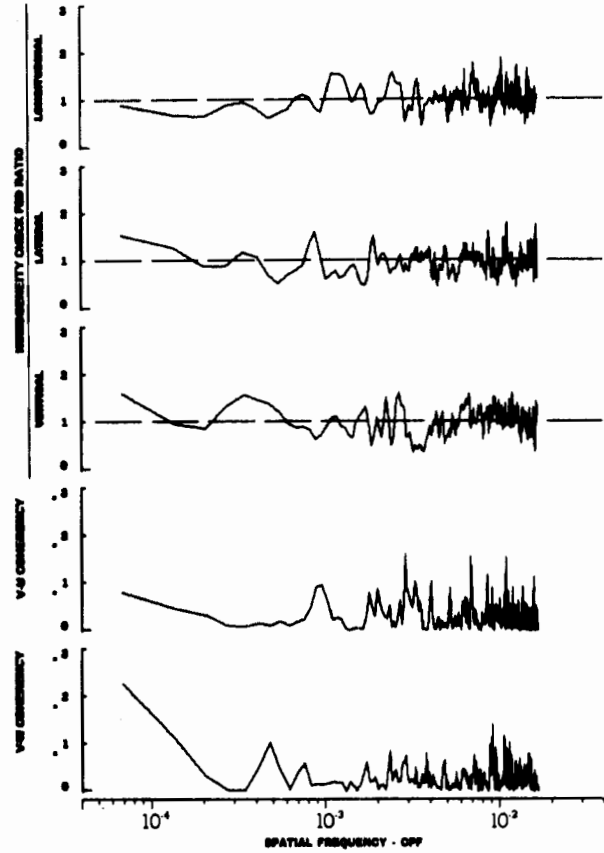
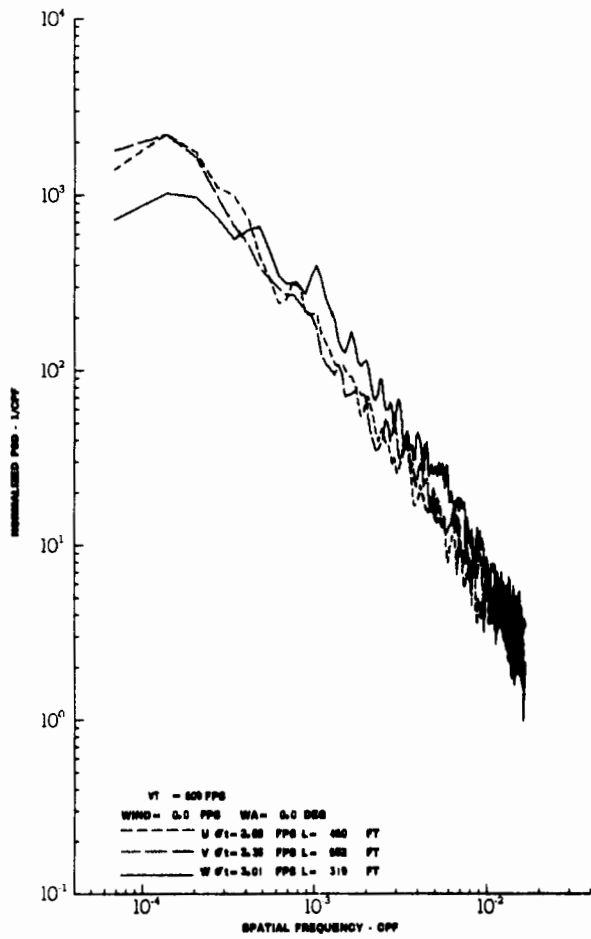
FIGURE IV-35

# Contrails



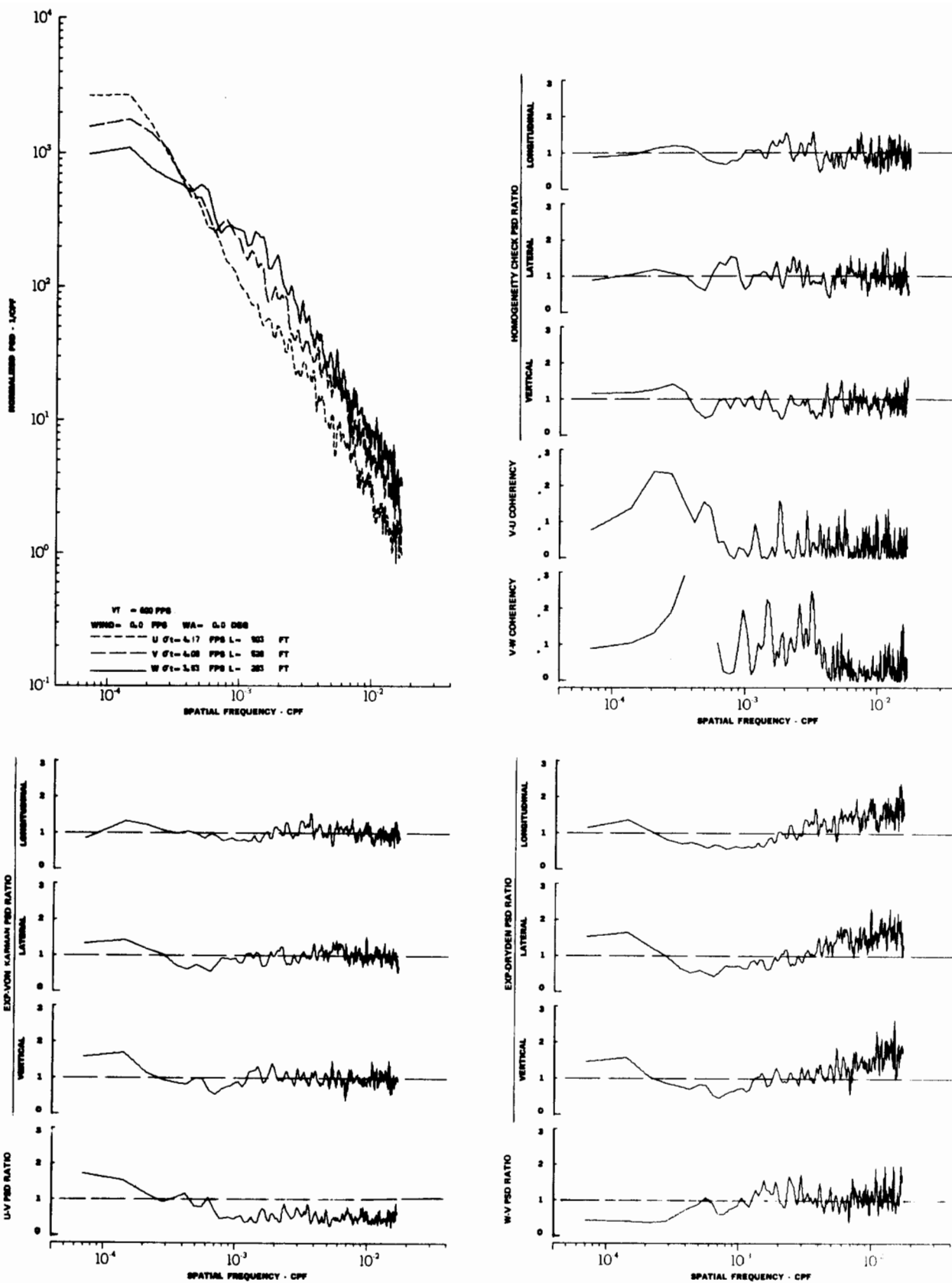
TURBULENCE SPECTRA DATA FOR TEST 40, LEG 8, CATEGORY 412234

FIGURE IV-36



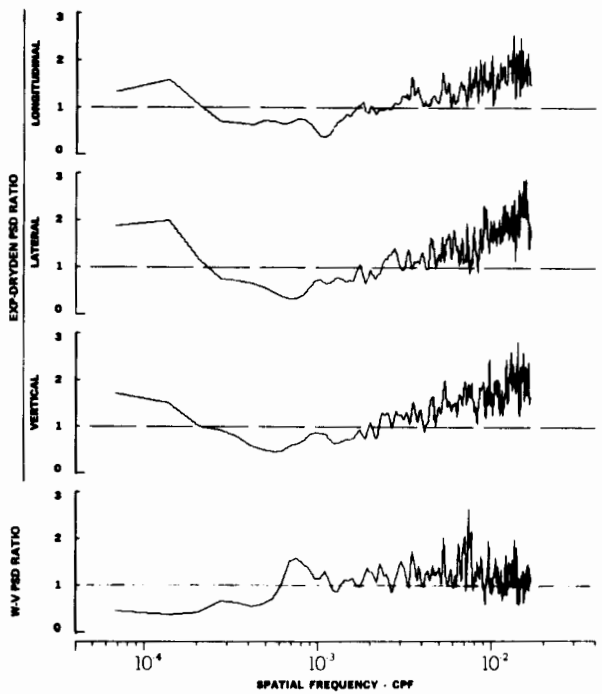
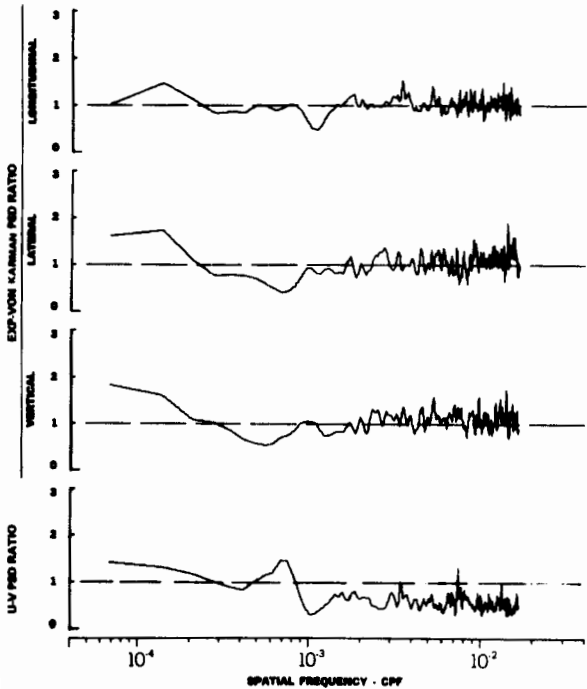
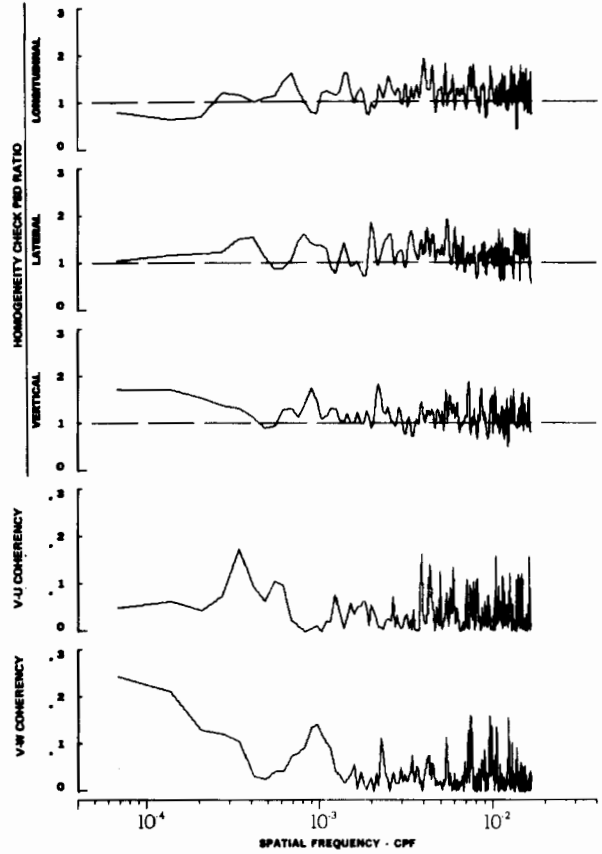
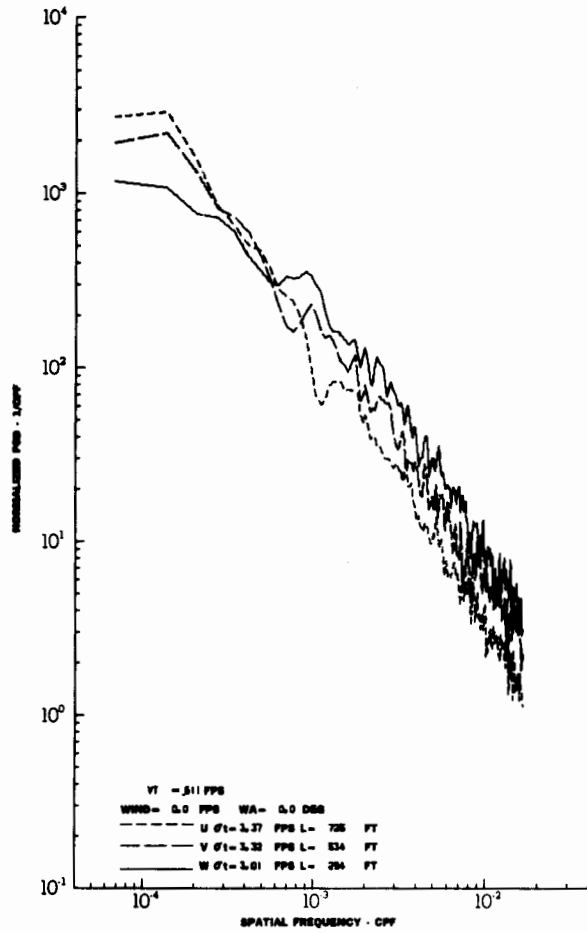
TURBULENCE SPECTRA DATA FOR TEST 41, LEG 1, CATEGORY 414324

FIGURE IV-37



TURBULENCE SPECTRA DATA FOR TEST 41, LEG 3, CATEGORY 414324

FIGURE IV-38

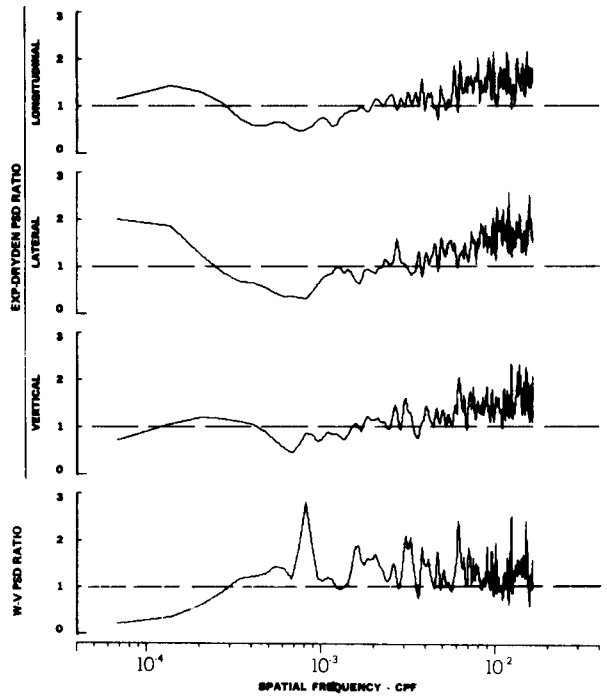
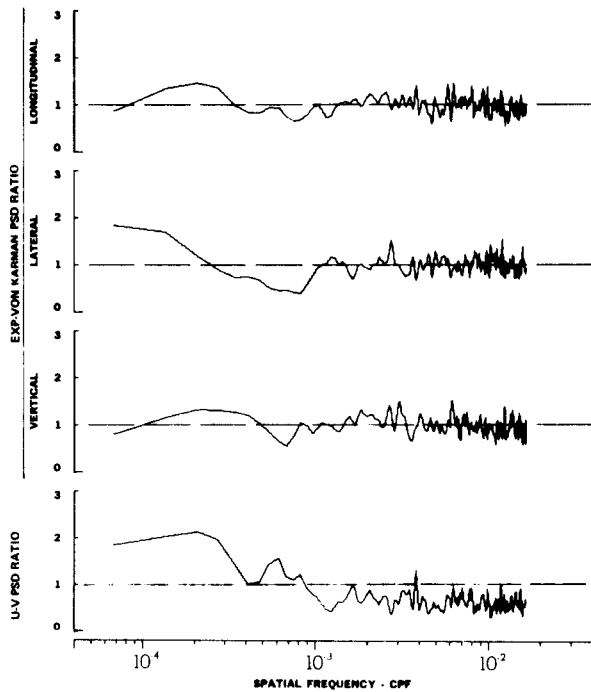
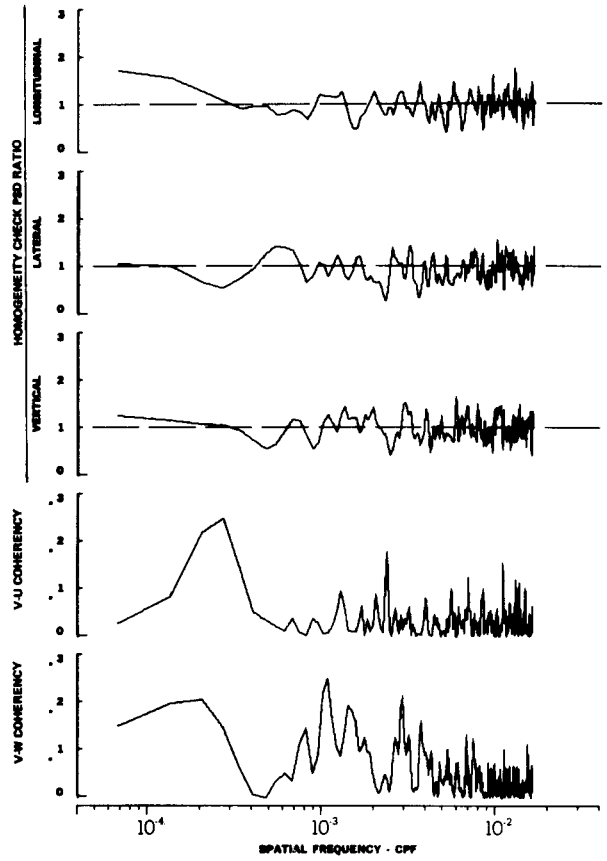
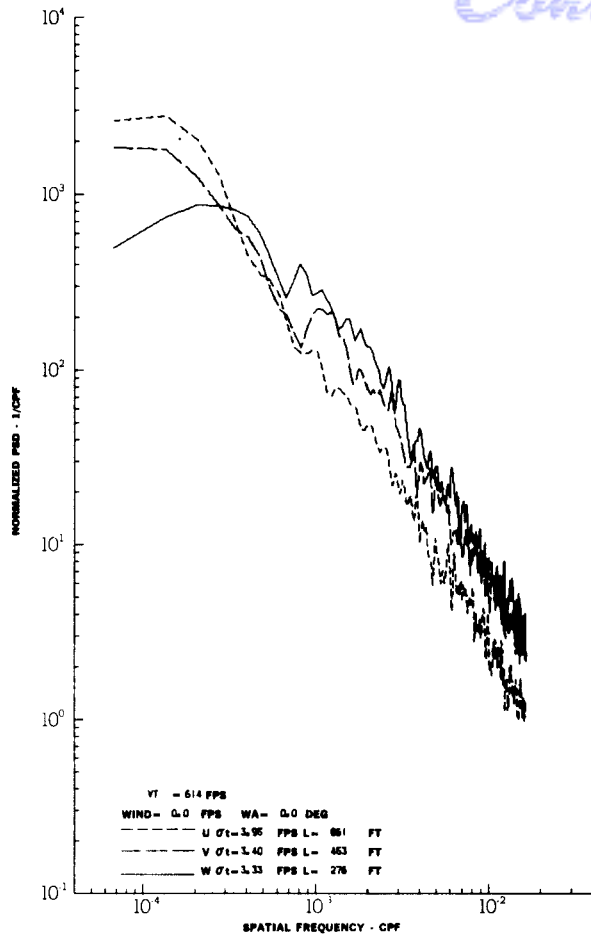


TURBULENCE SPECTRA DATA FOR TEST 41, LEG 5, CATEGORY 413324

FIGURE IV-39

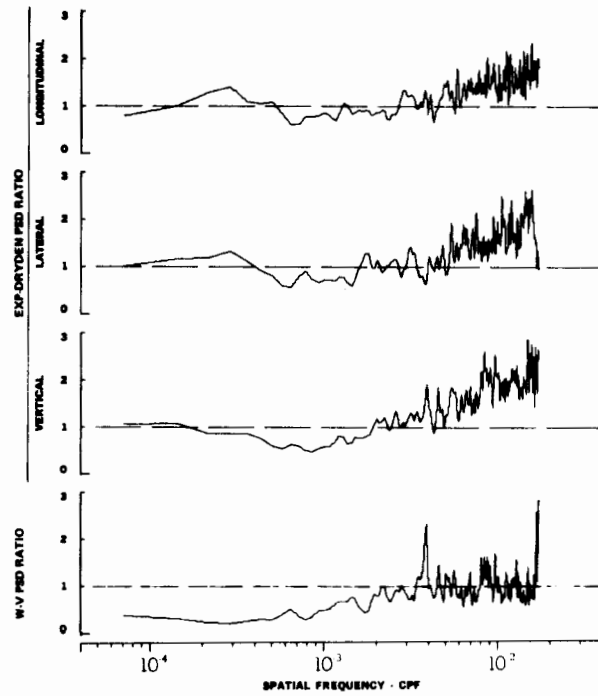
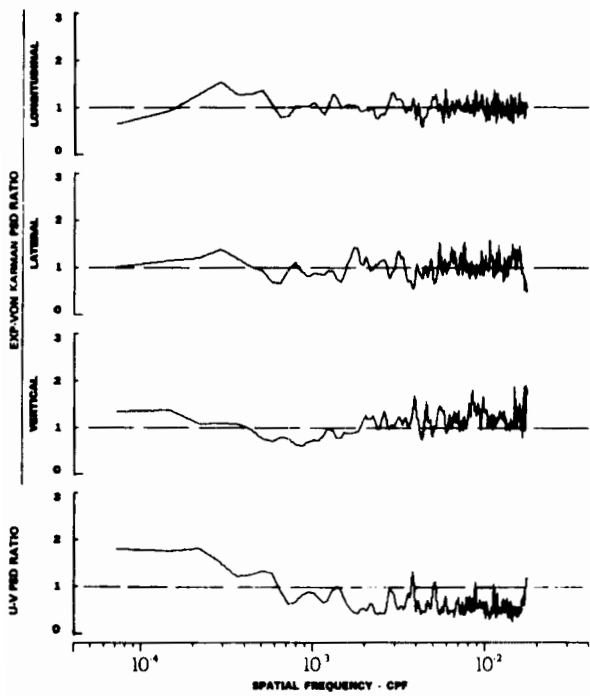
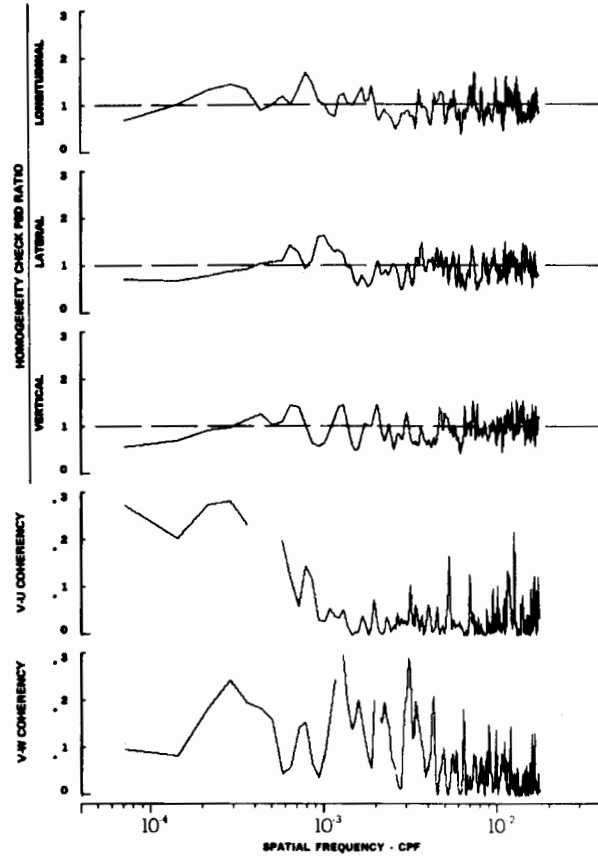
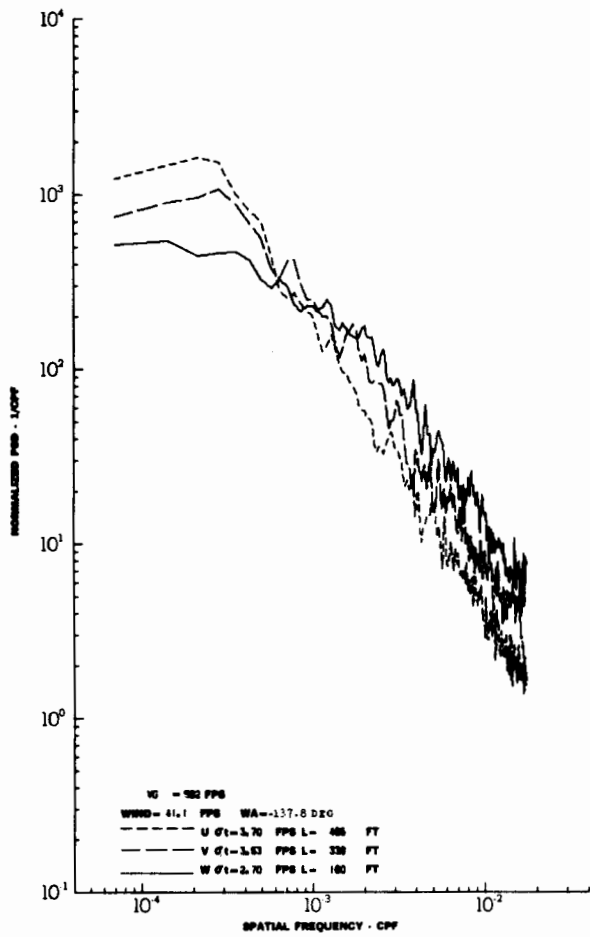


# Contrails



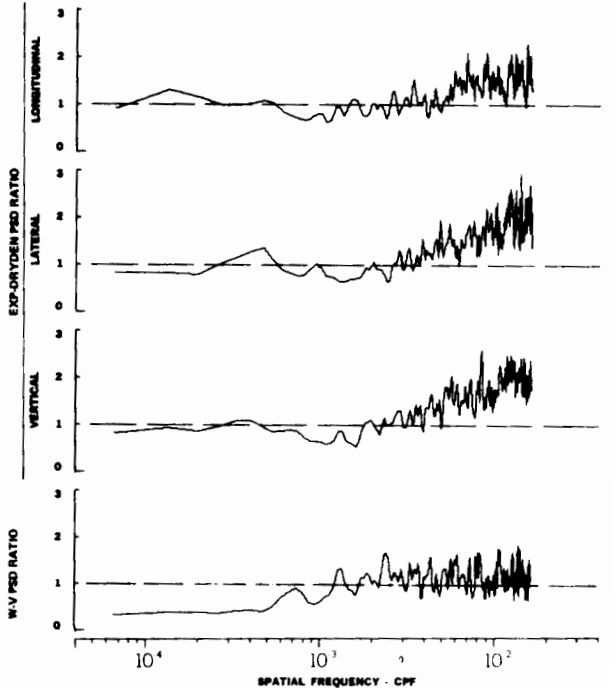
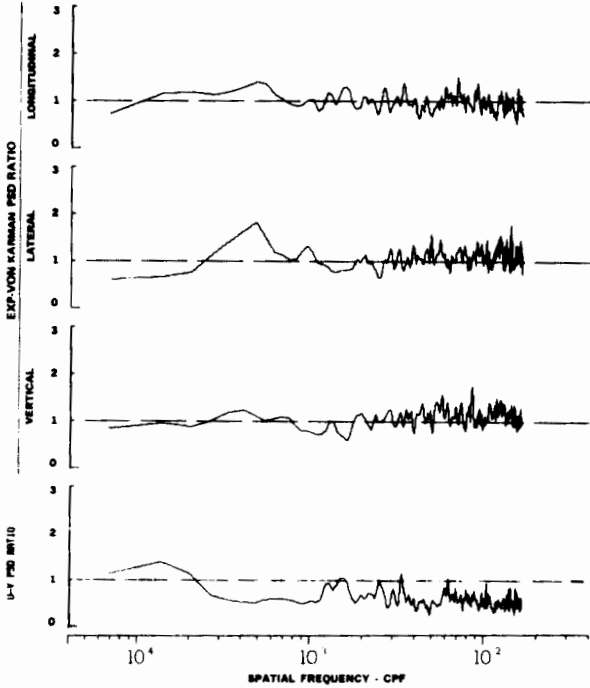
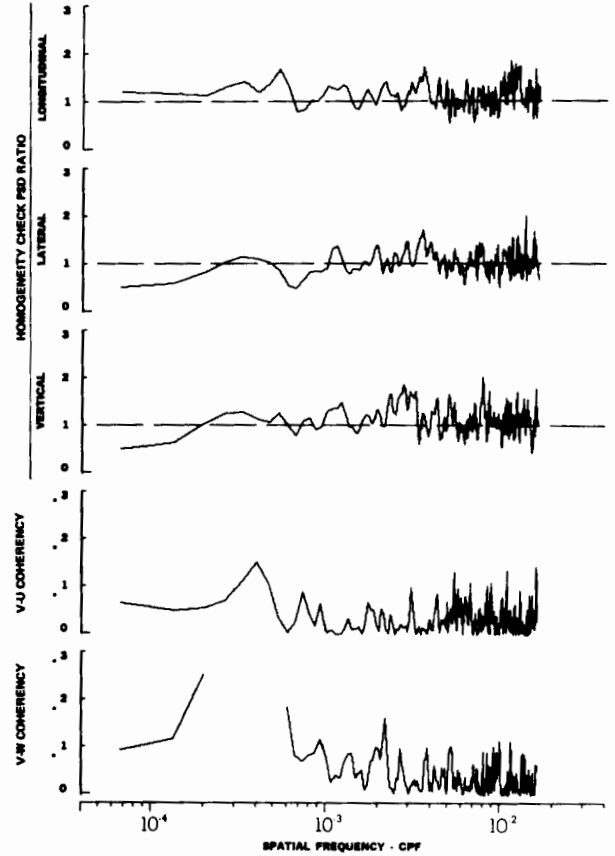
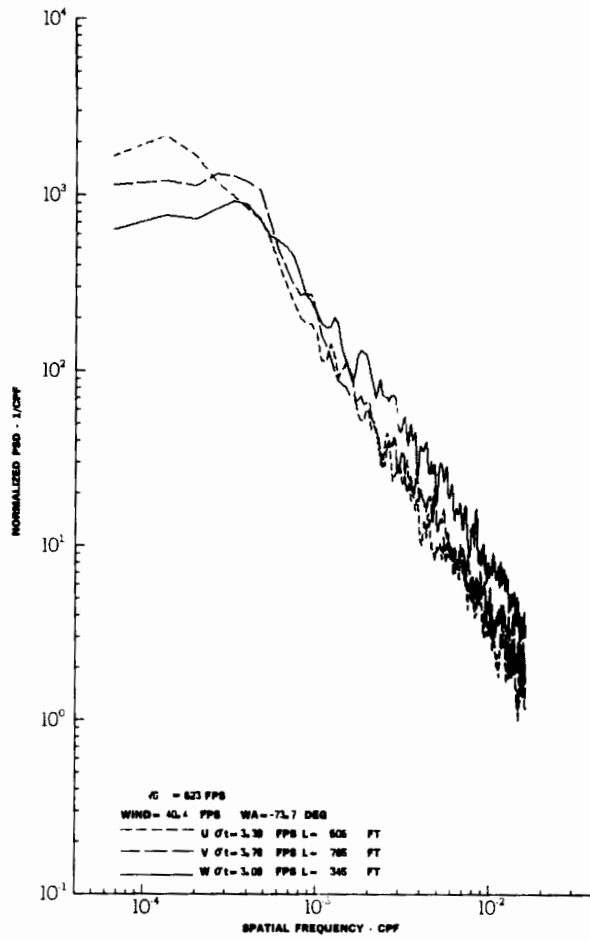
TURBULENCE SPECTRA DATA FOR TEST 41, LEG 7, CATEGORY 413324

FIGURE IV-40



TURBULENCE SPECTRA DATA FOR TEST 43, LEG 1, CATEGORY 424224

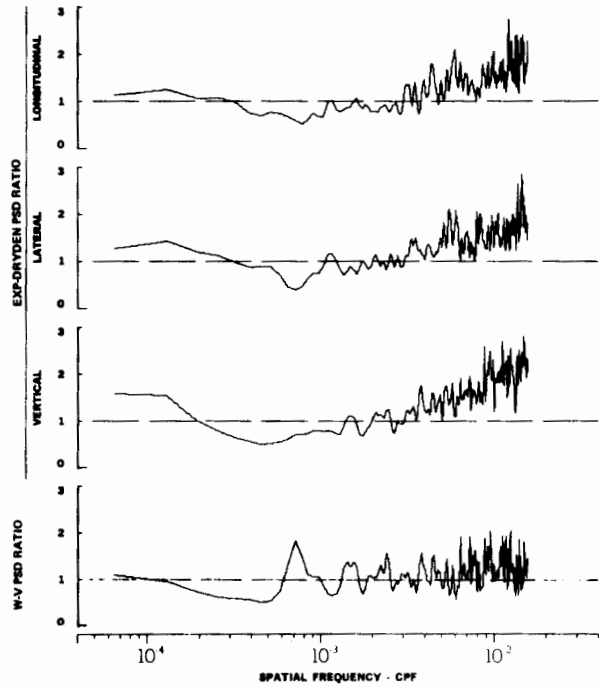
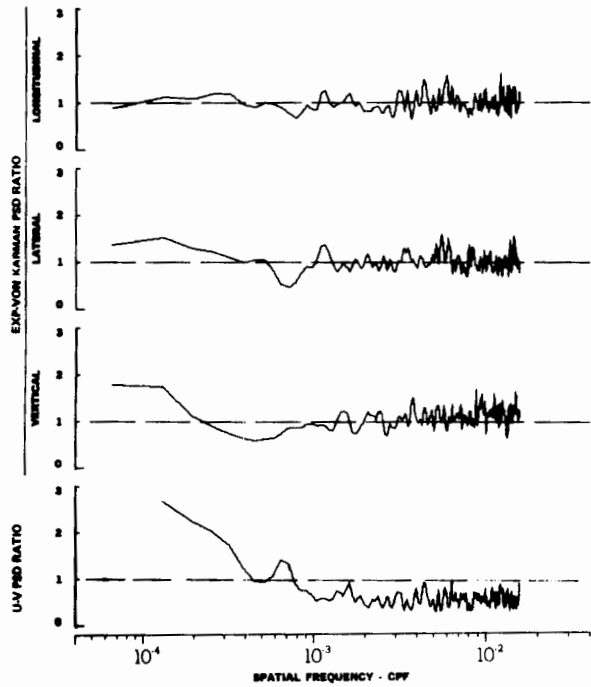
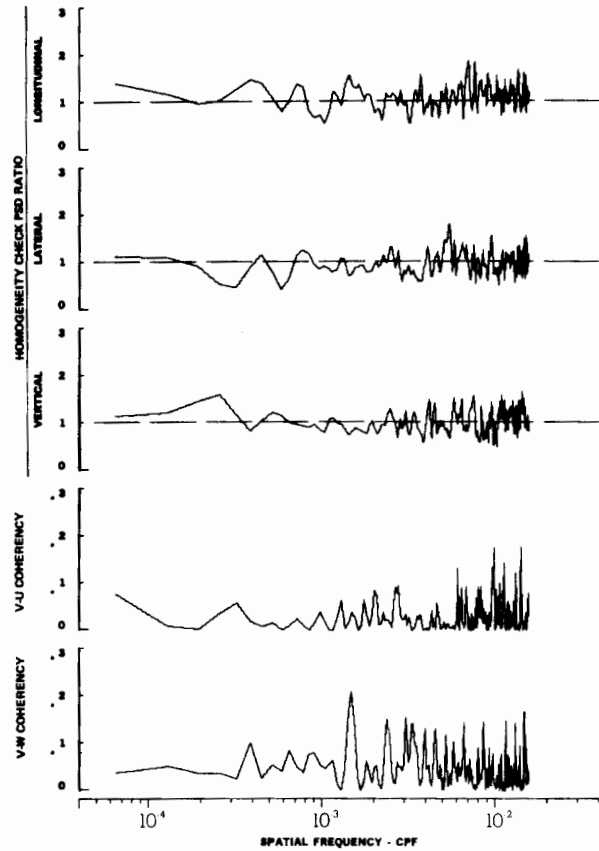
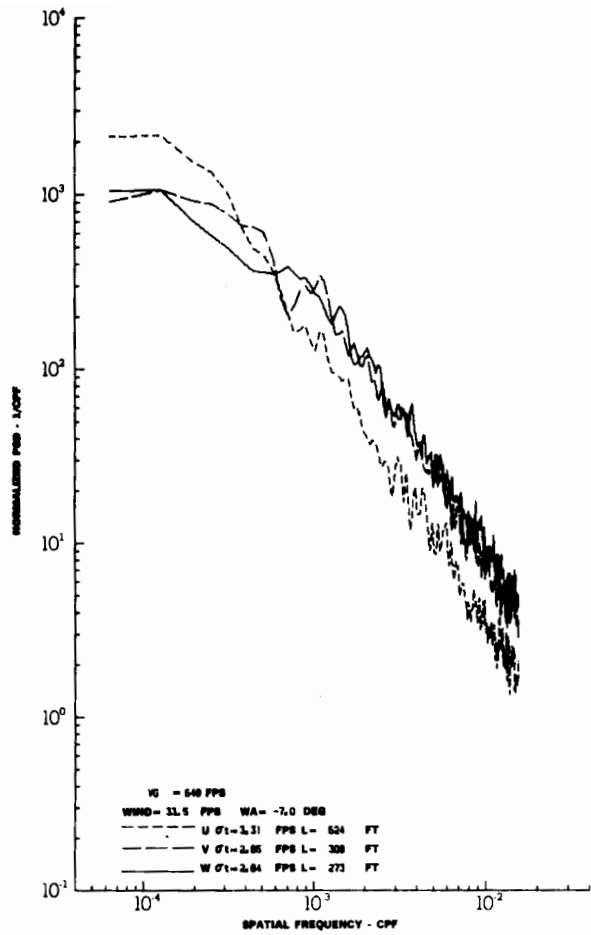
FIGURE IV-41



TURBULENCE SPECTRA DATA FOR TEST 43, LEG 3, CATEGORY 424224

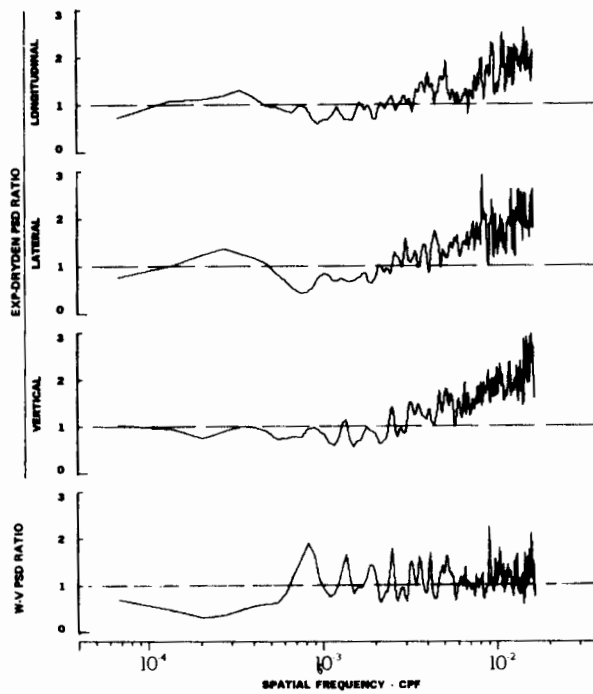
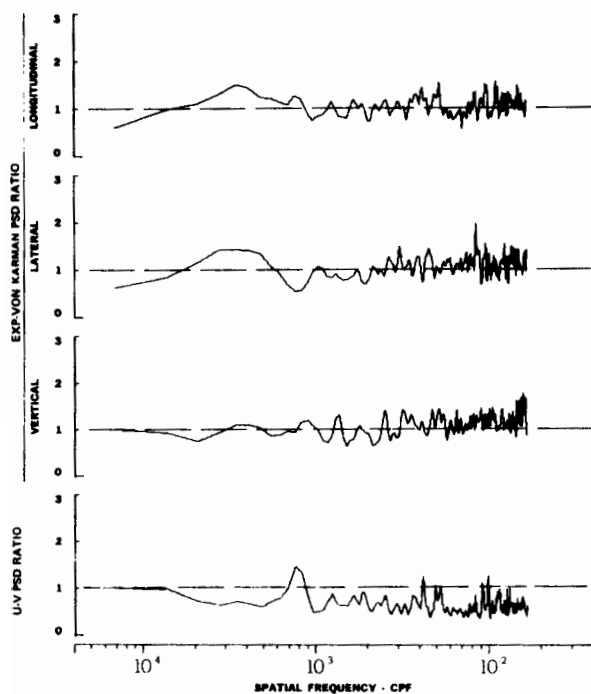
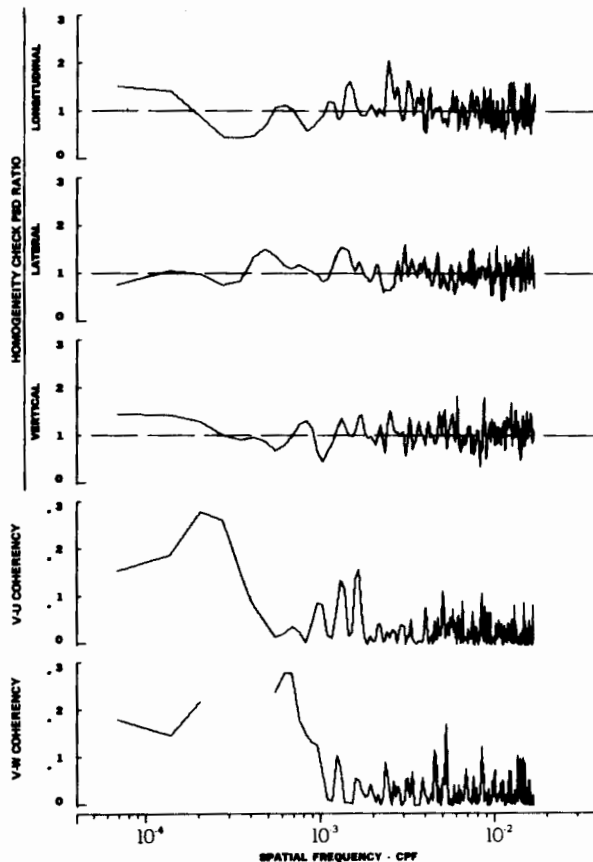
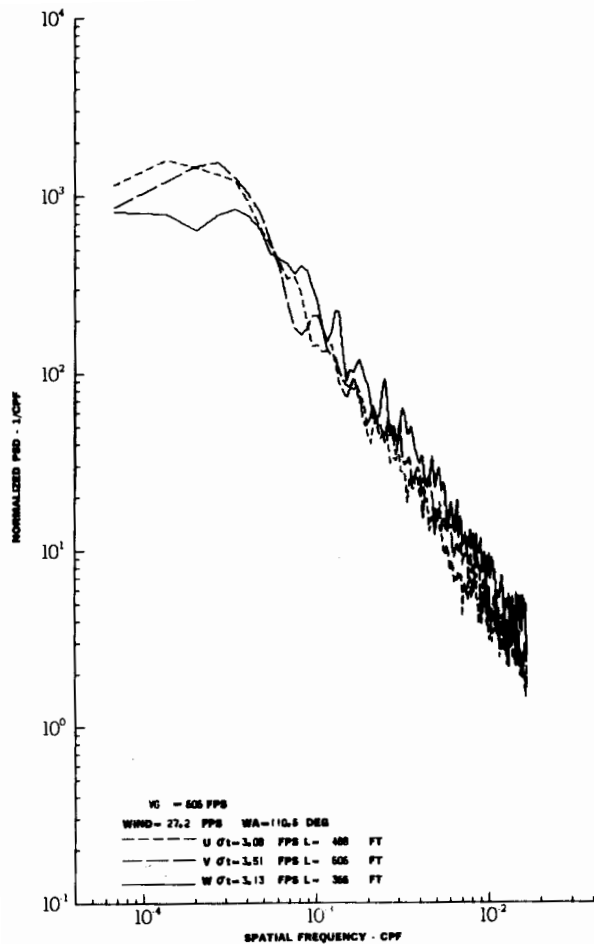
FIGURE IV-42

# Contrails



TURBULENCE SPECTRA DATA FOR TEST 43, LEG 5, CATEGORY 422224

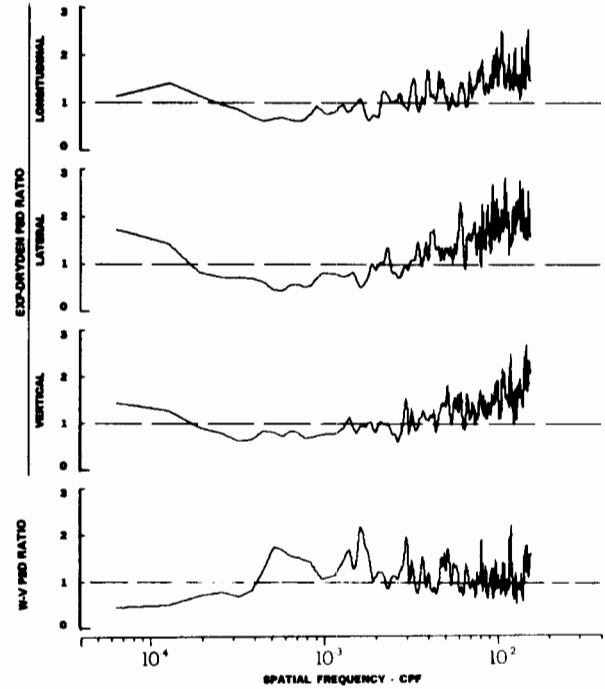
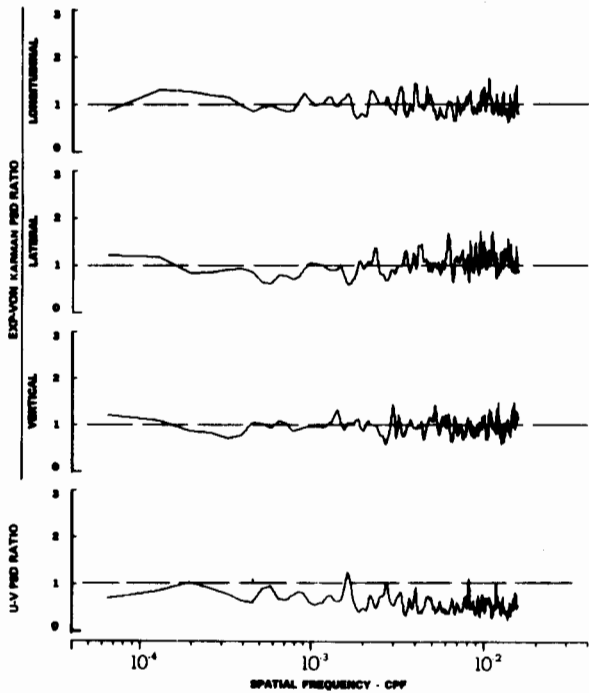
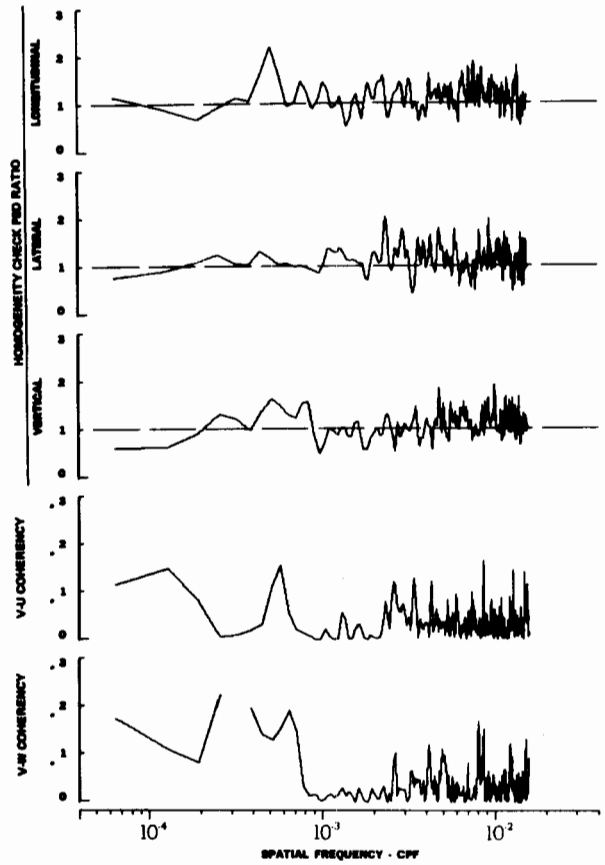
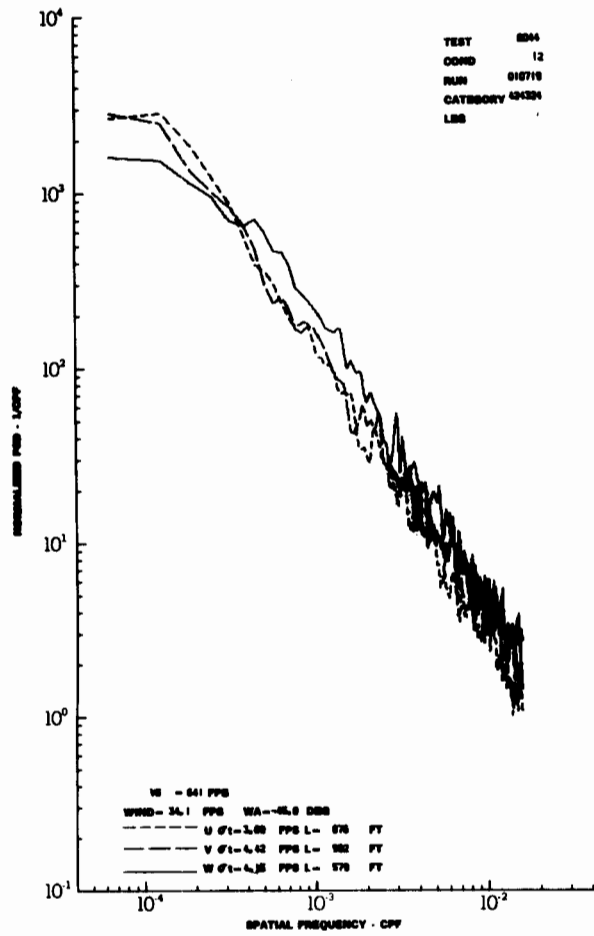
FIGURE IV-43



TURBULENCE SPECTRA DATA FOR TEST 43, LEG 7, CATEGORY 423224

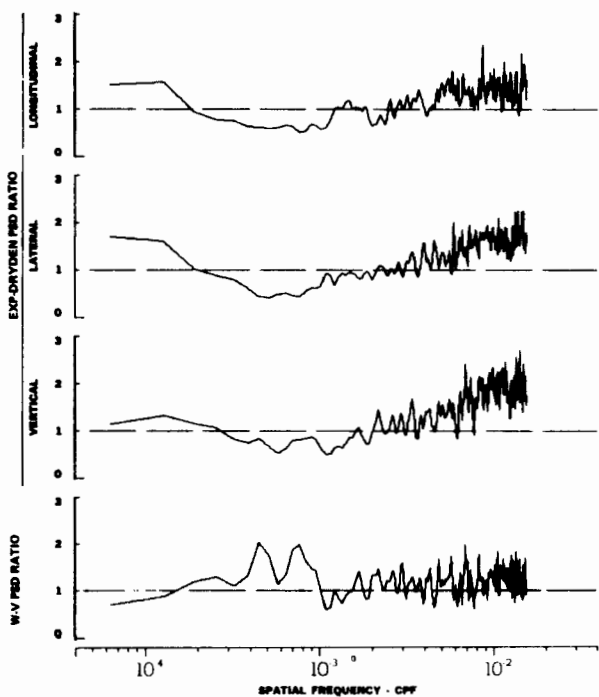
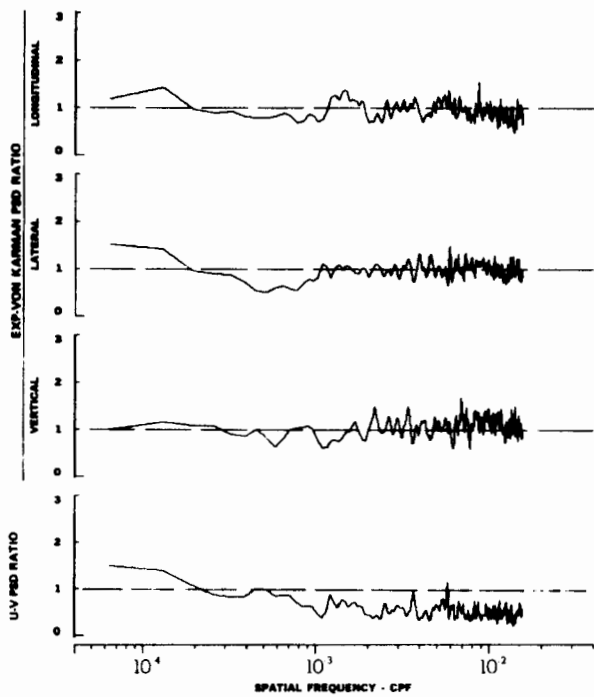
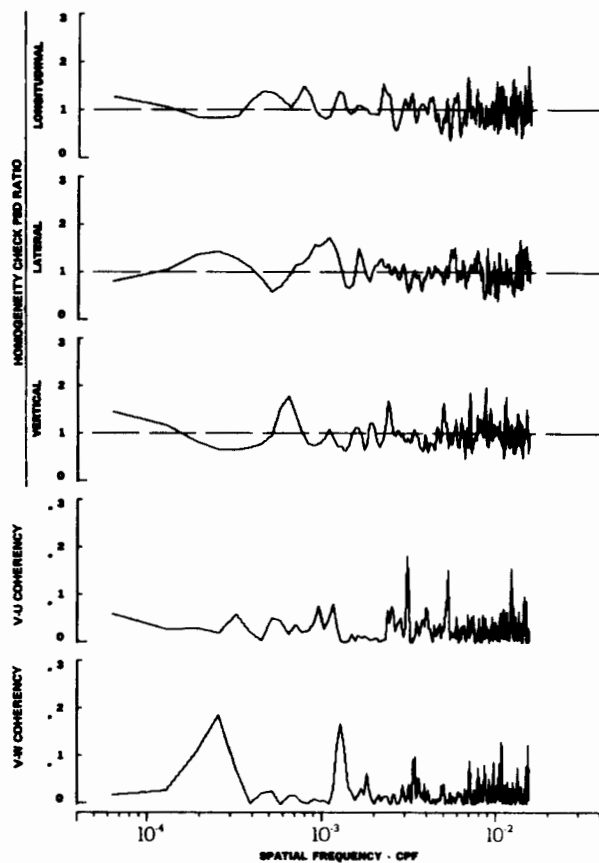
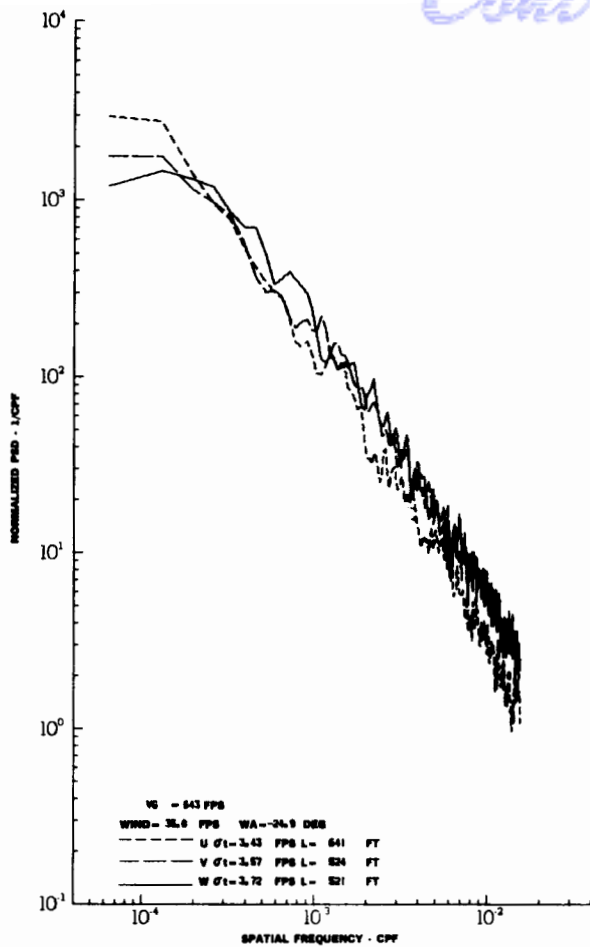
FIGURE IV-44

# Contrails



TURBULENCE SPECTRA DATA FOR TEST 44, LEG 4, CATEGORY 424324

FIGURE IV-45

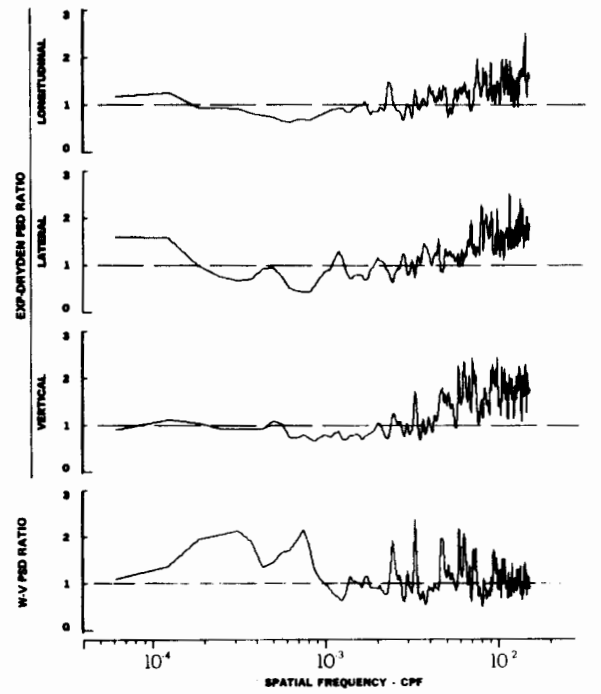
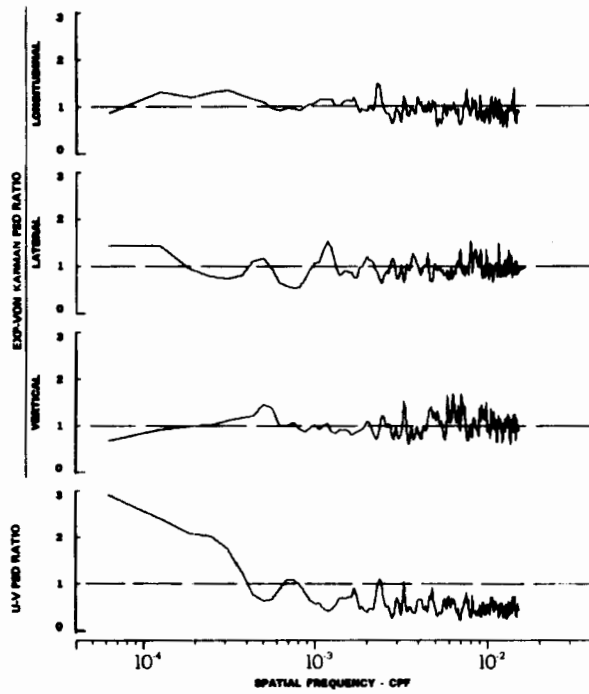
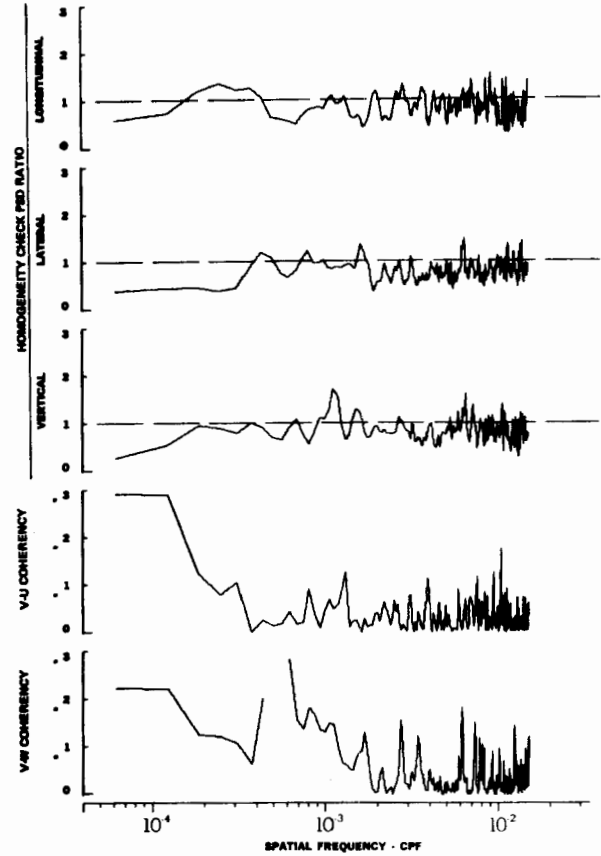
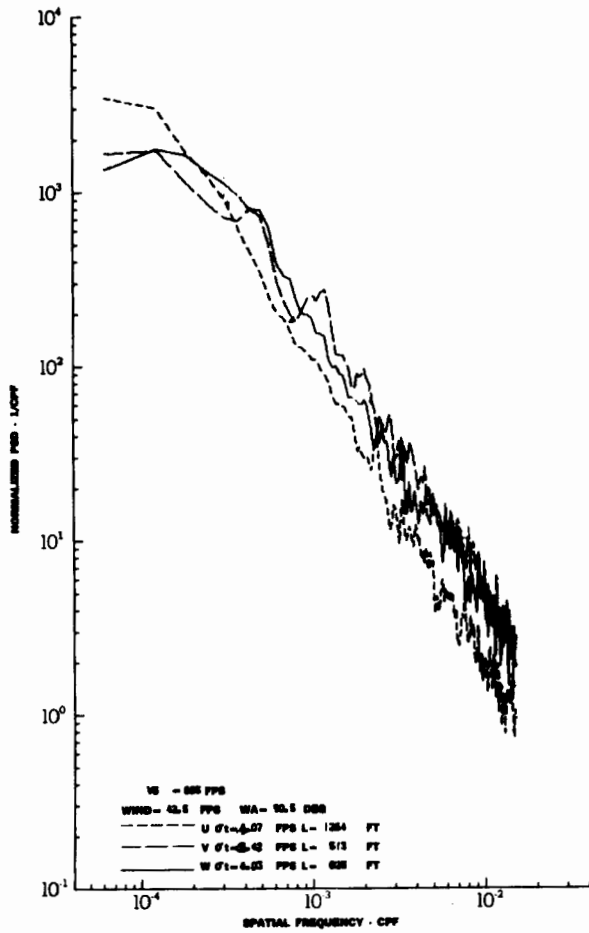


TURBULENCE SPECTRA DATA FOR TEST 44, LEG 6, CATEGORY 424324

FIGURE IV-46

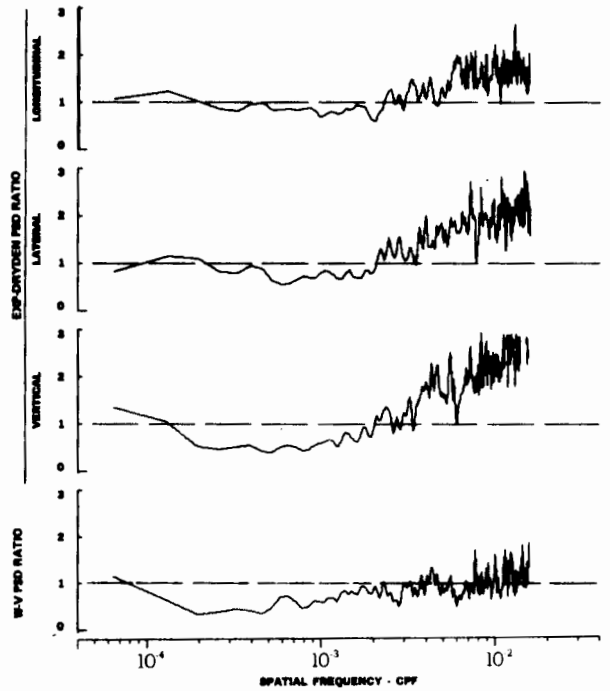
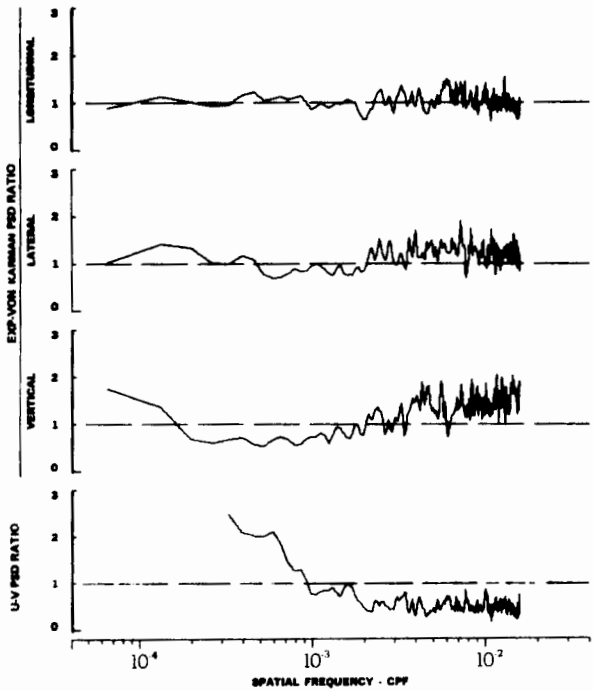
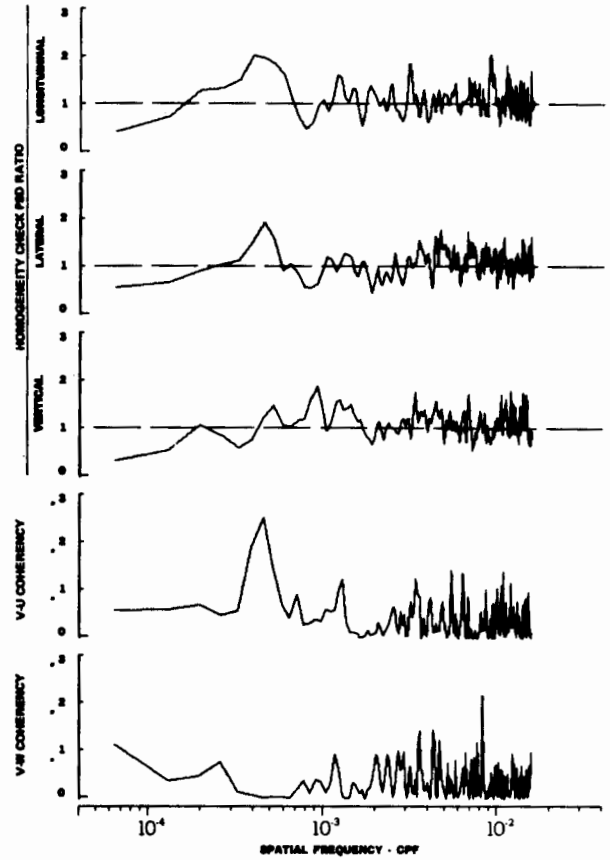
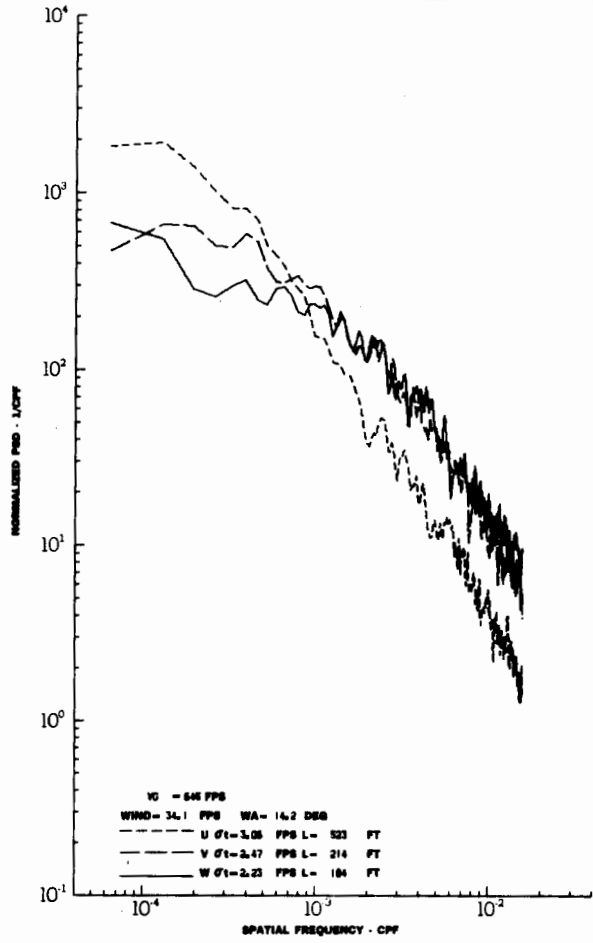


# Contrails



TURBULENCE SPECTRA DATA FOR TEST 44, LEG 8, CATEGORY 423324

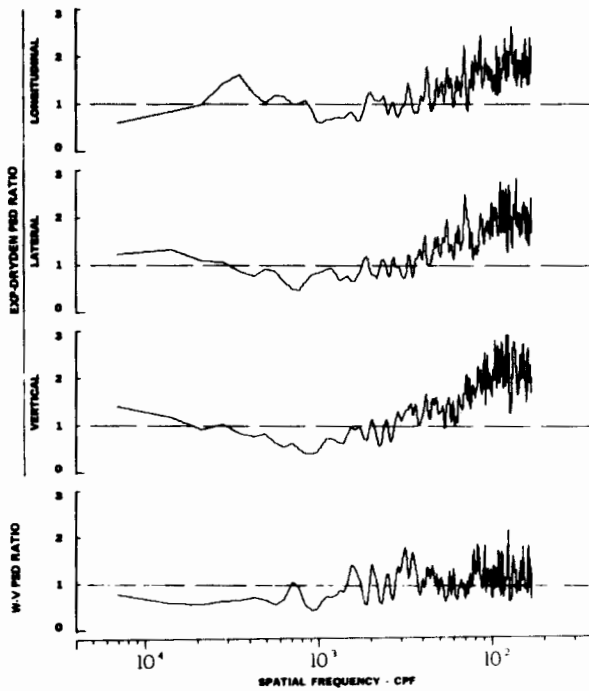
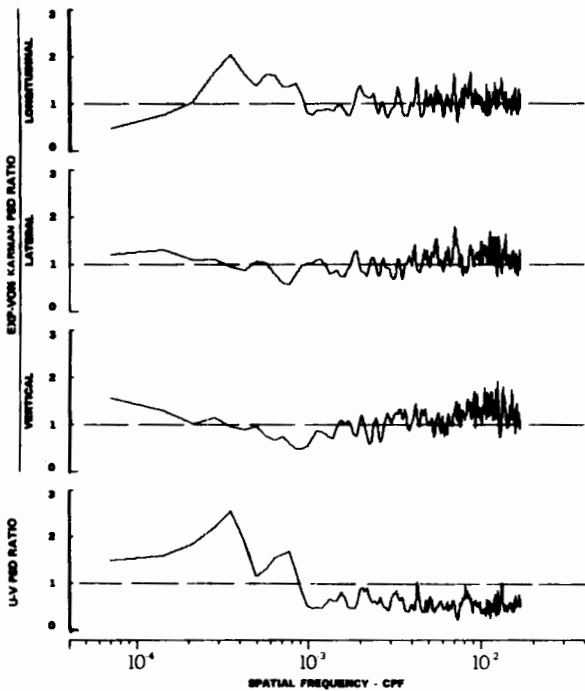
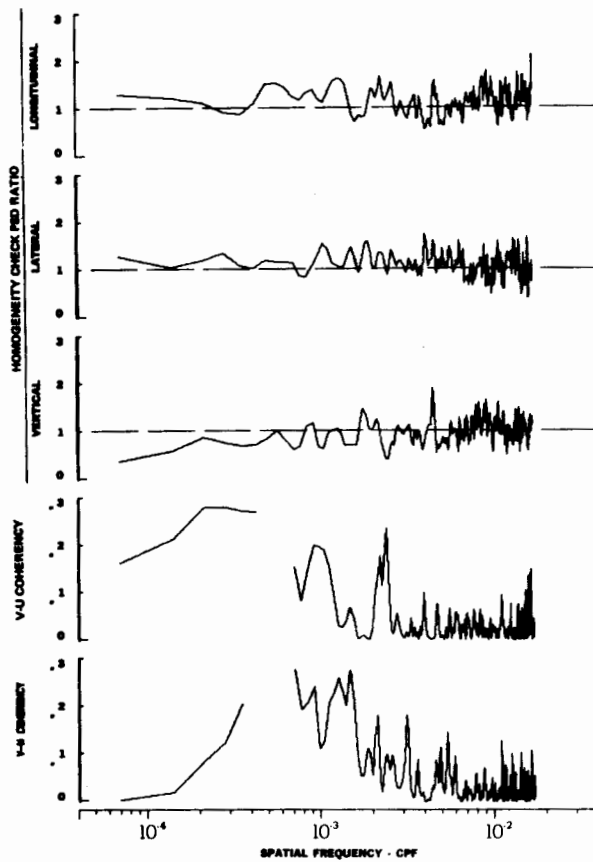
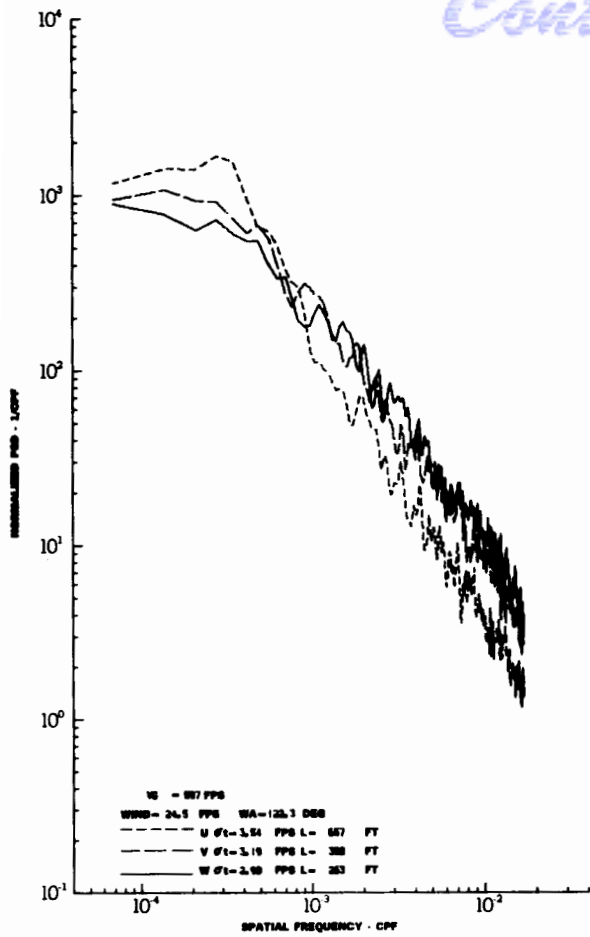
FIGURE IV-47



TURBULENCE SPECTRA DATA FOR TEST 46, LEG 2, CATEGORY 411234

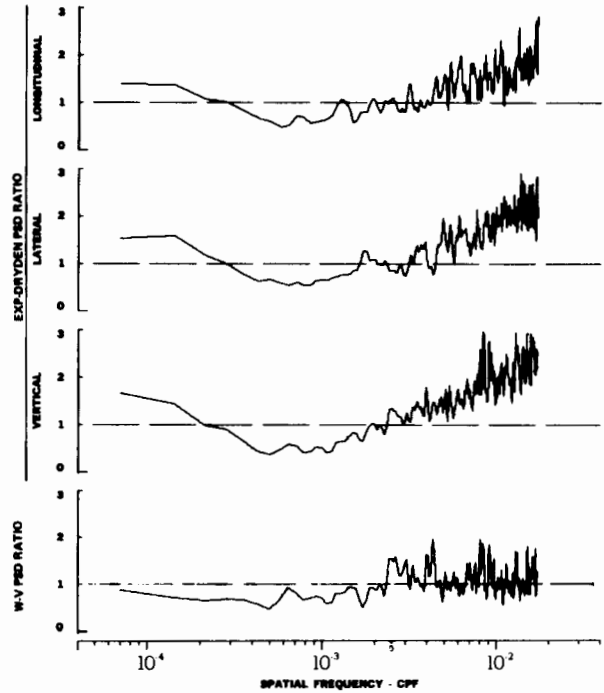
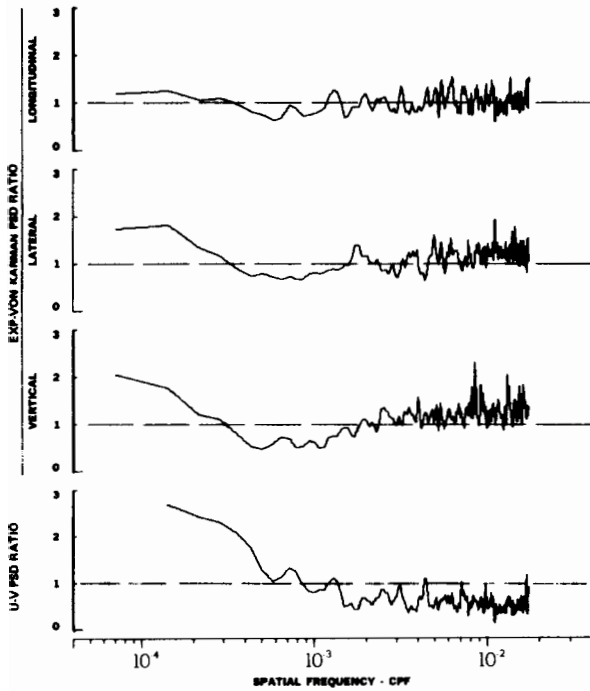
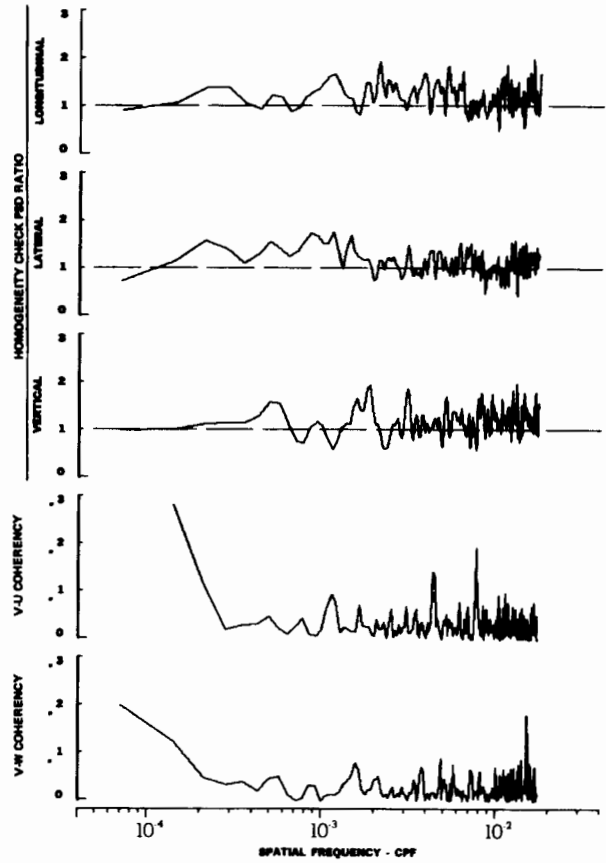
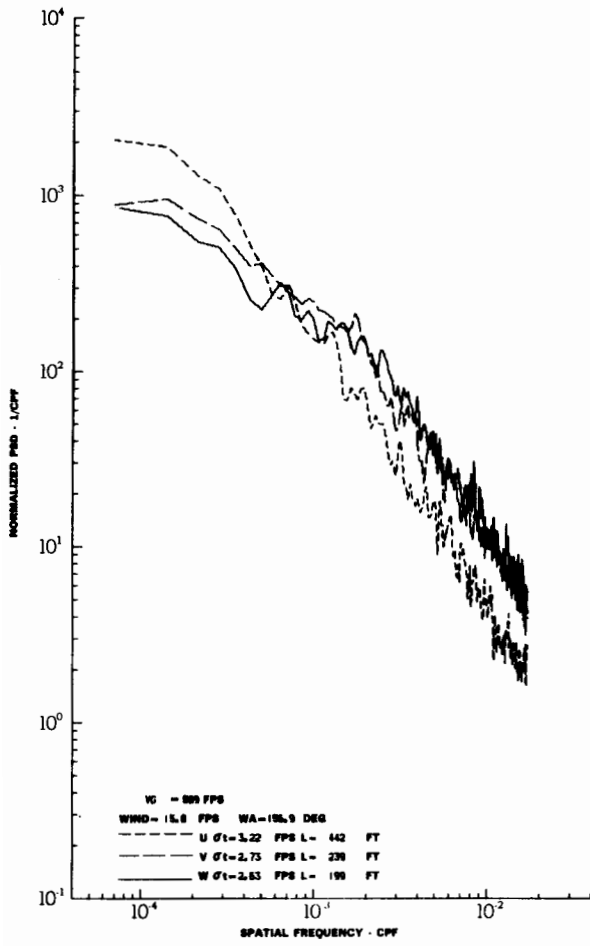
FIGURE IV-48

# Contrails

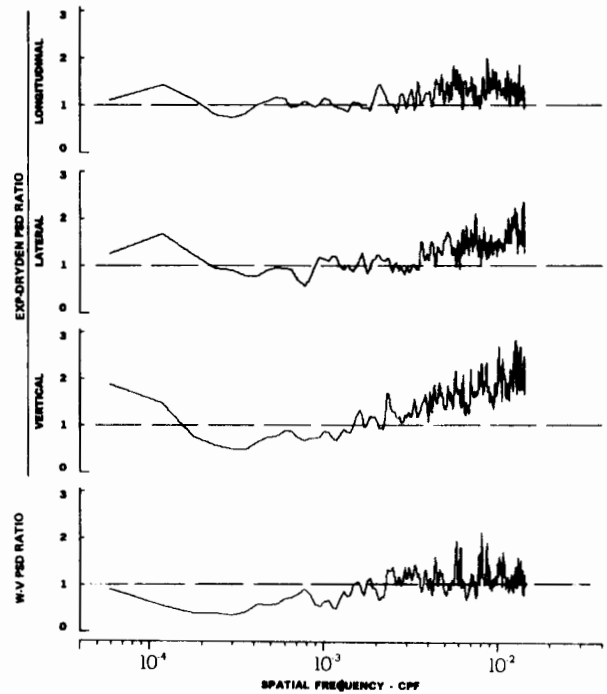
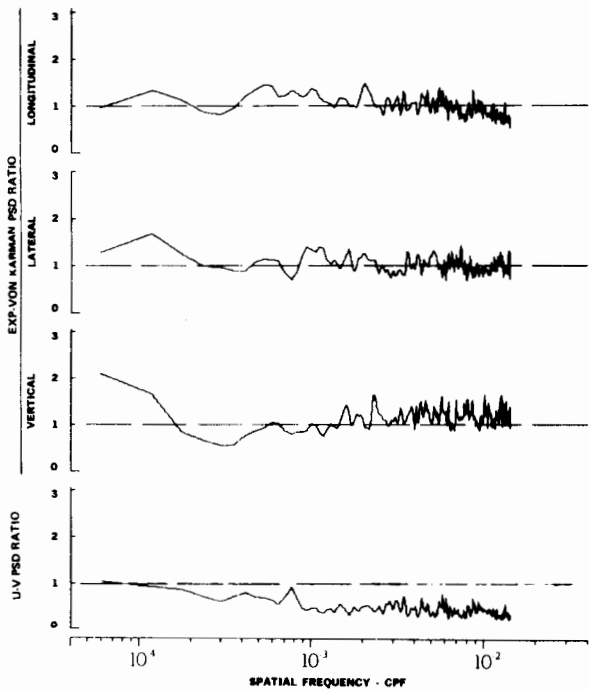
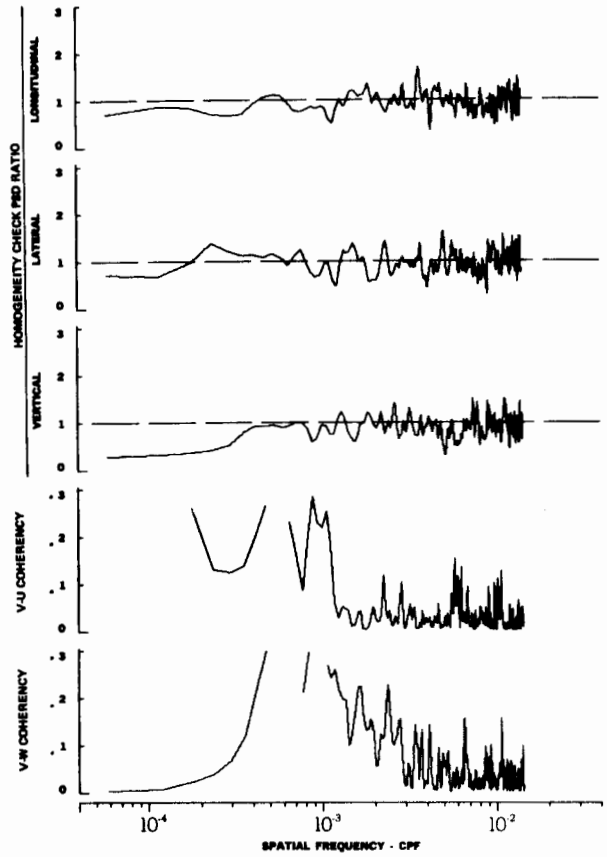
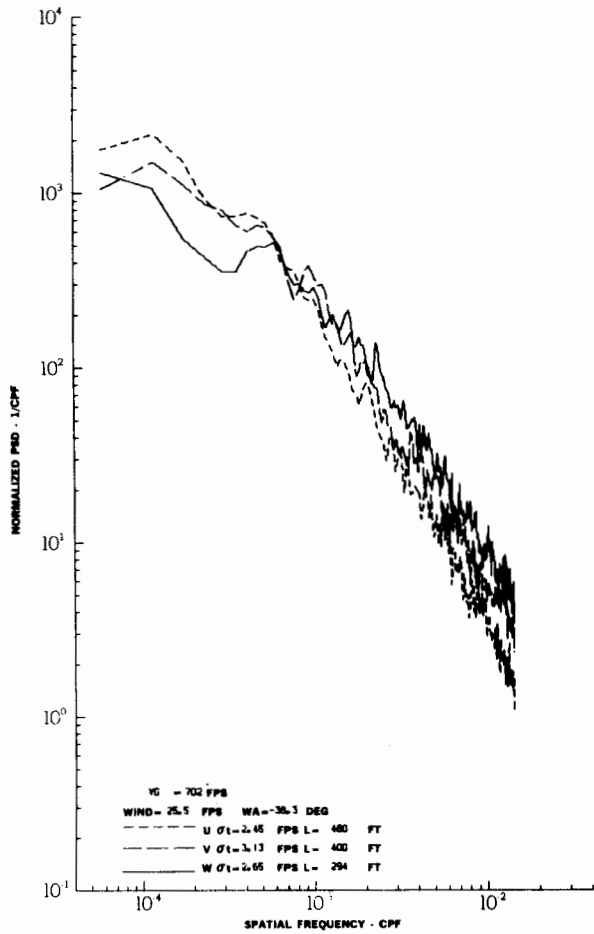


TURBULENCE SPECTRA DATA FOR TEST 46, LEG 4, CATEGORY 413234

FIGURE IV-49



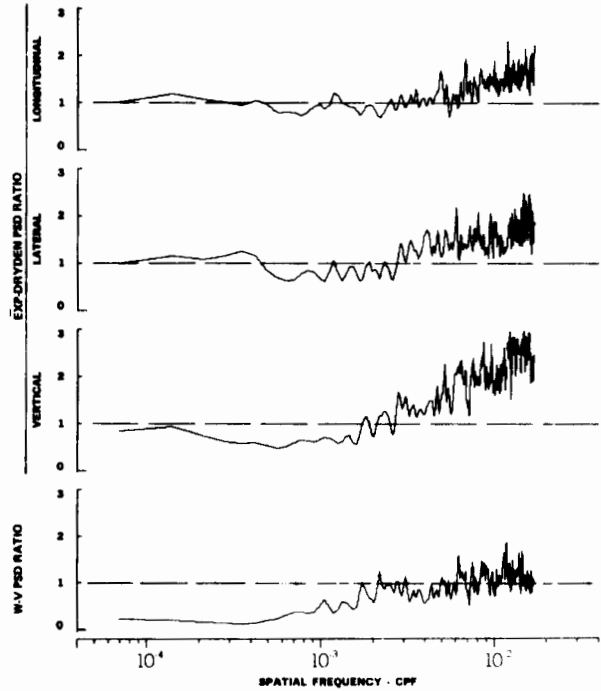
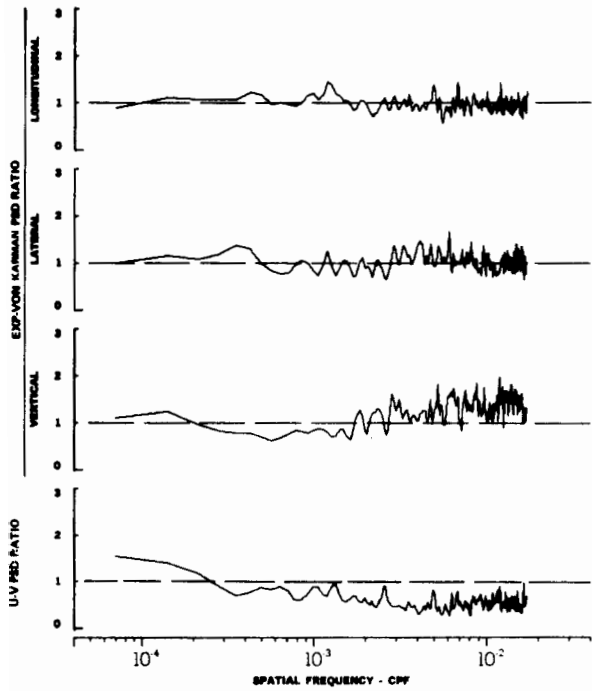
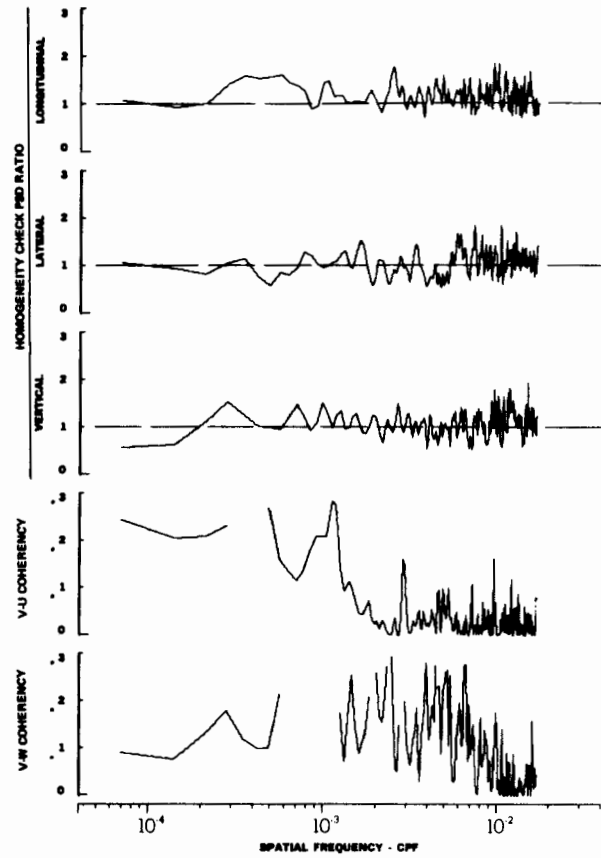
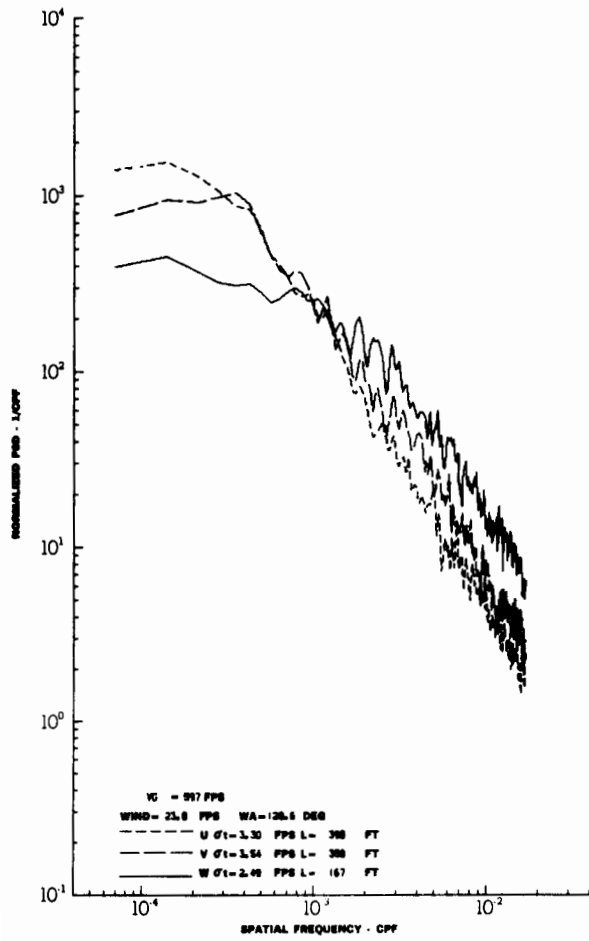
TURBULENCE SPECTRA DATA FOR TEST 46, LEG 6, CATEGORY 412234  
 FIGURE IV-50



TURBULENCE SPECTRA DATA FOR TEST 46, LEG 8, CATEGORY 412234

FIGURE IV-51

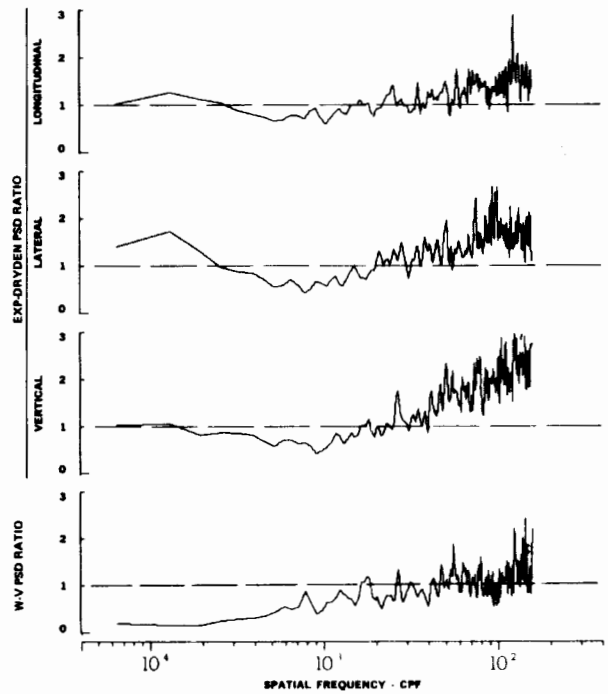
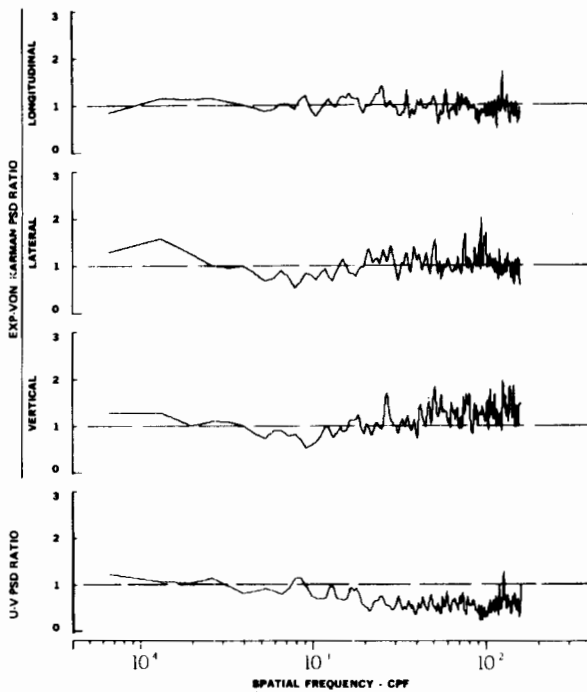
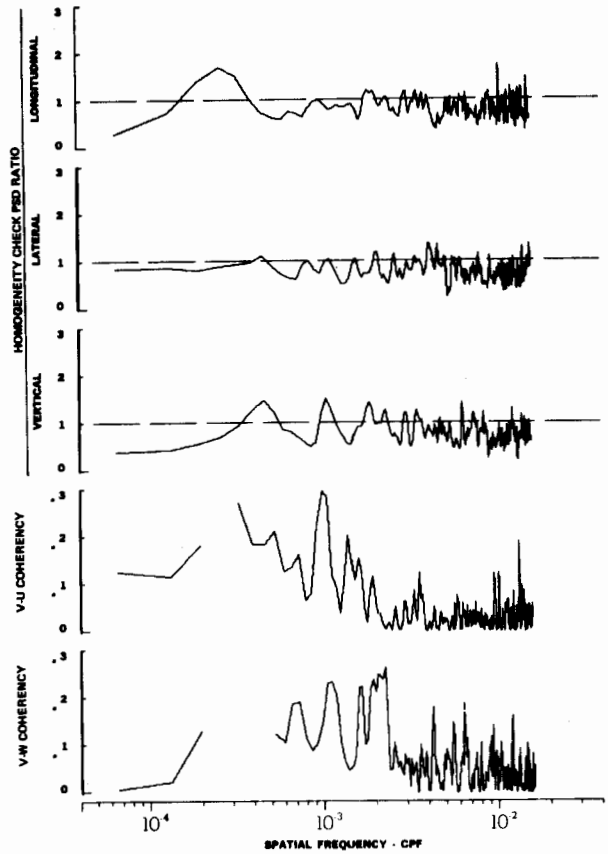
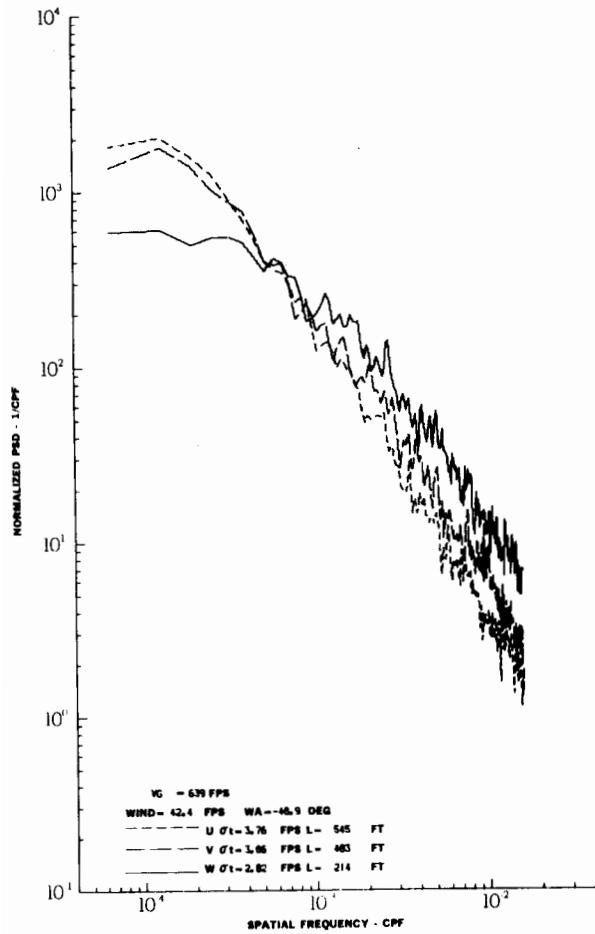
# Contrails



TURBULENCE SPECTRA DATA FOR TEST 47, LEG 3, CATEGORY 413334

FIGURE IV-52

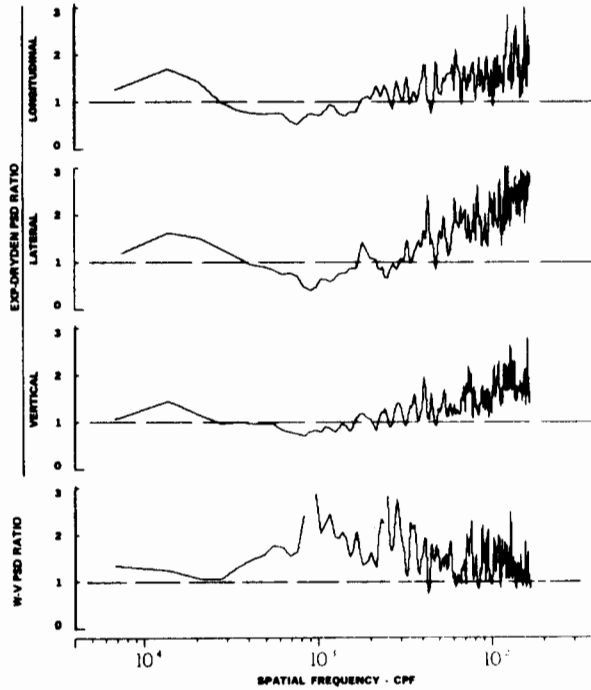
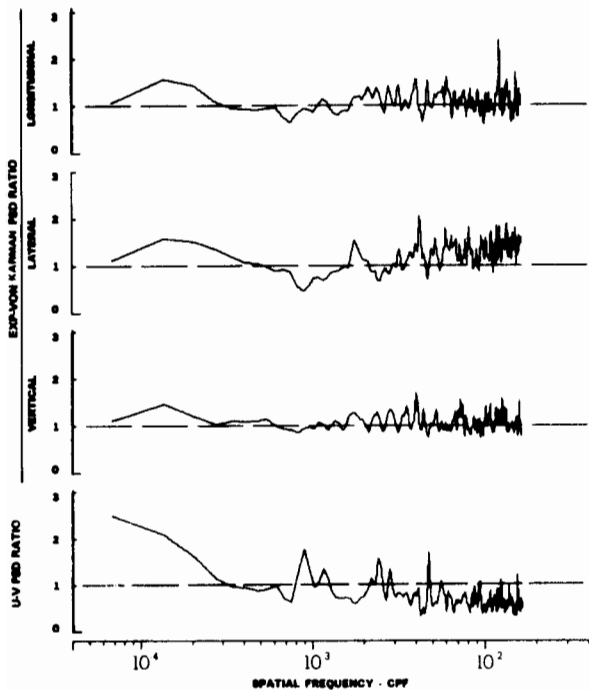
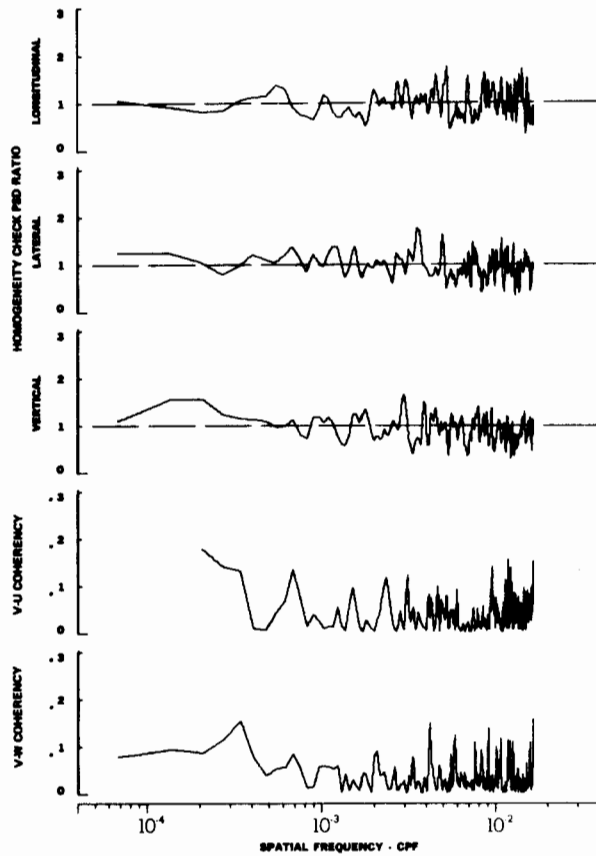
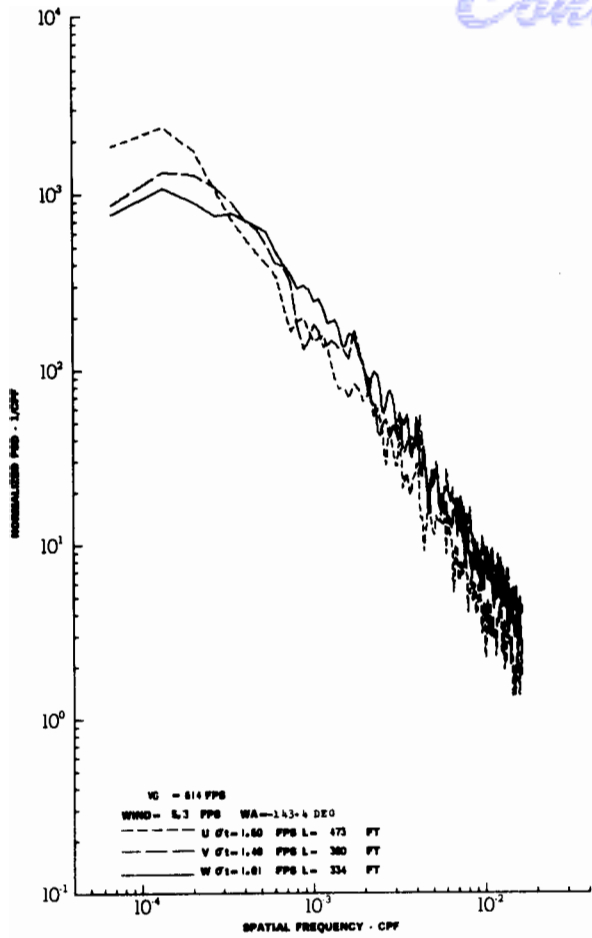
# Contrails



TURBULENCE SPECTRA DATA FOR TEST 47, LEG 7, CATEGORY 414334

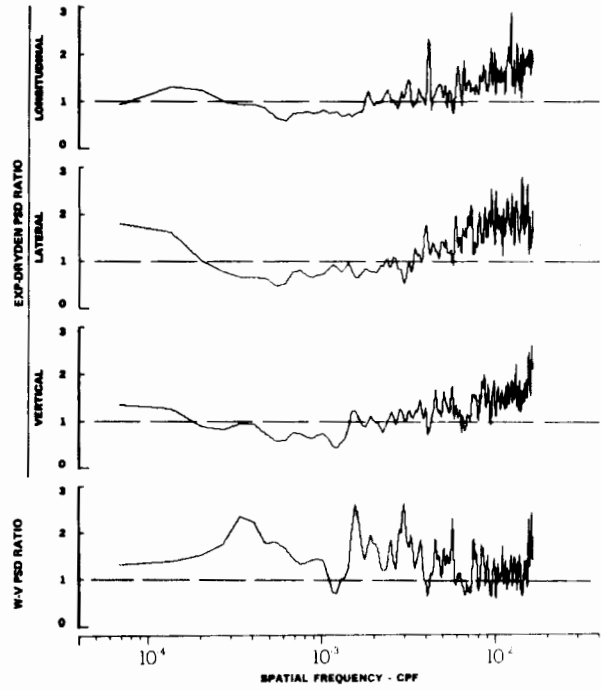
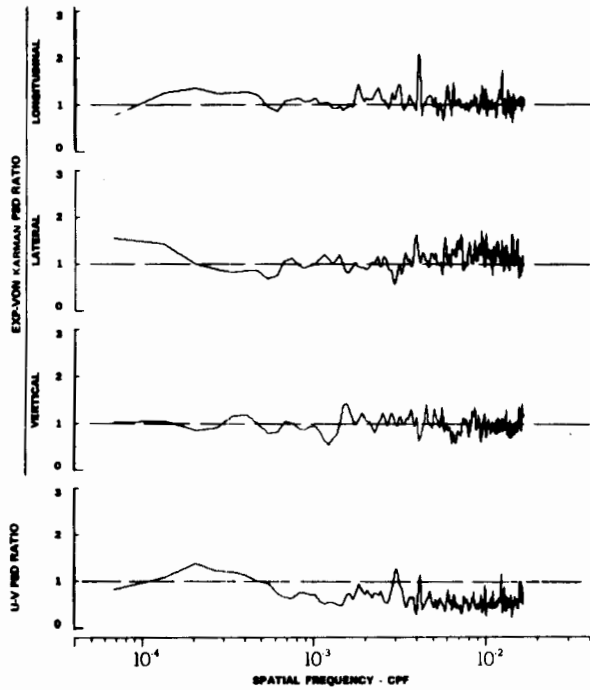
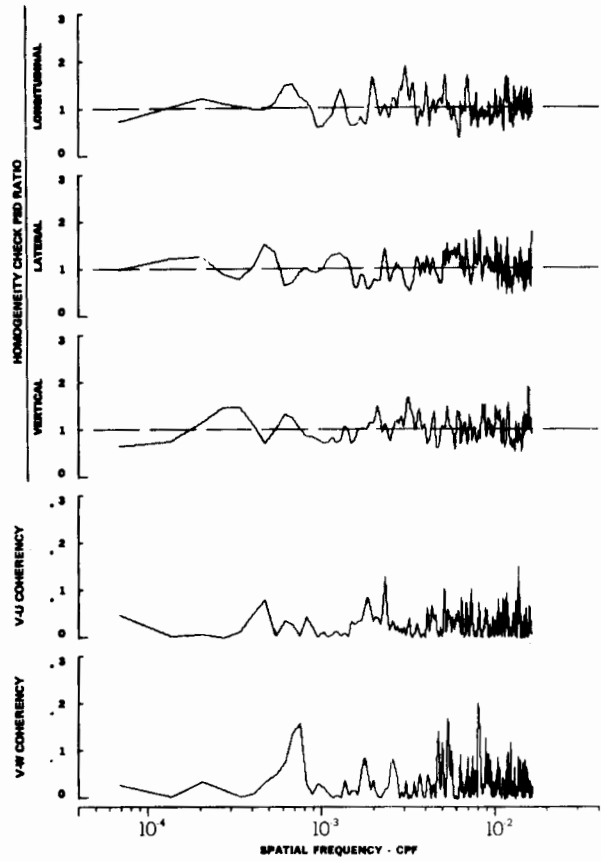
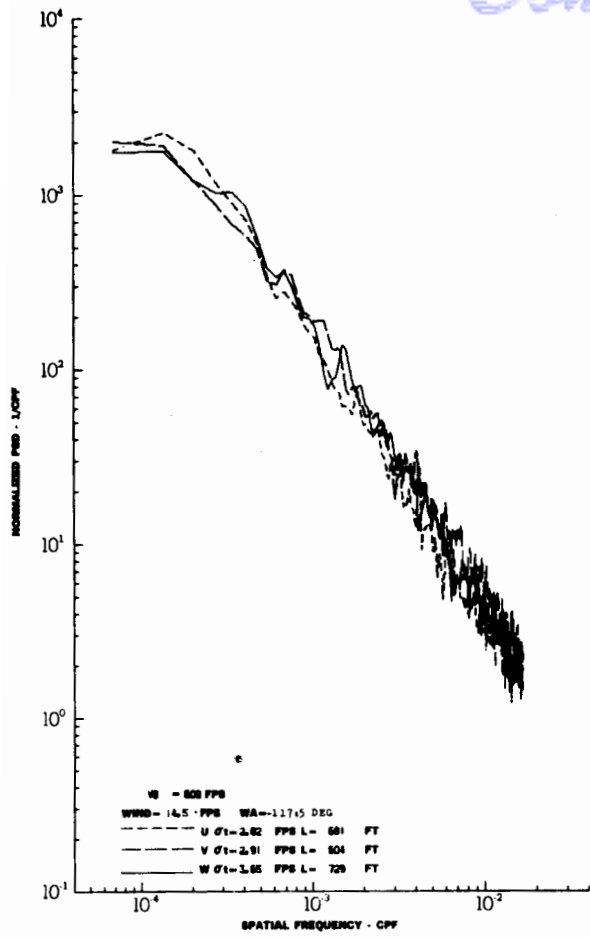
FIGURE IV-53





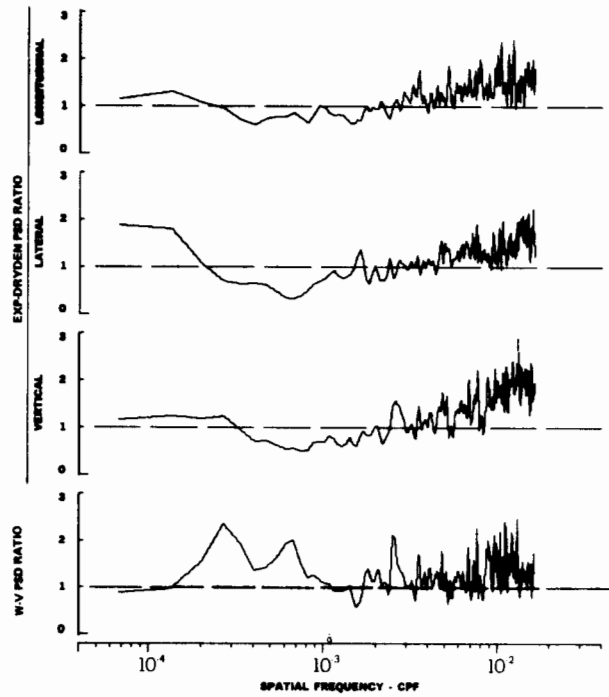
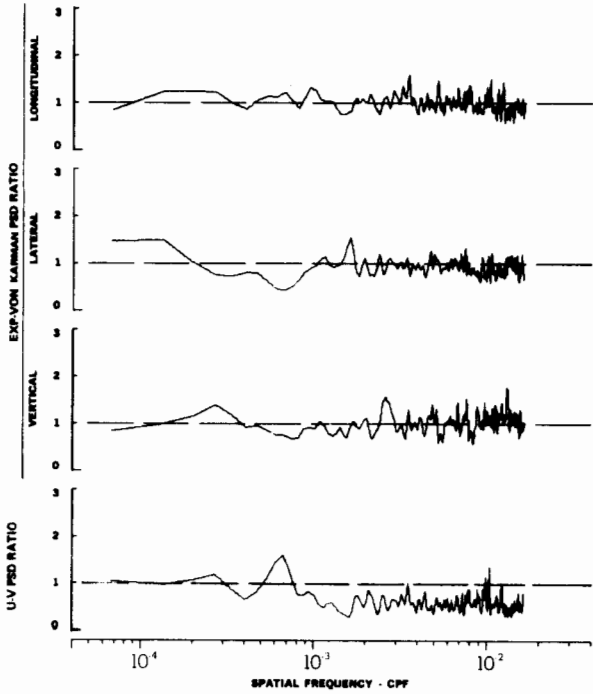
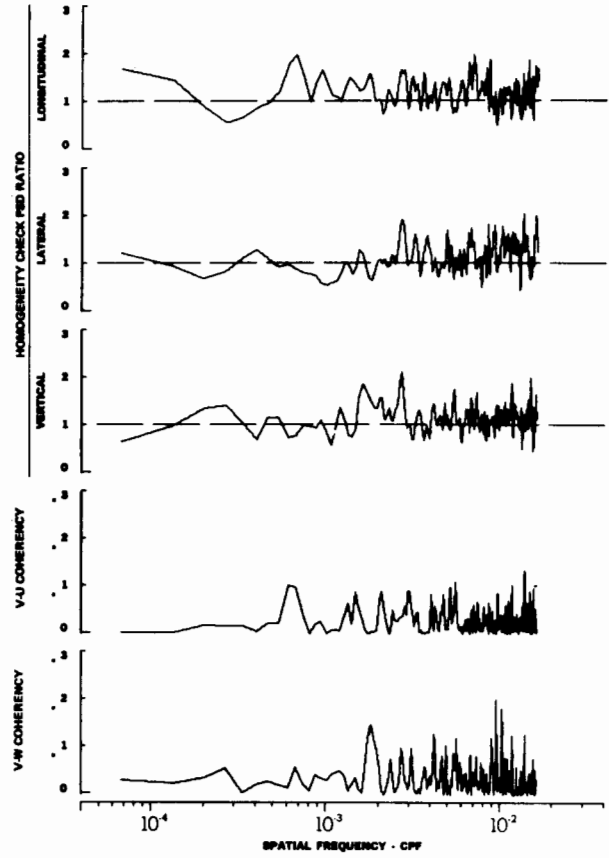
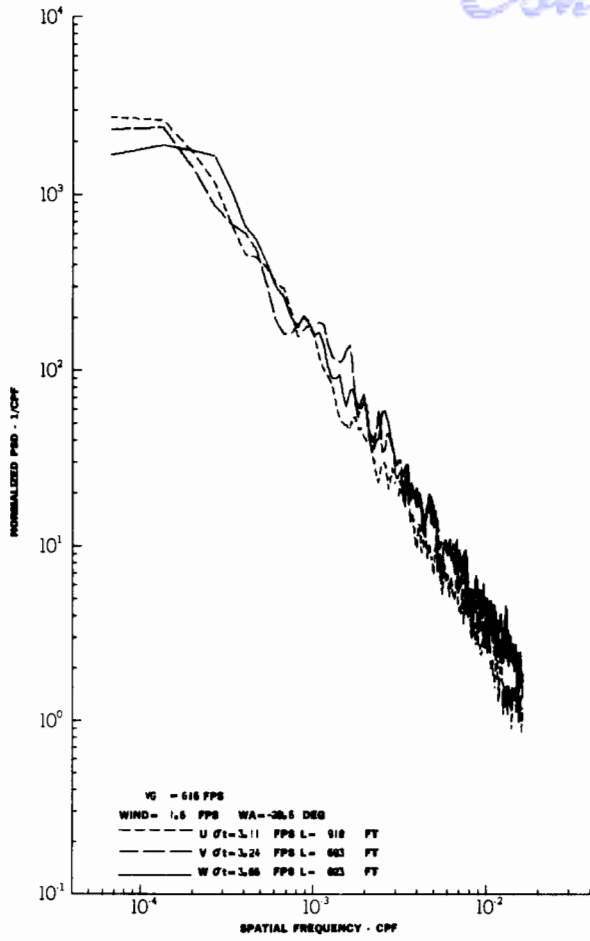
TURBULENCE SPECTRA DATA FOR TEST 49, LEG 7, CATEGORY 421234  
 FIGURE IV-54

# Contrails



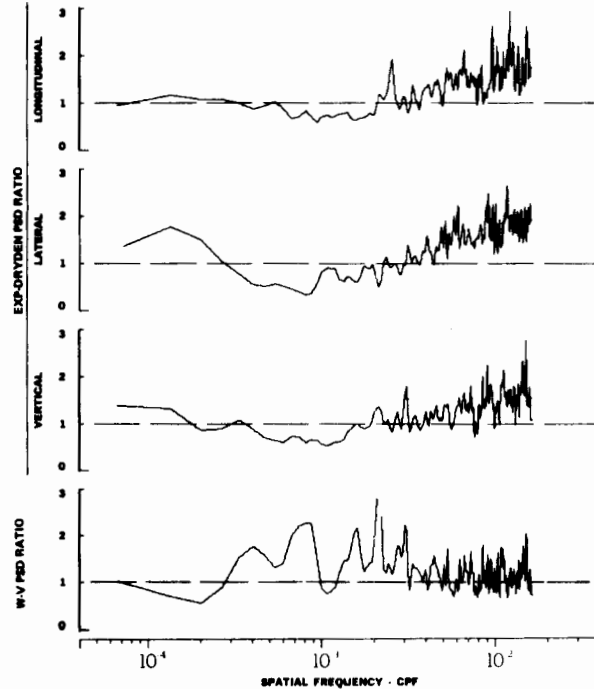
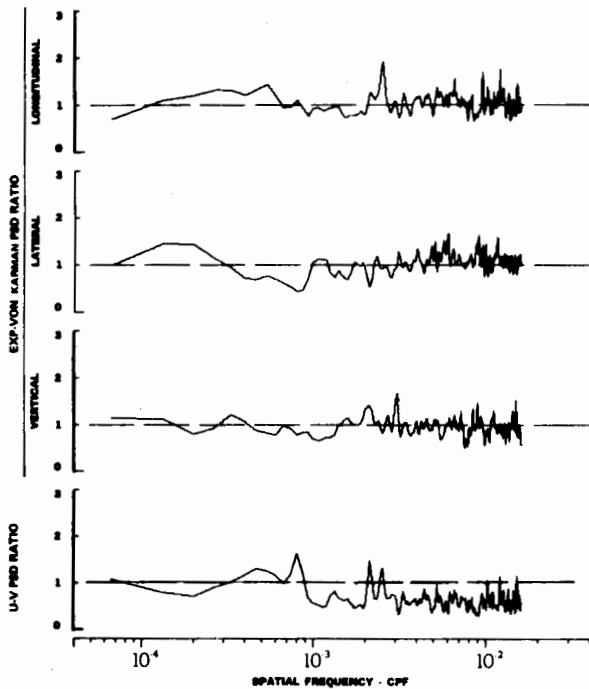
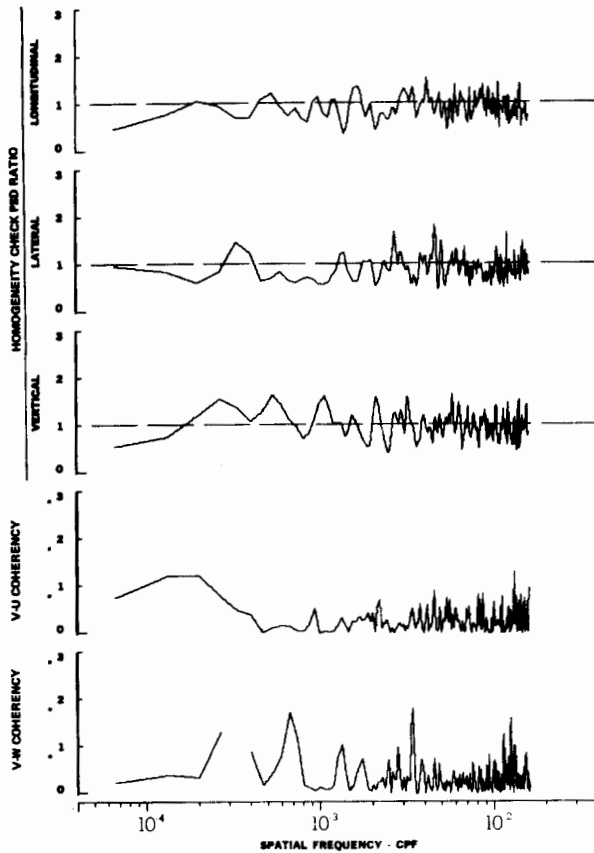
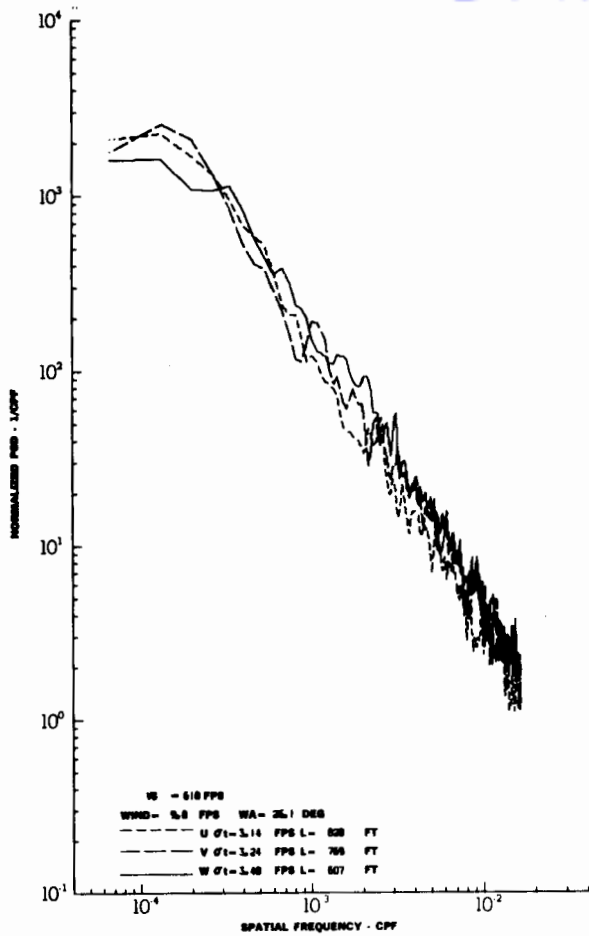
TURBULENCE SPECTRA DATA FOR TEST 50, LEG 2, CATEGORY 424334

FIGURE IV-55



TURBULENCE SPECTRA DATA FOR TEST 50, LEG 4, CATEGORY 424334

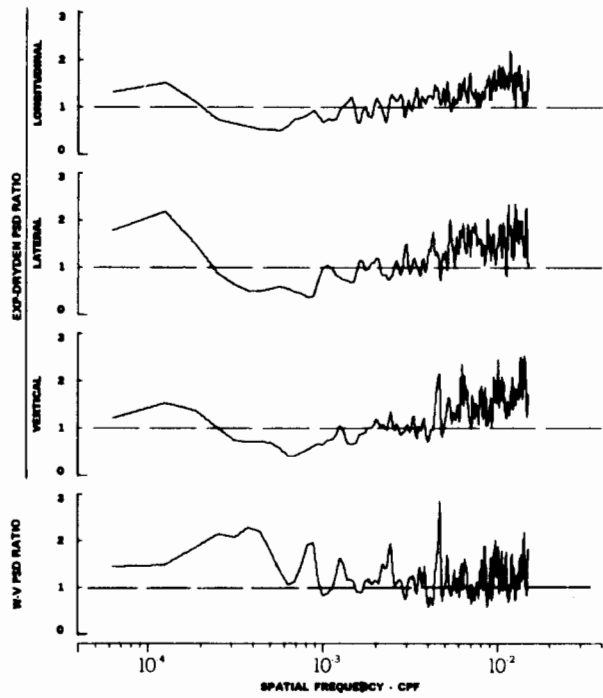
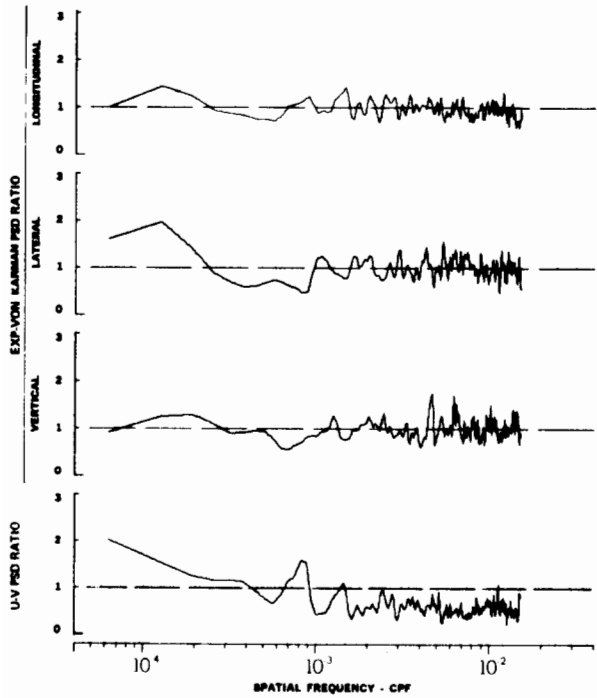
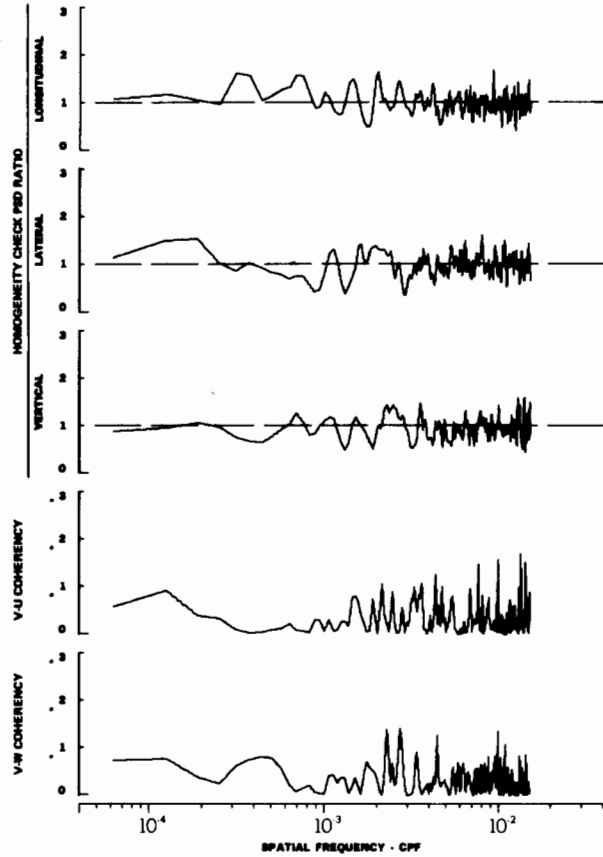
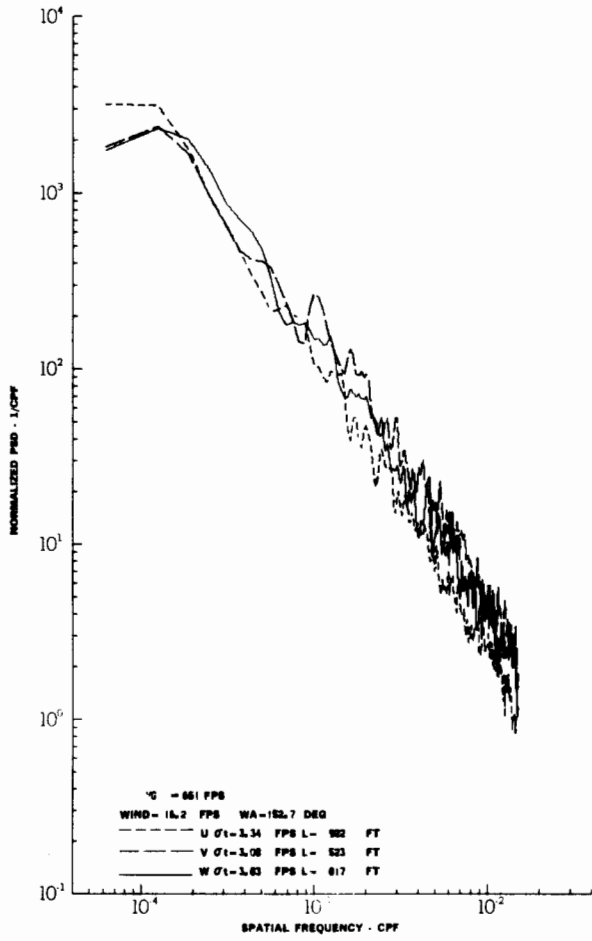
FIGURE IV-56



TURBULENCE SPECTRA DATA FOR TEST 50, LEG 6, CATEGORY 424334

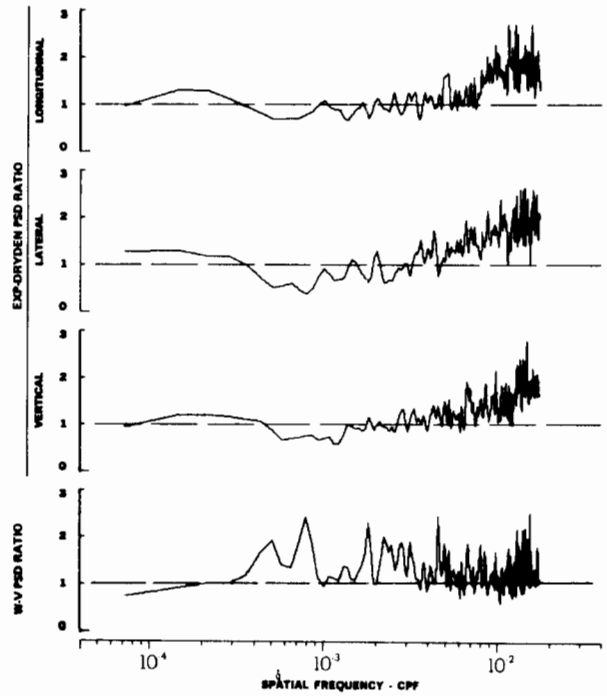
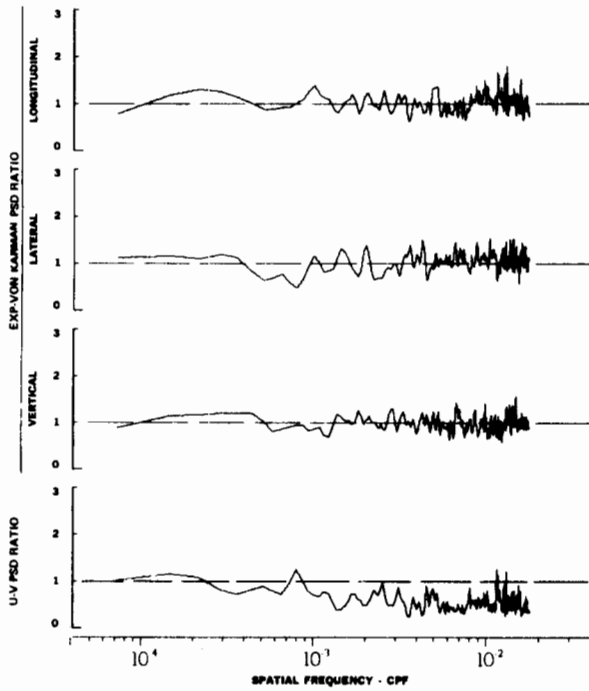
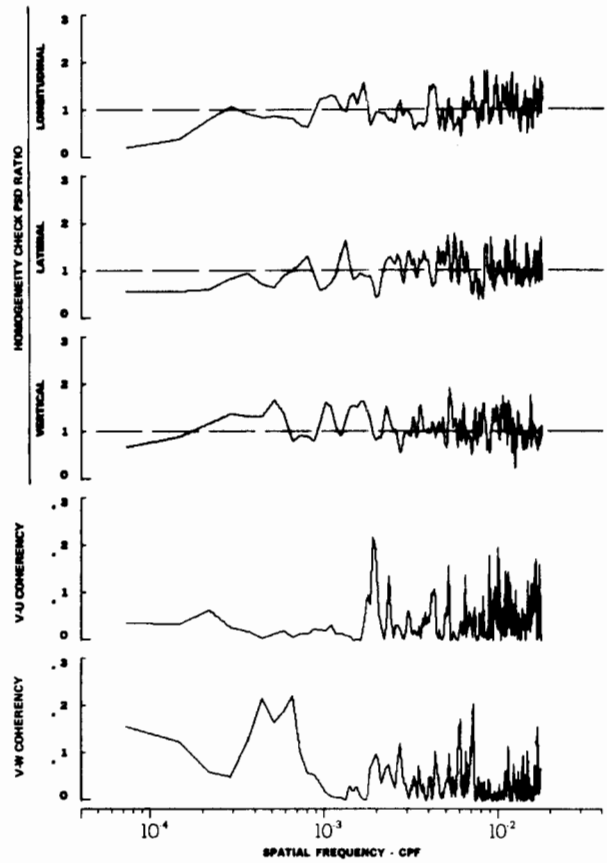
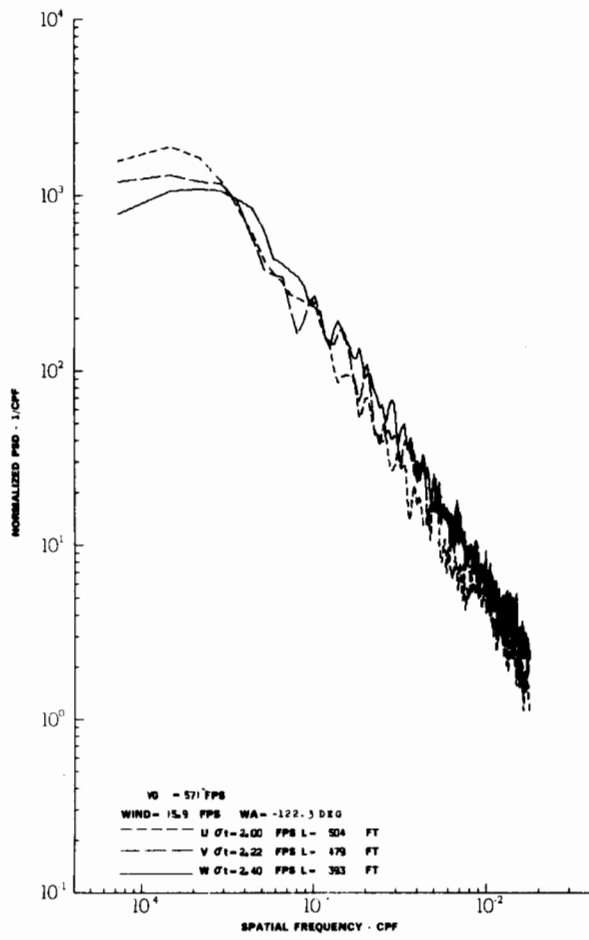
FIGURE IV-57

# Contrails

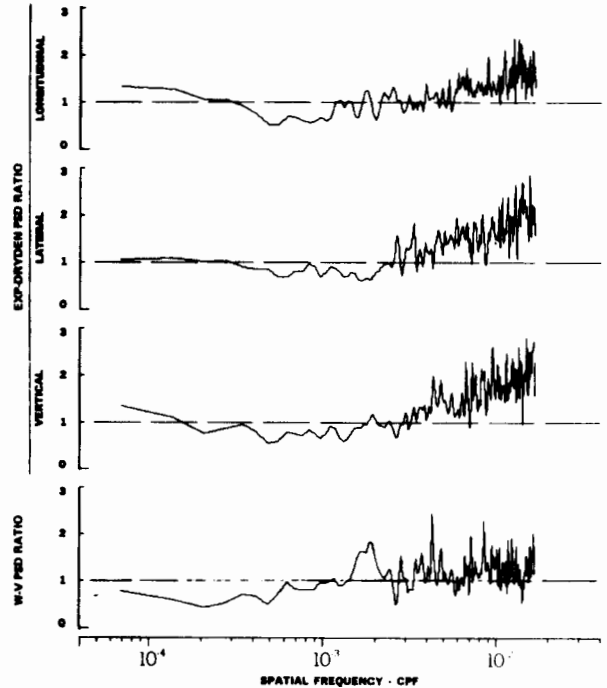
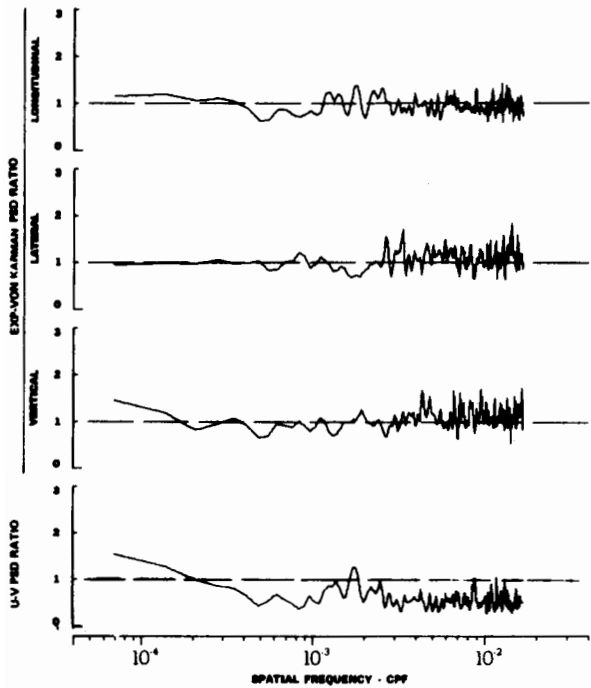
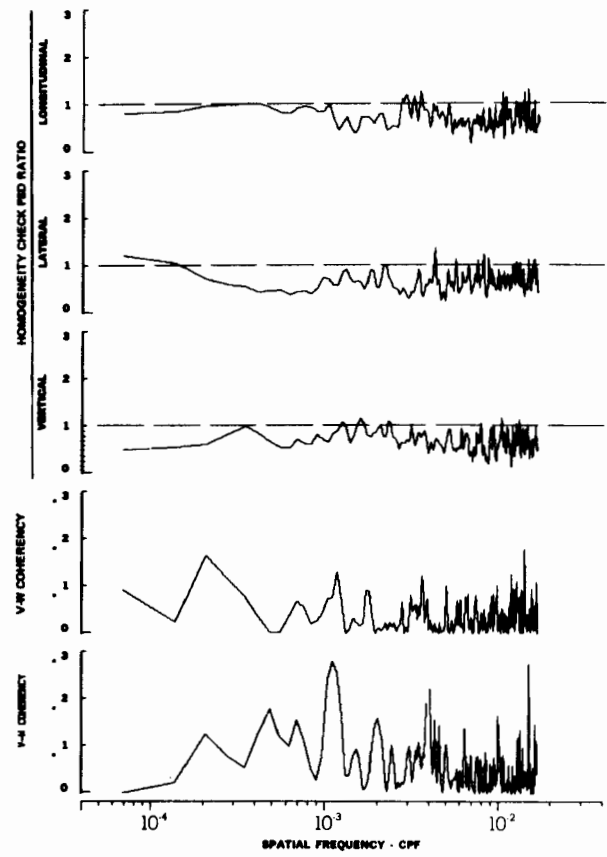
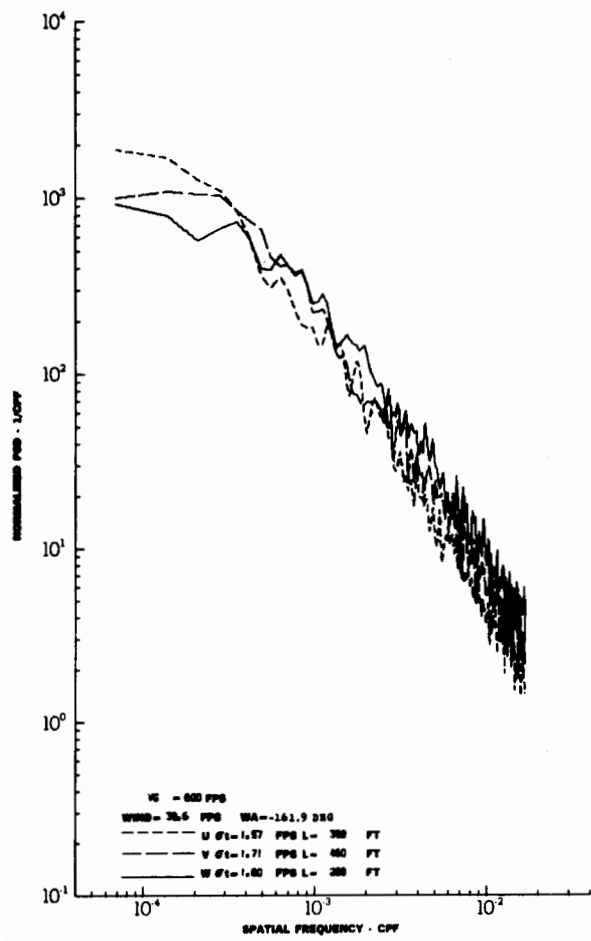


TURBULENCE SPECTRA DATA FOR TEST 50, LEG 8, CATEGORY 424334  
FIGURE IV-58

# Contrails

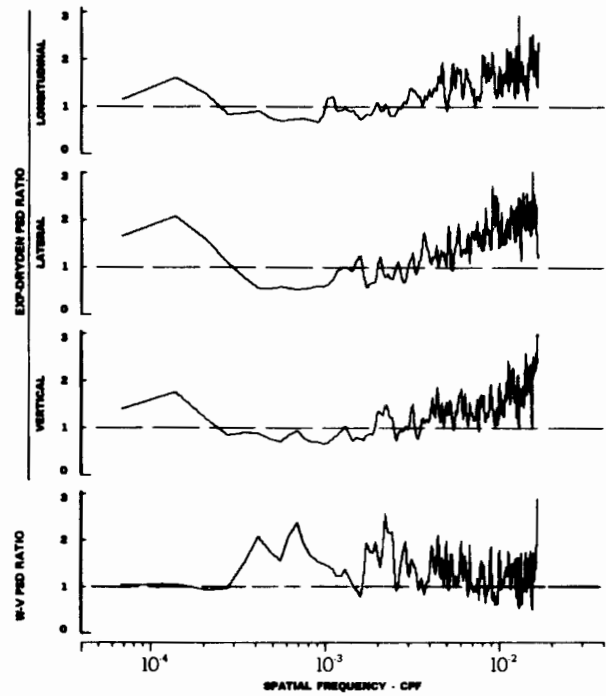
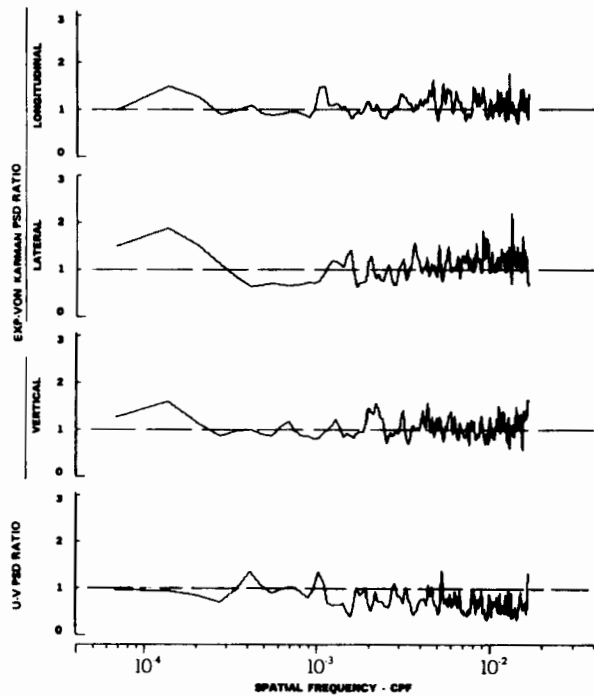
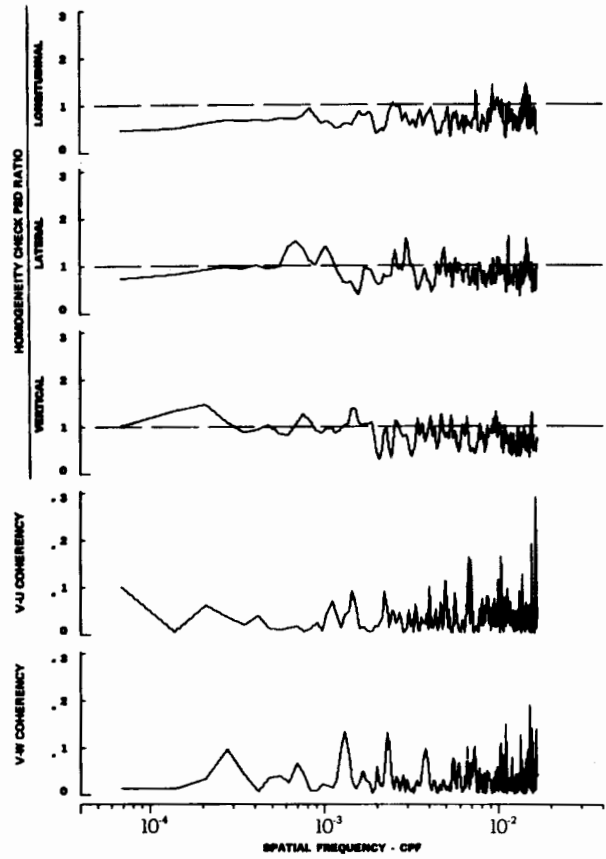
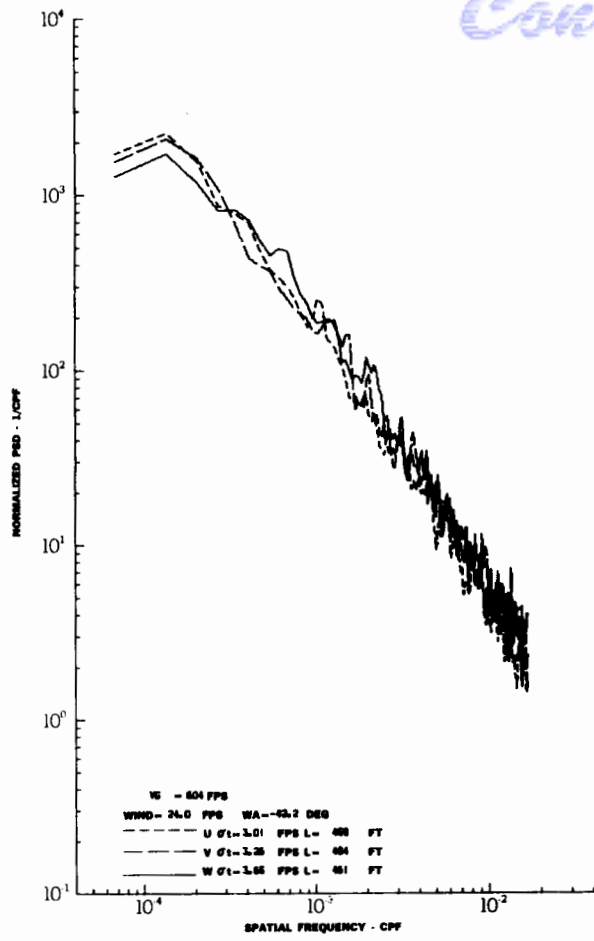


TURBULENCE SPECTRA DATA FOR TEST 51, LEG 3, CATEGORY 323231  
FIGURE IV-59

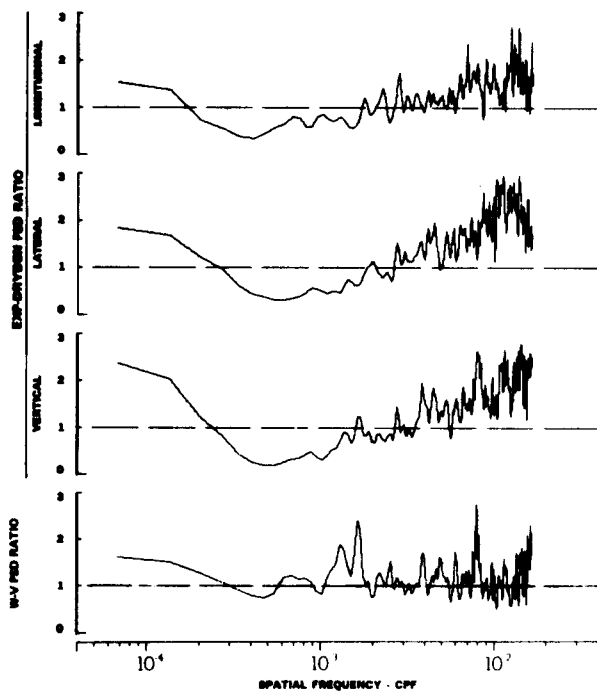
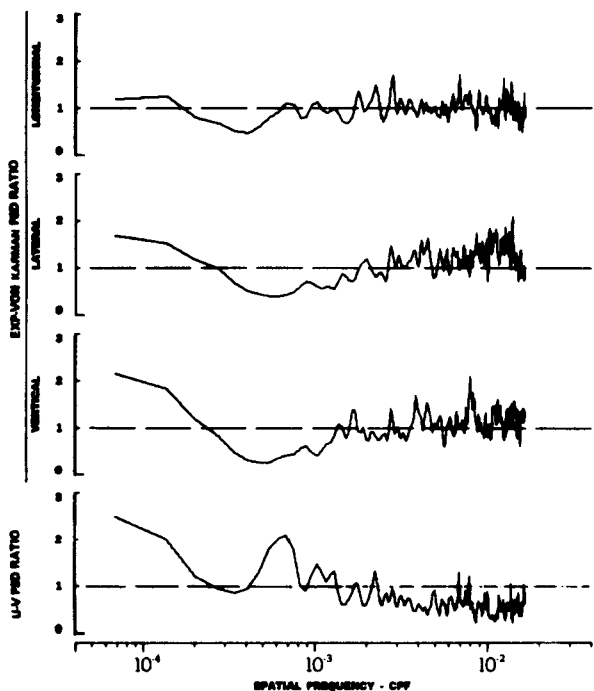
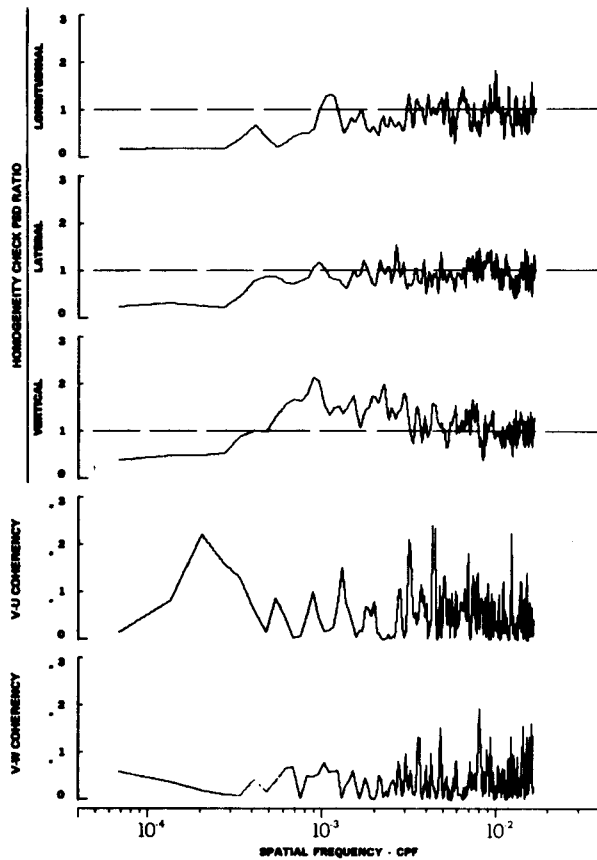
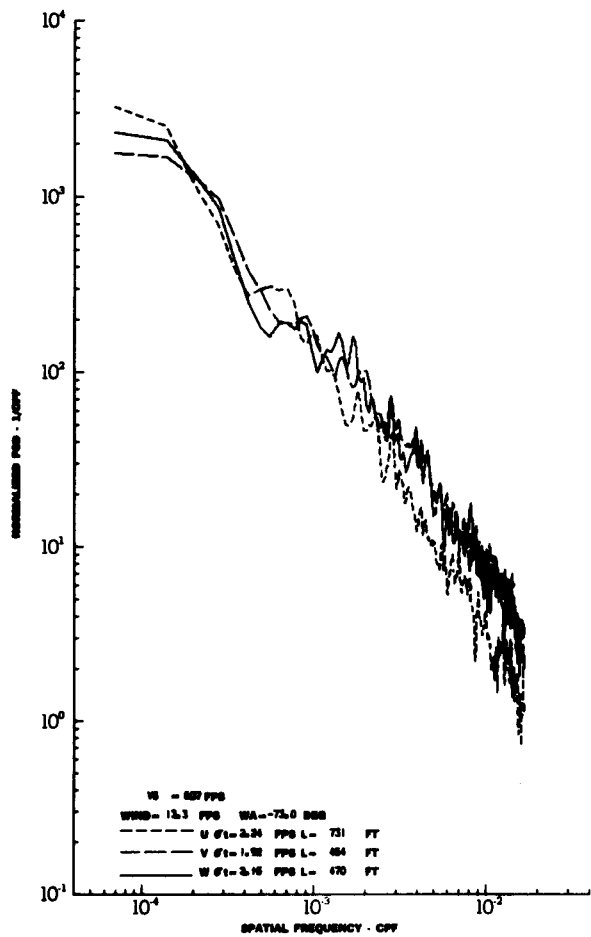


TURBULENCE SPECTRA DATA FOR TEST 53, LEG 3, CATEGORY 323231  
 FIGURE IV-60



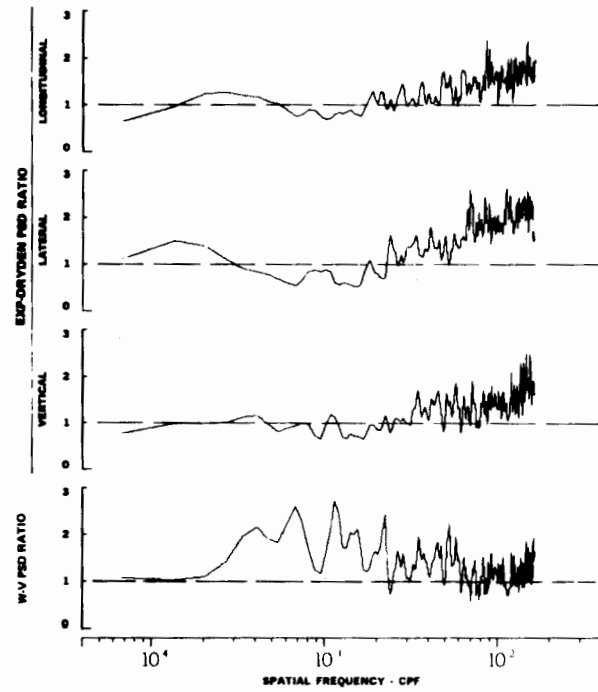
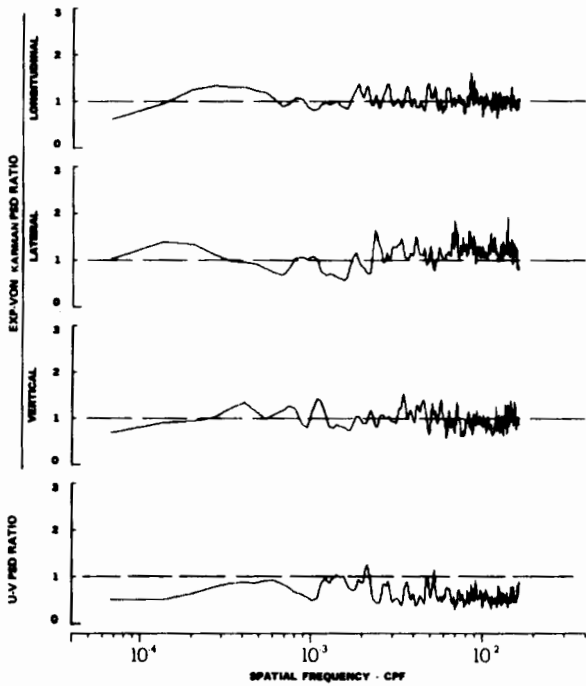
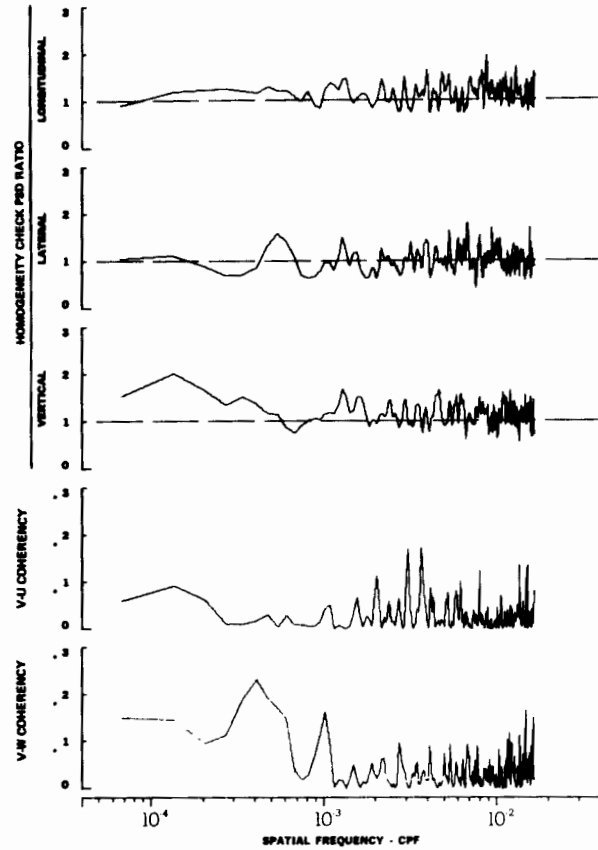
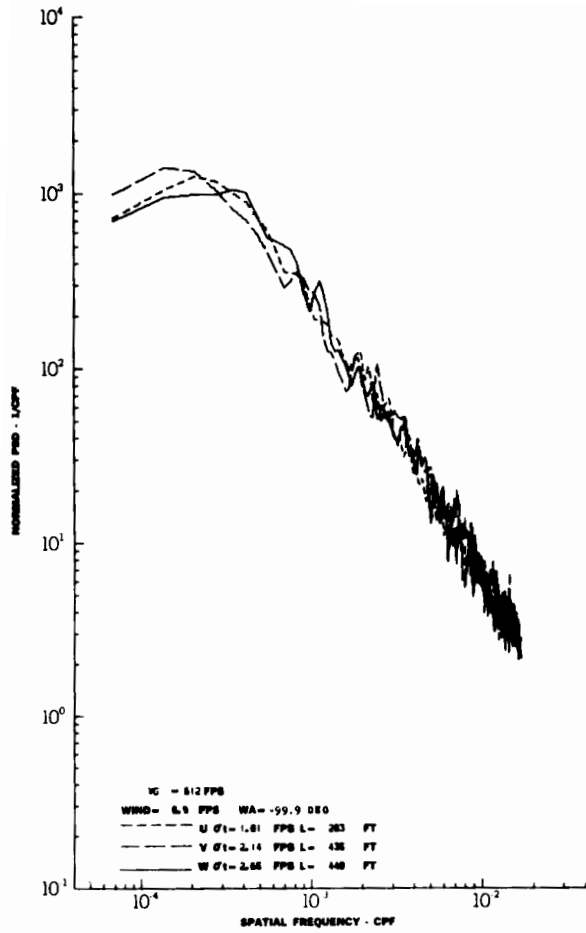


TURBULENCE SPECTRA DATA FOR TEST 57, LEG 1, CATEGORY 224331  
 FIGURE IV-61



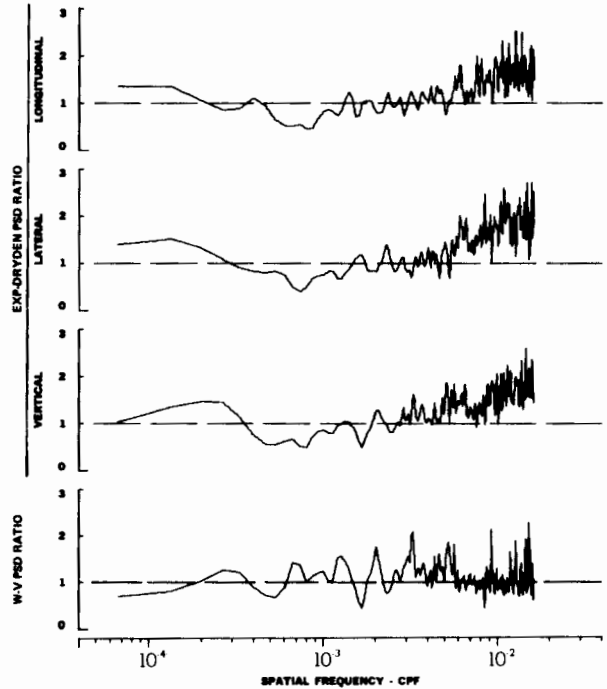
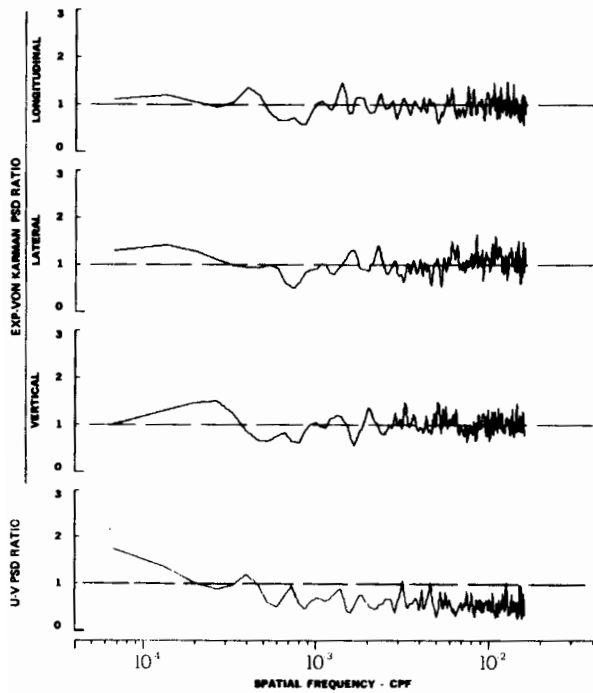
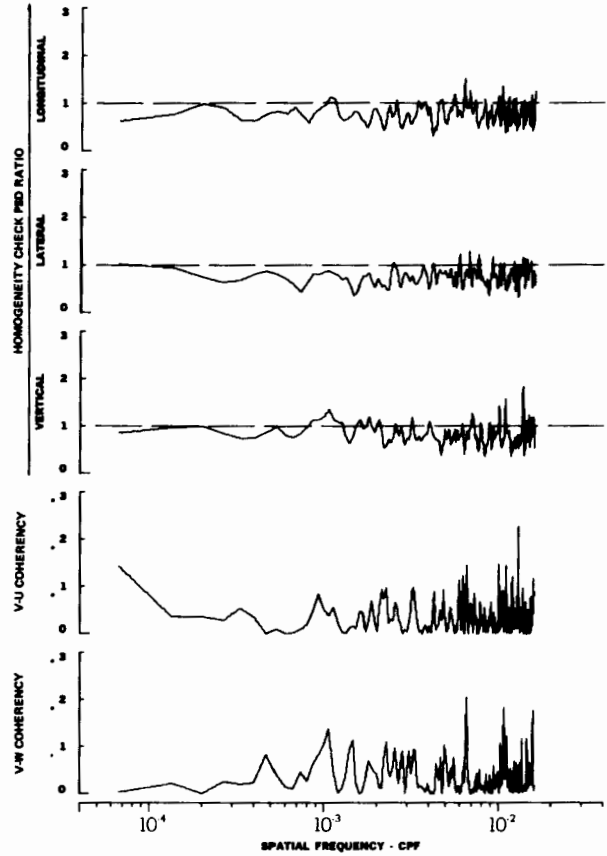
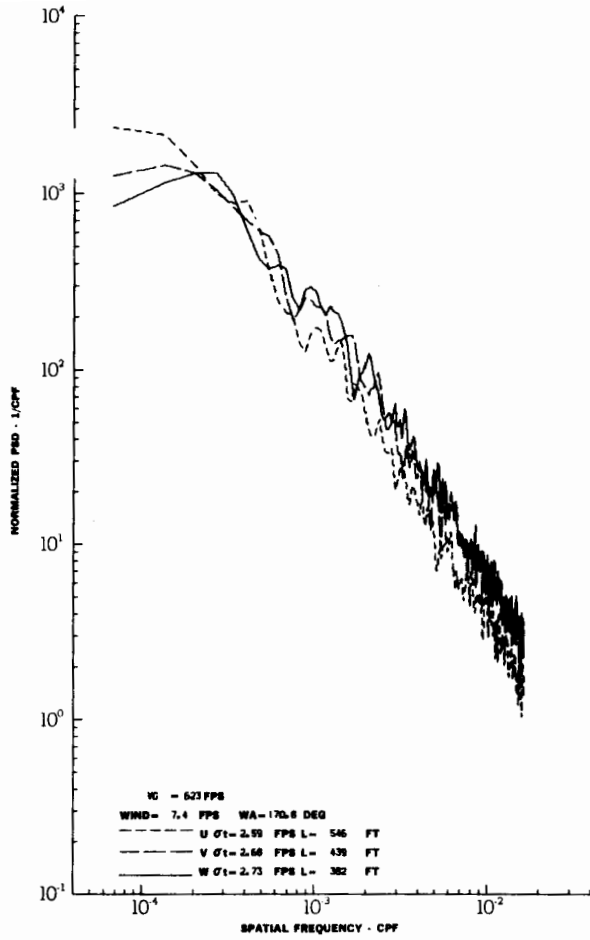
TURBULENCE SPECTRA DATA FOR TEST 59, LEG 1, CATEGORY 211231

FIGURE IV-62



TURBULENCE SPECTRA DATA FOR TEST 62, LEG 2, CATEGORY 322331

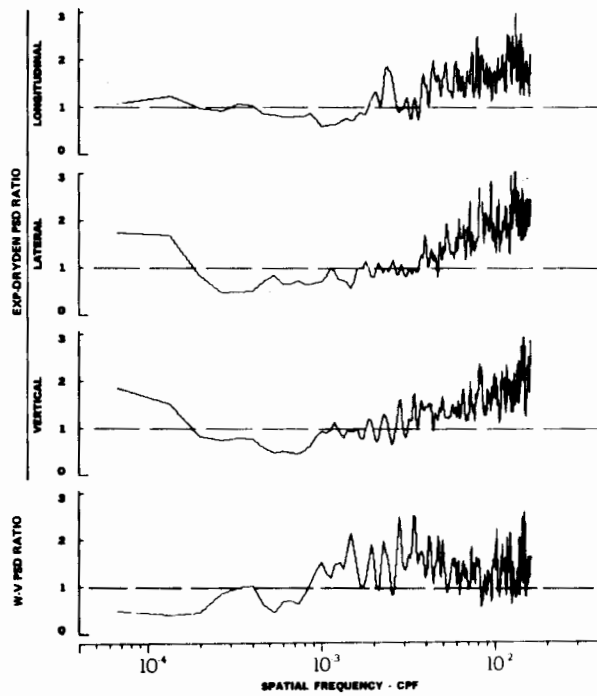
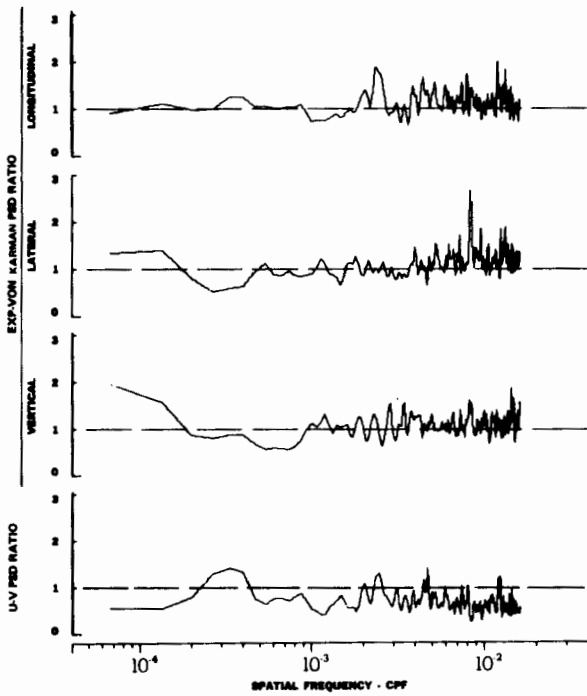
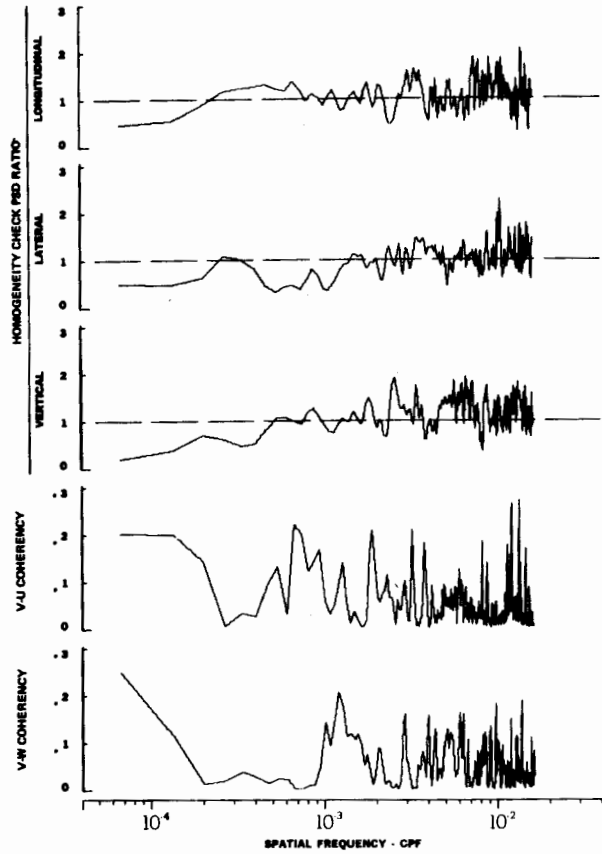
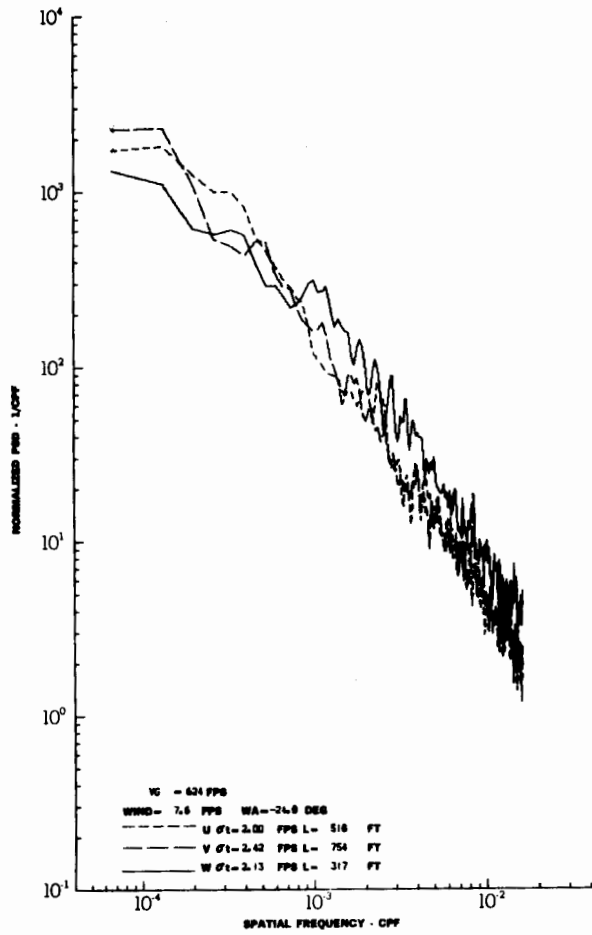
FIGURE IV-63



TURBULENCE SPECTRA DATA FOR TEST 62, LEG 6, CATEGORY 123331

FIGURE IV-64

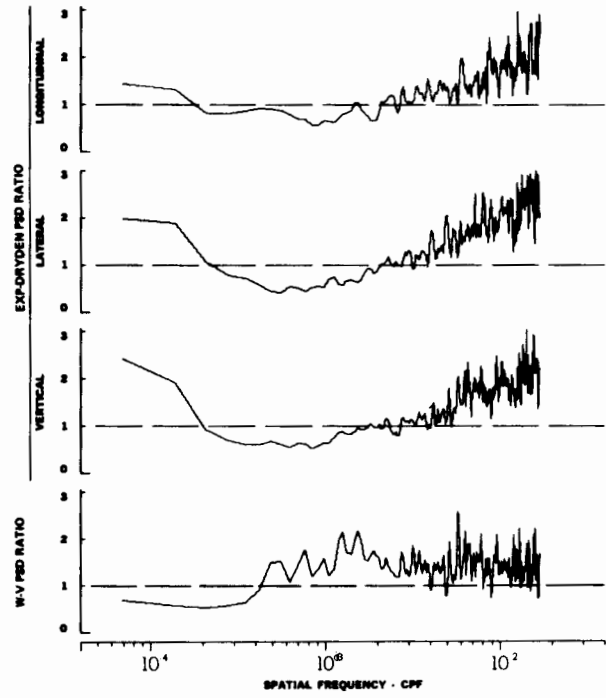
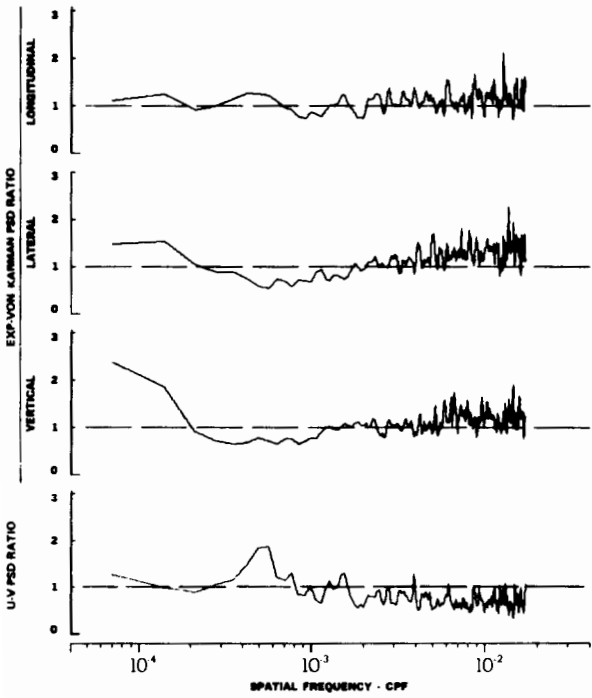
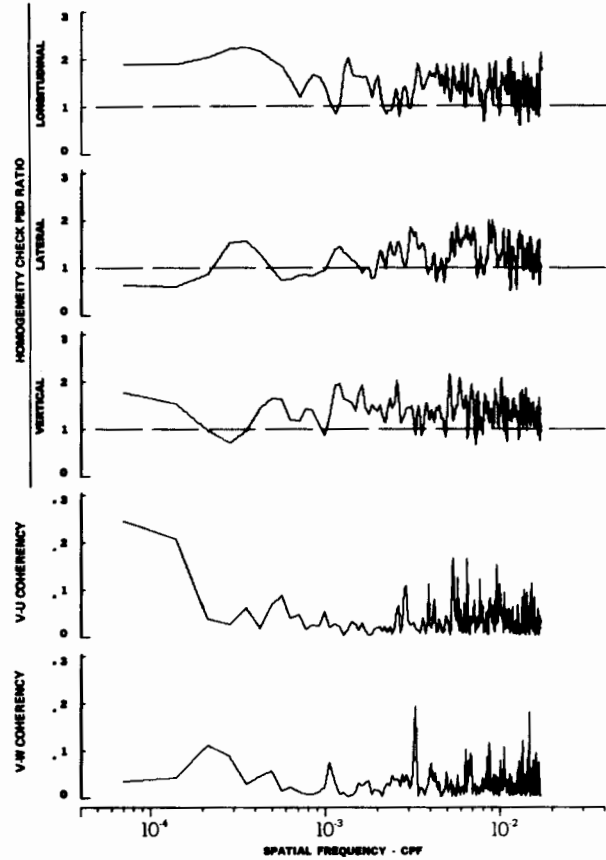
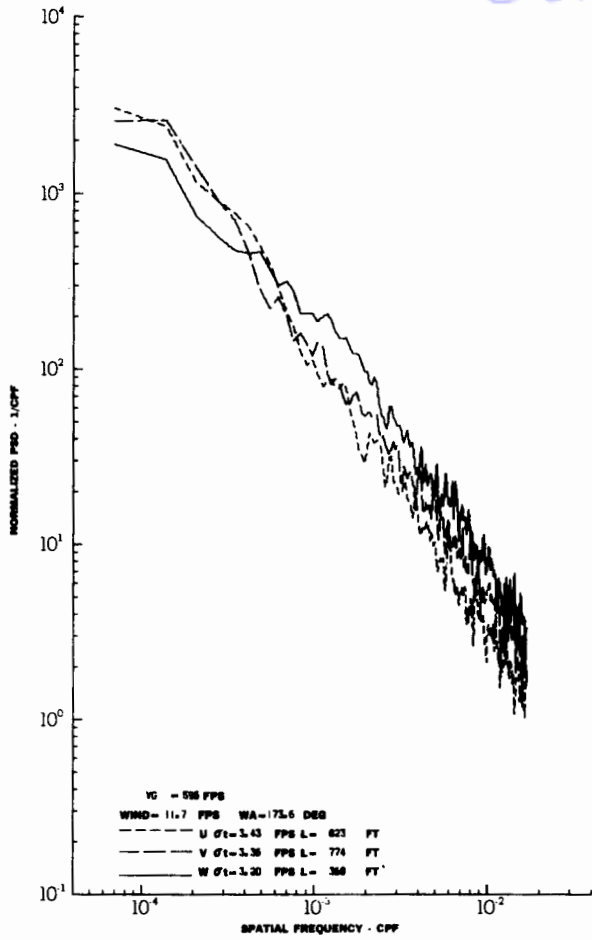
# Contrails



TURBULENCE SPECTRA DATA FOR TEST 64, LEG 6, CATEGORY 111231

FIGURE IV-65

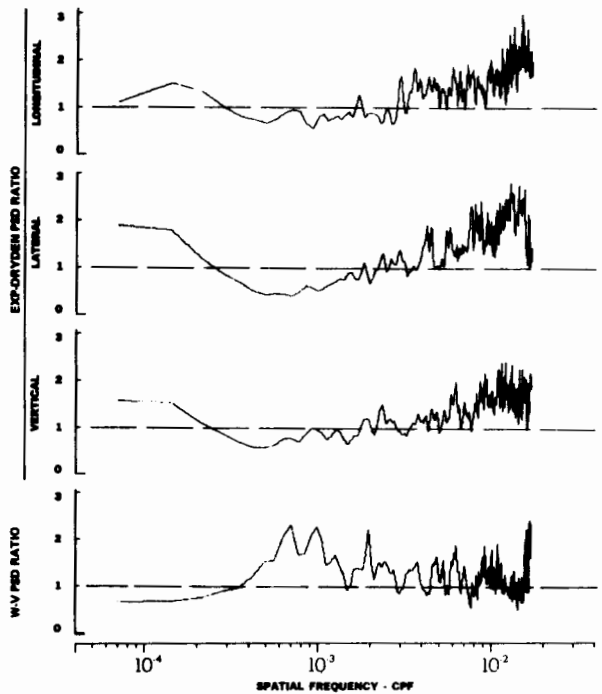
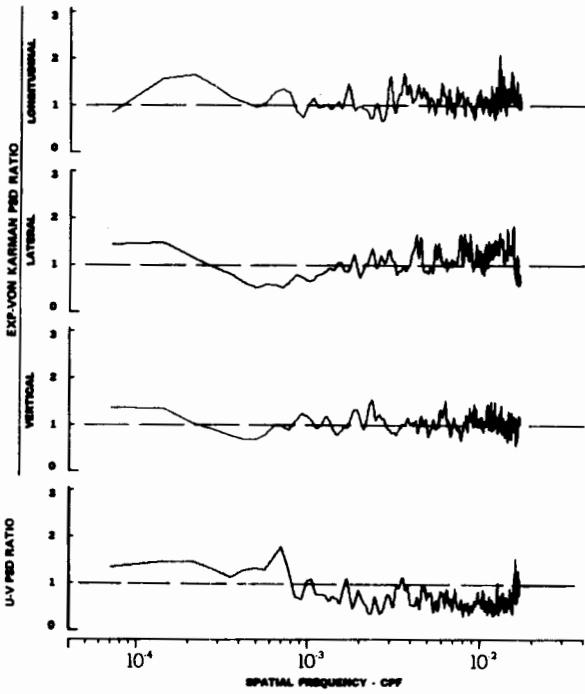
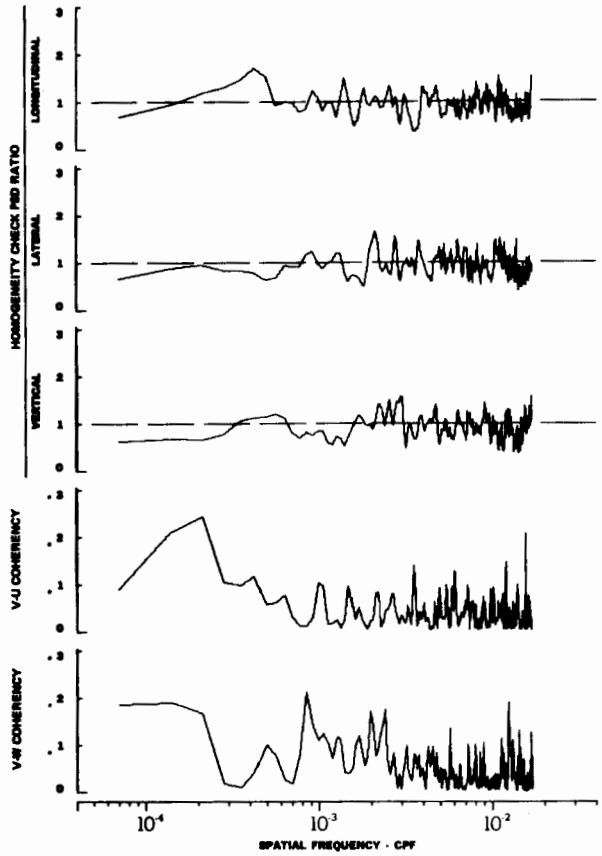
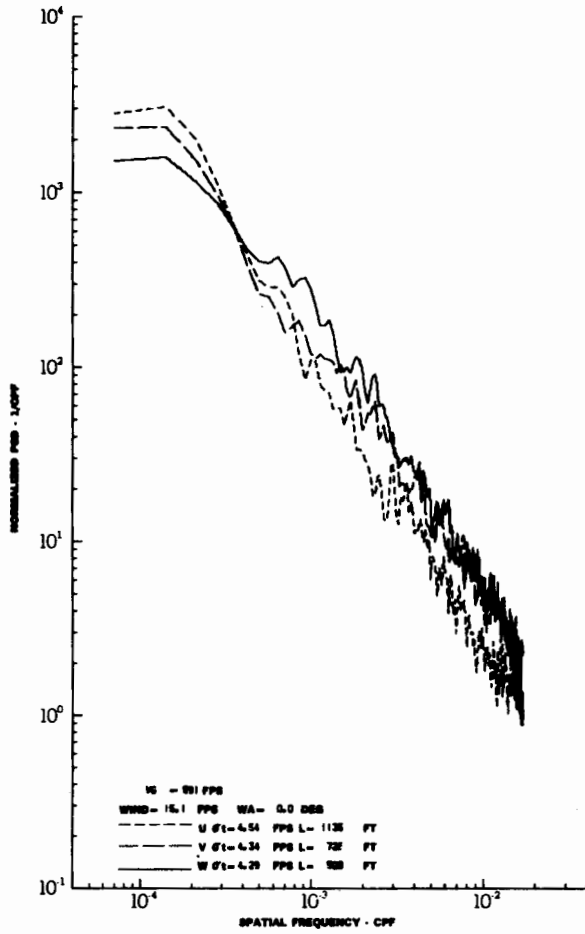
# Contrails



TURBULENCE SPECTRA DATA FOR TEST 64, LEG 8, CATEGORY 212231

FIGURE IV-66

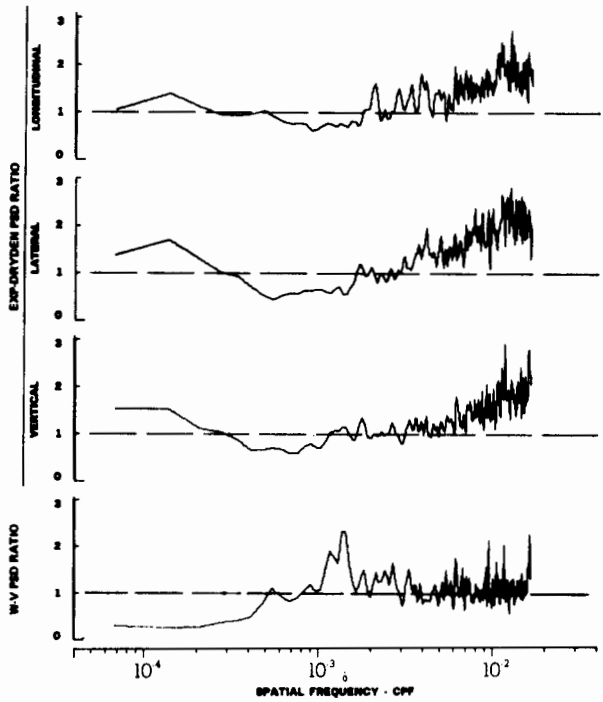
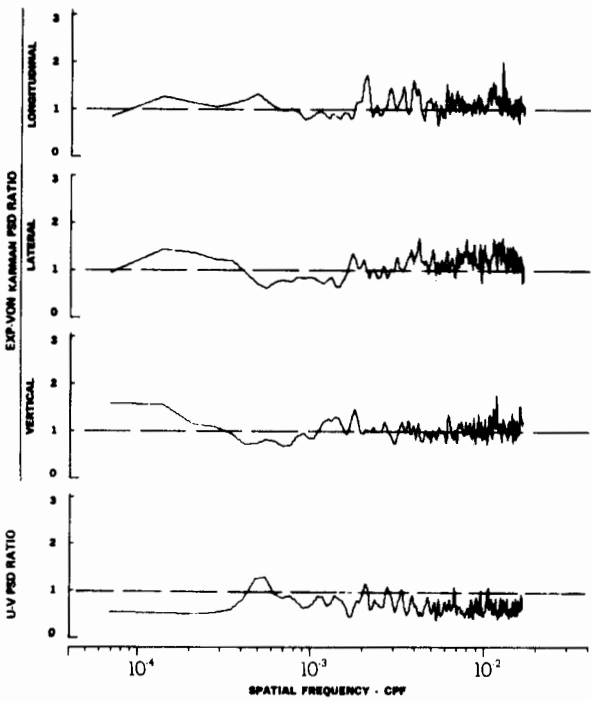
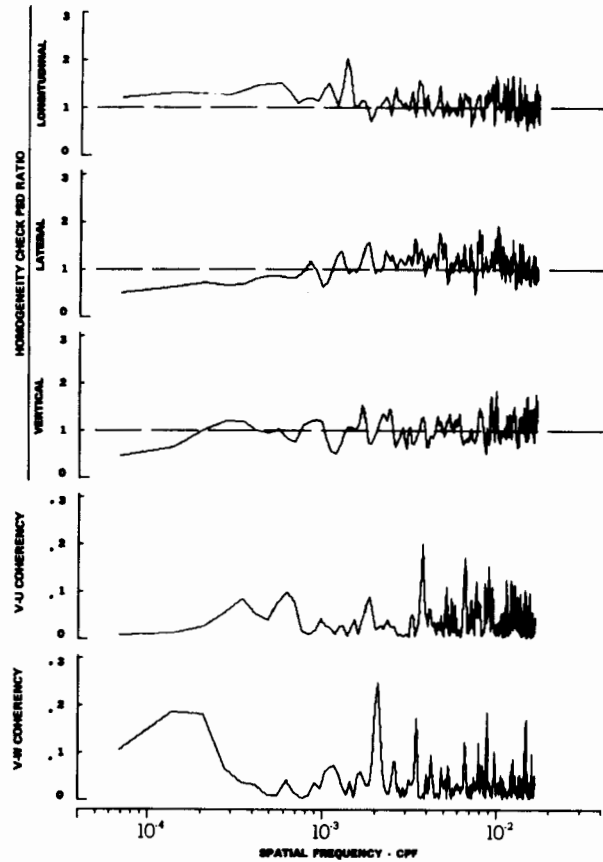
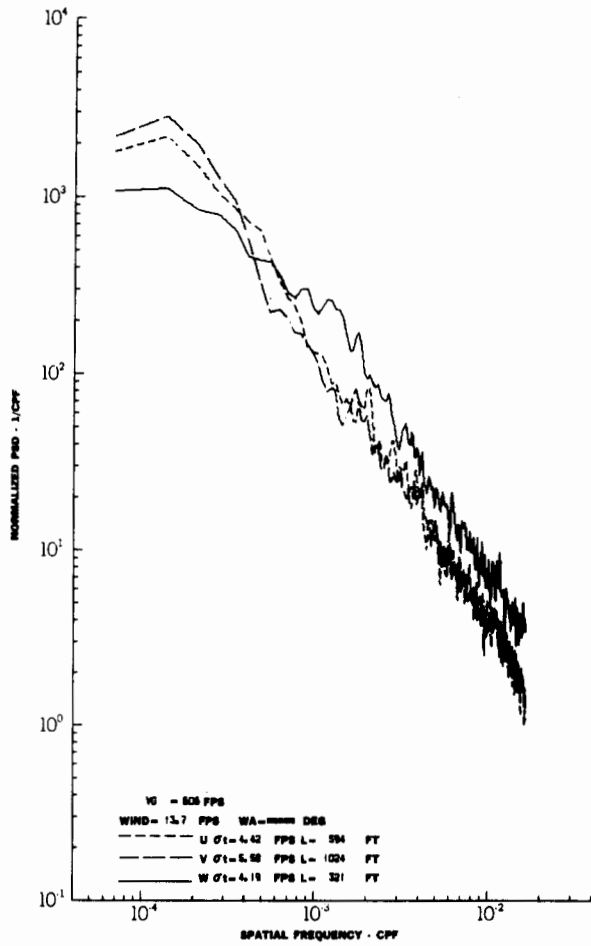
# Contrails



TURBULENCE SPECTRA DATA FOR TEST 65, LEG 1, CATEGORY 214331  
 FIGURE IV-67

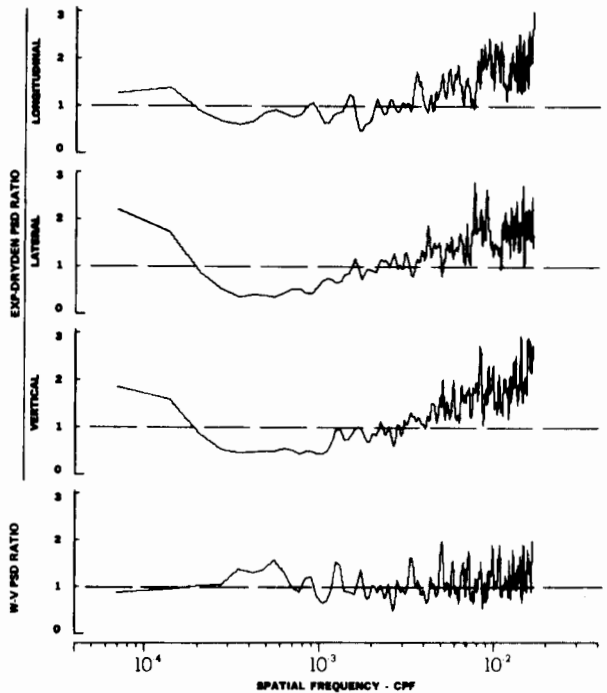
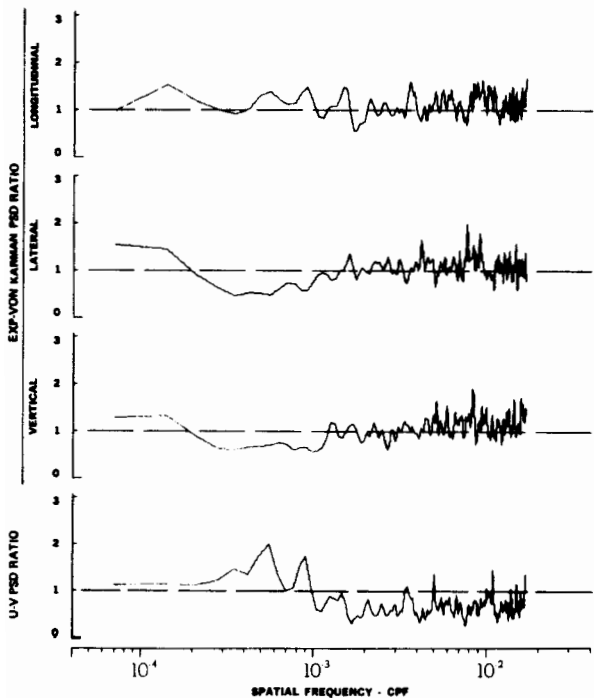
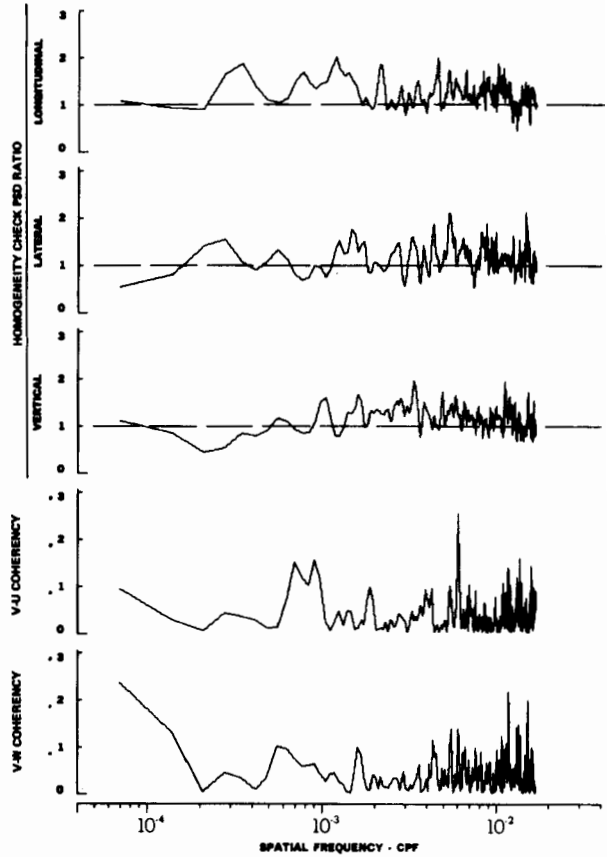
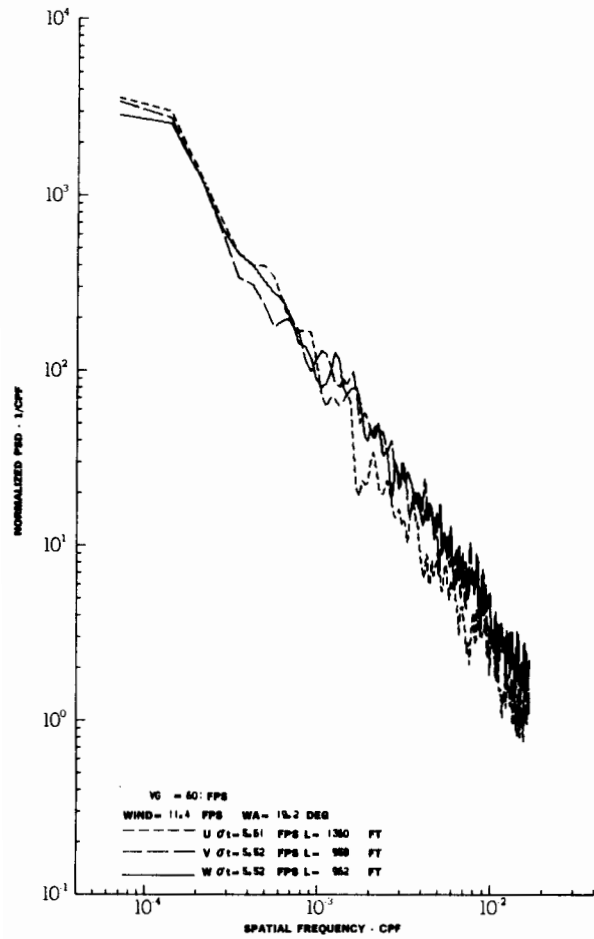


# Contrails



TURBULENCE SPECTRA DATA FOR TEST 65, LEG 3, CATEGORY 112331  
 FIGURE IV-68

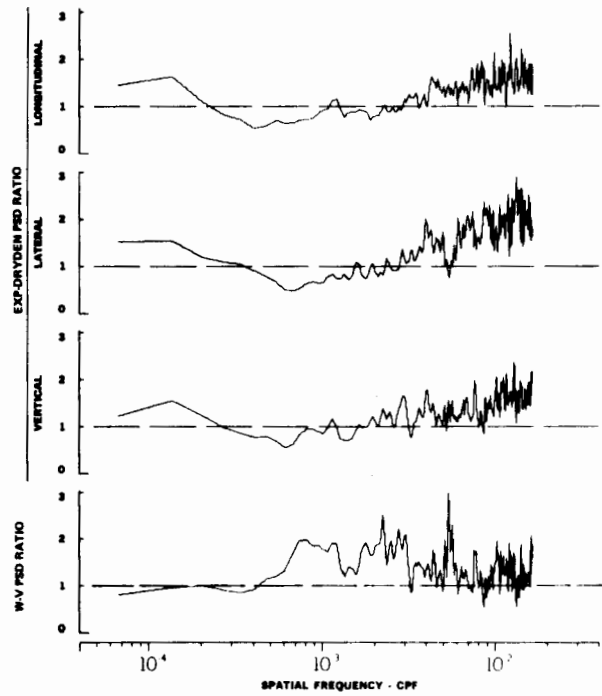
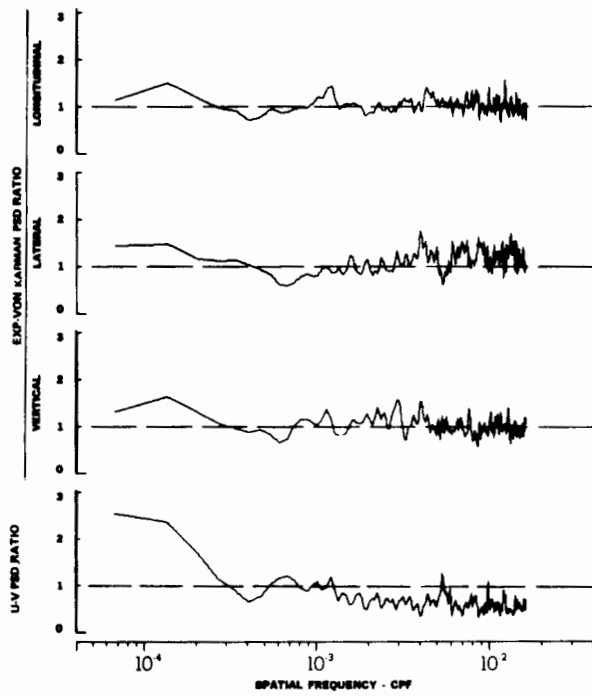
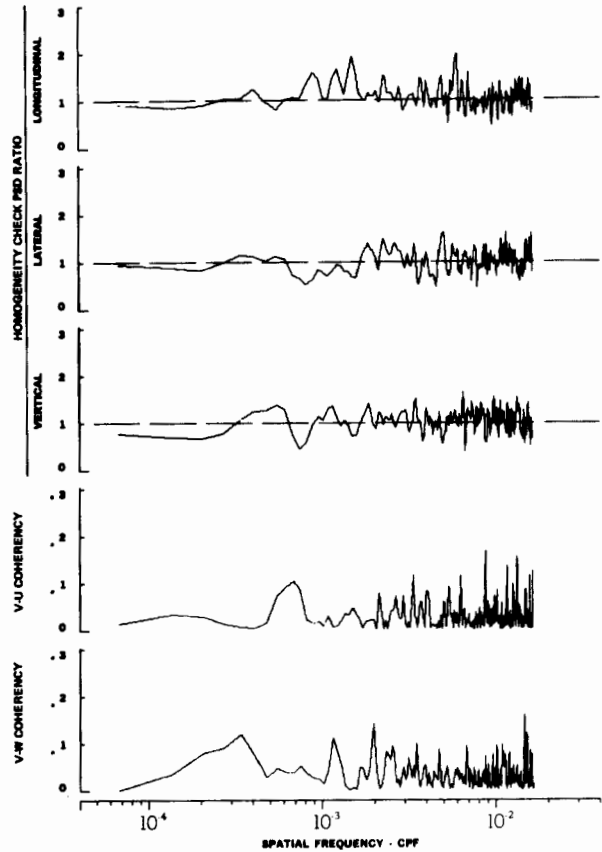
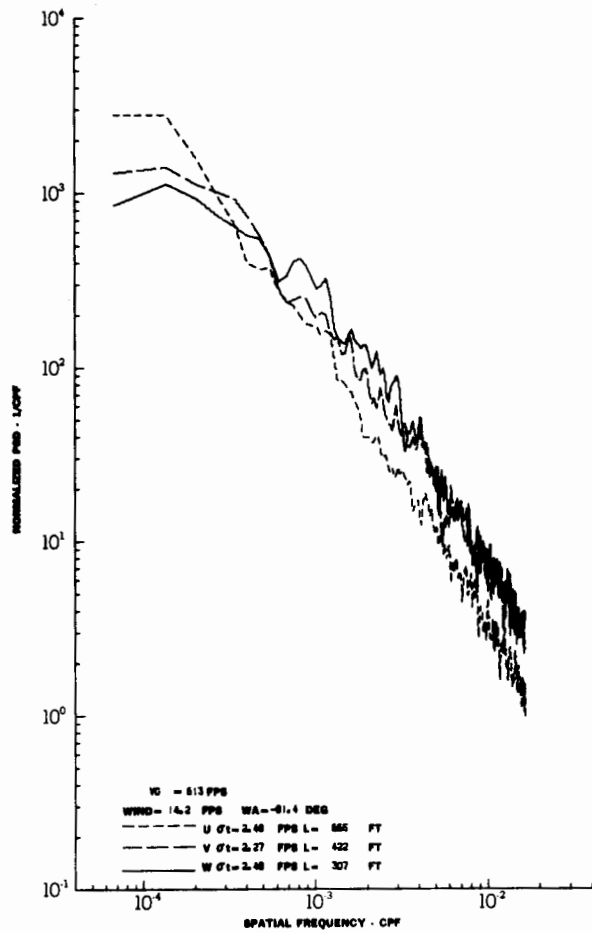
# Contrails



TURBULENCE SPECTRA DATA FOR TEST 65, LEG 5, CATEGORY 114331

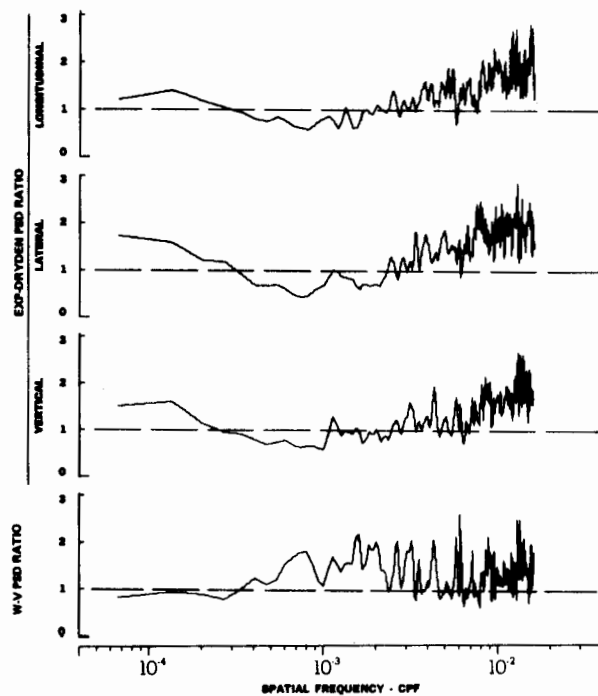
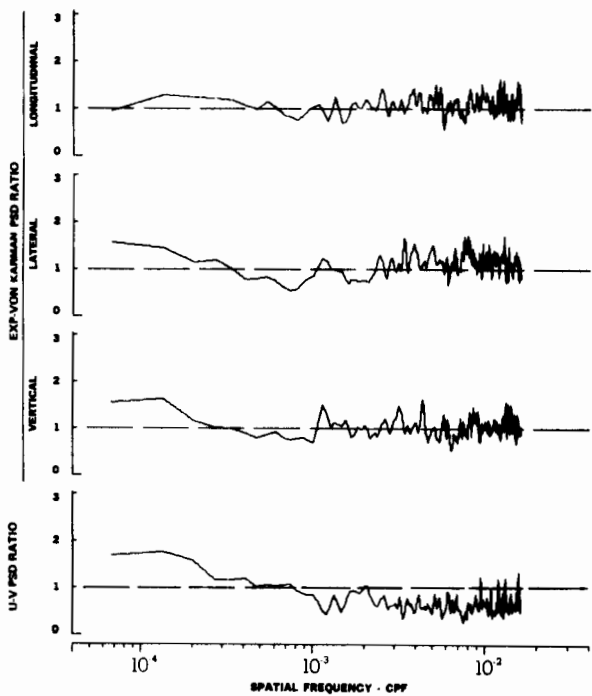
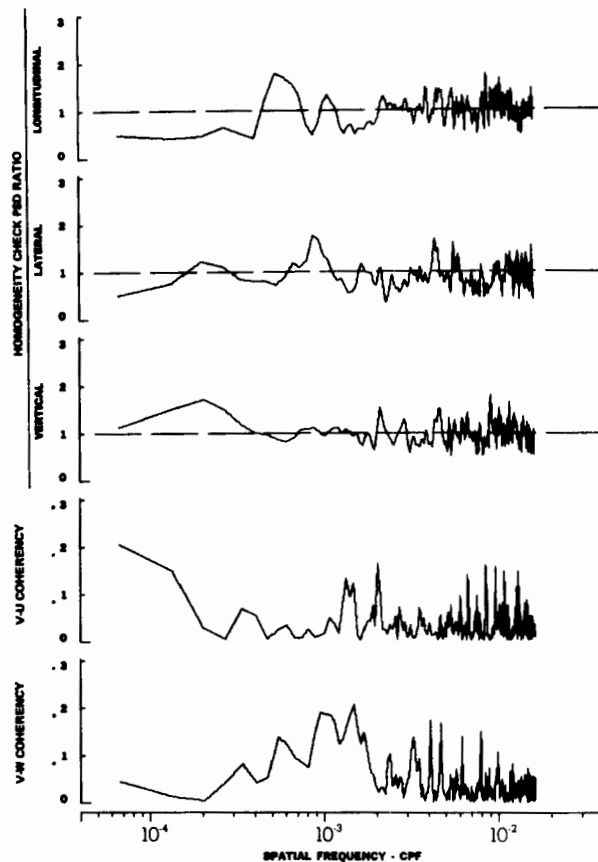
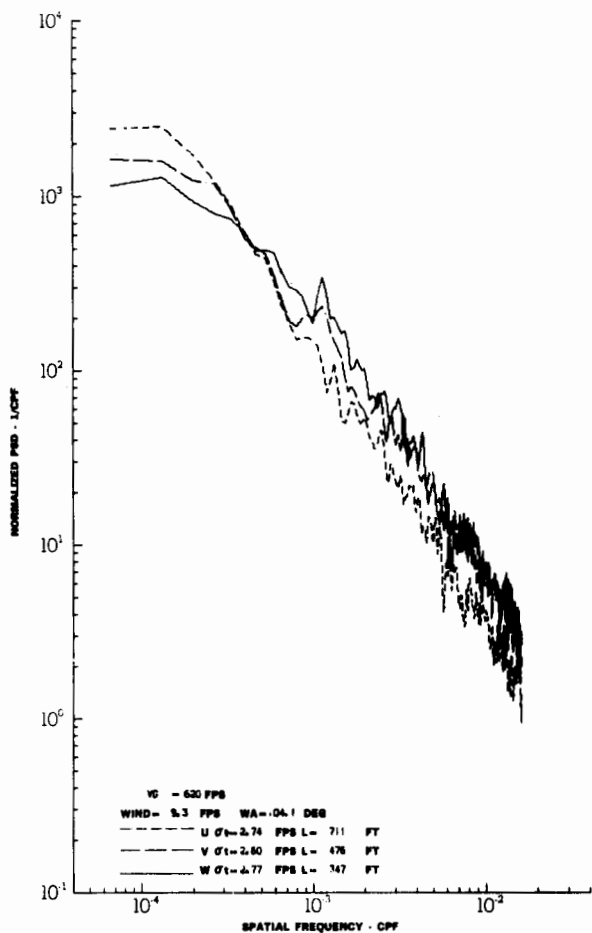
FIGURE IV-69

# Contrails



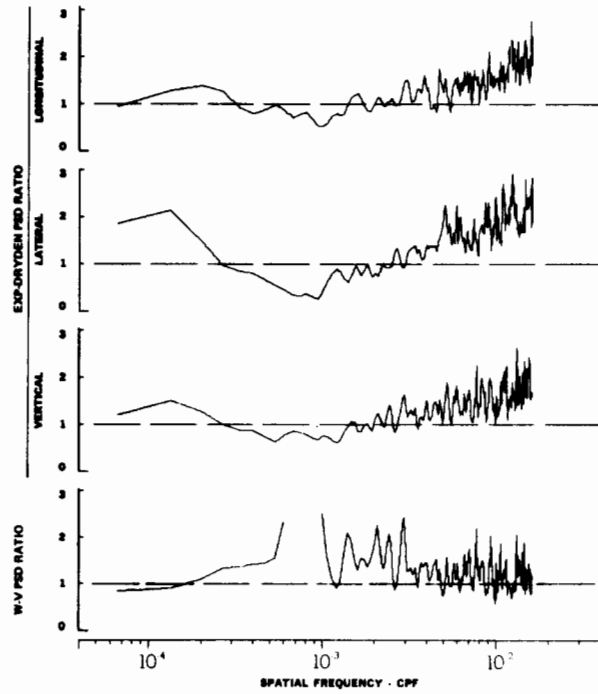
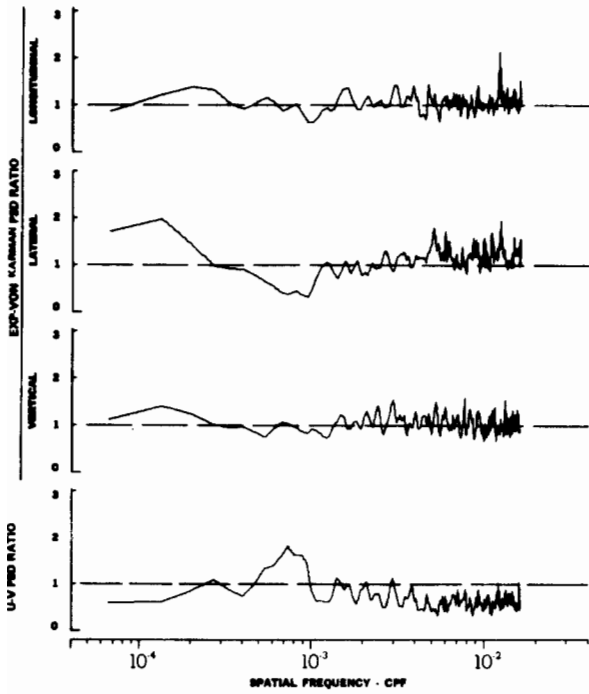
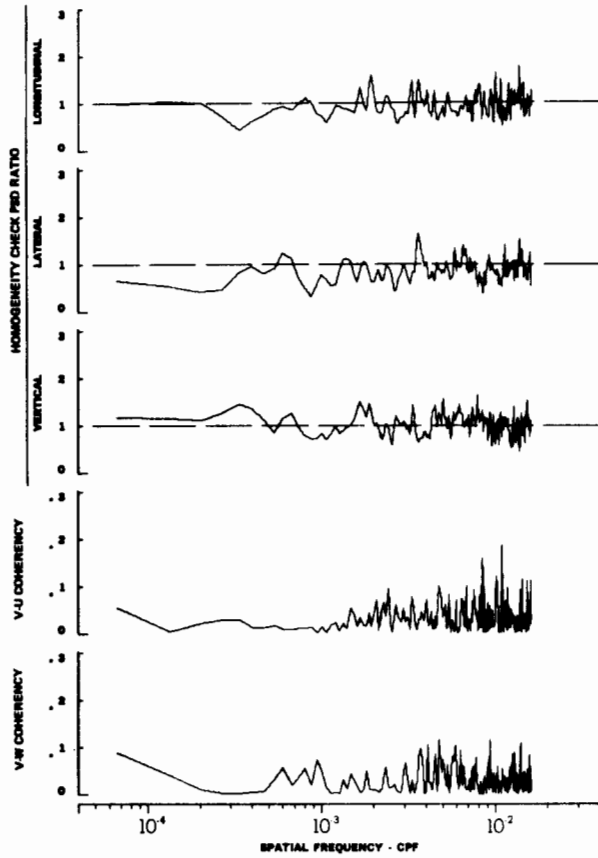
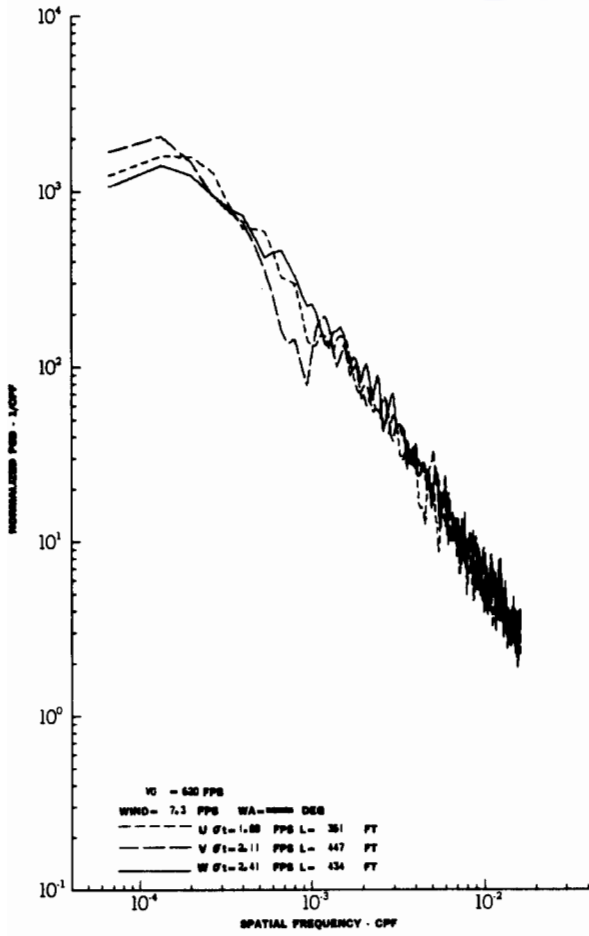
TURBULENCE SPECTRA DATA FOR TEST 66, LEG 2, CATEGORY 312331  
 FIGURE IV-70

# Contrails

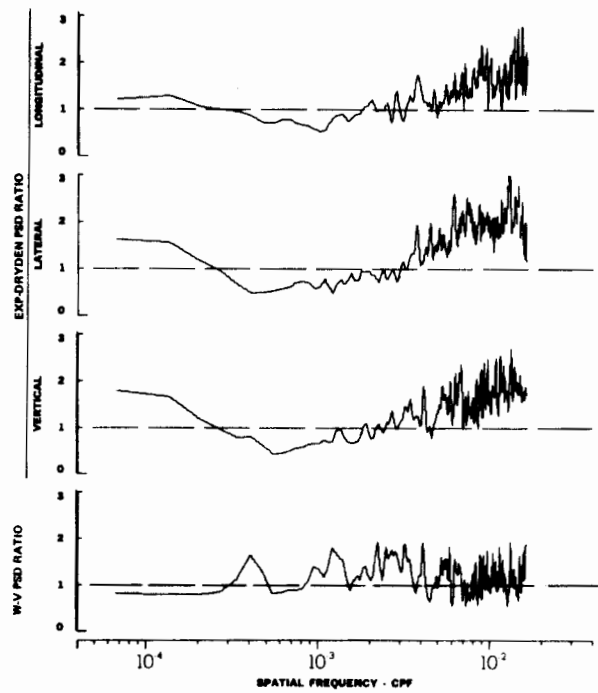
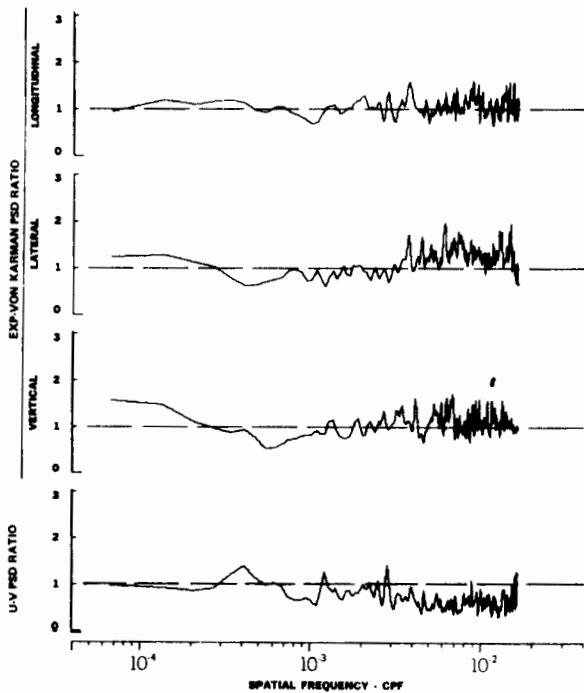
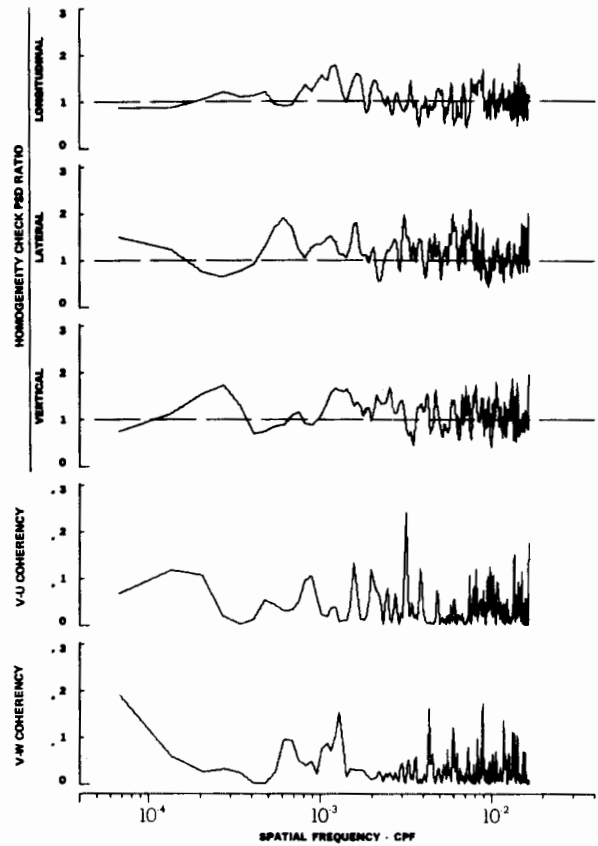
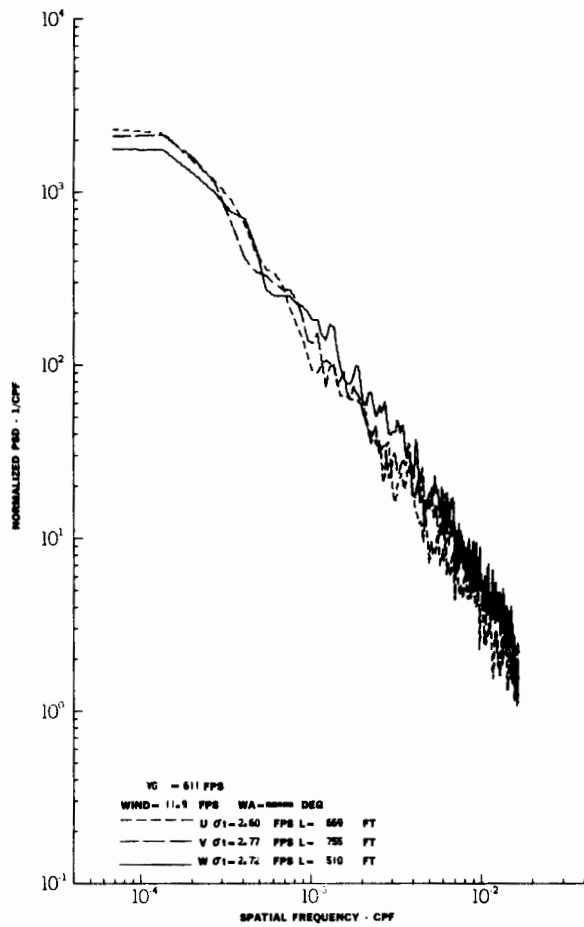


TURBULENCE SPECTRA DATA FOR TEST 66, LEG 6, CATEGORY 113331  
 FIGURE IV-71

# Contrails

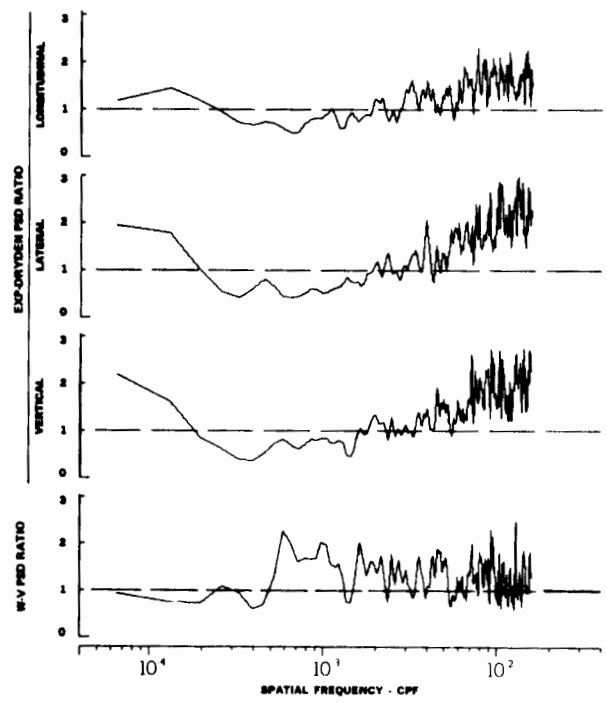
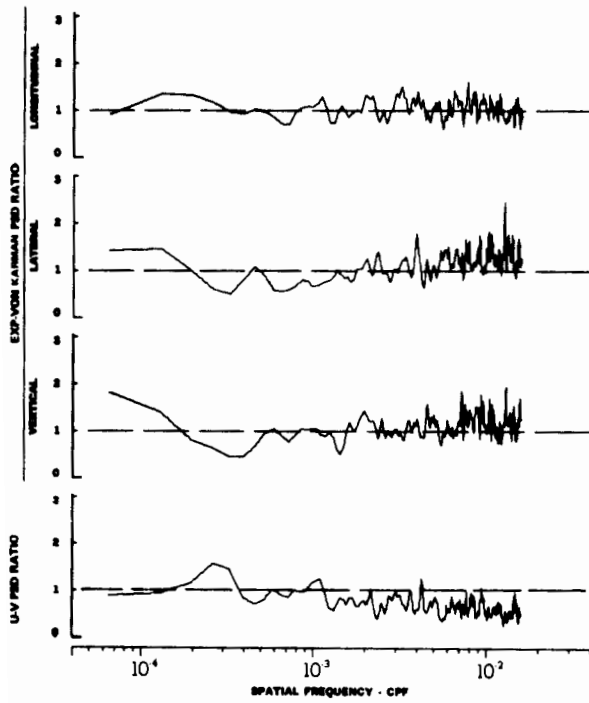
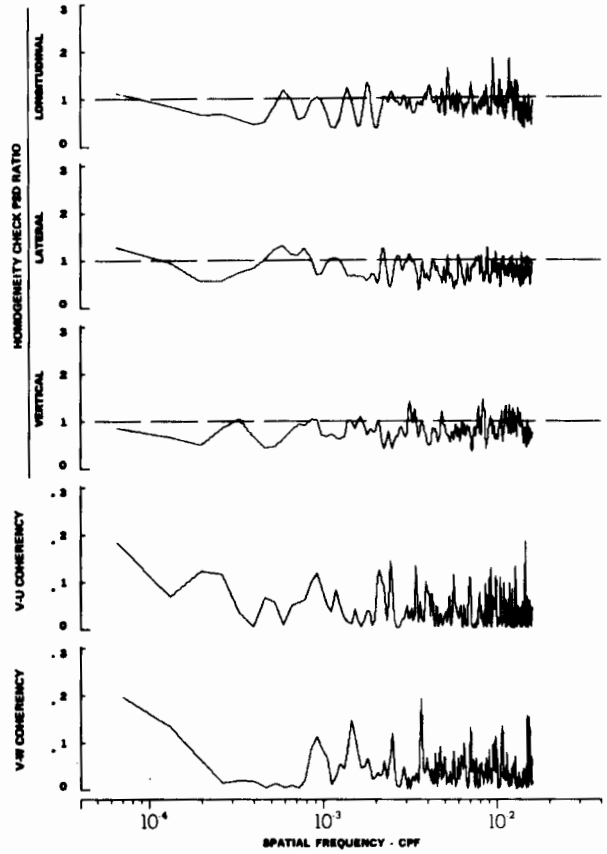
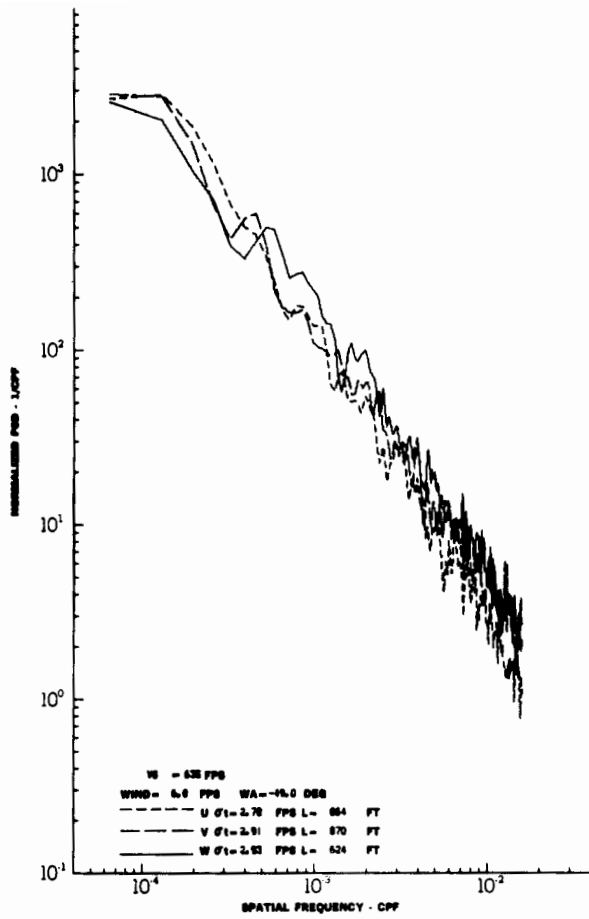


TURBULENCE SPECTRA DATA FOR TEST 68, LEG 6, CATEGORY 124231  
 FIGURE IV-72



TURBULENCE SPECTRA DATA FOR TEST 69, LEG 1, CATEGORY 224331

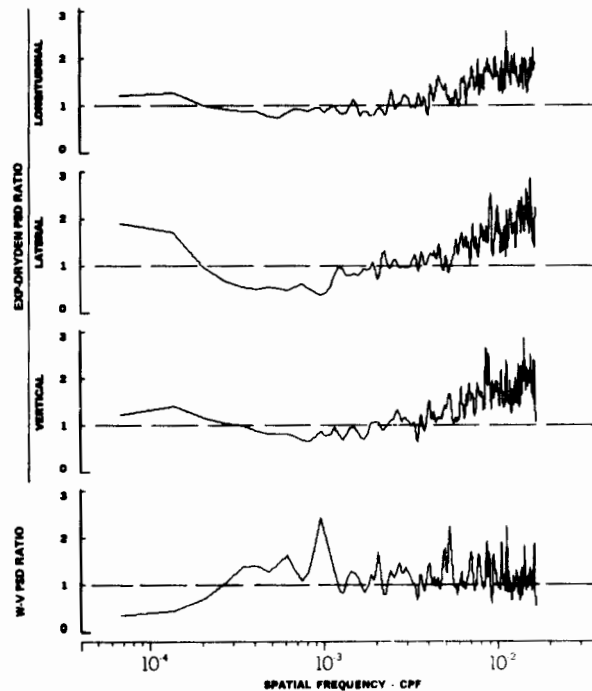
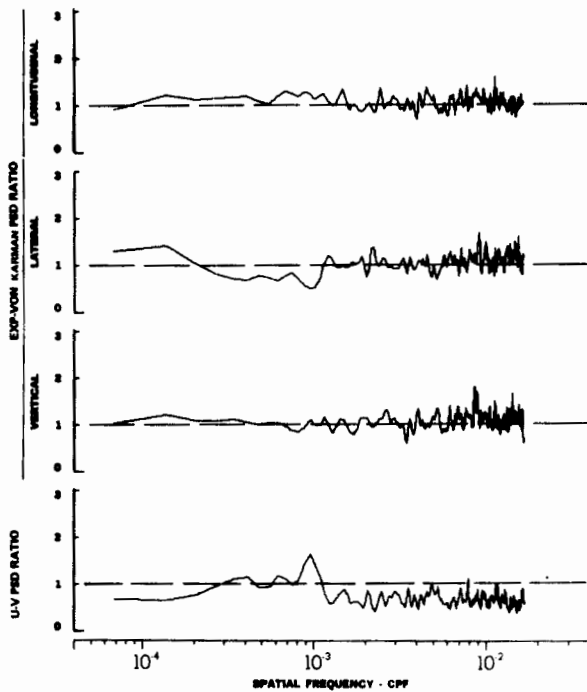
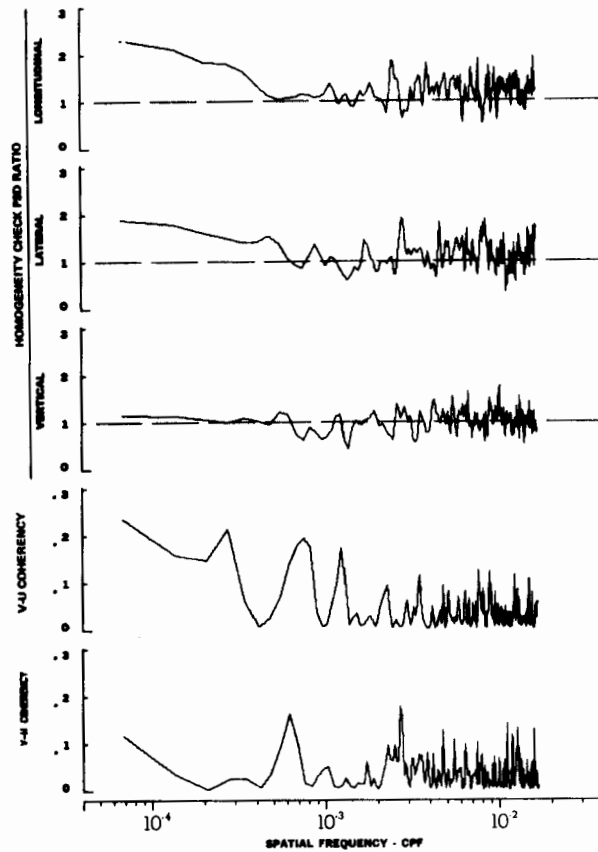
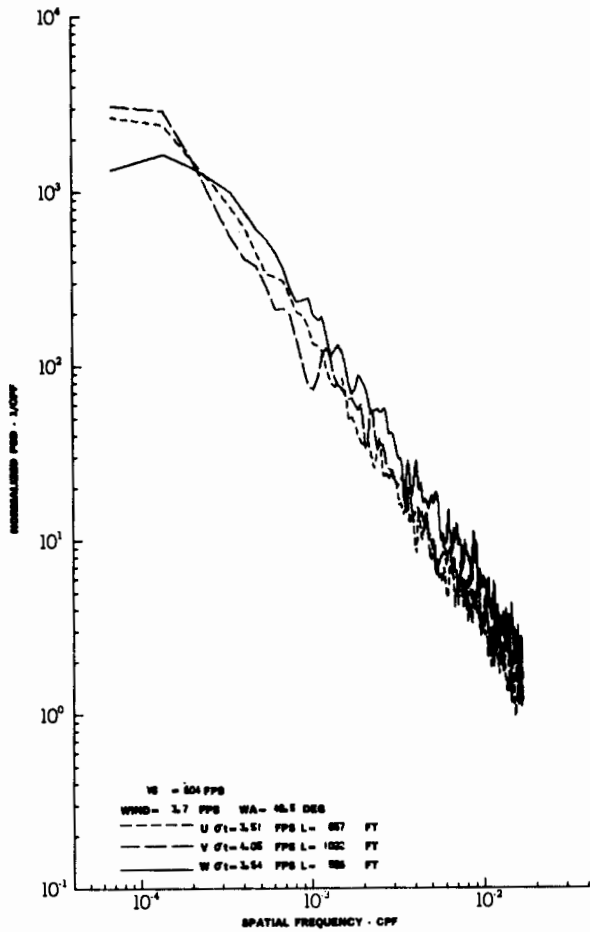
FIGURE IV-73



TURBULENCE SPECTRA DATA FOR TEST 69, LEG 3, CATEGORY 122331  
 FIGURE IV-74

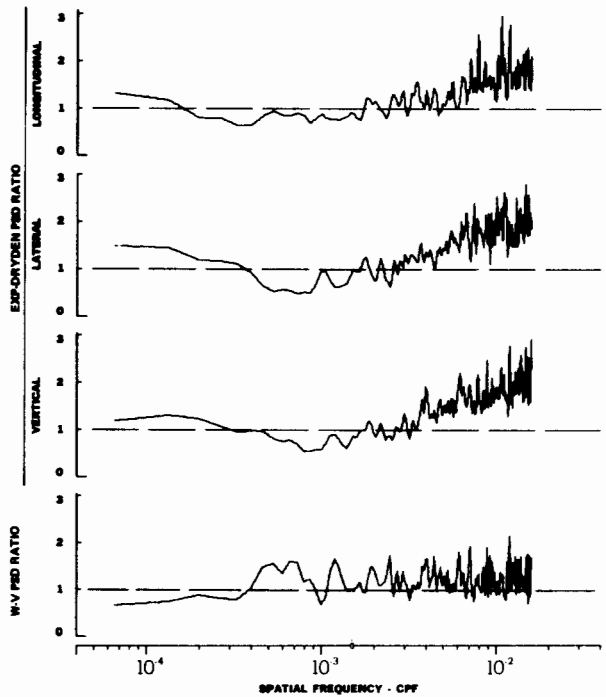
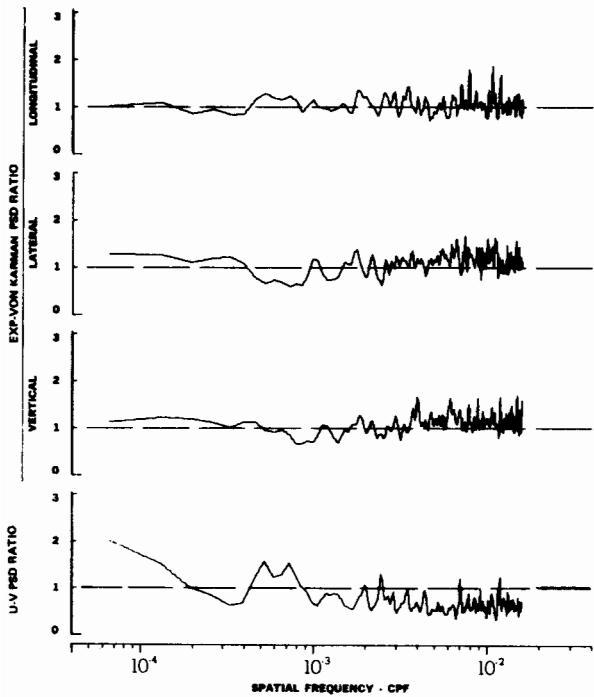
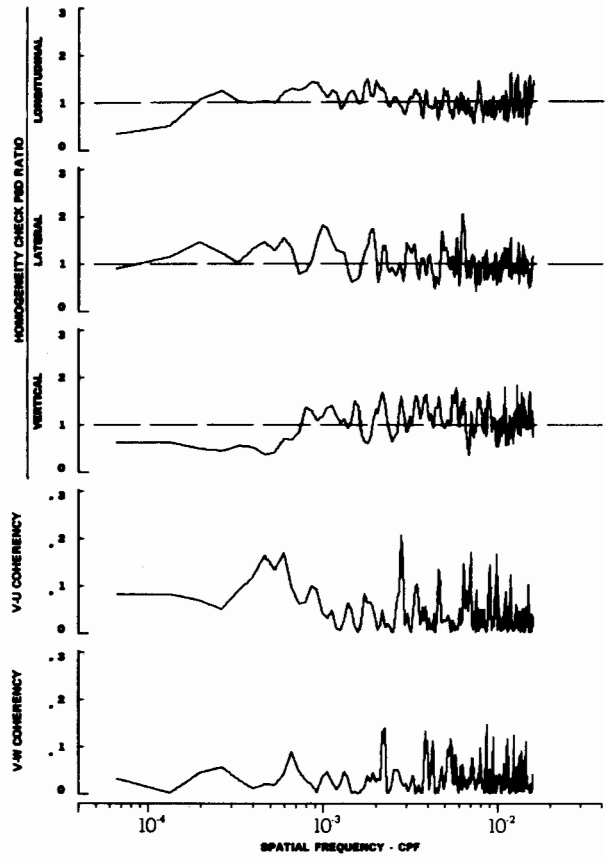
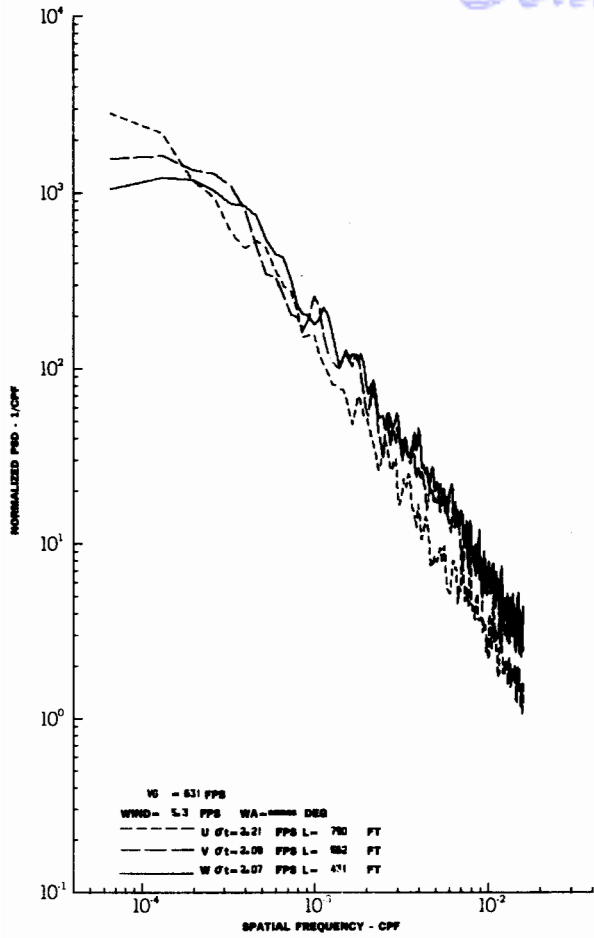


# Contrails



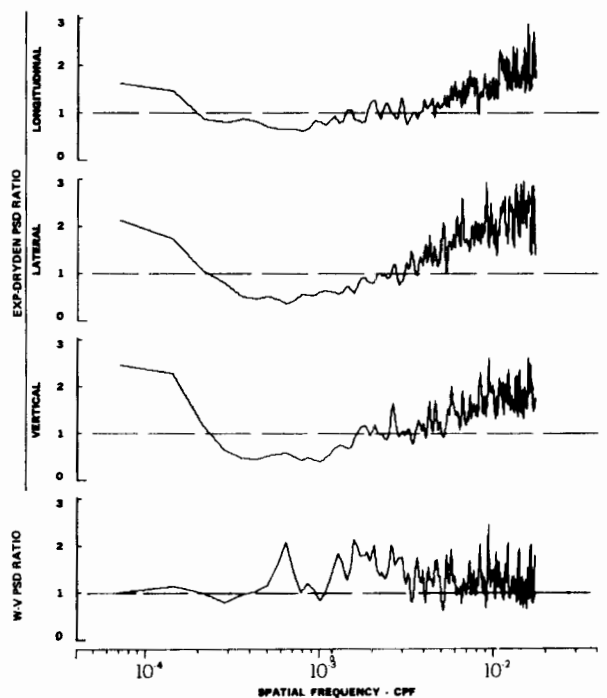
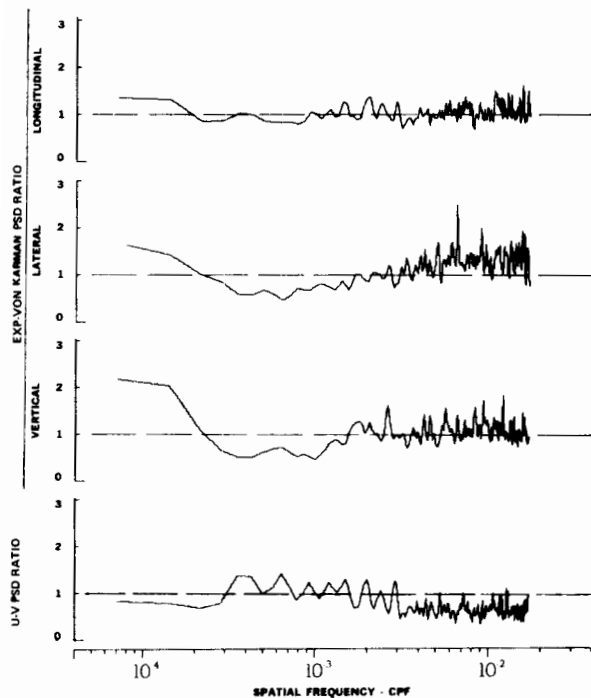
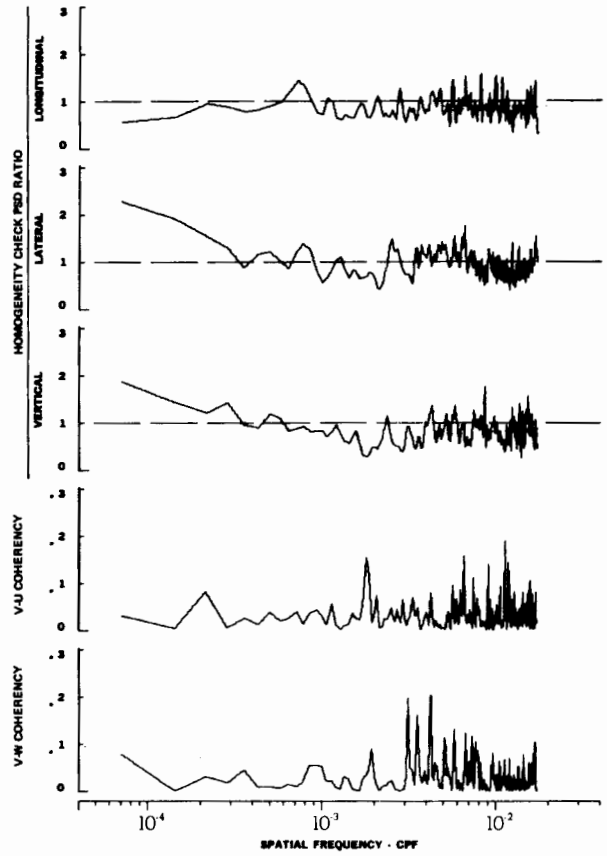
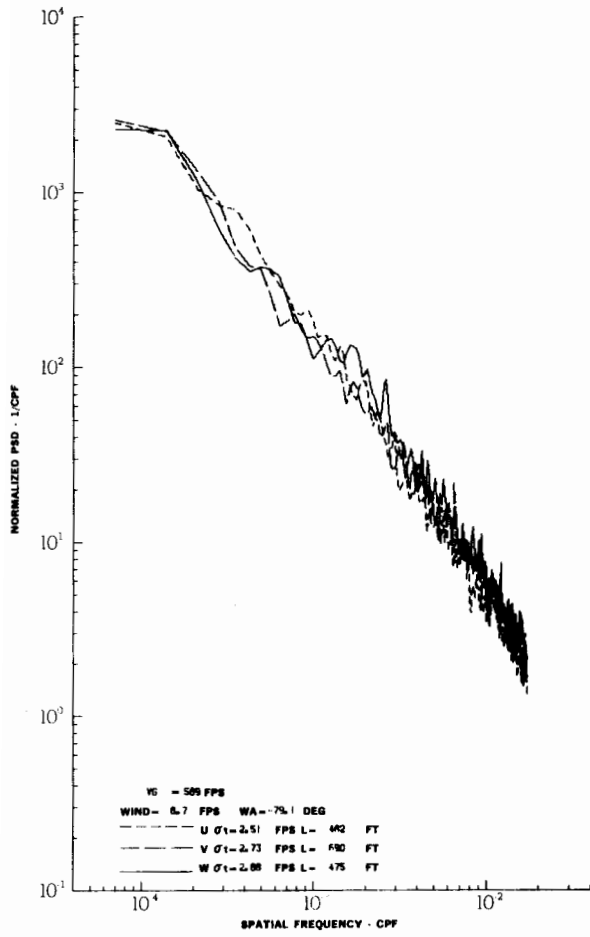
TURBULENCE SPECTRA DATA FOR TEST 69, LEG 5, CATEGORY 121331  
FIGURE IV-75

# Contrails



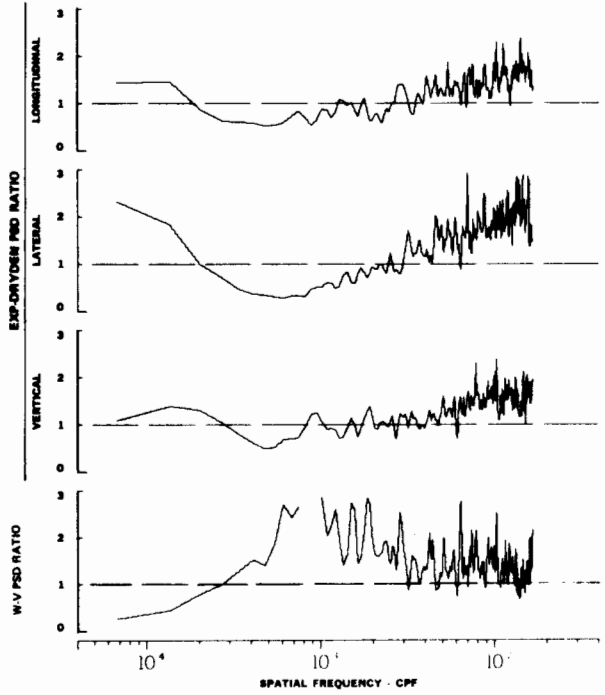
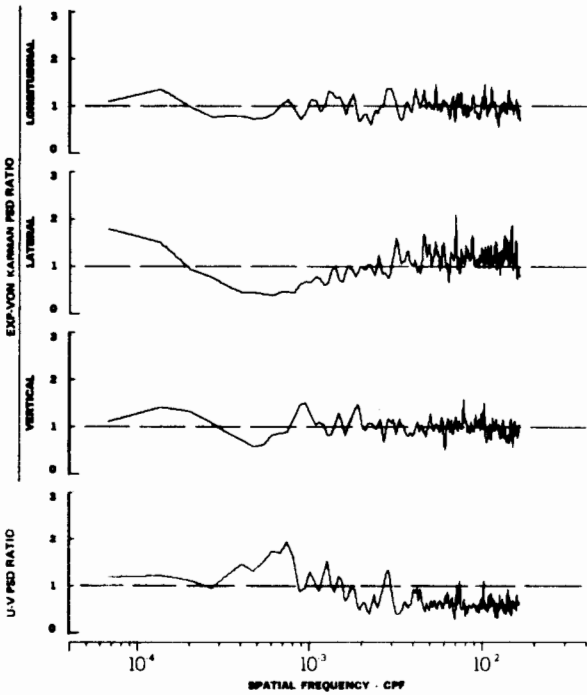
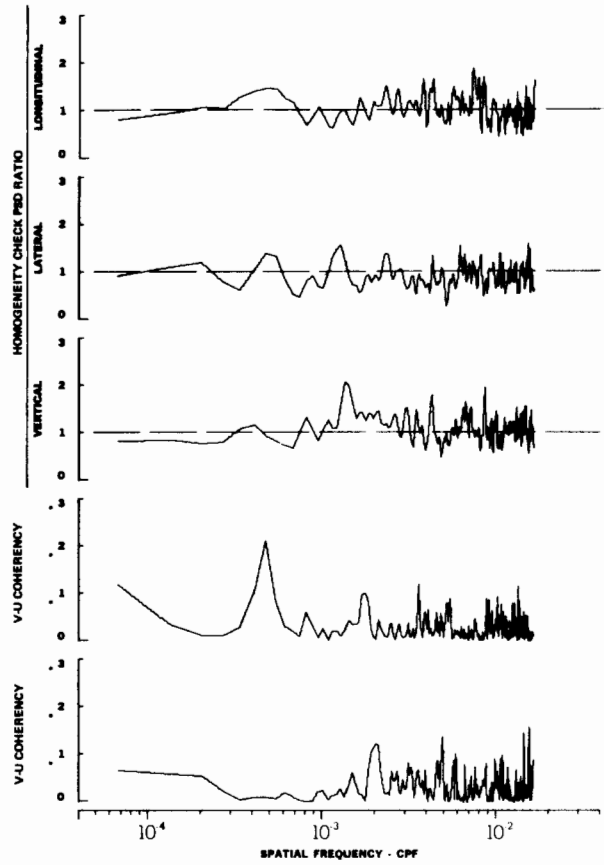
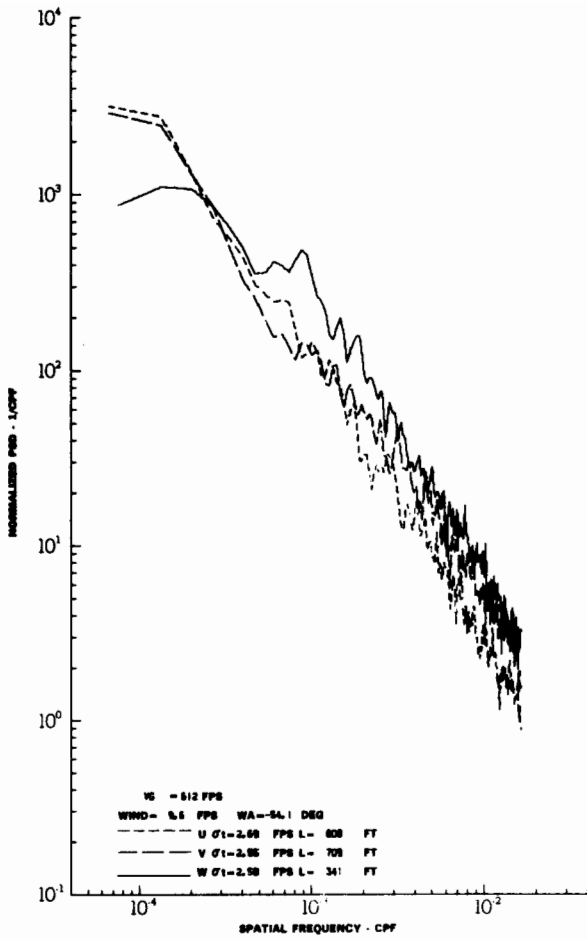
TURBULENCE SPECTRA DATA FOR TEST 69, LEG 7, CATEGORY 322331

FIGURE IV-76



TURBULENCE SPECTRA DATA FOR TEST 71, LEG 3, CATEGORY 112231  
 FIGURE IV-77

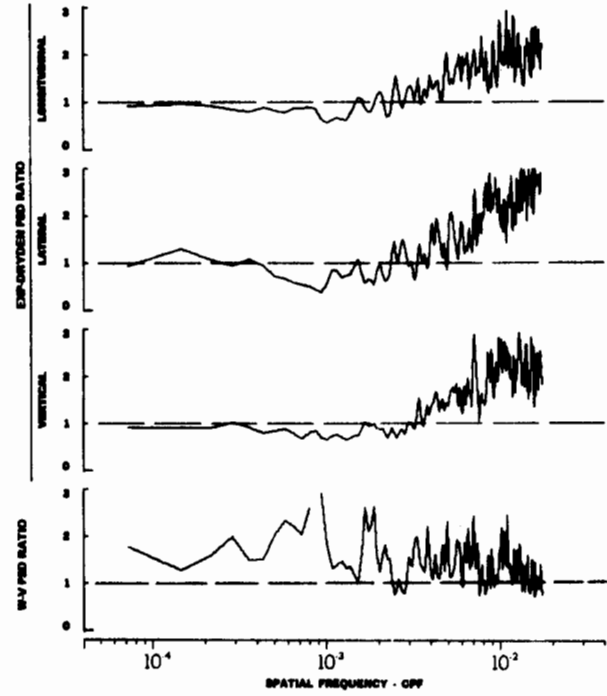
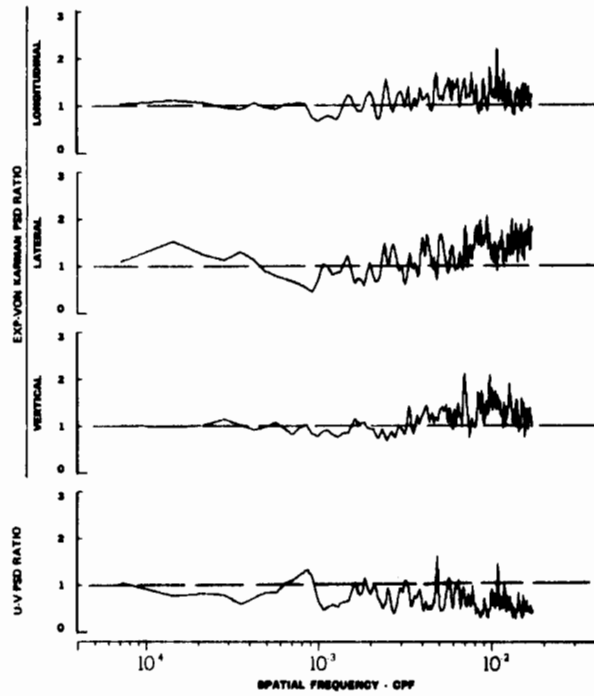
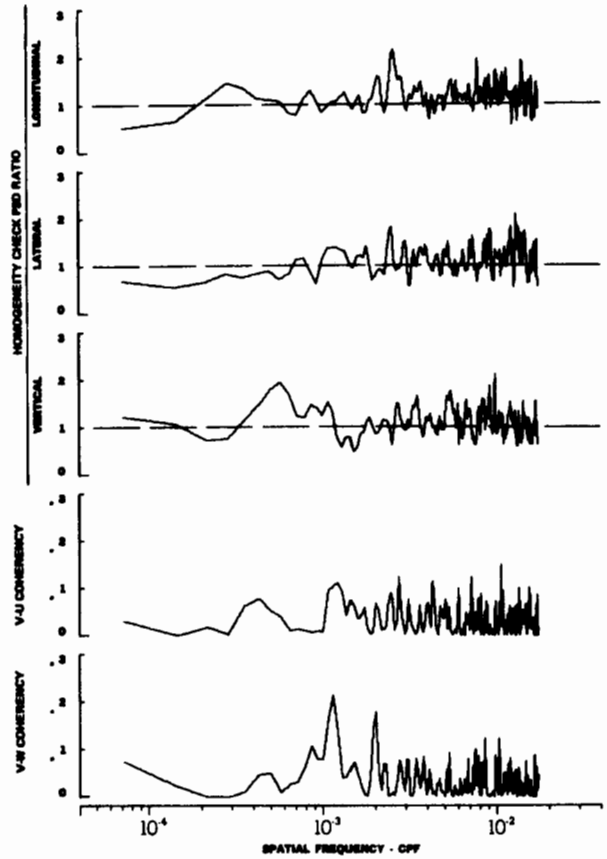
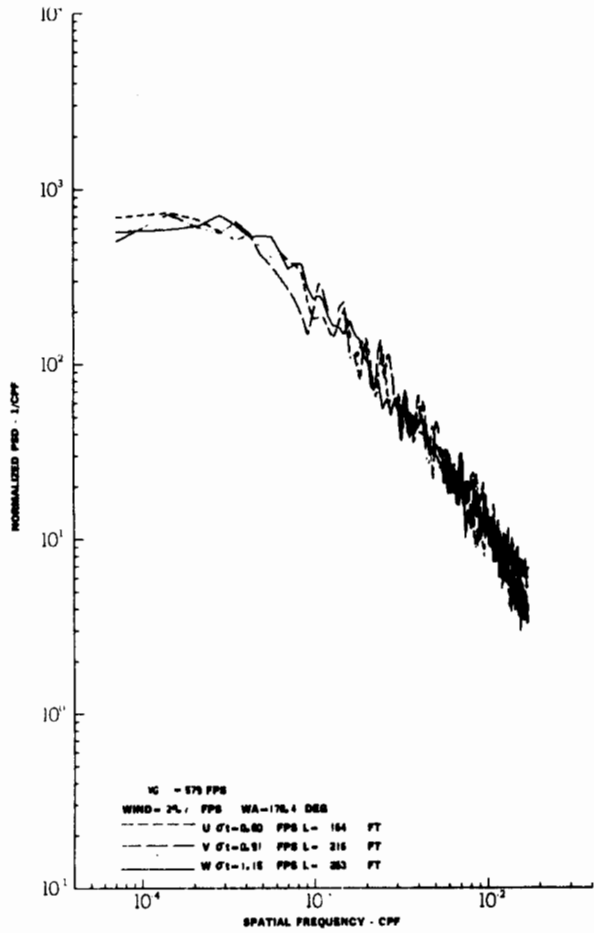
# Contrails



TURBULENCE SPECTRA DATA FOR TEST 72, LEG 2, CATEGORY 312331

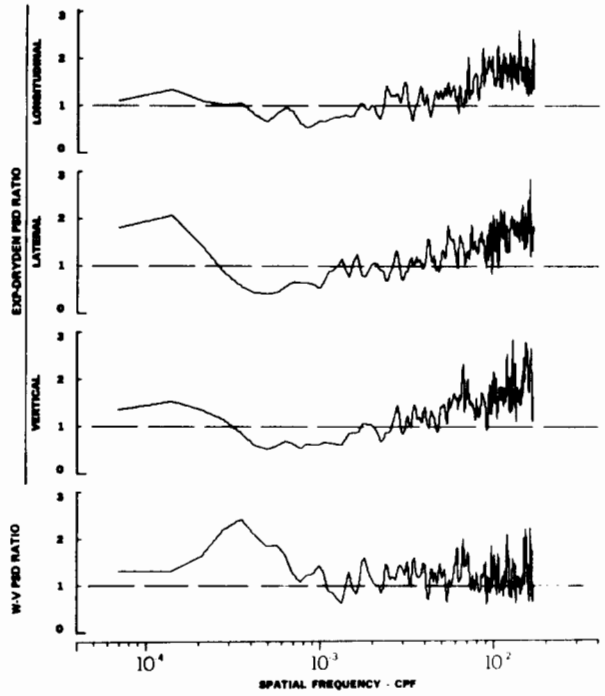
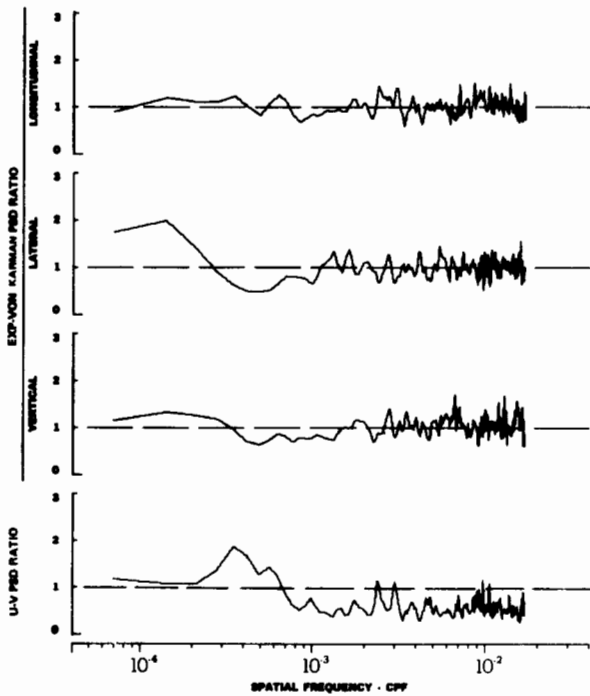
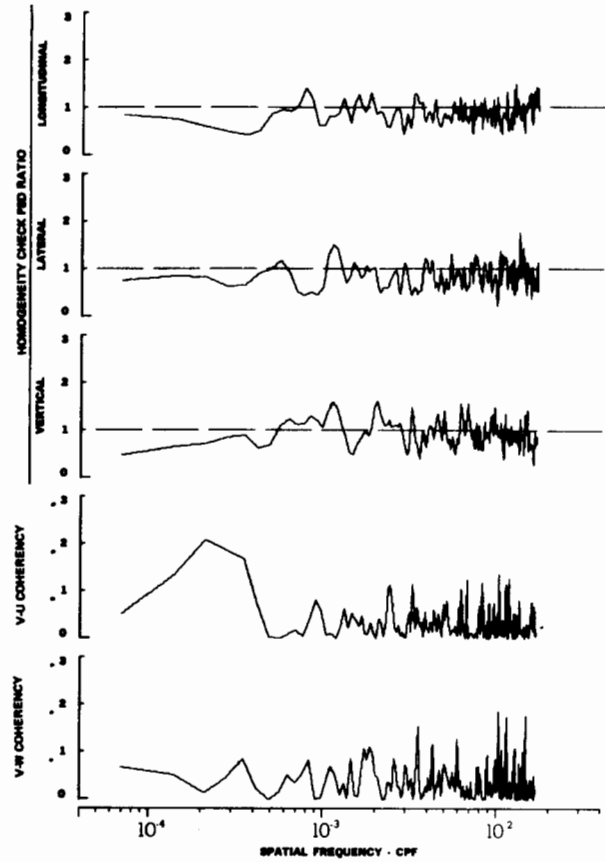
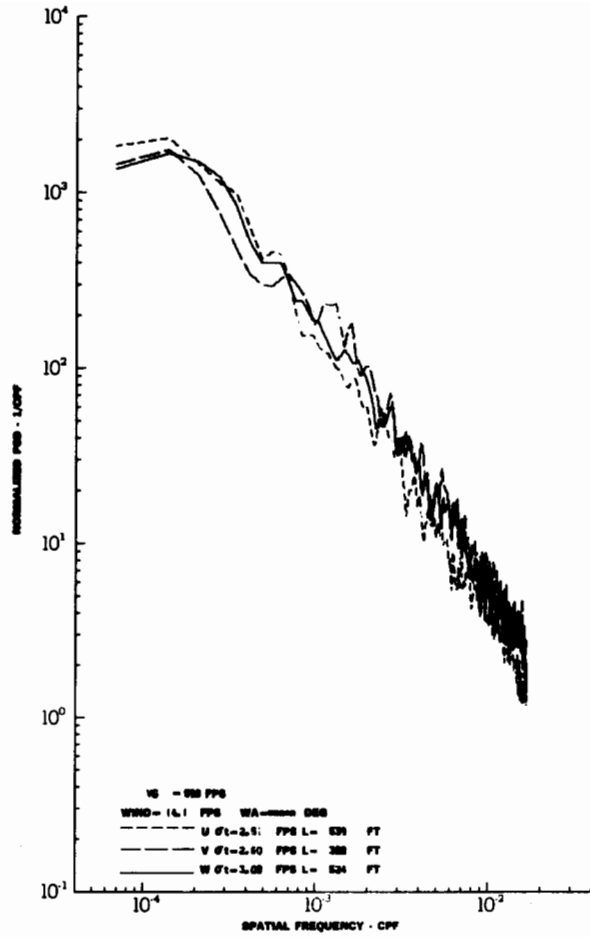
FIGURE IV-78

# Contrails



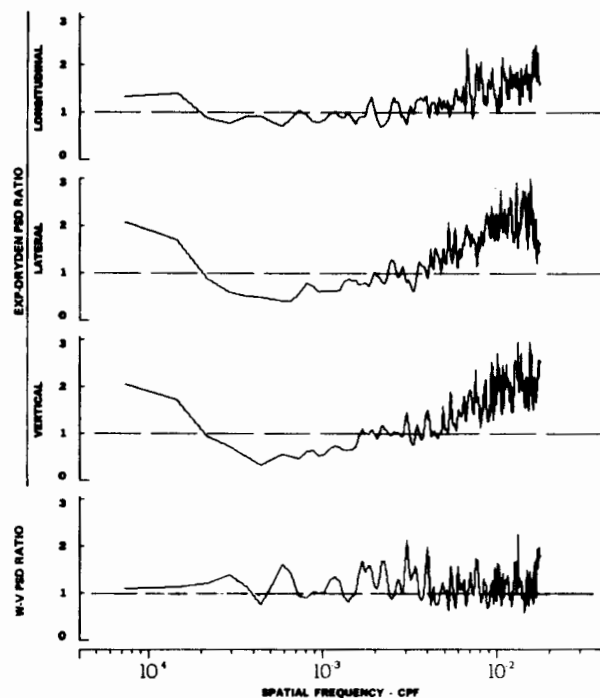
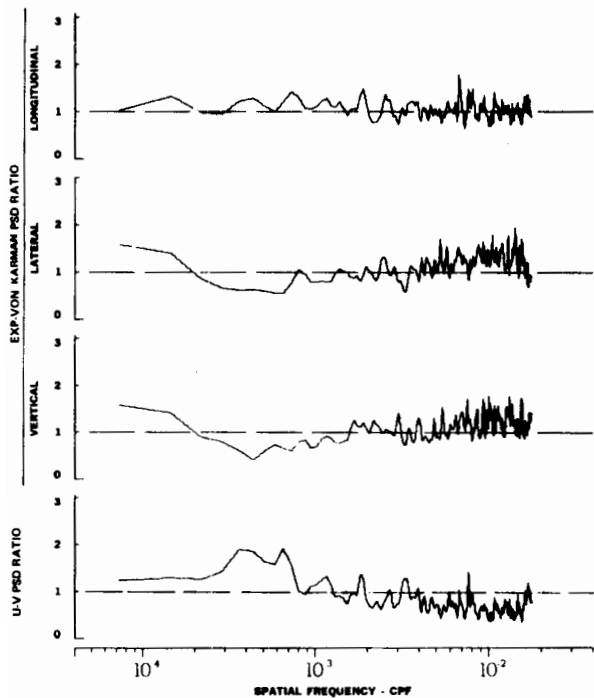
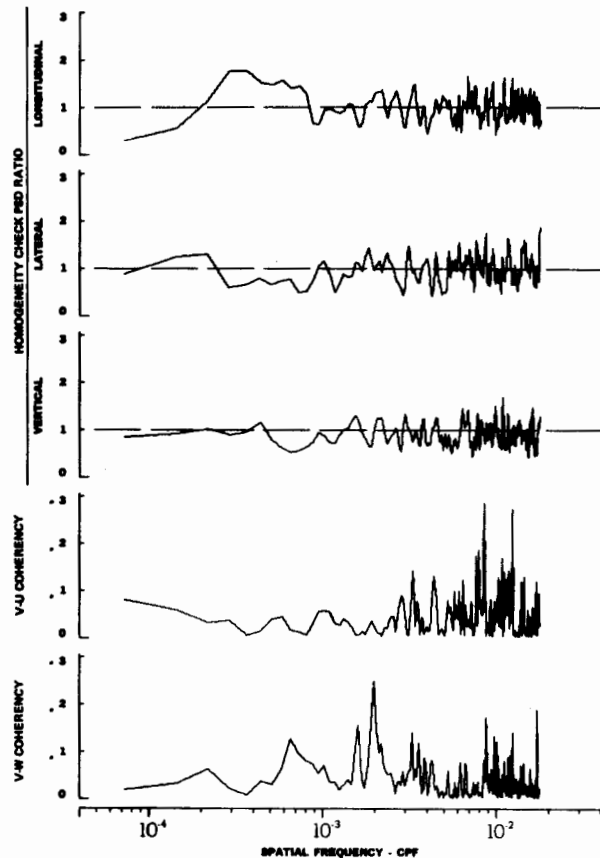
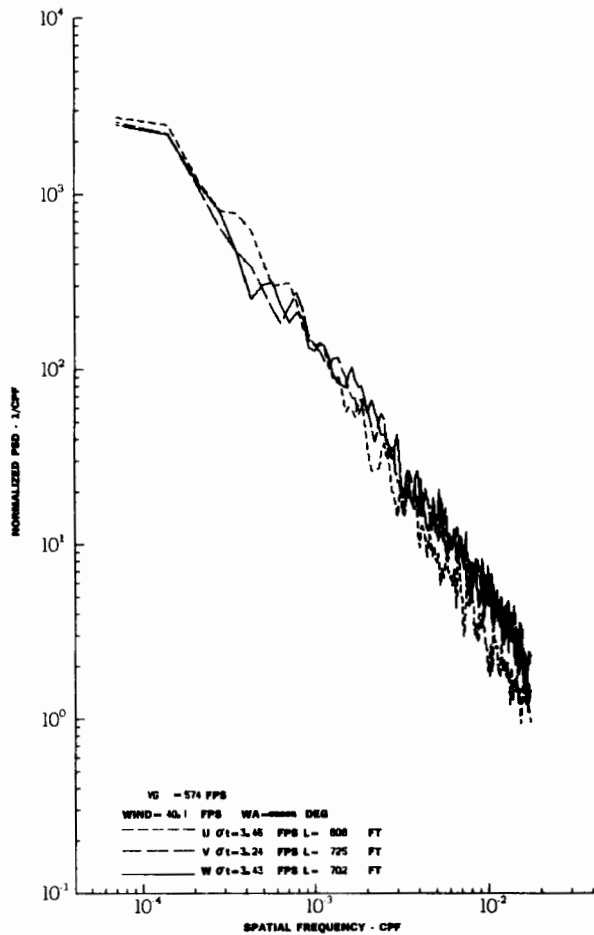
TURBULENCE SPECTRA DATA FOR TEST 72, LEG 4, CATEGORY 612331  
 FIGURE IV-79

# Contrails



TURBULENCE SPECTRA DATA FOR TEST 74, LEG 6, CATEGORY 123231

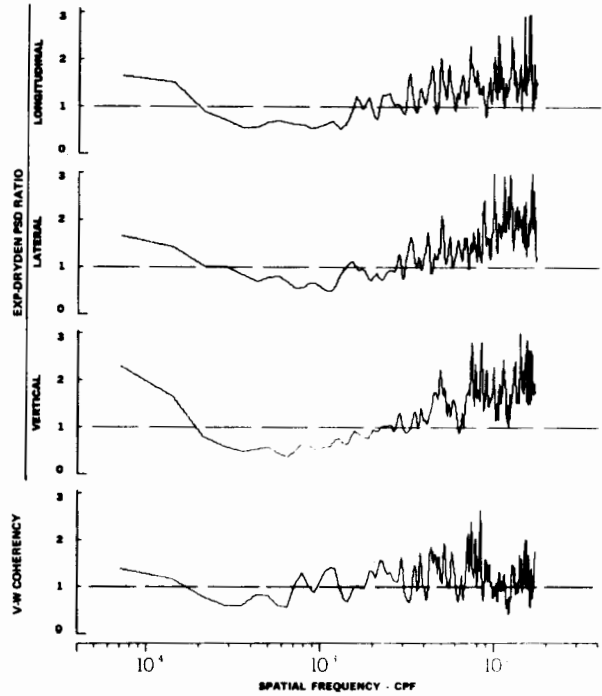
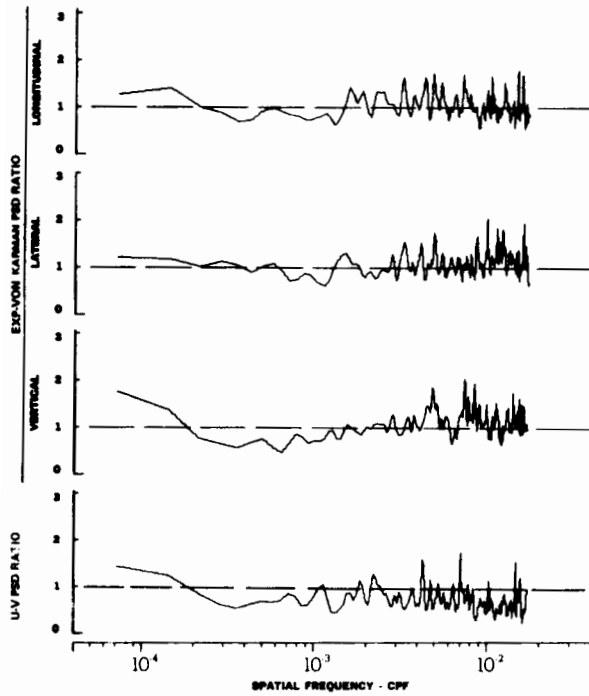
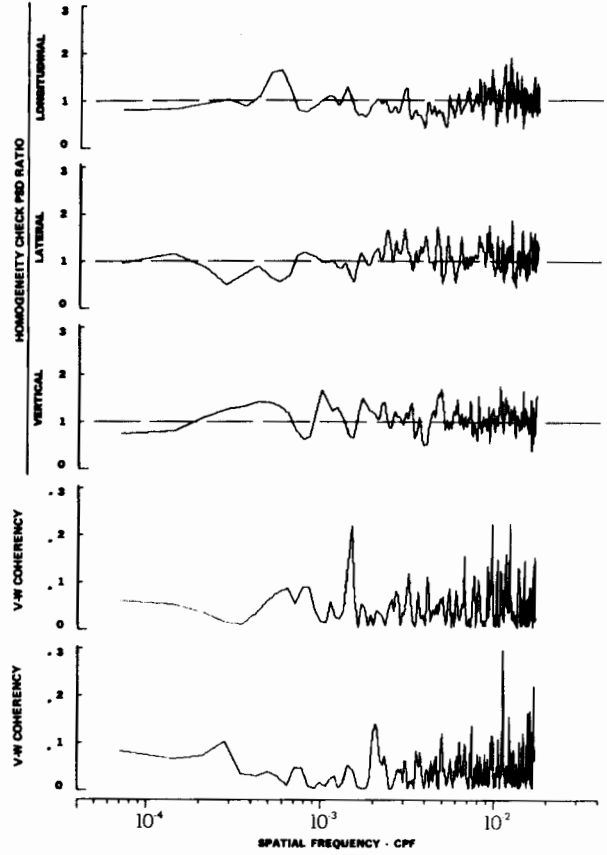
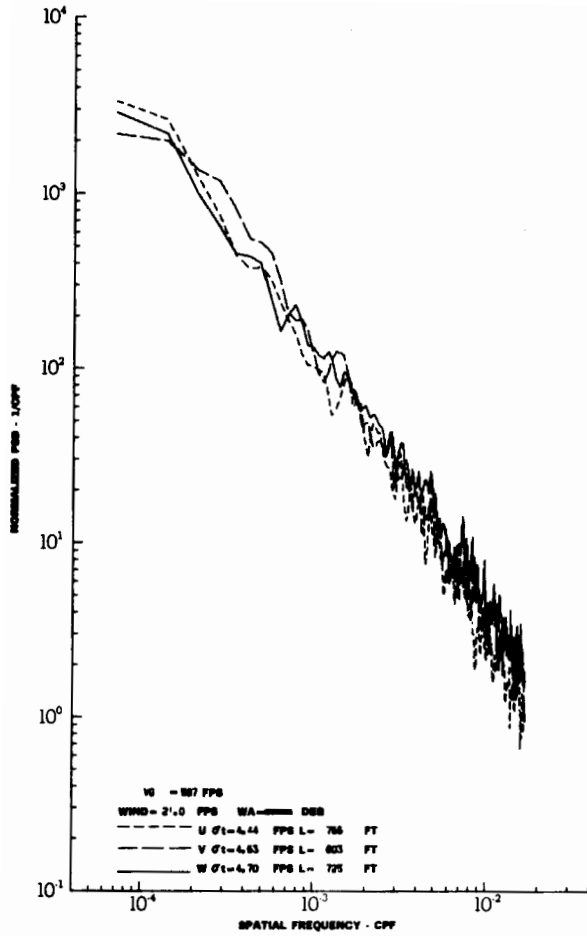
FIGURE IV-80



TURBULENCE SPECTRA DATA FOR TEST 75, LEG 1, CATEGORY 224331  
FIGURE IV-81

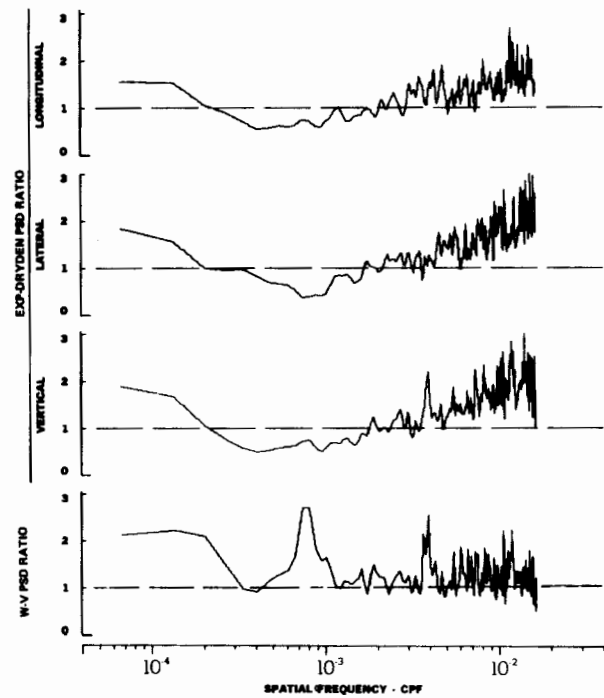
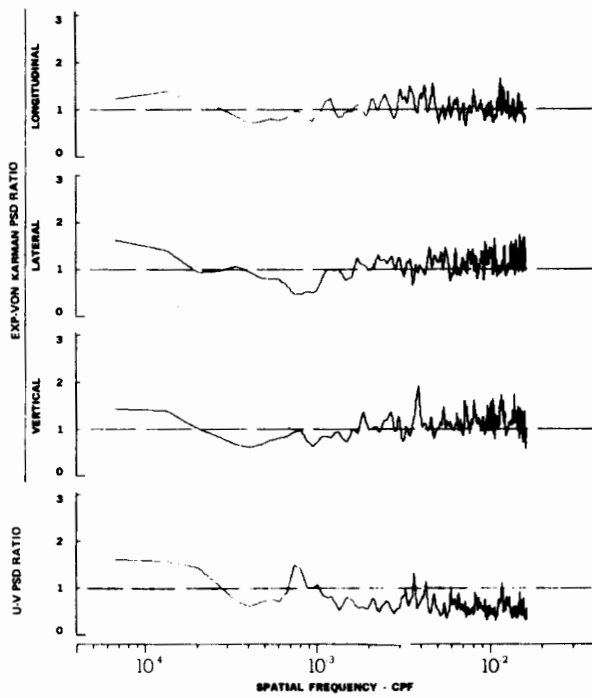
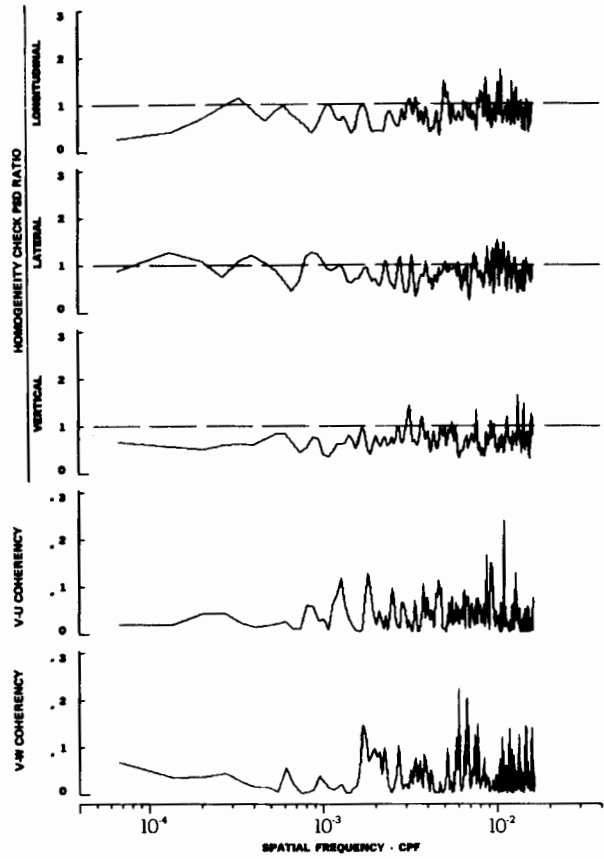
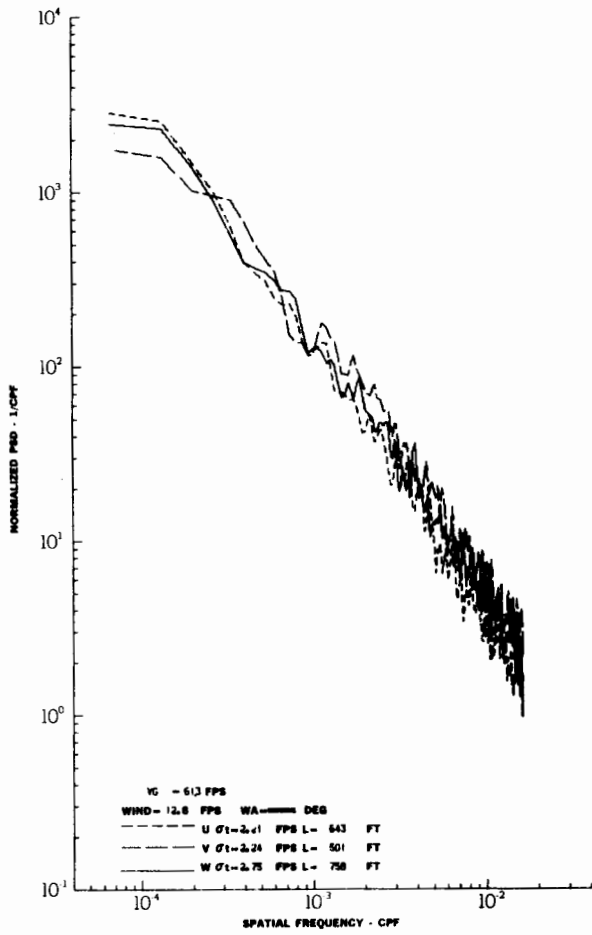


# Contrails



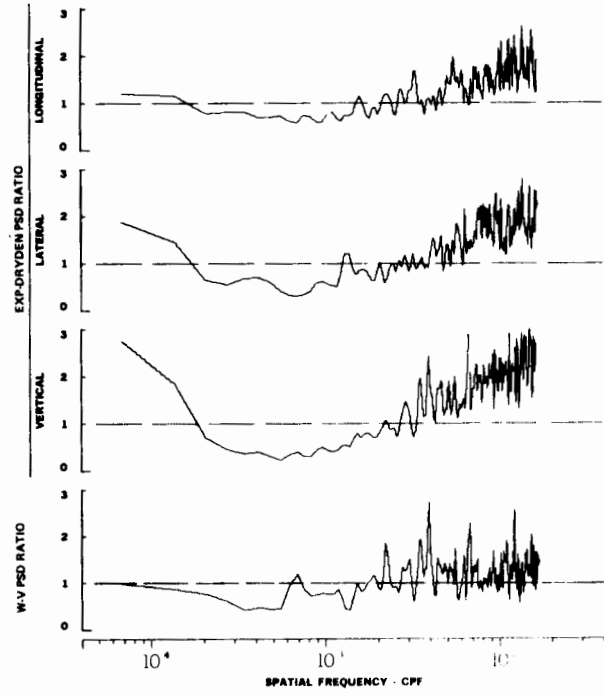
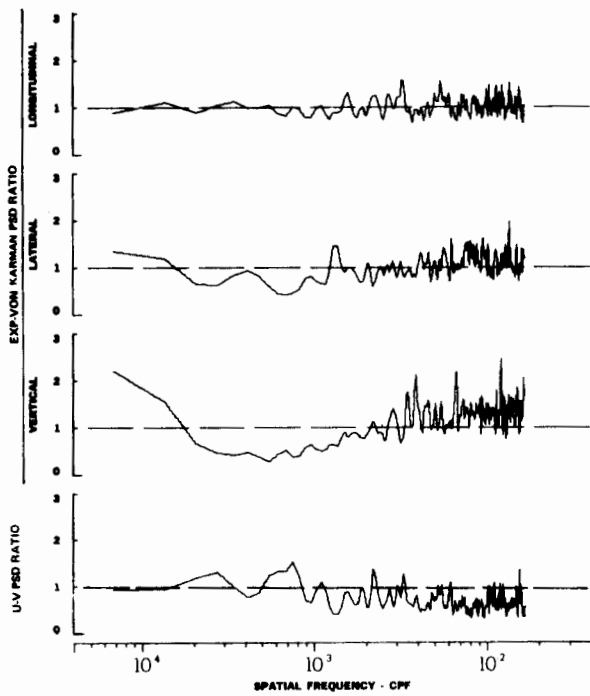
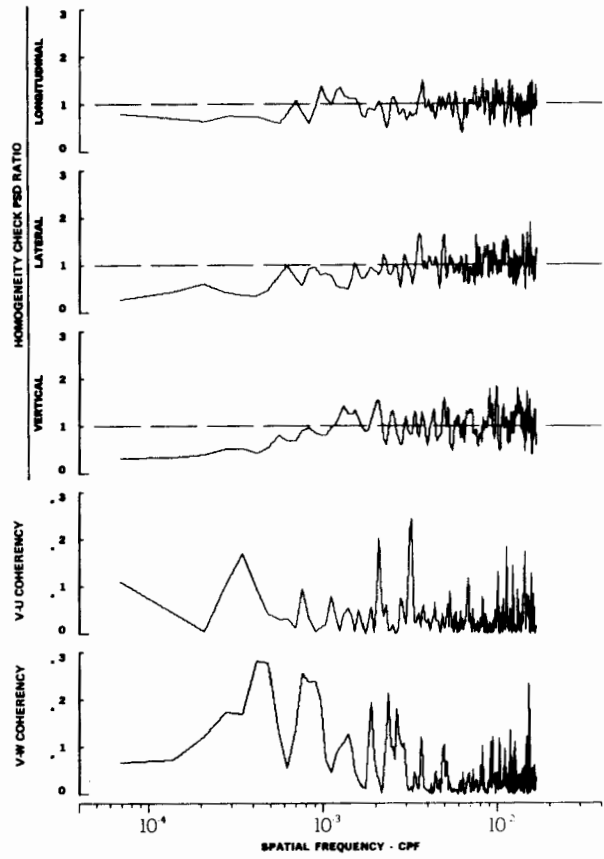
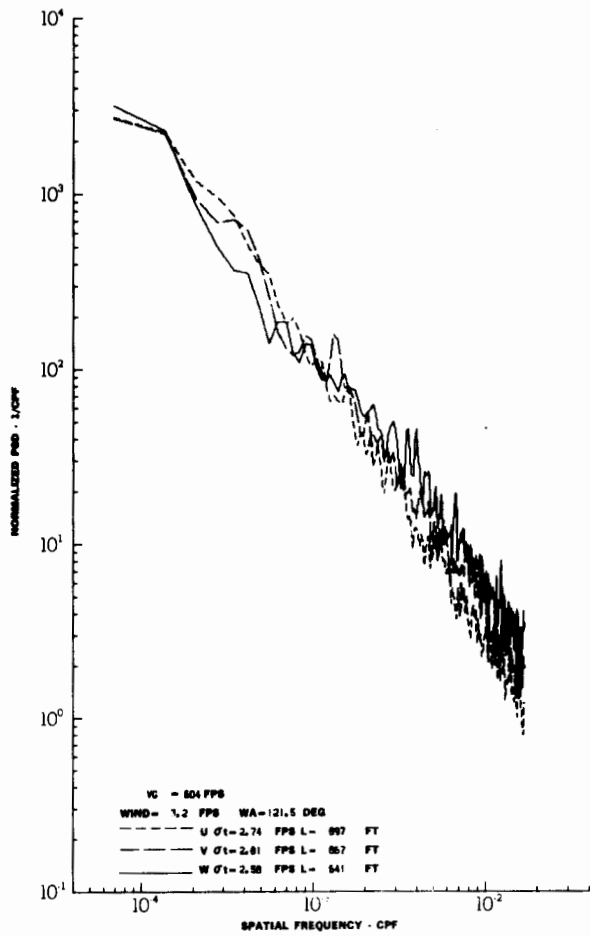
TURBULENCE SPECTRA DATA FOR TEST 75, LEG 5, CATEGORY 122331  
 FIGURE IV-82

# Contrails



TURBULENCE SPECTRA DATA FOR TEST 75, LEG 7, CATEGORY 322331  
 FIGURE IV-83

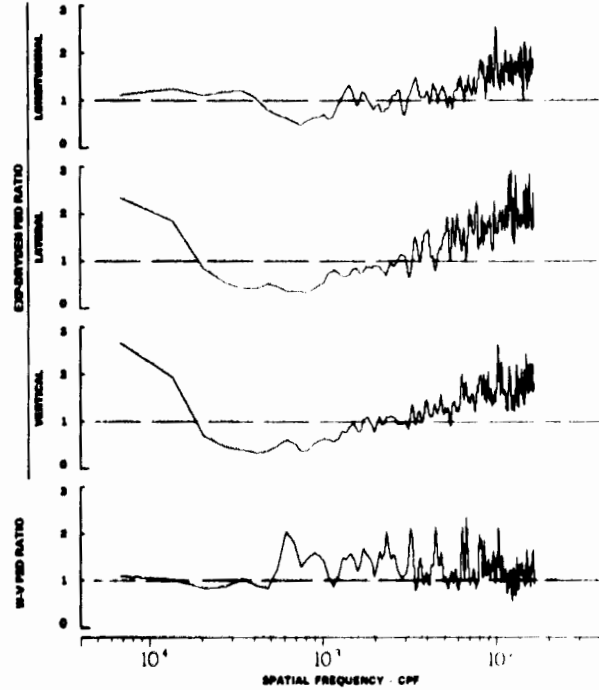
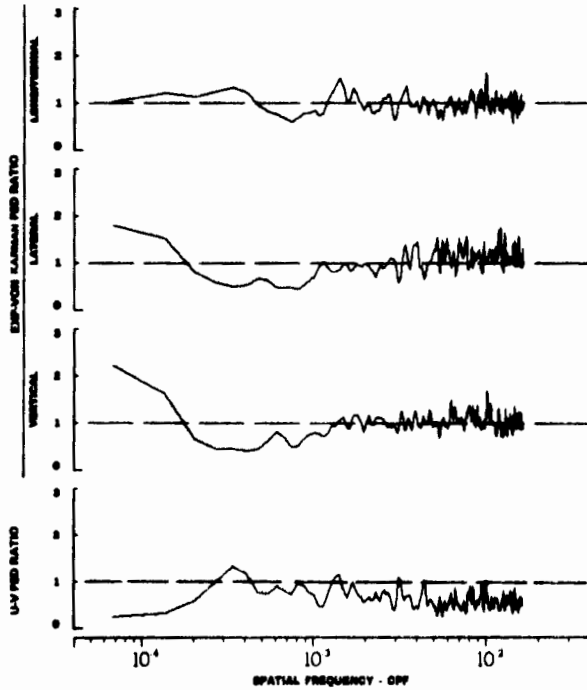
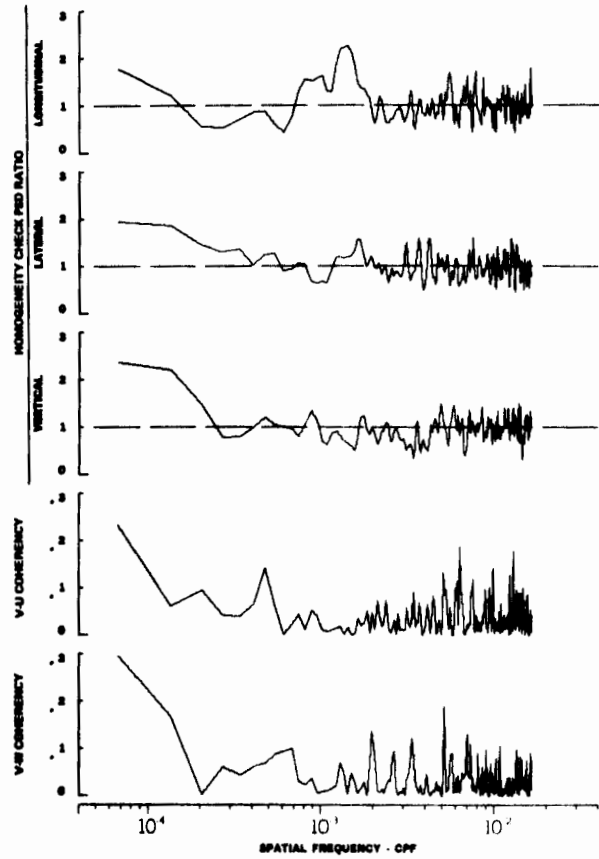
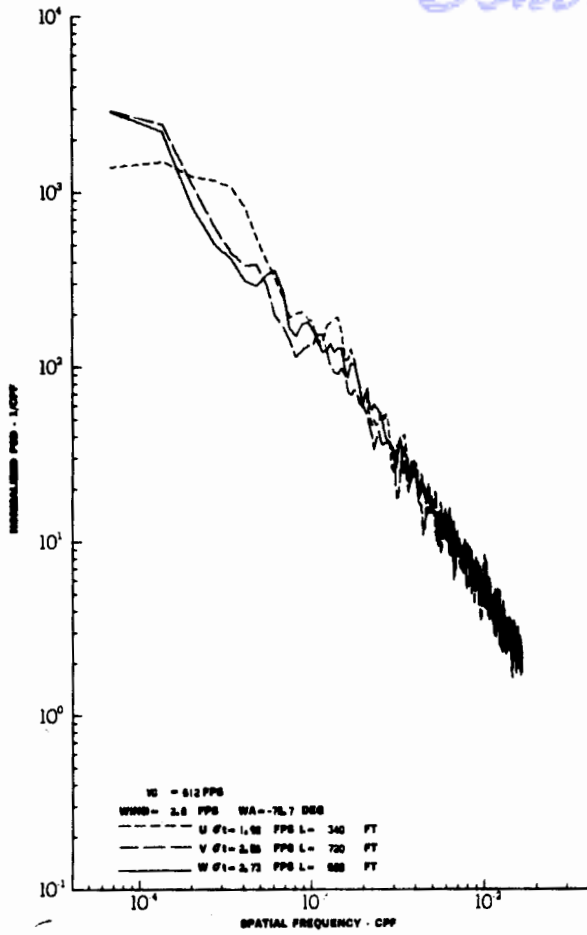
# Contrails



TURBULENCE SPECTRA DATA FOR TEST 77, LEG 3, CATEGORY 112231

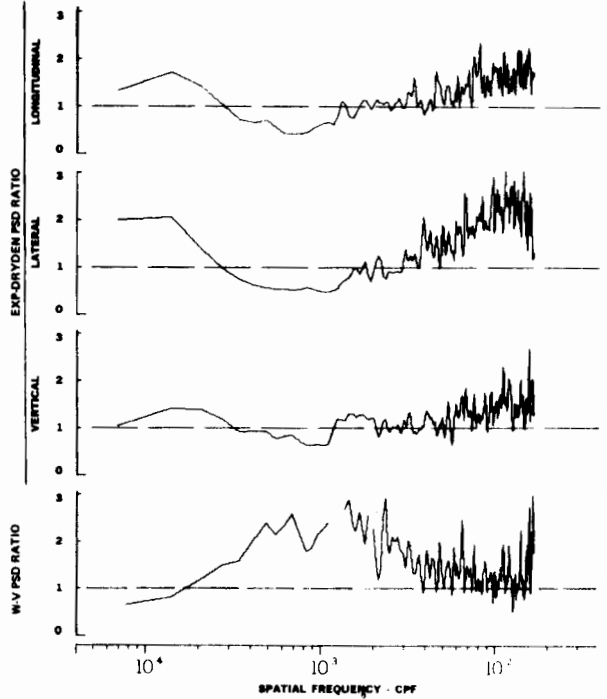
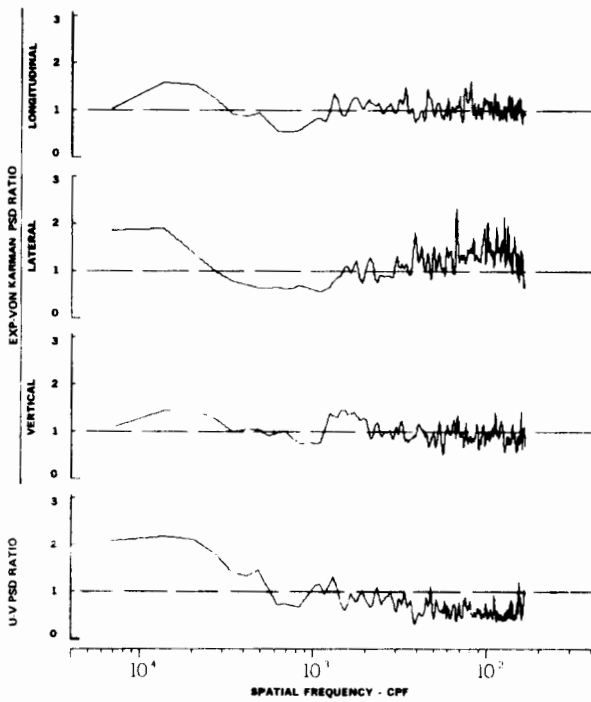
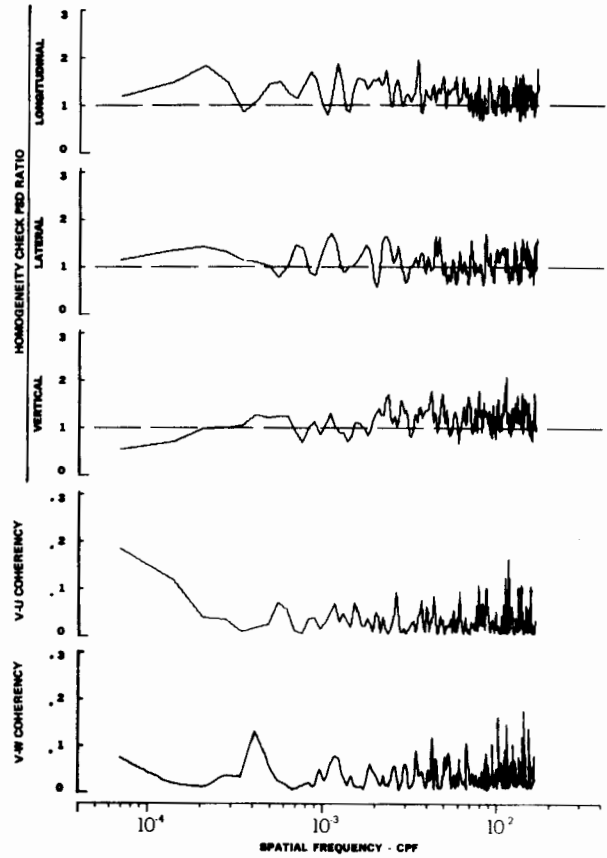
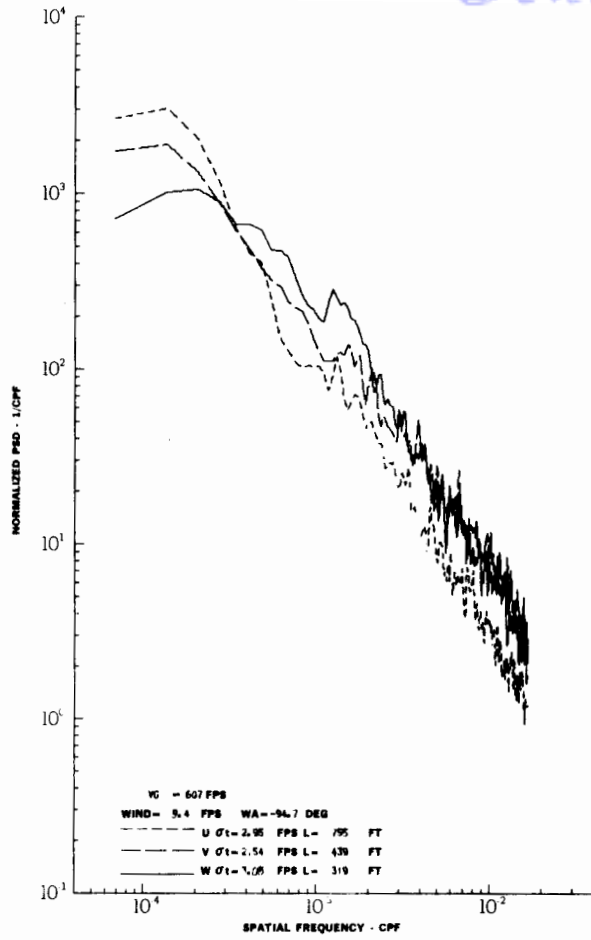
FIGURE IV-84

# Contrails



TURBULENCE SPECTRA DATA FOR TEST 77, LEG 7, CATEGORY 311231  
 FIGURE IV-85

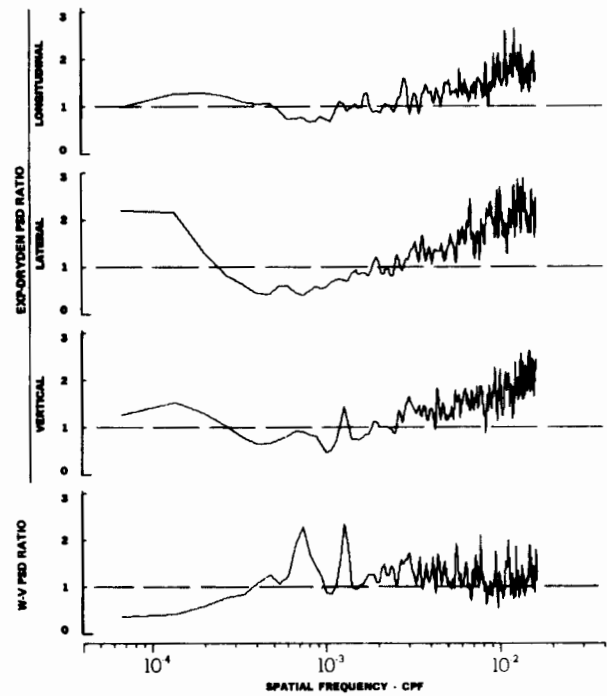
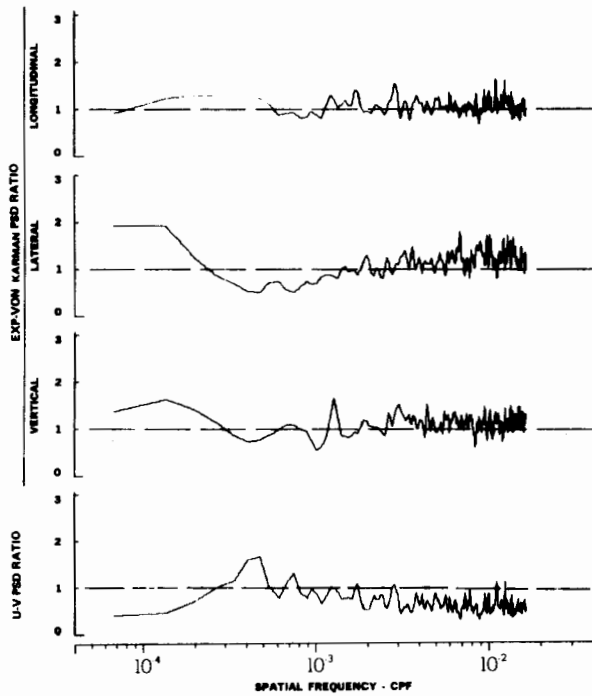
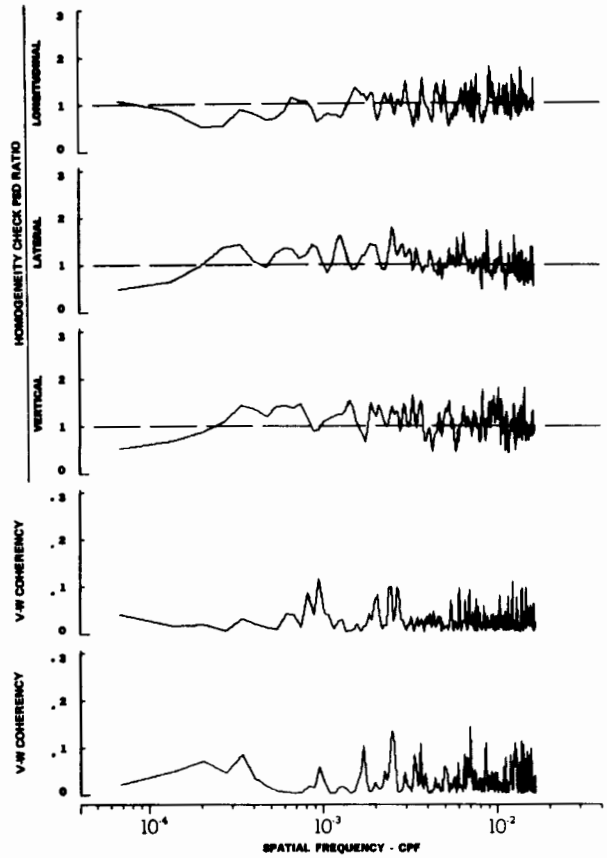
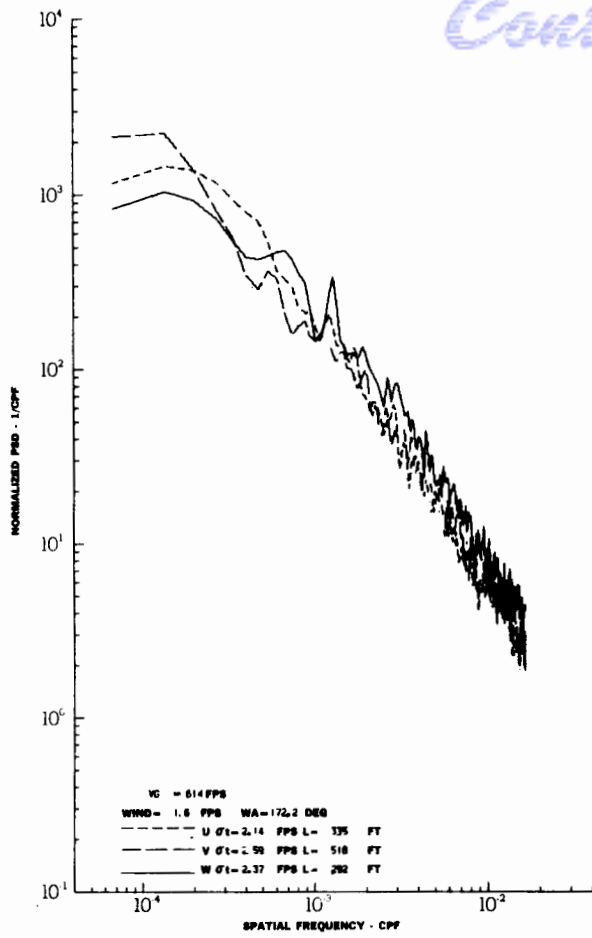
# Contrails



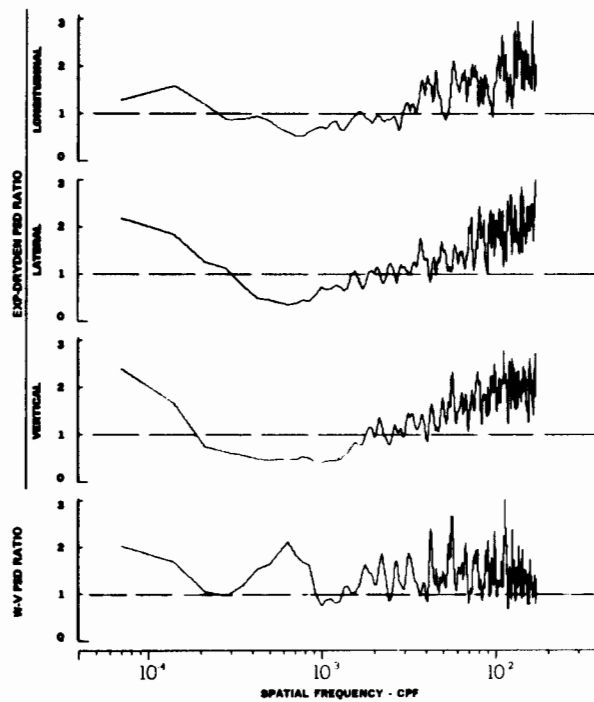
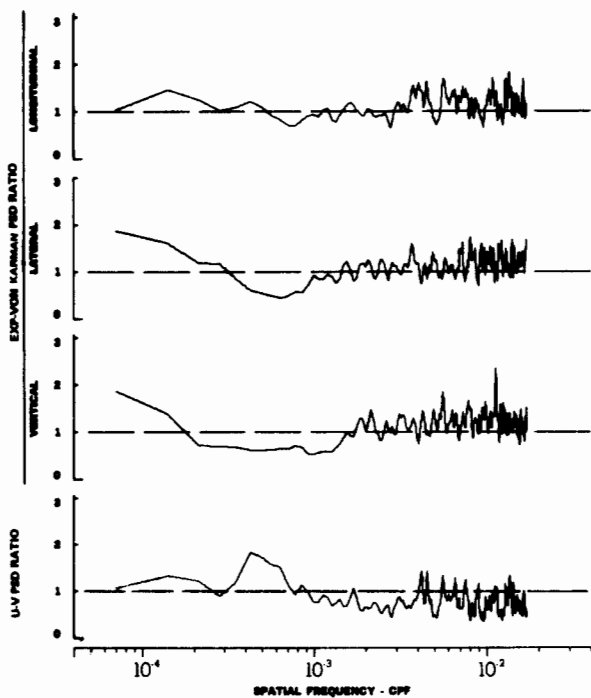
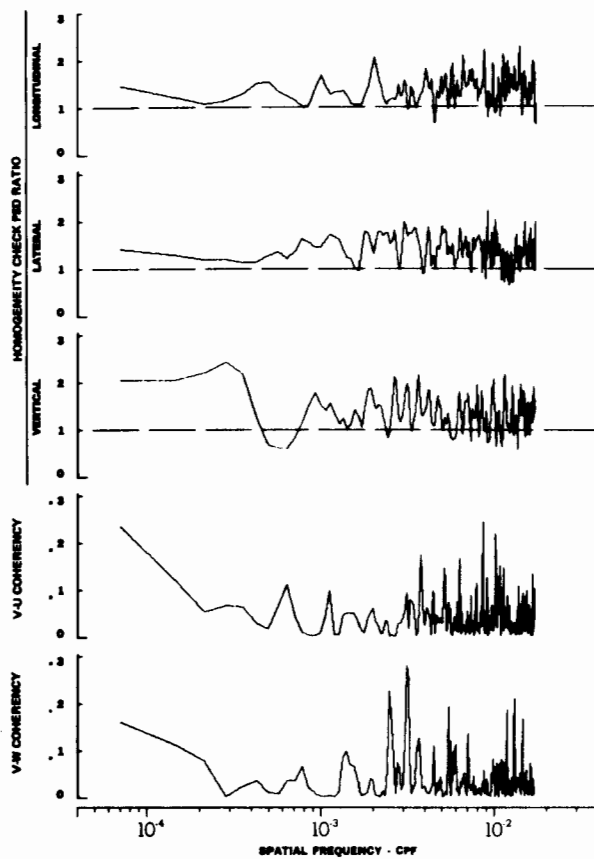
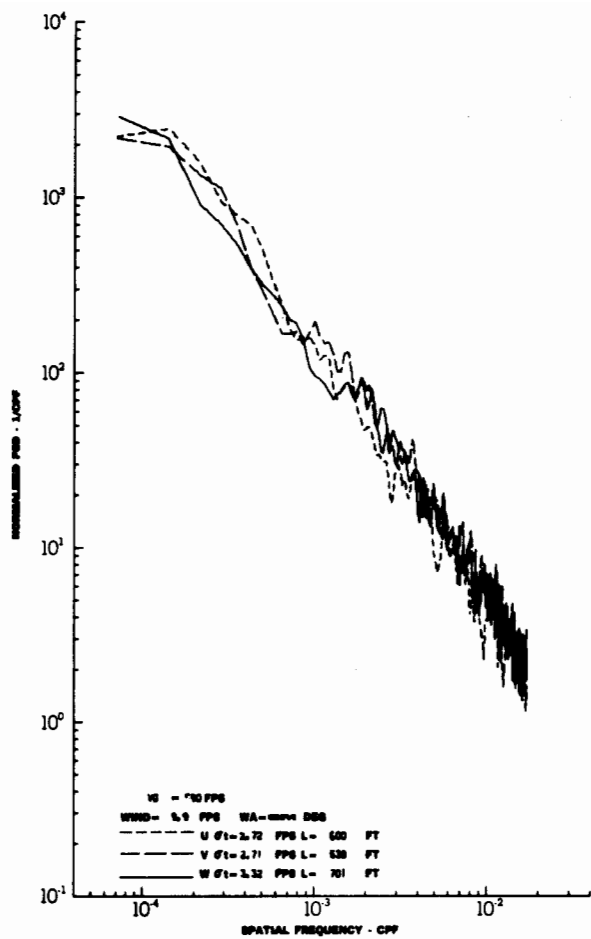
TURBULENCE SPECTRA DATA FOR TEST 78, LEG 2, CATEGORY 312331

FIGURE IV-86

# Contrails



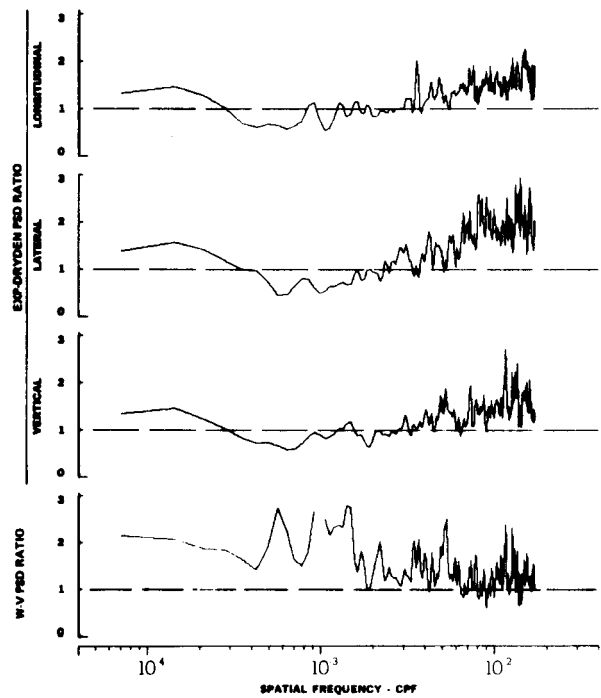
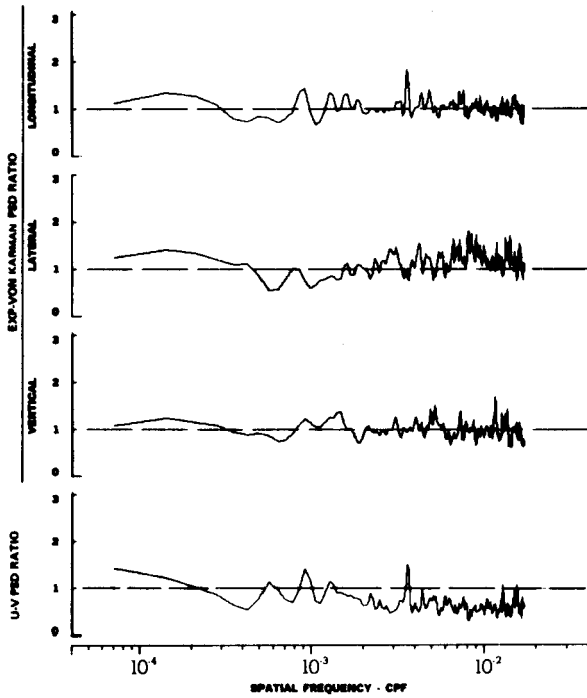
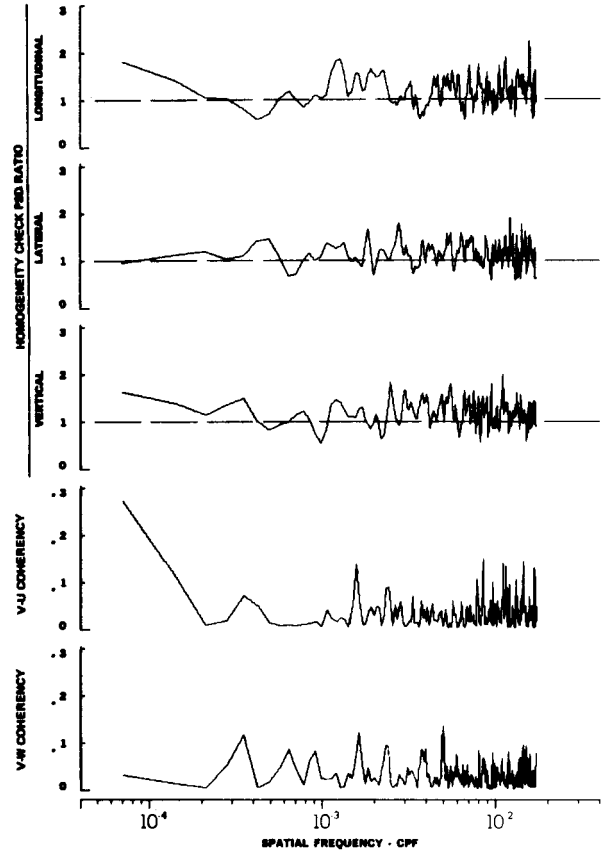
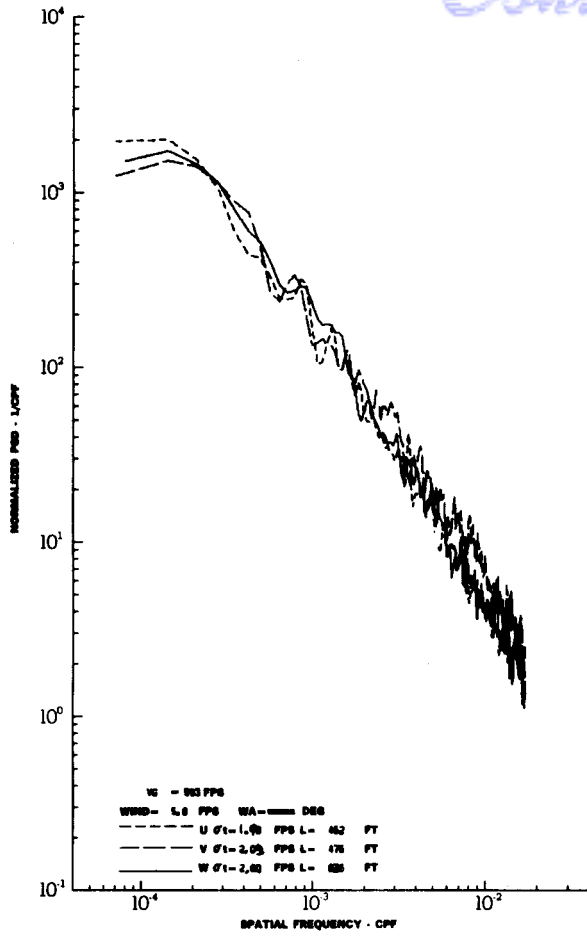
TURBULENCE SPECTRA DATA FOR TEST 78, LEG 6, CATEGORY 112331  
 FIGURE IV-87



TURBULENCE SPECTRA DATA FOR TEST 78, LEG 8, CATEGORY 213331  
FIGURE IV-88



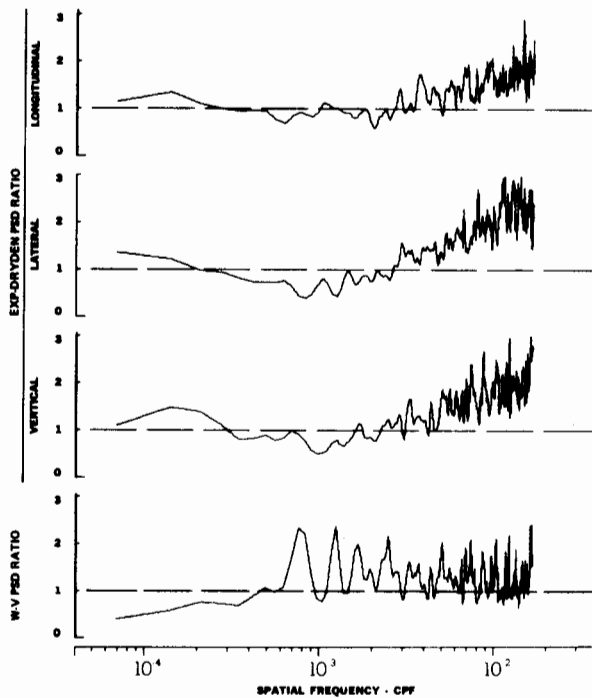
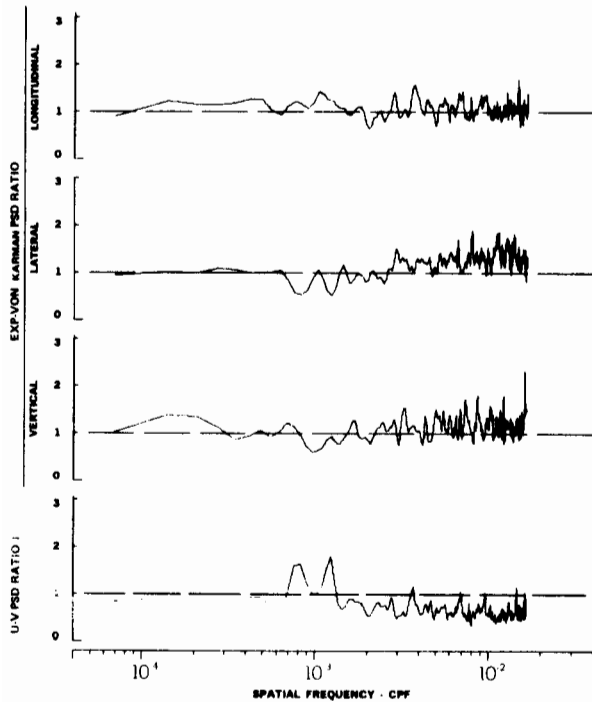
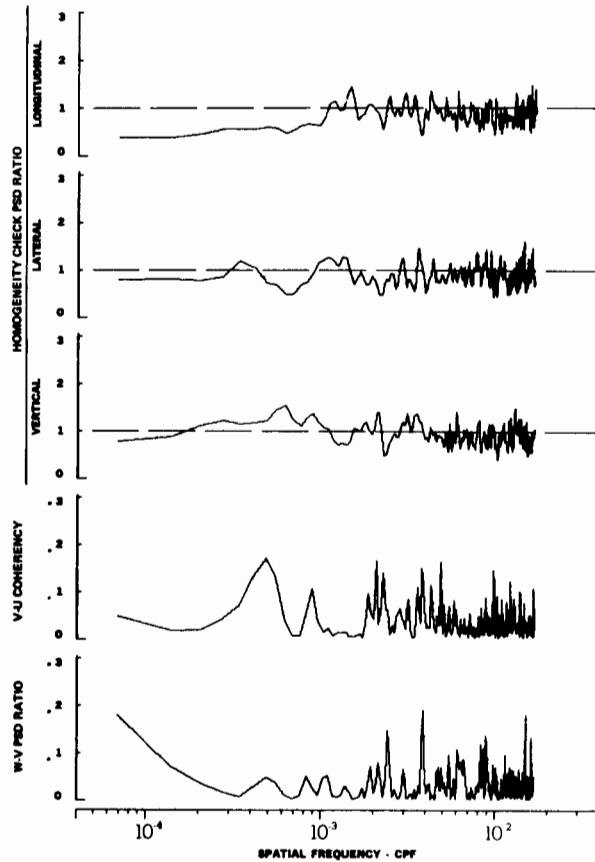
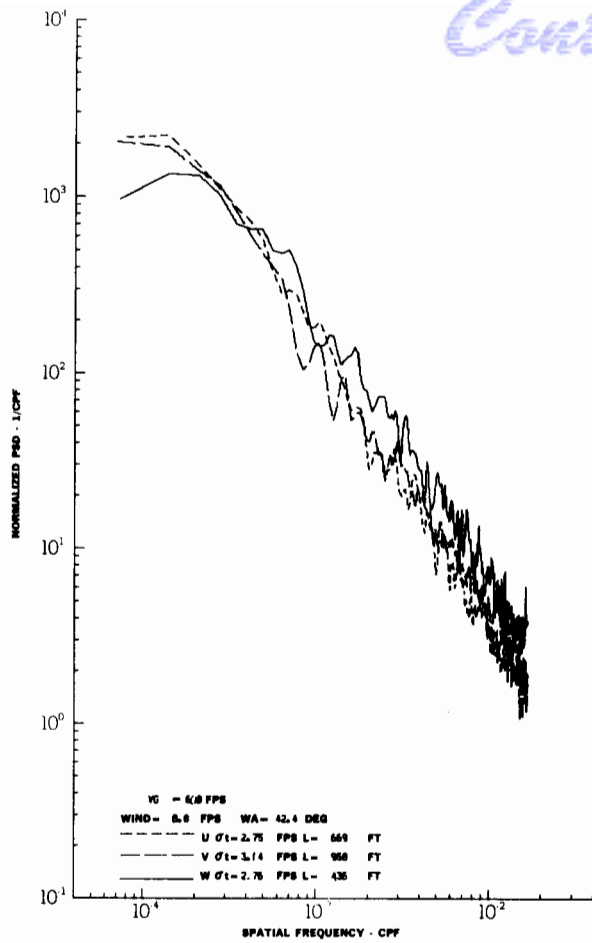
# Contrails



TURBULENCE SPECTRA DATA FOR TEST 80, LEG 2, CATEGORY 322331

FIGURE IV-89

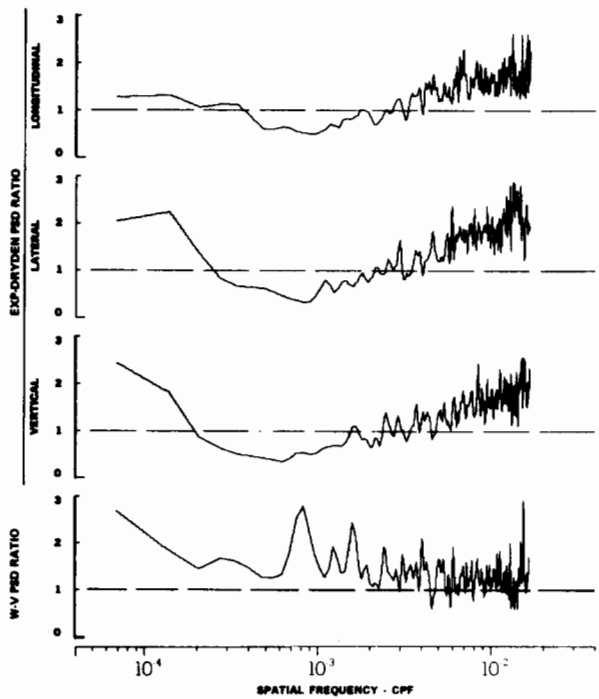
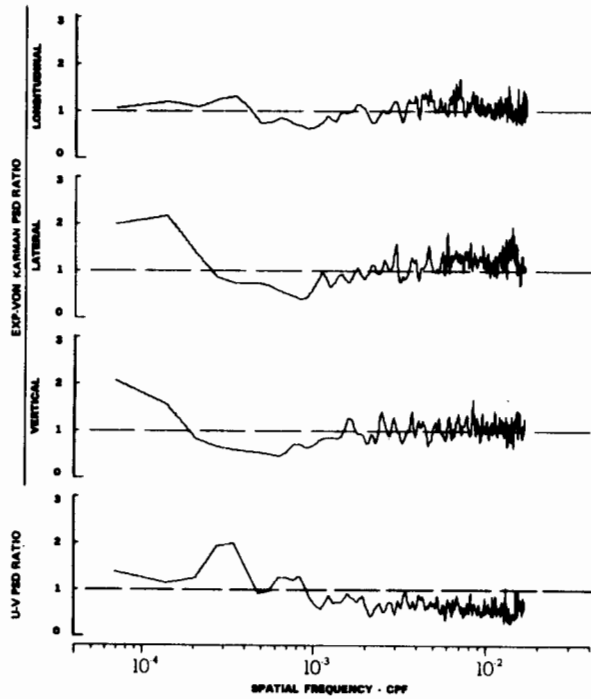
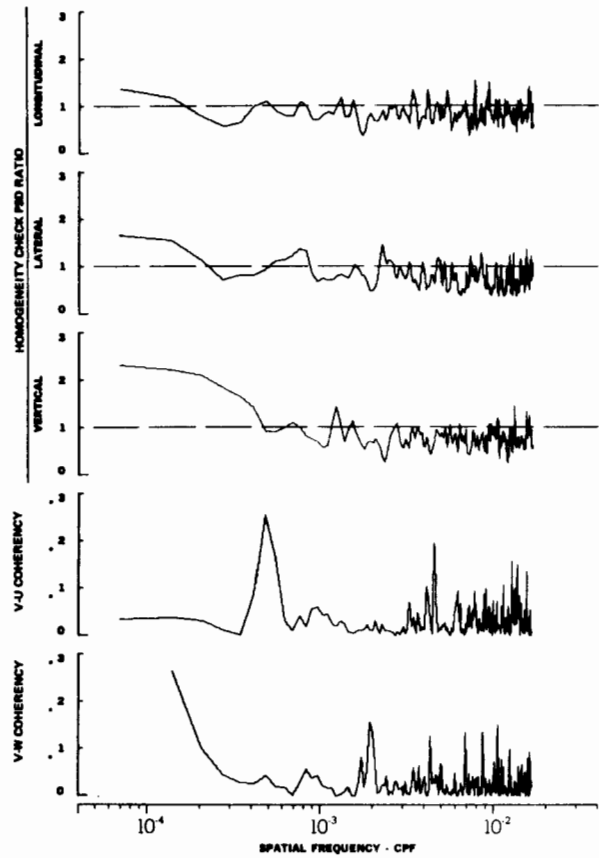
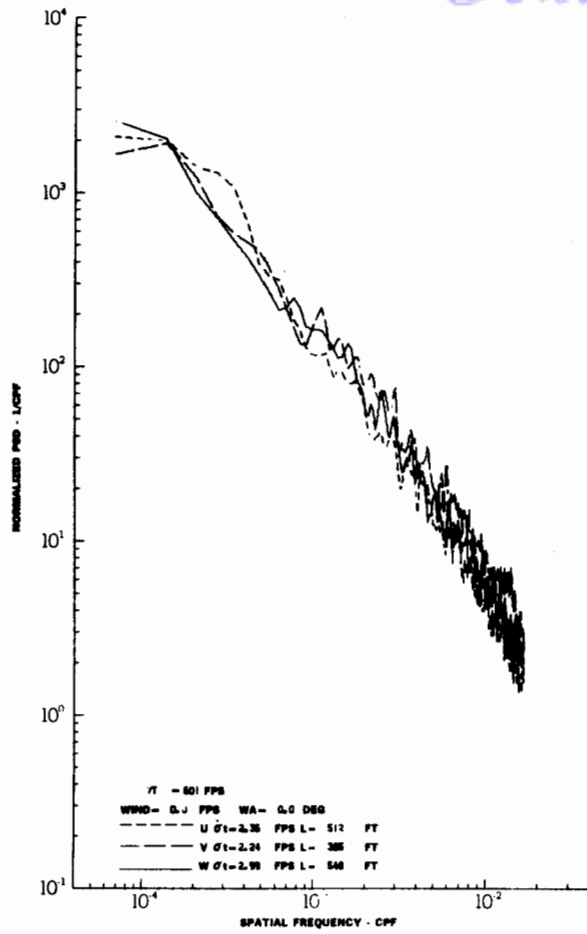
# Contrails



TURBULENCE SPECTRA DATA FOR TEST 80, LEG 6, CATEGORY 122331

FIGURE IV-90

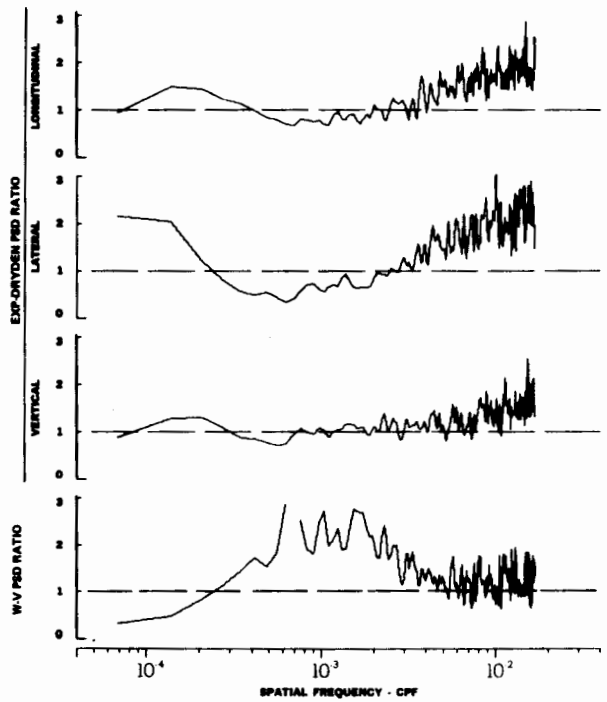
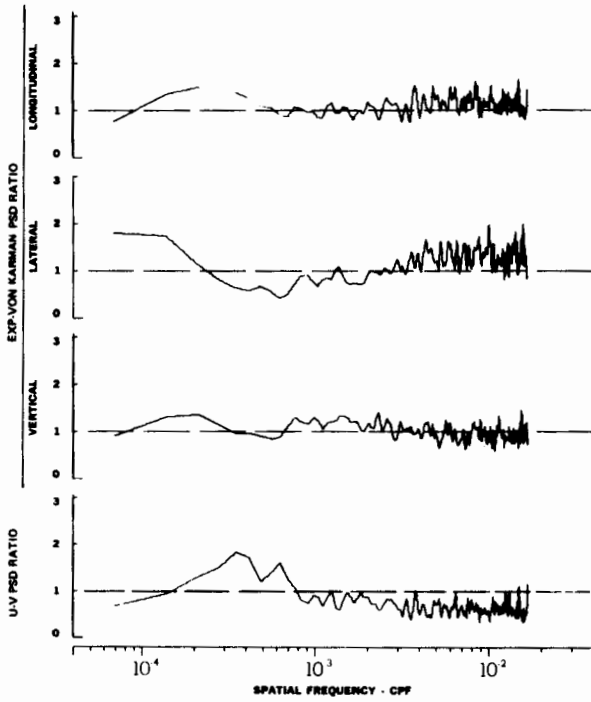
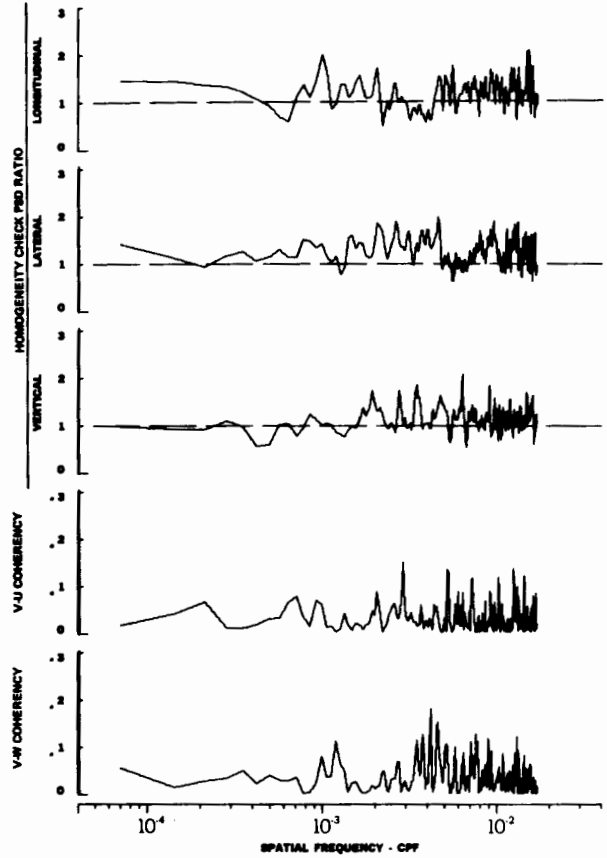
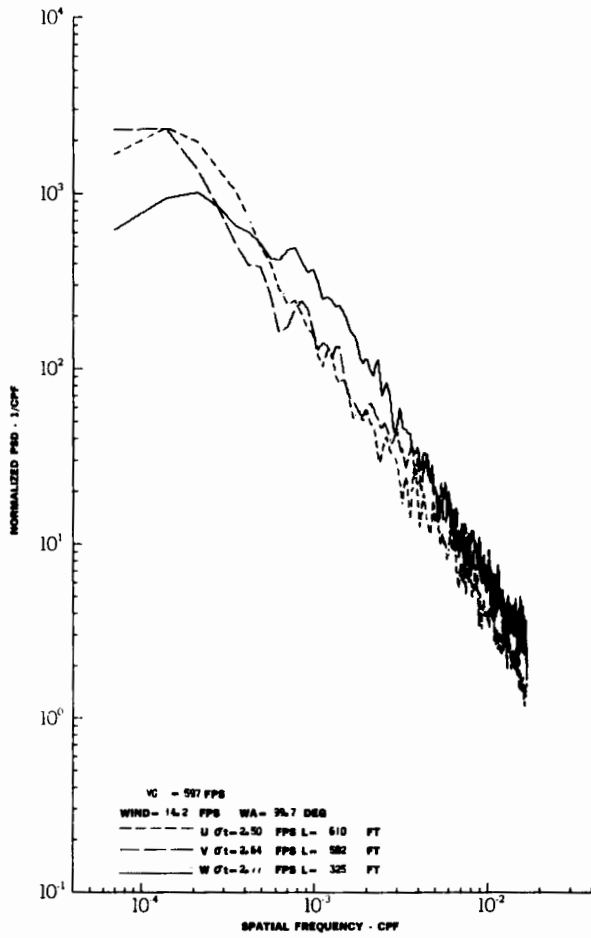
# Contrails



TURBULENCE SPECTRA DATA FOR TEST 81, LEG 7, CATEGORY 312231

FIGURE IV-91

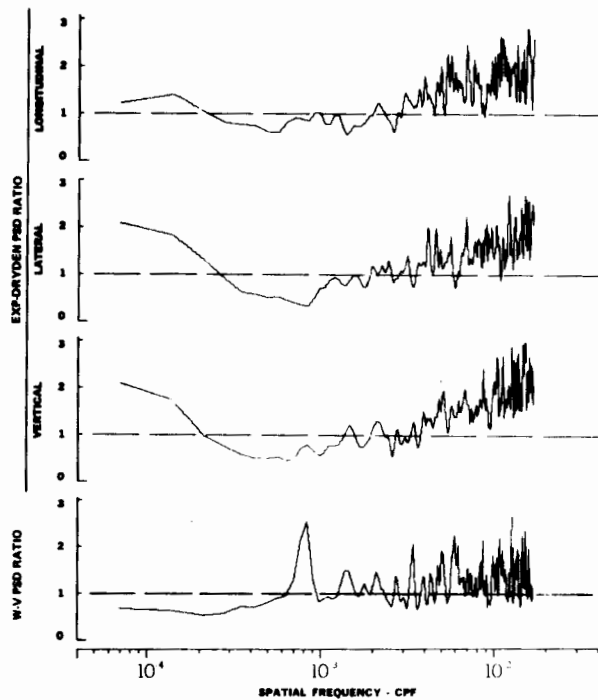
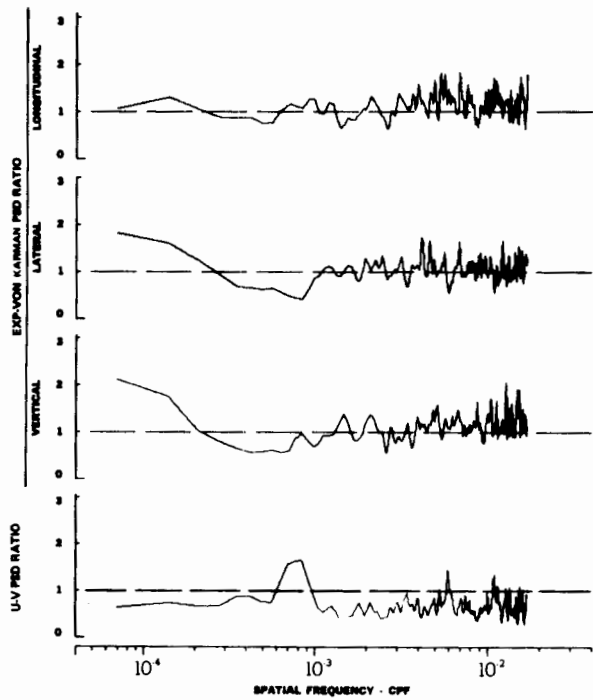
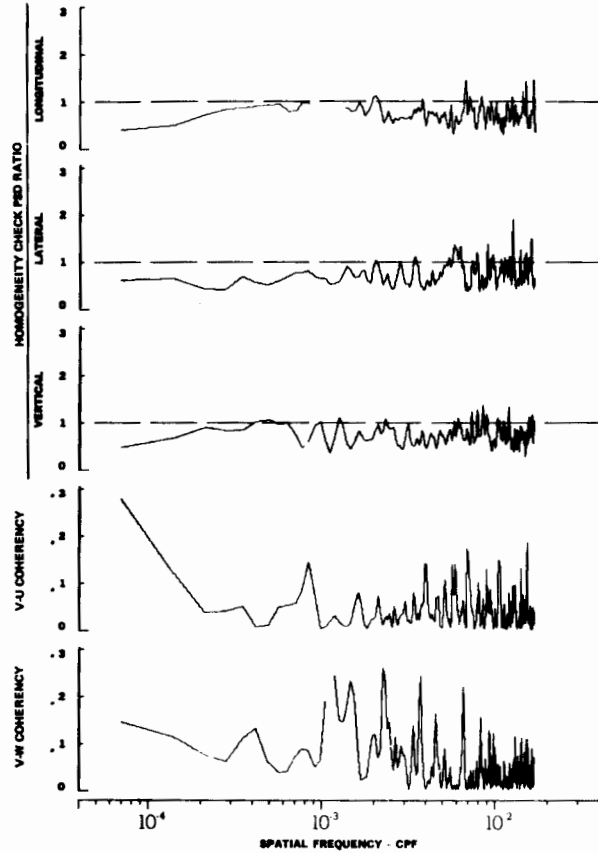
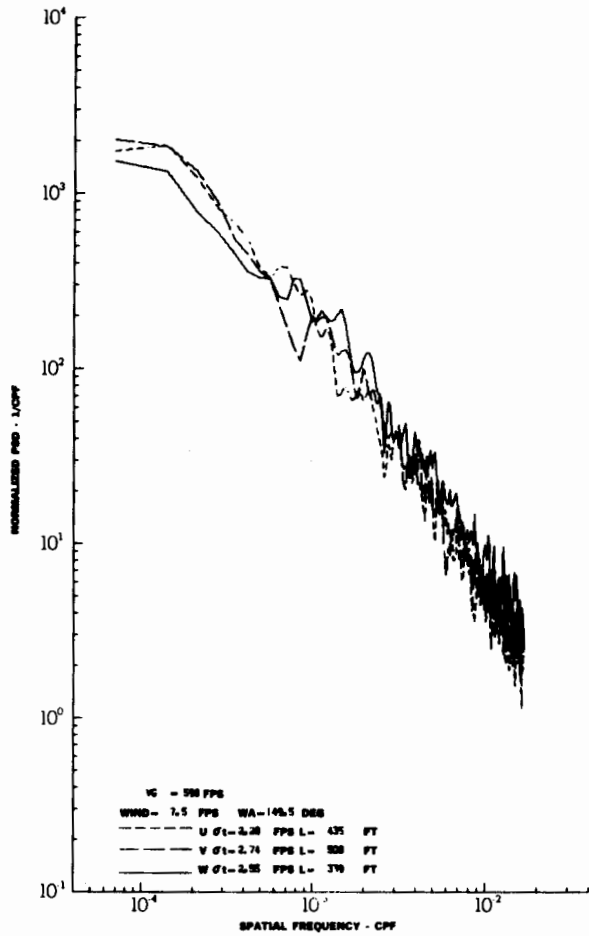
# Contrails



TURBULENCE SPECTRA DATA FOR TEST 82, LEG 2, CATEGORY 312331

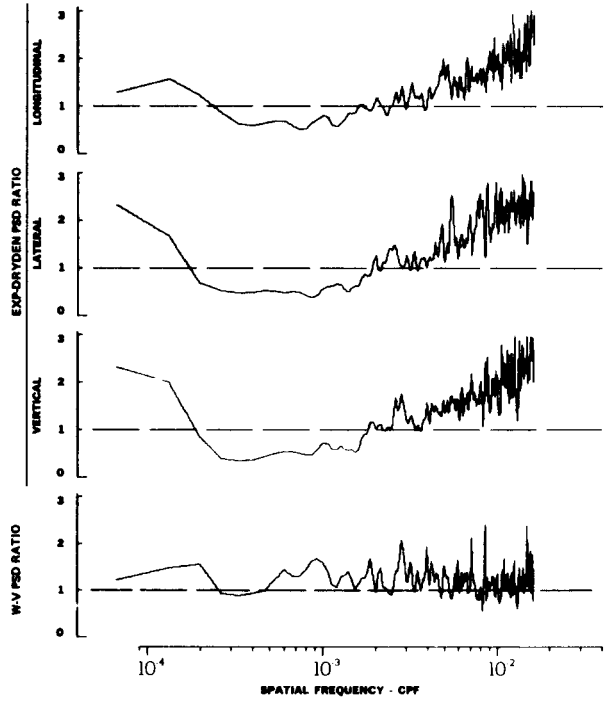
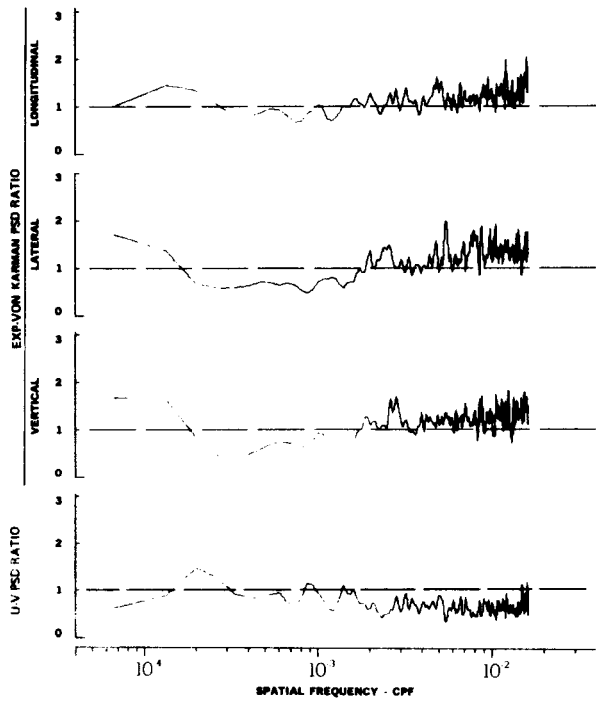
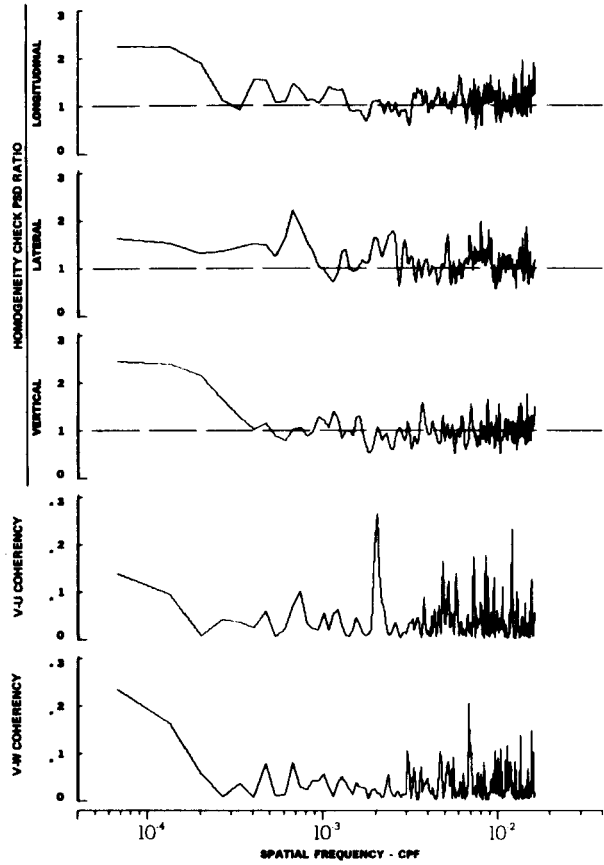
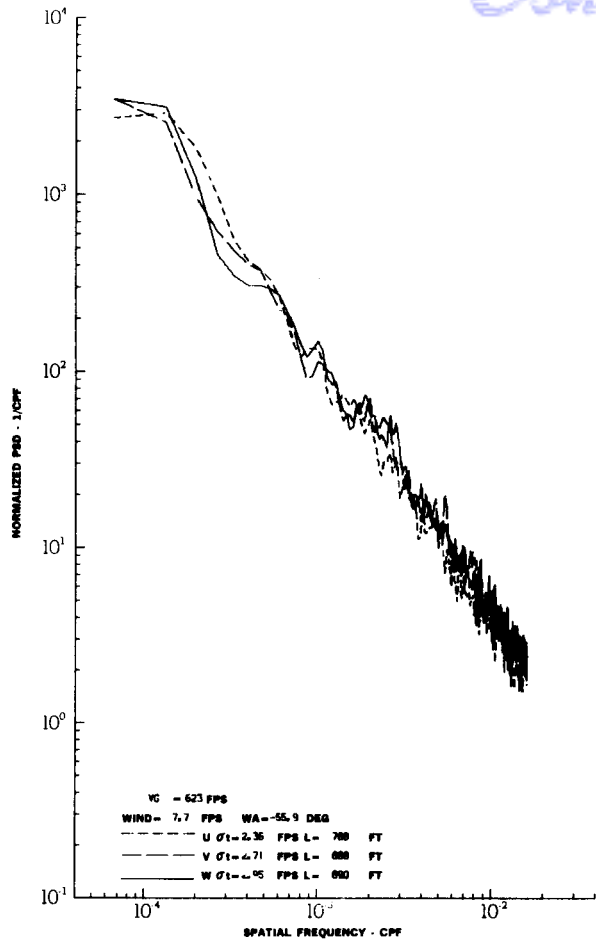
FIGURE IV-92

# Contrails



TURBULENCE SPECTRA DATA FOR TEST 82, LEG 6, CATEGORY 112331  
 FIGURE IV-93

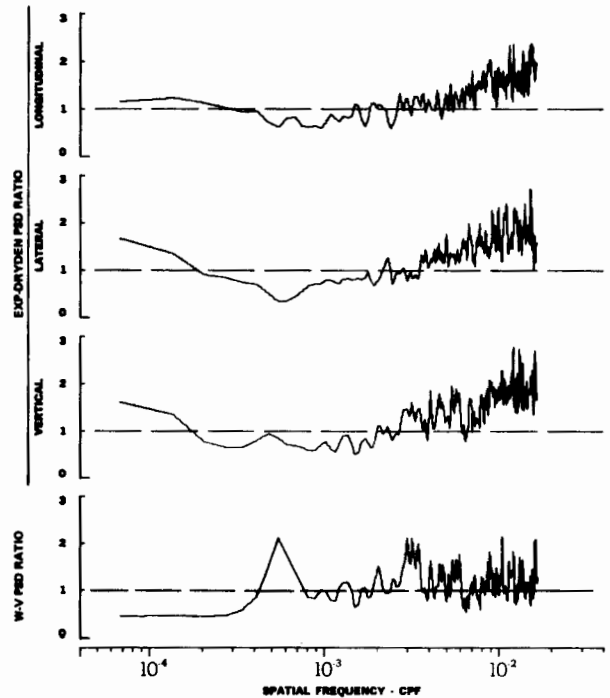
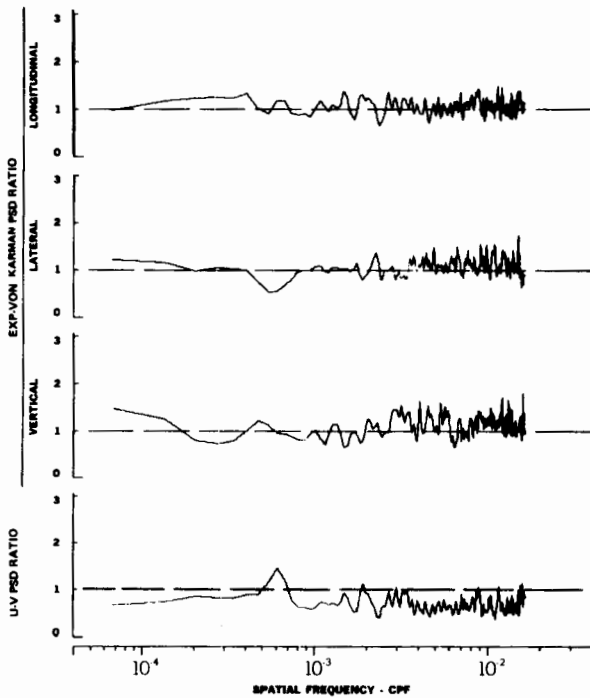
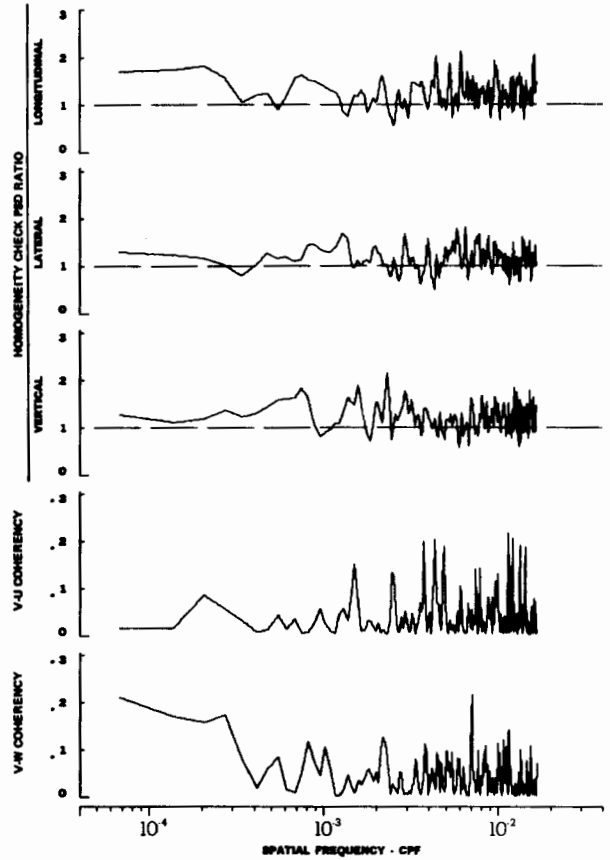
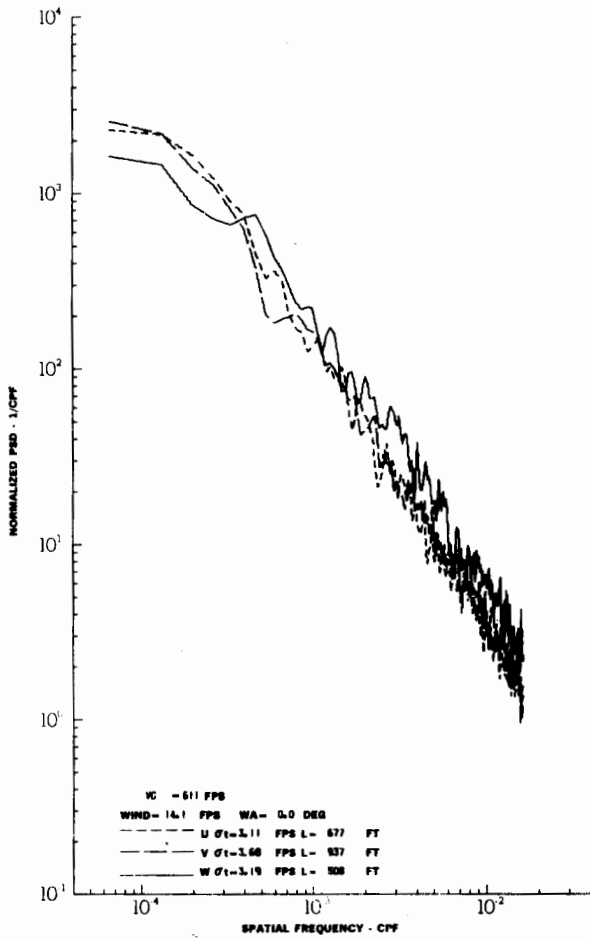
# Contrails



TURBULENCE SPECTRA DATA FOR TEST 82, LEG 8, CATEGORY 213331

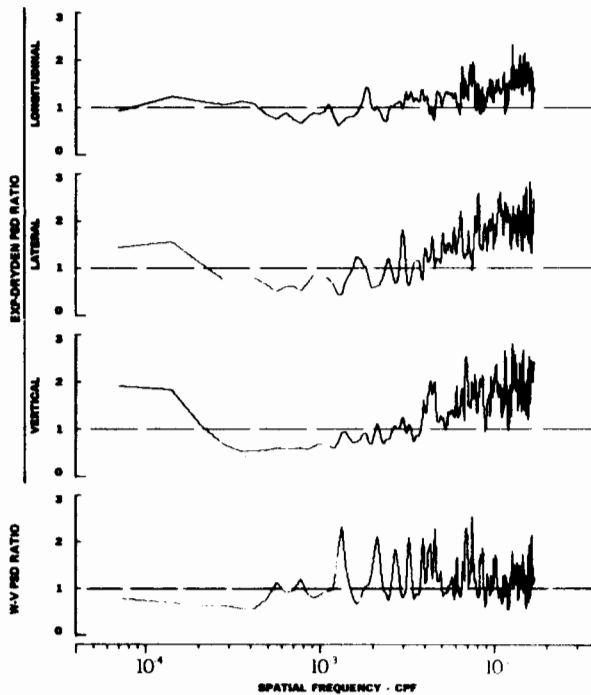
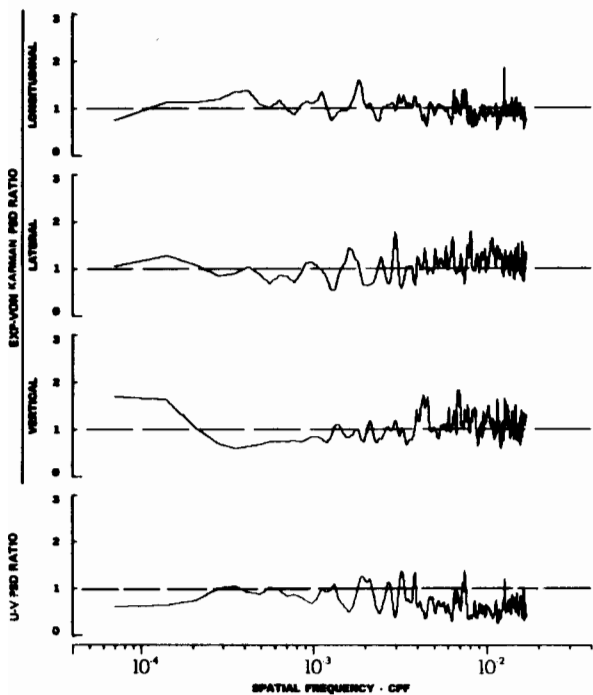
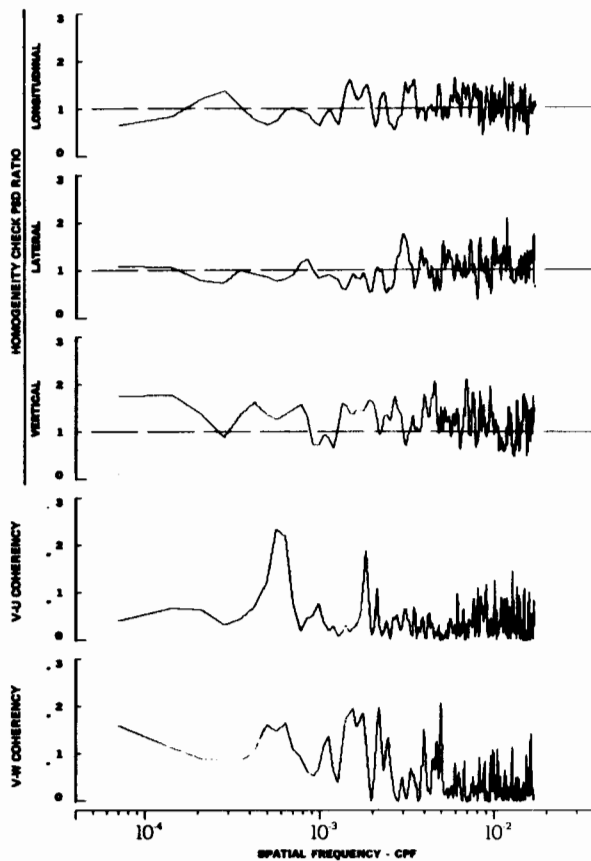
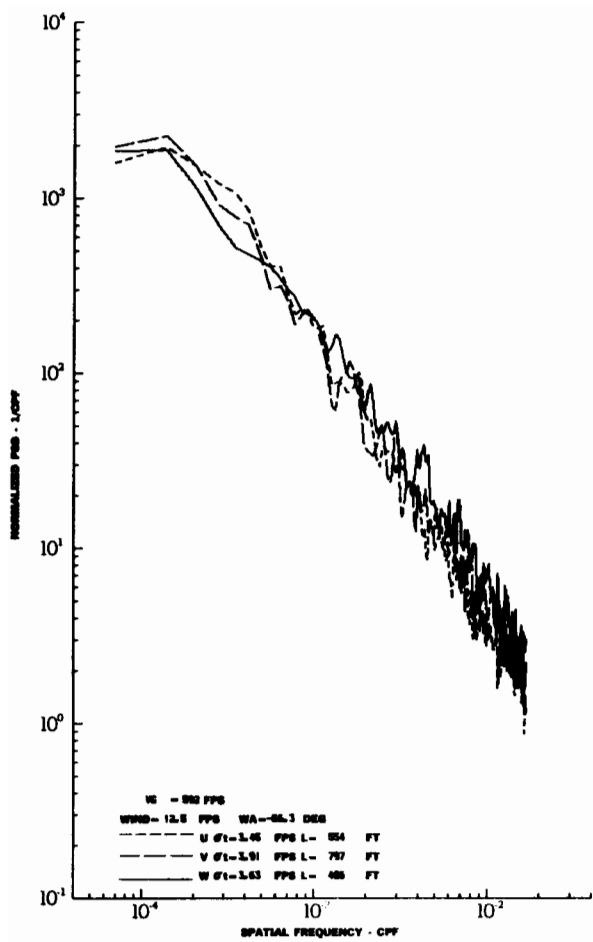
FIGURE IV-94

# Contrails



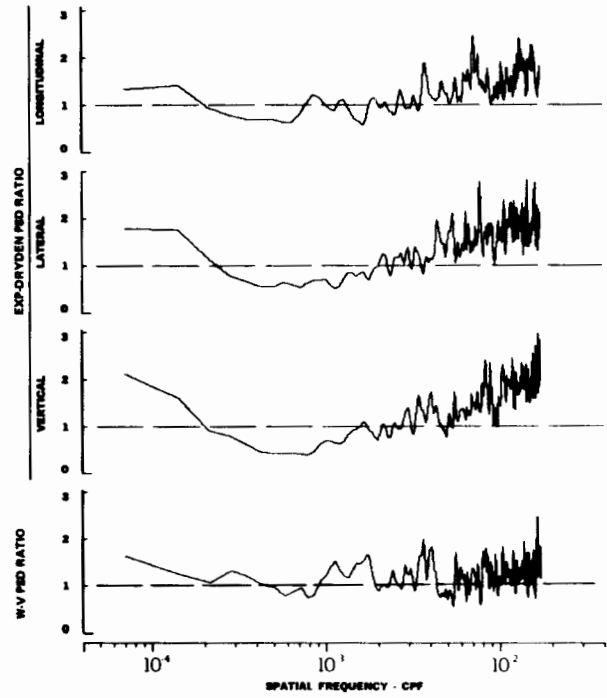
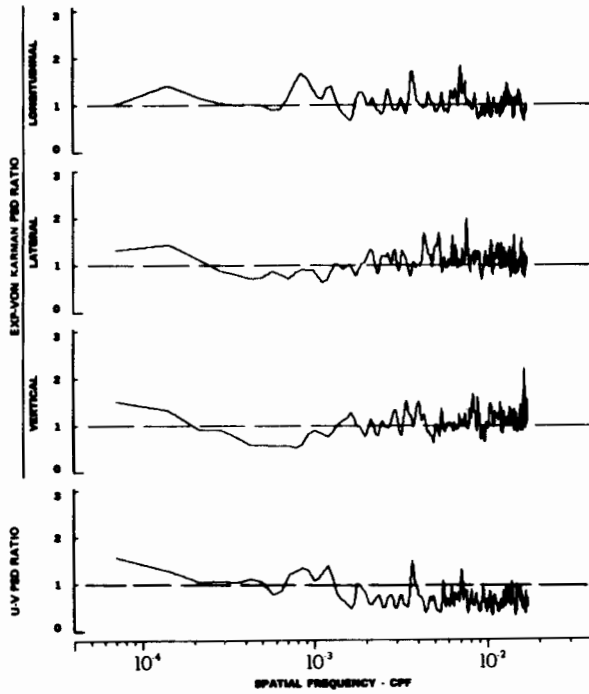
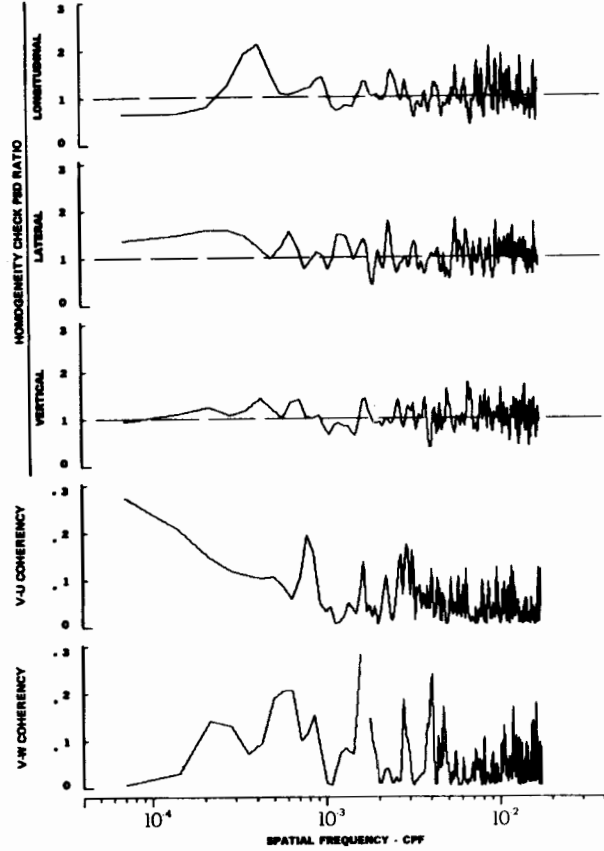
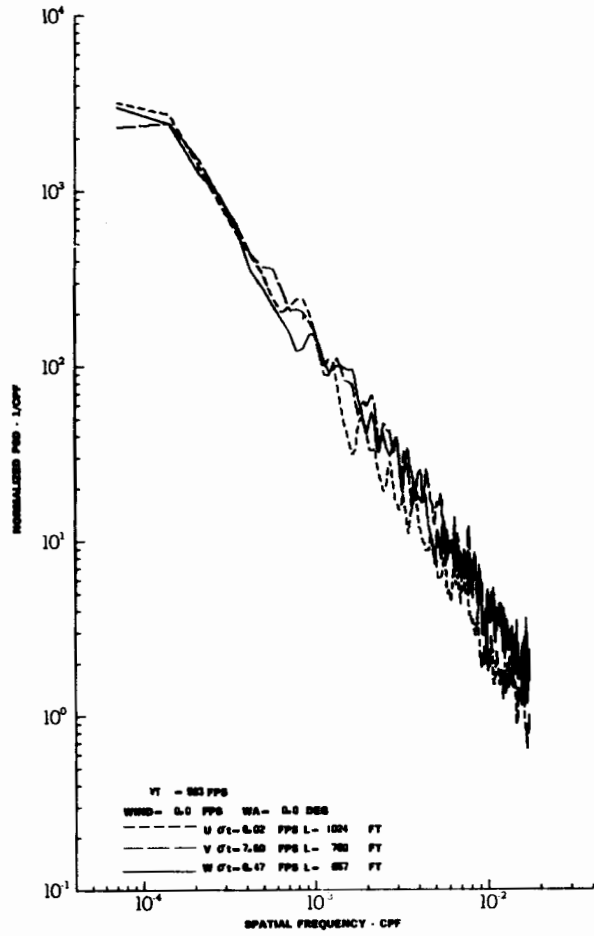
TURBULENCE SPECTRA DATA FOR TEST 85, LEG 1, CATEGORY 224331  
 FIGURE IV-95





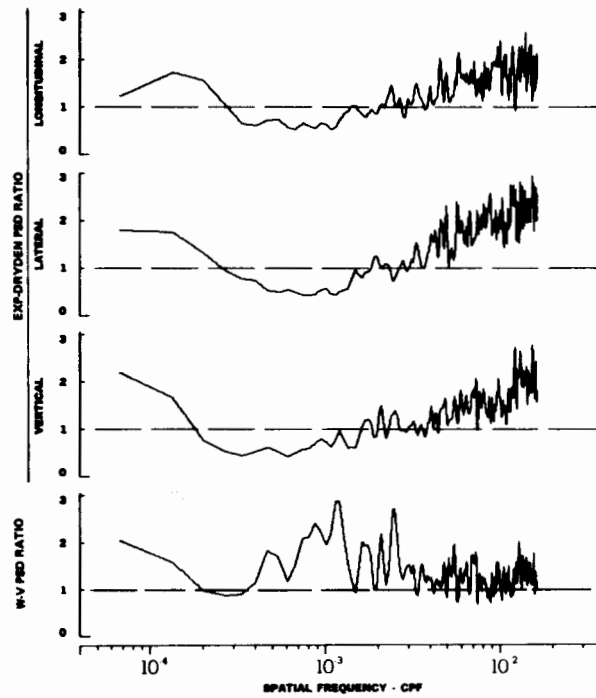
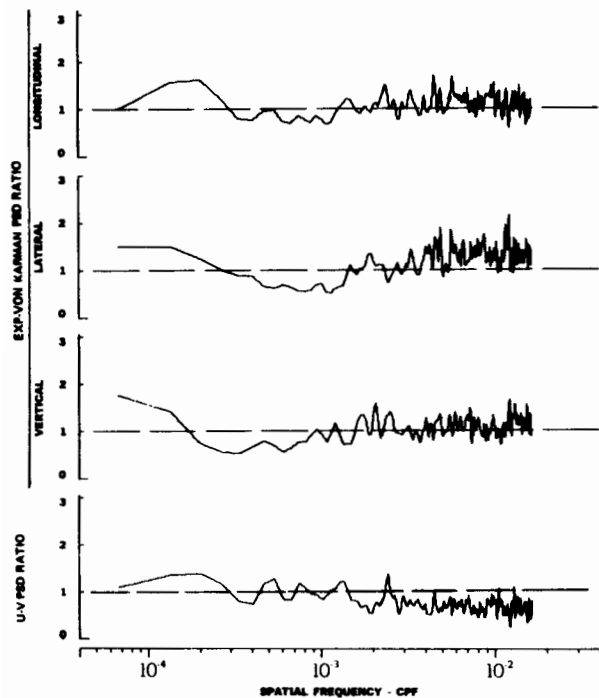
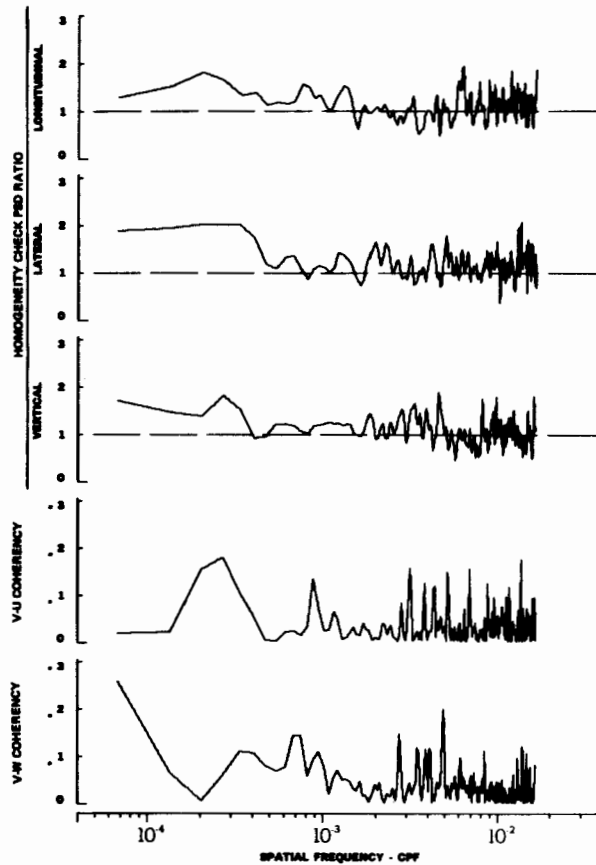
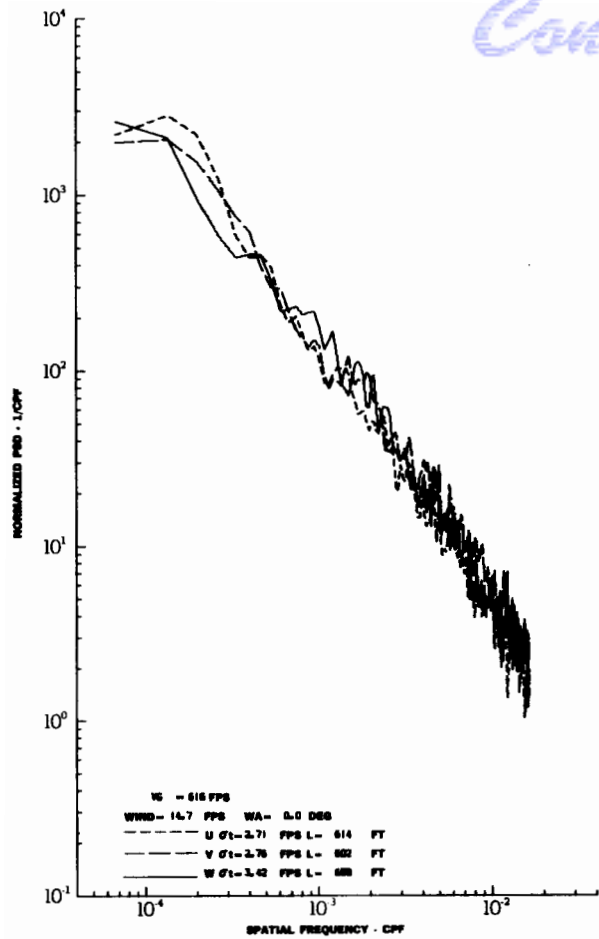
TURBULENCE SPECTRA DATA FOR TEST 85, LEG 5, CATEGORY 121331

FIGURE IV-96



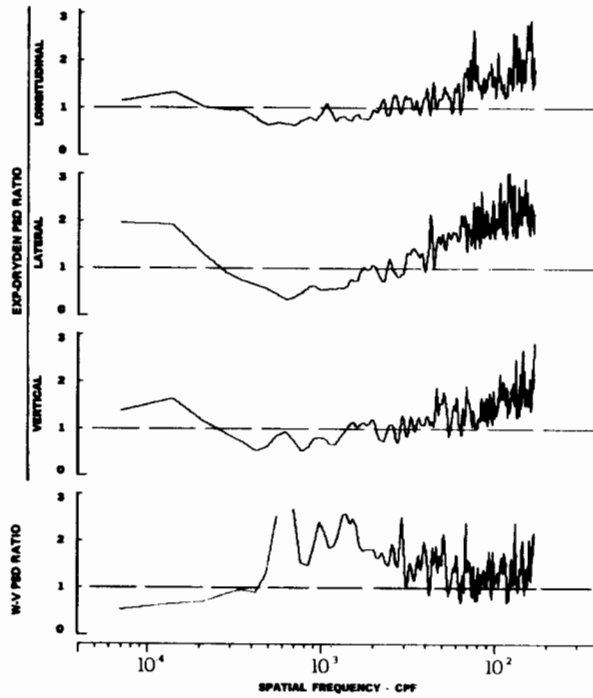
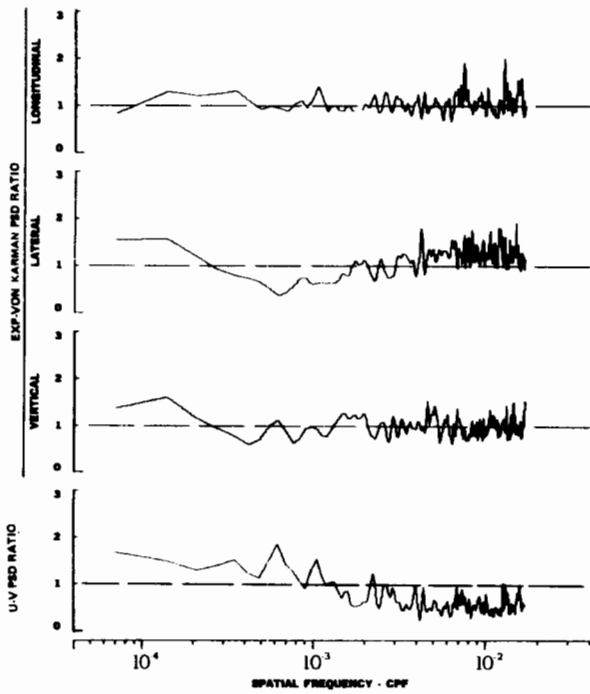
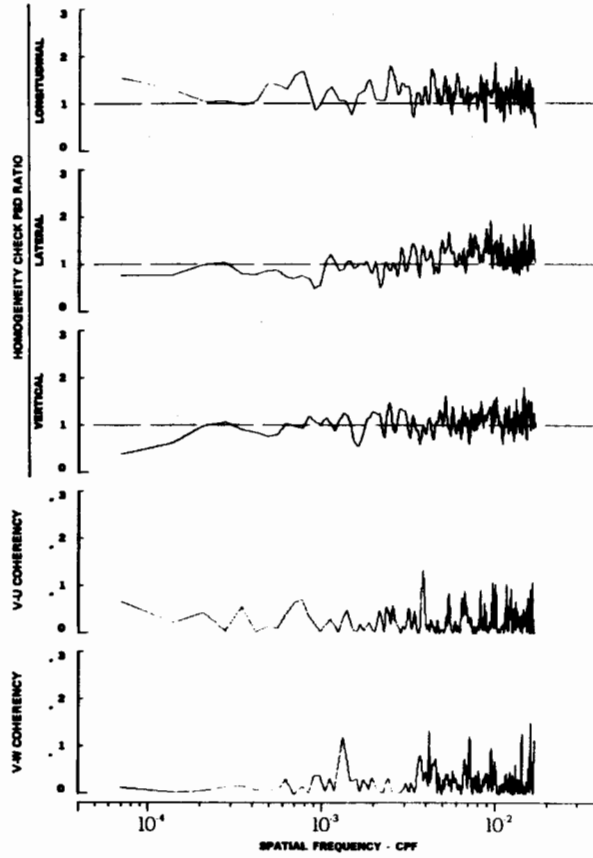
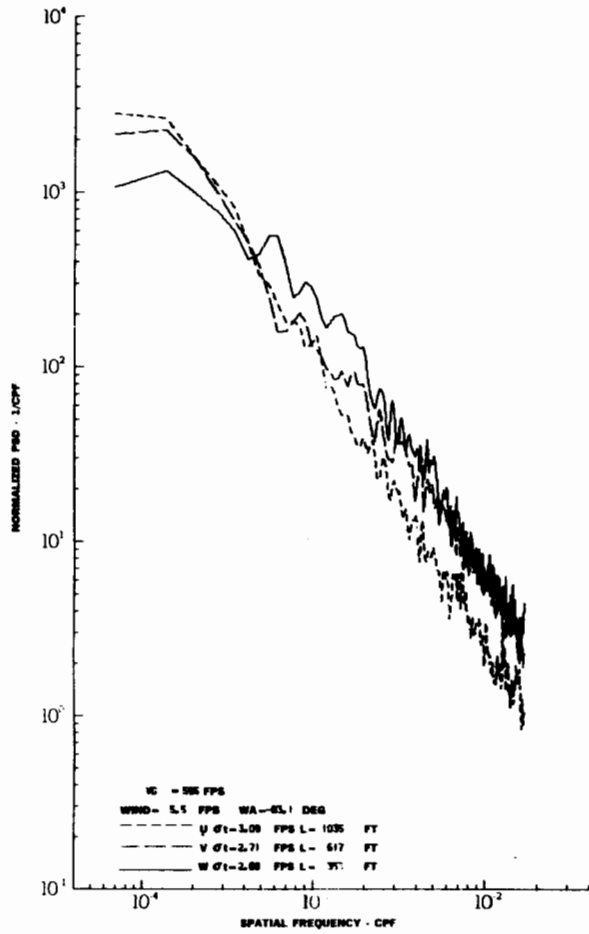
TURBULENCE SPECTRA DATA FOR TEST 87, LEG 5, CATEGORY 114231  
 FIGURE IV-97

# Contrails



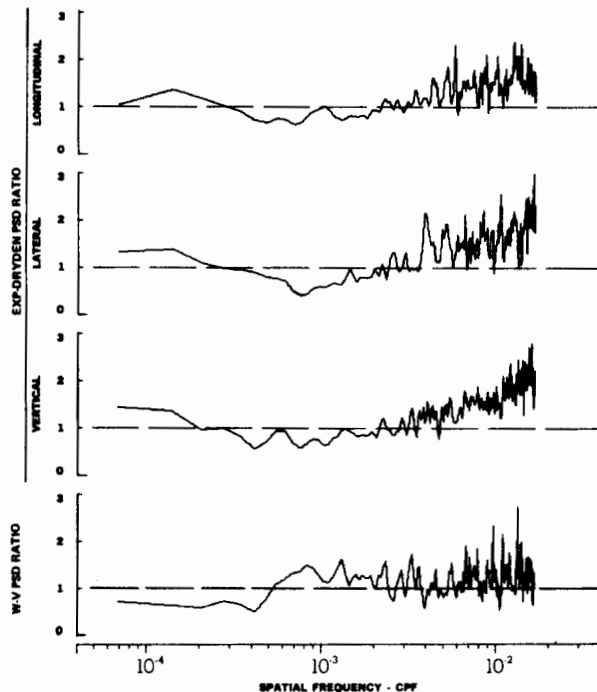
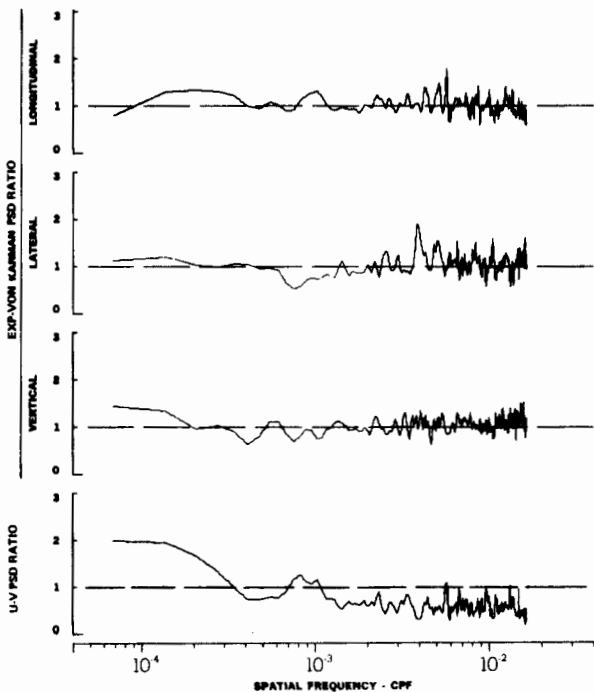
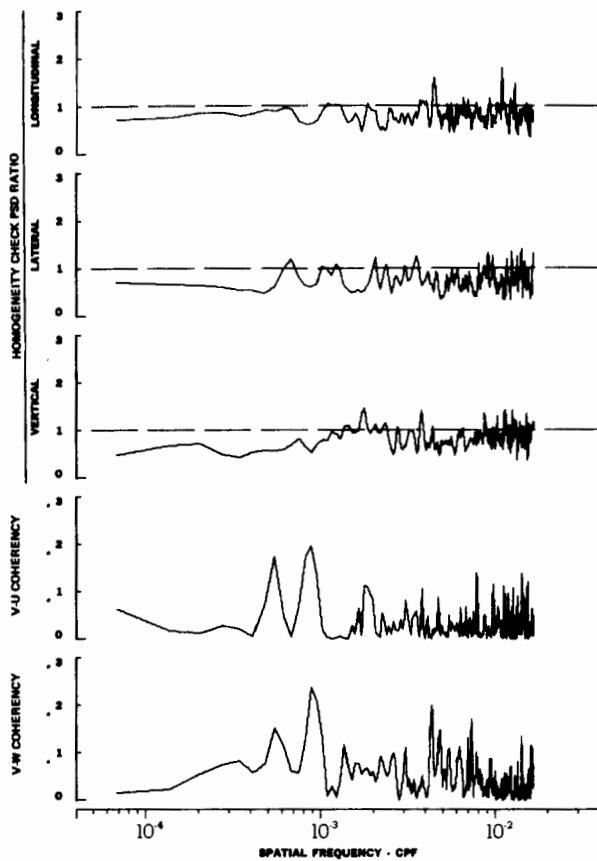
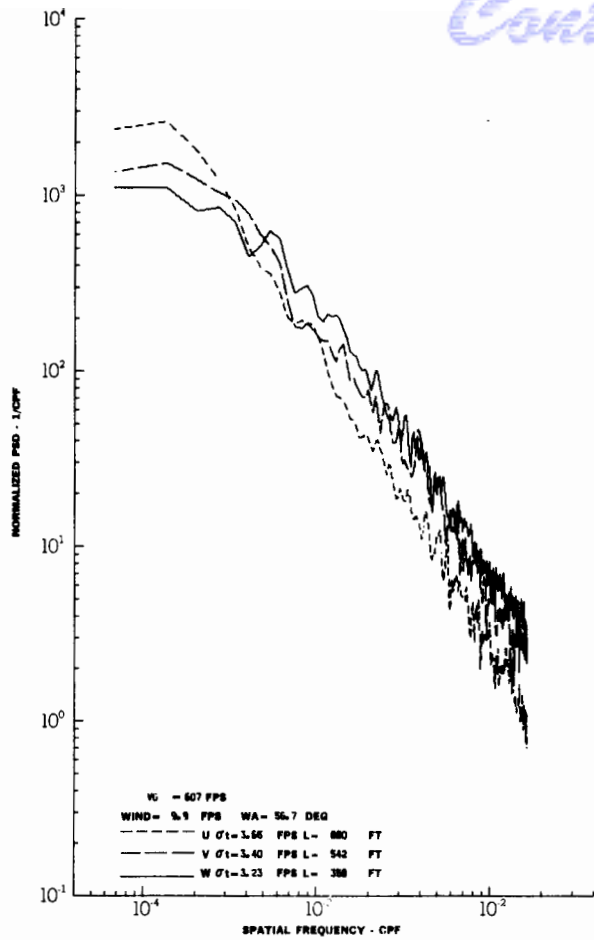
TURBULENCE SPECTRA DATA FOR TEST 87, LEG 7, CATEGORY 312231  
 FIGURE IV-98

# Contrails



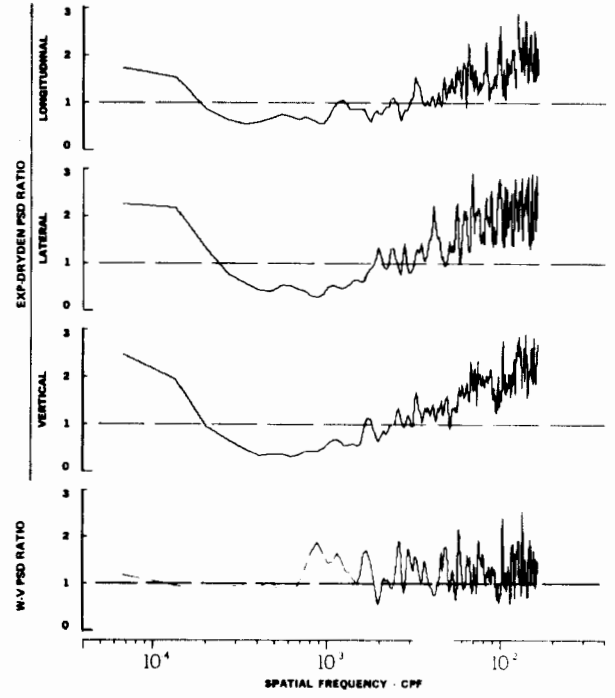
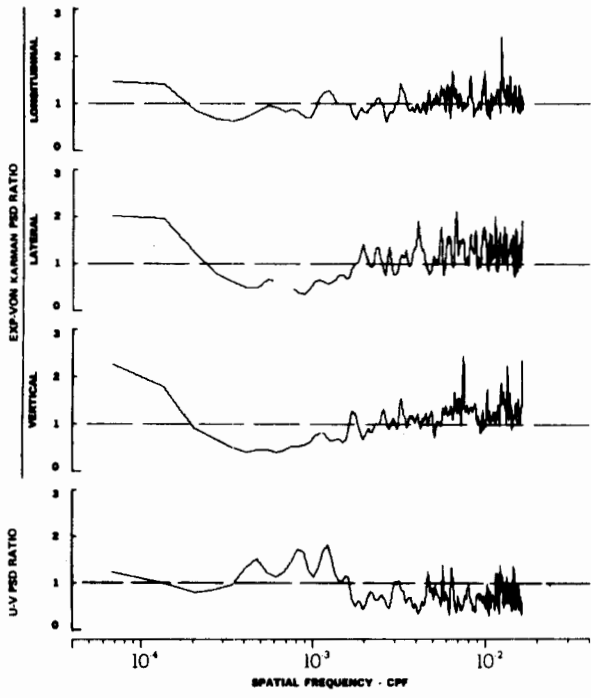
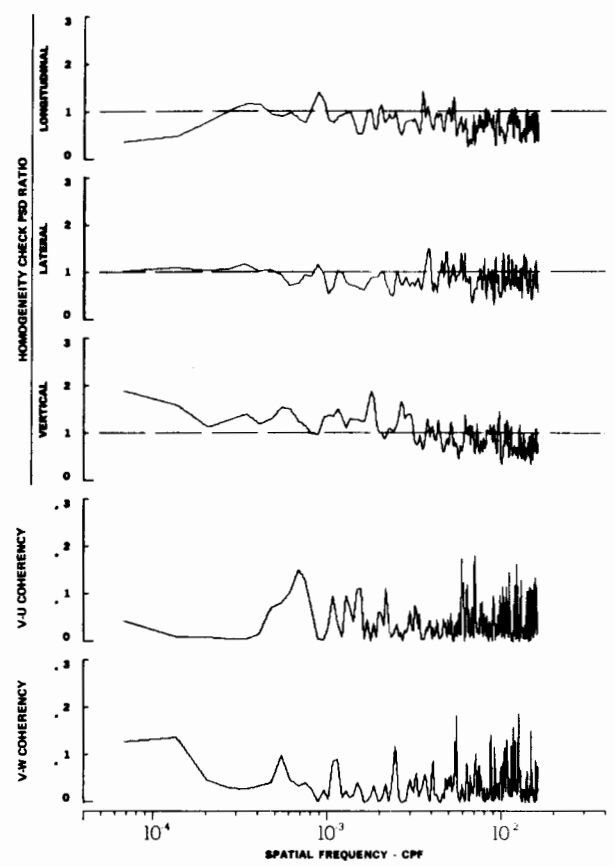
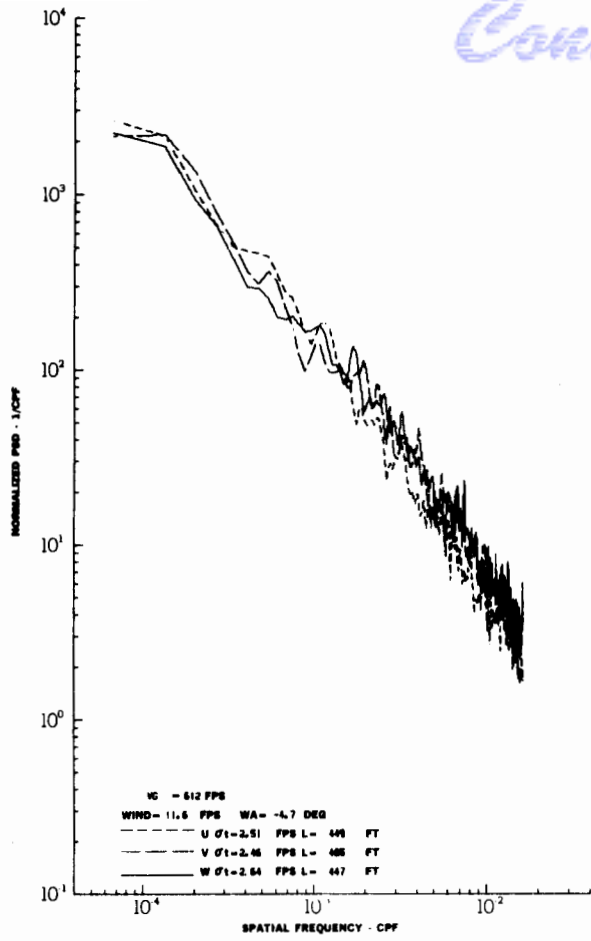
TURBULENCE SPECTRA DATA FOR TEST 88, LEG 2, CATEGORY 312331  
 FIGURE IV-99

# Contrails



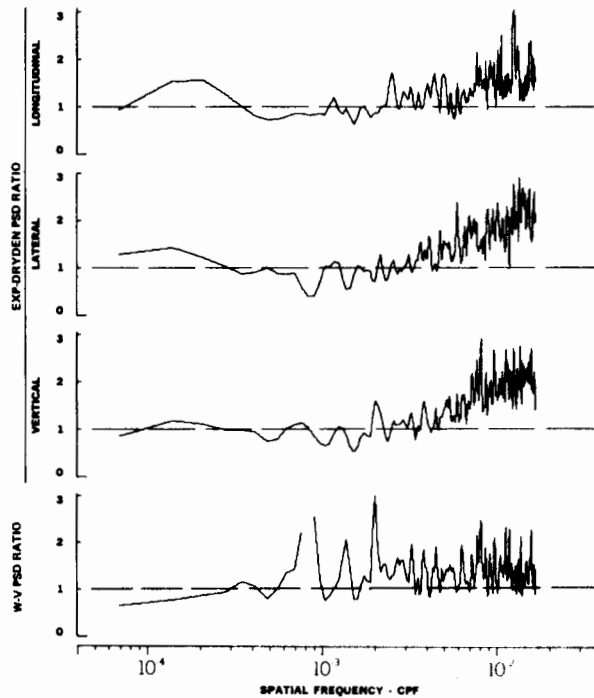
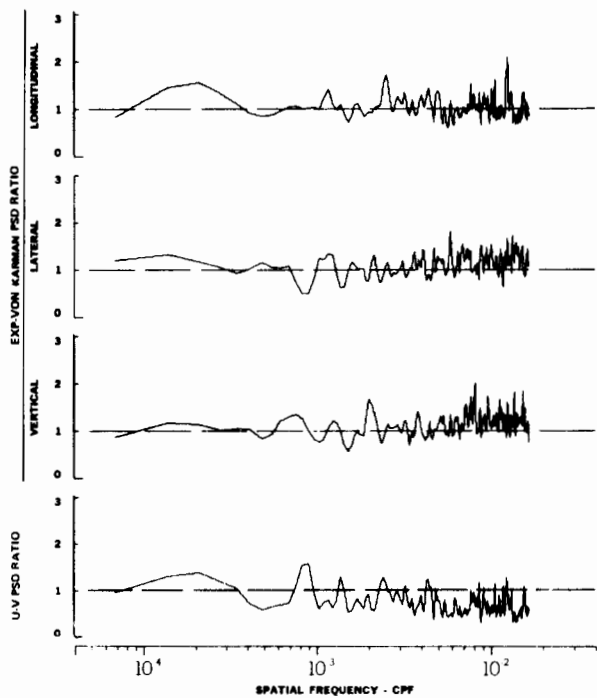
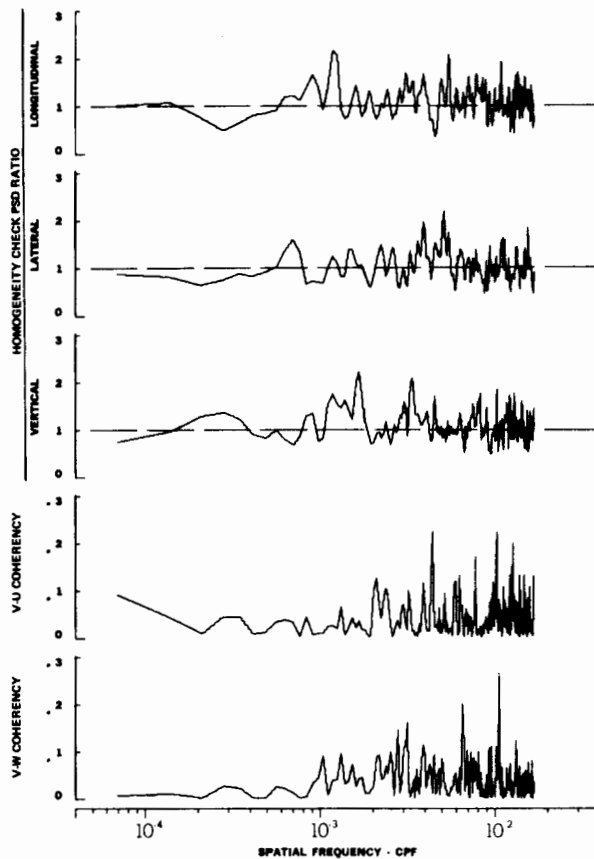
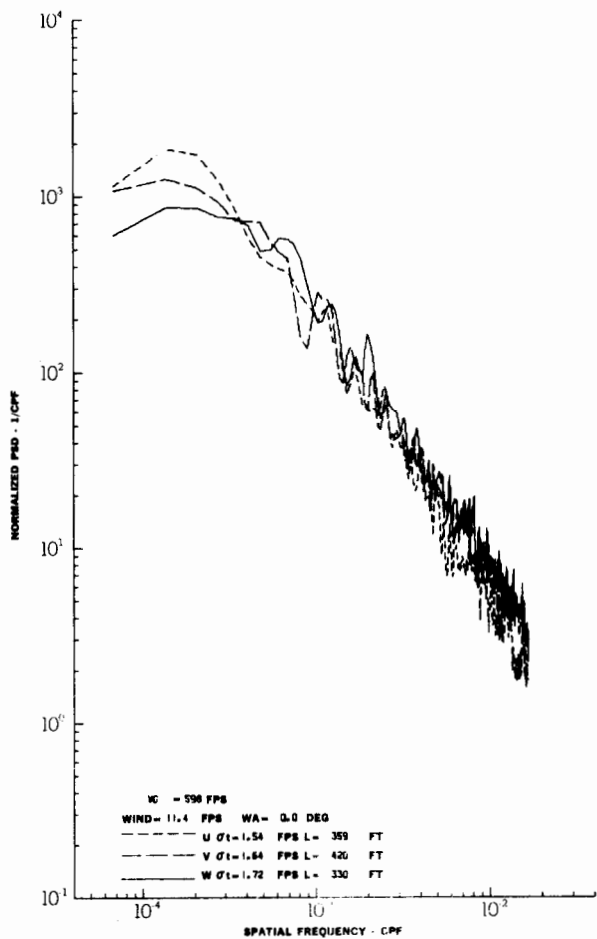
TURBULENCE SPECTRA DATA FOR TEST 88, LEG 6, CATEGORY 114331  
FIGURE IV-100

# Contrails



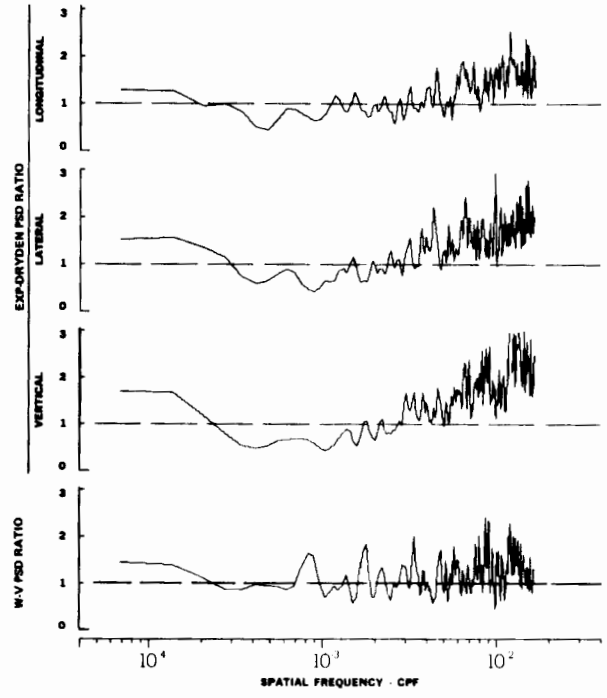
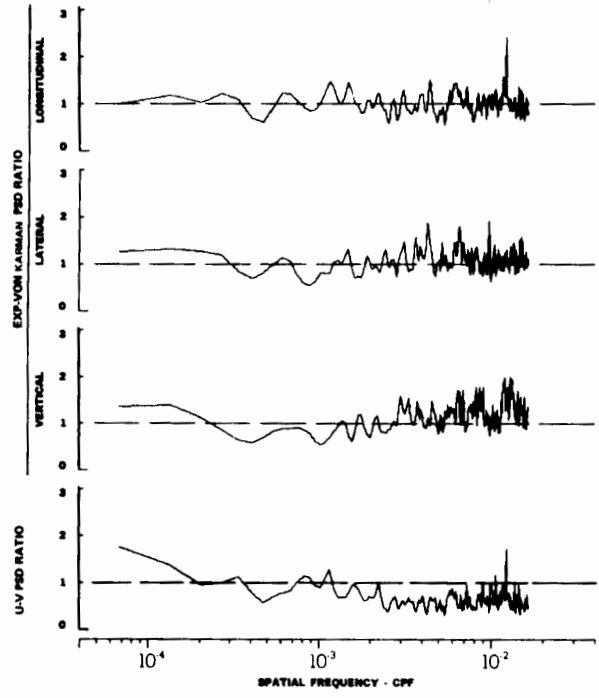
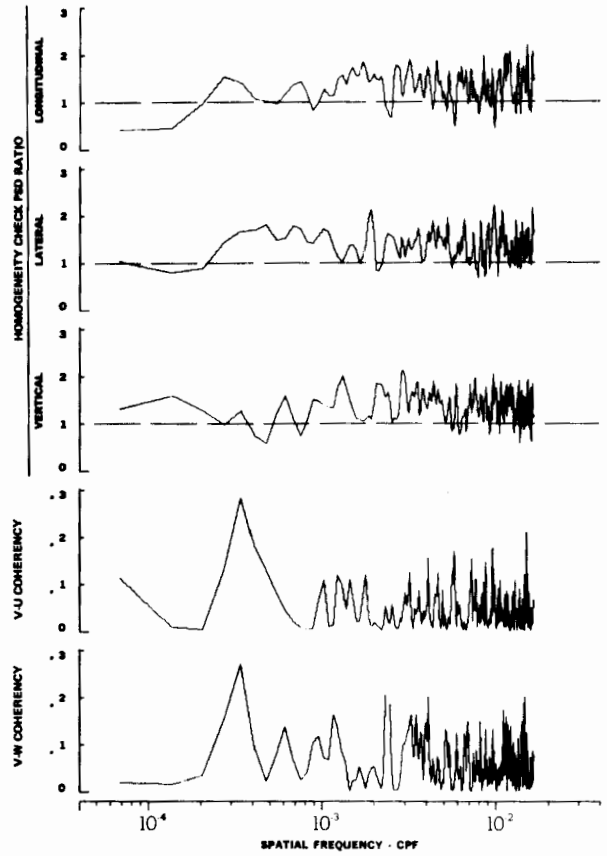
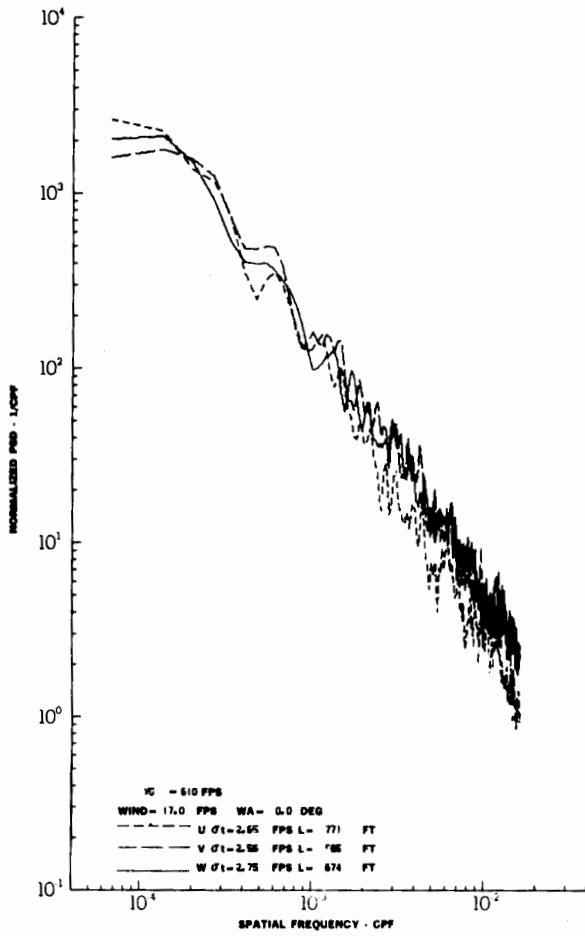
TURBULENCE SPECTRA DATA FOR TEST 88, LEG 8, CATEGORY 213331  
 FIGURE IV-101

# Contrails



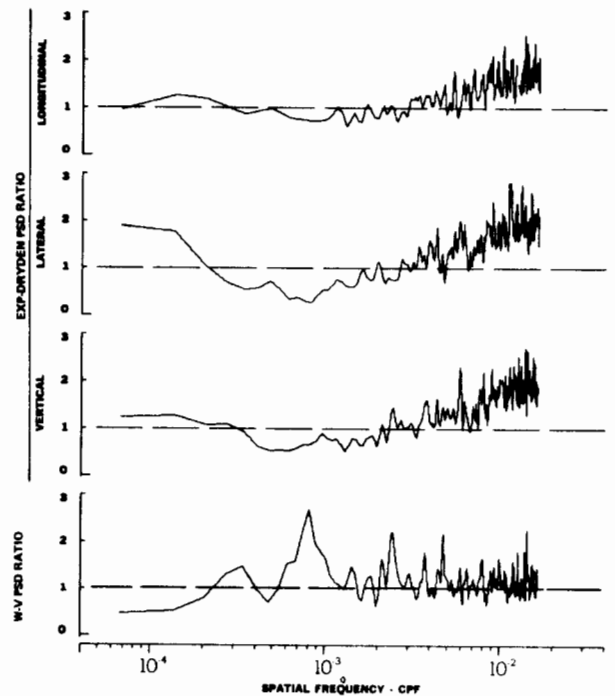
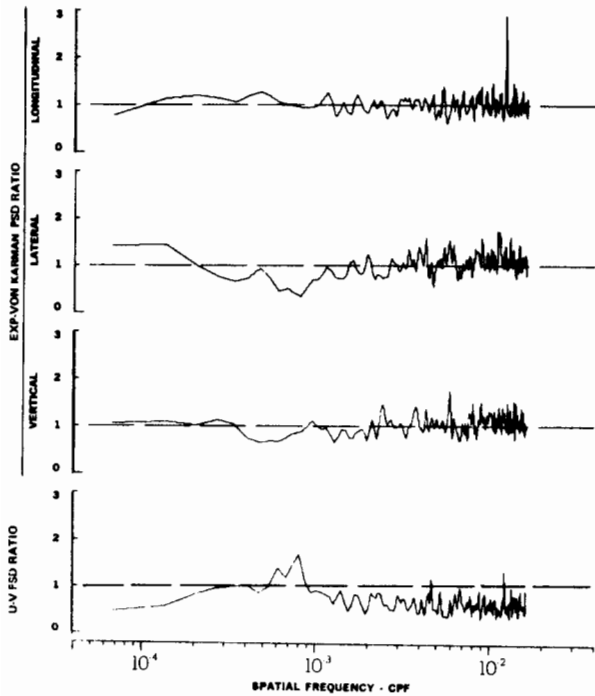
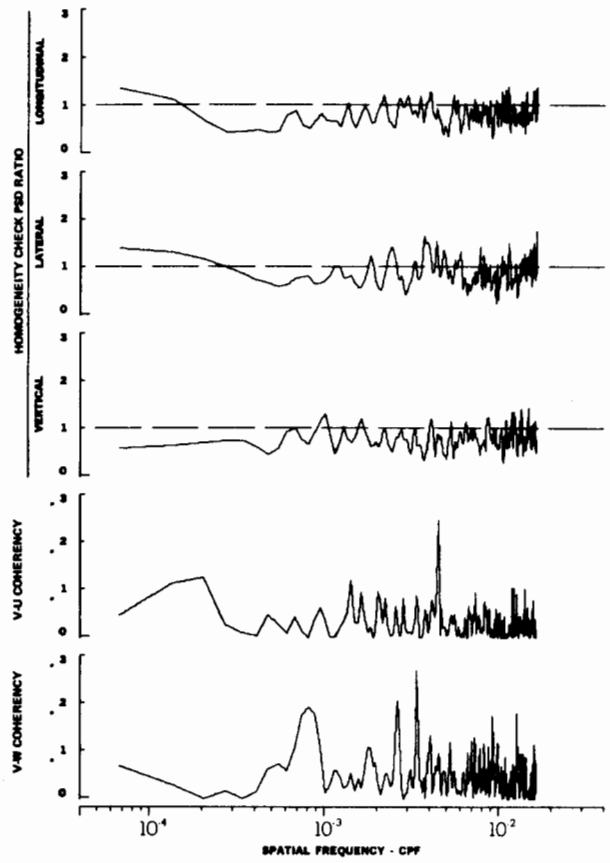
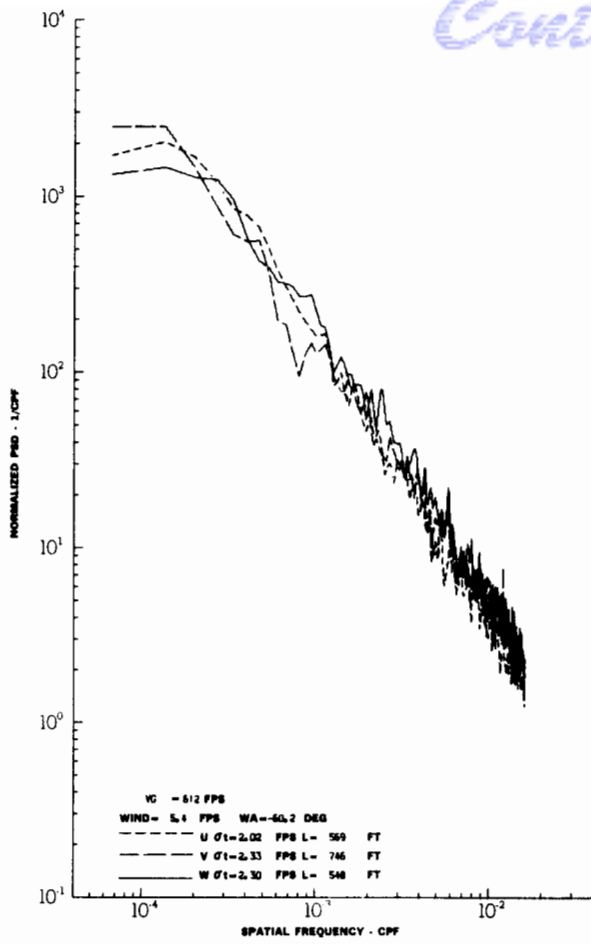
TURBULENCE SPECTRA DATA FOR TEST 90, LEG 6, CATEGORY 121231  
 FIGURE IV-102





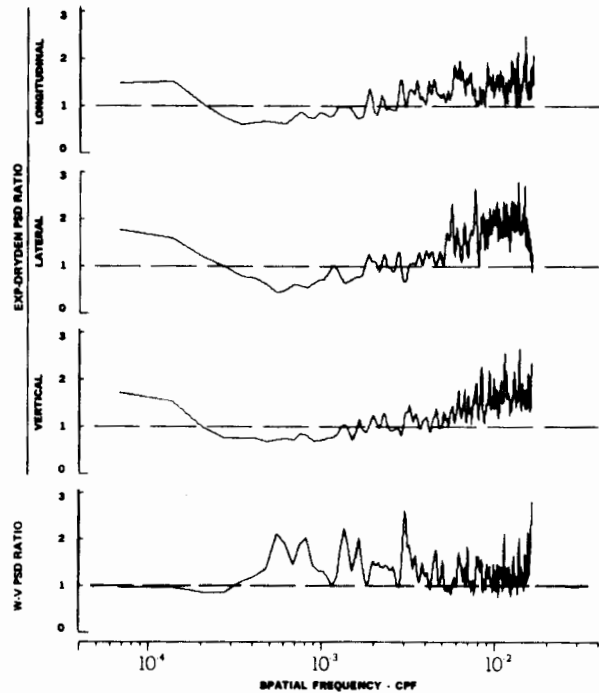
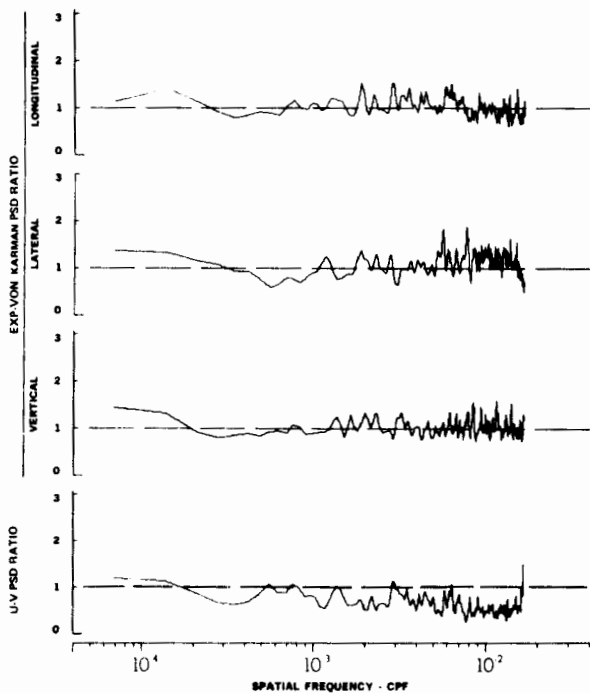
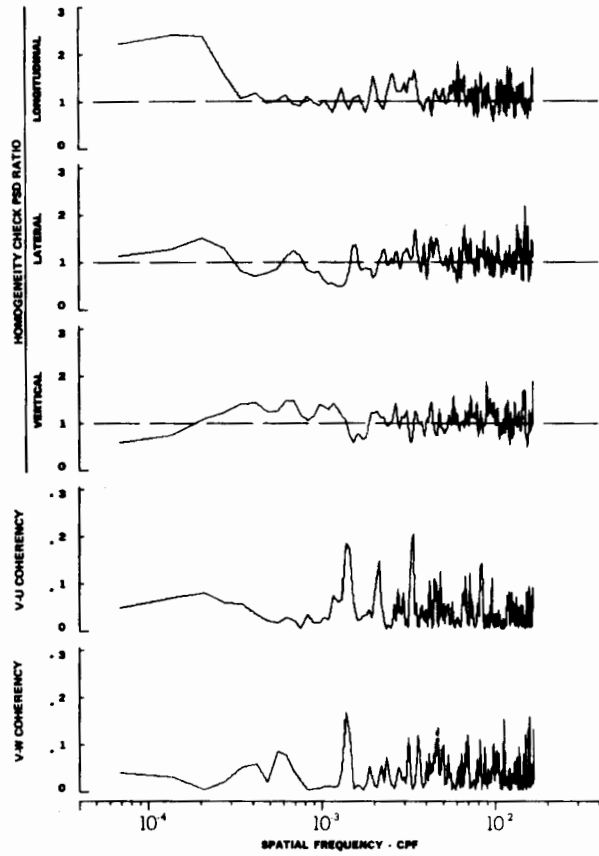
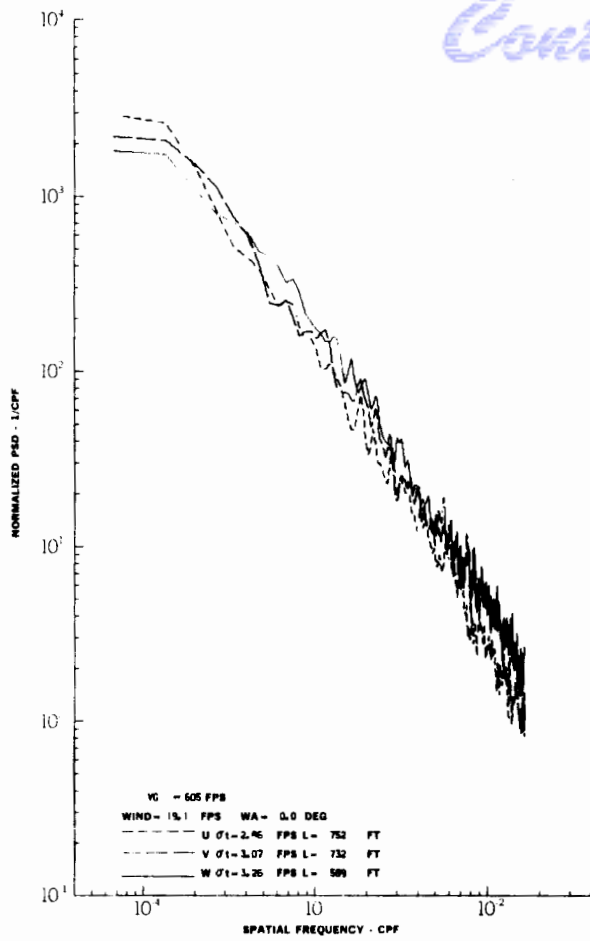
TURBULENCE SPECTRA DATA FOR TEST 90, LEG 8, CATEGORY 222231  
FIGURE IV-103

# Contrails



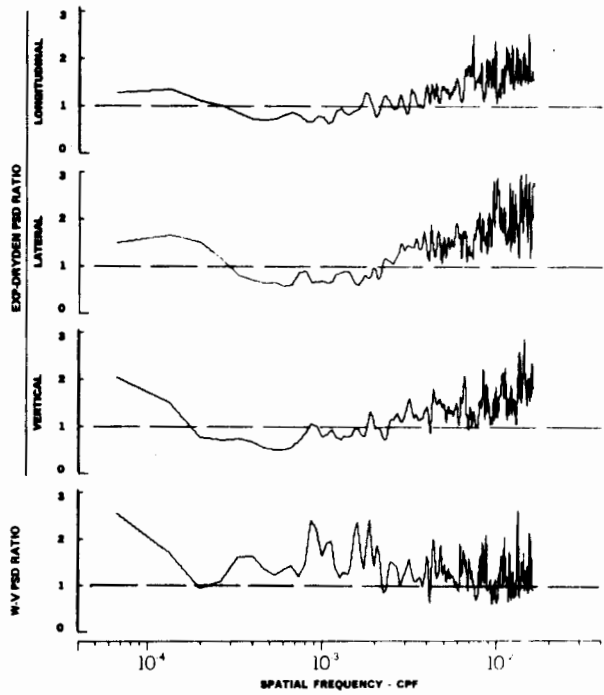
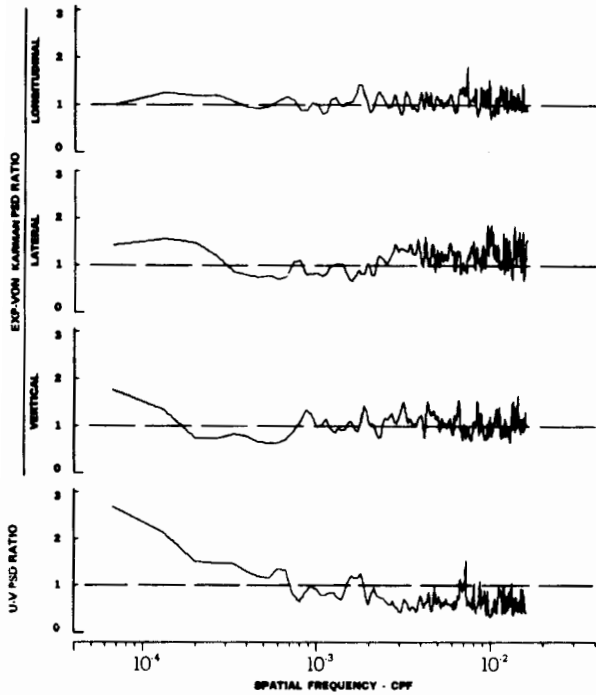
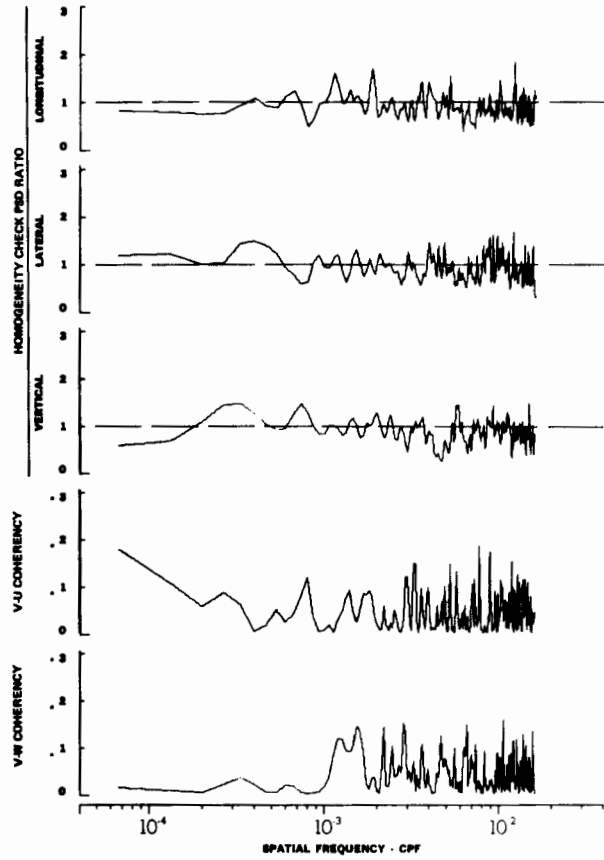
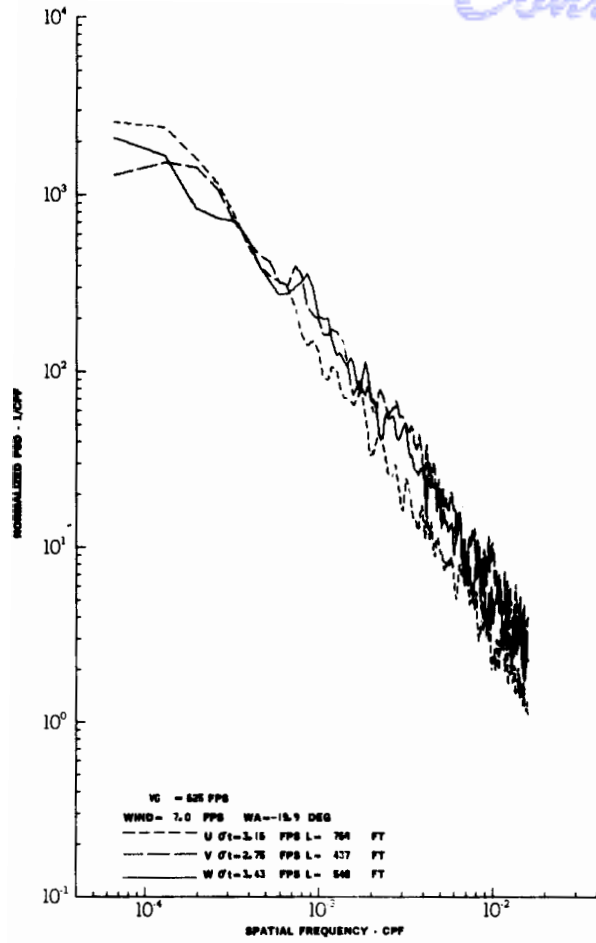
TURBULENCE SPECTRA DATA FOR TEST 94, LEG 8, CATEGORY 221231  
FIGURE IV-104

# Contrails



TURBULENCE SPECTRA DATA FOR TEST 95, LEG 1, CATEGORY 221331  
 FIGURE IV-105  
 212

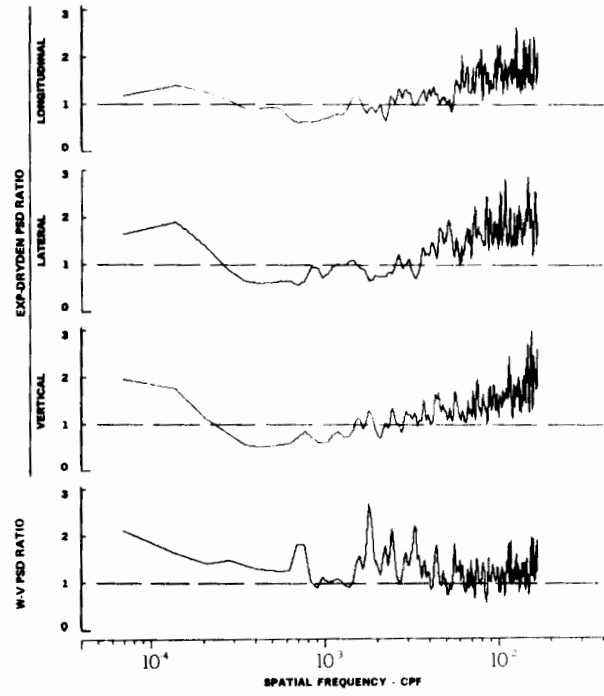
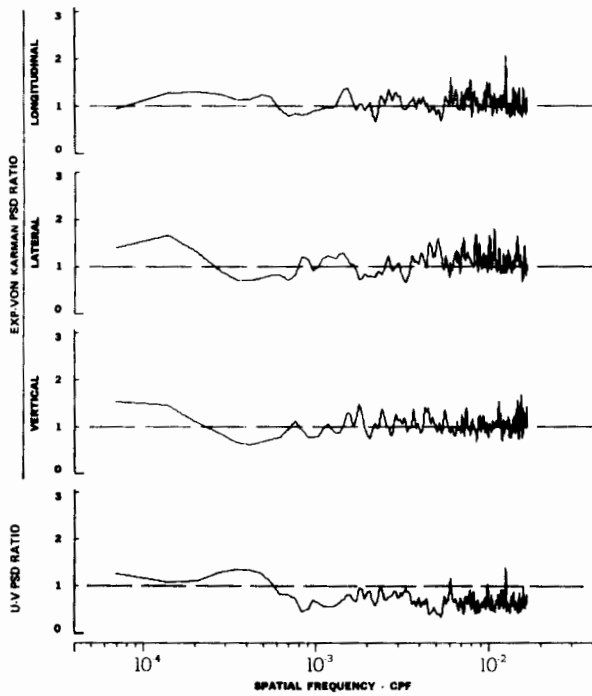
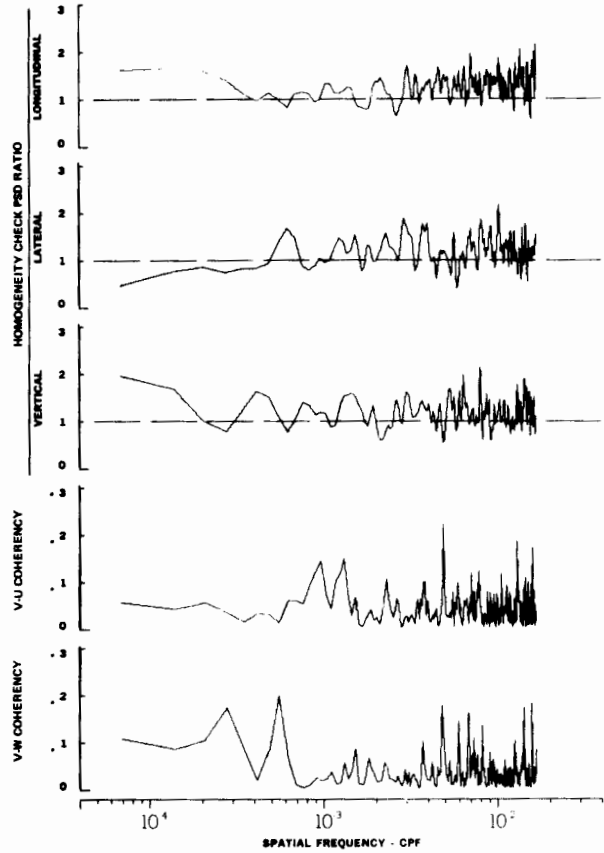
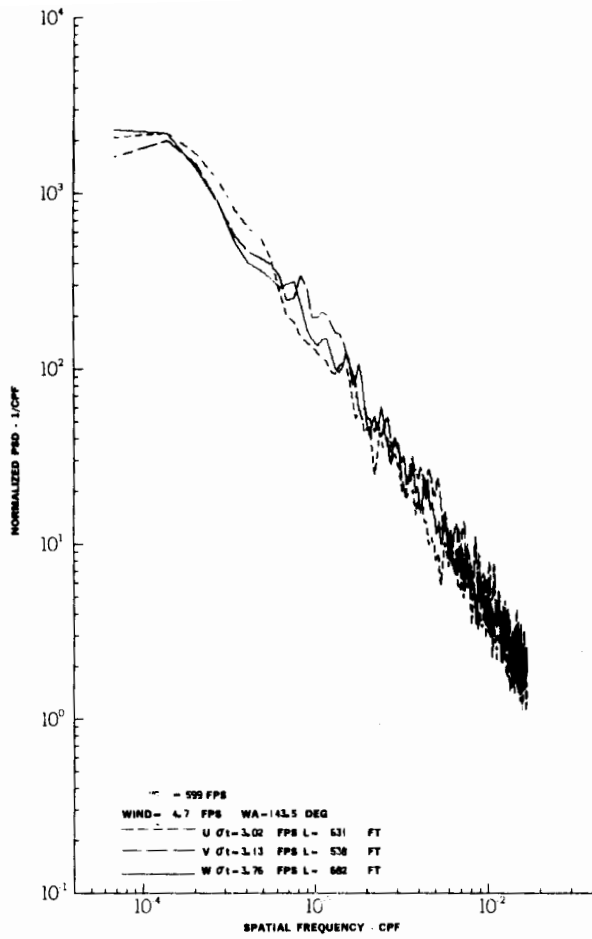
# Contrails



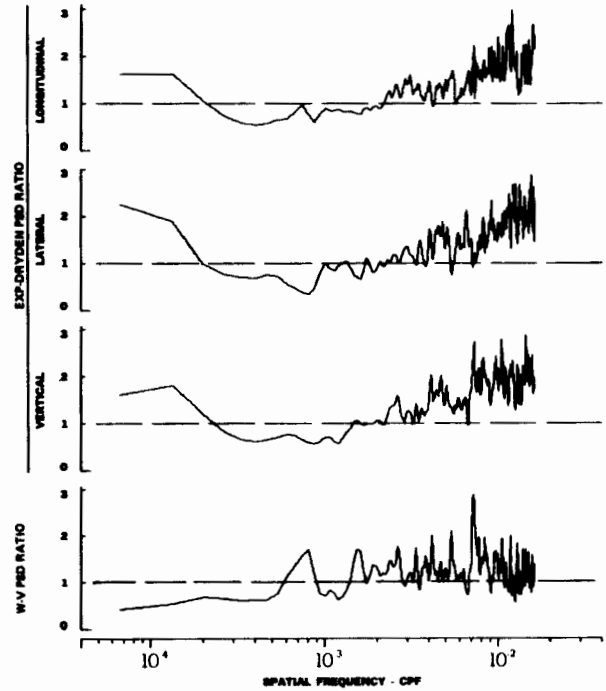
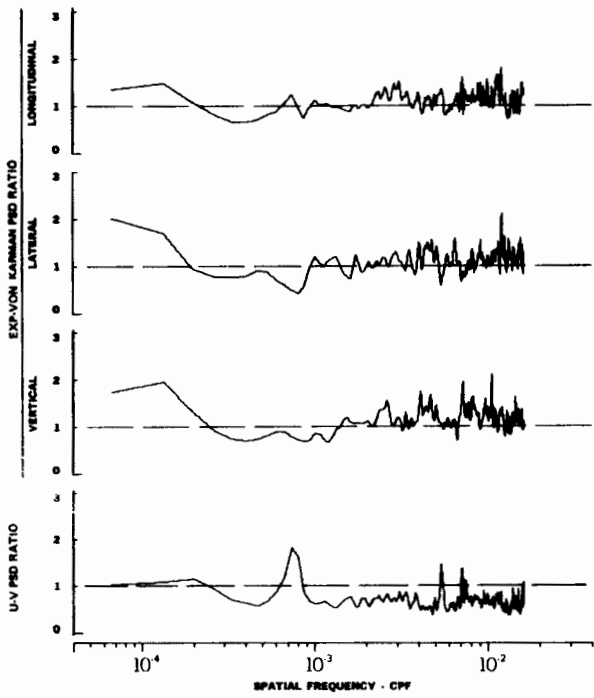
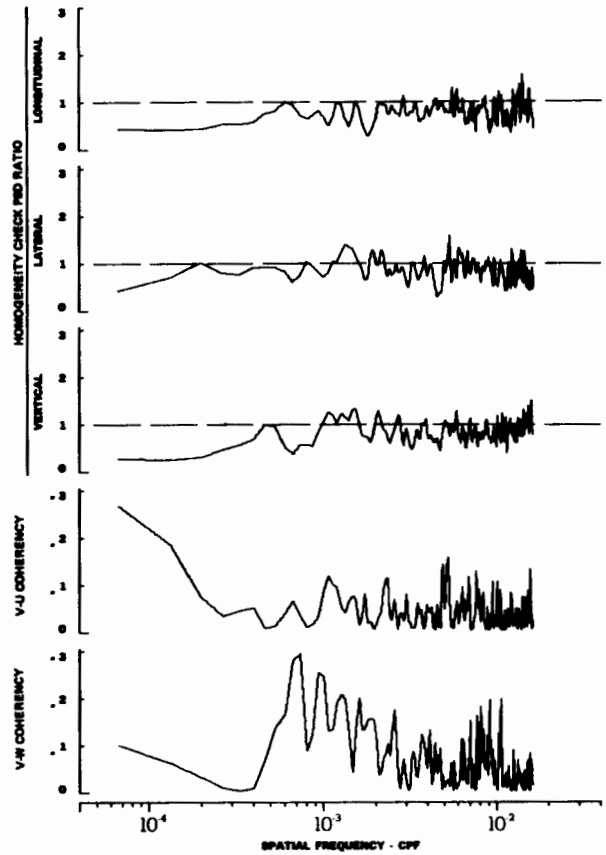
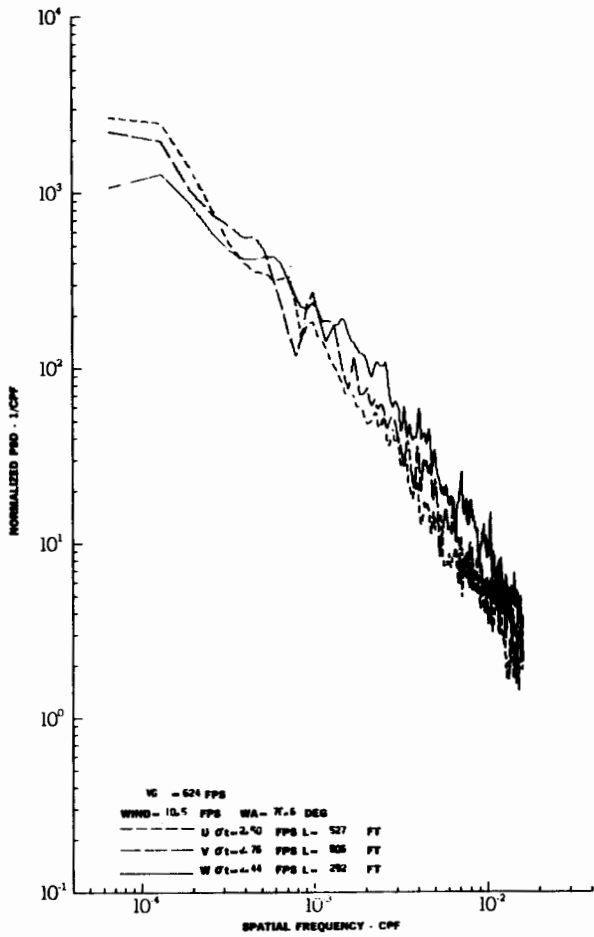
TURBULENCE SPECTRA DATA FOR TEST 95, LEG 3, CATEGORY 122331

FIGURE IV-106

# Contrails

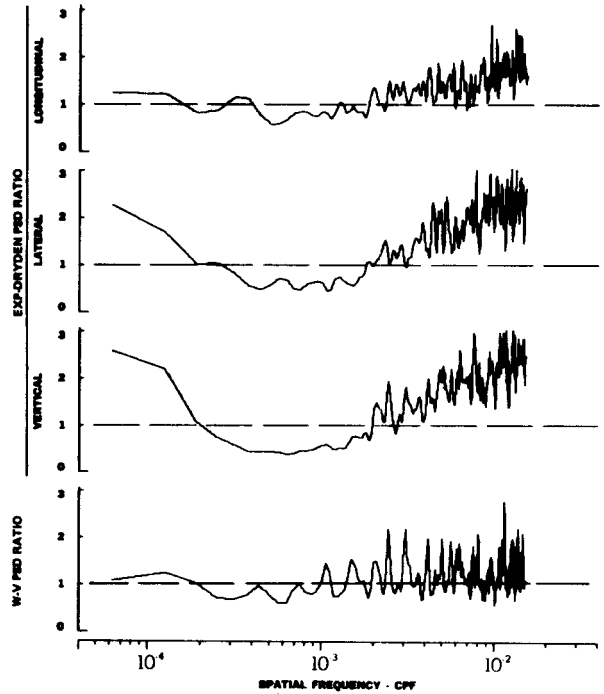
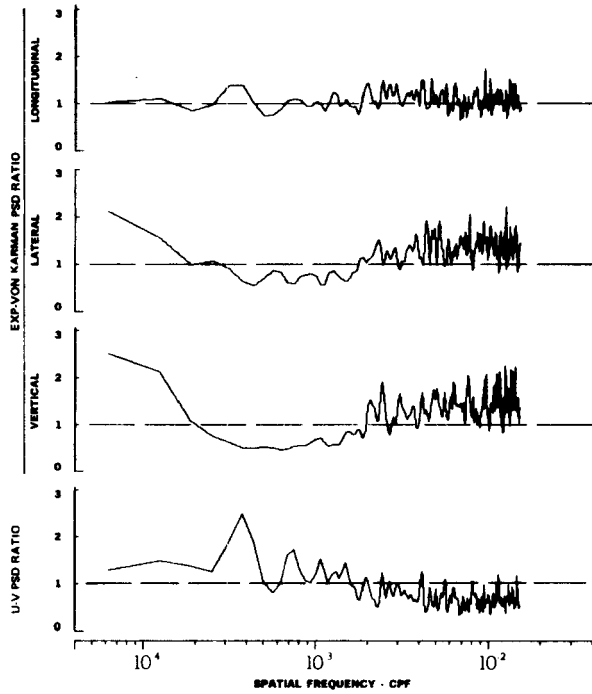
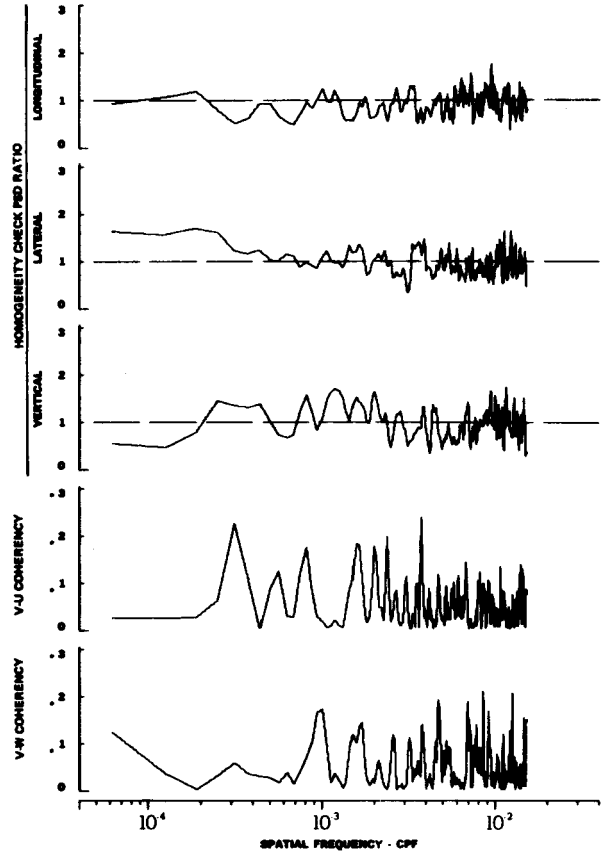
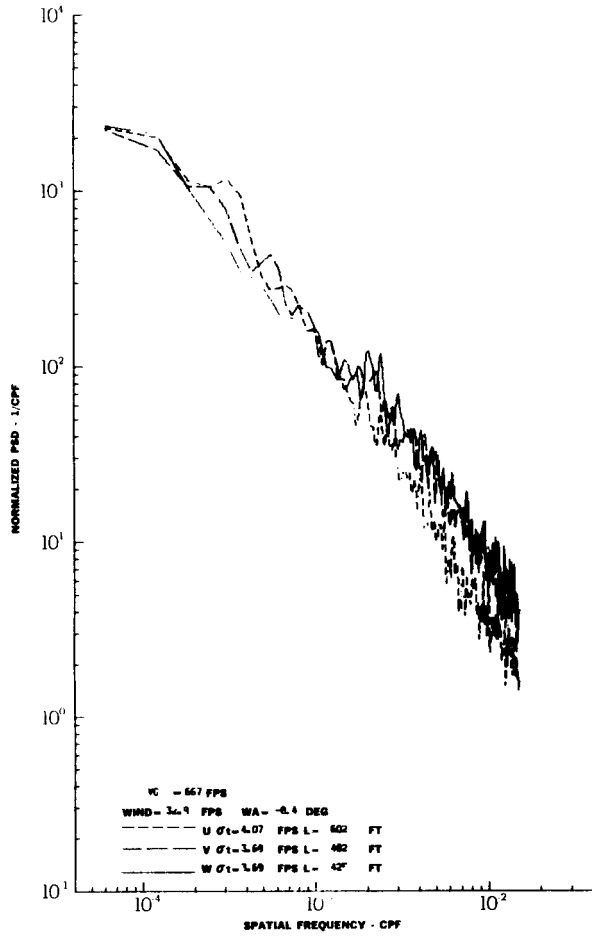


TURBULENCE SPECTRA DATA FOR TEST 95, LEG 5, CATEGORY 122331  
 FIGURE IV-107



TURBULENCE SPECTRA DATA FOR TEST 98, LEG 6, CATEGORY 212331  
 FIGURE IV-108

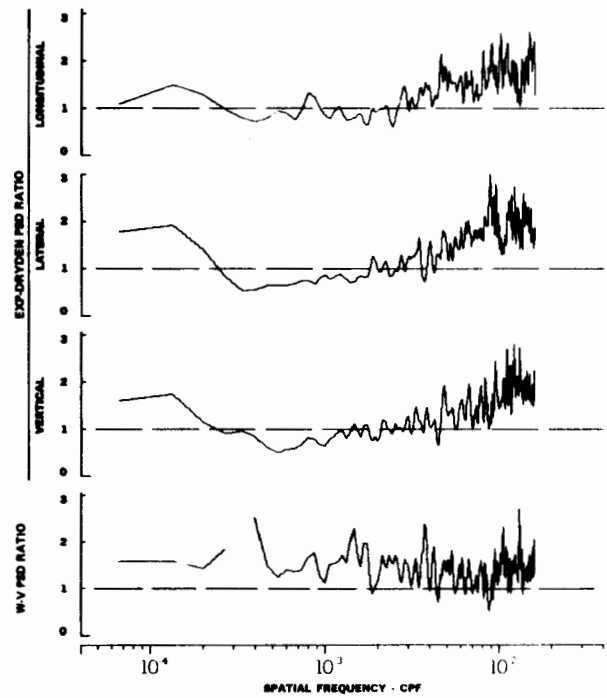
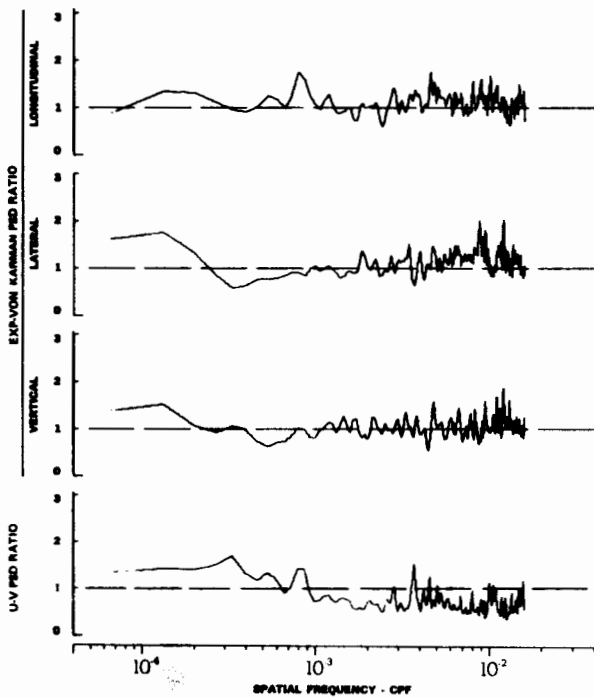
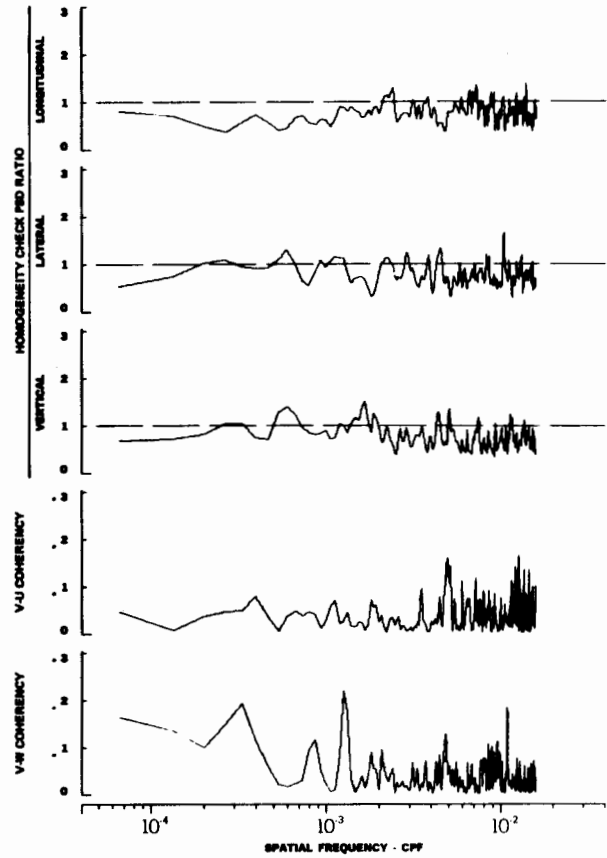
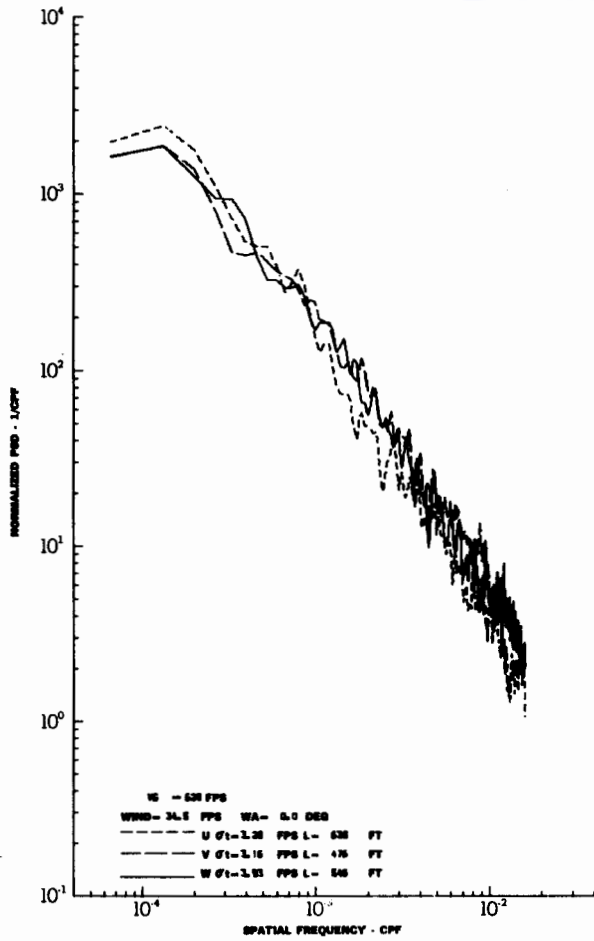
# Contrails



TURBULENCE SPECTRA DATA FOR TEST 98, LEG 8, CATEGORY 214331  
FIGURE IV-109

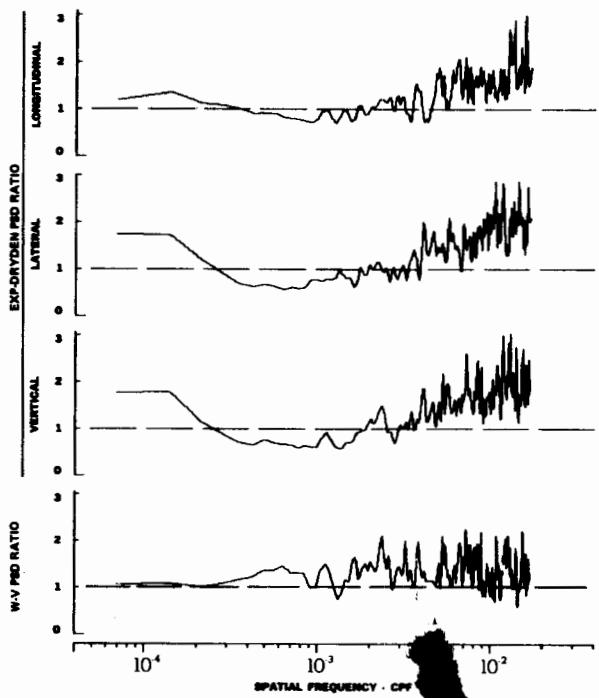
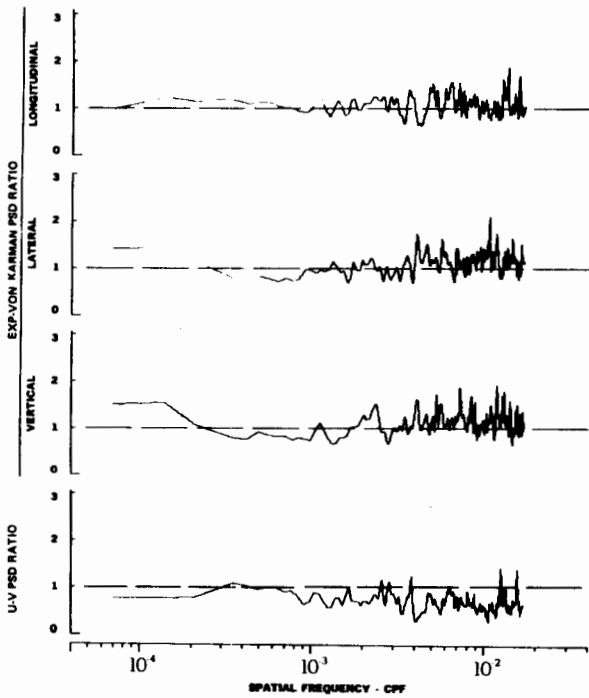
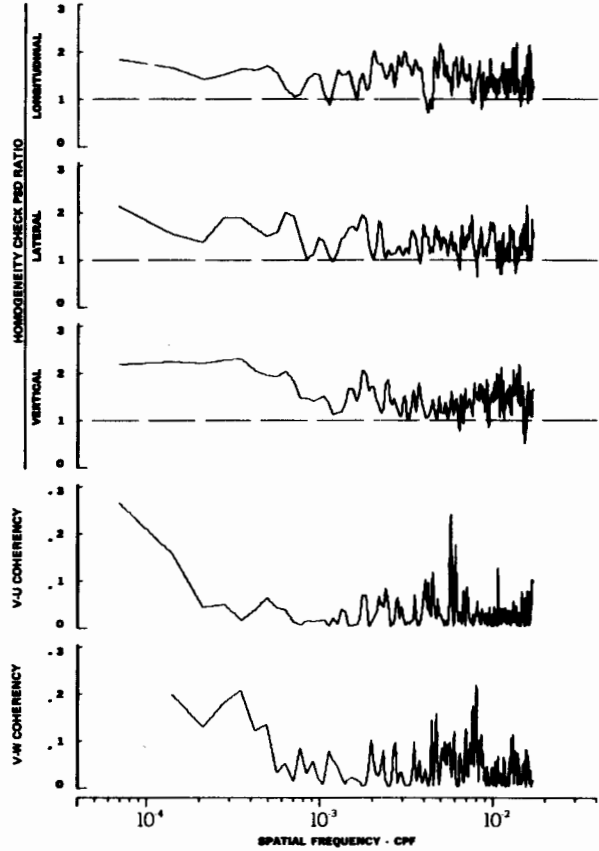
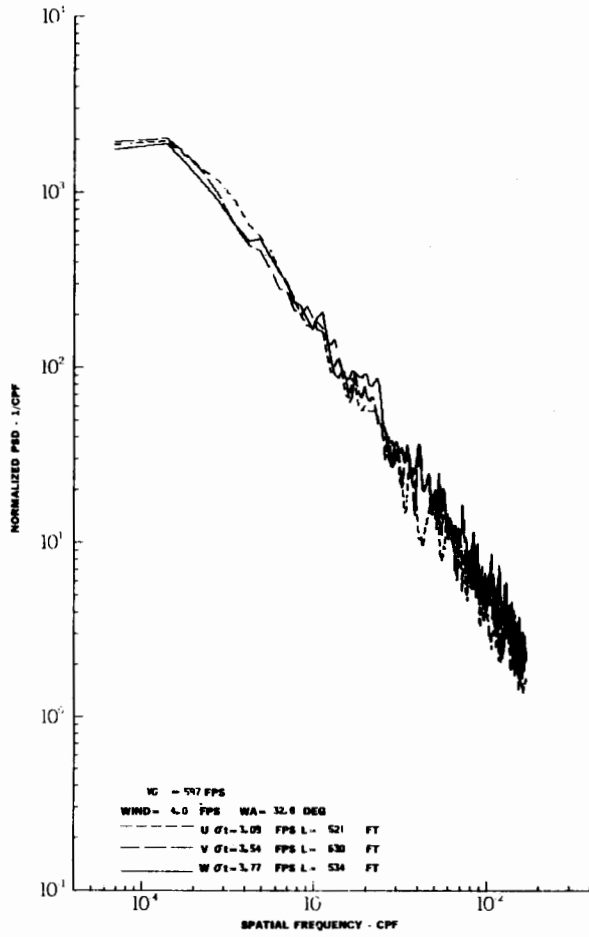


# Contrails



TURBULENCE SPECTRA DATA FOR TEST 101, LEG 1, CATEGORY 224331  
 FIGURE IV-110

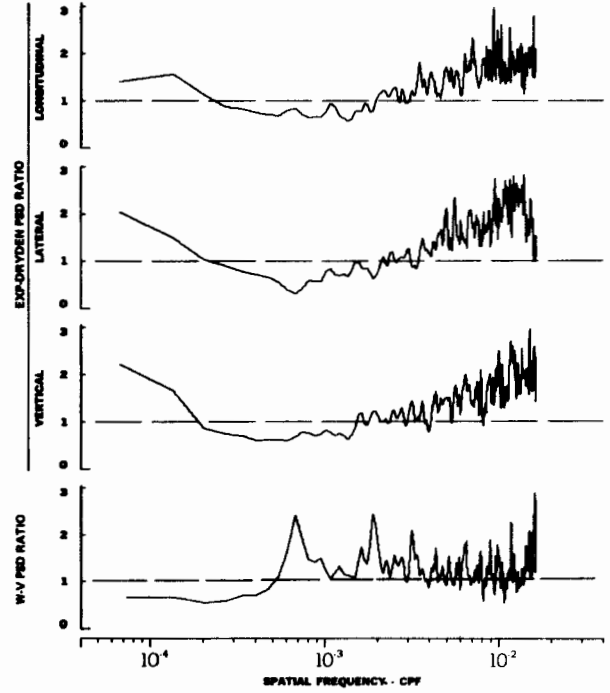
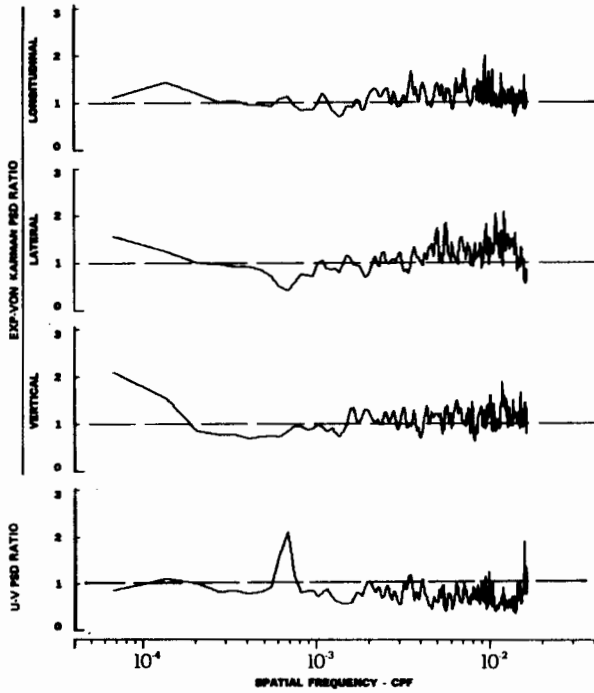
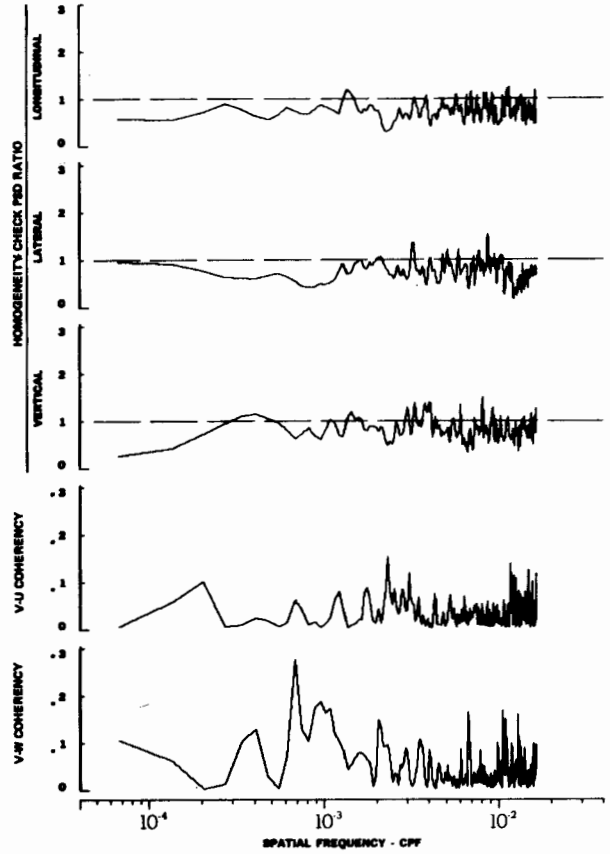
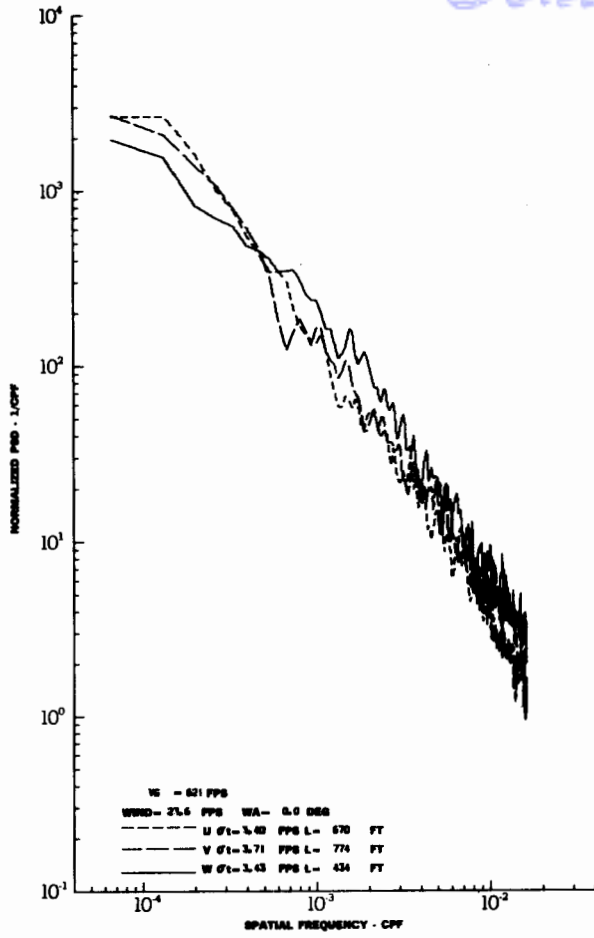
# Contrails



TURBULENCE SPECTRA DATA FOR TEST 101, LEG 5, CATEGORY 122331

FIGURE IV-111

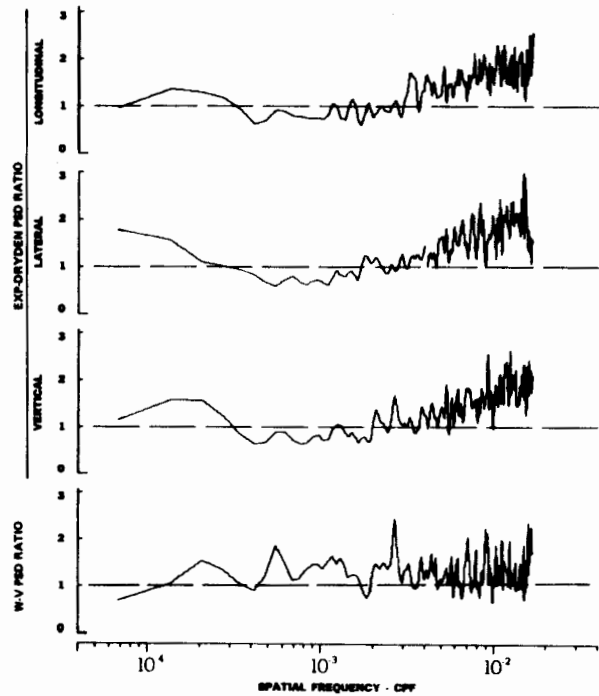
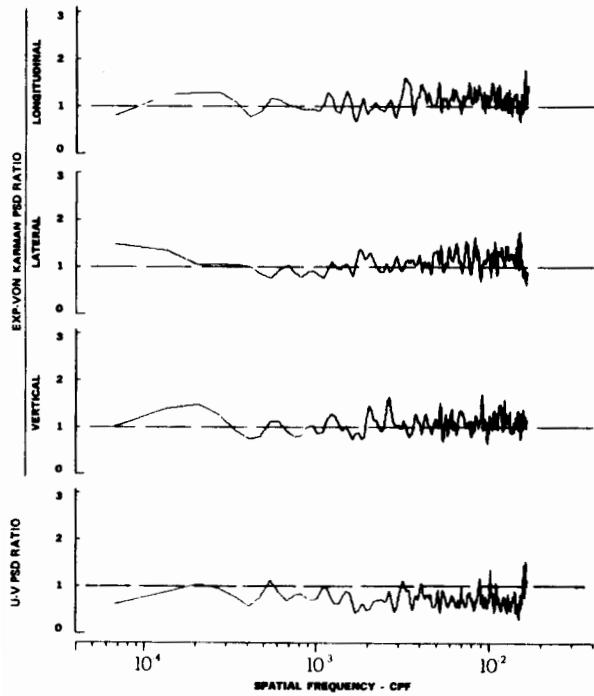
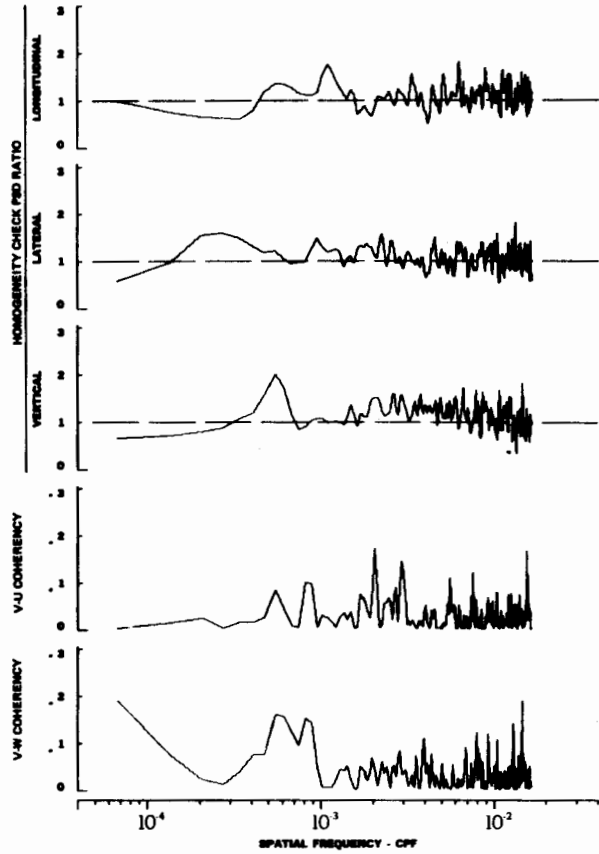
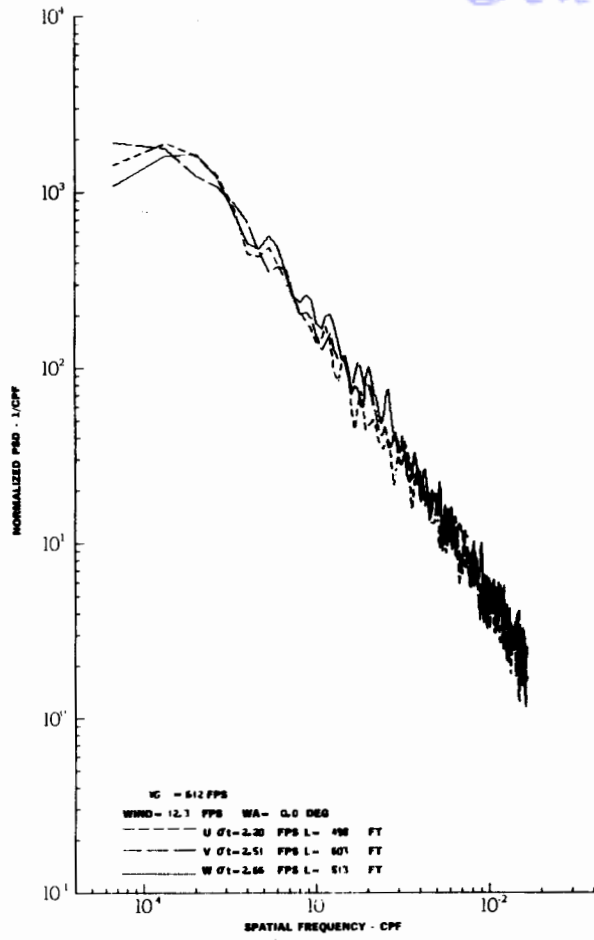
# Contrails



TURBULENCE SPECTRA DATA FOR TEST 103, LEG 1, CATEGORY 214231

FIGURE IV-112

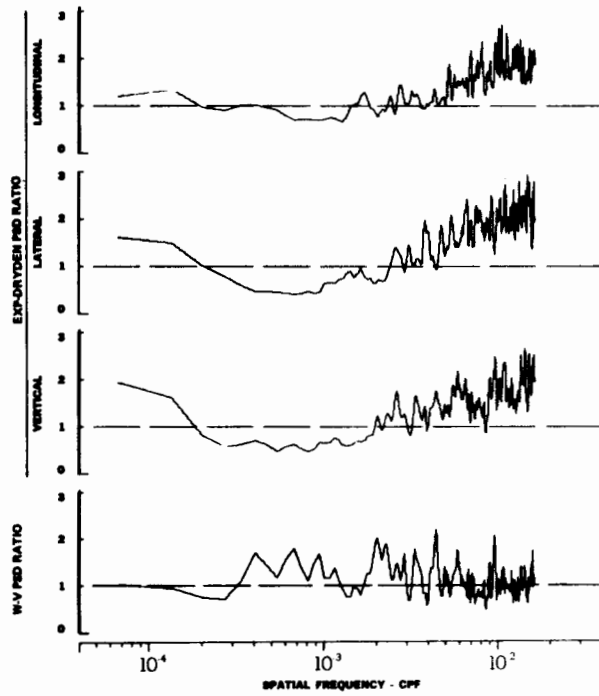
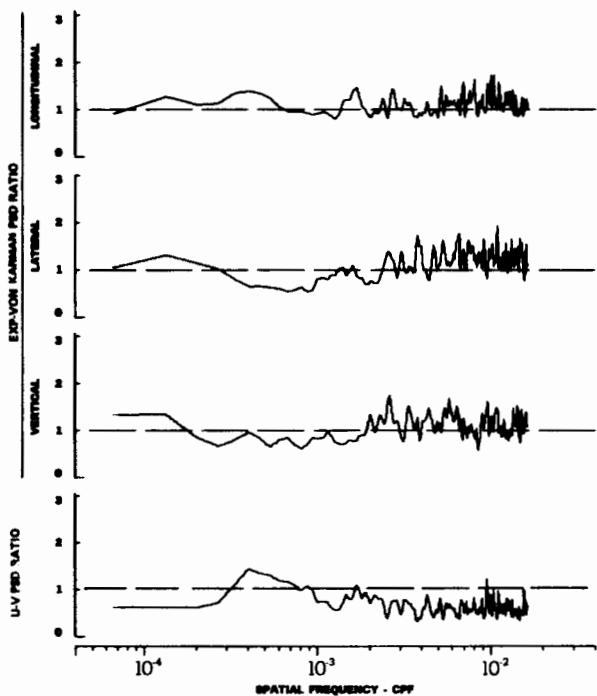
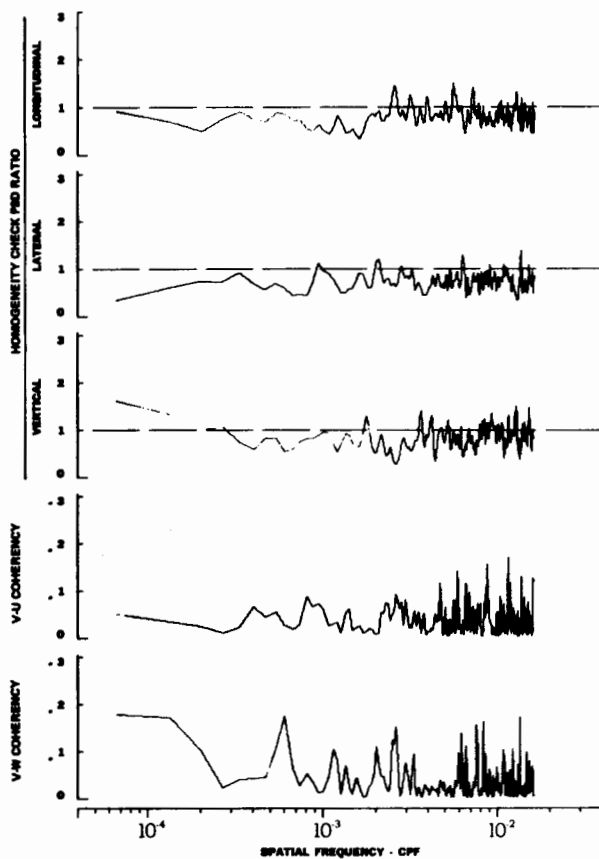
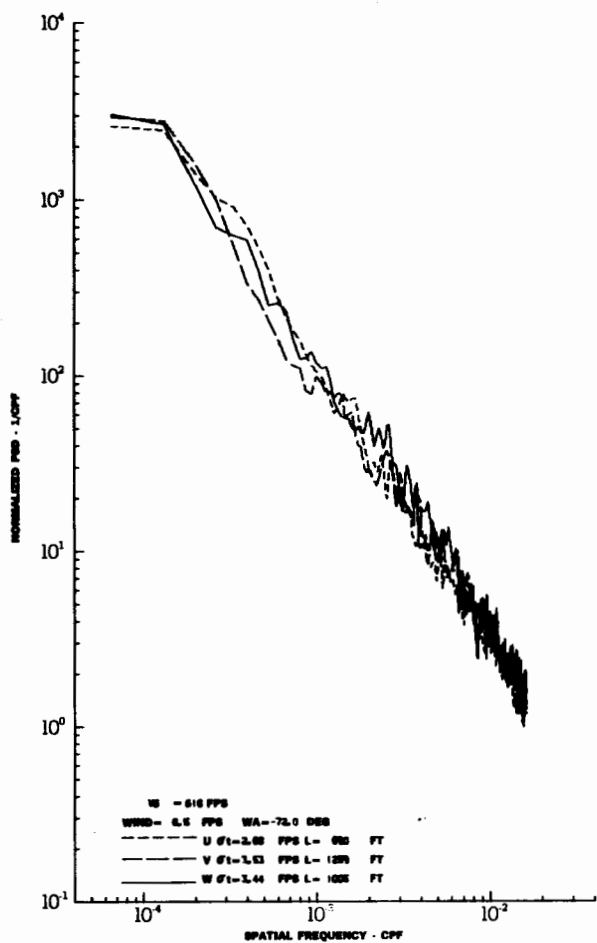
# Contrails



TURBULENCE SPECTRA DATA FOR TEST 107, LEG 1, CATEGORY 224331

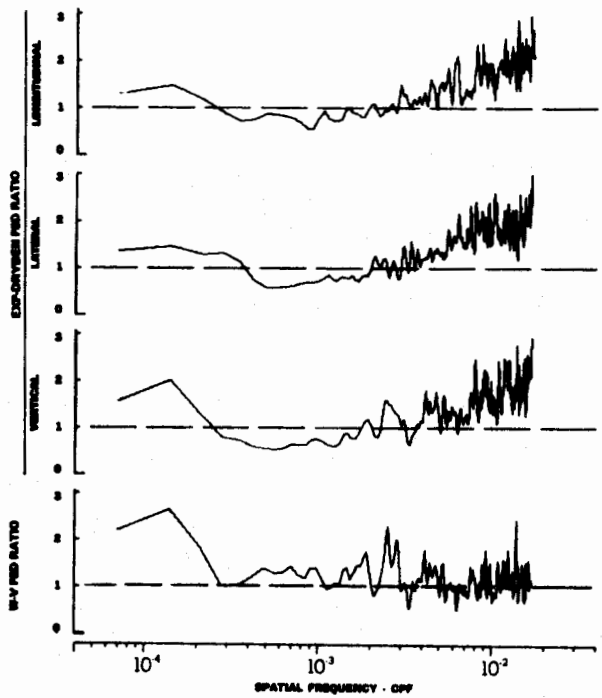
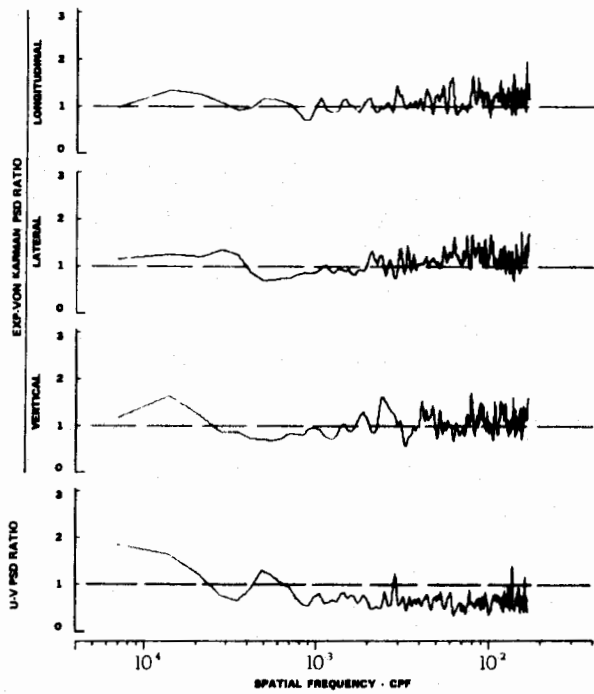
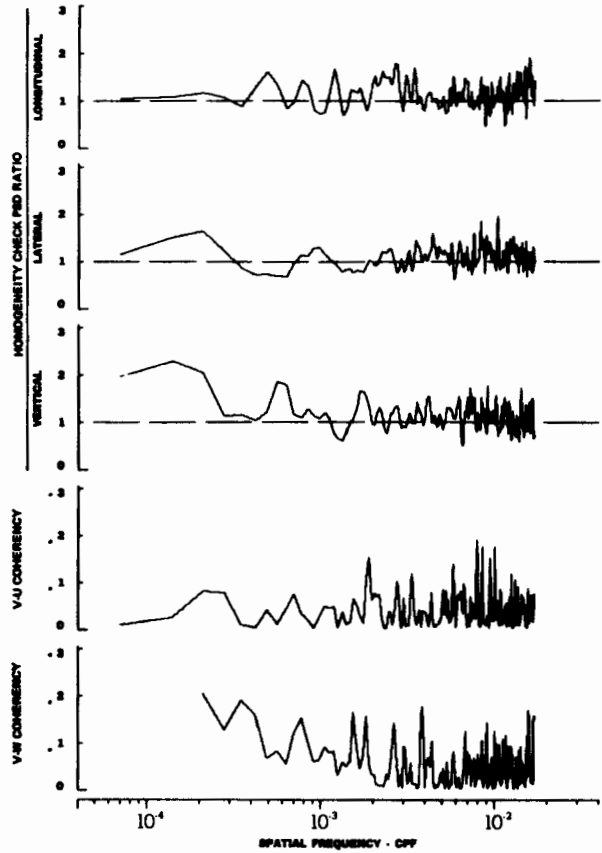
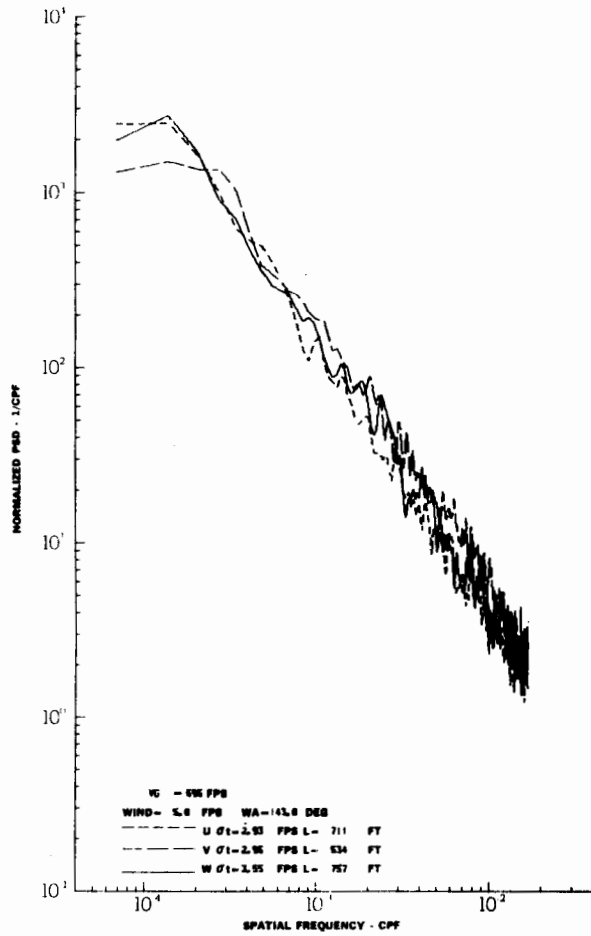
FIGURE IV-113

# Contrails



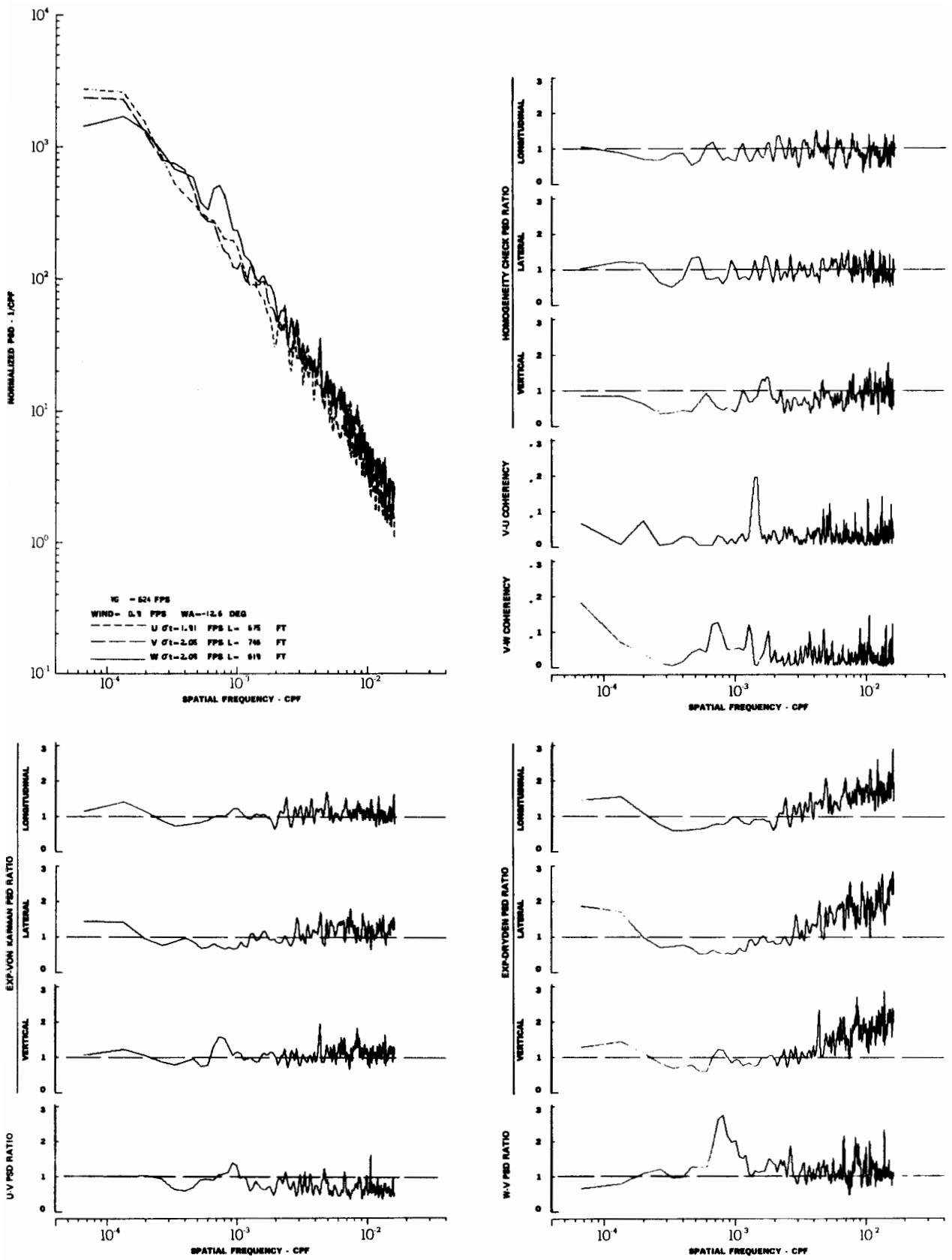
TURBULENCE SPECTRA DATA FOR TEST 107, LEG 3, CATEGORY 121331  
 FIGURE IV-114

# Contrails



TURBULENCE SPECTRA DATA FOR TEST 107, LEG 5, CATEGORY 123331  
 FIGURE IV-115

# Contrails

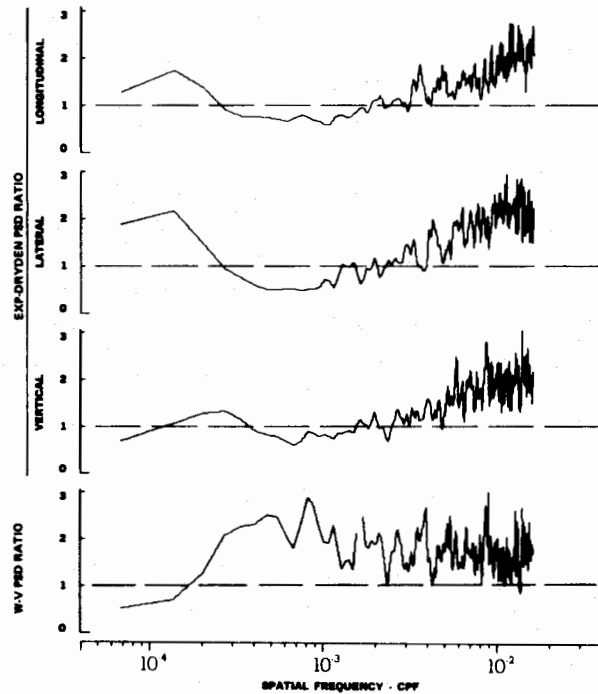
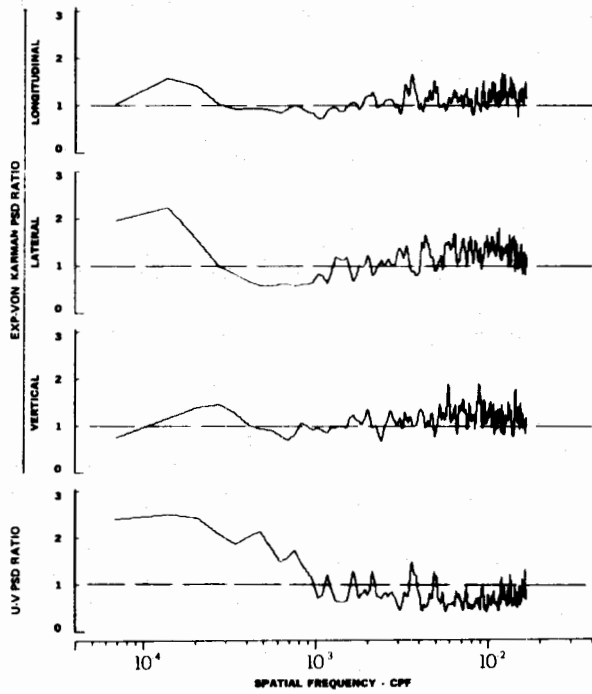
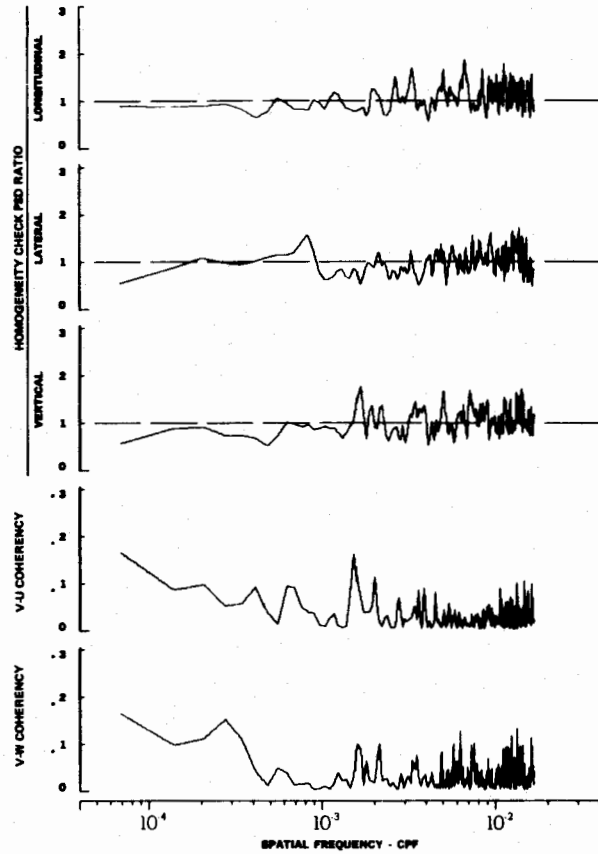
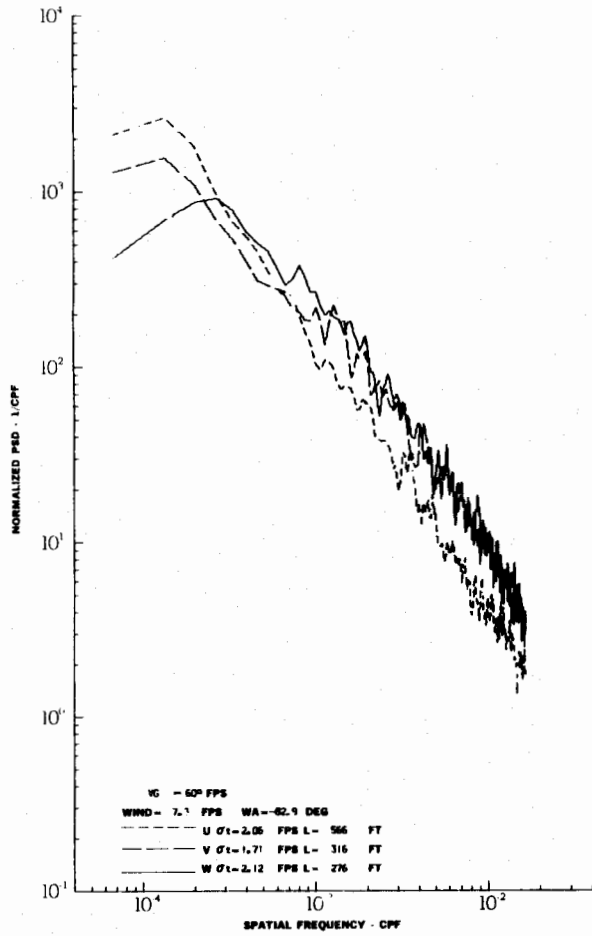


TURBULENCE SPECTRA DATA FOR TEST 107, LEG 7, CATAGORY 322331

FIGURE IV-116

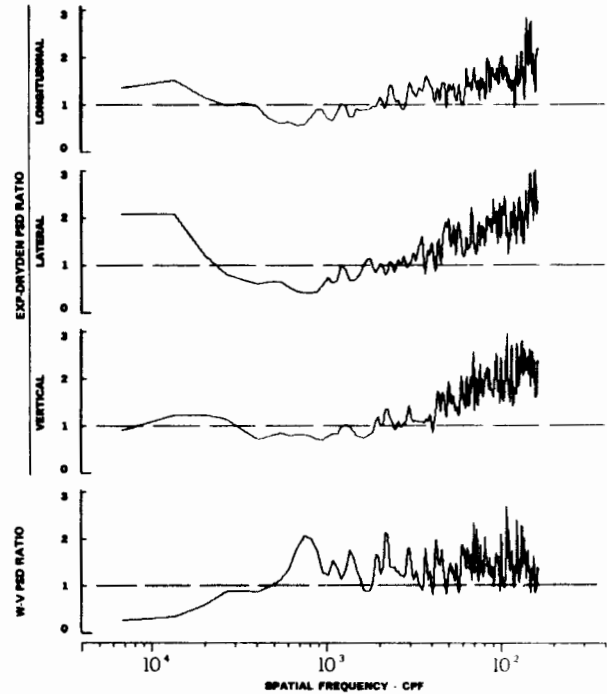
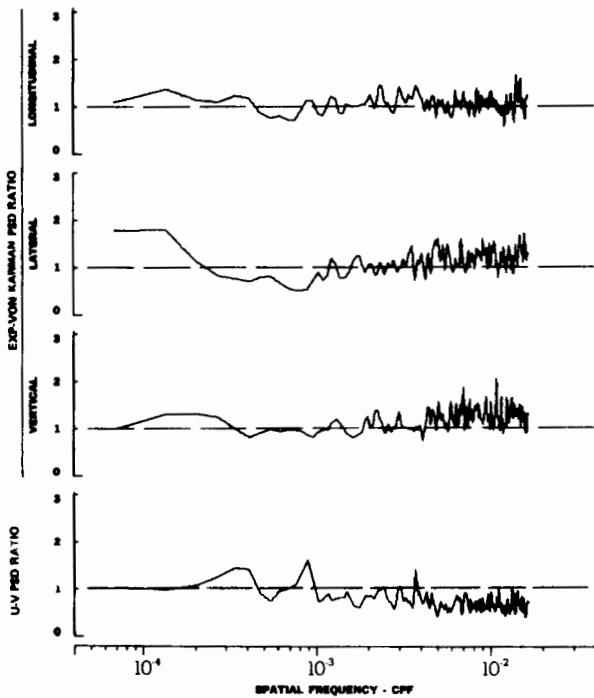
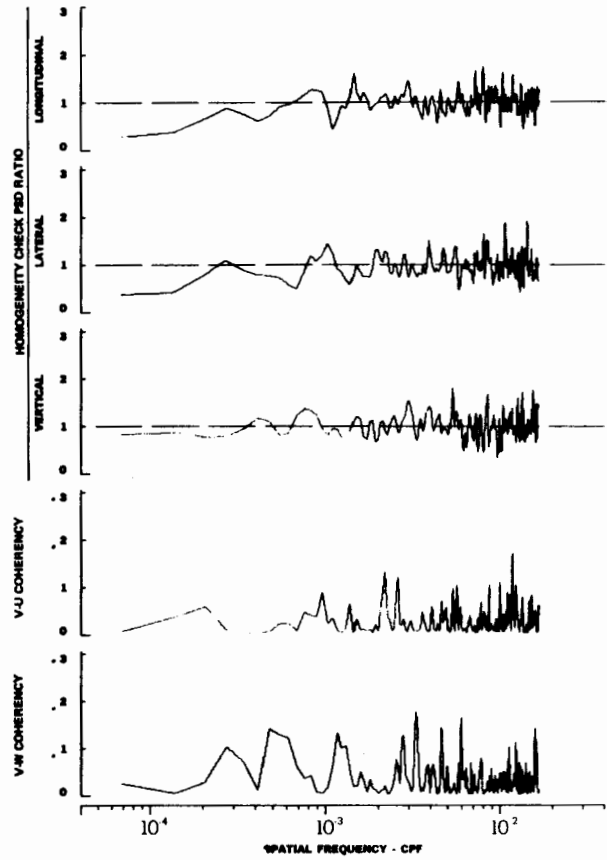
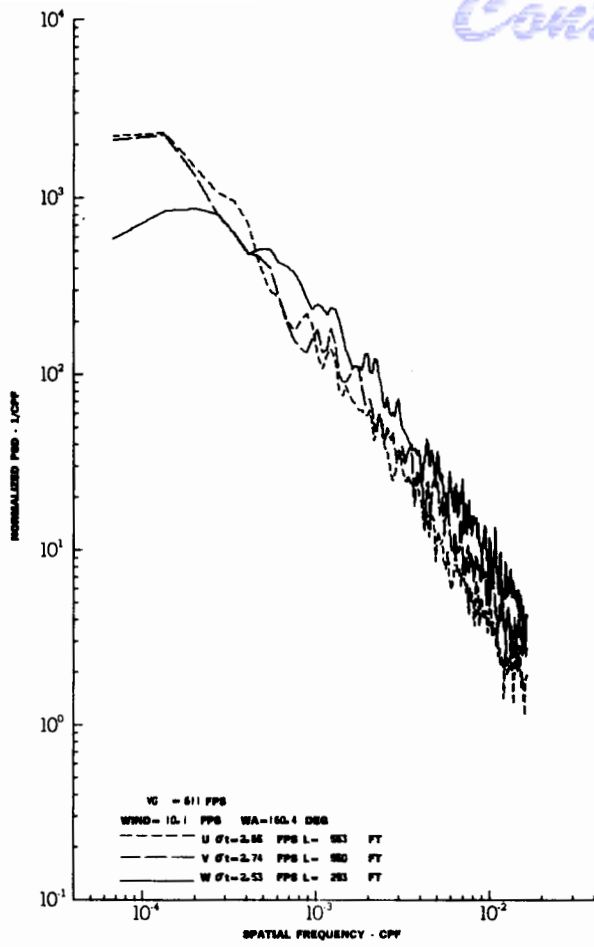


# Contrails

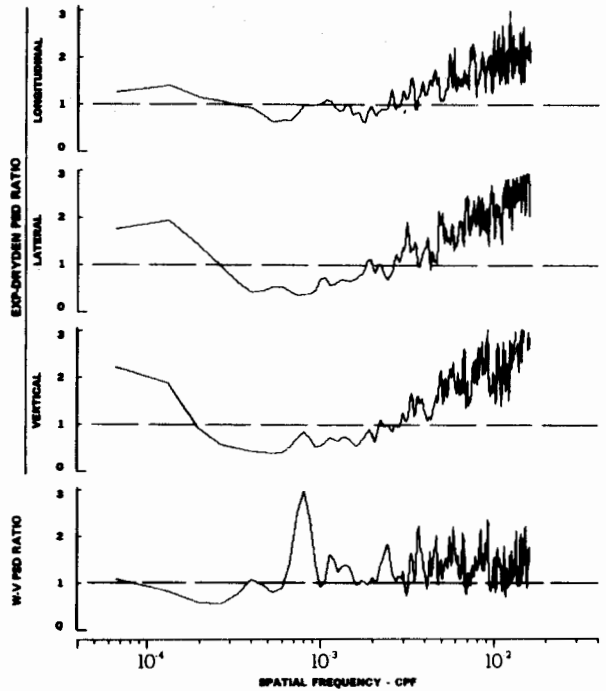
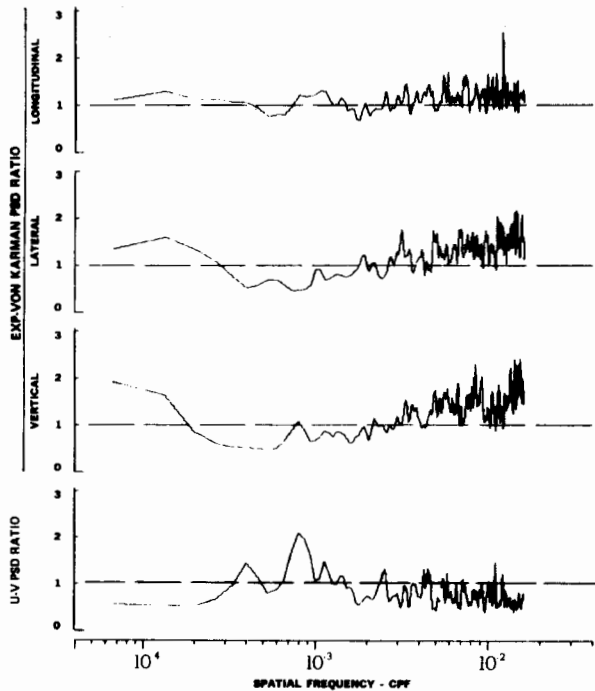
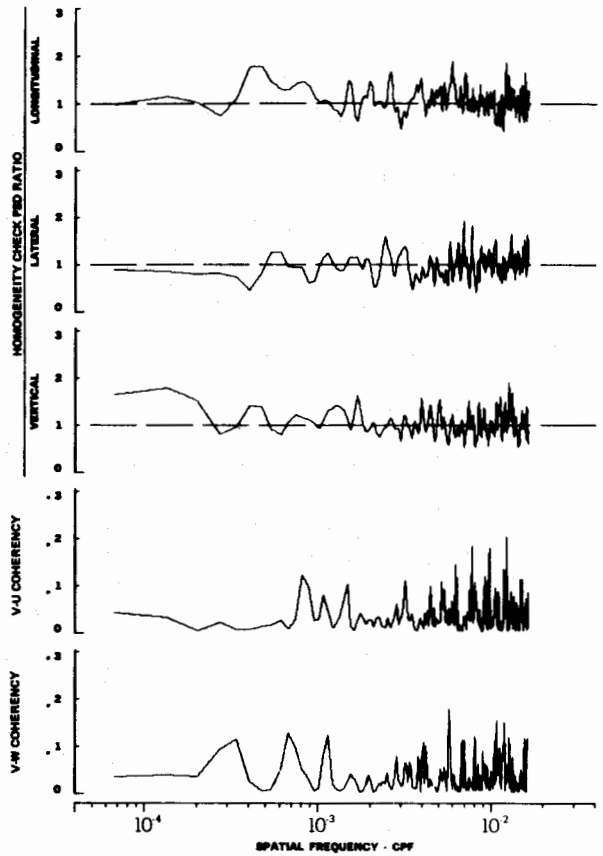
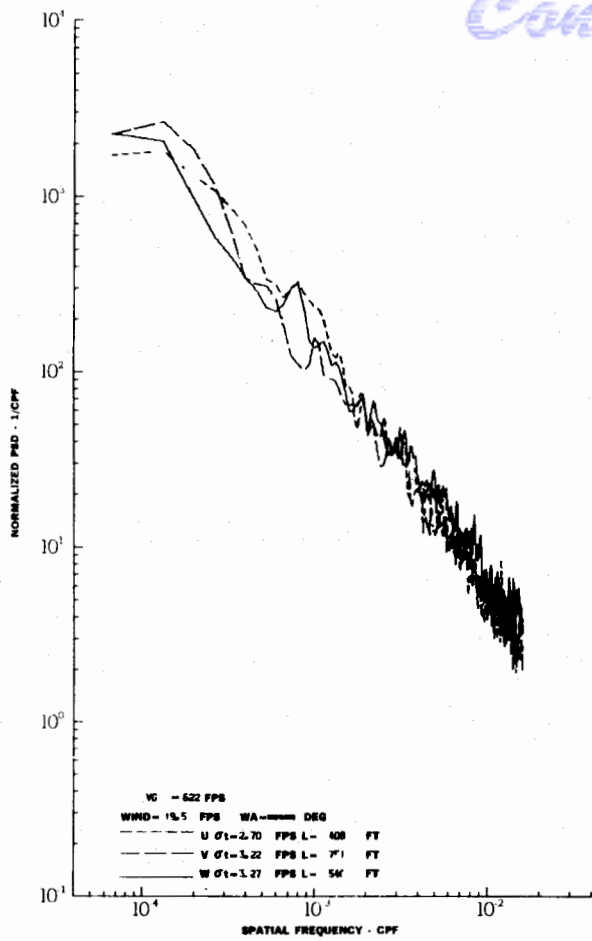


TURBULENCE SPECTRA DATA FOR TEST 108, LEG 2, CATEGORY 312231  
 FIGURE IV-117

# Contrails

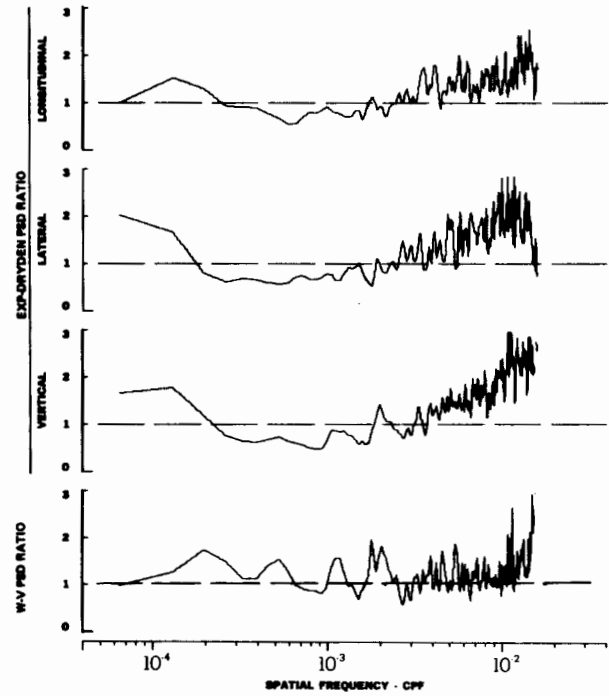
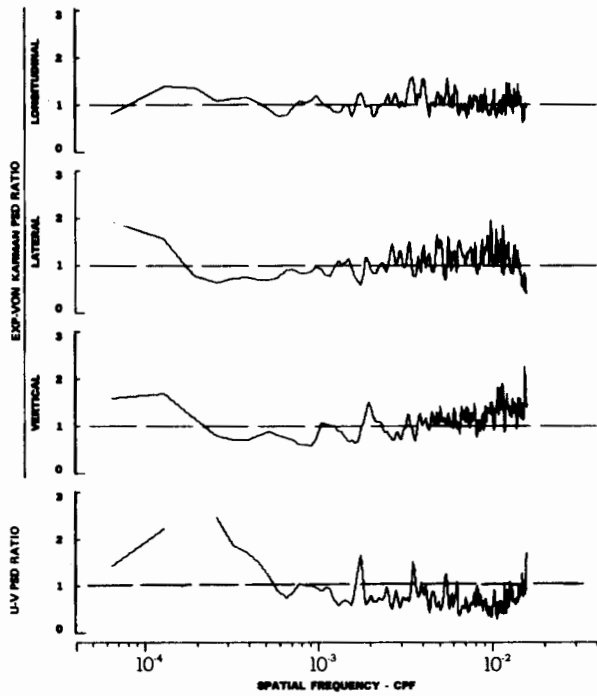
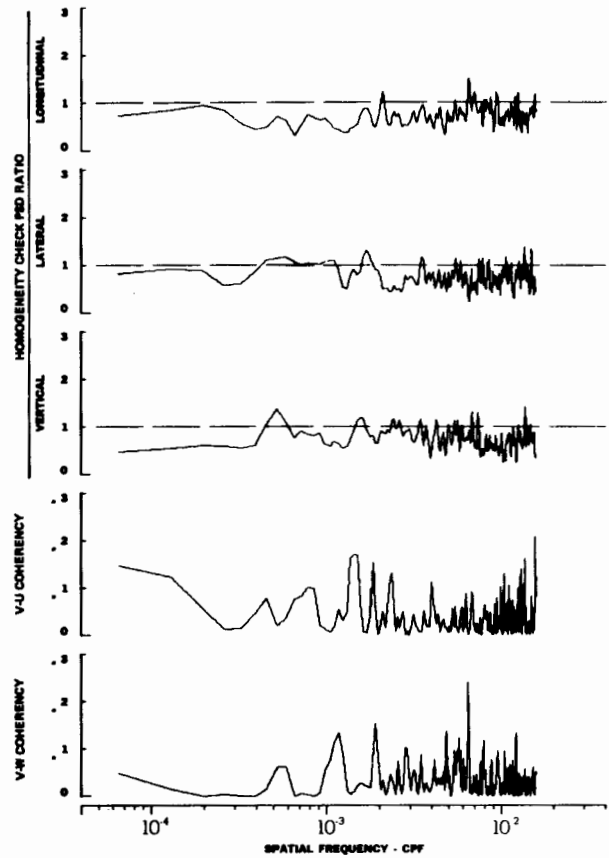
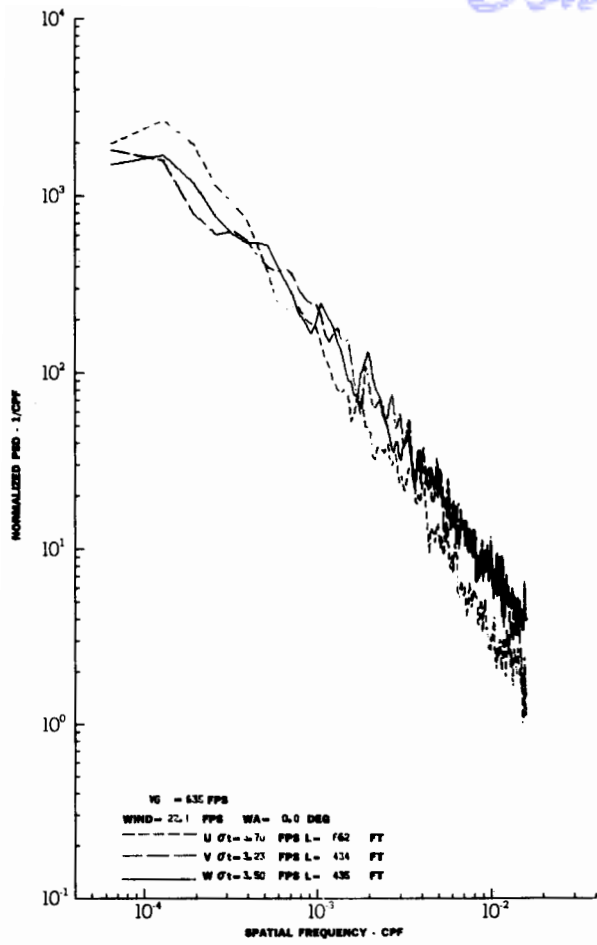


TURBULENCE SPECTRA DATA FOR TEST 108, LEG 6, CATEGORY 213231  
 FIGURE IV-118



TURBULENCE SPECTRA DATA FOR TEST 108, LEG 8, CATEGORY 212231  
 FIGURE IV-119

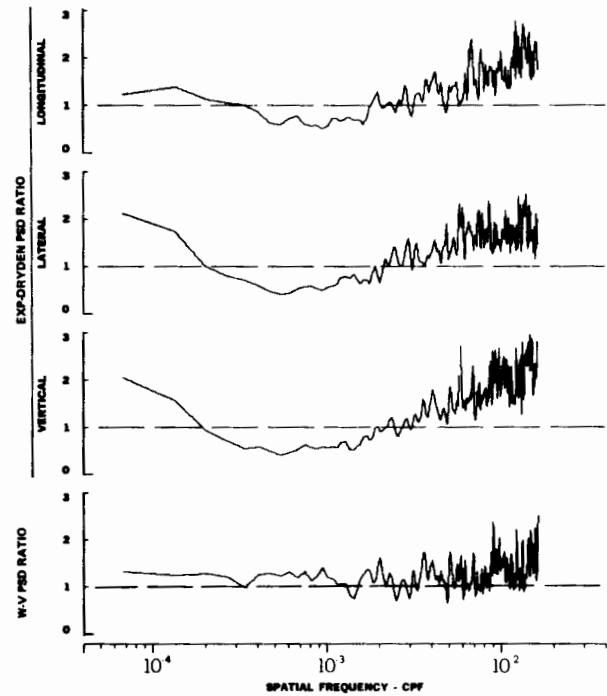
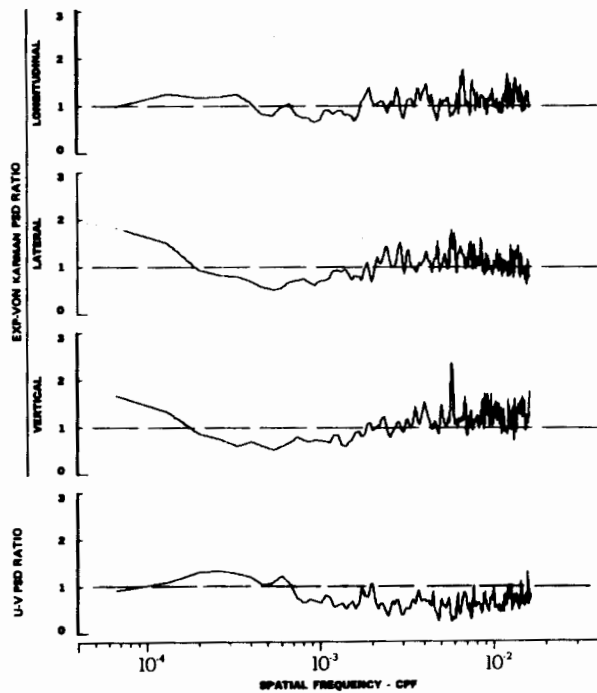
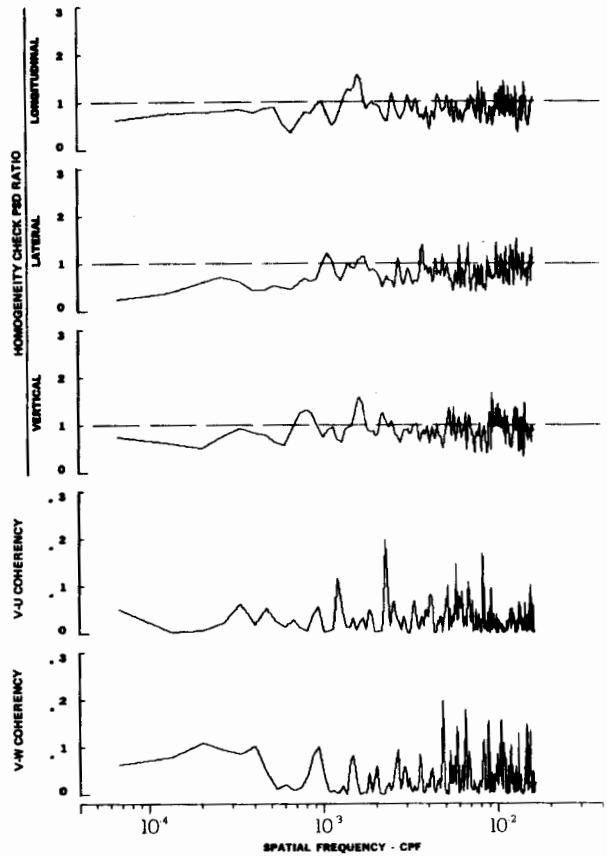
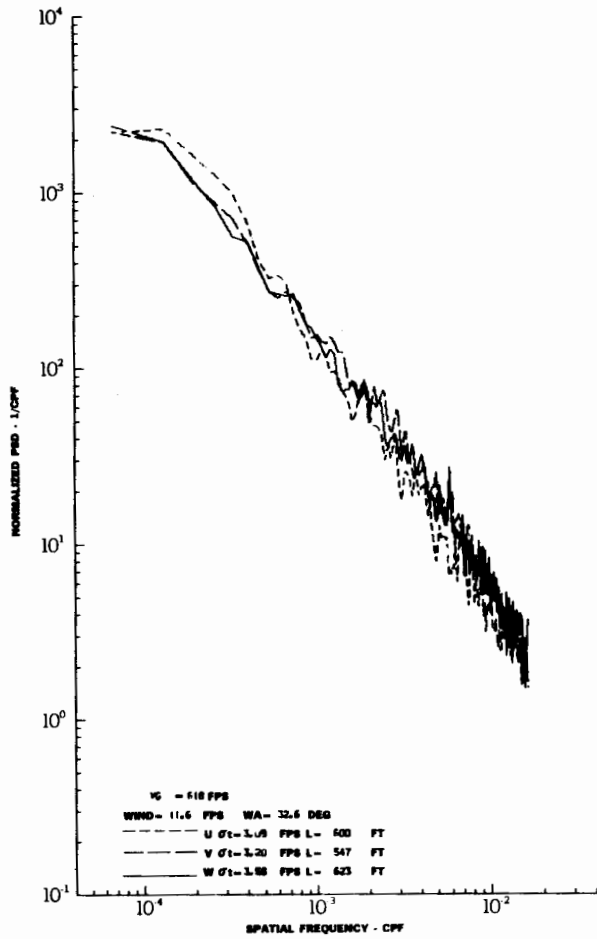
# Contrails



TURBULENCE SPECTRA DATA FOR TEST 109, LEG 1, CATEGORY 214331

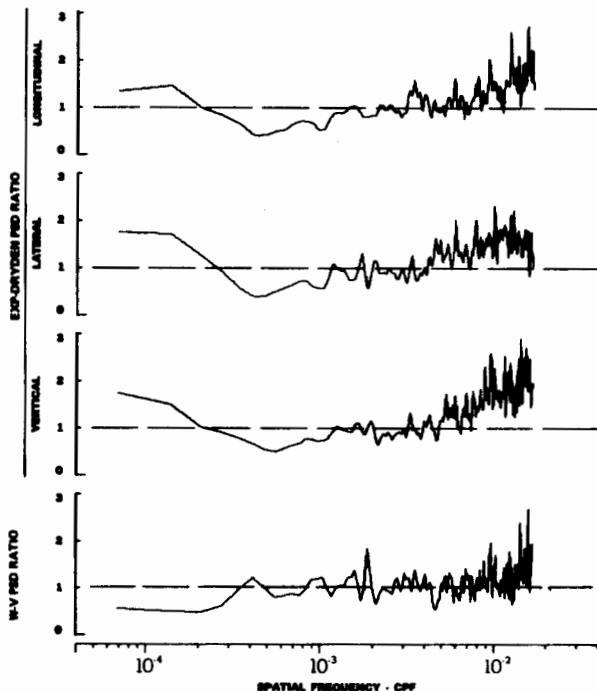
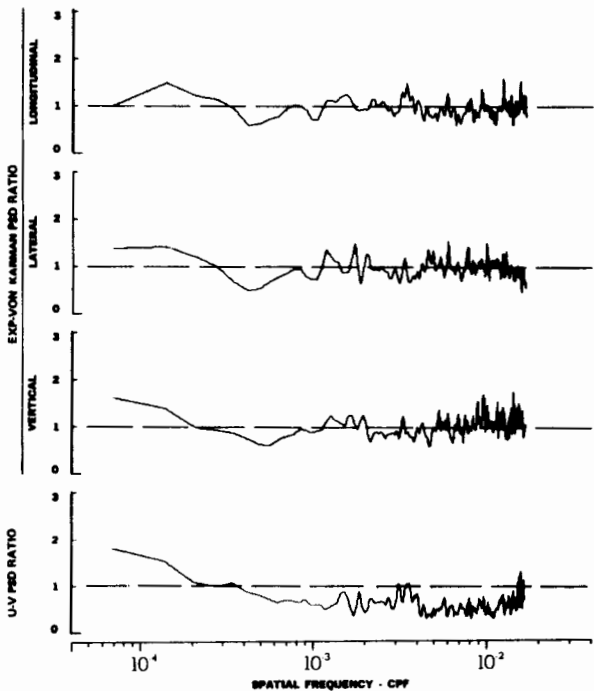
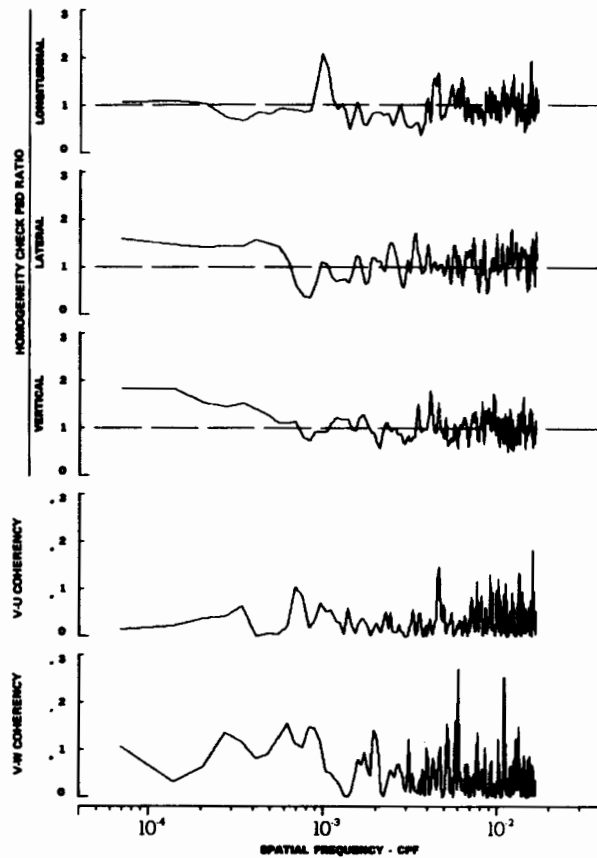
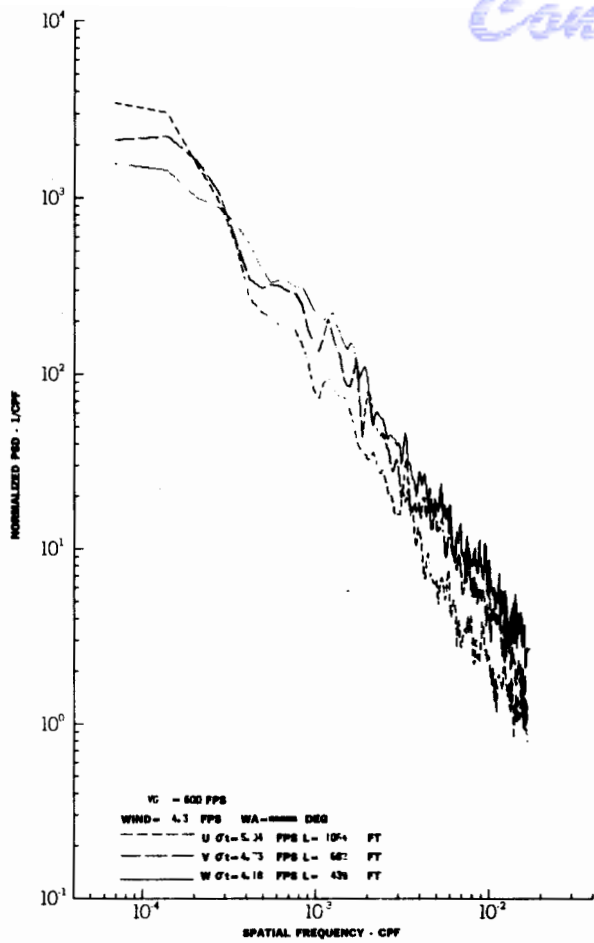
FIGURE IV-120

# Contrails



TURBULENCE SPECTRA DATA FOR TEST 109, LEG 3, CATEGORY 113331

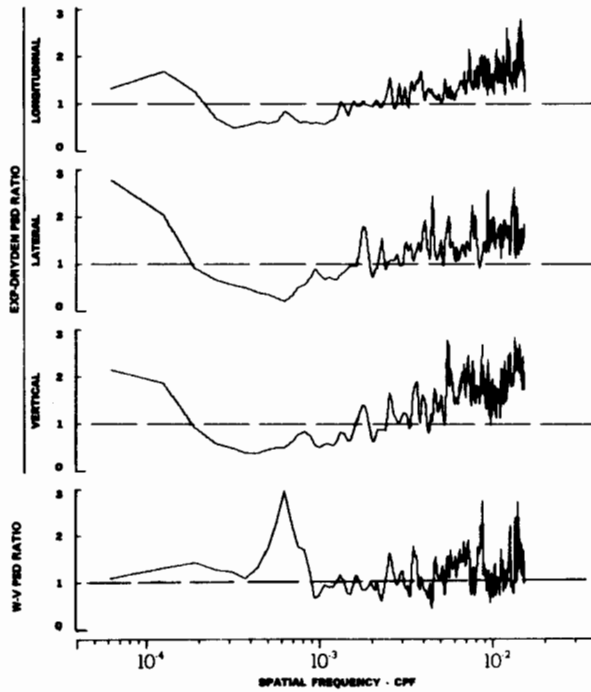
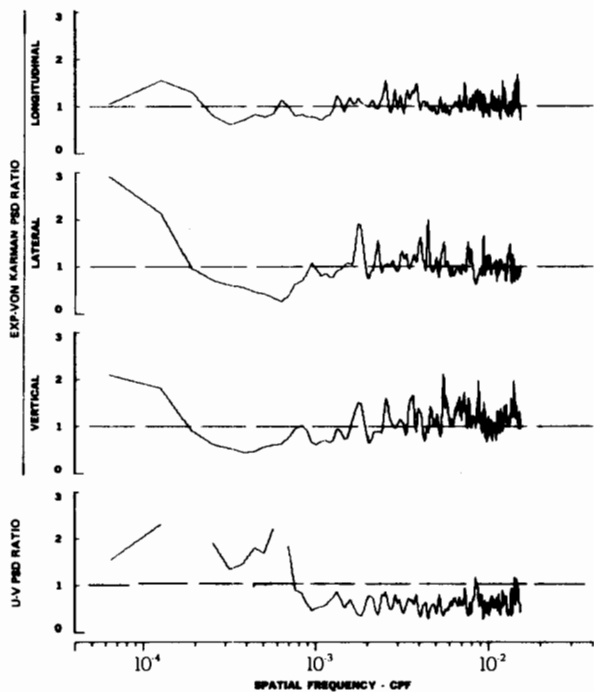
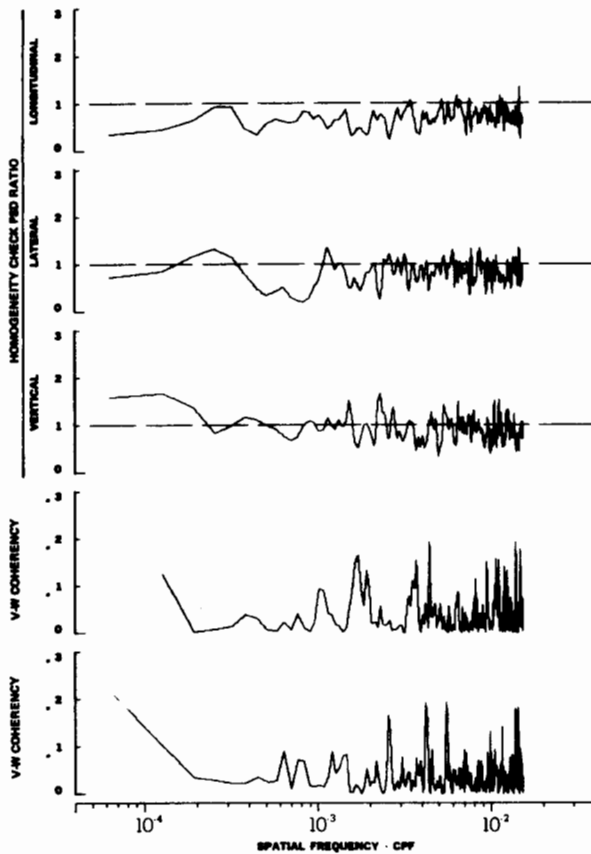
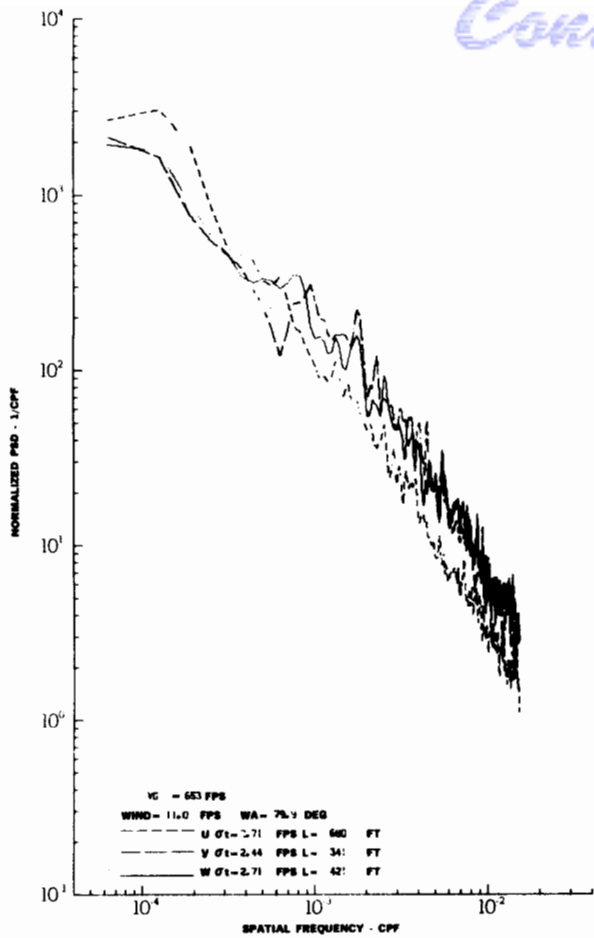
FIGURE IV-121



TURBULENCE SPECTRA DATA FOR TEST 109, LEG 5, CATEGORY 112331

FIGURE IV-122

# Contrails

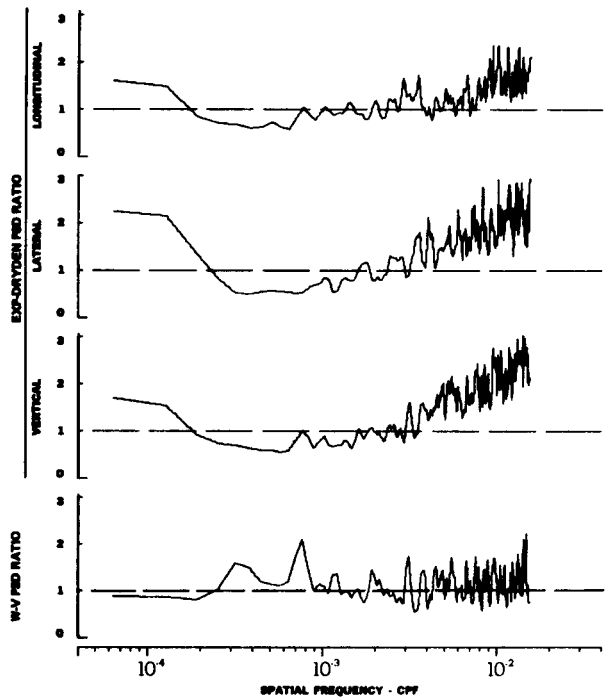
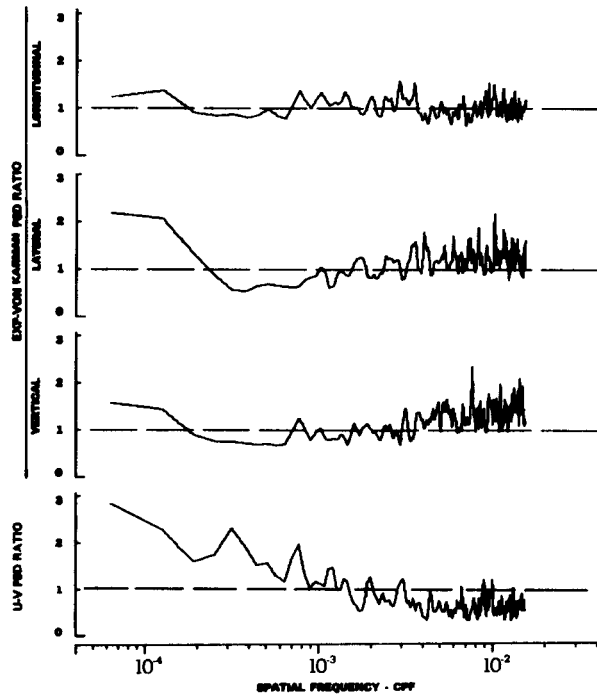
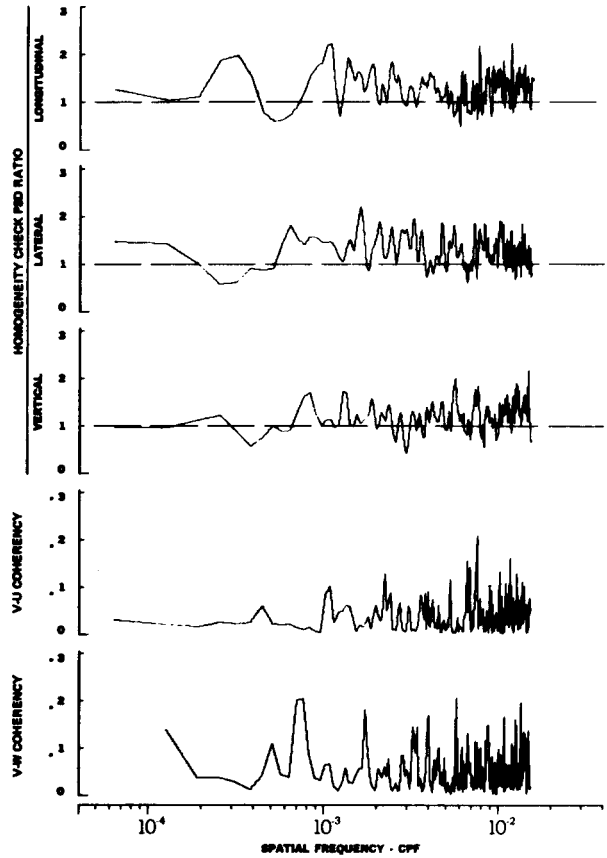
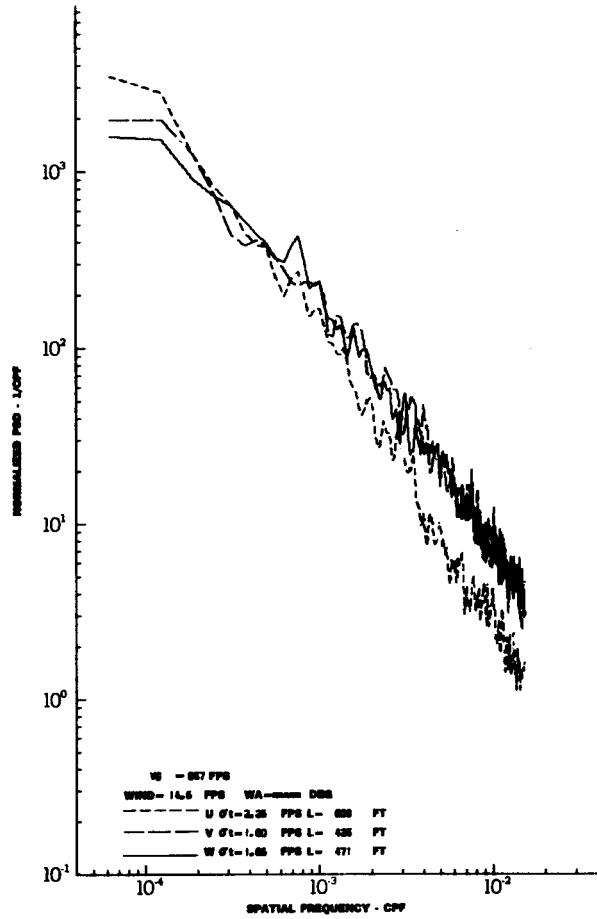


TURBULENCE SPECTRA DATA FOR TEST 109, LEG 7, CATEGORY 313331

FIGURE IV-123



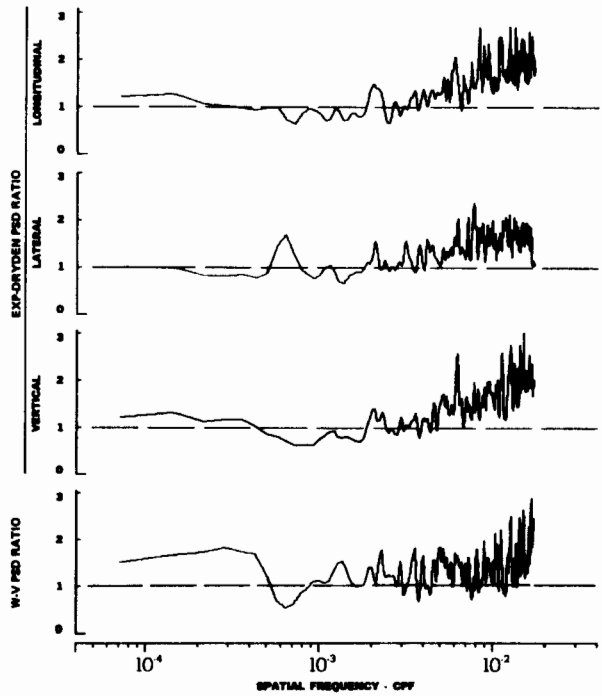
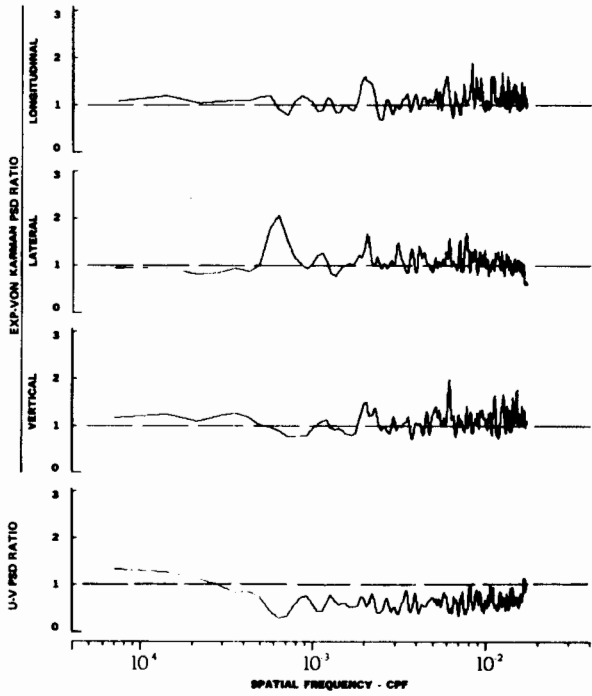
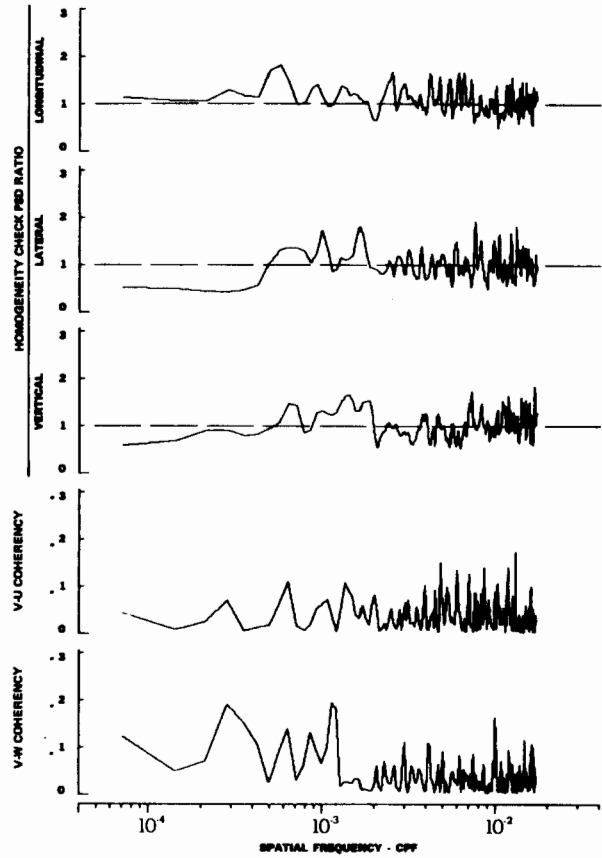
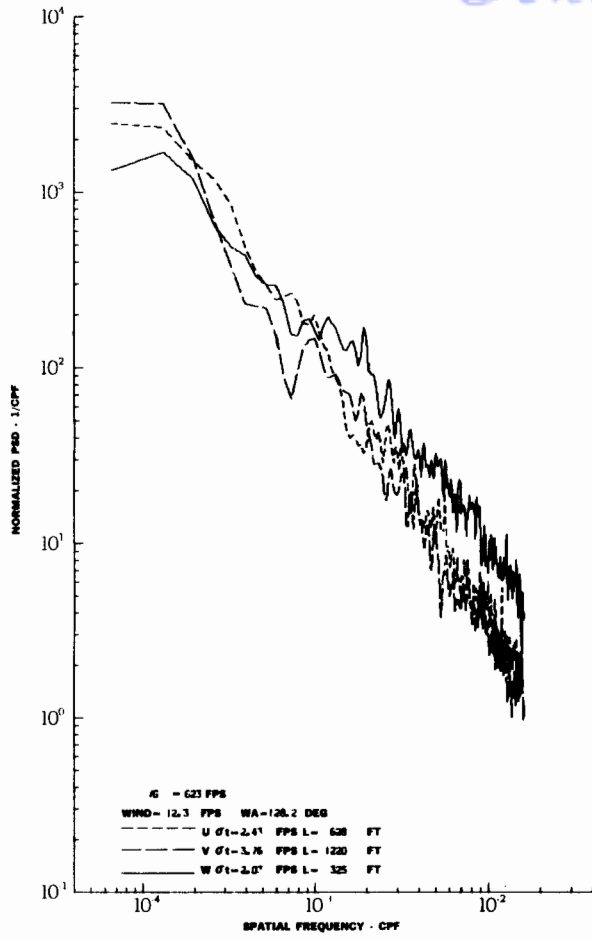
# Contrails



TURBULENCE SPECTRA DATA FOR TEST 111, LEG 7, CATEGORY 321231

FIGURE IV-124

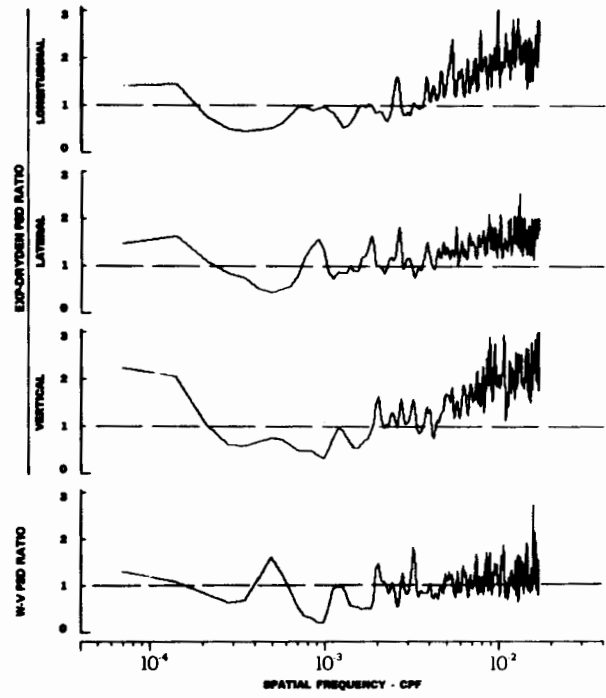
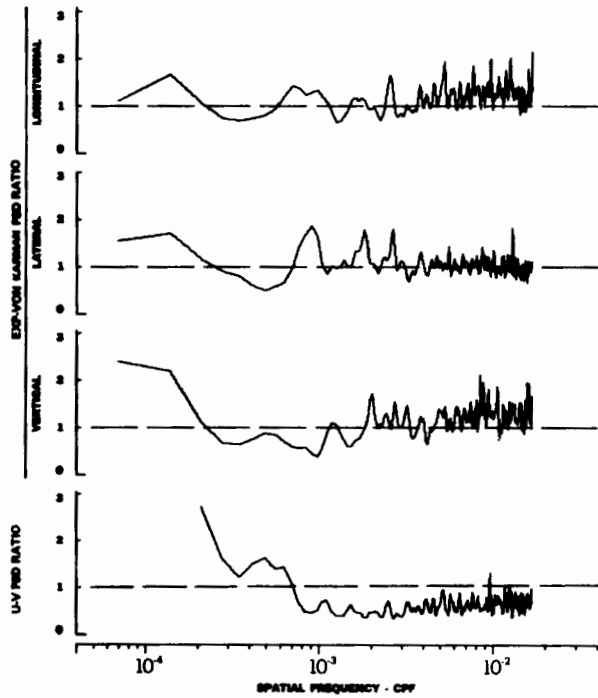
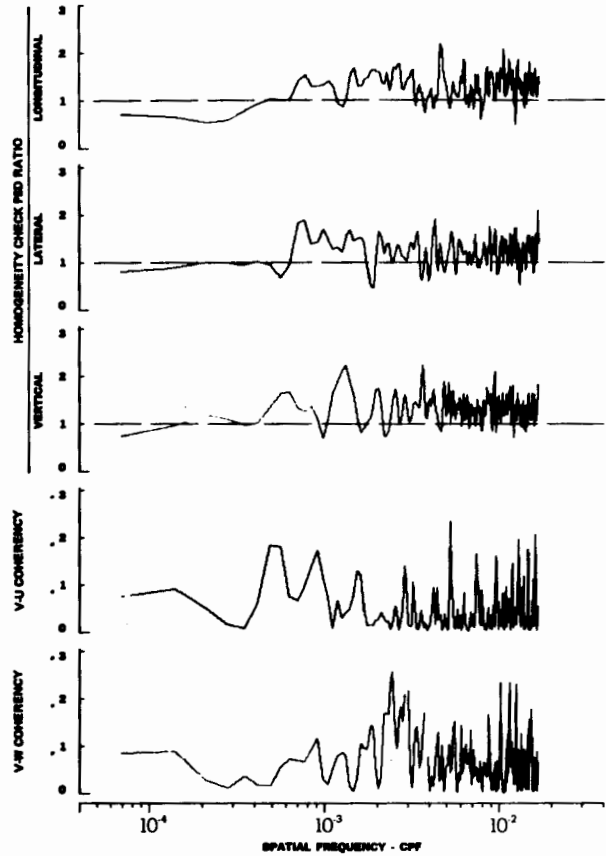
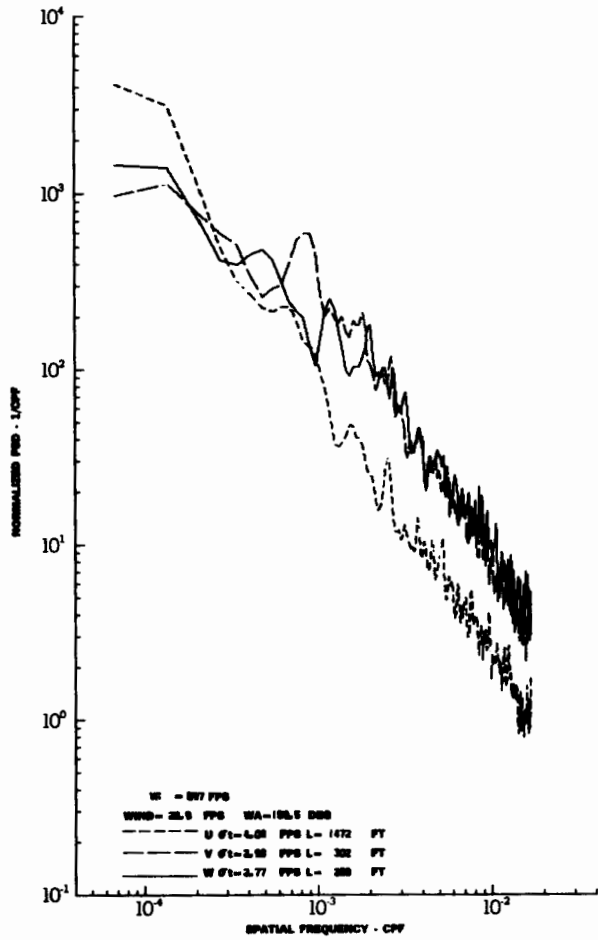
# Contrails



TURBULENCE SPECTRA DATA FOR TEST 112, LEG 6, CATEGORY 221331

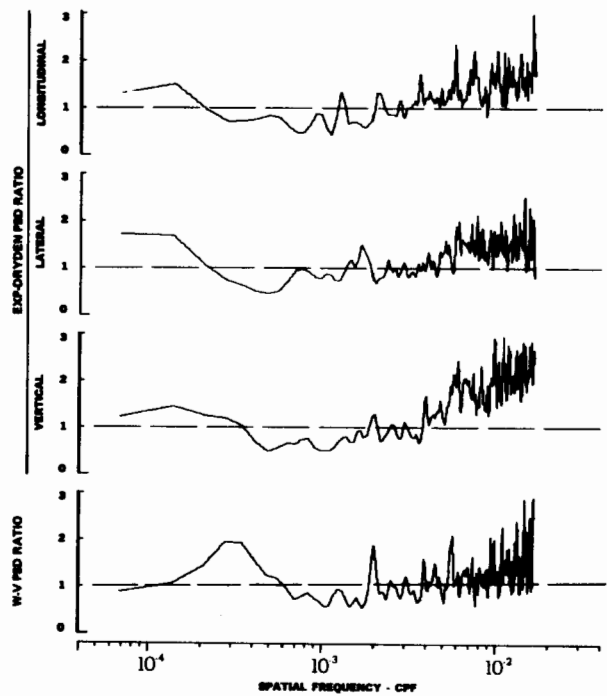
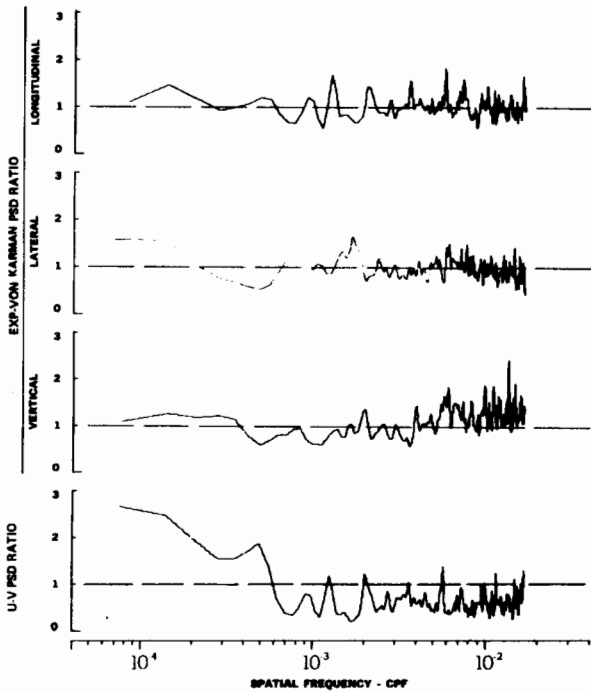
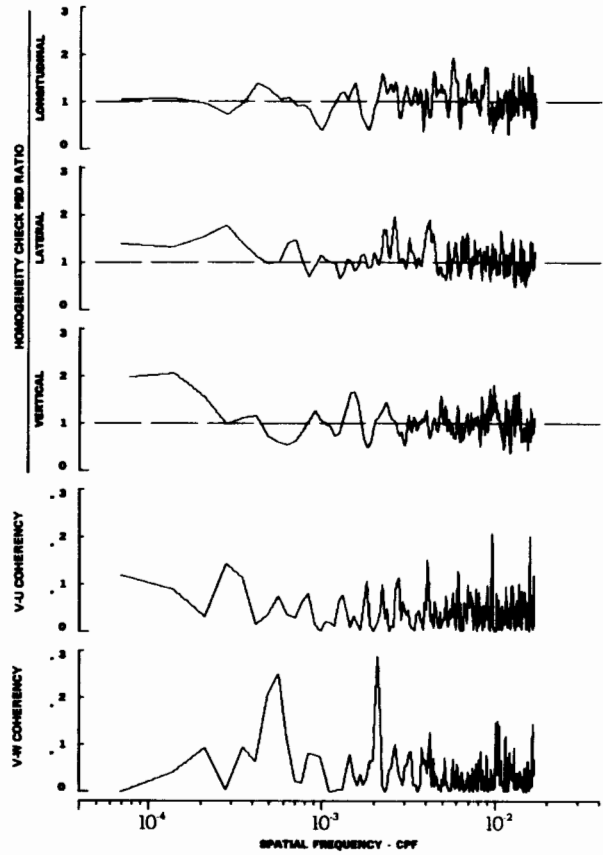
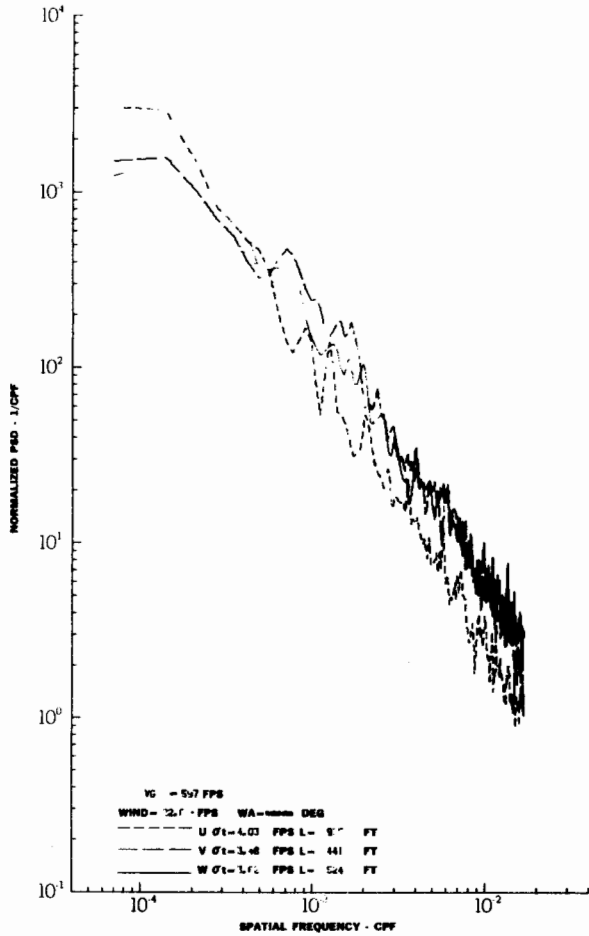
FIGURE IV-125

# Contrails



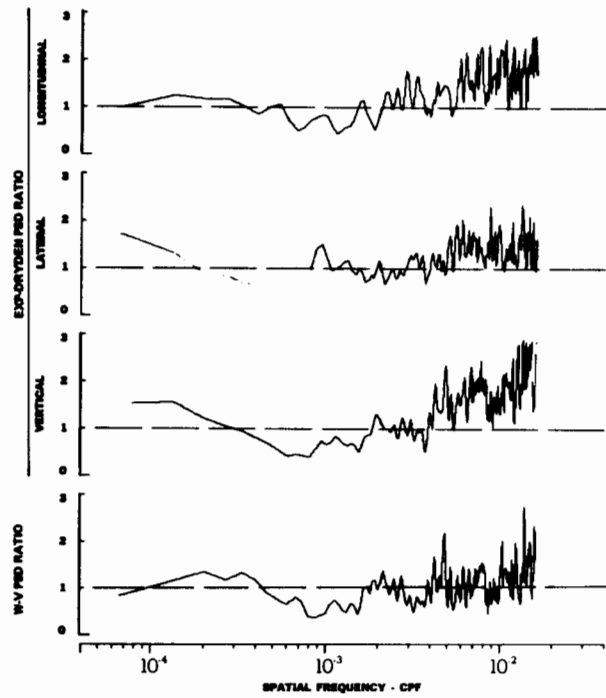
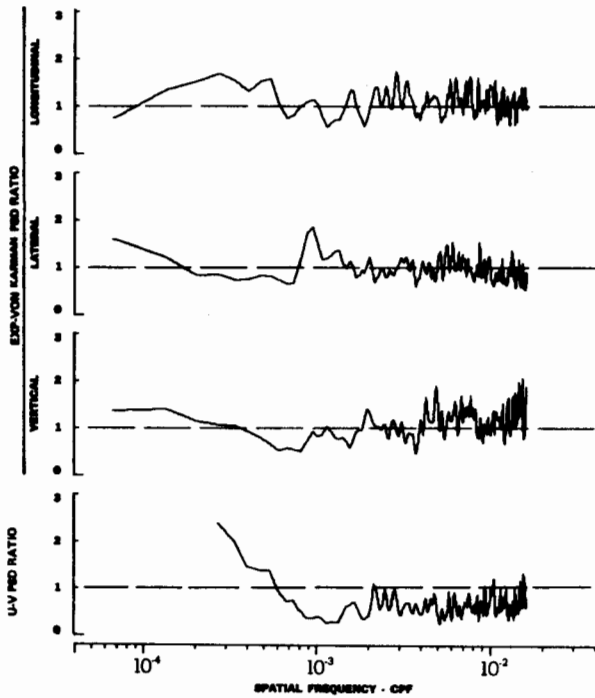
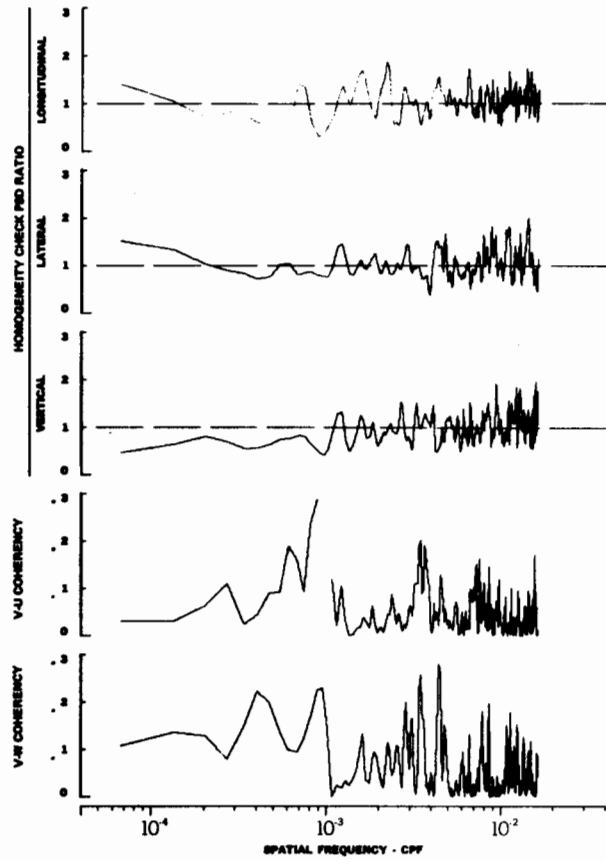
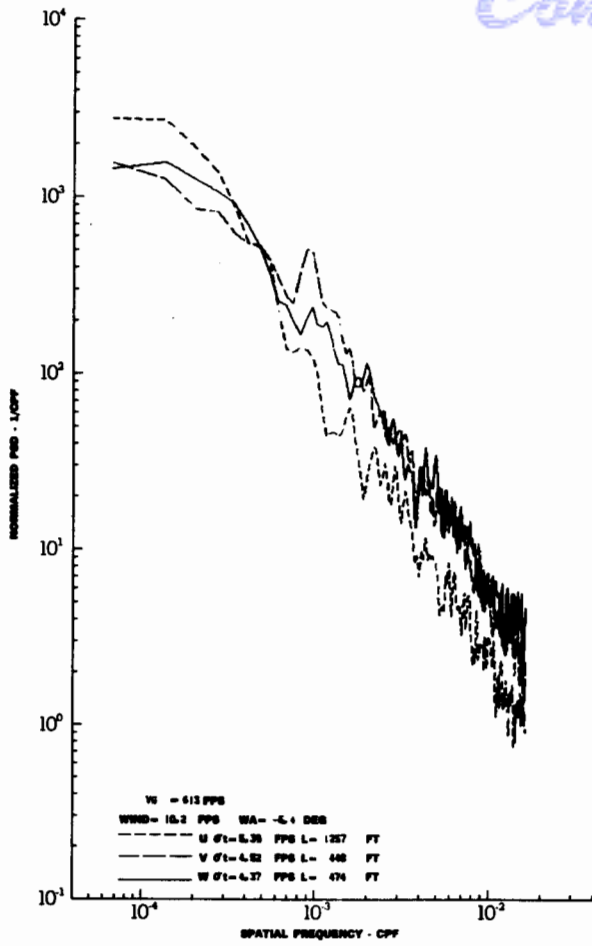
TURBULENCE SPECTRA DATA FOR TEST 112, LEG 8, CATEGORY 223331  
 FIGURE IV-126

# Contrails

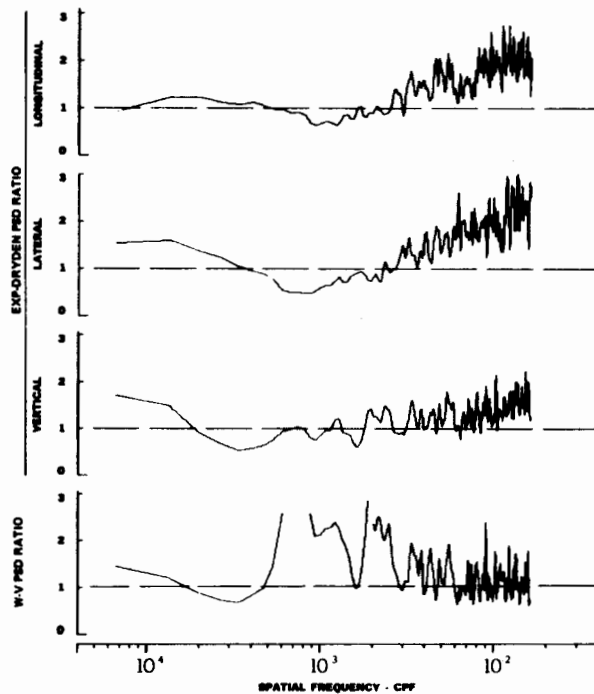
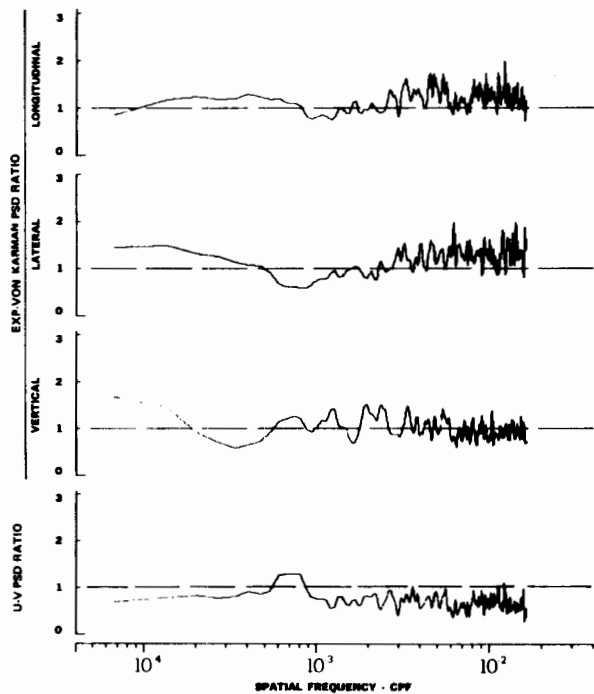
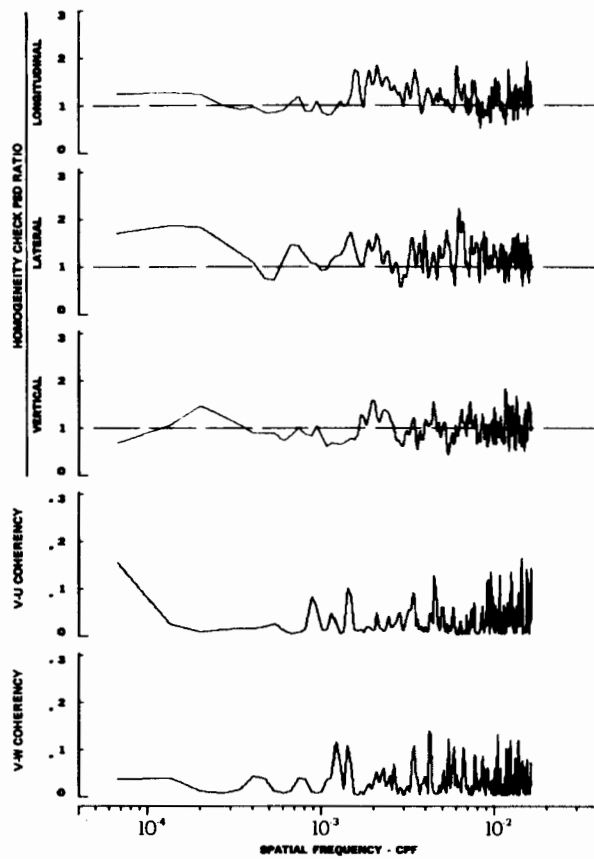
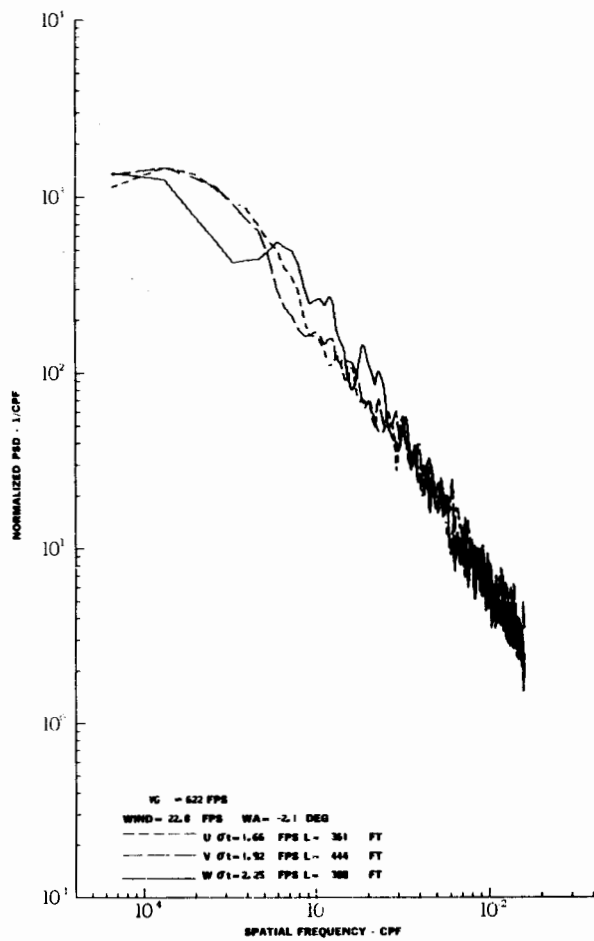


TURBULENCE SPECTRA DATA FOR TEST 123, LEG 3, CATEGORY 121331  
 FIGURE IV-127

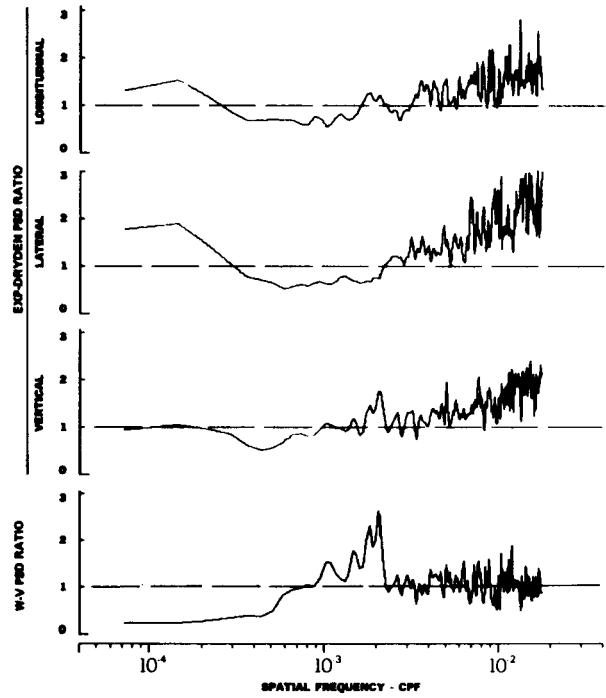
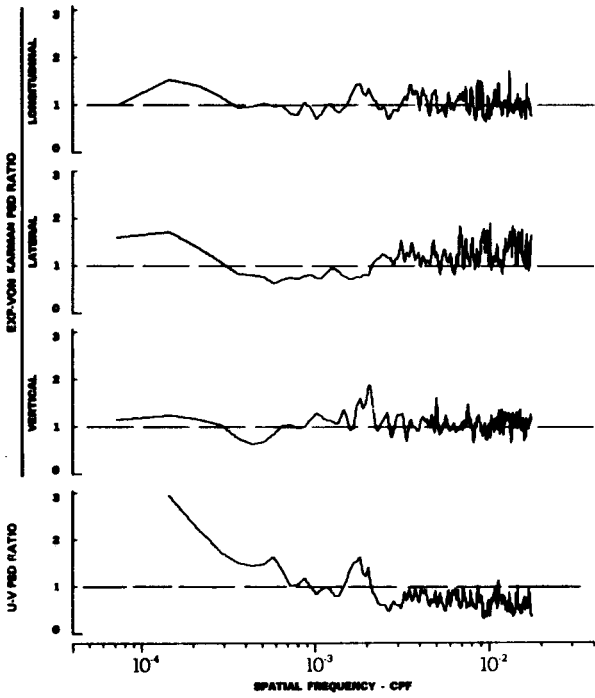
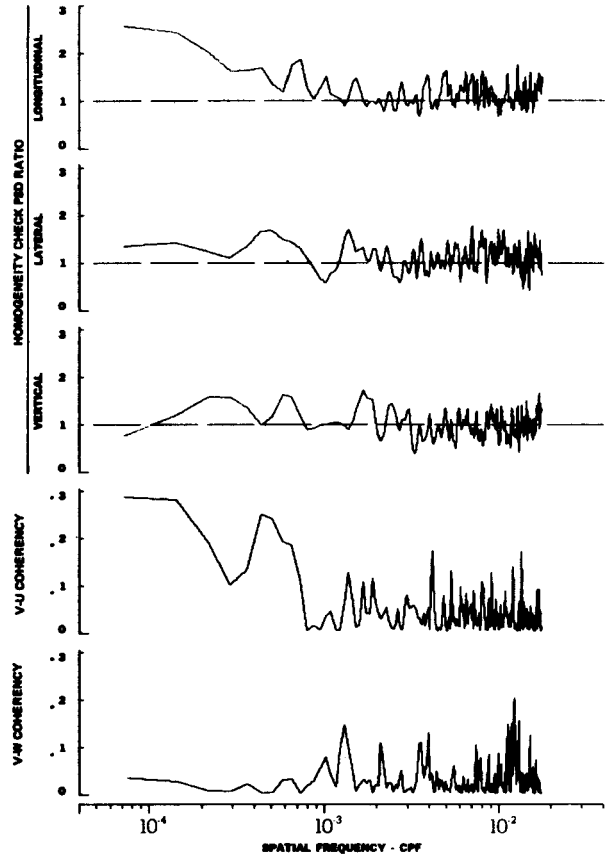
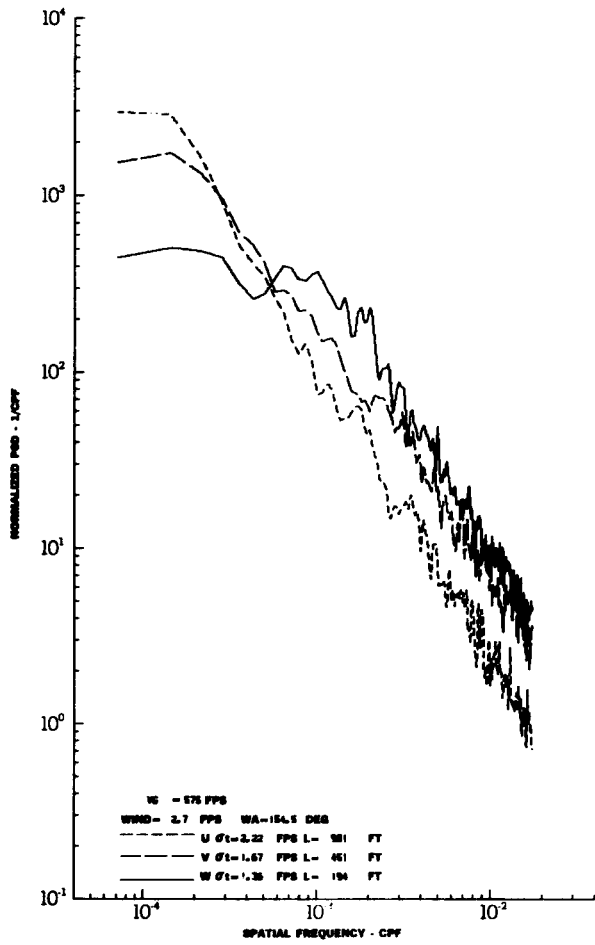
# Contrails



TURBULENCE SPECTRA DATA FOR TEST 123, LEG 5, CATEGORY 122331  
 FIGURE IV-128



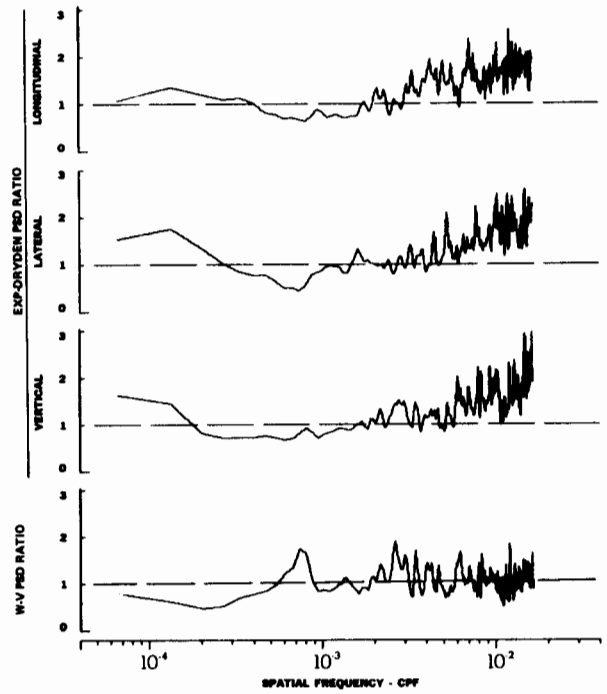
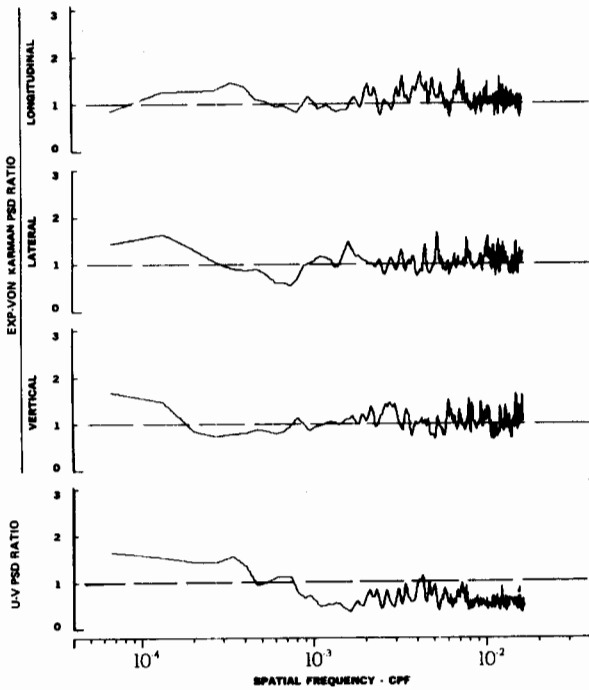
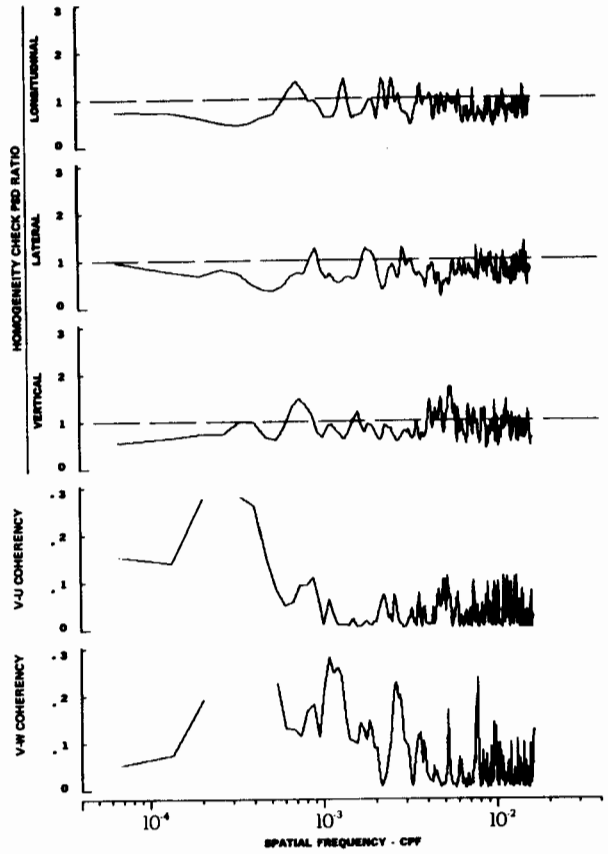
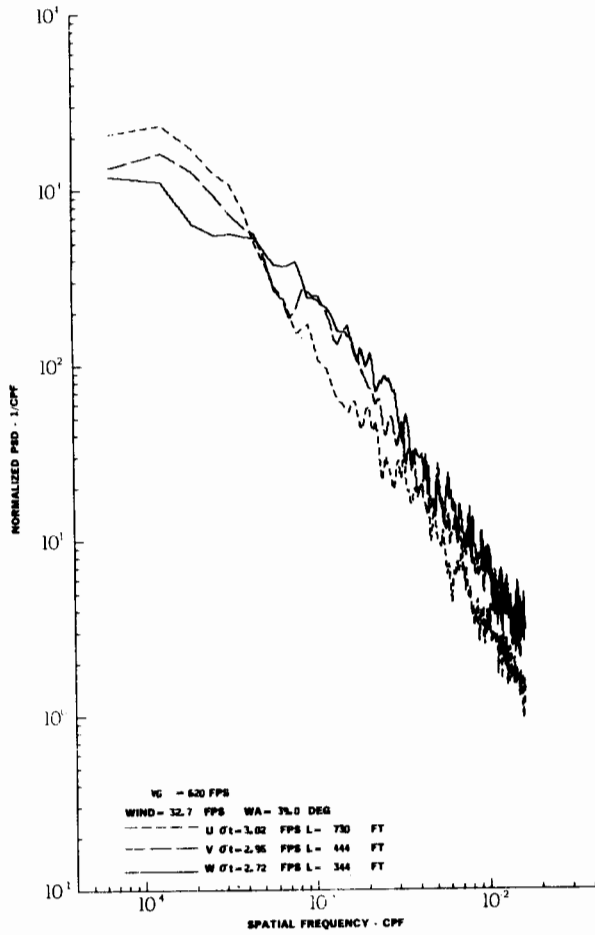
TURBULENCE SPECTRA DATA FOR TEST 124, LEG 2, CATEGORY 312231  
FIGURE IV-129



TURBULENCE SPECTRA DATA FOR TEST 124, LEG 4, CATEGORY 612231

FIGURE IV-130

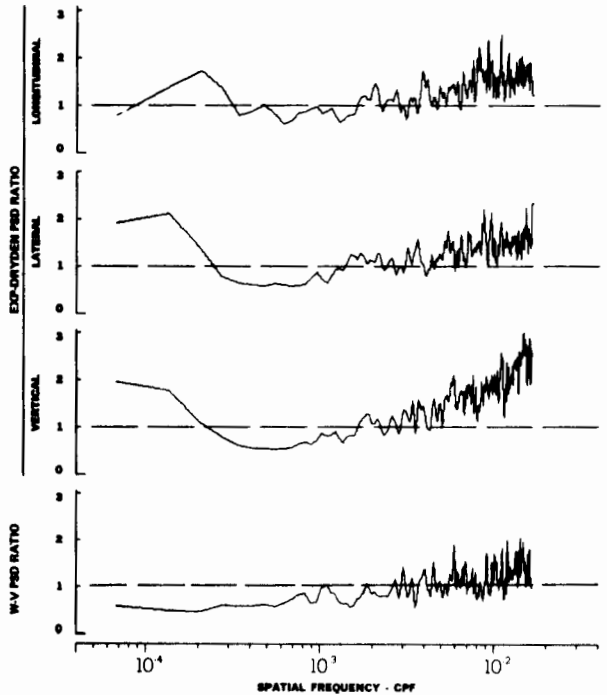
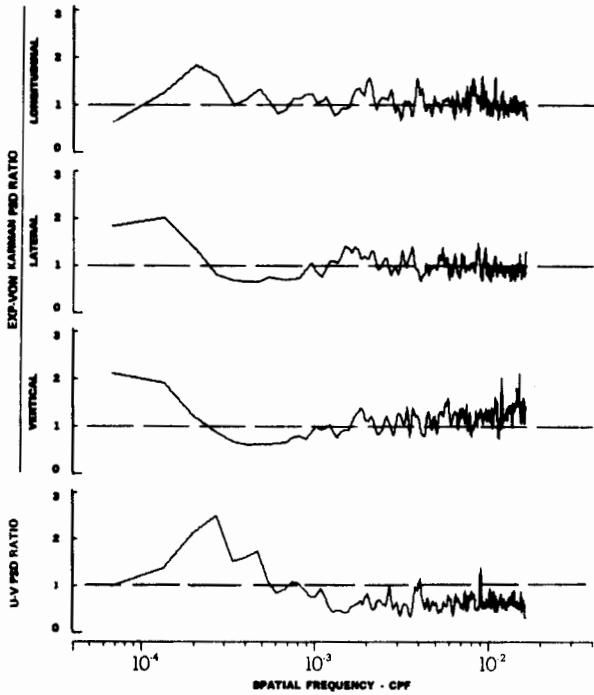
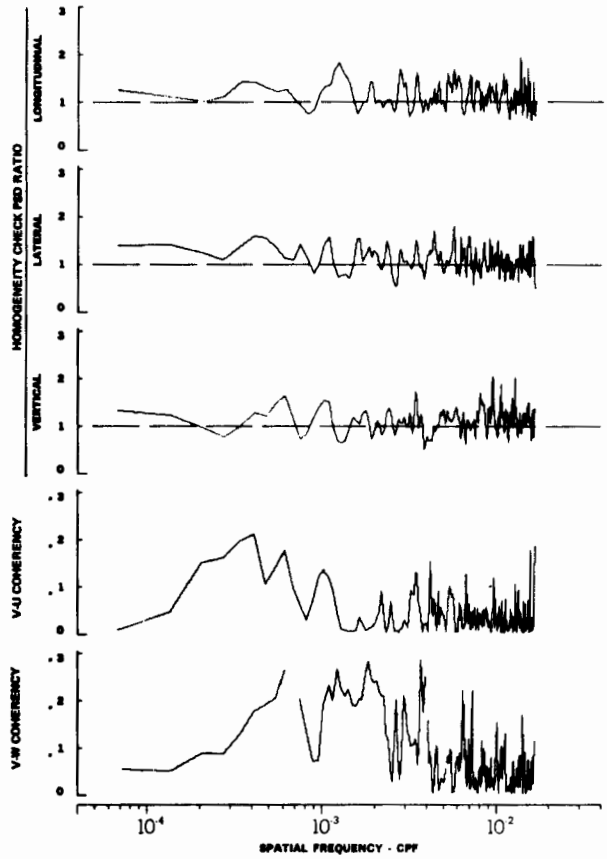
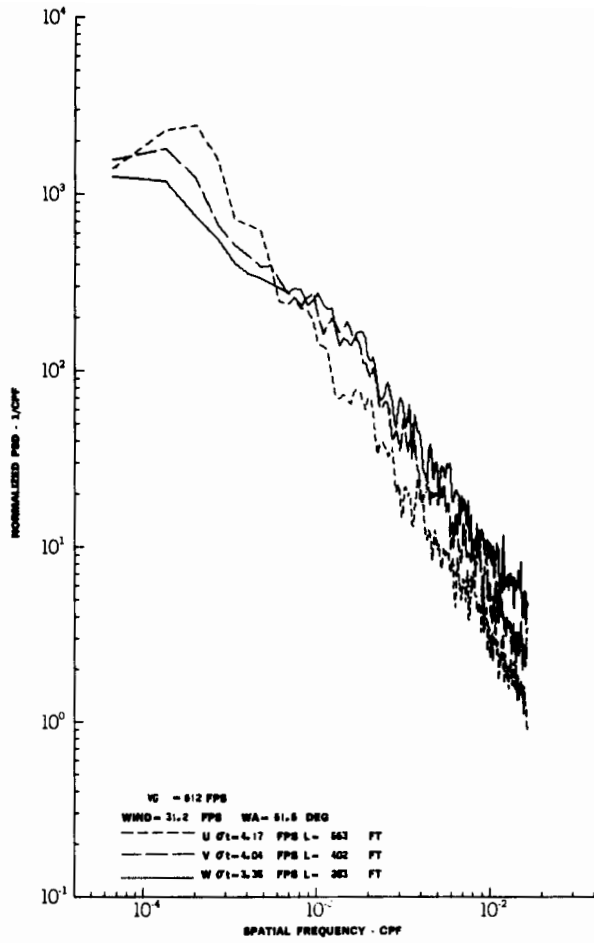




TURBULENCE SPECTRA DATA FOR TEST 124, LEG 6, CATEGORY 213231

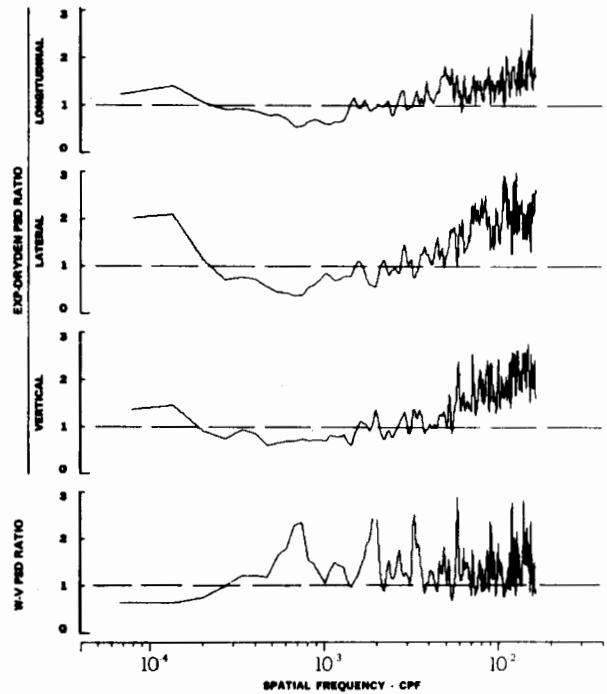
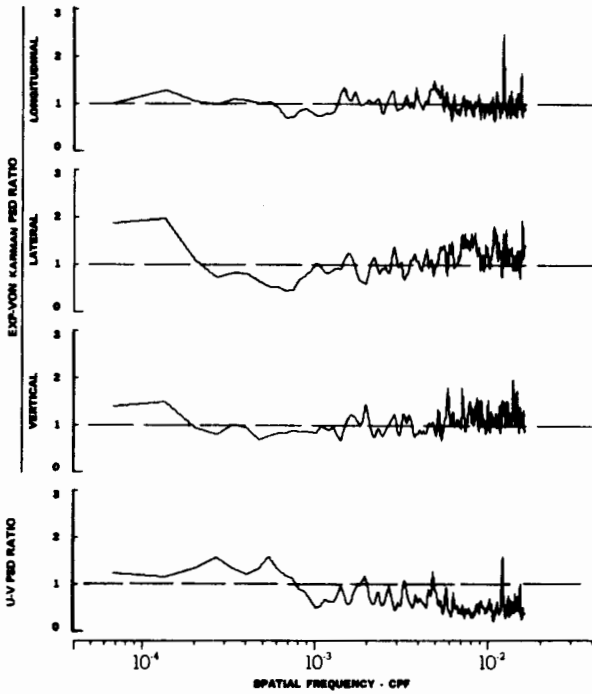
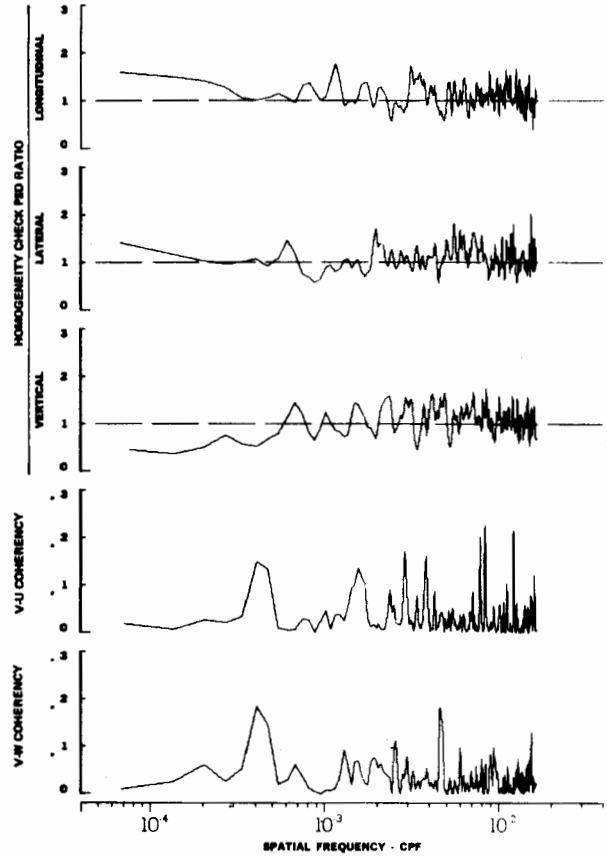
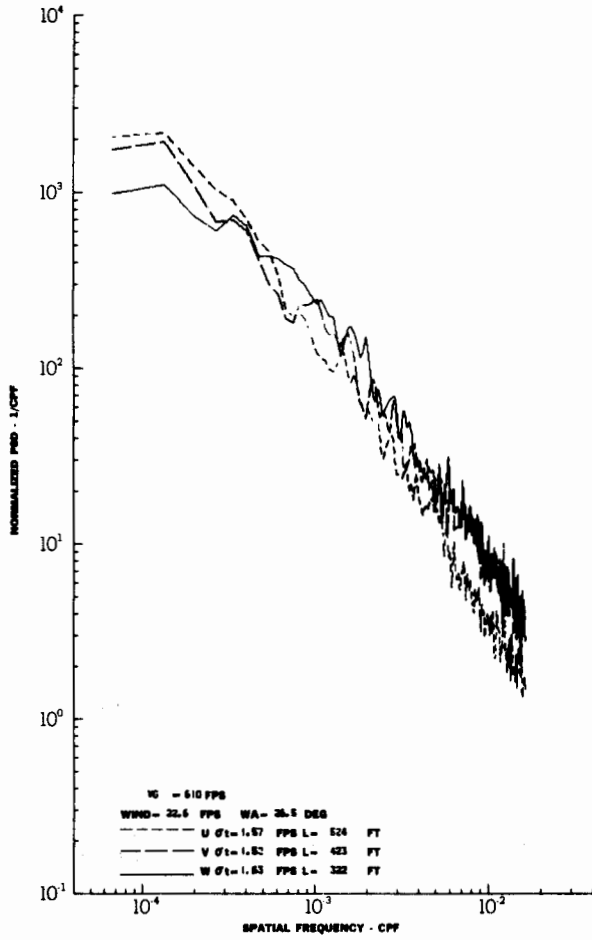
FIGURE IV-131

# Contrails



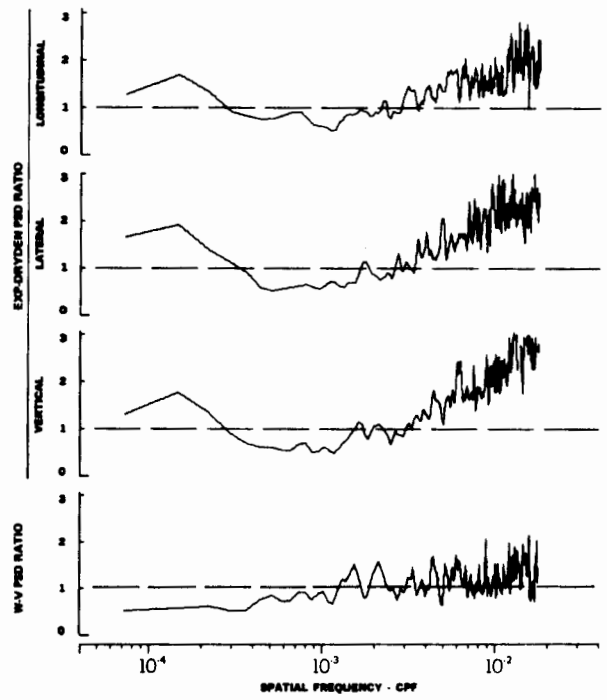
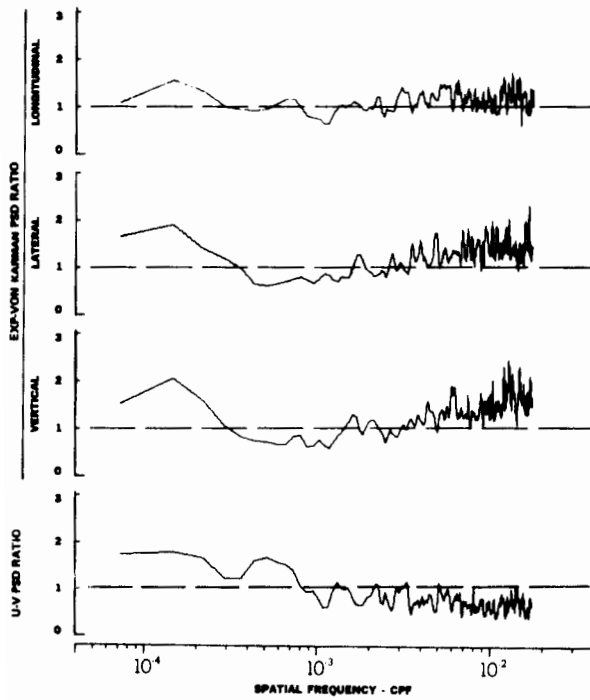
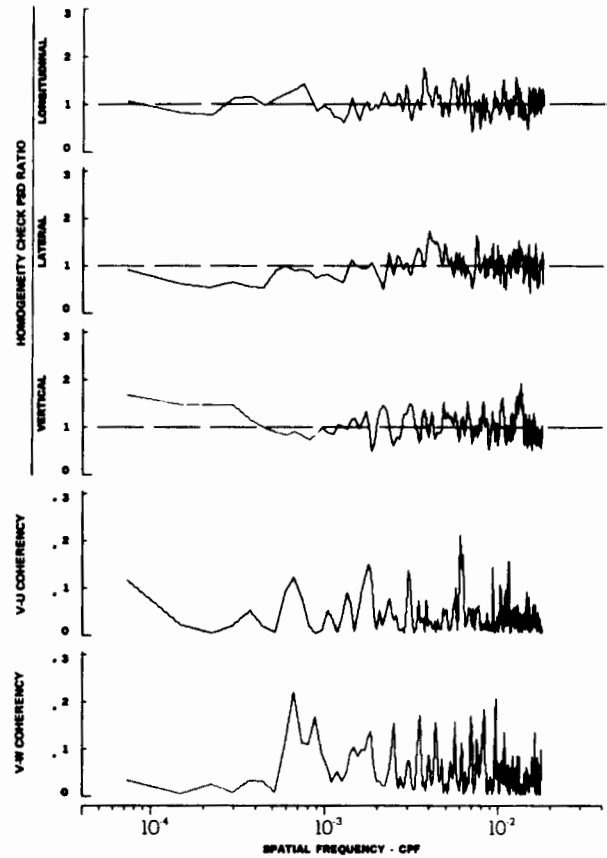
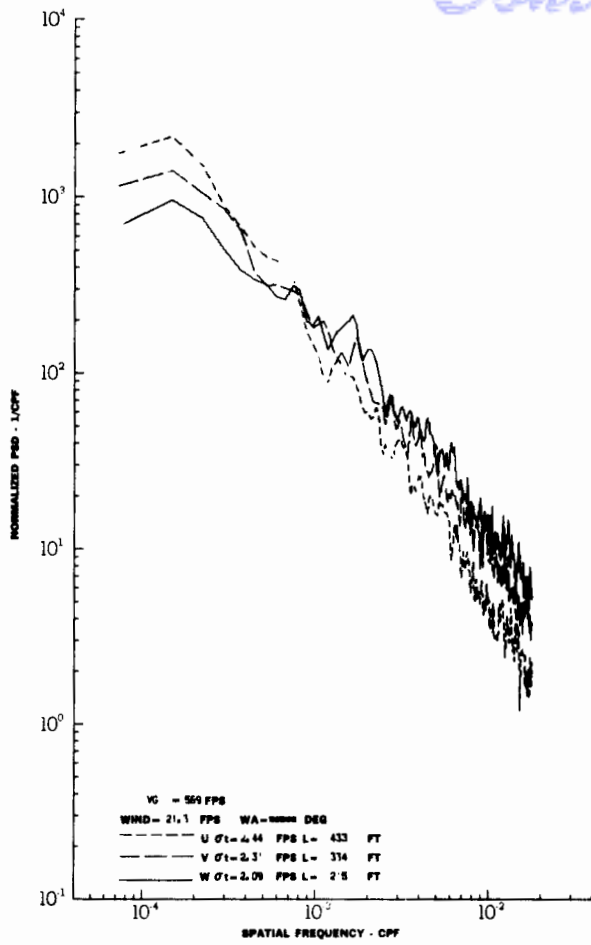
TURBULENCE SPECTRA DATA FOR TEST 124, LEG 8, CATEGORY 213231

FIGURE IV-132

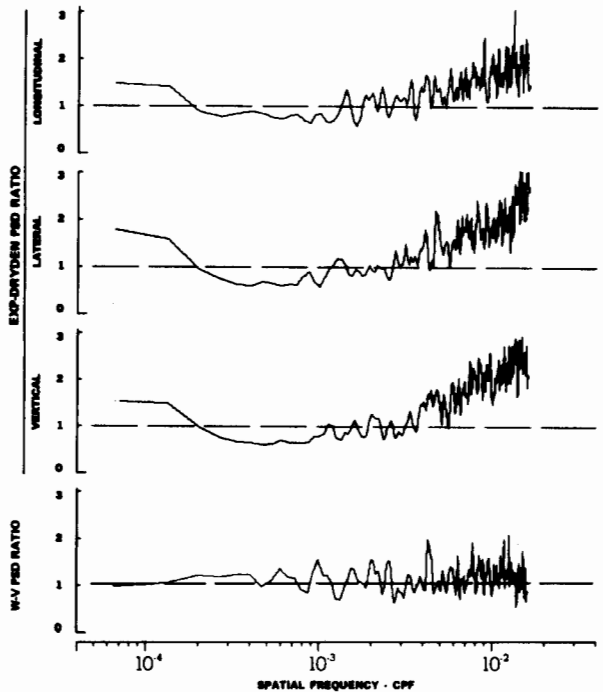
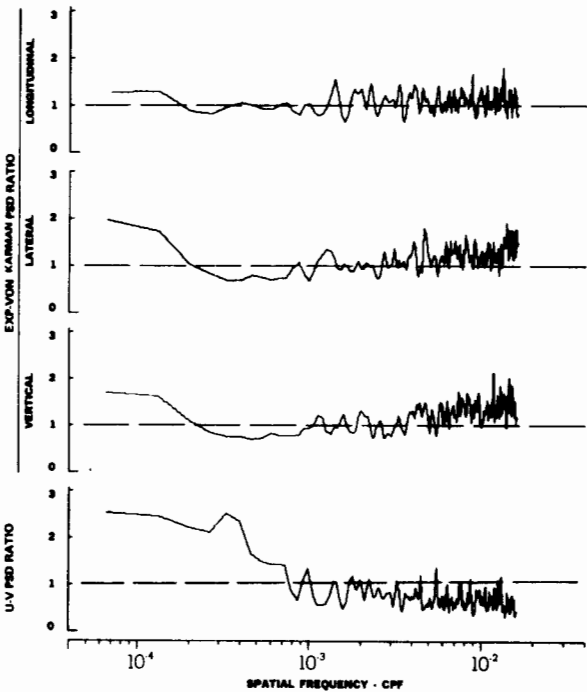
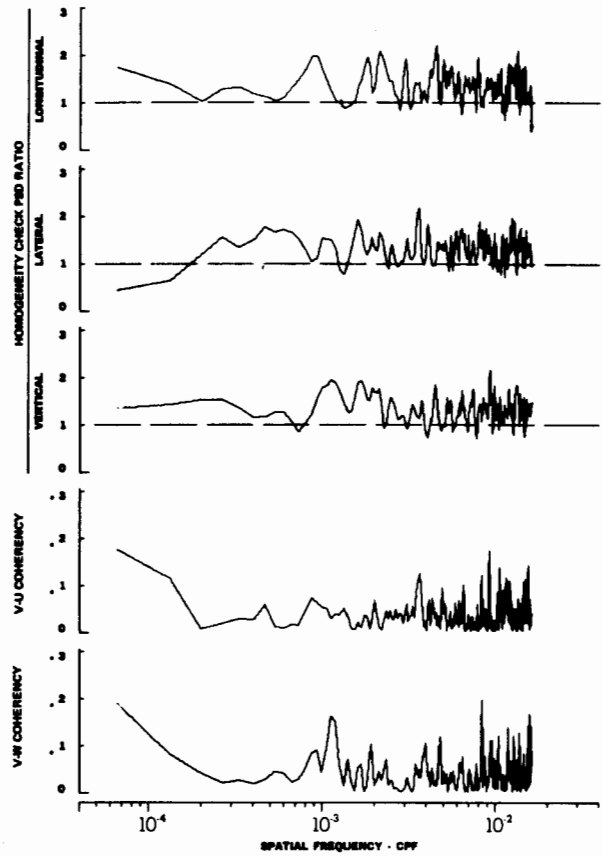
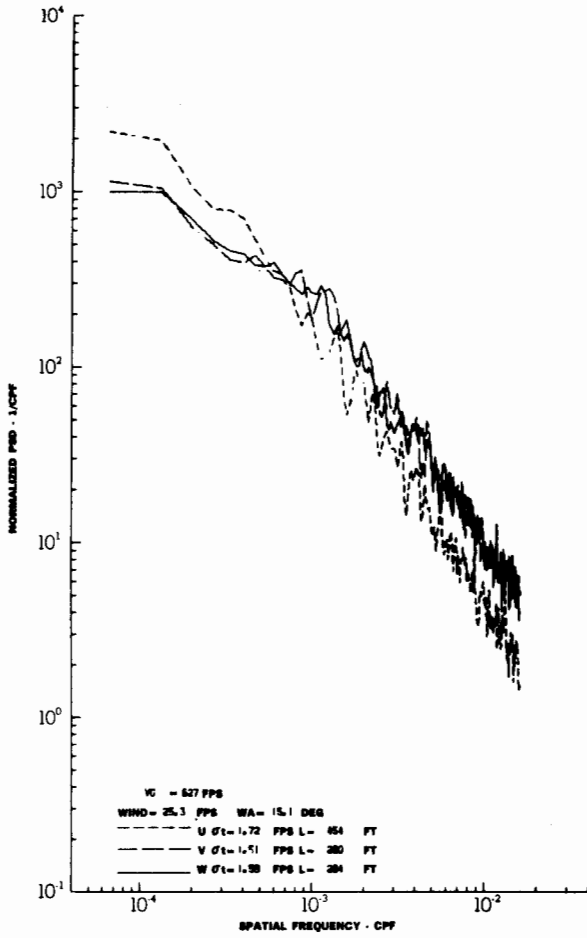


TURBULENCE SPECTRA DATA FOR TEST 125, LEG 7, CATEGORY 314331  
 FIGURE IV-133  
 240

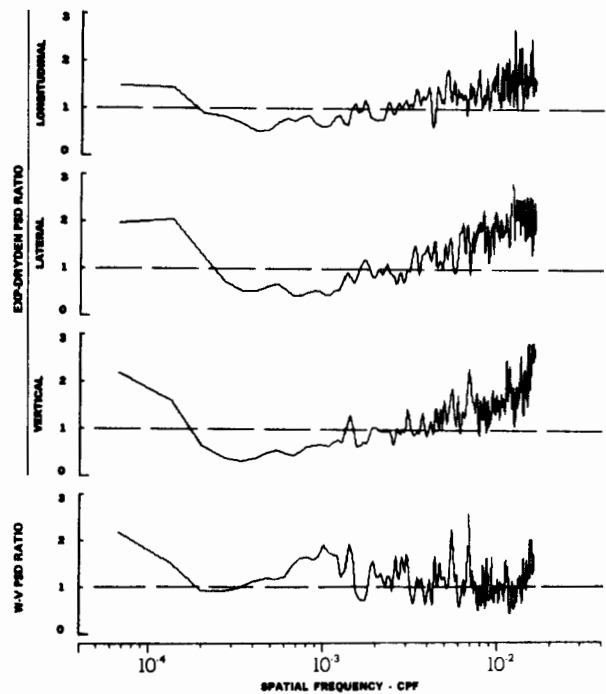
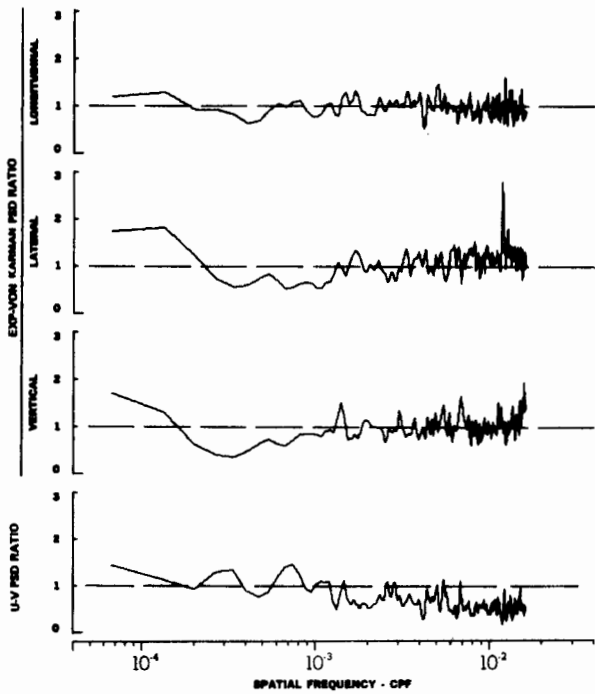
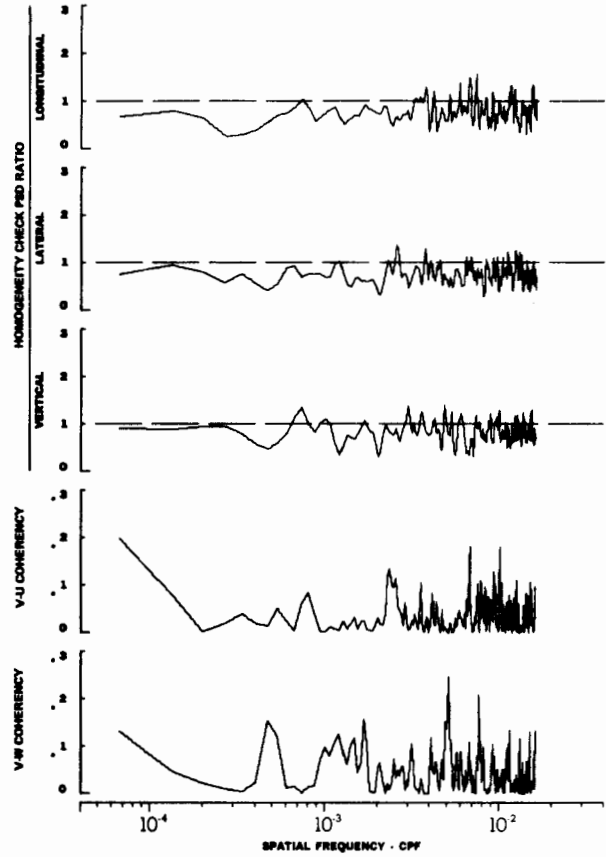
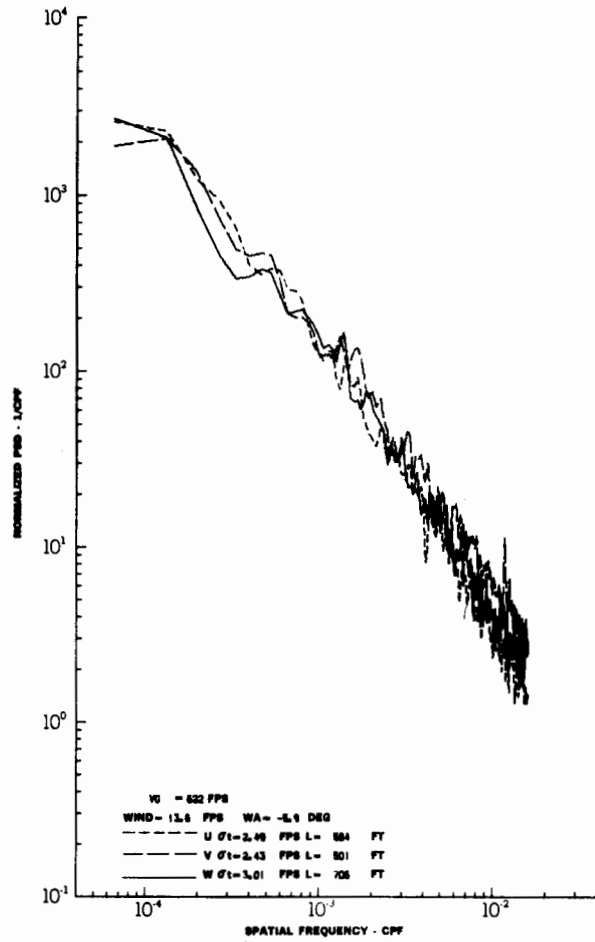
# Contrails



TURBULENCE SPECTRA DATA FOR TEST 130, LEG 4, CATEGORY 613231  
 FIGURE IV-134  
 241



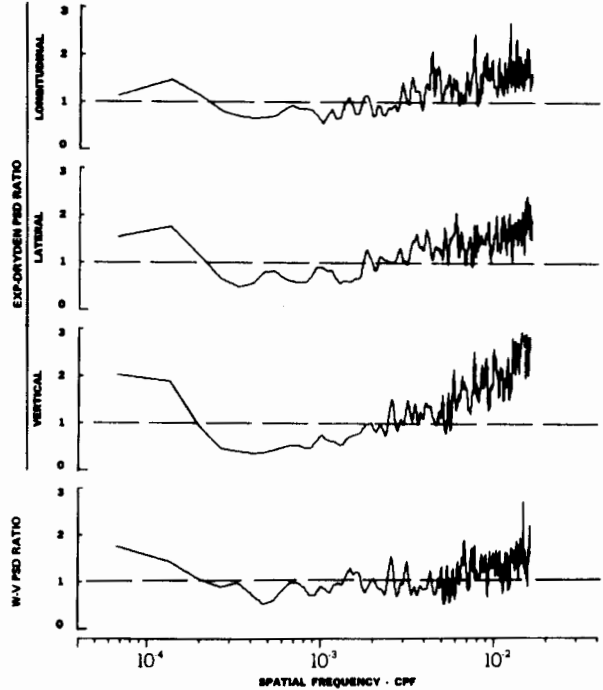
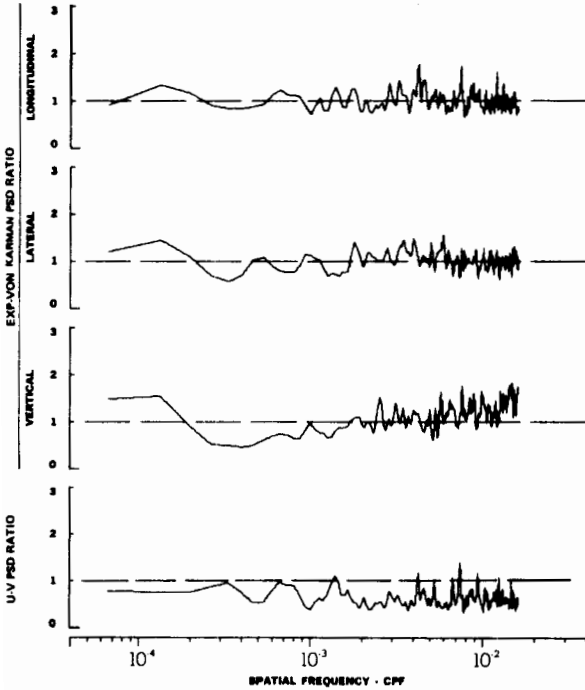
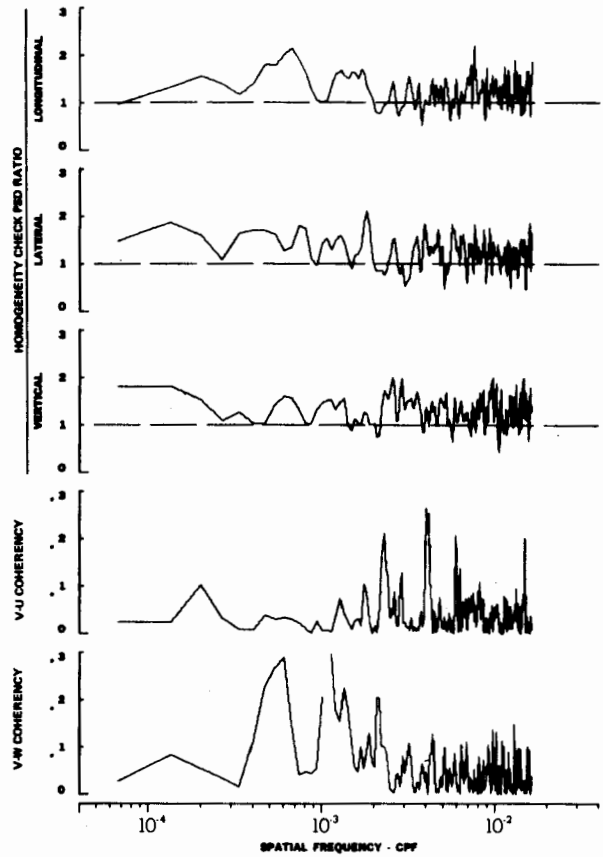
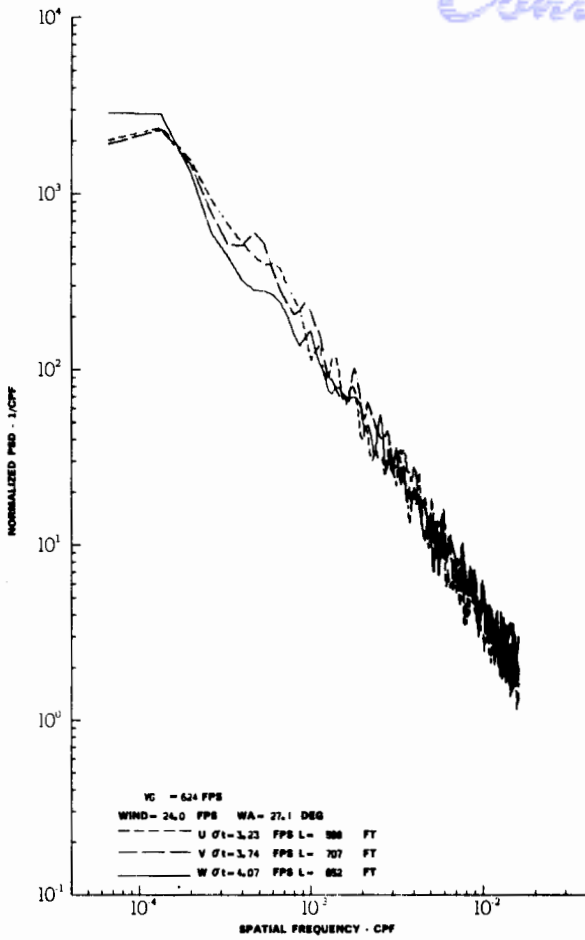
TURBULENCE SPECTRA DATA FOR TEST 130, LEG 6, CATEGORY 212231  
 FIGURE IV-135



TURBULENCE SPECTRA DATA FOR TEST 135, LEG 3, CATEGORY 111341

FIGURE IV-136

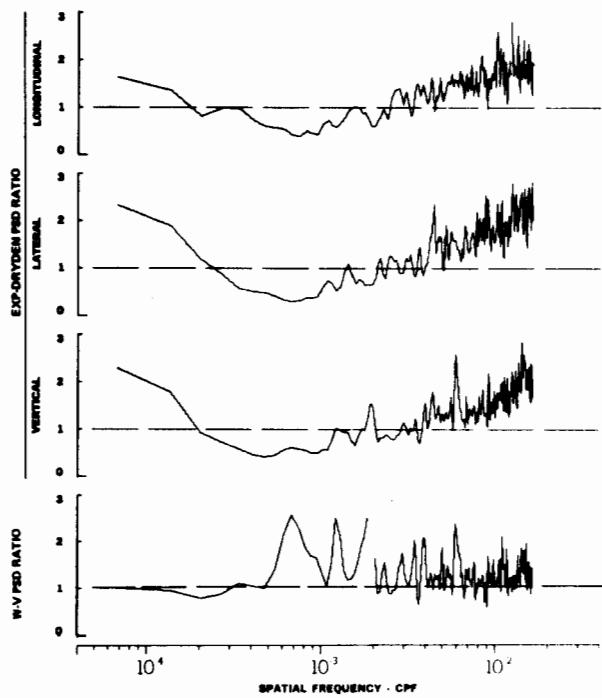
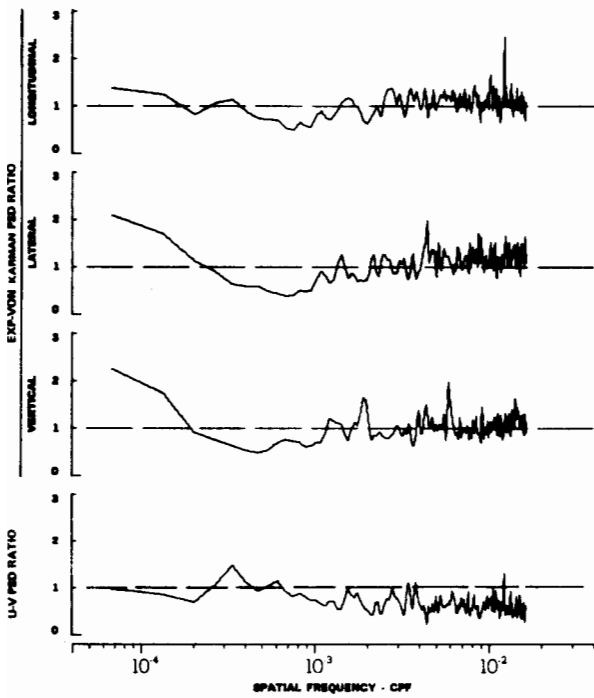
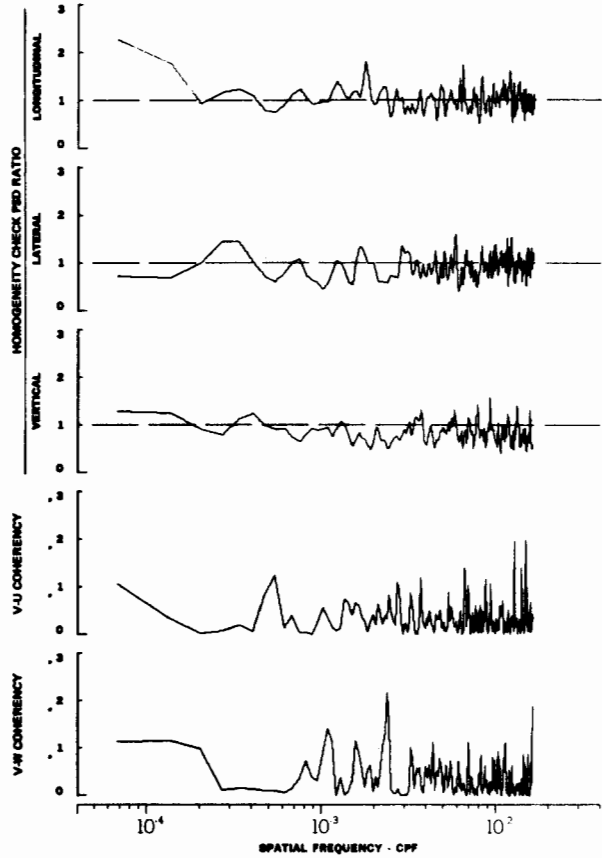
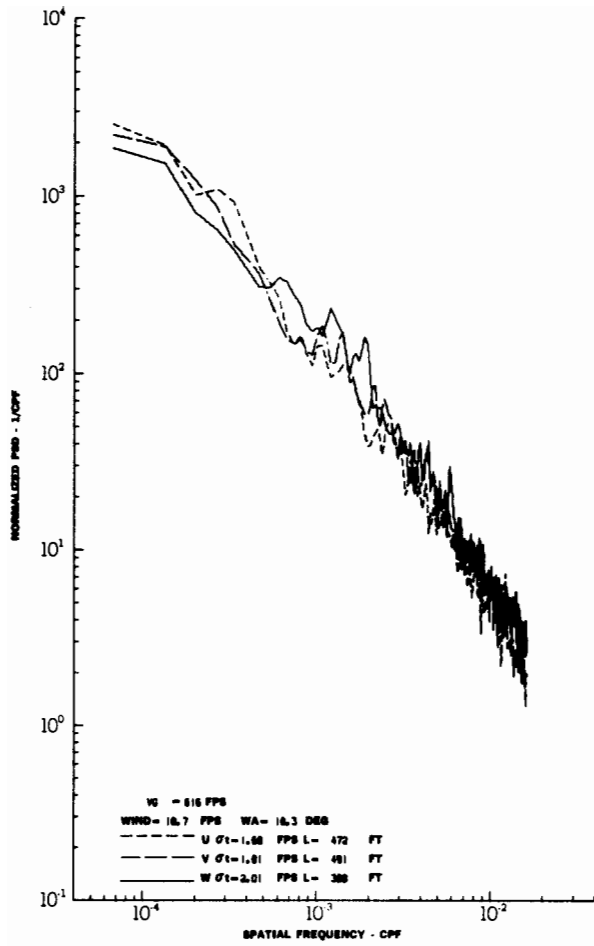
# Contrails



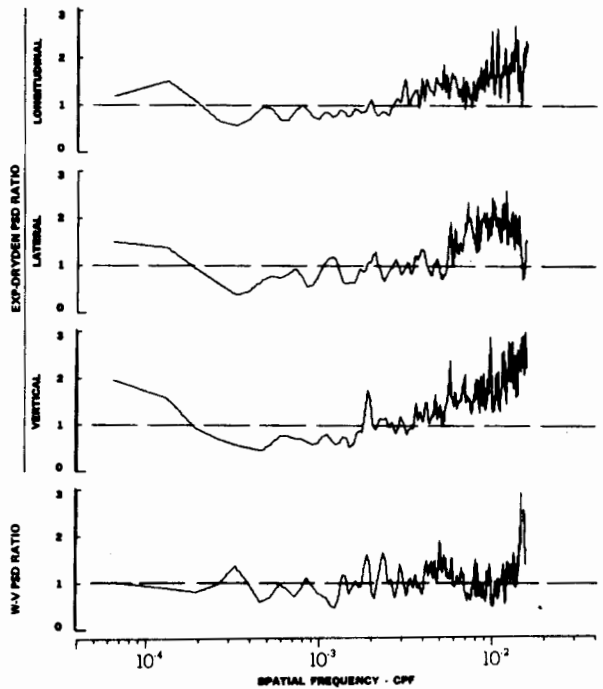
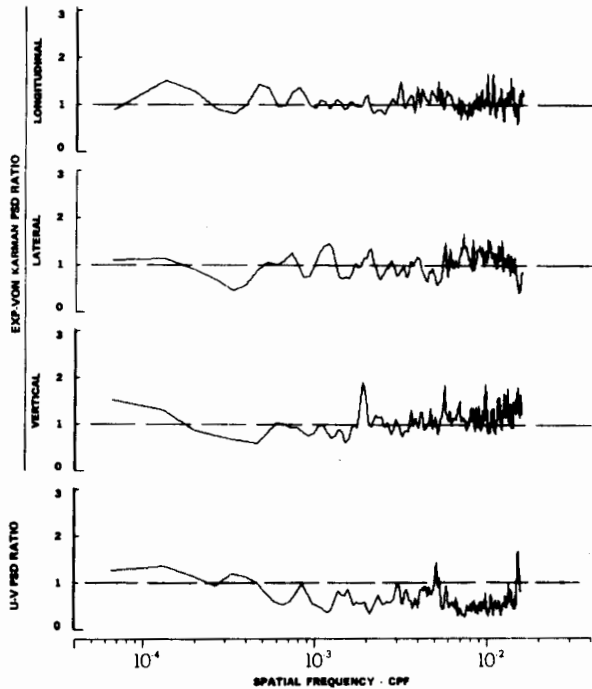
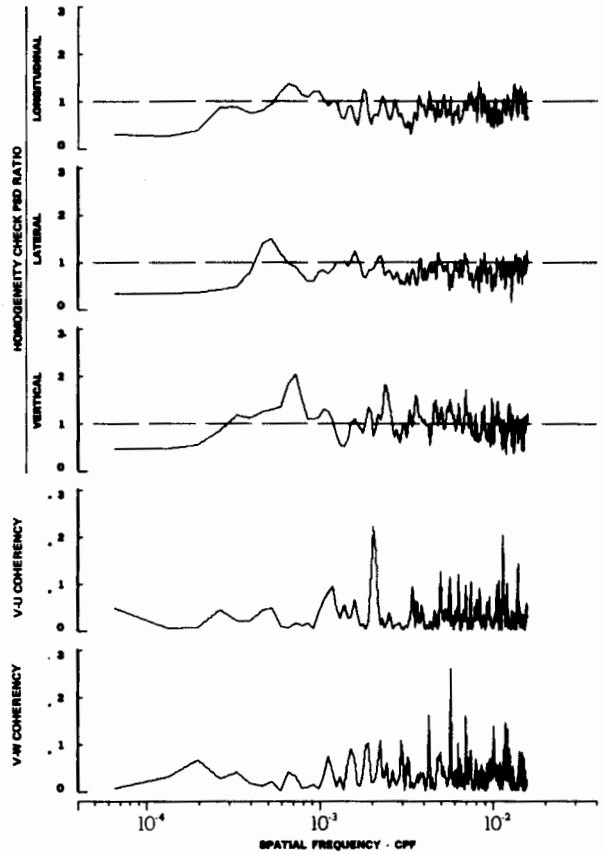
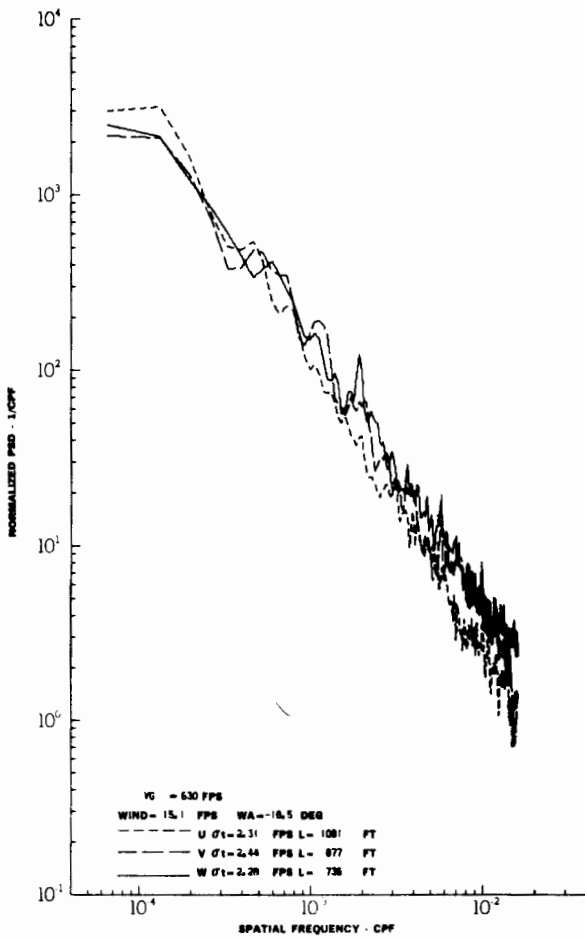
TURBULENCE SPECTRA DATA FOR TEST 135, LEG 5, CATEGORY 113341

FIGURE IV-137



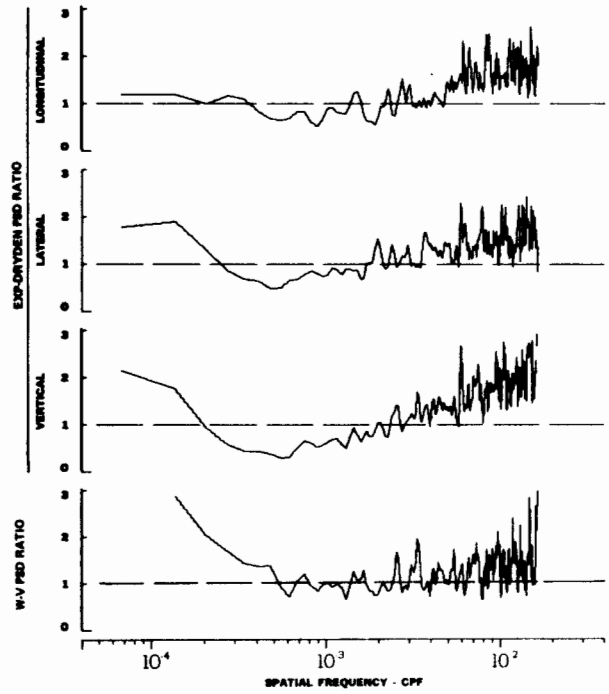
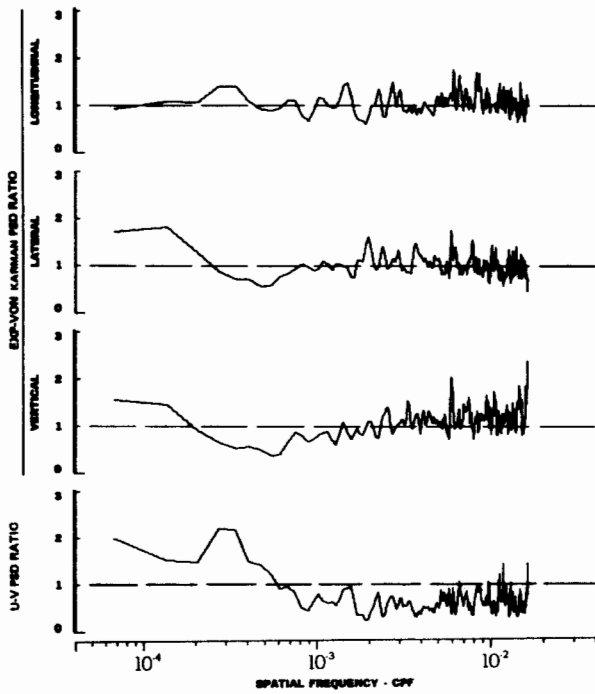
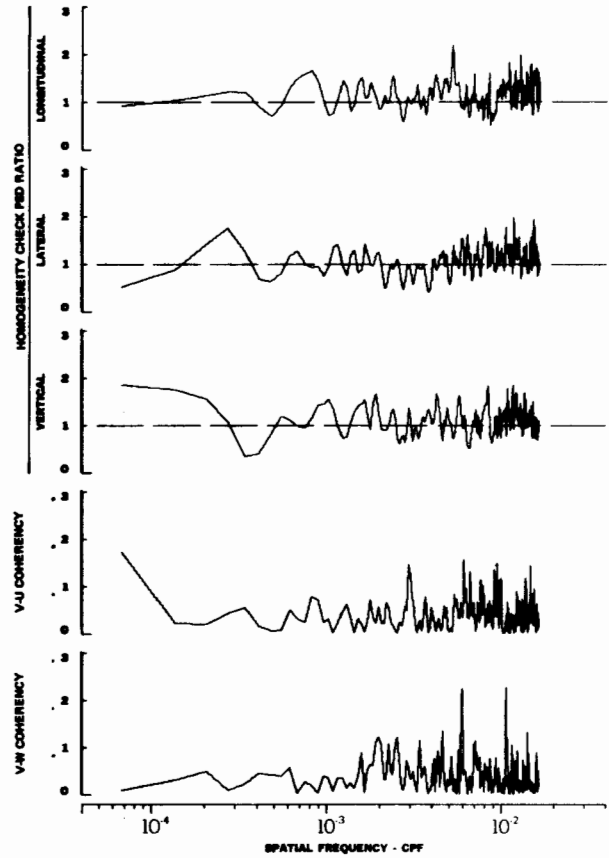
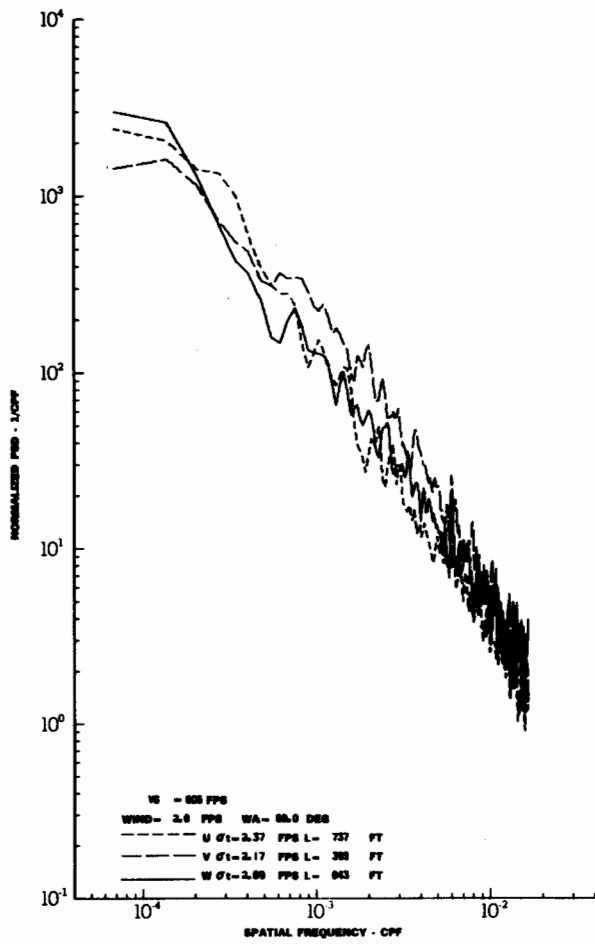


TURBULENCE SPECTRA DATA FOR TEST 135, LEG 7, CATEGORY 312341  
 FIGURE IV-138



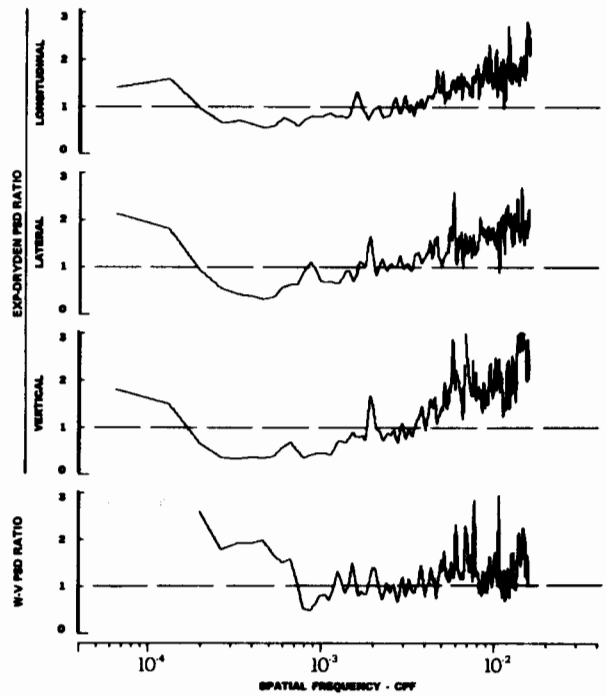
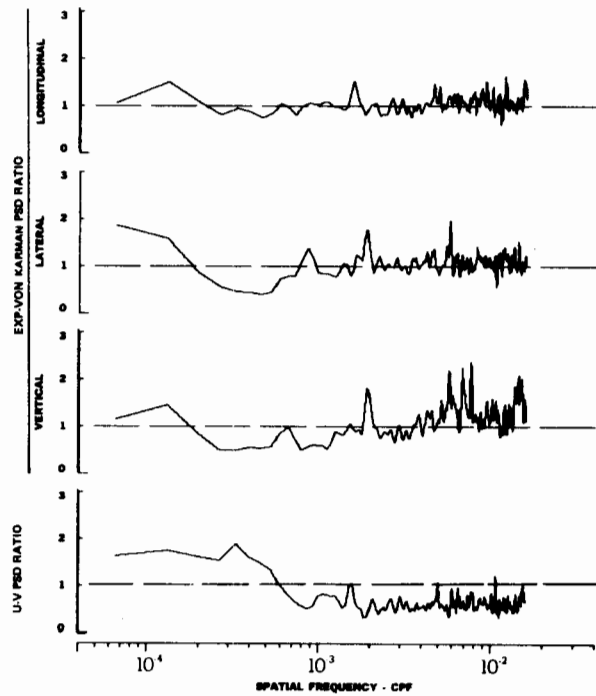
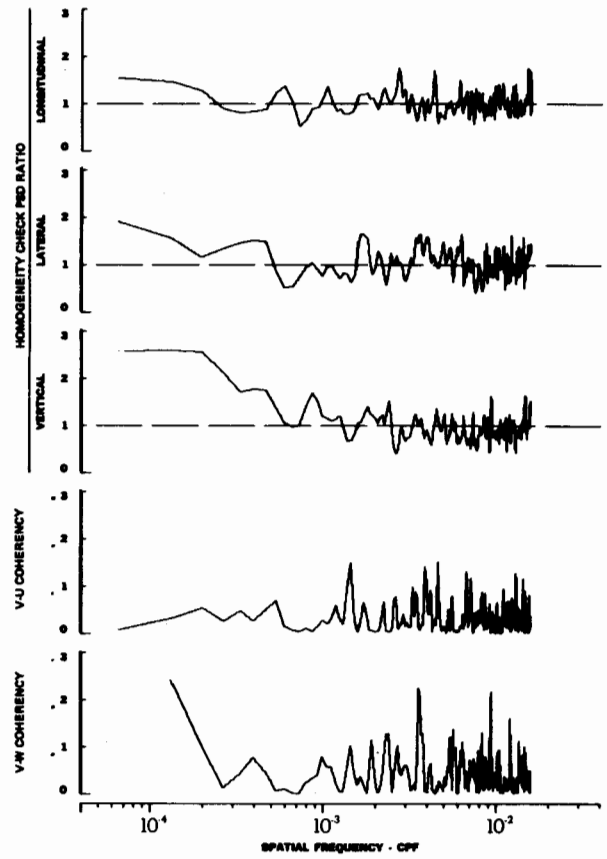
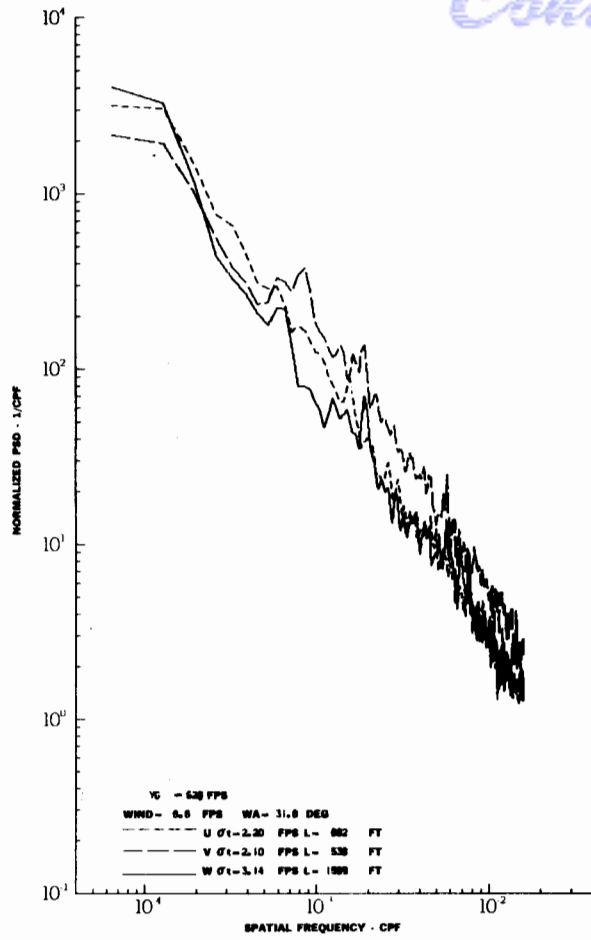
TURBULENCE SPECTRA DATA FOR TEST 141, LEG 1, CATEGORY 223341

FIGURE IV-139



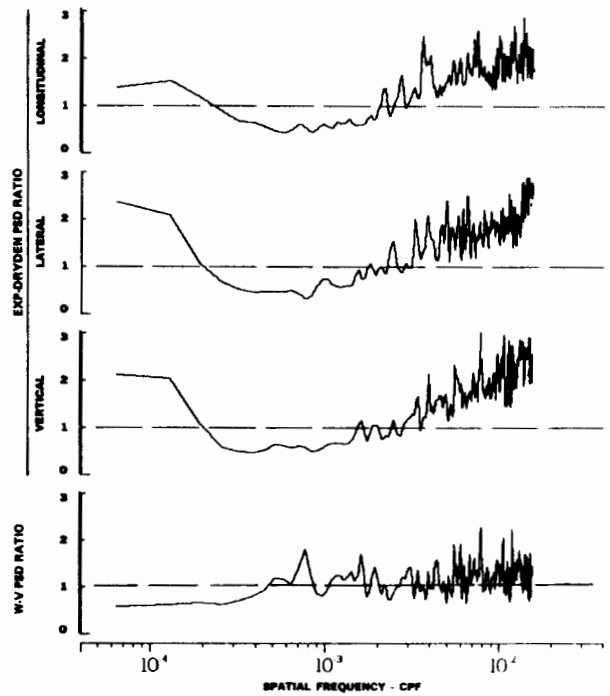
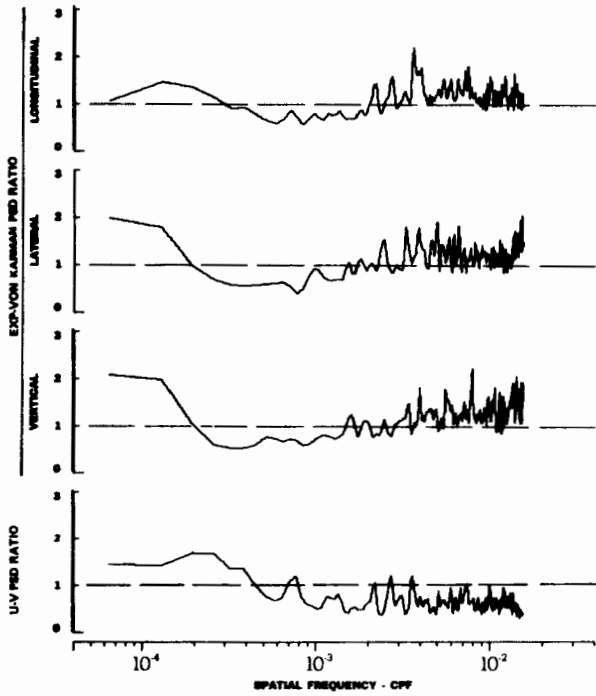
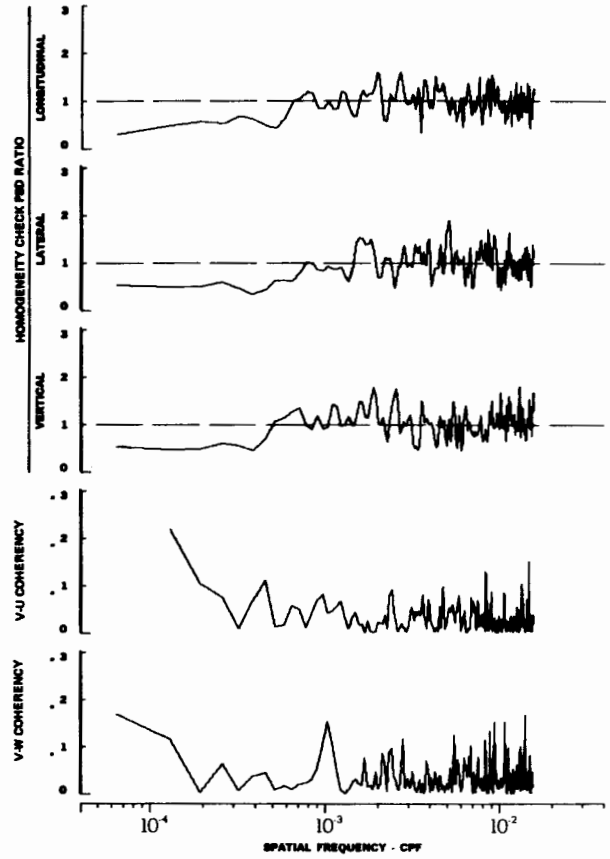
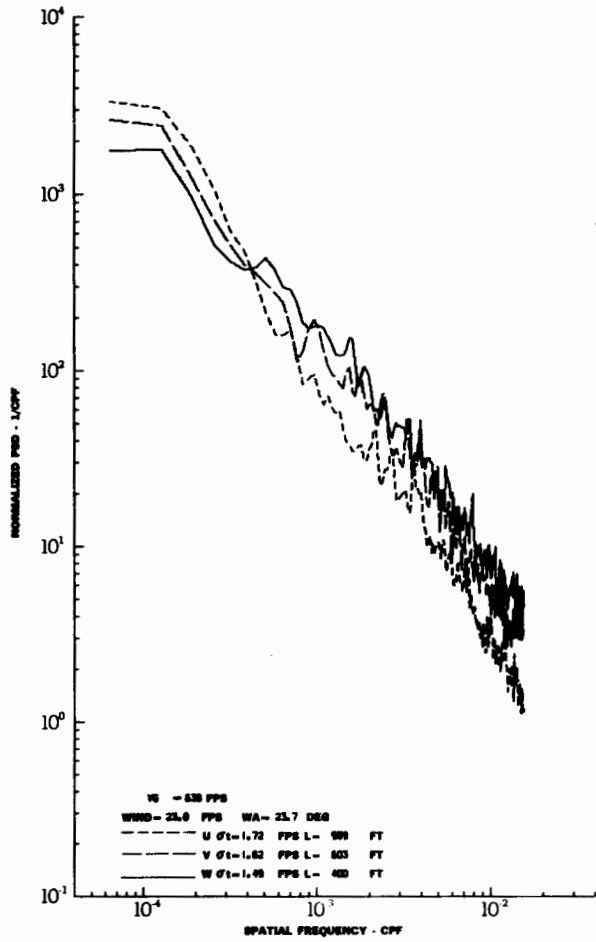
TURBULENCE SPECTRA DATA FOR TEST 141, LEG 3, CATEGORY 121341  
 FIGURE IV-140  
 247

# Contrails



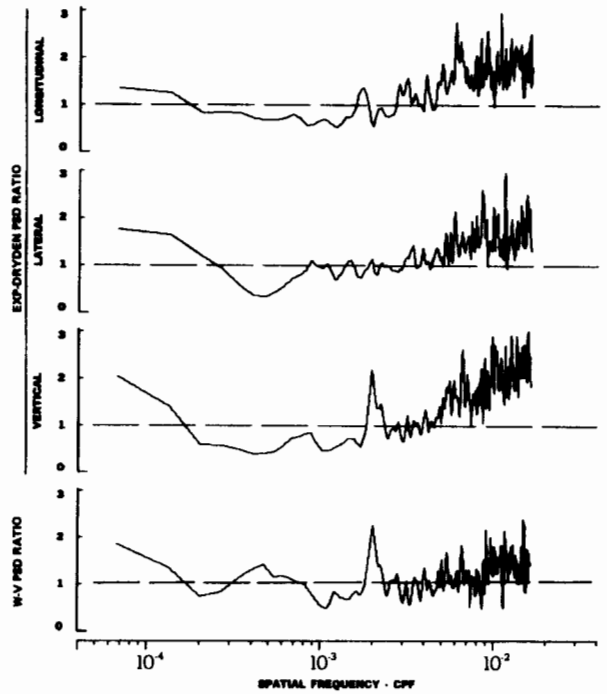
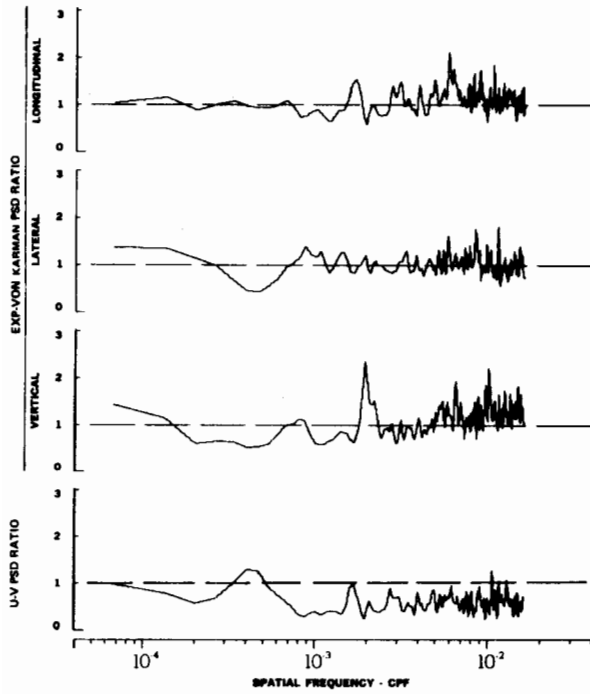
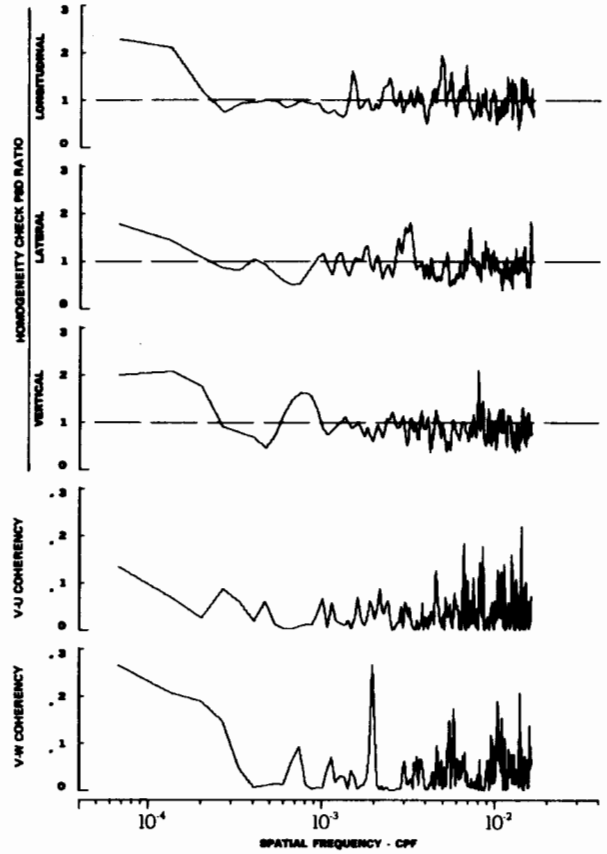
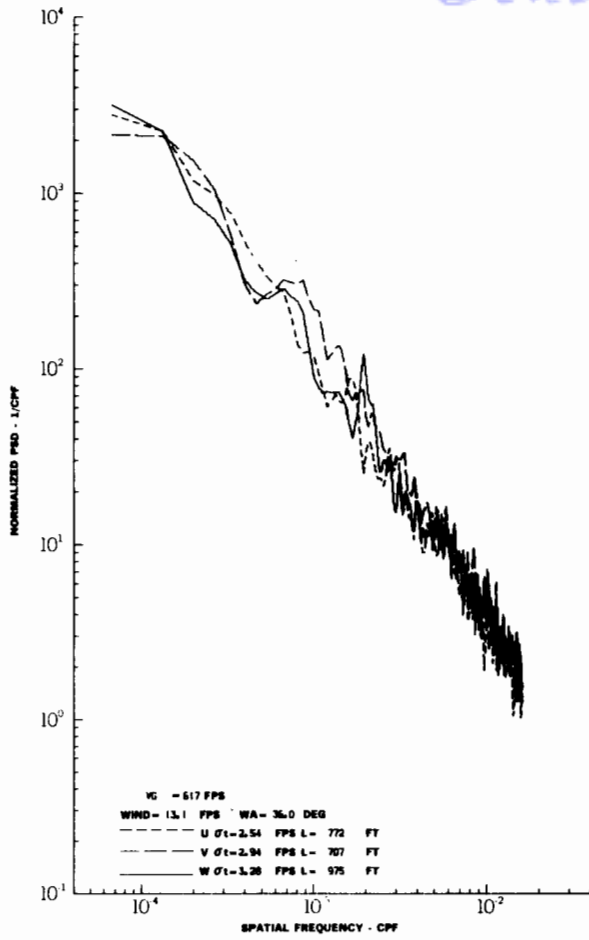
TURBULENCE SPECTRA DATA FOR TEST 141, LEG 5, CATEGORY 123341  
 FIGURE IV-141

# Contrails



TURBULENCE SPECTRA DATA FOR TEST 144, LEG 6, CATEGORY 212341  
 FIGURE IV-142

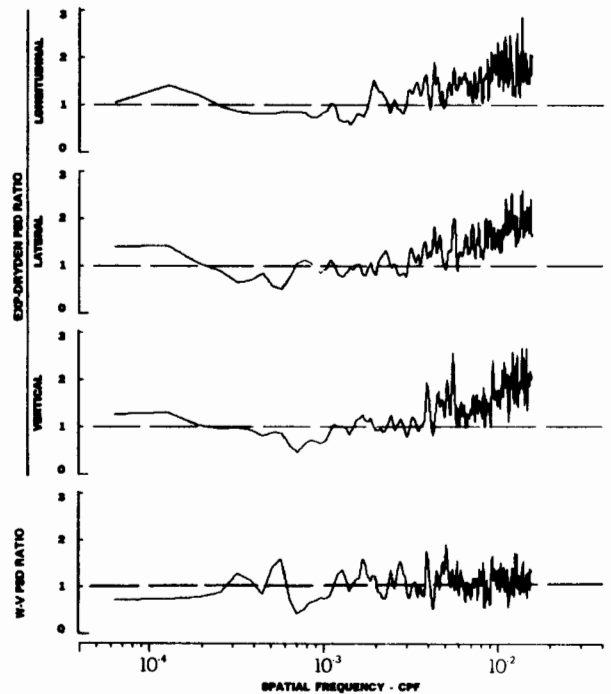
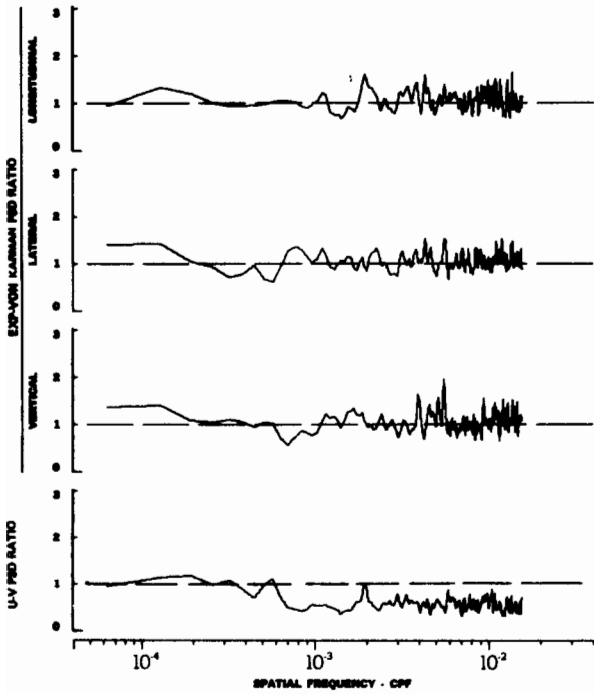
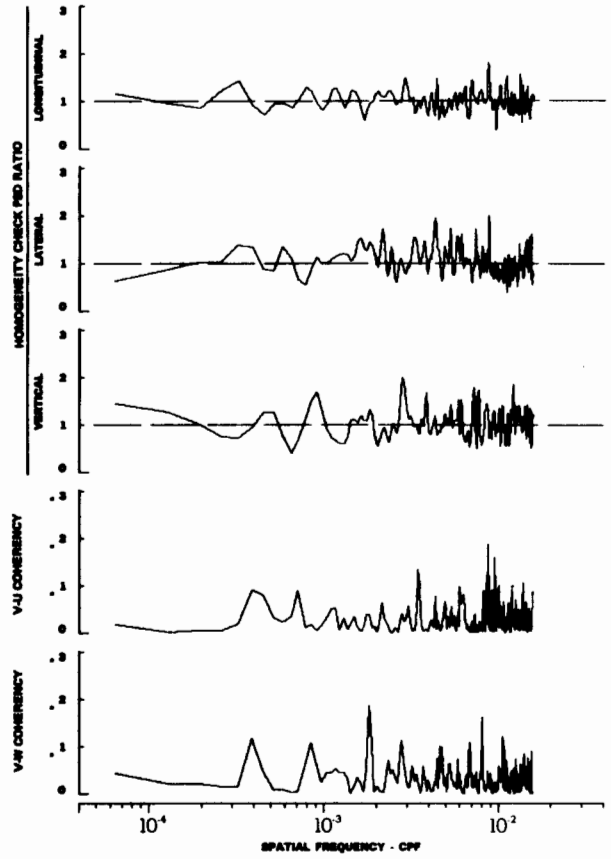
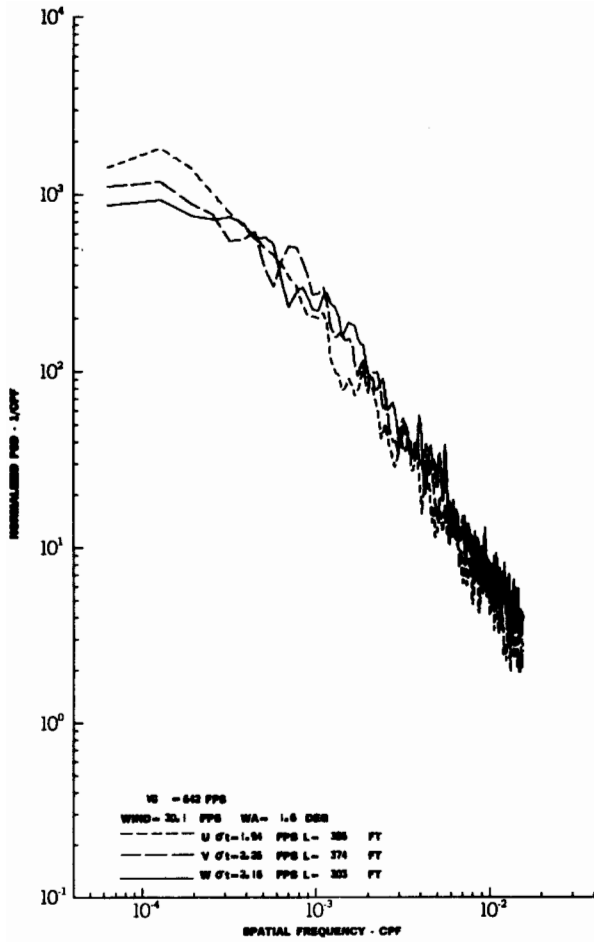
# Contrails



TURBULENCE SPECTRA DATA FOR TEST 147, LEG 5, CATEGORY 122341

FIGURE IV-143

# Contrails



TURBULENCE SPECTRA DATA FOR TEST 150, LEG 6, CATEGORY 214341  
 FIGURE IV-144



APPENDIX V

GUST VELOCITY PEAK, AMPLITUDE, AND LEVEL CROSSING COUNT DATA

Cumulative distribution and cumulative probability of gust velocities for the primary geophysical categories are shown in Figures V-1 through V-24. The category number, which is defined in Appendix IV of this report, is given on each figure. Zeros in the category number indicate that all numbers in that column have been combined. Therefore, category number 000000 indicates that all data available have been combined. All three components of gust velocity are given on each figure and cumulative miles represented are shown. Five plots are shown for each category presented. These plots are gust velocity cumulative peak distribution, level crossing distribution, amplitude count cumulative probability distribution, peak count cumulative probability distribution, and level crossing probability distribution, in that order.

CUMULATIVE  
MILES  
24676.9  
24267.0  
24267.0

U  
V  
W

CATEGORY 00000

LEVEL CROSSINGS PER STRUT MILE



GUST VELOCITY AMPLITUDE - FPS

GUST VELOCITY LEVEL CROSSING DISTRIBUTION

CUMULATIVE  
MILES  
24676.9  
24267.0  
24267.0

U  
V  
W

CATEGORY 00000

CUMULATIVE PEAKS PER STRUT MILE



GUST VELOCITY AMPLITUDE - FPS

GUST VELOCITY PEAK DISTRIBUTION

Figure V-1 Gust Velocity Peak and Level Crossing Distributions

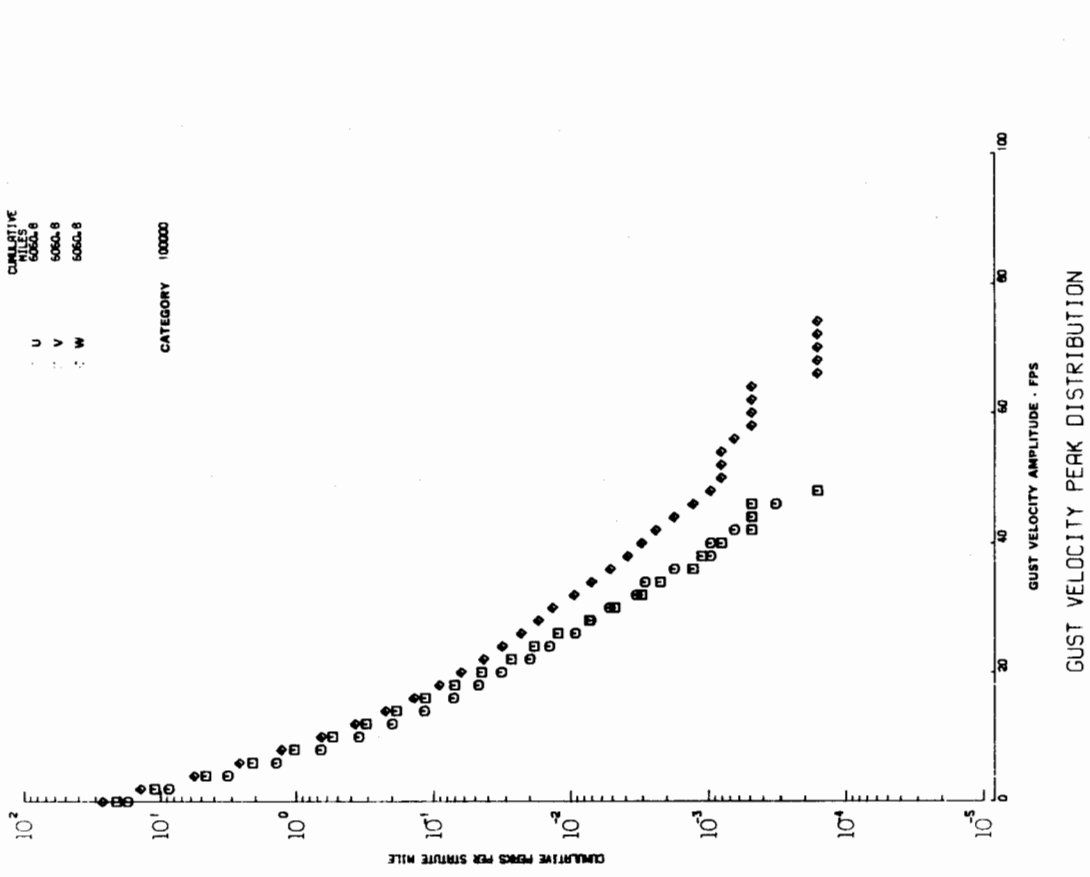
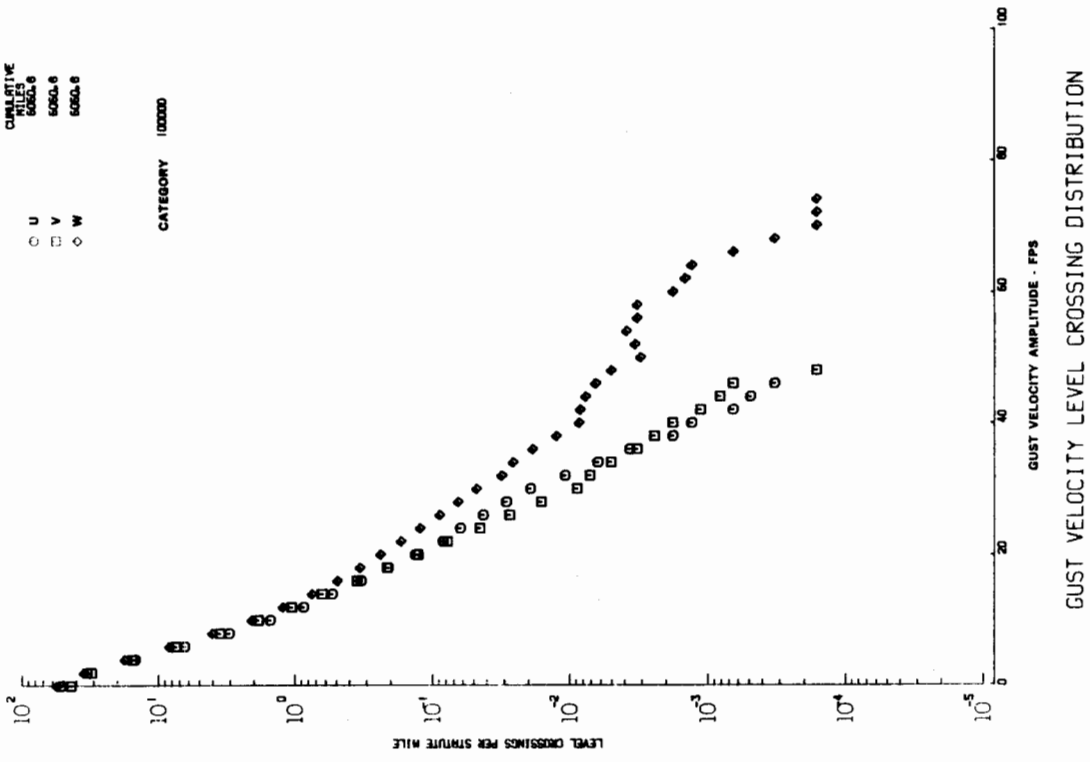


Figure V-2 Gust Velocity Peak and Level Crossing Distributions

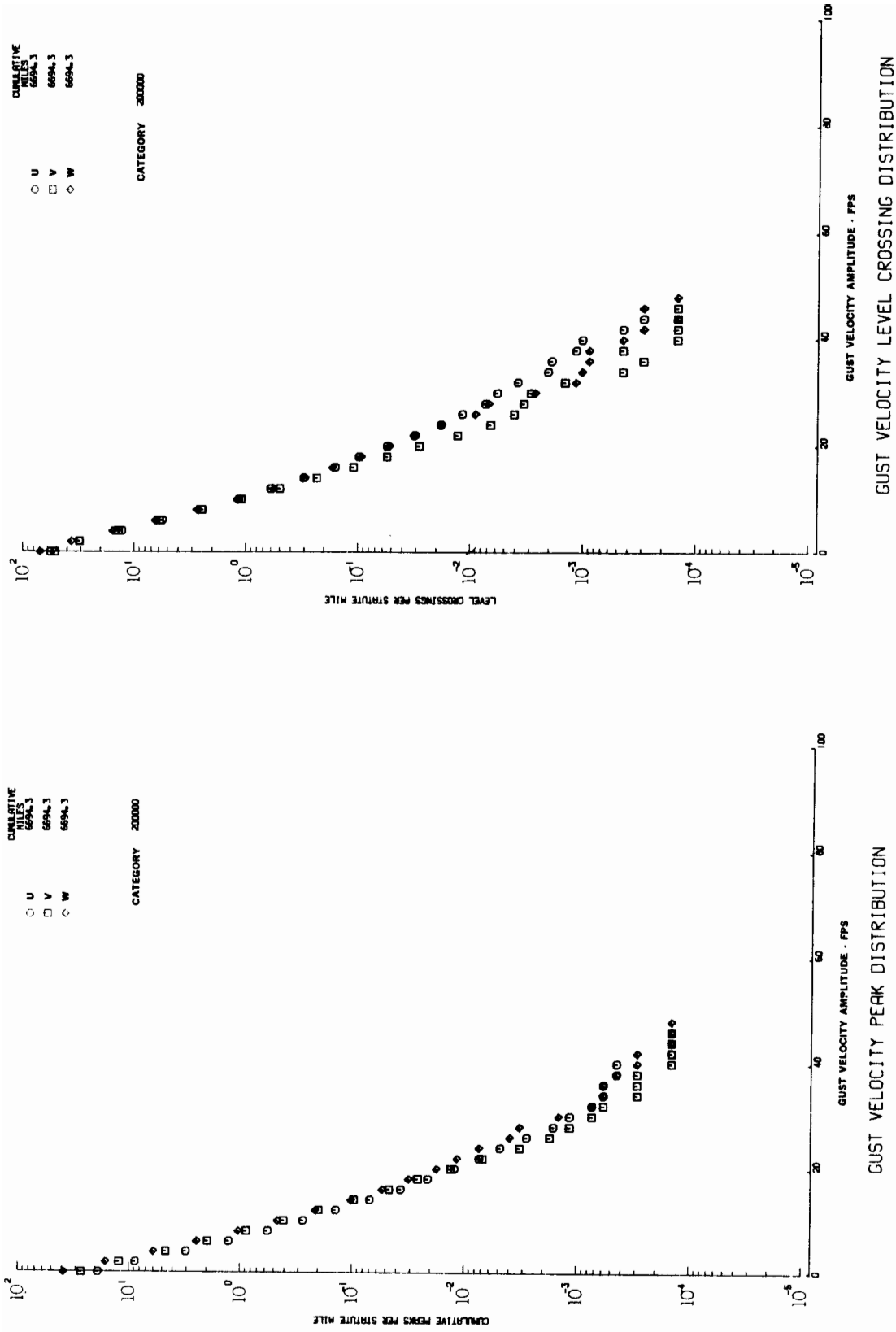


Figure V-3 Gust Velocity Peak and Level Crossing Distributions

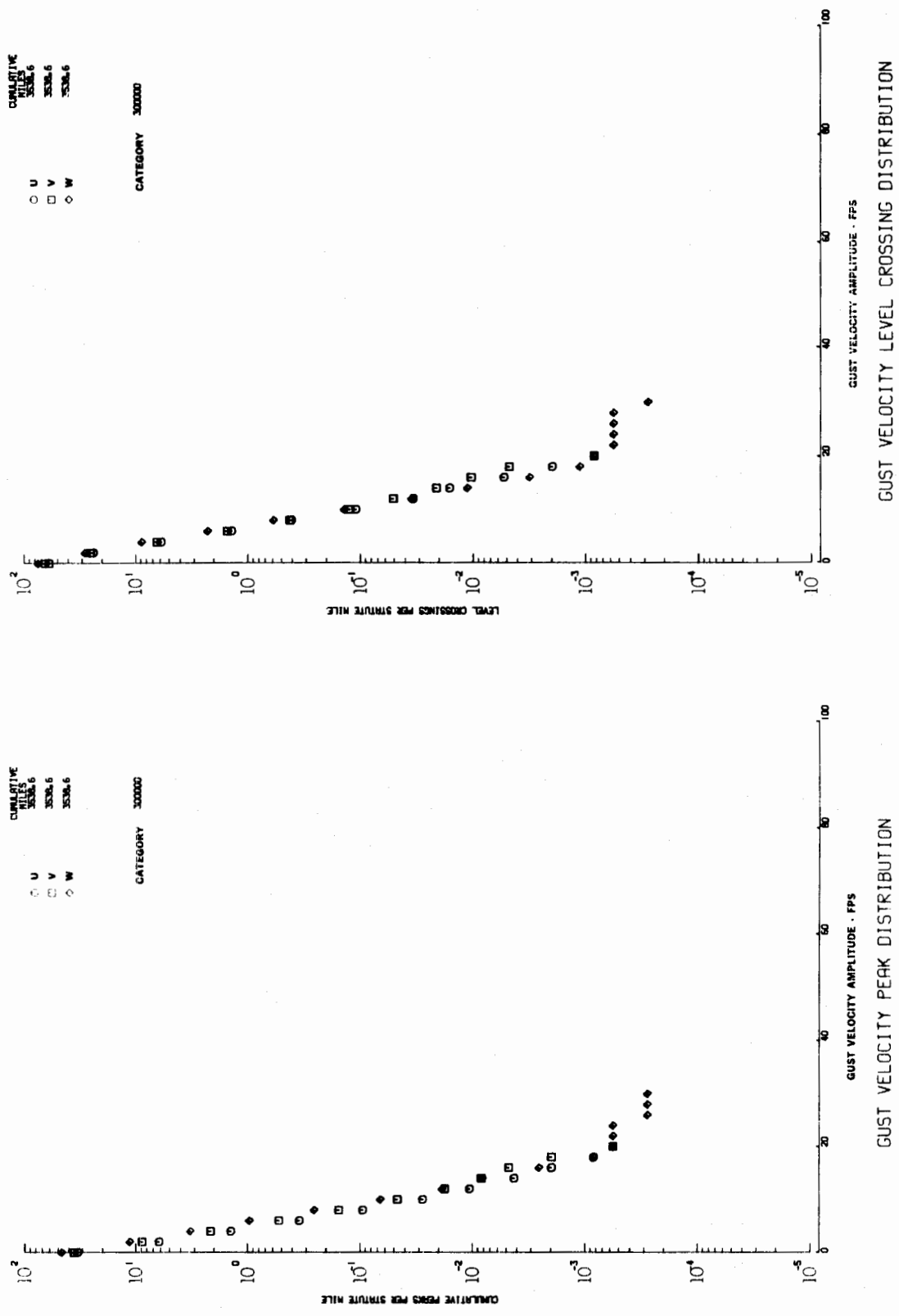


Figure V-4 Gust Velocity Peak and Level Crossing Distributions

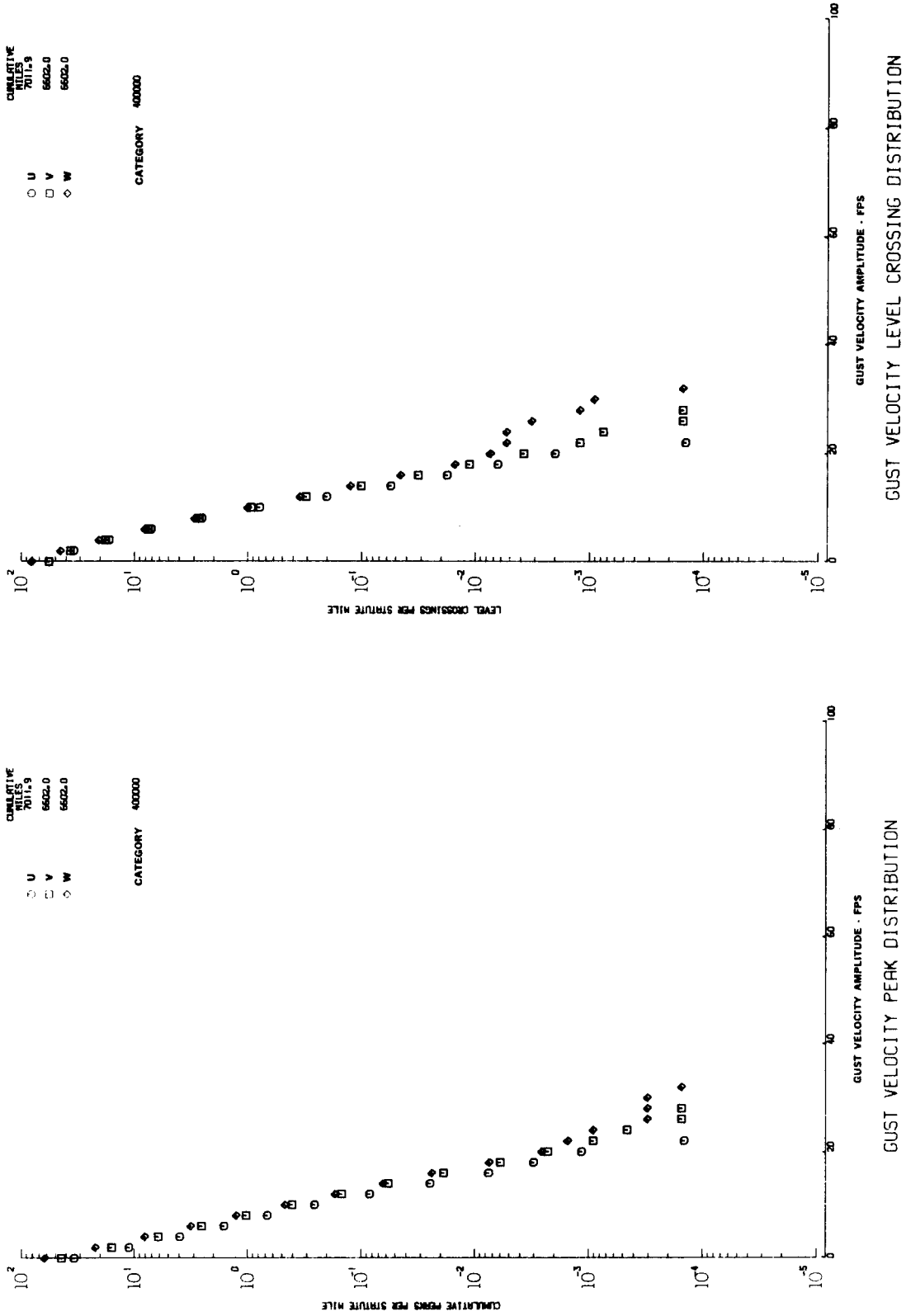


Figure V-5 Gust Velocity Peak and Level Crossing Distributions

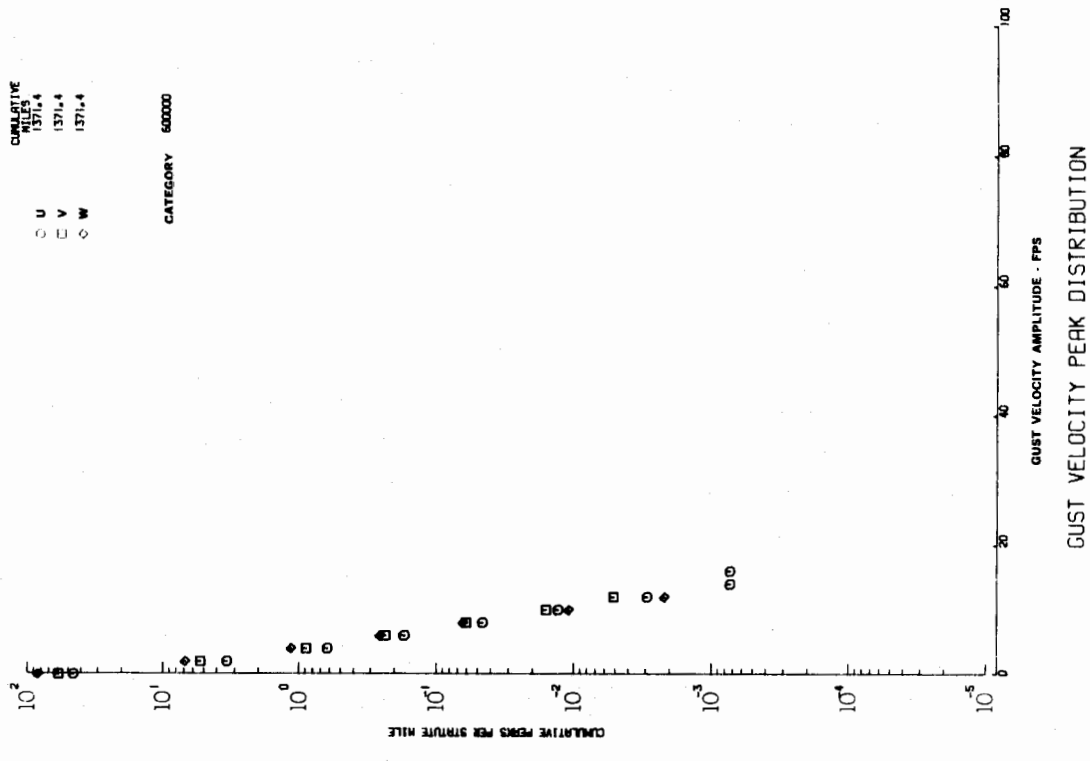
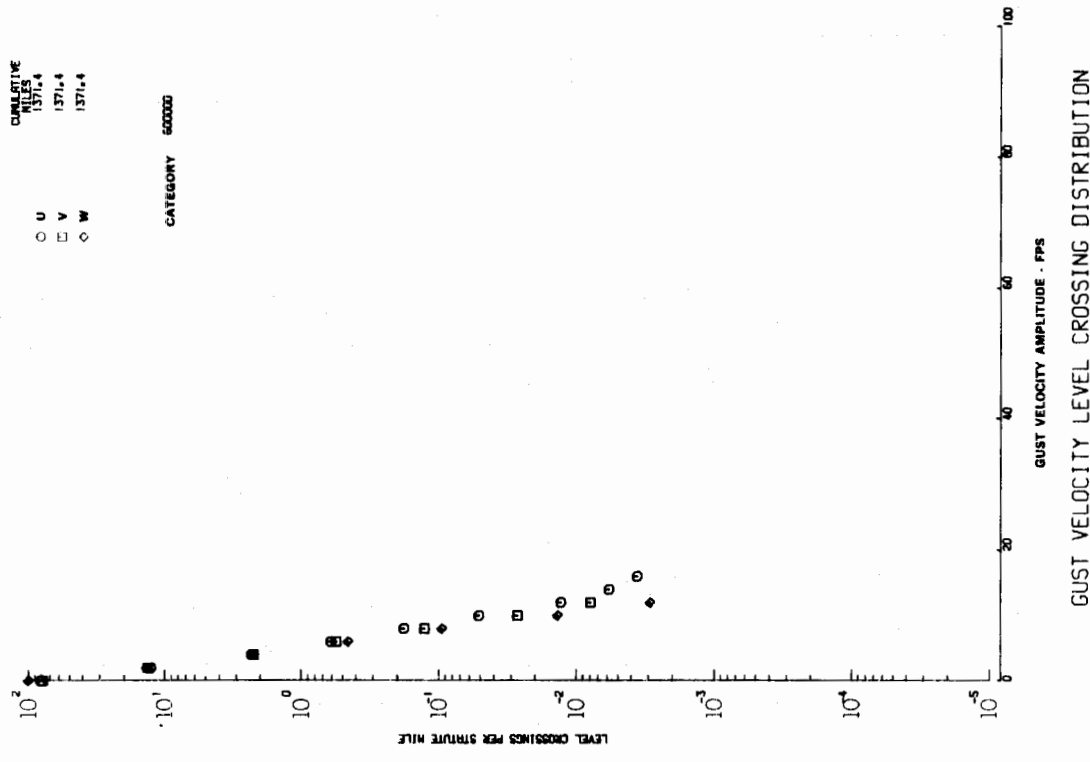


Figure V-6 Gust Velocity Peak and Level Crossing Distributions



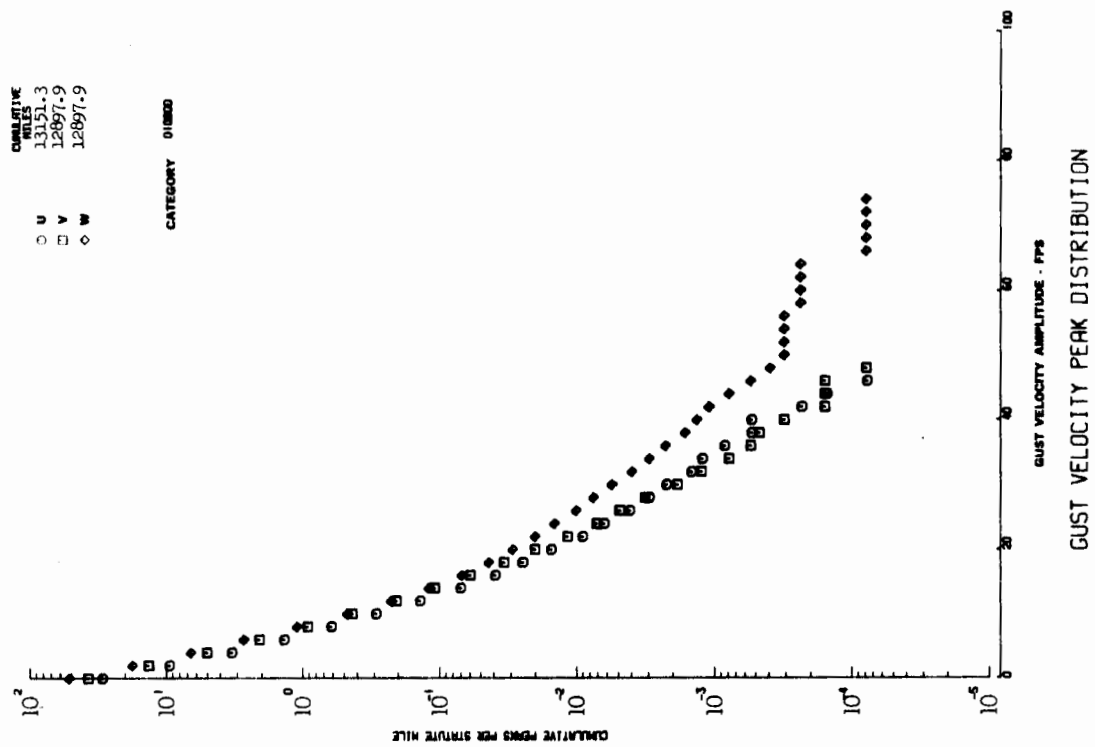
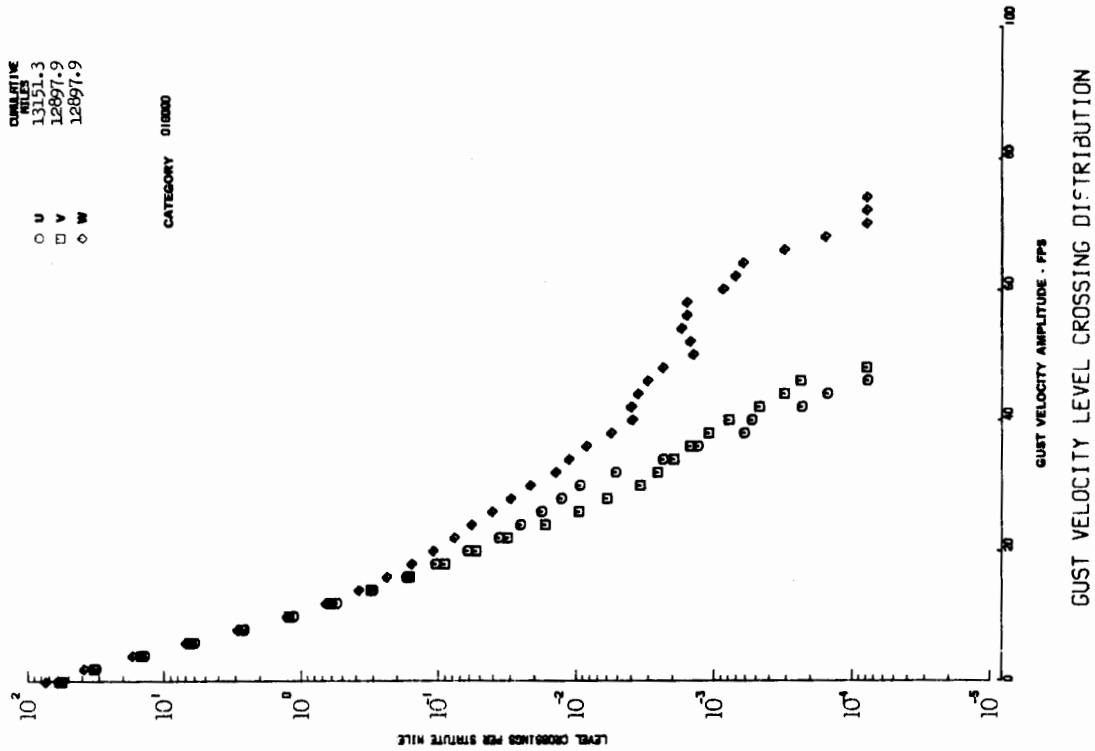


Figure V-7 Gust Velocity Peak and Level Crossing Distributions

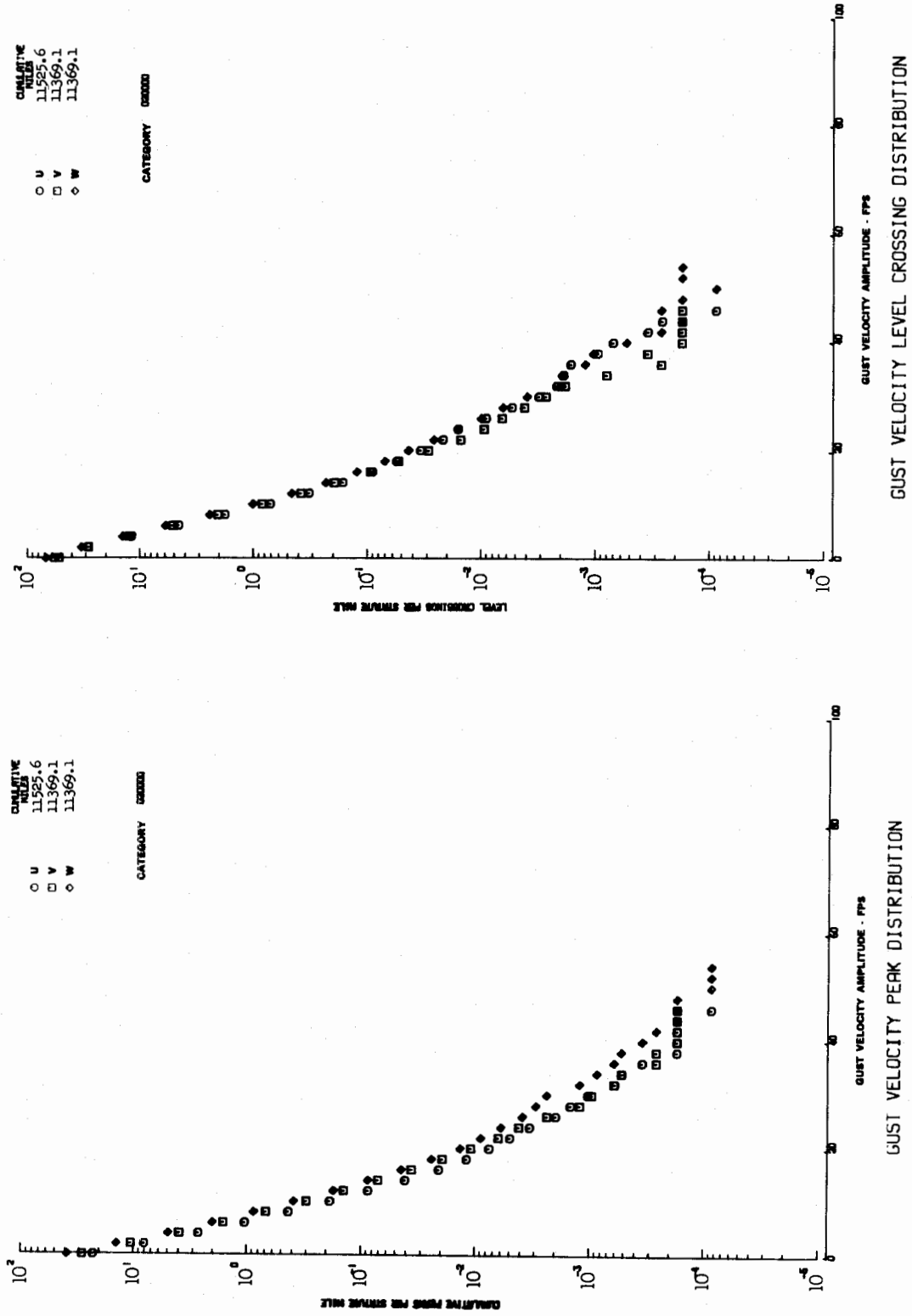
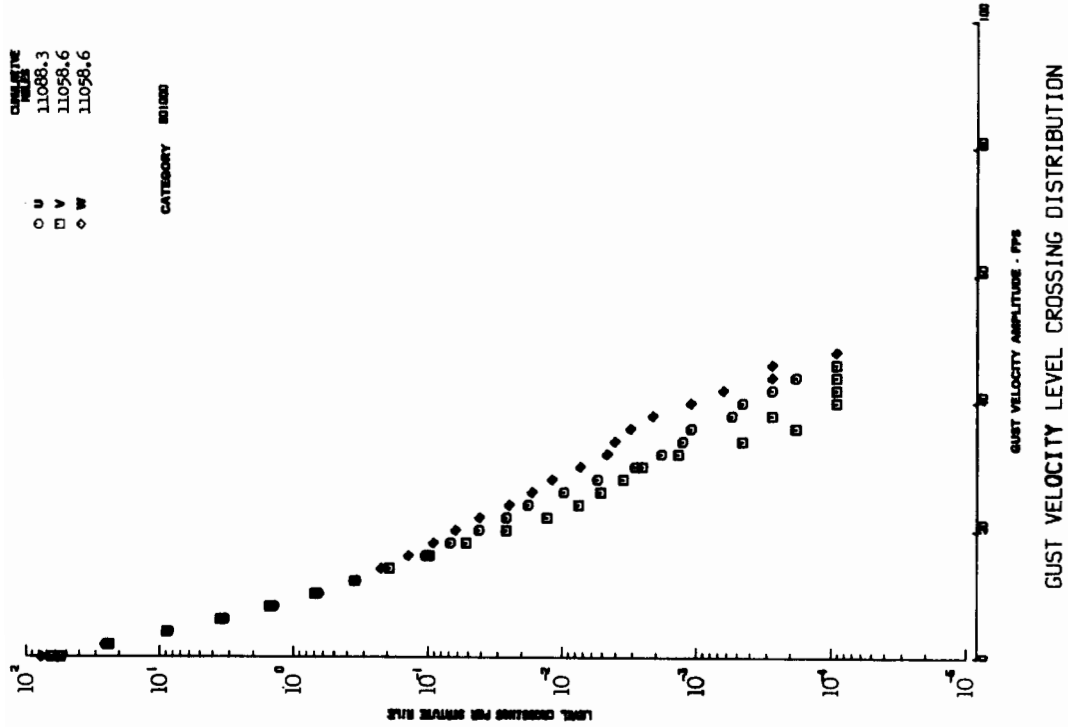
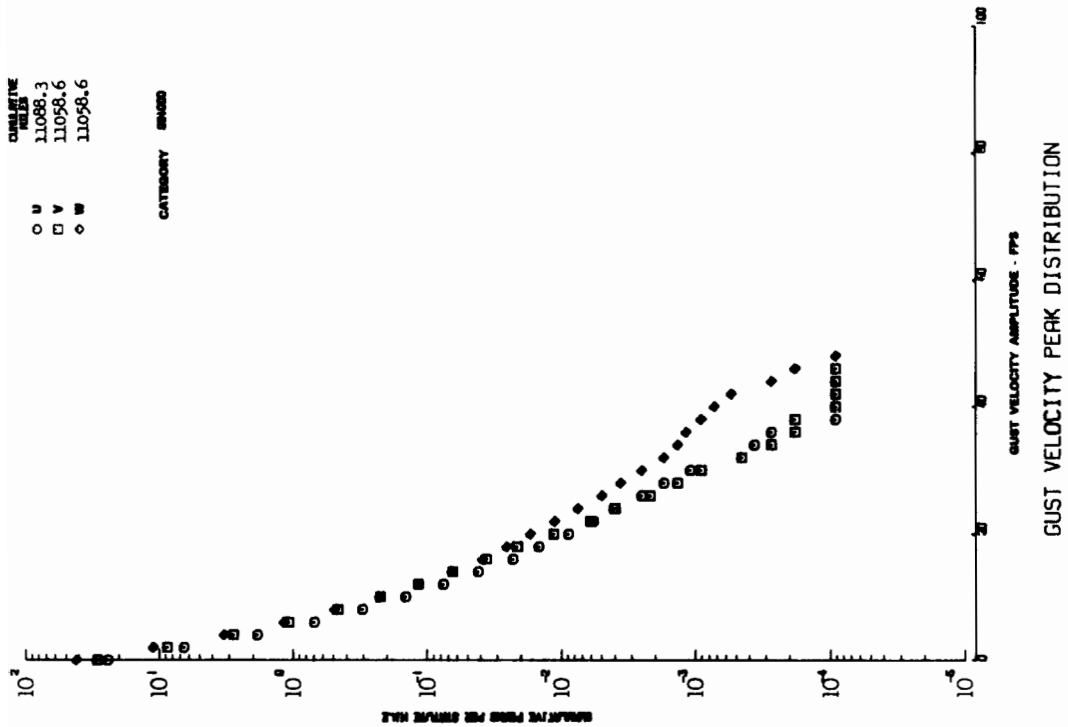


Figure V-8 Gust Velocity Peak and Level Crossing Distributions



GUST VELOCITY LEVEL CROSSING DISTRIBUTION



GUST VELOCITY PEAK DISTRIBUTION

Figure V-9 Gust Velocity Peak and Level Crossing Distributions

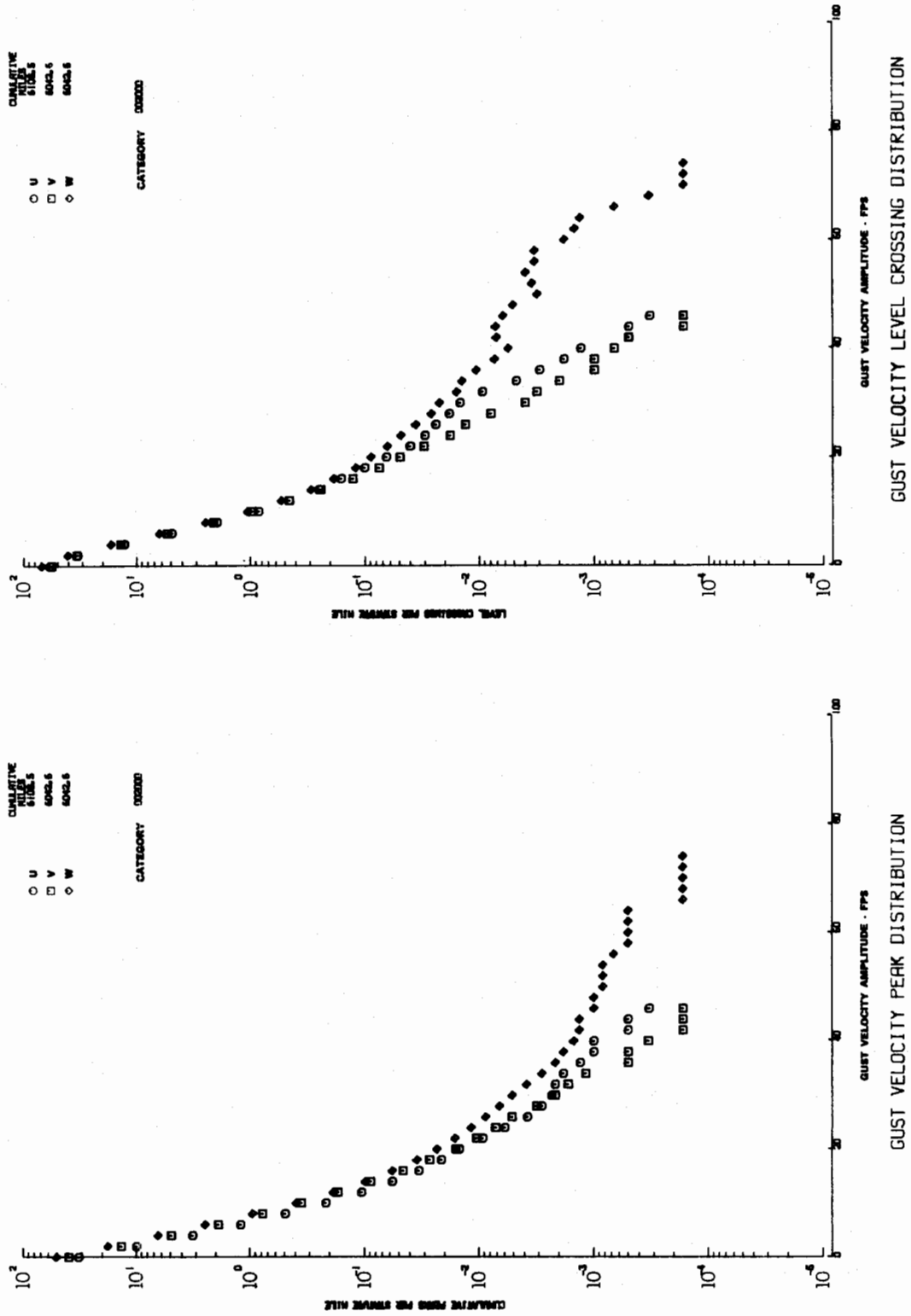


Figure V-10 Gust Velocity Peak and Level Crossing Distributions

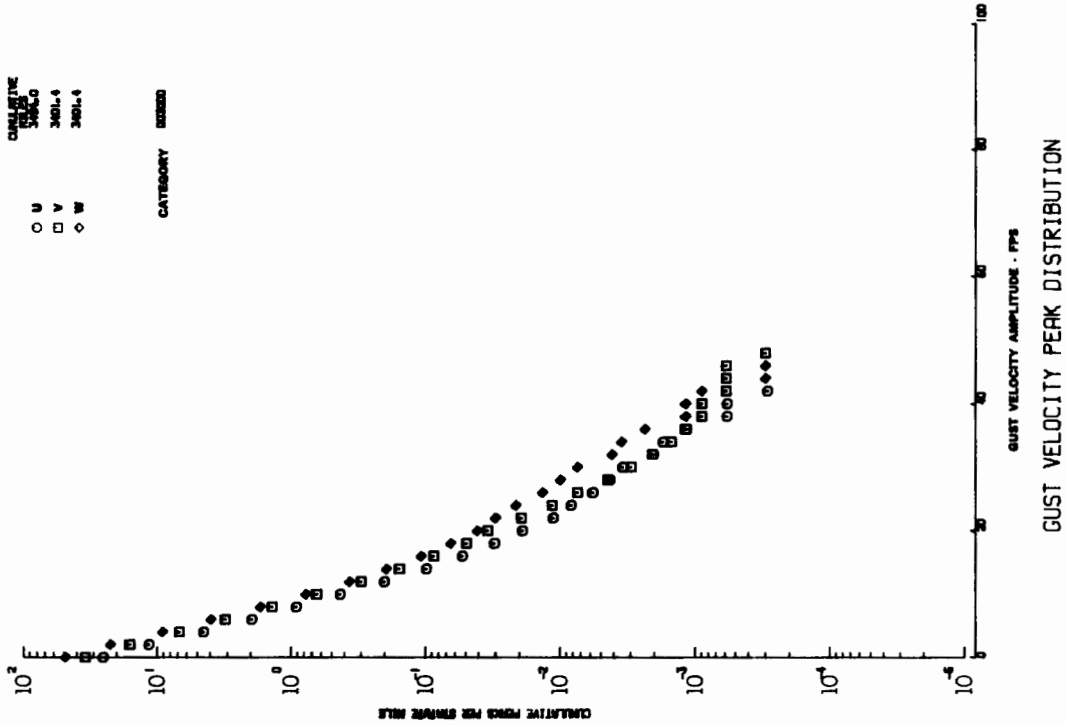
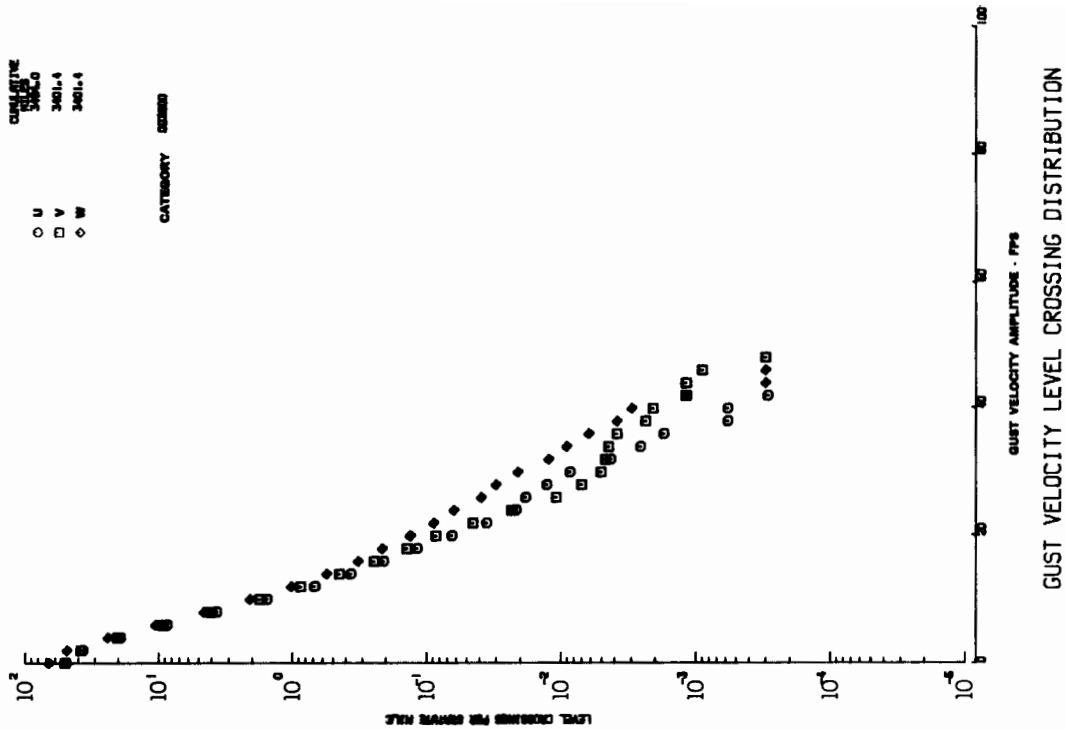


Figure V-11 Gust Velocity Peak and Level Crossing Distributions

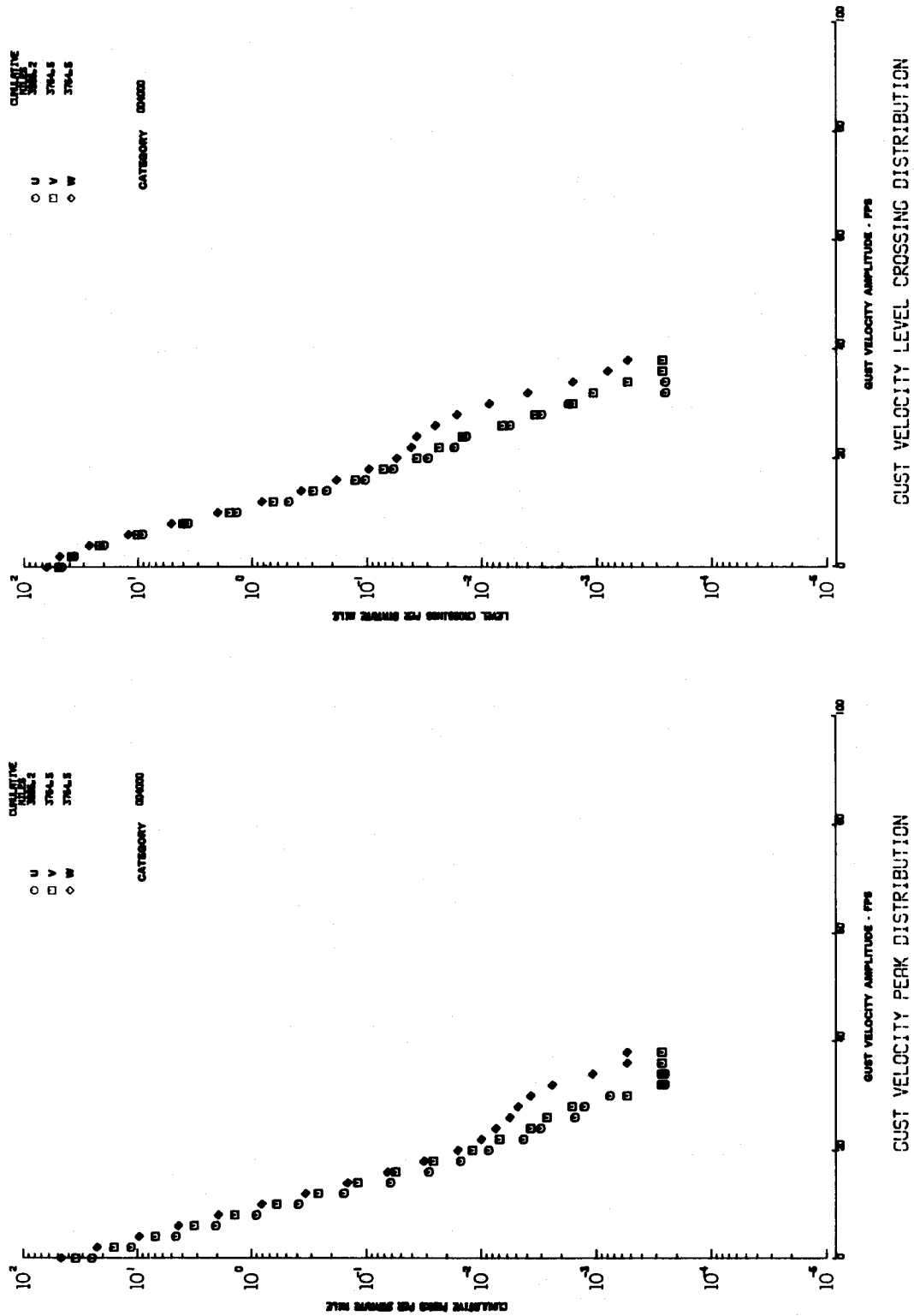


Figure V-12 Gust Velocity Peak and Level Crossing Distributions

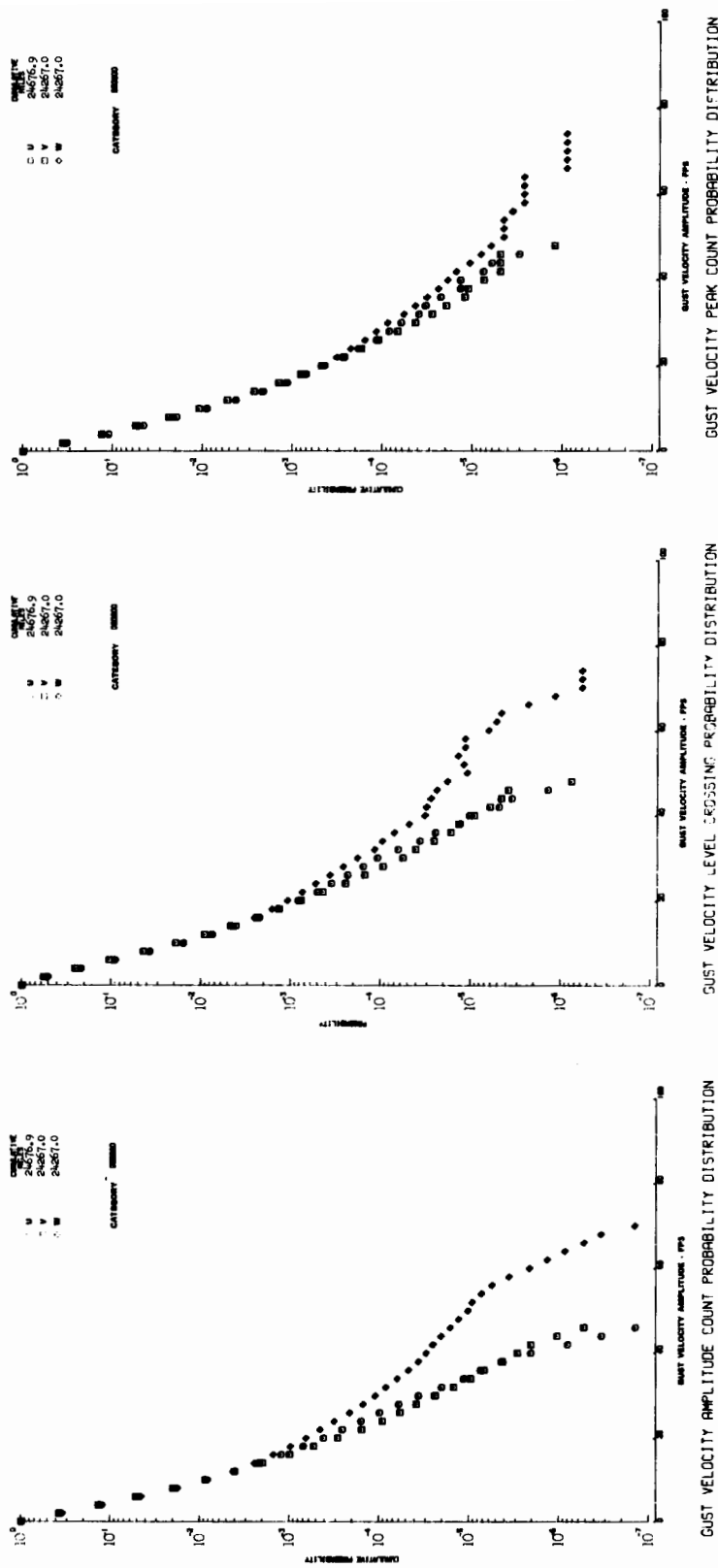


Figure V-13 Gust Velocity Peak, Amplitude and Level Crossing Probability Distributions

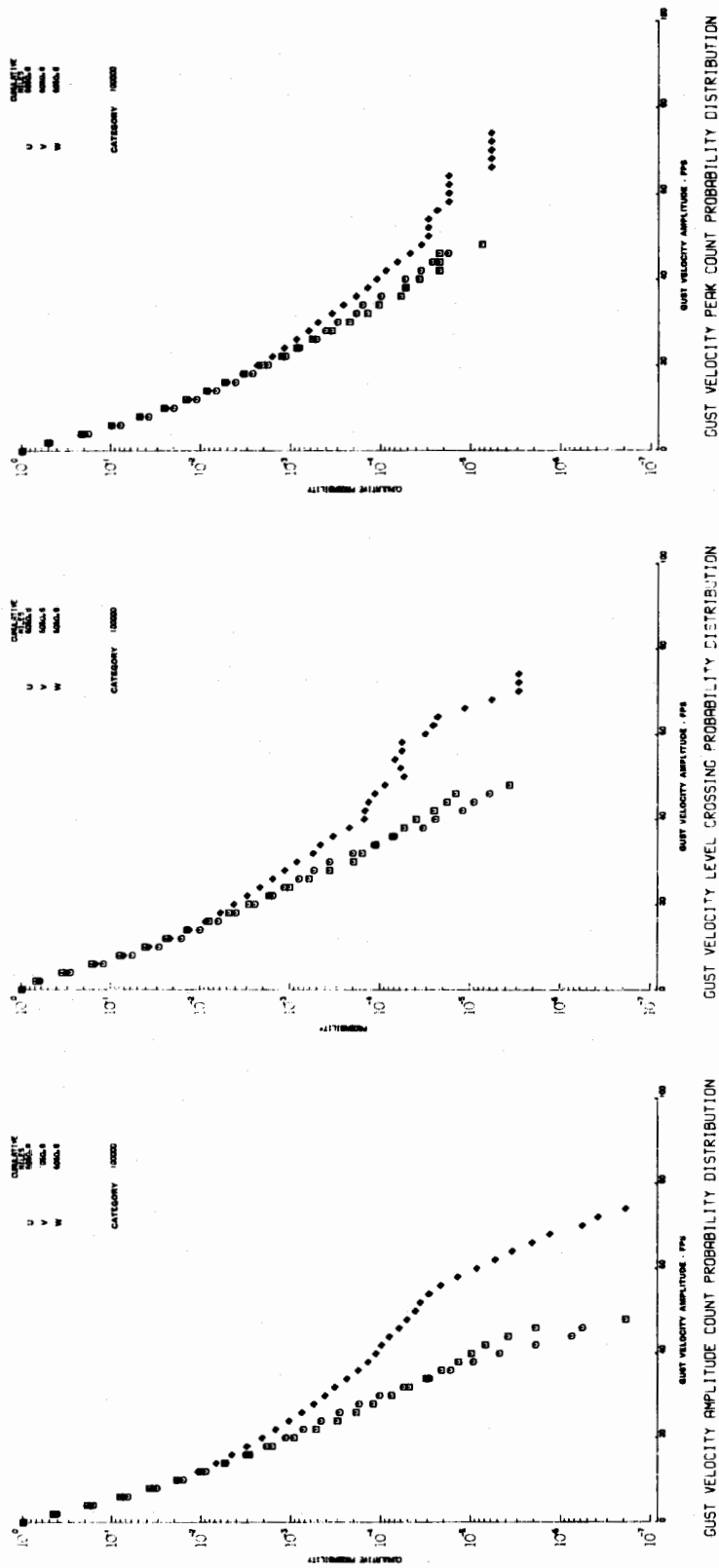


Figure V-14 Gust Velocity Peak, Amplitude and Level Crossing Probability Distributions



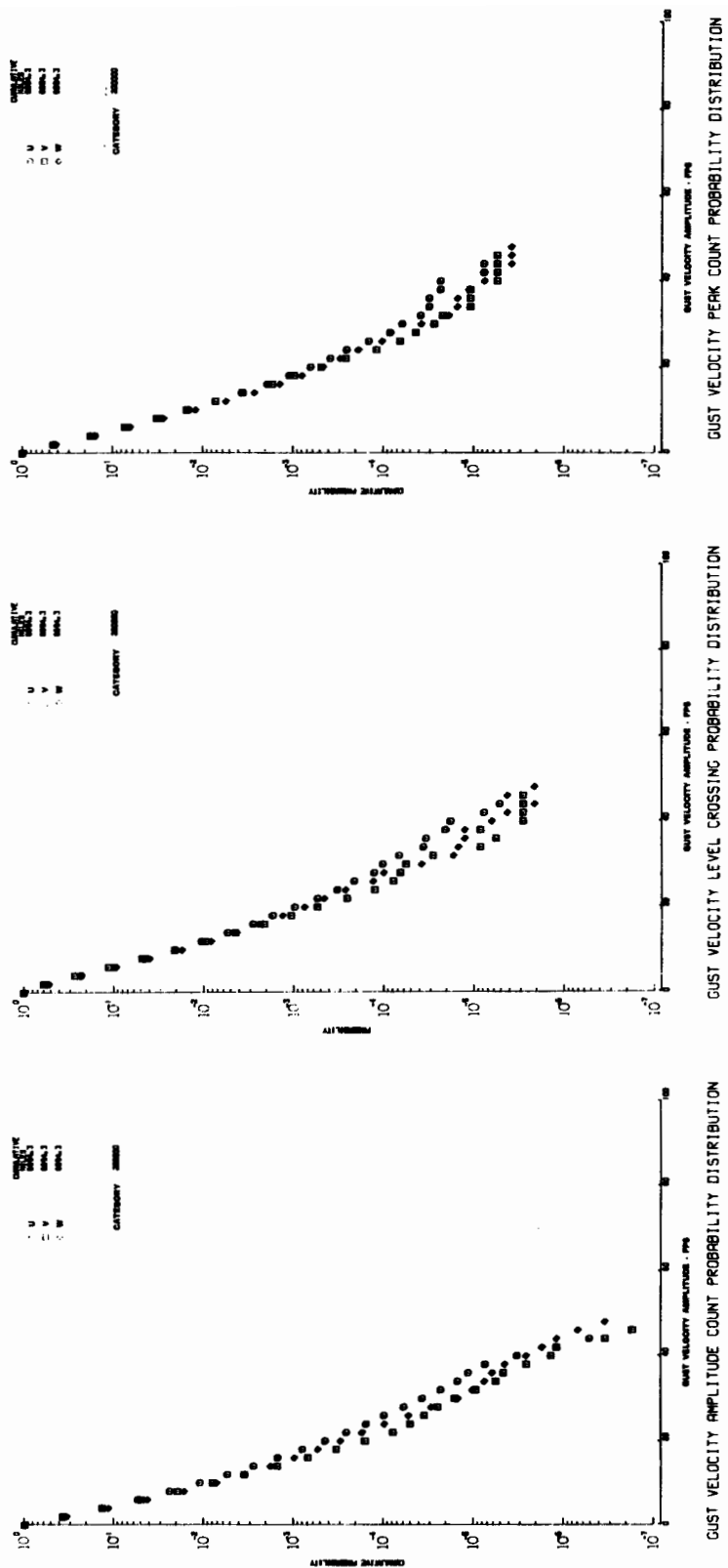


Figure V-15 Gust Velocity Peak, Amplitude and Level Crossing Probability Distributions

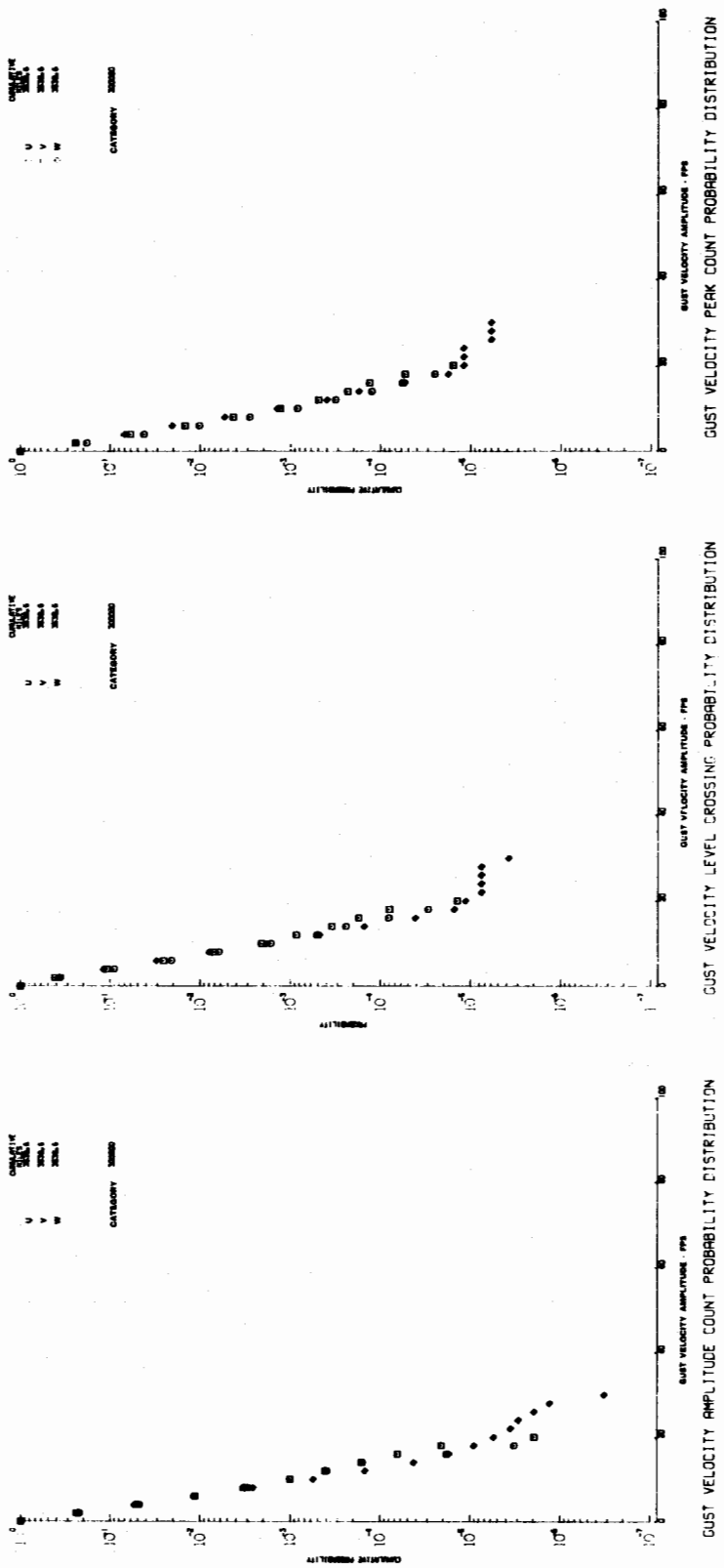


Figure V-16 Gust Velocity Peak, Amplitude and Level Crossing Probability Distributions

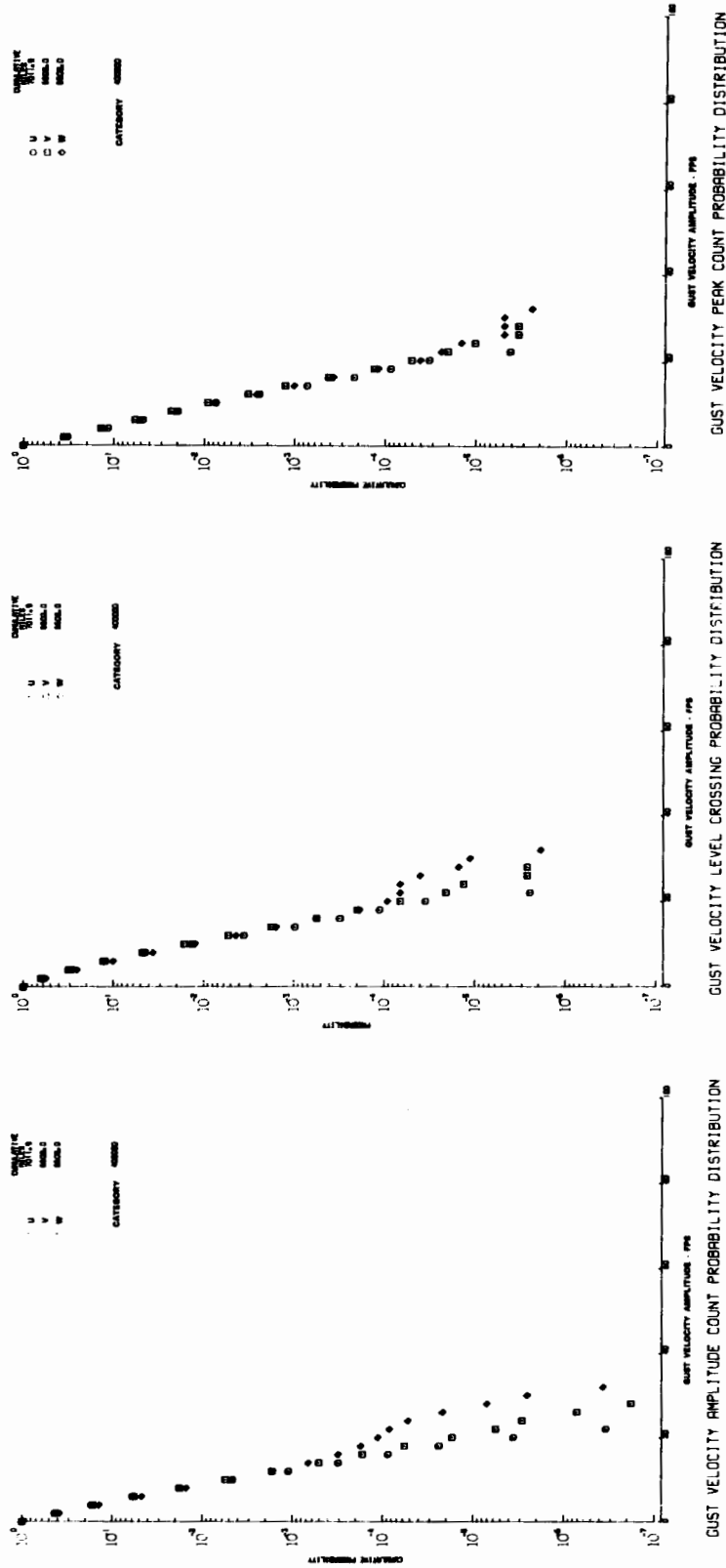


Figure V-17 Gust Velocity Peak, Amplitude and Level Crossing Probability Distributions

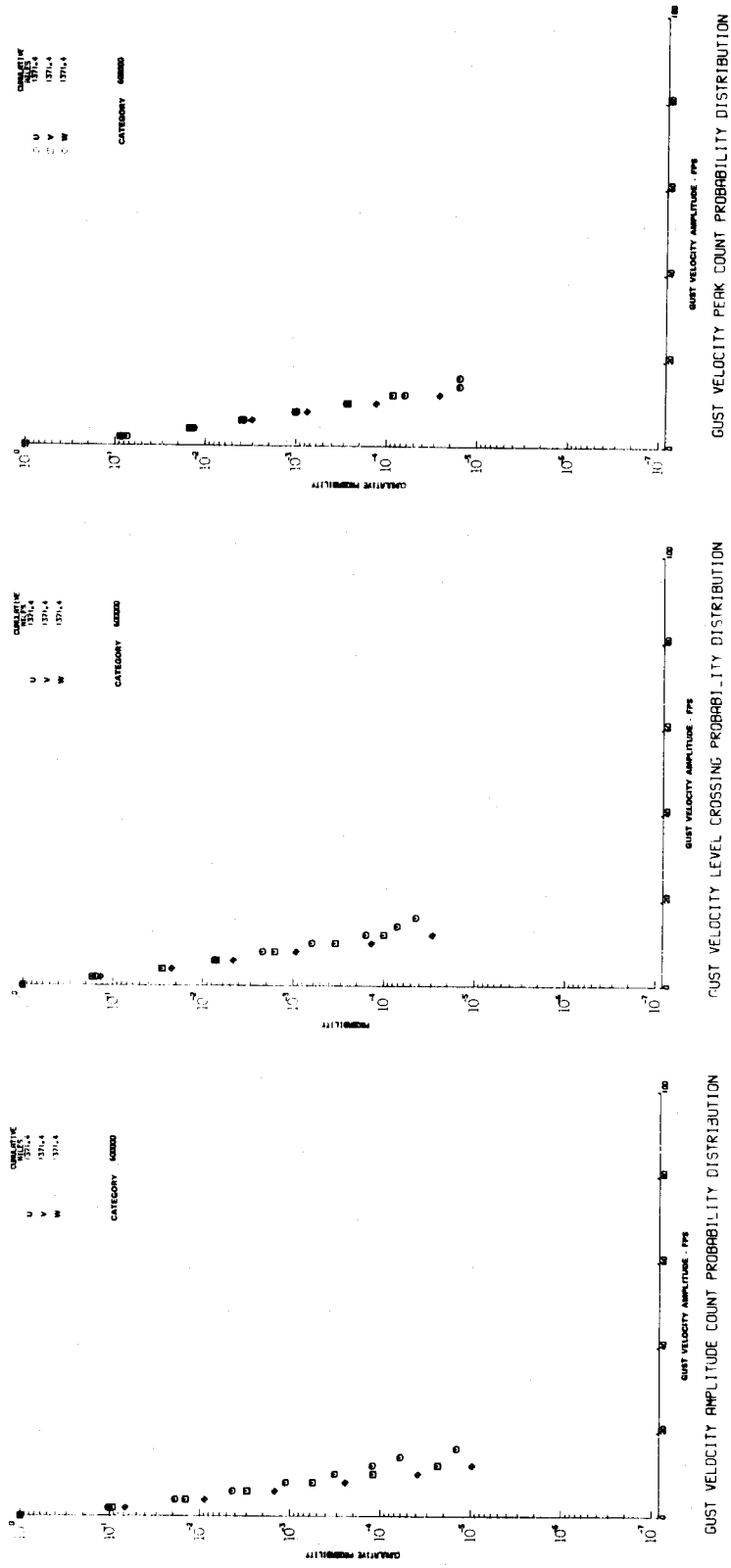


Figure V-18 Gust Velocity Peak, Amplitude and Level Crossing Probability Distributions

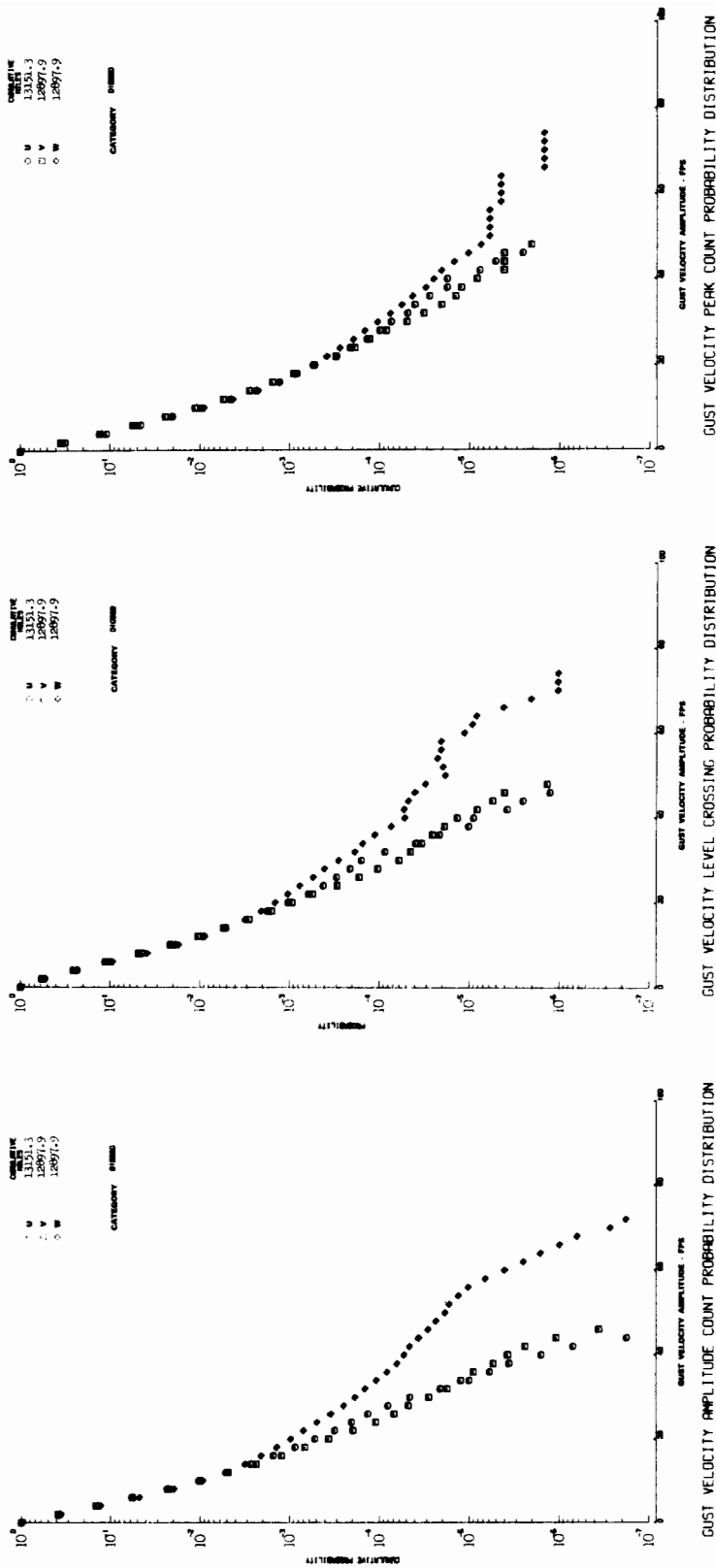


Figure V-19 Gust Velocity Peak, Amplitude and Level Crossing Probability Distributions

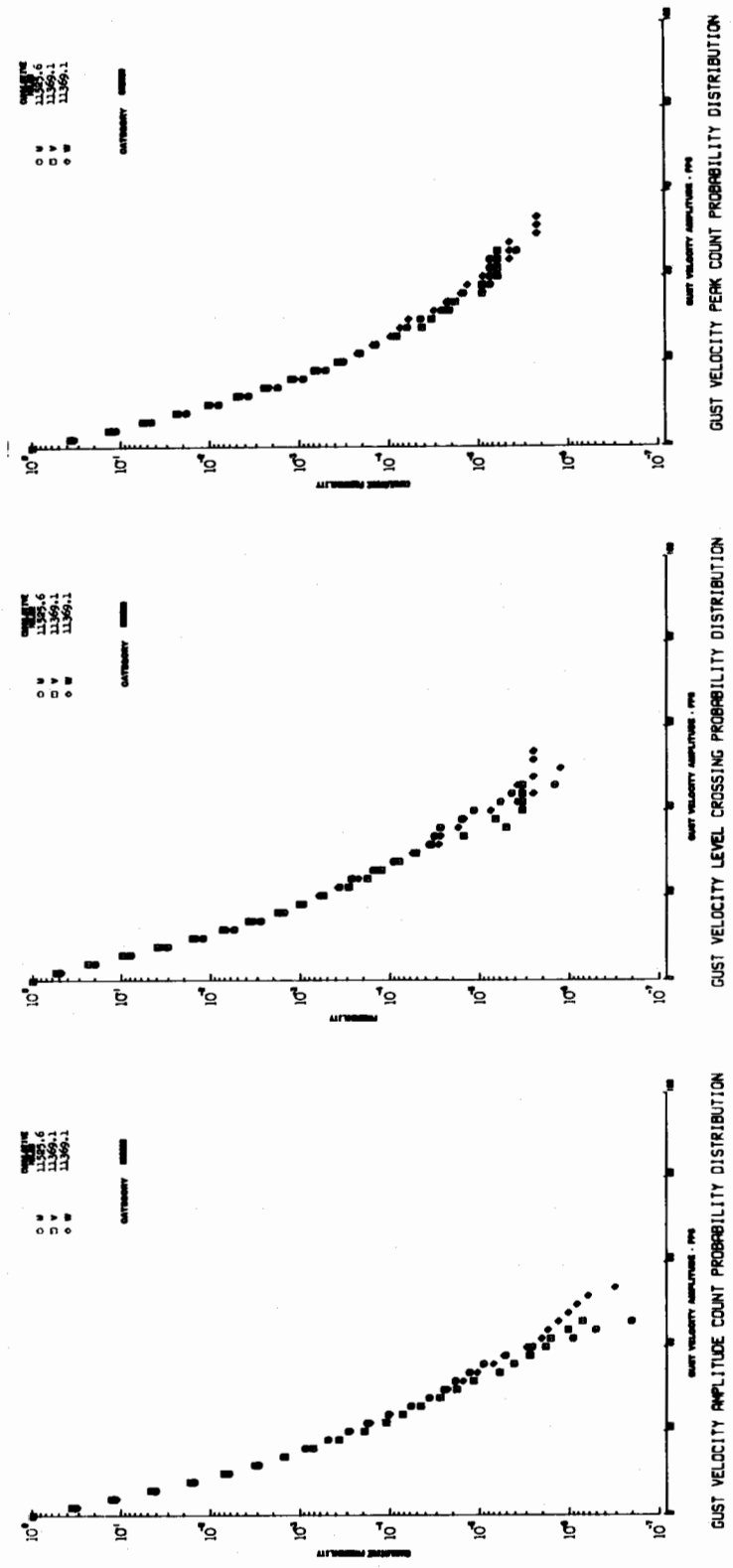


Figure V-20 Gust Velocity Peak, Amplitude and Level Crossing Probability Distributions

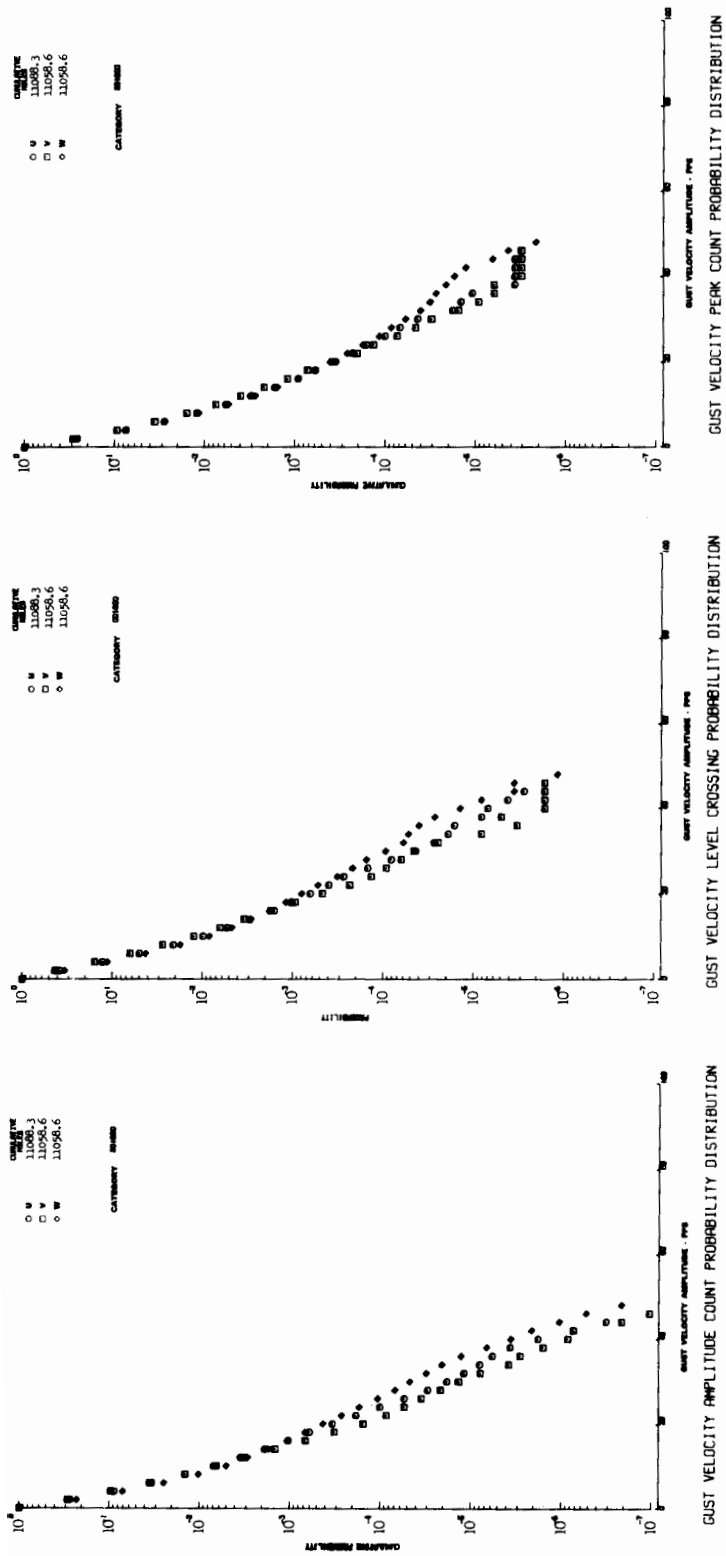


Figure V-21 Gust Velocity Peak, Amplitude and Level Crossing Probability Distributions

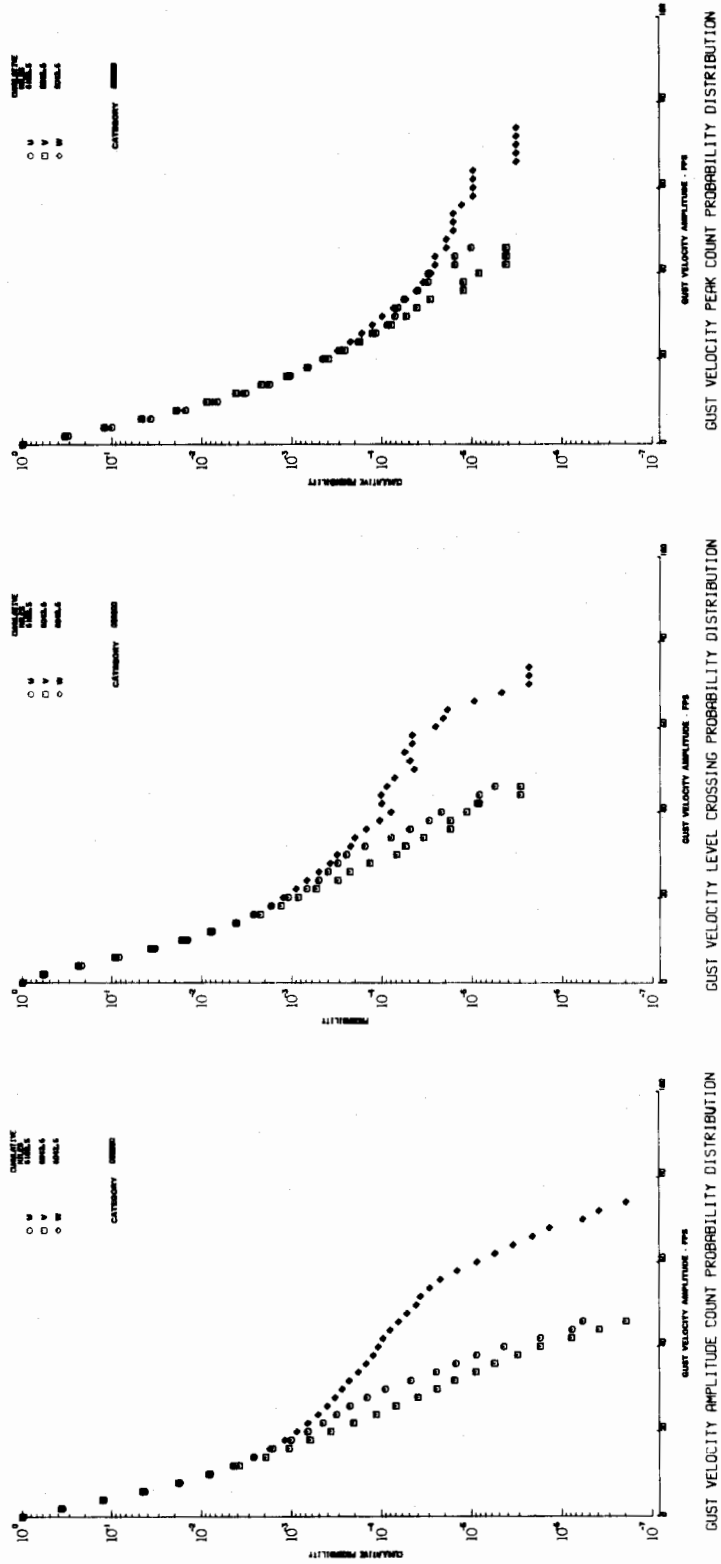


Figure V-22 Gust Velocity Peak, Amplitude and Level Crossing Probability Distributions



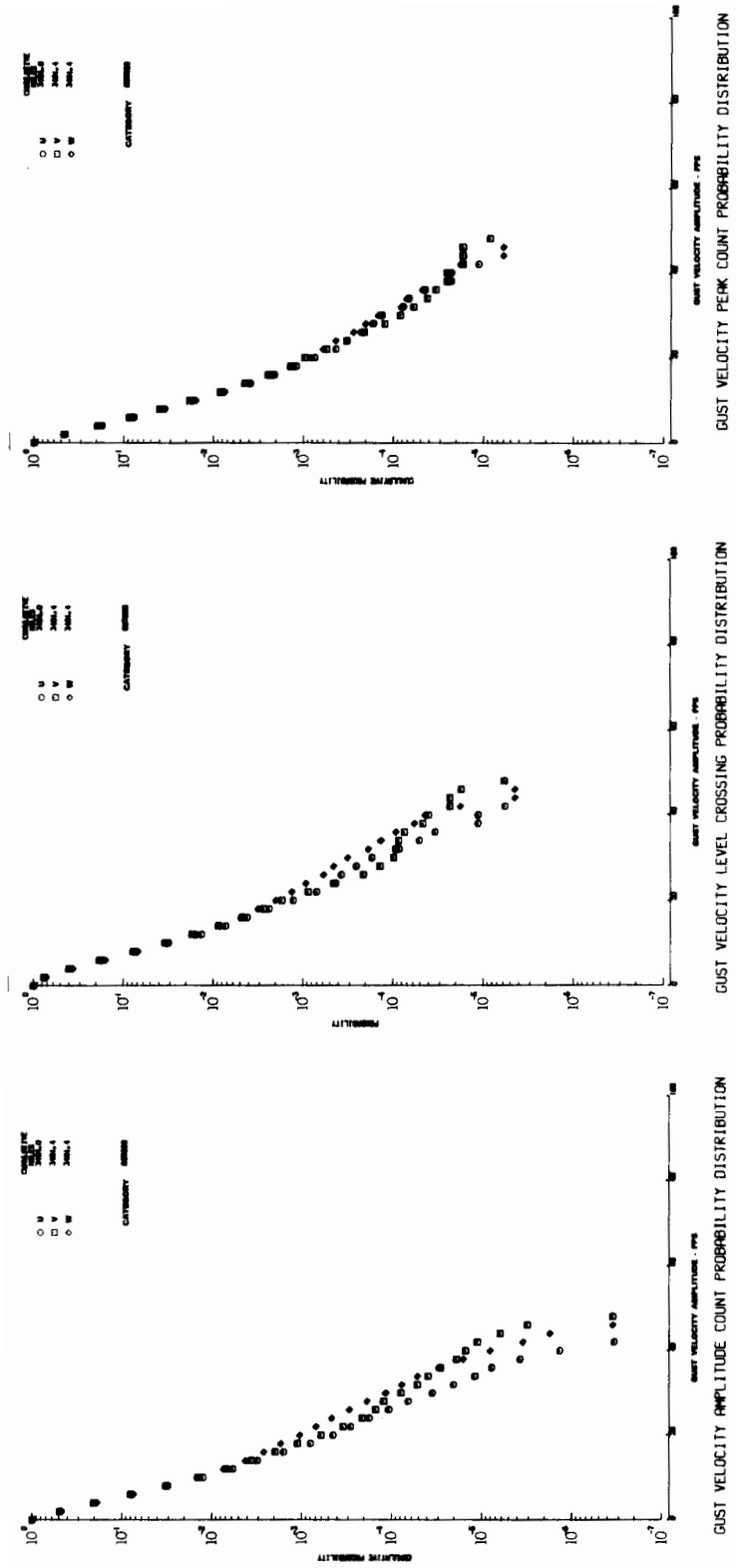


Figure V-23 Gust Velocity Peak, Amplitude and Level Crossing Probability Distributions

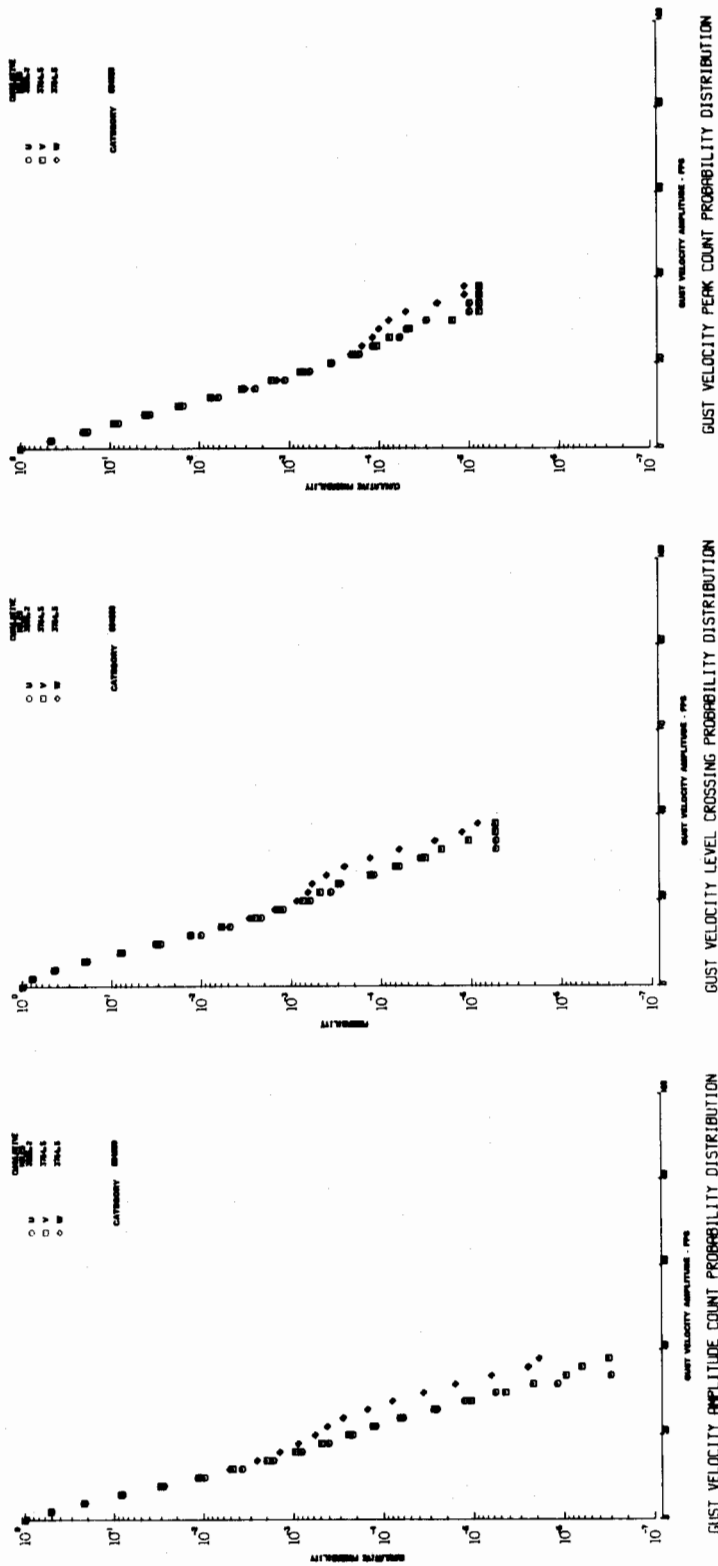


Figure V-24 Gust Velocity Peak, Amplitude and Level Crossing Probability Distributions

## APPENDIX VI

### TEST LOG

The test log presented in Table VI-1 contains test information and data obtained during LO-LOCAT flights originating from McConnell AFB and Edwards AFB. The data and information contained in this appendix consists of the following:

- Date of Test
- Test Number
- Length of Flight
- Leg Number
- Category Number
- Radar Altitude
- True Airspeed
- Airplane Heading
- Ambient Temperature
- von Karman Scale Length
- Ground Temperature
- Wind Velocity
- Wind Direction
- Maximum Calculated Gust Velocity Components
- Minimum Calculated Gust Velocity Components
- Time Series Sigma of Gust Velocity Components
- Maximum Absolute Derived Equivalent Gust Velocity
- Pilot Rated Turbulence Level
- Remarks

Most of the information in the test log is of a self-explanatory nature; however, a discussion to better clarify some items is presented in the following paragraphs.

LO-LOCAT data flights were normally accomplished on a 9 flights per week schedule. Deviations from this schedule were primarily caused by airplane and instrumentation maintenance and adverse weather conditions.

The test log contains test numbers for each flight conducted for the purpose of obtaining turbulence. It will be noted in many instances that one or more legs are omitted from the test log for a particular flight. These omissions are due to the fact that either the legs were not flown, instrumentation anomalies occurred during the test, or that the turbulence level was so low that processing of the data was not accomplished. In any case, the reasons for the omissions are given in the remarks section of the log.

A category number is assigned to each turbulence sample recorded to provide a means of grouping the data with respect to terrain, target altitude above terrain, atmospheric stability, time-of-day, season of year, and the location at which the flight originated. A definition of the category number is provided on each page of the test log.

Radar altitude, true airspeed, heading, ambient temperature, ground temperature, wind velocity, and wind direction were obtained by averaging data over the entire sample. Heading is corrected for local magnetic deviations and is the angle, measured clockwise, between true north and the direction which the airplane is pointed. Wind direction is the angle, measured clockwise, between true north and the direction from which the wind is blowing. Ground temperature is recorded from an airplane-installed radiometer, corrected for emissivity.

The maximum absolute derived equivalent gust velocity is determined as explained in Section V. The maximum absolute  $U_{de}$  does not necessarily occur simultaneously with the maximum or minimum vertical gust velocity component.

The pilot rated turbulence level is that experienced over each leg and reported by the pilot following each flight. Gaps in this test log column are indicative of legs flown where the pilot rated the turbulence to be less than light.

Approximately fifty percent of the data recorded were processed completely to obtain power spectra, homogeneity, coherency and von Karman scale length. Gaps in the test log column for von Karman scale length are indicative of conditions for which data were not completely processed. Conditions marked with an asterisk were completely processed but the scale length was invalid due to nonhomogeneous turbulence. Conditions marked with an X were completely processed but the scale lengths were invalid due to low signal-to-noise ratio or instrumentation anomalies.

Table VI-2 provides a listing of data samples successfully obtained but not processed, due to the low turbulence intensity. Included in Table VI-2 is the test number, route leg, category number and ground speed (where available) for each low turbulence sample. An X in the category number indicates that lapse rate could not be calculated.





















TEST LOG TABLE VI-1

DATE	TEST	FLIGHT TIME (HR:MIN)	CATEGORY	ALTIMETER	CLOCKED TIME (HRS)	TEMPERATURE (°F)	PRESSURE (IN. HG)	WIND VELOCITY (KTS)	WIND DIRECTION (DEG)	GUST VELOCITIES - U <sub>10</sub>			LOW BAROMETER SCALE LENGTH			REMARKS						
										U <sub>10</sub> (FPS)	U <sub>10</sub> (KTS)	U <sub>10</sub> (MPS)	L <sub>10</sub> (FEET)	L <sub>10</sub> (FEET)	L <sub>10</sub> (FEET)							
10-26-66	0065	1:15	1	122331	416.7	606.1	179.8	17.1	13.7	229.7	17.1	40.18	23.24	-25.31	-22.80	24.5	1	594	1024	321		
			2	114331	654.8	601.0	541.2	105.4	11.4	196.7	25.69	29.61	33.11	-19.90	-20.67	24.3	1	1360	958	982		
			3	114331	884.0	614.2	135.4	82.4	22.0	251.1	14.43	19.29	17.26	-16.24	-18.35	-12.21	3.77	5.99	5.35	16.2	1	
			4	114331	884.0	614.2	135.4	82.4	22.0	251.1	14.43	19.29	17.26	-16.24	-18.35	-12.21	3.77	5.99	5.35	16.2	1	
			5	114331	884.0	614.2	135.4	82.4	22.0	251.1	14.43	19.29	17.26	-16.24	-18.35	-12.21	3.77	5.99	5.35	16.2	1	
			6	114331	884.0	614.2	135.4	82.4	22.0	251.1	14.43	19.29	17.26	-16.24	-18.35	-12.21	3.77	5.99	5.35	16.2	1	
			7	114331	884.0	614.2	135.4	82.4	22.0	251.1	14.43	19.29	17.26	-16.24	-18.35	-12.21	3.77	5.99	5.35	16.2	1	
			8	114331	884.0	614.2	135.4	82.4	22.0	251.1	14.43	19.29	17.26	-16.24	-18.35	-12.21	3.77	5.99	5.35	16.2	1	
10-30-68	0066	1:25	1	122331	267.2	605.6	49.8	40.3	49.3	20.20	23.63	25.43	-40.21	-20.26	-23.69	5.43	4.25	5.05	17.6	1		
			2	112331	682.1	612.5	247.7	80.4	14.2	1.1	8.89	9.72	12.04	-12.97	-9.41	-7.63	2.69	2.81	4.00	31.8	1-M	
			3	112331	411.7	618.3	180.3	50.1	13.1	14.4	24.64	27.35	24.82	-27.26	-24.71	3.85	4.81	4.00	31.8	1-M		
			4	112331	411.7	618.3	180.3	50.1	13.1	14.4	24.64	27.35	24.82	-27.26	-24.71	3.85	4.81	4.00	31.8	1-M		
			5	112331	411.7	618.3	180.3	50.1	13.1	14.4	24.64	27.35	24.82	-27.26	-24.71	3.85	4.81	4.00	31.8	1-M		
			6	112331	411.7	618.3	180.3	50.1	13.1	14.4	24.64	27.35	24.82	-27.26	-24.71	3.85	4.81	4.00	31.8	1-M		
			7	112331	411.7	618.3	180.3	50.1	13.1	14.4	24.64	27.35	24.82	-27.26	-24.71	3.85	4.81	4.00	31.8	1-M		
			8	112331	411.7	618.3	180.3	50.1	13.1	14.4	24.64	27.35	24.82	-27.26	-24.71	3.85	4.81	4.00	31.8	1-M		
0067	1:35	1:20	1	122331	607.9	607.9	368.8	51.1	65.1	117.5	12.22	11.29	19.62	-14.12	-17.42	-19.45	2.13	2.49	2.29	11.8	1	
			2	122331	607.9	607.9	368.8	51.1	65.1	117.5	12.22	11.29	19.62	-14.12	-17.42	-19.45	2.13	2.49	2.29	11.8	1	
			3	122331	607.9	607.9	368.8	51.1	65.1	117.5	12.22	11.29	19.62	-14.12	-17.42	-19.45	2.13	2.49	2.29	11.8	1	
			4	122331	607.9	607.9	368.8	51.1	65.1	117.5	12.22	11.29	19.62	-14.12	-17.42	-19.45	2.13	2.49	2.29	11.8	1	
			5	122331	607.9	607.9	368.8	51.1	65.1	117.5	12.22	11.29	19.62	-14.12	-17.42	-19.45	2.13	2.49	2.29	11.8	1	
			6	122331	607.9	607.9	368.8	51.1	65.1	117.5	12.22	11.29	19.62	-14.12	-17.42	-19.45	2.13	2.49	2.29	11.8	1	
			7	122331	607.9	607.9	368.8	51.1	65.1	117.5	12.22	11.29	19.62	-14.12	-17.42	-19.45	2.13	2.49	2.29	11.8	1	
			8	122331	607.9	607.9	368.8	51.1	65.1	117.5	12.22	11.29	19.62	-14.12	-17.42	-19.45	2.13	2.49	2.29	11.8	1	
0068	1:25	1:20	1	222331	717.8	603.4	286.5	54.3	75.7	17.7	332.7	11.91	13.48	14.74	-16.71	-10.71	-12.64	2.42	1.89	0.82	10.4	1
			2	222331	717.8	603.4	286.5	54.3	75.7	17.7	332.7	11.91	13.48	14.74	-16.71	-10.71	-12.64	2.42	1.89	0.82	10.4	1
			3	222331	717.8	603.4	286.5	54.3	75.7	17.7	332.7	11.91	13.48	14.74	-16.71	-10.71	-12.64	2.42	1.89	0.82	10.4	1
			4	222331	717.8	603.4	286.5	54.3	75.7	17.7	332.7	11.91	13.48	14.74	-16.71	-10.71	-12.64	2.42	1.89	0.82	10.4	1
			5	222331	717.8	603.4	286.5	54.3	75.7	17.7	332.7	11.91	13.48	14.74	-16.71	-10.71	-12.64	2.42	1.89	0.82	10.4	1
			6	222331	717.8	603.4	286.5	54.3	75.7	17.7	332.7	11.91	13.48	14.74	-16.71	-10.71	-12.64	2.42	1.89	0.82	10.4	1
			7	222331	717.8	603.4	286.5	54.3	75.7	17.7	332.7	11.91	13.48	14.74	-16.71	-10.71	-12.64	2.42	1.89	0.82	10.4	1
			8	222331	717.8	603.4	286.5	54.3	75.7	17.7	332.7	11.91	13.48	14.74	-16.71	-10.71	-12.64	2.42	1.89	0.82	10.4	1
11-4-68	0070	1:00	1	212331	349.5	616.5	282.5	43.5	53.6	22.2	321.7	12.31	11.80	12.32	-16.94	-11.20	-12.26	3.25	2.42	2.13	17.0	1
			2	212331	349.5	616.5	282.5	43.5	53.6	22.2	321.7	12.31	11.80	12.32	-16.94	-11.20	-12.26	3.25	2.42	2.13	17.0	1
			3	212331	349.5	616.5	282.5	43.5	53.6	22.2	321.7	12.31	11.80	12.32	-16.94	-11.20	-12.26	3.25	2.42	2.13	17.0	1
			4	212331	349.5	616.5	282.5	43.5	53.6	22.2	321.7	12.31	11.80	12.32	-16.94	-11.20	-12.26	3.25	2.42	2.13	17.0	1
			5	212331	349.5	616.5	282.5	43.5	53.6	22.2	321.7	12.31	11.80	12.32	-16.94	-11.20	-12.26	3.25	2.42	2.13	17.0	1
			6	212331	349.5	616.5	282.5	43.5	53.6	22.2	321.7	12.31	11.80	12.32	-16.94	-11.20	-12.26	3.25	2.42	2.13	17.0	1
			7	212331	349.5	616.5	282.5	43.5	53.6	22.2	321.7	12.31	11.80	12.32	-16.94	-11.20	-12.26	3.25	2.42	2.13	17.0	1
			8	212331	349.5	616.5	282.5	43.5	53.6	22.2	321.7	12.31	11.80	12.32	-16.94	-11.20	-12.26	3.25	2.42	2.13	17.0	1
11-5-68	0073	1:25	1	222331	287.9	596.4	271.0	48.2	83.2	32.7	312.7	12.40	14.09	13.35	-16.44	-13.78	-13.46	3.26	3.26	3.56	18.3	1
			2	222331	287.9	596.4	271.0	48.2	83.2	32.7	312.7	12.40	14.09	13.35	-16.44	-13.78	-13.46	3.26	3.26	3.56	18.3	1
			3	222331	287.9	596.4	271.0	48.2	83.2	32.7	312.7	12.40	14.09	13.35	-16.44	-13.78	-13.46	3.26	3.26	3.56	18.3	1
			4	222331	287.9	596.4	271.0	48.2	83.2	32.7	312.7	12.40	14.09	13.35	-16.44	-13.78	-13.46	3.26	3.26	3.56	18.3	1
			5	222331	287.9	596.4	271.0	48.2	83.2	32.7	312.7	12.40	14.09	13.35	-16.44	-13.78	-13.46	3.26	3.26	3.56	18.3	1
			6	222331	287.9	596.4	271.0	48.2	83.2	32.7	312.7	12.40	14.09	13.35	-16.44	-13.78	-13.46	3.26	3.26	3.56	18.3	1
			7	222331	287.9	596.4	271.0	48.2	83.2	32.7	312.7	12.40	14.09	13.35	-16.44	-13.78	-13.46	3.26	3.26	3.56	18.3	1
			8	222331	287.9	596.4	271.0	48.2	83.2	32.7	312.7	12.40	14.09	13.35	-16.44	-13.78	-13.46	3.26	3.26	3.56	18.3	1
0074	1:25	1:20	1	222331	703.1	608.0	272.7	47.6	80.6	40.6	322.9	21.20	16.64	31.36	-29.27	-24.53	-31.79	4.39	3.74	4.56	18.9	1
			2	222331	703.1	608.0	272.7	47.6	80.6	40.6	322.9	21.20	16.64	31.36	-29.27	-24.53	-31.79	4.39	3.74	4.56	18.9	1
			3	222331	703.1	608.0	272.7	47.6	80.6	40.6	322.9	21.20	16.64	31.36	-29.27	-24.53	-31.79	4.39	3.74	4.56	18.9	1
			4	222331	703.1	608.0	272.7	47.6	80.6	40.6	322.9	21.20	16.64	31.36	-29.27	-24.53	-31.79	4.39	3.74	4.56	18.9	1
			5	222331	703.1	608.0	272.7	47.6	80.6	40.6	322.9	21.20	16.64	31.36	-29.27	-24.53	-31.79	4.39	3.74	4.56	18.9	1
			6	222331	703.1	608.0	272.7	47.6	80.6	40.6	322.9	21.20	16.64	31.36	-29.27	-24.53	-31.79	4.39	3.74	4.56	18.9	1
			7	222331	703.1	608.0	272.7	47.6	80.6	40.6	322.9	21.20	16.64	31.36	-29.27	-24.53	-31.79	4.39	3.74	4.56	18.9	1
			8	222331	703.1	608.0	272.7	47.6	80.6	40.6	322.9	21.20	16.64	31.36	-29.27	-24.53	-31.79	4.39	3.74	4.56	18.9	1

REMARKS ARE GOLF LENGTHS





TEST LOG TABLE VI-1

DATE	TEST	FLIGHT TIME (HR:MIN)	LEAD CATEGORY	ALTITUDE (FEET)	TEMPERATURE (°F)	VELOCITY (KNOTS)	WIND VELOCITY (KNOTS)	WIND		VELOCITY		VELOCITY		VELOCITY		VELOCITY		PILOT TOLERANCE (PERCENT)	% MAXIMUM ALTITUDE (PERCENT)	% MAXIMUM VELOCITY (PERCENT)	REMARKS		
								TEMPERATURE (°F)	WIND VELOCITY (KNOTS)	WIND VELOCITY (KNOTS)	WIND VELOCITY (KNOTS)	WIND VELOCITY (KNOTS)	WIND VELOCITY (KNOTS)	WIND VELOCITY (KNOTS)	WIND VELOCITY (KNOTS)	WIND VELOCITY (KNOTS)	WIND VELOCITY (KNOTS)						
11-14-68	CORR	1:20	1	11-14-68	601.9	617.7	179.4	60.1	87.5	18.1	384.3	10.87	17.48	18.30	-17.78	-13.84	-13.68	3.13	4.28	5.99	27.0		
			2	11-14-68	531.7	546.3	343.6	87.8	8.5	84.94	28.73	-27.74	-23.94	-24.04	-24.04	-24.04	-24.04	-24.04	5.08	6.86	8.81	37.7	
			3	11-14-68	289.5	303.9	134.0	81.7	7.5	118.4	11.80	11.80	11.80	11.80	11.80	11.80	11.80	11.80	2.30	2.78	3.57	18.3	
			4	11-14-68	168.1	168.1	60.8	86.8	8.9	108.4	11.89	-12.87	-8.48	-8.78	-8.78	-8.78	-8.78	-8.78	2.47	2.87	3.58	28.3	
			5	11-14-68	114.5	114.5	57.3	81.0	7.7	884.8	13.18	11.77	16.87	-10.53	-10.56	-10.90	-10.90	-10.90	8.37	8.75	8.87	21.8	
			6	11-14-68	100.0	100.0	43.7	80.7	12.9	80.7	8.70	10.33	7.82	-8.08	-18.08	-8.86	-8.86	-8.86	1.41	1.61	1.61	14.8	
			7	11-14-68	84.1	84.1	36.8	80.8	8.0	80.0	8.71	6.21	3.78	8.08	8.08	8.08	8.08	8.08	0.82	0.84	0.75	18.1	
			8	11-14-68	68.6	68.6	27.8	80.8	179.8	80.8	179.8	179.8	179.8	179.8	179.8	179.8	179.8	179.8	179.8	8.81	8.87	8.78	28.4
CORR	1:20	1	11-14-68	606.8	606.8	170.7	70.8	68.1	18.1	318.0	12.42	12.42	12.42	12.42	12.42	12.42	12.42	3.18	3.28	3.28	25.6		
		2	11-14-68	546.0	546.0	137.5	70.8	68.1	11.5	164.2	7.81	6.82	9.21	-13.80	-8.19	-8.19	-8.19	1.81	1.78	1.84	10.8		
		3	11-14-68	464.1	464.1	108.1	68.1	71.3	9.3	185.1	10.86	14.87	10.08	-8.08	-10.83	-8.45	-8.45	1.41	1.36	1.38	13.3		
		4	11-14-68	431.9	431.9	114.9	65.7	78.2	9.0	148.1	18.42	11.94	8.38	-13.18	-15.08	-12.28	-12.28	2.70	2.98	3.07	13.8		
		5	11-14-68	388.7	388.7	81.2	101.4	101.4	18.1	18.1	18.1	18.1	18.1	18.1	18.1	18.1	18.1	18.1	3.31	3.31	3.31	18.2	
		6	11-14-68	348.8	348.8	68.8	81.8	81.8	11.2	179.7	3.58	5.68	6.68	6.08	-4.18	-3.42	-3.42	0.84	1.01	0.80	8.1		
		7	11-14-68	310.8	310.8	51.0	81.8	81.8	11.2	179.7	18.48	16.34	13.18	-20.18	-20.08	-20.08	-20.08	6.18	5.37	5.85	21.8		
		8	11-14-68	271.8	271.8	33.9	84.4	84.4	8.7	180.1	18.48	16.34	13.18	-20.18	-20.08	-20.08	-20.08	6.18	5.37	5.85	21.8		
CORR	1:20	1	11-14-68	231.8	231.8	11.9	87.0	101.2	16.1	18.48	16.34	13.18	-20.18	-20.08	-20.08	-20.08	-20.08	6.18	5.37	5.85	21.8		
		2	11-14-68	191.8	191.8	7.4	88.8	88.8	6.7	204.8	18.48	16.34	13.18	-20.18	-20.08	-20.08	-20.08	6.18	5.37	5.85	21.8		
		3	11-14-68	151.8	151.8	18.7	88.8	88.8	8.1	188.8	18.48	16.34	13.18	-20.18	-20.08	-20.08	-20.08	6.18	5.37	5.85	21.8		
		4	11-14-68	111.8	111.8	11.9	88.8	88.8	17.3	188.8	18.48	16.34	13.18	-20.18	-20.08	-20.08	-20.08	6.18	5.37	5.85	21.8		
		5	11-14-68	71.8	71.8	84.4	88.8	88.8	18.8	188.8	18.48	16.34	13.18	-20.18	-20.08	-20.08	-20.08	6.18	5.37	5.85	21.8		
		6	11-14-68	31.8	31.8	137.8	88.8	88.8	1.7	38.0	8.11	8.04	11.71	-8.89	-11.80	-8.89	-8.89	8.28	8.40	8.18	17.8		
		7	11-14-68	17.8	17.8	48.4	88.8	88.8	3.1	88.8	8.81	14.28	8.02	-10.86	-12.84	-12.77	-12.77	8.02	8.88	1.84	13.8		
		8	11-14-68	7.8	7.8	117.1	87.0	87.0	24.8	188.8	18.48	16.34	13.18	-20.18	-20.08	-20.08	-20.08	6.18	5.37	5.85	21.8		
CORR	1:20	1	11-14-68	287.0	287.0	179.4	68.5	75.8	18.1	318.0	12.42	12.42	12.42	12.42	12.42	12.42	12.42	3.18	3.28	3.28	25.6		
		2	11-14-68	247.0	247.0	137.5	68.5	75.8	11.5	164.2	7.81	6.82	9.21	-13.80	-8.19	-8.19	-8.19	1.81	1.78	1.84	10.8		
		3	11-14-68	165.1	165.1	108.1	68.5	75.8	9.3	185.1	10.86	14.87	10.08	-8.08	-10.83	-8.45	-8.45	1.41	1.36	1.38	13.3		
		4	11-14-68	125.1	125.1	81.9	68.5	75.8	9.0	148.1	18.42	11.94	8.38	-13.18	-15.08	-12.28	-12.28	2.70	2.98	3.07	13.8		
		5	11-14-68	85.1	85.1	61.2	101.2	101.2	18.1	18.1	18.1	18.1	18.1	18.1	18.1	18.1	18.1	18.1	3.31	3.31	3.31	18.2	
		6	11-14-68	45.1	45.1	41.8	88.8	88.8	11.2	179.7	3.58	5.68	6.68	6.08	-4.18	-3.42	-3.42	0.84	1.01	0.80	8.1		
		7	11-14-68	5.1	5.1	179.7	88.8	88.8	11.2	179.7	18.48	16.34	13.18	-20.18	-20.08	-20.08	-20.08	6.18	5.37	5.85	21.8		
		8	11-14-68	1.1	1.1	179.7	88.8	88.8	11.2	179.7	18.48	16.34	13.18	-20.18	-20.08	-20.08	-20.08	6.18	5.37	5.85	21.8		

\* NUMERICAL VALUES ARE SCALE LIMITS FOR ONLY HOMOGENEOUS AND MARCINALLY HOMOGENEOUS TURBULENCE  
 \* - SCALE LIMITS INVALID BECAUSE OF NON-HOMOGENEOUS TURBULENCE  
 \* X - SCALE LIMITS INVALID BECAUSE OF LOW SIGNAL TO NOISE RATIO OR INSTRUMENTATION PROBLEMS.

1. LIGHT  
 2. MODERATE  
 3. SEVERE  
 4. EXTREME

1. REMAINS ALIVE  
 2. DROPPED ALTITUDE  
 3. EXCEEDED ALTITUDE  
 4. EXCEEDED ALTITUDE  
 5. EXCEEDED ALTITUDE

1. QUALITY  
 2. VERY POOR  
 3. POOR  
 4. FAIR  
 5. GOOD  
 6. EXCELLENT



TEST LOG TABLE VI-1

DATE	TEST	FLIGHT TIME (HR-MIN)	LATE CATEGORY	ALTITUDE (FEET)	AVERAGE TRUE ALTITUDE (FEET)	TEMPERATURE (°F)	TEMPERATURE (°F)	WIND VELOCITY (KTS)	WIND DIRECTION (DEG)	CROSS VELOCITIES				PILOT WING LEVEL	VOR KAIMA SCALE LENGTH	REMARKS								
										W (FPS)	V (FPS)	Y (FPS)	Z (FPS)											
11-25-68	0086	1:20	1	214531	606.4	64.3	85.3	17.3	14.4	15.09	17.69	20.88	-28.74	-319.24	4.14	5.90	4.29	20.9	L	LANS 2 AND 7 NOT FLAM DUE TO WATER				
			4	611331	397.1	61.0	68.7	3.98	3.55	4.16	6.34	3.69	3.47											
			5	113331	377.8	60.5	70.8	84.0	16.7	35.8	15.11	27.12	34.39	-54.31	-28.41	4.70	4.74	5.63	32.6	M				
			6	213331	621.2	65.9	89.1	10.5	43.2	10.57	17.08	9.85	-14.57	-11.51	2.52	2.77	2.46	18.6	L	587	508	292		
			8	214531	550.4	65.9	60.8	81.2	52.9	298.8	18.06	21.06	23.88	-12.64	-18.94	4.08	3.70	3.74	26.1	L	602	682	682	
			1	221131	626.5	66.9	56.9	56.7	24.0	8.01	9.42	10.80	-10.19	-9.77	-6.50	1.55	1.78	1.19	9.1	X	X	X	LANS 2, 5, 6 AND 7 NOT FLAM DUE TO WATER.	
			5	121131	815.4	67.1	66.9	66.9	35.83	34.95	29.81	-25.31	-32.13	-25.62	5.29	6.69	5.37	31.5	M	*	*			
			6	221131	623.2	67.1	69.2	69.2	12.7	12.07	11.76	-13.89	-15.60	-15.70	2.79	3.10	2.22	13.0	L					
0100	1:20	3	224531	689.1	67.4	84.3	64.0	6.5	275.1	14.94	15.67	18.88	-11.35	-16.26	2.40	2.88	2.85	23.5	L	LANS 2, 6 AND 7 NOT FLAM DUE TO WATER.				
		5	121231	761.0	62.3	178.3	64.0	17.2	80.6	19.66	20.82	23.73	-14.87	-17.94	2.40	2.88	2.85	23.5	L	NOT FLAM DUE TO WATER.				
		8	224531	683.6	62.3	65.9	65.9	29.2	133.4	18.33	20.49	23.55	-17.42	-18.61	3.26	4.08	4.56	31.3	L	NOT FLAM DUE TO WATER.				
		1	224531	681.0	60.5	60.1	81.8	24.5	24.5	13.84	13.87	22.57	-13.56	-18.36	3.29	3.18	3.95	18.5	L	NOT FLAM DUE TO WATER.				
		5	121331	759.4	62.0	178.5	64.2	89.3	12.8	266.2	16.32	16.47	20.79	-17.42	-18.61	3.29	3.18	3.95	18.5	L	NOT FLAM DUE TO WATER.			
		5	121331	765.5	62.0	66.8	66.8	64.5	6.0	205.3	14.56	12.44	20.29	-16.13	-22.88	3.11	3.55	3.79	30.2	L	NOT FLAM DUE TO WATER.			
		6	221331	750.5	61.8	131.5	61.8	82.3	6.8	202.1	7.15	9.43	9.17	-6.73	-7.23	1.79	1.67	1.49	10.4	L	NOT FLAM DUE TO WATER.			
		8	221331	697.3	63.7	111.8	60.4	82.3	34.0	127.4	14.91	19.00	20.01	-16.17	-17.52	3.19	3.61	3.23	19.6	L	NOT FLAM DUE TO WATER.			
11-26-68	0102	1:20	1	212131	286.5	63.5	63.2	6.3	17.0	12.58	16.25	17.52	-16.10	-15.79	3.30	3.27	2.66	16.2	L	LANS 2 AND 7 NOT FLAM DUE TO WATER.				
			2	312131	240.5	60.6	84.5	68.5	4.3	17.0	4.88	4.46	3.12	-5.10	-4.51	3.01	1.12	1.00	0.54	5.2	X	NOT FLAM DUE TO WATER.		
			3	112131	415.6	59.5	178.3	60.8	44.6	20.17	20.53	24.28	-23.87	-18.43	-25.64	3.82	4.32	4.51	37.7	L	NOT FLAM DUE TO WATER.			
			4	612131	239.1	60.5	58.7	66.5	58.7	66.5	3.08	5.98	3.03	-4.07	-4.15	-3.19								
			5	112131	506.1	64.9	546.1	64.9	54.0	15.32	30.46	46.86	-25.07	-23.34	-29.21	4.37	5.83	5.42	32.4	M				
			6	211331	282.2	62.5	139.8	60.0	44.7	8.01	8.59	6.07	-8.91	-10.82	-10.55	1.68	1.56	0.88	10.8	X	X			
			7	311331	256.6	54.9	47.4	50.5	1.2	7.12	8.41	5.23	-9.24	-14.23	-6.54	1.80	2.15	1.29	21.0	X	X			
			8	211331	376.7	62.0	106.2	60.4	68.4	10.87	12.75	8.59	-8.81	-9.08	-7.68	6.75	2.75	2.15	28.6	L	X			
0104	1:20	1	214531	286.0	62.9	64.0	71.0	23.6	15.05	14.55	13.67	-13.58	-18.35	-15.08	3.42	3.73	3.45	16.2	L	NOT FLAM DUE TO WATER.				
		2	312331	248.6	60.1	241.6	68.2	74.1	14.0	326.2	7.24	6.43	6.78	-6.21	-6.13	-5.92	1.50	2.04	10.8	X				
		3	112331	383.1	60.5	177.9	66.3	68.6	10.0	76.1	15.66	19.55	17.55	-12.06	-14.48	2.80	4.55	4.08	36.4	L	X			
		5	112331	446.0	58.2	545.8	53.1	80.5	10.0	10.0	11.74	22.80	31.48	-13.22	-31.31	3.06	5.20	5.42	24.3	L	X			
		6	212331	287.4	62.6	129.8	67.7	76.5	6.8	158.2	6.11	11.55	10.17	-7.43	-8.48	1.82	2.05	2.25	14.8	X	X			
		7	312331	275.1	61.8	65.0	64.9	74.1	3.4	186.2	5.60	7.89	12.52	-10.53	-8.07	-8.05	1.88	2.01	2.47	24.3	X	X		
		8	212331	341.7	62.8	110.2	47.2	72.9	15.7	136.8	17.06	21.54	-16.02	-18.18	-14.88	3.79	3.87	4.01	21.6	L	X			
		1	214531	286.7	61.9	53.1	63.7	63.7	25.0	21.06	17.06	21.54	-16.02	-18.18	-14.88	3.79	3.87	3.52	16.2	L	X			
0106	1:20	2	312331	236.4	62.1	242.2	54.0	98.6	11.2	348.8	9.24	9.40	11.12	-9.47	-9.48	-10.08	2.53	2.32	2.64	12.1	X	X		
		3	121331	305.8	60.5	178.0	61.7	79.8	5.6	346.4	11.96	15.94	21.91	-21.70	-19.78	-17.33	3.36	2.98	3.41	24.3	L	X		
		5	113331	547.8	60.8	545.3	58.4	85.5	4.1	31.0	11.74	22.80	31.48	-13.22	-31.31	3.06	5.20	5.42	24.3	L	X			
		6	213331	278.5	62.2	128.6	54.0	78.7	8.1	135.3	11.96	10.07	12.67	-10.86	-11.81	-11.86	2.49	2.34	2.43	20.2	L	X		
		7	313331	257.7	61.7	42.1	50.6	77.1	6.7	106.5	8.12	16.51	12.05	-11.86	-14.13	2.89	2.51	2.75	-	X	X			
		8	213331	311.5	62.6	107.7	51.2	72.4	9.8	135.8	13.00	21.52	20.36	-16.68	-18.25	-12.71	3.46	3.75	3.03	-	L	X		
		1	224531	681.9	61.2	52.7	83.0	12.3	6.08	9.06	12.56	-10.27	-10.81	-11.51	2.21	2.55	2.68	16.2	L	X				
		2	322331	715.6	60.9	246.9	52.8	82.4	12.9	337.2	6.15	6.34	12.03	-7.43	-7.73	1.62	1.81	2.32	10.8	X	X			
11-27-68	0106	1:20	3	121331	605.2	61.6	55.8	83.5	299.8	10.98	13.59	14.54	-11.36	-14.91	-10.81	2.88	3.54	3.46	17.5	X	X			
			5	123331	767.6	59.2	85.7	85.7	5.8	320.8	11.92	11.40	18.72	-11.47	-16.80	-14.63	2.95	2.97	3.57	26.6	X	X		
			6	222331	738.7	63.5	131.2	55.3	71.7	7.3	296.2	12.65	9.89	8.75	-8.18	-10.61	-7.46	1.89	1.70	13.5	X	X		
			7	322331	622.2	62.2	44.4	62.2	77.4	0.2	210.7	5.27	3.44	2.52	-7.22	-5.35	1.52	2.02	2.12	14.0	X	X		
			8	222331	684.4	60.6	106.3	51.8	72.6	9.7	211.0	8.72	6.48	8.16	-6.50	-9.01	-7.29	1.90	2.10	1.90	13.5	X	X	

REMARKS: VALUES ARE LOCAL LENGTHS FOR ONLY NON-ROTATIONAL AND NON-ROTATIONAL TUMBLING  
 \* - SCALE LENGTHS INVALID BECAUSE OF NON-ROTATIONAL TUMBLING  
 X - SCALE LENGTHS TRIMMED BECAUSE OF LOW SIGNAL TO NOISE RATIO OR INSTRUMENTATION PROBLEMS.

1 LIGHT  
 2 MEDIUM  
 3 SEVERE  
 4 EXTREME

1 FORWARD AFB  
 2 GUTTERS AFB  
 3 STATION  
 4 RECOVERY FIELD  
 5 RECOVERY AFB  
 6 WPTD

1 250 FEET  
 2 150 FEET  
 3 STABLE  
 4 UNSTABLE

1 250 FEET  
 2 150 FEET  
 3 STABLE  
 4 UNSTABLE



DATE	TEST	FLIGHT TIME (MIN:SEC)	LRC CATEGORY	ALTITUDE (FEET)	AERIAL SPEED (KTS)	HEADWIND (KTS)	TEMPERATURE AIR (°F)	TEMPERATURE GROUND (°F)	TEMPERATURE SURFACE (°F)	VELOCITY (KTS)	DIRECTION (DEG)	CROSS VELOCITIES				USE MAXIMUM WIND CORRECTION	CROSS VELOCITIES - $\theta_c$				REMARKS			
												U (KTS)	V (KTS)	W (KTS)	WIND (KTS)		U (KTS)	V (KTS)	W (KTS)	WIND (KTS)				
12-2-68	0108	1:20	1	214231	391.5	810.5	37.1	64.1	13.6	13.6	13.6	11.17	-10.35	-15.81	-9.62	2.59	2.73	2.43	24.8					
			2	312321	252.4	608.3	242.1	47.1	74.4	7.3	352.6	7.3	352.6	7.95	-7.00	-9.47	1.72	1.72	1.14	11.7				
			3	113231	372.7	686.9	176.8	50.7	66.8	10.9	9.2	41.47	29.11	45.94	-23.49	-24.79	-20.20	4.36	4.31	6.38	31.3	L		
			4	812331	245.8	617.4	57.7	64.3	64.3	28.7	4.99	5.88	4.37	-5.35	-3.97	-4.18				7.8		X		
			5	113231	245.8	596.0	346.8	44.4	72.8	20.9	47.1	42.35	49.59	37.44	-40.04	-26.53	7.41	8.28	6.68	41.8	M			
			6	213231	283.2	620.0	130.5	41.9	73.5	10.1	126.4	10.55	10.48	11.46	-12.23	-13.70	-10.09	2.66	2.75	2.56	15.0	L		
			7	313231	283.2	625.9	45.1	42.3	72.2	14.6	57.6	14.6	57.6	14.6	-16.04	-16.48	-9.08	2.42	2.56	2.55	35.2			
			8	213231	325.3	640.9	110.0	37.0	67.5	19.5	131.6	14.85	20.14	16.78	-14.82	-10.85	-21.02	2.72	3.24	3.31	11.0	L		
0109	1:20	1:20	1	214331	295.6	618.2	42.7	73.5	22.1	22.88	14.15	17.24	-14.86	-12.64	-14.05	3.72	3.54	3.70	17.0	L				
			2	314331	251.4	606.4	843.2	51.5	86.1	1.9	100.2	9.47	12.87	-11.64	-12.73	-10.89	2.65	2.88	2.77	14.4				
			3	114331	300.7	628.5	176.7	44.3	74.8	11.6	46.0	13.07	13.75	16.72	-15.41	-13.00	-15.52	3.10	3.22	3.60	22.2	L		
			4	611331	234.1	597.6	50.0	58.8	50.1	30.1	3.67	5.78	3.02	-5.00	-5.43				7.8					
			5	114331	325.3	628.5	246.0	50.6	77.6	6.3	6.1	13.94	26.72	37.10	-29.75	-14.45	5.05	4.75	4.21	37.8	L			
			6	214331	276.2	605.6	129.6	46.4	75.0	16.5	43.9	15.50	12.08	18.85	-20.16	-14.62	3.46	2.73	2.87	19.8	L			
			7	314331	251.4	631.6	43.2	46.4	74.4	11.0	323.0	10.26	10.98	15.82	-13.94	-16.62	-10.43	2.72	2.46	2.73	23.5			
			8	214331	300.3	633.5	108.4	42.4	64.5	16.7	90.1	12.67	15.23	15.24	-14.86	-12.81	-14.05	3.04	3.08	3.08	26.1	L		
0110	1:20	1:20	1	221131	683.7	625.5	41.6	42.9	19.6	26.48	17.85	16.51	-12.25	-18.91	-16.83	3.34	3.13	2.89	17.5	L				
			3	121131	787.8	626.4	176.7	53.1	49.0	70.7	119.1	23.25	16.94	18.62	-22.00	-16.25	3.00	3.92	3.13	20.2	L			
			4	121131	650.6	621.6	346.4	55.8	54.3	21.1	125.5	7.70	10.15	7.43	-9.03	-7.72	1.69	1.81	1.80	15.6	L			
			5	321131	712.5	621.5	45.2	47.2	49.0	6.5	22.0	6.07	6.05	4.55	-8.98	-8.47	1.62	1.38	0.89	10.8				
			6	221131	686.1	623.2	112.7	44.4	50.8	34.1	119.1	21.25	16.94	18.62	-22.00	-16.25	3.00	3.92	3.13	20.2	L			
			7	321131	712.5	621.5	45.2	47.2	49.0	6.5	22.0	6.07	6.05	4.55	-8.98	-8.47	1.62	1.38	0.89	10.8				
			8	221131	686.1	623.2	112.7	44.4	50.8	34.1	119.1	21.25	16.94	18.62	-22.00	-16.25	3.00	3.92	3.13	20.2	L			
			9	321131	712.5	621.5	45.2	47.2	49.0	6.5	22.0	6.07	6.05	4.55	-8.98	-8.47	1.62	1.38	0.89	10.8				
0111	1:20	1:20	1	224231	731.9	615.0	42.7	74.1	11.5	308.3	5.48	6.10	-7.24	-5.45	-5.67	1.83	1.30	1.04						
			3	141231	721.2	614.0	61.7	64.4	64.4	11.5	308.3	5.48	6.10	-7.24	-5.45	-5.67	1.83	1.30	1.04					
			4	141231	721.2	614.0	61.7	64.4	64.4	11.5	308.3	5.48	6.10	-7.24	-5.45	-5.67	1.83	1.30	1.04					
			5	121231	760.2	626.8	434.7	55.7	55.7	18.2	148.5	8.44	10.42	14.76	-10.37	-10.87	-8.43	2.00	2.38	1.82	14.4	L		
			6	221231	690.3	626.8	434.7	55.7	55.7	18.2	148.5	8.44	10.42	14.76	-10.37	-10.87	-8.43	2.00	2.38	1.82	14.4	L		
			7	321231	760.2	626.8	434.7	55.7	55.7	18.2	148.5	8.44	10.42	14.76	-10.37	-10.87	-8.43	2.00	2.38	1.82	14.4	L		
			8	221231	701.0	618.1	111.8	46.9	71.0	30.9	130.5	26.83	22.61	17.58	-22.47	-24.82	-17.54	5.53	4.41	3.83	17.0	L		
			9	321231	701.0	618.1	111.8	46.9	71.0	30.9	130.5	26.83	22.61	17.58	-22.47	-24.82	-17.54	5.53	4.41	3.83	17.0	L		
0112	1:20	1:20	1	224331	730.1	613.6	50.5	77.7	24.4	16.08	15.30	15.42	-12.62	-14.64	-16.61	3.55	3.18	2.87	17.0	L				
			2	324331	730.1	613.6	50.5	77.7	24.4	16.08	15.30	15.42	-12.62	-14.64	-16.61	3.55	3.18	2.87	17.0	L				
			3	124331	730.1	613.6	50.5	77.7	24.4	16.08	15.30	15.42	-12.62	-14.64	-16.61	3.55	3.18	2.87	17.0	L				
			4	224331	730.1	613.6	50.5	77.7	24.4	16.08	15.30	15.42	-12.62	-14.64	-16.61	3.55	3.18	2.87	17.0	L				
			5	124331	730.1	613.6	50.5	77.7	24.4	16.08	15.30	15.42	-12.62	-14.64	-16.61	3.55	3.18	2.87	17.0	L				
			6	224331	730.1	613.6	50.5	77.7	24.4	16.08	15.30	15.42	-12.62	-14.64	-16.61	3.55	3.18	2.87	17.0	L				
			7	324331	730.1	613.6	50.5	77.7	24.4	16.08	15.30	15.42	-12.62	-14.64	-16.61	3.55	3.18	2.87	17.0	L				
			8	224331	730.1	613.6	50.5	77.7	24.4	16.08	15.30	15.42	-12.62	-14.64	-16.61	3.55	3.18	2.87	17.0	L				
0113	1:20	1:20	1	211131	476.3	603.4	178.8	54.5	51.8	2.5	226.4	28.16	25.42	42.17	-19.31	-27.86	-28.86	4.11	3.88	5.45	25.6	M		
			2	311131	247.8	604.2	59.9	55.9	85.5	6.0	6.78	6.41	4.14	-3.33	-5.58	-4.50				5.4				
			3	111131	397.3	618.2	346.3	58.0	58.9	21.4	38.8	16.86	24.44	40.02	-26.63	-22.43	-26.44	5.08	4.87	4.76	40.4	M		
			4	211131	297.0	620.4	131.5	48.8	45.1	8.5	160.3	5.92	10.23	9.56	-6.02	-1.58	1.54	0.78	9.4					
			5	311131	330.5	620.0	110.5	48.3	54.9	2.7	281.4	27.50	25.57	34.62	-20.10	-22.82	-24.06	5.03	4.01	5.30	32.4	M		
			6	211131	289.6	613.6	52.3	71.5	34.0	24.6	23.30	22.61	28.03	-19.66	-23.06	-5.55	4.06	4.21	12.1	L				
			7	111131	416.3	603.0	178.8	55.9	60.1	17.6	30.47	26.67	34.40	-26.70	-27.38	-27.10	4.76	4.38	4.89	28.6	M			
			8	211131	287.0	628.0	134.5	52.6	58.8	4.3	36.4	11.10	10.50	11.08	-8.32	-11.83	-7.16	2.05	2.41	2.10	14.8	L		
0114	1:20	1:20	1	212231	346.5	631.9	106.2	53.6	78.5	60.20	22.50	30.17	-22.89	-24.92	-28.40	6.28	4.17	4.84	20.2	L				
			2	312231	346.5	631.9	106.2	53.6	78.5	60.20	22.50	30.17	-22.89	-24.92	-28.40	6.28	4.17	4.84	20.2	L				
			3	112231	346.5	631.9	106.2	53.6	78.5	60.20	22.50	30.17	-22.89	-24.92	-28.40	6.28	4.17	4.84	20.2	L				
			4	212231	346.5	631.9	106.2	53.6	78.5	60.20	22.50	30.17	-22.89	-24.92	-28.40	6.28	4.17	4.84	20.2	L				
			5	312231	346.5	631.9	106.2	53.6	78.5	60.20	22.50	30.17	-22.89	-24.92	-28.40	6.28	4.17	4.84	20.2	L				
			6	212231	346.5	631.9	106.2	53.6	78.5	60.20	22.50	30.17	-22.89	-24.92	-28.40	6.28	4.17	4.84	20.2	L				
			7	312231	346.5	631.9	106.2	53.6	78.5	60.20	22.50	30.17	-22.89	-24.92	-28.40	6.28	4.17	4.84	20.2	L				
			8	212231	346.5	631.9	106.2	53.6	78.5	60.20	22.50	30.17	-22.89	-24.92	-28.40	6.28	4.17	4.84	20.2	L				

NUMERICAL VALUES ARE SCALE LIMITS FOR ONLY IMMEDIATE AND MAXIMALLY PROBABILISTIC TOLERANCE.  
 \* - SCALE LIMITS SPYALIZED BECAUSE OF NON-DETERMINISTIC PROBABILITIES.  
 X - SCALE LIMITS INVALID BECAUSE OF LOW PROBABILITY OF OCCURRENCE.



TEST LOG TABLE VI-1

DATE	TIME	FLIGHT TIME (MIN)	ALTITUDE (FEET)	AIRSPEED (KTS)	TEMPERATURE (°F)	TEMPERATURE (°F)	TEMPERATURE (°F)	VELOCITY (KTS)	DIRECTION (DEG)	WIND			GUST VELOCITIES - G			% MAXIMUM ALLOWABLE			PILOT COMMENTS			
										U	V	W	U	V	W	U	V	W		U	V	W
12-10-66	0123	1:05	7	22133	660.1	54.6	50.0	64.0	18.2	133.1	16.49	12.10	13.15	-11.96	-11.41	2.42	2.71	1.40	10.4			
			8	22133	639.9	63.3	55.2	56.0	11.7	145.0	13.79	11.90	8.12	-11.89	-12.26	2.36	2.69	1.43	18.6			
			9	22133	705.2	62.4	57.1	66.2	10.2	131.0	14.92	14.34	6.96	-8.95	-12.26	2.02	2.86	1.07	9.4			
			10	22133	744.3	60.8	57.2	54.3	31.0	131.0	16.30	16.11	25.25	-18.89	-18.30	3.89	3.69	3.25	21.6			
			11	22133	761.6	59.6	57.4	61.1	47.14	131.0	17.39	16.71	29.41	-20.41	-20.41	4.33	4.49	36.0				
			12	22133	762.4	57.6	70.1	61.1	187.0	11.83	13.53	11.15	-12.71	-13.43	2.85	2.41	1.49	10.8				
			13	22133	674.9	62.3	64.9	64.5	15.1	121.0	12.43	14.48	17.41	-10.47	-15.21	2.38	2.89	2.20	29.8			
			14	22133	664.9	62.3	55.7	71.0	22.0	167.5	10.81	10.86	8.94	-13.77	-15.21	2.53	1.89	1.33	13.5			
12-17-66	0124	1:05	1	22133	665.0	62.1	55.3	78.4	27.0	124.0	12.40	14.01	-9.71	-21.96	-13.38	2.45	3.03	2.46	33.5			
			2	22133	750.0	63.4	56.7	61.7	89.5	4.7	212.2	7.72	7.39	8.46	-7.42	-7.41	1.44	1.49	9.4			
			3	22133	843.5	63.2	57.1	56.7	173.1	22.6	202.3	20.40	18.09	15.45	-20.76	-18.47	4.04	3.54	3.44	21.6		
			4	22133	889.8	62.3	55.7	71.5	10.2	183.7	10.35	17.46	14.74	-20.28	-27.32	3.89	3.49	6.40	20.6			
			5	22133	728.8	62.7	62.4	62.4	22.2	211.9	15.06	16.11	24.33	-21.88	-23.42	5.41	6.54	6.40	20.6			
			6	22133	750.0	61.4	50.8	61.4	81.2	9.0	192.7	10.13	11.96	11.18	-12.64	-10.57	2.53	2.37	1.46	14.9		
			7	22133	750.0	61.4	50.8	61.4	81.2	9.0	192.7	10.13	11.96	11.18	-12.64	-10.57	2.53	2.37	1.46	14.9		
			8	22133	643.8	60.6	101.4	56.1	74.4	6.2	211.0	8.49	11.71	11.32	-8.41	-14.71	1.87	2.41	1.81	18.2		
12-18-66	0126	1:00	1	22133	750.0	60.1	60.4	60.4	18.1	44.4	16.00	16.06	14.44	-18.45	-15.07	3.47	3.00	2.87	14.6			
			2	22133	853.9	59.9	62.7	72.8	22.8	67.4	7.08	10.50	7.59	-7.83	-7.11	1.87	1.85	2.27	10.8			
			3	22133	889.8	57.1	56.4	66.3	2.7	297.8	9.12	9.00	7.34	-8.46	-6.73	1.49	1.39	1.39	10.8			
			4	22133	889.8	57.1	56.4	66.3	2.7	297.8	9.12	9.00	7.34	-8.46	-6.73	1.49	1.39	1.39	10.8			
			5	22133	750.0	61.4	50.8	61.4	81.2	9.0	192.7	10.13	11.96	11.18	-12.64	-10.57	2.53	2.37	1.46	14.9		
			6	22133	750.0	61.4	50.8	61.4	81.2	9.0	192.7	10.13	11.96	11.18	-12.64	-10.57	2.53	2.37	1.46	14.9		
			7	22133	750.0	61.4	50.8	61.4	81.2	9.0	192.7	10.13	11.96	11.18	-12.64	-10.57	2.53	2.37	1.46	14.9		
			8	22133	750.0	61.4	50.8	61.4	81.2	9.0	192.7	10.13	11.96	11.18	-12.64	-10.57	2.53	2.37	1.46	14.9		
12-18-66	0127	1:00	1	22133	750.0	60.1	60.4	60.4	18.1	44.4	16.00	16.06	14.44	-18.45	-15.07	3.47	3.00	2.87	14.6			
			2	22133	853.9	59.9	62.7	72.8	22.8	67.4	7.08	10.50	7.59	-7.83	-7.11	1.87	1.85	2.27	10.8			
			3	22133	889.8	57.1	56.4	66.3	2.7	297.8	9.12	9.00	7.34	-8.46	-6.73	1.49	1.39	1.39	10.8			
			4	22133	889.8	57.1	56.4	66.3	2.7	297.8	9.12	9.00	7.34	-8.46	-6.73	1.49	1.39	1.39	10.8			
			5	22133	750.0	61.4	50.8	61.4	81.2	9.0	192.7	10.13	11.96	11.18	-12.64	-10.57	2.53	2.37	1.46	14.9		
			6	22133	750.0	61.4	50.8	61.4	81.2	9.0	192.7	10.13	11.96	11.18	-12.64	-10.57	2.53	2.37	1.46	14.9		
			7	22133	750.0	61.4	50.8	61.4	81.2	9.0	192.7	10.13	11.96	11.18	-12.64	-10.57	2.53	2.37	1.46	14.9		
			8	22133	750.0	61.4	50.8	61.4	81.2	9.0	192.7	10.13	11.96	11.18	-12.64	-10.57	2.53	2.37	1.46	14.9		

NUMERICAL VALUES ARE SCALE LIMITS  
 1 - LIMIT  
 2 - EXCEEDED  
 3 - EXCEEDED  
 4 - EXCEEDED  
 5 - EXCEEDED  
 6 - EXCEEDED  
 7 - EXCEEDED  
 8 - EXCEEDED  
 9 - EXCEEDED  
 X - EXCEEDED

NUMERICAL VALUES ARE SCALE LIMITS  
 1 - LIMIT  
 2 - EXCEEDED  
 3 - EXCEEDED  
 4 - EXCEEDED  
 5 - EXCEEDED  
 6 - EXCEEDED  
 7 - EXCEEDED  
 8 - EXCEEDED  
 9 - EXCEEDED  
 X - EXCEEDED

NUMERICAL VALUES ARE SCALE LIMITS  
 1 - LIMIT  
 2 - EXCEEDED  
 3 - EXCEEDED  
 4 - EXCEEDED  
 5 - EXCEEDED  
 6 - EXCEEDED  
 7 - EXCEEDED  
 8 - EXCEEDED  
 9 - EXCEEDED  
 X - EXCEEDED

NUMERICAL VALUES ARE SCALE LIMITS  
 1 - LIMIT  
 2 - EXCEEDED  
 3 - EXCEEDED  
 4 - EXCEEDED  
 5 - EXCEEDED  
 6 - EXCEEDED  
 7 - EXCEEDED  
 8 - EXCEEDED  
 9 - EXCEEDED  
 X - EXCEEDED

NUMERICAL VALUES ARE SCALE LIMITS  
 1 - LIMIT  
 2 - EXCEEDED  
 3 - EXCEEDED  
 4 - EXCEEDED  
 5 - EXCEEDED  
 6 - EXCEEDED  
 7 - EXCEEDED  
 8 - EXCEEDED  
 9 - EXCEEDED  
 X - EXCEEDED

NUMERICAL VALUES ARE SCALE LIMITS  
 1 - LIMIT  
 2 - EXCEEDED  
 3 - EXCEEDED  
 4 - EXCEEDED  
 5 - EXCEEDED  
 6 - EXCEEDED  
 7 - EXCEEDED  
 8 - EXCEEDED  
 9 - EXCEEDED  
 X - EXCEEDED

NUMERICAL VALUES ARE SCALE LIMITS  
 1 - LIMIT  
 2 - EXCEEDED  
 3 - EXCEEDED  
 4 - EXCEEDED  
 5 - EXCEEDED  
 6 - EXCEEDED  
 7 - EXCEEDED  
 8 - EXCEEDED  
 9 - EXCEEDED  
 X - EXCEEDED

NUMERICAL VALUES ARE SCALE LIMITS  
 1 - LIMIT  
 2 - EXCEEDED  
 3 - EXCEEDED  
 4 - EXCEEDED  
 5 - EXCEEDED  
 6 - EXCEEDED  
 7 - EXCEEDED  
 8 - EXCEEDED  
 9 - EXCEEDED  
 X - EXCEEDED

NUMERICAL VALUES ARE SCALE LIMITS  
 1 - LIMIT  
 2 - EXCEEDED  
 3 - EXCEEDED  
 4 - EXCEEDED  
 5 - EXCEEDED  
 6 - EXCEEDED  
 7 - EXCEEDED  
 8 - EXCEEDED  
 9 - EXCEEDED  
 X - EXCEEDED

NUMERICAL VALUES ARE SCALE LIMITS  
 1 - LIMIT  
 2 - EXCEEDED  
 3 - EXCEEDED  
 4 - EXCEEDED  
 5 - EXCEEDED  
 6 - EXCEEDED  
 7 - EXCEEDED  
 8 - EXCEEDED  
 9 - EXCEEDED  
 X - EXCEEDED











Contracts

TABLE VI-2  
LOW TURBULENCE DATA SAMPLES

TEST	LEG	CATEGORY NO.	GROUND SPEED (fps)	TEST	LEG	CATEGORY NO.	GROUND SPEED (fps)	TEST	LEG	CATEGORY NO.	GROUND SPEED (fps)	
15	1	421124	543.8	30	6	421124	644.6	81	3	11X231	-	
	2	422124	586.5		7	421124	639.6		82	4	611331	581.8
	3	42X124	634.8		8	421124	708.1		92	4	611331	557.7
	4	42X124	647.1		1	42X224	587.2		93	4	621131	-
	5	42X124	663.7		4	41X324	650.0		94	4	621231	-
	6	42X124	661.3		6	41X324	652.4		95	4	621331	563.8
	7	42X124	598.2		1	42X124	602.0		97	4	621231	-
	8	42X124	615.4		2	42X124	598.0		99	4	621131	-
25	1	424124	631.2	3	42X124	671.2	100	4	621231	585.0		
	2	421124	653.2	4	42X124	678.1	101	4	621331	-		
	3	421124	620.8	5	42X124	664.1	103	4	611231	-		
	4	421124	617.5	6	42X124	669.6	104	4	612331	571.0		
	5	421124	608.3	7	42X124	598.2	107	4	621331	587.8		
	6	421124	615.1	8	42X124	662.2	110	2	321131	597.1		
	7	421124	648.5	1	421134	605.0	112	4	621131	-		
	8	421124	648.3	2	421134	629.9	117	4	621331	581.9		
26	1	42X224	626.5	3	421134	603.8	121	4	621231	-		
	2	42X224	646.2	4	421134	602.5	127	4	621231	-		
27	1	411124	611.8	5	421134	620.0	137	4	611141	-		
	2	411124	623.4	6	421134	626.1	138	4	611241	-		
30	3	412124	624.4	7	421134	620.1	139	4	621141	-		
	5	411124	627.5	8	421134	685.1	140	4	621241	-		
	6	411124	626.4	1	421234	614.4	141	4	621341	-		
	8	411124	699.0	2	421234	615.2	142	4	611141	-		
	1	421124	586.4	3	421234	617.4	144	4	612341	-		
	2	421124	604.6	4	421234	615.6	145	4	621141	583.8		
	3	421124	624.9	4	62X231	-	146	4	621241	-		
	4	421124	627.4	4	61X331	631.8	147	4	621341	600.2		
5	421124	642.7	4	62X131	478.4							



## REFERENCES

- I-1 R. J. Niemann and C. J. Gamm (The Boeing Company), Installation, Operation and Maintenance Instrumentation Report - LO-LOCAT Phase III T-33A, AF57-0550, Boeing Document D3-7793, The Boeing Company, Wichita, Kansas, August, 1968.
- I-2 William R. Rogers and C. J. Gamm (The Boeing Company), Mobile Data Van - Flight Test Instrumentation, Boeing Document D3-7906, The Boeing Company, Wichita, Kansas, January, 1969.
- II-1 D. L. Millikan, Subsonic Wind Tunnel Tests of Two Full Scale Gust Probes for the Boeing Company, Wichita Division Report No. AA-2005-W, Cornell Aeronautical Laboratory, Inc., Buffalo, New York, December 1964.
- II-2 J. Gault, et al., Dynamic Loads Survey - B-52 with ECP 1050 (WFT 1217), B-52 Flight Test Activities Report, Boeing Document D3-13273-361A, The Boeing Company, Wichita, Kansas, May, 1966.
- II-3 A. M. Zarem and D. D. Erway, Introduction to the Utilization of Solar Energy, McGraw-Hill Book Co., Inc., 1963.
- III-1 Joseph F. A. Ormsby, "Design of Numerical Filters with Applications to Missile Data Processing," Journal of the Association for Computing Machinery, Vol. 8, No. 3, July, 1961.
- III-2 Marcel A. Martin, Digital Filters for Data Processing, G. E. Technical Information Series, 62SD484, October, 1962.
- III-3 Ronald J. Graham, Determination and Analysis of Numerical Smoothing Weights, NASA Technical Report R-179, December, 1963.
- III-4 Edward B. Anders, Digital Filters, NASA Technical Report CR-136, December, 1964.
- III-5 E. U. Condon and H. Odishaw, Handbook of Physics, McGraw-Hill Book Co., Inc., 1958.
- III-6 A. Ralston and H. S. Wilf, Mathematical Methods for Digital Computers, Wiley and Sons, Inc., 1958.
- III-7 H. A. Panofsky and G. W. Brier, Some Applications of Statistics to Meteorology, Pennsylvania State University, 1958.
- III-8 U. O. Lappe, A Climatological-Wind Turbulence Model for Estimating Low Altitude Gust Loads, AFFDL-TR-67-122, Wright-Patterson Air Force Base, Ohio, January, 1968.

Security Classification		
DOCUMENT CONTROL DATA - R & D		
<i>(Security classification of title, body of abstract and indexing annotation must be entered when the overall report is classified)</i>		
1. ORIGINATING ACTIVITY (Corporate author) The Boeing Company Wichita Division Wichita, Kansas 67210		2a. REPORT SECURITY CLASSIFICATION Unclassified
		2b. GROUP
3. REPORT TITLE Low Altitude Atmospheric Turbulence LO-LOCAT Phase III Interim Report Volume II		
4. DESCRIPTIVE NOTES (Type of report and inclusive dates) R&D Interim Report - 17 April 1968 to 8 January 1969		
5. AUTHOR(S) (First name, middle initial, last name) K. R. Monson, G. W. Jones, R. H. Mielke, et al.		
6. REPORT DATE August 1969	7a. TOTAL NO. OF PAGES 298	7b. NO. OF REFS 13
8a. CONTRACT OR GRANT NO. F33615-68-C-1498	9a. ORIGINATOR'S REPORT NUMBER(S) NONE	
b. PROJECT NO. ADP682E	9b. OTHER REPORT NO(S) (Any other numbers that may be assigned this report) AFFDL-TR-69-63, Volume II	
c.		
d.		
10. DISTRIBUTION STATEMENT This document is subject to special export controls and each transmittal to foreign governments or foreign nationals may be made only with prior approval of Air Force Flight Dynamics Laboratory (FTDE), Wright-Patterson AFB, Ohio 45433		
11. SUPPLEMENTARY NOTES		12. SPONSORING MILITARY ACTIVITY Air Force Flight Dynamics Laboratory, FDTE Wright-Patterson AFB, Ohio 45433
13. ABSTRACT The contents of this report describe accomplishments during the first half of the Low-Level Critical Air Turbulence (LO-LOCAT) Phase III program. Data that were obtained during flight over routes near McConnell Air Force Base, Kansas, and Edwards Air Force Base, California, are presented. Also included are time histories of some of the larger magnitude gust velocities recorded over the Peterson Field, Colorado route. Approximately 72 hours of low-level (0-1000 feet) turbulence and associated meteorological data recorded from August 16, 1968, through January 8, 1969, are presented. The turbulence environment is analyzed in terms of gust velocity primary peaks, amplitude samples, rms values, maximum values and derived equivalent gusts. Mathematical expressions for turbulence spectra and scale length statistics, and correlations between atmospheric gust velocities and meteorological and geophysical phenomena are shown. The most predominant characteristics of these data are the increases in rms values, scale lengths, Taylor micro scales and maximum gust values as compared to the LO-LOCAT Phases I and II data. These differences are attributed to the increased speed of the Phase III airplane which is providing a better definition of the longer wavelengths of atmospheric turbulence. This report consists of two volumes. Volume I contains a discussion of data acquisition and quality, along with a preliminary analysis of turbulence and meteorological data. Instrumentation details, calibrations and checks, data processing, gust velocity data (power spectra, peak and amplitude count, etc.) and test logs are presented in Volume II.  (Distribution of this abstract is unlimited)		

UNCLASSIFIED

Security Classification

14. KEY WORDS	LINK A		LINK B		LINK C	
	ROLE	WT	ROLE	WT	ROLE	WT
LO-LOCAT (Low-Low Altitude Critical Atmospheric Turbulence) Low Level Turbulence (0-1000 feet) Clear Air Turbulence Gust Velocity Statistics Gust Velocity Power Spectra Low Level Turbulence Models Meteorology (Turbulence) Turbulence Forecasting						

UNCLASSIFIED

Security Classification